SECONDARY METABOLISM AND FRUIT QUALITY

EDITED BY: M. Teresa Sanchez-Ballesta, Carlos R. Figueroa and Itay Maoz
PUBLISHED IN: Frontiers in Plant Science

frontiers Research Topics

frontiers

ISSN 1664-8714
ISBN 978-2-83250-878-7
DOI 10.3389/978-2-83250-878-7

About Frontiers

Frontiers is more than just an open-access publisher of scholarly articles: it is a pioneering approach to the world of academia, radically improving the way scholarly research is managed. The grand vision of Frontiers is a world where all people have an equal opportunity to seek, share and generate knowledge. Frontiers provides immediate and permanent online open access to all its publications, but this alone is not enough to realize our grand goals.

Frontiers Journal Series

The Frontiers Journal Series is a multi-tier and interdisciplinary set of open-access, online journals, promising a paradigm shift from the current review, selection and dissemination processes in academic publishing. All Frontiers journals are driven by researchers for researchers; therefore, they constitute a service to the scholarly community. At the same time, the Frontiers Journal Series operates on a revolutionary invention, the tiered publishing system, initially addressing specific communities of scholars, and gradually climbing up to broader public understanding, thus serving the interests of the lay society, too.

Dedication to Quality

Each Frontiers article is a landmark of the highest quality, thanks to genuinely collaborative interactions between authors and review editors, who include some of the world's best academicians. Research must be certified by peers before entering a stream of knowledge that may eventually reach the public - and shape society; therefore, Frontiers only applies the most rigorous and unbiased reviews.
Frontiers revolutionizes research publishing by freely delivering the most outstanding research, evaluated with no bias from both the academic and social point of view. By applying the most advanced information technologies, Frontiers is catapulting scholarly publishing into a new generation.

What are Frontiers Research Topics?

Frontiers Research Topics are very popular trademarks of the Frontiers Journals Series: they are collections of at least ten articles, all centered on a particular subject. With their unique mix of varied contributions from Original Research to Review Articles, Frontiers Research Topics unify the most influential researchers, the latest key findings and historical advances in a hot research area! Find out more on how to host your own Frontiers Research Topic or contribute to one as an author by contacting the Frontiers Editorial Office: frontiersin.org/about/contact

SECONDARY METABOLISM AND FRUIT QUALITY

Topic Editors:
M. Teresa Sanchez-Ballesta, Institute of Science and Technology of Food and Nutrition, Spanish National Research Council (CSIC), Spain
Carlos R. Figueroa, University of Talca, Chile
Itay Maoz, Agricultural Research Organization (ARO), Israel

Citation: Sanchez-Ballesta, M. T., Figueroa, C. R., Maoz, I., eds. (2022). Secondary Metabolism and Fruit Quality. Lausanne: Frontiers Media SA.
doi: 10.3389/978-2-83250-878-7

Table of Contents

frontiers | Frontiers in Plant Science

TYPE Editorial
PUBLISHED 14 November 2022
DOI 10.3389/fpls.2022.1072193

OPEN ACCESS

EDITED AND REVIEWED BY
Reuben J. Peters,
Iowa State University, United States

*CORRESPONDENCE
María Teresa Sanchez-Ballesta
mballesta@ictan.csic.es

SPECIALTY SECTION
This article was submitted to Plant Metabolism and Chemodiversity, a section of the journal Frontiers in Plant Science

RECEIVED 17 October 2022
ACCEPTED 20 October 2022
PUBLISHED 14 November 2022

CITATION
Sanchez-Ballesta MT, Maoz I and Figueroa CR (2022) Editorial: Secondary metabolism and fruit quality.
Front. Plant Sci. 13:1072193.
doi: 10.3389/fpls.2022.1072193

Editorial: Secondary metabolism and fruit quality

María Teresa Sanchez-Ballesta[1]*, Itay Maoz[2] and Carlos R. Figueroa[3,4]

[1]Department of Characterization, Quality, and Safety, Institute of Food Science, Technology and Nutrition (ICTAN-CSIC), Ciudad Universitaria, Madrid, Spain, [2]Department of Postharvest Science, Agricultural Research Organization, Volcani Institute, Rishon LeZion, Israel, [3]Laboratory of Plant Molecular Physiology, Institute of Biological Sciences, Campus Talca, Universidad de Talca, Talca, Chile, [4]Millennium Nucleus for the Development of Super Adaptable Plants (MN-SAP), Santiago, Chile

KEYWORDS

anthocyanin biosynthesis, fruit ripening, fruit volatiles, gene expression, metabolomics, phytohormones, polyphenolic metabolism, transcription factors

Editorial on the Research Topic
Secondary metabolism and fruit quality

Fruits produce a wide array of secondary metabolites, which perform essential physiological and biochemical functions. These metabolites are essential to interacting with the environment during development and postharvest storage, coping with biotic and abiotic stresses. Secondary metabolites are also of utmost importance in fruit quality from the point of view of consumer acceptability, affecting the color/appearance and the flavor, and their implication in fruit nutritional characteristics. The "*SECONDARY METABOLISM AND FRUIT QUALITY*" Research Topic is a compilation of 12 research articles, one review, and one perspective article covering the most recent advances and integrative insights into genes and compounds from the secondary metabolism related to quality traits of non-climacteric and climacteric fruit, such as apricot, grape, cucumber, kumquat, different citrus species, fig, and eggplant.

The importance of secondary metabolism to the environmental adaptation of grapes has been reflected in the four articles studying pre-harvest treatments (Li et el.; Martins et al.) or climate change (Lu et al.; Gashu et al.) that affect berry quality. Abscisic acid (ABA) plays an important role in non-climacteric fruit quality. Taking advantage of the availability of a new table grape cultivar, 'Ruiduhongyu', pink in color and muscatel in flavor, on which the effect of ABA had not yet been explored, Li et al., contributes to our current understanding that exogenous ABA improves fruit quality by mediating the endogenous phytohormone levels in grape. Thus, the endogenous biosynthesis of ABA, auxins, and cytokinins regulated by exogenous ABA was correlated with the improvement in appearance parameters, sugars, anthocyanins, and fatty acids. Pre- and postharvest applications of calcium (Ca) have been increasingly used in grapes to maintain fruit quality, improve fruit firmness, and control total decay. Martins et al.

combined integrated metabolomics and directed transcriptomic analysis to study the pre-harvest effect of spraying Ca in white wine grapes (cv. Loureiro) over key genes involved in polyphenol biosynthesis and metabolic profile at harvest time. Authors suggested a specific integrated effect of Ca over biochemical and structural properties of white berries down- and up-regulating the expression of *PG1* and *PAL1*, respectively, leading to increased firmness and higher levels of flavonols, at the expense of fruit size and °Brix.

Climate change modifies environmental conditions for fruit production worldwide. Two research articles studied grapes to understand how climatic changes affect fruit quality, either by exploiting the seasonal climatic variations under the double cropping system (Lu et al.) or differences in temperature and radiation in two experimental vineyards (Gashu et al.). Metabolomic and transcriptomic analysis revealed that under the double cropping system, winter wine and table grape berries presented higher concentrations of different volatiles such as terpenes and norisoprenoids correlated with the accumulation of *VviDXS*s, *VviPSY*s, and *VviCCD*s at the transcriptional level (Lu et al.). However, the metabolomic analysis carried out on ten white wine grape cultivars over three years showed that the effect of radiation and temperature on carotenoid and phenylpropanoid contents during ripening was seasonal and varietal-dependent (Gashu et al.), highlighting the potential of crop plasticity to resist elevated temperatures. Savoi et al. presented a perspective article exploring the universe of omics studies conducted on grapes. The authors presented the first integrated grapevine transcriptomics and metabolomics database developed within the *Vitis* Visualization platform to understand berry quality and secondary metabolism.

The spatiotemporal changes of the secondary metabolism in plants are regulated by a complex network of transcription factors, including AP2/ERF, WRKY, bHLH, bZIP, MYB, and NAC. Two research articles lay the foundation for understanding the role of the bHLH transcription factor family in anthocyanin biosynthesis in fruit. Song et al. identified 118 hypothetical bHLH genes in the fig genome; phylogenetic analysis indicated their classification into 25 subfamilies. Transcriptomic data obtained from the re-mined three fig fruit RNA-seq libraries allowed them to screen *FcbHLH42* as a candidate gene related to anthocyanin synthesis. Indeed, further yeast-two hybrid experiments showed the interaction between FcbHLH42 and anthocyanin synthesis-related proteins and its transient expression in tobacco leaves, which led to an apparent anthocyanin accumulation. However, this does not seem to be a shared role of all bHLHs, since *SmbHLH1* from eggplant was identified as a potential repressor of anthocyanin biosynthesis in eggplant fruit peel (Duan et al.). *SmbHLH1* presented a high identity with *SmTT8*, a *SmMYB113*-dependent positive regulator of anthocyanin-biosynthesis in plants, but results indicated different action mechanisms. Thus, *in vitro* and *in vivo* experiments showed that SmbHLH1 could not interact with SmMYB113, whereas SmTT8 could. In addition, SmbHLH1 inhibited anthocyanin biosynthesis, probably by repressing *SmDFR* and *SmANS* expression.

Integrative studies are a valuable tool for discovering new metabolic pathways, genes, and/or traits. In this special issue, a cucumber (Jo et al.) and kumquat (Ma et al.) fruit quality were investigated using metabolomic and transcriptomic approaches. In the first study, Jo et al. compared the peel and flesh of three different cucumber cultivars (Chuichung, White Dadagi, and Mini), including one (Mini) recently developed in Korea. Results indicated differences between tissues and cultivars. Thus, fruit from the cultivar Mini, which is the smallest, presented higher levels of flavonoids and carotenoids in the pulp. However, these were higher in the peel of Chuichung, which is the largest one. Moreover, the antioxidant activity assays, flavonoid-(*CHS* and *4CL*), and carotenoid-related (*PSY* and *ZDS*) genes followed the same tendency in both cultivars.

By taking advantage of the availability of a spontaneous seedling mutant named 'Huapi' from 'Rongan' kumquat, having desirable traits such as glossy peel, fewer seeds, and less spicy flavor in comparison to the wild type, Ma et al. investigated the mechanisms related to its unique phenotype. The authors indicated that differences could be explained at the transcriptional and biochemical levels and attributed to the high levels of glycosylated flavonoid and low lysophospholipid accumulation in the mutant. Since this cultivar accumulates large amounts of flavones, Tian et al. carried out a molecular characterization of *FcFNSII-2* to lay the foundations for improving its composition in kumquat fruit. *In vivo* and *in vitro* results confirmed that FNSII-2 could be a good candidate for engineering the pathway since it was able to activate the transcription of structural genes of the flavonoid-biosynthesis pathway, interact with *CHS* and *CHI* genes and convert flavanones into corresponding flavones.

Rey et al. comprehensively addressed a comparative metabolomic and transcriptional study of tocopherol accumulation during fruit maturation of four *Citrus* species, namely orange, mandarin, lemon, and grapefruit. Tocopherol contents were higher in the flavedo and increased in this tissue during maturation, paralleled by the induction of genes *TAT1* and *VTE4*, which regulate homogentisate availability and the conversion of γ- to α-tocopherol, respectively. However, the contents decreased or remained constant in the pulp, reflecting changes in the expression of genes *VTE6*, *DXS2*, and *GGDR*, which regulate phytyl pyrophosphate availability.

Apricot fruits' aromatic profile consists of a large number of volatile compounds. Among the diverse chemical groups of compounds, esters are considered key odorants that influence

flavor quality, similar to other fruits, such as apples. Zhou et al. identified *PaAAT1* as a new candidate gene involved in the biosynthesis of volatiles in apricot fruit. Specifically, transient expression of *PaAAT1* in apricot fruit, together with *in vitro* assays using the recombinant protein, suggest its involvement in the biosynthesis of C_6 esters during fruit ripening.

There is a growing interest in using rapid, accurate, and cost-effective methods in the food industry and research instead of classic methods, which involve a high amount of chemicals, some of which are often hazardous and costly. Hssaini et al. obtained promising results using the Fourier transform infrared with attenuated total reflectance (FTIR-ATR) spectra coupled with partial least square regression (PLSR) model to predict the amounts of phenolic acids and flavonoids concerning their partitioning between the peel and pulp of fresh figs.

Finally, this Research Topic brings a review article about the molecular biology underlying the branched-chain volatiles (BCVs), essential to the characteristic flavor and aroma profiles of many edible fruits, such as bananas and melons. The authors paid attention to the diversity of BCV compounds identified in edible fruits and reviewed the four general hypotheses concerning the mechanisms of BCV biosynthesis. They also explored whether the regulatory mechanisms known to control similar pathways in mammals could offer potential avenues for altering the BCV content of fruit.

Understanding how secondary metabolism affects fruit quality is necessary to develop novel approaches aiming to reduce losses during pre- and postharvest. We hope readers will find this Research Topic a valuable reference to further explore secondary metabolism regulation and its implication in fruit quality.

Author contributions

MTS-B wrote the first draft of the manuscript. All authors have revised and approved the manuscript for publication.

Funding

MTS-B's work was supported by the CICYT project PID2020-113965RB-I00/AEI/10.13039/501100011033. CRF was supported by the National Research and Development Agency (ANID) – Millenium Science Initiative Program – NCN2021_010 and FONDECYT/Regular 1210941.

Conflict of interest

The authors declare that the research was conducted in the absence of any commercial or financial relationships that could be construed as a potential conflict of interest.

Publisher's note

frontiers in Plant Science

ORIGINAL RESEARCH
published: 27 August 2021
doi: 10.3389/fpls.2021.742887

Exogenous Calcium Delays Grape Berry Maturation in the White cv. Loureiro While Increasing Fruit Firmness and Flavonol Content

Viviana Martins[1,2], Marianne Unlubayir[3], António Teixeira[1], Arnaud Lanoue[3] and Hernâni Gerós[1,2,4]*

[1] Department of Biology, Centre of Molecular and Environmental Biology, University of Minho – Campus de Gualtar, Braga, Portugal, [2] Centre for the Research and Technology of Agro-Environmental and Biological Sciences, University of Trás-os-Montes and Alto Douro, Vila Real, Portugal, [3] EA 2106 Biomolécules et Biotechnologie Végétales, UFR des Sciences Pharmaceutiques, Université de Tours, Tours, France, [4] Department of Biological Engineering, Centre of Biological Engineering (CEB), University of Minho – Campus de Gualtar, Braga, Portugal

OPEN ACCESS

Edited by:
M. Teresa Sanchez-Ballesta, Instituto de Ciencia y Tecnología de Alimentos y Nutrición (ICTAN), Spain

Reviewed by:
Michaela Griesser, University of Natural Resources and Life Sciences Vienna, Austria
Nazareth Torres, University of California, Davis, United States

***Correspondence:**
Viviana Martins
vmartins@bio.uminho.pt

Specialty section:
This article was submitted to Plant Metabolism and Chemodiversity, a section of the journal Frontiers in Plant Science

Received: *16 July 2021*
Accepted: *09 August 2021*
Published: *27 August 2021*

Citation:
Martins V, Unlubayir M, Teixeira A, Lanoue A and Gerós H (2021) Exogenous Calcium Delays Grape Berry Maturation in the White cv. Loureiro While Increasing Fruit Firmness and Flavonol Content. Front. Plant Sci. 12:742887. doi: 10.3389/fpls.2021.742887

Vineyard calcium (Ca) sprays have been increasingly used by grape growers to improve fruit firmness and thus maintain quality, particularly in periods of heavy rains and hail. The observation that Ca visibly modified berry size, texture, and color in the most prominent white cultivar of the DOC region 'Vinhos Verdes', cultivar (cv.) Loureiro, led us to hypothesize that Ca induced metabolic rearrangements that resulted in a substantial delay in fruit maturation. Targeted metabolomics by ultra-performance liquid chromatography coupled to mass spectrometry and directed transcriptomics were thus combined to characterize the metabolic and transcriptional profiles of cv. Loureiro berries that, together with firmness, °Brix, and fruit weight measurements, allowed to obtain an integrated picture of the biochemical and structural effects of Ca in this cultivar. Results showed that exogenous Ca decreased amino acid levels in ripe berries while upregulating *PAL1* expression, and stimulated the accumulation of caftaric, coutaric, and fertaric acids. An increase in the levels of specific stilbenoids, namely *E*-piceid and *E*-ω-viniferin, was observed, which correlated with the upregulation of *STS* expression. Trace amounts of anthocyanins were detected in berries of this white cultivar, but Ca treatment further inhibited their accumulation. The increased berry flavonol content upon Ca treatment confirmed that Ca delays the maturation process, which was further supported by an increase in fruit firmness and decrease in weight and °Brix at harvest. This newly reported effect may be specific to white cultivars, a topic that deserves further investigation.

Keywords: anthocyanins, amino acids, calcium, flavonols, fruit firmness, grape berry ripening, polyphenolic metabolism, white grape cultivars

INTRODUCTION

Calcium (Ca) supplements have been increasingly used in fresh fruits and vegetables toward improved fitness, sanitation, nutritional enrichment, and decay prevention (Martín-Diana et al., 2007). Diverse supplementation strategies have been optimized, from routinely spraying the fruits throughout their development in the tree, applying a single treatment at pre-harvest, or supplying

Ca only at postharvest, through spraying, dipping, or even impregnation techniques (Saftner et al., 1997; Martín-Diana et al., 2005, 2007; Manganaris et al., 2007; Wang et al., 2014; Correia et al., 2019). The refinement of these methodologies showed that the beneficial effects of Ca can be achieved at both preharvest and postharvest stages, supporting its potential to protect the grape berries against abiotic and biotic stresses (Alcaraz-López et al., 2005; Romanazzi et al., 2012; Ciccarese et al., 2013; González-Fontes et al., 2017; Aldon et al., 2018). Accordingly, increased fruit resistance to infection by *Botrytis cinerea* during storage was achieved by Ca dips after harvest (Fu et al., 2020), an effect that was also reported upon vineyard Ca sprays between fruit set and veraison stages (Amiri et al., 2009; Ciccarese et al., 2013). In line with these observations, Ca sprays during berry development reduce the incidence of microcracks on the fruit surface and the lodging of filamentous fungi in these structures, reducing fruit decay at postharvest (Martins et al., 2020b, 2021a).

The effects of Ca on fruit texture are connected to its structural function in the cell wall and membranes, mediating cross-links between pectin molecules, and inhibiting the activity of polygalacturonases responsible for fruit softening (Hocking et al., 2016; Martins et al., 2020b), but a myriad of developmental and stress–response processes mediated by Ca may occur because it is a pivotal secondary messenger (González-Fontes et al., 2017; Aldon et al., 2018). Recent studies reported increased bulk anthocyanin content in berries cultivar (cv.) Manicure Finger sprayed with Ca around veraison stage (Yu et al., 2020). In contrast, a general repression in the synthesis of anthocyanins in the grape berry was shown through a targeted metabolomics approach, following Ca treatments throughout the entire fruiting season in vineyards cv. Vinhão (Martins et al., 2020a). This effect was also reported in grape cell cultures cv. Gamay Fréaux var. Teinturier, which became significantly less pigmented upon Ca treatment, due to a general repression of the entire flavonoid pathway (Martins et al., 2018, 2020a). These effects were underlaid by the Ca-driven regulation of core enzymes of secondary metabolism, at gene expression and protein activity levels, besides vacuolar transporters mediating anthocyanin accumulation (Martins et al., 2018). Transcriptomics studies in berries cv. Manicure Finger also showed the involvement of Ca-activated transcription factors in the regulation of anthocyanin levels (Yu et al., 2020). In cv. Vinhão berries, the inhibition of anthocyanin synthesis was accompanied by a general accumulation of stilbenoids, including *E*-resveratrol, *E*-ε-viniferin, *E*-piceid, and pallidol, demonstrating the powerful ability of Ca in diverting polyphenolic biosynthetic routes (Martins et al., 2020a).

The studies reported above provided a good overview of the effects of Ca over the metabolism of red wine grape cultivars (Martins et al., 2018, 2020a; Yu et al., 2020); however, how the phenolics metabolism of berries from white cultivars is affected by Ca is still puzzling. Previous studies indicated a qualitative improvement in the general color of grape berries of the white cv. Asgari (Amiri et al., 2009), but information on the metabolic mechanisms underlying these effects is lacking. The present study aimed at filling a gap in the literature, following the observation that Ca visibly modified berry size, texture, and color in the white cv. Loureiro, in two consecutive seasons. Our main hypothesis is that Ca induces specific metabolic rearrangements that result in a substantial delay in fruit maturation. Integrated metabolomics and directed transcriptomics were combined to study the effect of Ca over key genes involved in polyphenol biosynthesis and in grape berry metabolic profile at harvest time. The determination of technical and biochemical parameters such as firmness, °Brix, and fruit weight further enlightened the mechanisms of Ca-driven modulation of fruit structure and metabolism in cv. Loureiro, possibly posing as a model for other white cultivars.

MATERIALS AND METHODS

Vineyard Treatments and Sample Collection

Field trials were performed in grapevines cv. Loureiro, the most prominent white cultivar of the Portuguese DOC region of 'Vinhos Verdes' (edaphoclimatic conditions specified in **Supplementary Figure 1**), cultivated in a commercial vineyard with coordinates: N41°28′28″ latitude, W8°34′59″ longitude, 165 m altitude. The plants were oriented in southwest to northeast, spaced at 2.2 m between rows, 1.0 m along the row and trained on a vertical shoot position trellis system, uniformly pruned on a unilateral Royat cordon. Grapevine aerial parts were evenly sprayed with a solution of 2% (w/v) $CaCl_2$ and 0.1% (v/v) Silwet L-77 used as a surfactant, as previously optimized (Saftner et al., 1997; Martins et al., 2020a,b, 2021a). Treatments were performed in the early morning, and 3 L of the solution was used for every 10 plants. Three applications were performed throughout the fruiting season, every 30 days, the first performed at the pea size (E-L 31; Coombe, 1995), the second performed at veraison stage (E-L 35), and the last performed 1 week before harvest (E-L 38). Control plants were sprayed with a solution containing the surfactant agent only. Both control and Ca-treated grapevines were healthy, cultivated under the same microclimate, and subjected to the same routine phytosanitary treatments with Topaze and Ridomil Gold R WG, according to the instructions of the suppliers. Rows of control and Ca-treated vines were intercalated with vines with no treatment At the harvest time, berries were randomly collected from 10 Ca-treated and control grapevines. Six independent sets ($n = 6$) of approximately 30 berries each were frozen immediately in liquid nitrogen and stored at −80°C for further characterization of metabolite profile. The determination of technical/biochemical parameters and gene expression analysis were performed in three pools of two independent sets ($n = 3$).

Determination of Berry Weight, Ca Content, °Brix, and Firmness

Grape berry fresh weight was assessed with an analytical scale Mettler Toledo AG245 (Martins et al., 2020a). Ca content was determined in profusely washed berries, using a previously optimized adaptation of the technique described by Spare (1964). Briefly, berries were ground in liquid nitrogen and 200 mg of fresh weight were used for extraction of soluble contents in

1.5 mL milli-Q H_2O. After centrifuging the extracts at 12,000 × *g* for 3 min, 300 μL of 0.008% (w/v) murexide reagent was added to 500 μl of the supernatant. Following incubation for 15 min at RT, the OD_{490nm} was recorded and Ca concentration was determined through a calibration curve of $CaCl_2$ solution at 2–150 μM (Martins et al., 2020b). The °Brix was determined in aliquots of grape juice using a digital wine refractometer Hanna HI 96813, as described previously (Martins et al., 2020c). Fruit firmness was assessed in 24 intact fruits containing the pedicel, by determining the tension necessary to perforate the fruit skin. Tests were performed on a Shimadzu (model AG-IS) equipped with a 50-N load cell and a 1-mm diameter needle. Force–stroke plots were assembled in Trapezium 2.0 Software and results were expressed in MPa, as described previously (Martins et al., 2020b).

Characterization of the Grape Berry Metabolic Profile

Grape berries were ground in liquid nitrogen and converted into a fine powder. Metabolites were extracted from freeze-dried samples, using a proportion of 1 mL of 80% (v/v) methanol per 25 mg of dry weight. Samples were sonicated for 30 min and macerated overnight at 4°C in the dark, centrifuged at 18,000*g* for 10 min, and the supernatants were recovered. Ultra-performance liquid chromatography coupled to mass spectrometry (UPLC–MS)-targeted metabolomic analysis was performed as optimized previously (Billet et al., 2018a,b,c; Martins et al., 2020a), using an ACQUITY UPLC system coupled to a photo diode array detector and a Xevo TQD mass spectrometer (Waters, Milford, MA, United States) equipped with an electrospray ionization source controlled by Masslynx 4.1 software (Waters, Milford, MA, United States). Analyte separation was achieved by using a Waters Acquity HSS T3 C18 column (150 × 2.1 mm, 1.8 μm) with a flow rate of 0.4 mL/min at 55°C. Chromatographic separation and identification of analytes were achieved as optimized previously, using the same standards specified by Martins et al. (2020a, 2021b). UPLC–MS analyses were achieved using the selected ion monitoring (SIM) mode of the targeted molecular ions. SIM chromatograms were integrated using the subroutine QuanLynx 4.1 for data mining. Peak integration was performed using the ApexTrack algorithm with a mass window of 0.1 Da and relative retention time window of 1 min followed by Savitzky–Golay smoothing (iteration = 1 and width = 1). To evaluate the robustness of measurements and analytical variability, a pool of all samples was prepared to obtain a quality control sample and the samples were randomly injected. Relative quantification was determined for L-proline (m1), L-leucine (m2), L-isoleucine (m3), L-phenylalanine (m4), L-tyrosine (m5), L-tryptophan (m6), cyanidin-3-*O*-glucoside (m7), peonidin-3-*O*-glucoside (m8), delphinidin-3-*O*-glucoside (m9), cyanidin-3-*O*-(6-*O*-acetyl)-glucoside (m10), malvidin-3-*O*-glucoside (m11), malvidin-3-*O*-(6-*O*-acetyl)-glucoside (m12), petunidin-3-*O*-(6-*p*-coumaroyl)-glucoside (m13), malvidin-3-*O*-(6-*p*-coumaroyl)-glucoside (m14), malvidin-3,5-*O*-diglucoside (m15), gallic acid (m16), citric acid (m17), *E*-resveratrol (m18), *E*-piceatannol (m19), catechin (m20), epicatechin (m21), coutaric acid (m22), caftaric acid (m23), fertaric acid (m24), *E*-piceid (m25), kaempferol-3-*O*-glucoside (m26), pallidol (m27), *E*-ε-viniferin (m28), *E*-ω-viniferin (m29), *E*-δ-viniferin (m30), quercetin-3-*O*-glucoside (m31), quercetin-3-*O*-glucuronide (m32), myricetin-hexoside 1 (m33), myricetin-hexoside 2 (m34), quercetin derivative (m35), procyanidin B1 (m36), procyanidin B2 (m37), procyanidin B3 (m38), procyanidin B4 (m39), kaempferol-3-*O*-rutinoside (40), procyanidin gallate (41), procyanidin trimer 1 (42), and procyanidin trimer 2 (43).

RNA Extraction and Quantitative Real-Time PCR Analysis

Total RNA was extracted from 0.3 g of freshly ground samples according to the method of Reid et al. (2006), as previously optimized (Martins et al., 2020a,b). RNA was purified with the GRS Total RNA kit – Plant (Grisp Research Solutions, Porto, Portugal), and the cDNA was obtained from 1 μg of mRNA by reverse transcription with an Xpert cDNA Synthesis Kit and oligo (dT) primers (Grisp Research Solutions). Quantitative real-time PCR (qRT-PCR) reactions were performed in triplicate, as previously described (Martins et al., 2020a,b). The sequences of the gene-specific primers used are detailed in **Supplementary Table 1**. Genes encoding core enzymes of secondary metabolism were selected, namely, *PAL1* (phenylalanine ammonia lyase), *STS* (stilbene synthase), *CHS3* (chalcone synthase), *CHI1* (chalcone isomerase), *F3′5′H* (flavonoid 3′,5′-hydroxylase), *F3H1* (flavanone 3-hydroxylase), *FLS1* (flavonol synthase), *DFR* (dihydroflavonol 4-reductase), *LAR1* (leucoanthocyanidin reductase), *ANS* (anthocyanidin synthase), *BAN* and *ANR* (anthocyanidin reductases), and UDP–glucose:flavonoid-3-O-glucosyltransferase (*UFGT*) (Jeong et al., 2004; Bogs et al., 2005; Castellarin et al., 2007; Tavares et al., 2013; Martins et al., 2018). The expression of *LAC* encoding a laccase involved in the oxidation of *E*-resveratrol was also studied, together with key genes involved in cell wall and cuticle structure, namely, *PME1* (pectin methylesterase), *PG1* (polygalacturonase), *EXP6* (expansin), *CesA3* (cellulose synthase), *CER9* (E3 ubiquitin ligase), and *CYP15* (cytochrome P450 monooxygenase/hydroxylase) (Martins et al., 2018, 2020b). Dissociation curves allowed confirmation of the specificity of the PCR reactions. Expression of target genes was normalized to that of the reference genes glyceraldehyde 3-phosphate dehydrogenase (*GAPDH*) and actin (*ACT1*) (Martins et al., 2020a) using the ΔΔCq method in CFX Manager Software 3.1 (Bio-Rad Laboratories, Inc., Hercules, CA, United States).

General Statistical Analysis

Results were statistically analyzed through the Student's *t*-test in Prism6 (GraphPad Software, Inc.). The significance level of differences between the control and the Ca-treated samples is marked in graphs with asterisks: $^{*}P \leq 0.05$; $^{**}P \leq 0.01$; $^{***}P \leq 0.001$; $^{****}P \leq 0.0001$. A multivariate statistical data analysis (MVA) of the samples was performed with SIMCA P+ version 15 (Umetrics AB, Umeå, Sweden), after mean-centering all variables and scaling unit-variance. Metabolic variables affected by Ca treatment were revealed through the principal component analysis (PCA) applied as the unsupervised MVA method.

RESULTS

Results showed that Ca treatment throughout the fruiting season visibly modified the size (decreased), texture, and color of the berries at harvest time, and these effects were consistent in two consecutive seasons (**Figure 1A**). Accordingly, the fresh weight of berries from Ca-treated plants was 35% lower than that of the control fruits. In parallel, Ca sprays increased fruit Ca content by 30% and decreased the °Brix from 18.4 to 16.7 °B, in line with the immature appearance of the fruits (**Figure 1B**). In addition, the force necessary to perforate the skin of berries from Ca-treated plants, expressed as tension, was significantly higher than that of the control fruits (**Figure 2A**). This change was associated to a 56-fold increase in the expression of cell wall *PME1* (**Figure 2B**). Likewise, transcript levels of *EXP6* also increased by 5.6-fold. In contrast, the expression of *PG1* decreased by 66% upon Ca treatment. The same effect was observed for *CYP15* involved in the cuticle structure, that was downregulated by 82%. Other genes involved in the cell wall and cuticle structures, namely *CesA3* and *CER9* were not significantly affected by the Ca treatment.

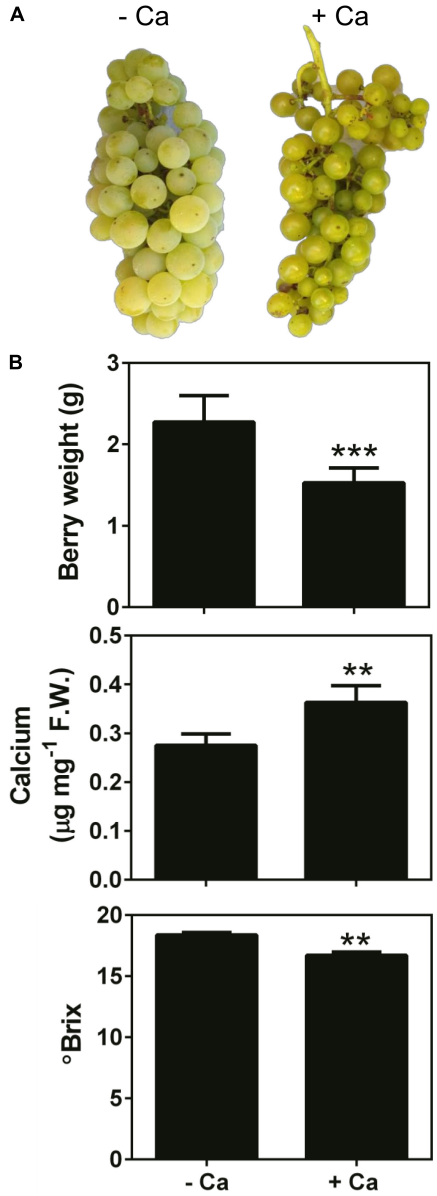

FIGURE 1 | Appearance **(A)**, weight, Ca content, and °Brix **(B)** of mature berries from vines cv. Loureiro treated with Ca (+ Ca) or without treatment (– Ca). Images in panel **(A)** are representative of two consecutive seasons. Results are expressed as mean ± SD and asterisks denote statistical significance as compared to control (– Ca): $^{**}P \leq 0.01$; $^{***}P \leq 0.001$; $n = 3$.

Targeted metabolomics analysis by UPLC–MS allowed the detection of 44 metabolites, including 5 phenolic and organic acids, 6 amino acids, 9 flavan-3-ols, 7 flavonols, 9 anthocyanins, and 7 stilbenoids (**Supplementary Table 2**). Unsupervised PCA score plot of the first two components explained 52.9% of the variance and readily discriminated the metabolic profiles of berries from control and Ca-treated vines (**Figure 3A**). In general, amino acids and anthocyanins di-OH mostly accumulated in control berries, while most phenolic acids were more abundant in berries from Ca-treated vines (**Figure 3B**). A detailed analysis of berry metabolic profiles showed that all amino acids detected, including L-phenylalanine, were significantly reduced in berries from Ca-treated vines, decreasing by up to 40% in comparison to the control fruits (**Figure 4**). In contrast, phenolic acids increased by up to 1.9-fold, among which coutaric, caftaric, and fertaric acids. The levels of citric and gallic acids were not affected by Ca treatment. Regarding stilbenoids, a significant increase of 1.8-fold was observed in *E*-piceid levels upon Ca treatment, together with a 6.5-fold increase in *E*-ω-viniferin content. For the remaining stilbenoids, which included *E*-resveratrol, *E*-ε-viniferins, and *E*-δ-viniferins, a tendential but not significant decrease was observed. Regarding flavan-3-ols, only the content in epicatechin was significantly affected by Ca treatment, for which a reduction of 20% was observed. Thus, the apparent increase in procyanidin levels observed in the loading plot was not statistically significant (**Figure 3B**). The accumulation of specific flavonols, namely kaempferol-3-*O*-rutinoside, quercetin-3-*O*-glucuronide, and myricetin-hexoside 2, was favored by the Ca treatment and their content increased by up to 2.8-fold in comparison to the control fruits. The corresponding glucosides were not significantly affected by the Ca treatment, nor myricetin-hexoside 1 (**Figure 4**). Anthocyanins detected in berries of cv. Loureiro included cyanidin, peonidin, petunidin, delphinidin, and malvidin conjugates, the latter being the most diverse. The Ca treatment specifically reduced cyanidin-3-*O*-glucoside levels by 40% and malvidin-3-*O*-(6-*p*-coumaroyl)-glucoside content by 60%. The effect of Ca on the remaining anthocyanins was not statistically significant.

The molecular nature of the metabolic shifts triggered by Ca in berries of cv. Loureiro vines was investigated through the analysis of transcript levels of genes encoding key enzymes of secondary metabolism. The expression of *PAL1*, encoding PAL, was upregulated by 63% upon Ca treatment (**Figure 5**). Likewise, *STS* encoding stilbene synthases was upregulated by 62%. Coincidentally, the expression of *CHS3* encoding chalcone synthase was 62% lower in berries from Ca-treated vines than in the control berries. The same effect was observed

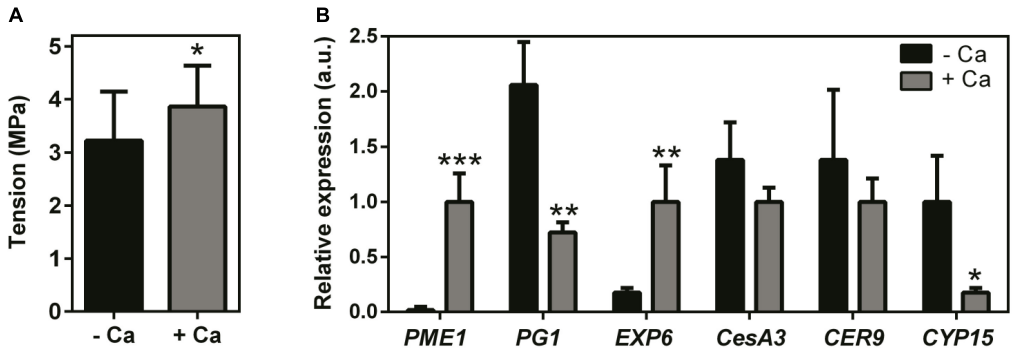

FIGURE 2 | Firmness **(A)** and transcript levels of genes involved in cell wall and cuticle structures **(B)**, in berries from vines cv. Loureiro treated with Ca (+ Ca) or without treatment (– Ca). Firmness is expressed as the tension necessary to perforate the fruit skin; $n = 24$. Transcript levels are shown for pectin methylesterase (*PME1*), polygalacturonase (*PG1*), expansin (*EXP6*), cellulose synthase (*CesA3*), E3 ubiquitin ligase (*CER9*), and cytochrome P450 monooxygenase/hydroxylase (*CYP15*). Results are expressed as mean ± SD and asterisks denote statistical significance as compared to control (– Ca): $^{*}P \leq 0.05$; $^{**}P \leq 0.01$; $^{***}P \leq 0.001$; $n = 3$.

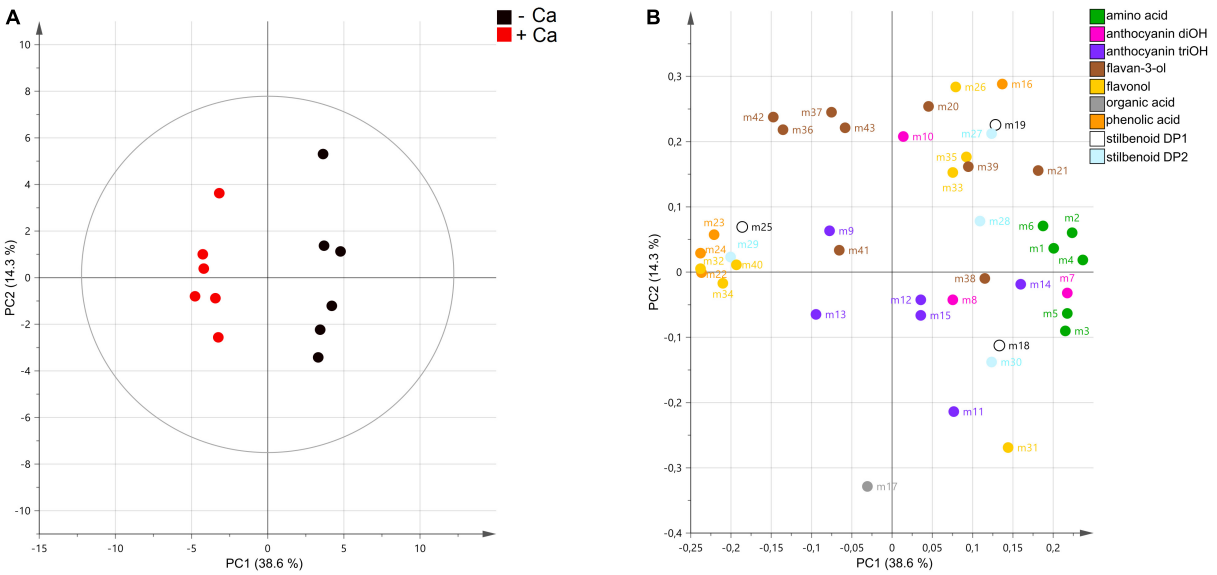

FIGURE 3 | Unsupervised classification using the principal component analysis on metabolomic data from grape berries from vines cv. Loureiro treated with Ca (+ Ca) or without treatment (– Ca) ($n = 6$). Variables in the score plot **(A)** were colored according to the treatment, and variables in loading plot **(B)** were colored according to the metabolic class. Numbers indicate the ID of metabolites, as follows: L-proline (m1), L-leucine (m2), L-isoleucine (m3), L-phenylalanine (m4), L-tyrosine (m5), L-tryptophan (m6), cyanidin-3-*O*-glucoside (m7), peonidin-3-*O*-glucoside (m8), delphinidin-3-*O*-glucoside (m9), cyanidin-3-*O*-(6-*O*-acetyl)-glucoside (m10), malvidin-3-*O*-glucoside (m11), malvidin-3-*O*-(6-*O*-acetyl)-glucoside (m12), petunidin-3-*O*-(6-*p*-coumaroyl)-glucoside (m13), malvidin-3-*O*-(6-*p*-coumaroyl)-glucoside (m14), malvidin-3,5-*O*-diglucoside (m15), gallic acid (m16), citric acid (m17), *E*-resveratrol (m18), *E*-piceatannol (m19), catechin (m20), epicatechin (m21), coutaric acid (m22), caftaric acid (m23), fertaric acid (m24), *E*-piceid (m25), kaempferol-3-*O*-glucoside (m26), pallidol (m27), *E*-ε-viniferin (m28), *E*-ω-viniferin (m29), *E*-δ-viniferin (m30), quercetin-3-*O*-glucoside (m31), quercetin-3-*O*-glucuronide (m32), myricetin-hexoside 1 (m33), myricetin-hexoside 2 (m34), quercetin derivative (m35), procyanidin B1 (m36), procyanidin B2 (m37), procyanidin B3 (m38), procyanidin B4 (m39), kaempferol-3-*O*-rutinoside (40), procyanidin gallate (41), procyanidin trimer 1 (42), and procyanidin trimer 2 (43).

for *F3H1* encoding flavanone 3-hydroxylase, whose transcript levels decreased by 50% upon Ca treatment. Further in the flavonoid pathway, *DFR* encoding dihydroflavonol reductase was upregulated by 30% upon Ca treatment, whereas *ANS* encoding anthocyanidin synthase was downregulated by 49%. Seven other genes of the flavonoid pathway including *UFGT* were not significantly affected by the Ca treatment, nor did *LAC* (laccase) was involved in the *E*-resveratrol oxidation. An overview of the effects of Ca in cv. Loureiro berries is shown in **Figure 6**.

DISCUSSION

Results in the present study demonstrated the beneficial effect of Ca sprays over the firmness of berries cv. Loureiro, complementing the few studies conducted in other white cultivars, namely Thompson Seedless, Asgari, and Italia (Amiri et al., 2009; Bonomelli and Ruiz, 2010; Ciccarese et al., 2013), and are in agreement with some previous reports on red cultivars such as Vinhão and Crimson (Alcaraz-López et al., 2005;

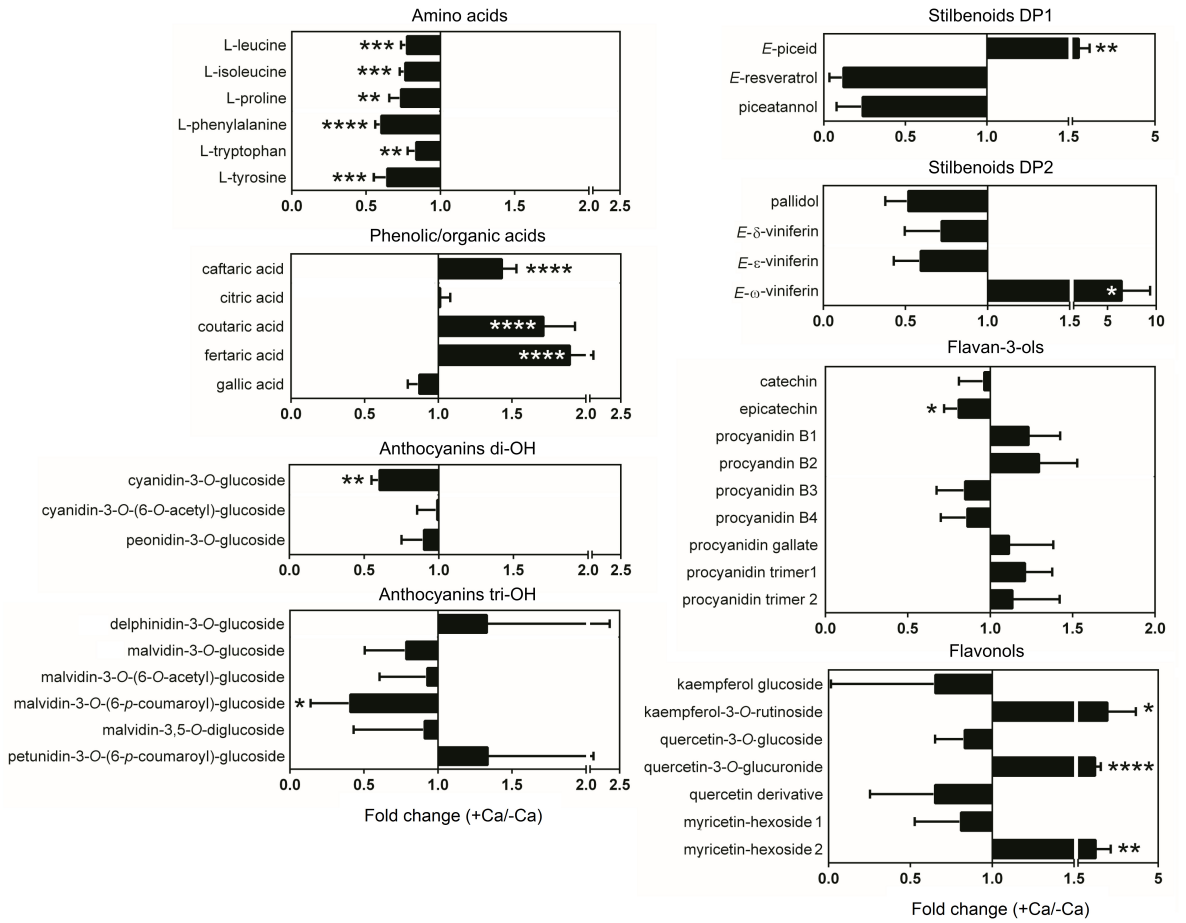

FIGURE 4 | Effect of Ca on the metabolite profile of grape berries cv. Loureiro. Results are expressed as fold changes of the mean ± SD values obtained for Ca treatment (+ Ca) relative to the control (– Ca), and asterisks indicate statistical significance of + Ca *vs.* – Ca for each metabolite: $^{*}P \leq 0.05$; $^{**}P \leq 0.01$; $^{***}P \leq 0.001$; $^{****}P \leq 0.0001$; $n = 6$.

Martins et al., 2020b). Electron microscopy studies on cv. Vinhão berries showed that increased firmness was accompanied by a reduction in the incidence of microcracks on the fruit surface which became smoother than that of the control fruits (Martins et al., 2020b). The tight regulation of genes involved in the cell wall and cuticle structures by Ca in berries cv. Loureiro likely explained the improved fruit firmness. The observed inhibition of *PG1* and *CYP15* expression was in accordance to previous results in cv. Vinhão berries (Martins et al., 2020b), thus it seems that both white and red varieties share the same targets related to the prevention of fruit softening in response to Ca. PGs degrade pectin molecules in the cell wall and a particularly close correlation between *PG1* levels and grape berry softening has been reported (Deytieux-Belleau et al., 2008). In turn, cuticular CYPs such as *CYP15* are involved in the synthesis of wax triterpenoids, which also determine the fruit quality (Fukushima et al., 2011; Lara et al., 2014). Contrary to previous studies in cv. Vinhão berries (Martins et al., 2020b), *PME1* and *EXP6* were upregulated upon Ca treatment in cv. Loureiro. PME and EXP are involved in various physiological processes underlying both reproductive and vegetative plant development, including seed germination, root tip elongation, and soft fruit ripening (Sampedro and Cosgrove, 2005; Pelloux et al., 2007). PME effects on the latter process arise from its contribution in the degree of demethylated polygalacturonans that are prone to degradation by PGs and the availability of homogalacturonan carboxylic groups for Ca^{2+} binding (Deytieux-Belleau et al., 2008). Accordingly, the induction of PME mRNAs has been associated to the decrease in the degree of methyl-esterification of insoluble pectins during grape berry development (Barnavon et al., 2001).

Results in the present study showed a reduction in the weight and °Brix of mature berries from vines sprayed with Ca, suggesting a delay in fruit maturation, which could be anticipated from the immature appearance of the fruits. This result was not observed in vines of the red cultivar Vinhão subjected to the same Ca application protocol (Martins et al., 2020b). However, decreased °Brix following Ca treatment was reported previously for another white grape cv. Asgari (Amiri et al., 2009). This effect was accompanied by a change in fruit skin color, berries remaining greener, and not attaining the characteristic golden color of ripe fruits (Amiri et al., 2009), much like the observations in the present study with the cv. Loureiro.

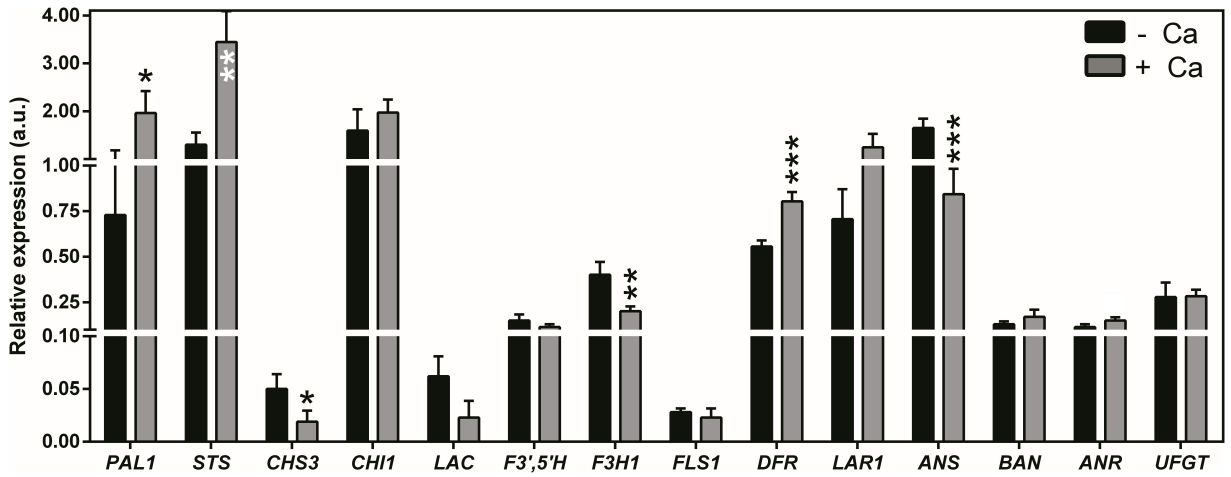

FIGURE 5 | Transcript levels of genes encoding enzymes of secondary metabolism core branches in berries from vines cv. Loureiro treated with Ca (+ Ca) or without treatment (– Ca). Transcript levels are shown for phenylalanine ammonia lyase (*PAL1*), stilbene synthase (*STS*), polyphenol oxidase/laccase (*LAC*), chalcone synthase (*CHS3*), chalcone isomerase (*CHI1*), flavonoid 3′,5′-hydroxylase (*F3′,5′H*), flavanone 3-hydroxylase (*F3H1*), flavonol synthase (*FLS1*), dihydroflavonol 4-reductase (*DFR*), leucoanthocyanidin reductase (*LAR1*), anthocyanidin synthase (*ANS*), anthocyanidin reductases (*BAN* and *ANR*), and anthocyanidin 3-*O*-glucosyltransferase (UDP–glucose:flavonoid-3-*O*-glucosyltransferase, *UFGT*). Expression levels were normalized to the transcript levels of *GAPDH* and (*ACT1*) (housekeeping genes). Results are expressed as mean ± SD and asterisks denote statistical significance as compared to control (– Ca): $^{*}P \leq 0.05$; $^{**}P \leq 0.01$; and $^{***}P \leq 0.001$; $n = 3$.

In this study, trace amounts of anthocyanins were detected by UPLC–MS in cv. Loureiro berries, as reported in other white cultivars such as Chardonnay, Sauvignon Blanc, Riesling, Pinot Blanc, and Muscat Blanc, also by chromatographic methods (Arapitsas et al., 2015; Niu et al., 2017). In contrast, earlier studies (Boss et al., 1996) reported the absence of these pigments in white cultivars; however, the quantification methods were much less sensitive. Results in the present study and in previous reports suggested that anthocyanin diversity is similar in both white and red grape varieties (Arapitsas et al., 2015; Niu et al., 2017; Martins et al., 2020a). The inhibitory effect of Ca over the anthocyanins malvidin-3-*O*-(6-*p*-coumaroyl)-glucoside and cyanidin-3-*O*-glucoside observed in the present study for fruits cv. Loureiro is in line with previous studies in cv. Vinhão, and is consistent with the downregulation of *ANS* and *UFGT* (Martins et al., 2020a).

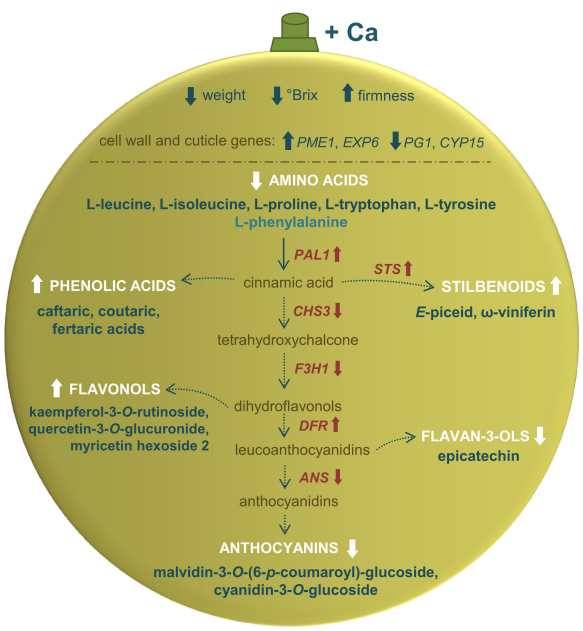

FIGURE 6 | Physiological, metabolic, and transcriptional changes driven by exogenous Ca in grape berries from vines cv. Loureiro. Arrows pointing upward indicate increase in comparison to control berries, while arrows pointing downward indicate decrease. The pathway was based on the information from Kyoto Encyclopedia of Genes and Genomes – KEGG database.

The consistent decrease in fruit amino acid levels upon Ca treatment observed in the present study might bring about changes during wine fermentation, as many of these metabolites constitute the yeast assimilable nitrogen fraction of the must (Vilanova et al., 2007). In particular, the decrease in L-phenylalanine levels was tightly linked to the upregulation of *PAL1* encoding the enzyme responsible for its conversion to cinnamic acid, the first catalytic step of plant secondary metabolism (Teixeira et al., 2013). This effect correlated with the increase in phenolic acids, produced in downstream routes initially fed by this substrate. Caftaric acid is known to account for the color of white wines, as it can be hydrolyzed to caffeic acid during the wine-making process, the oxidation of the latter contributing to wine browning (Cilliers and Singleton, 1990). Caftaric acid and other hydroxycinnamates including coutaric acid, also detected in the present study, were shown to be effective markers of wine differentiation, together with resveratrol, piceid, and epicatechin (Andrés-Lacueva et al., 2002; Lampír, 2013). In the present study, Ca treatment induced *STS* expression and consequently, stilbenoid synthesis, in analogy to previous reports in berries of cv. Vinhão

vines located in the same vineyard (Martins et al., 2020a). Although in cv. Vinhão a general increase in most stilbenoids including *E*-resveratrol and *E*-ε-viniferin was reported, in cv. Loureiro a targeted accumulation of *E*-piceid and *E*-ω-viniferin was observed, suggesting a specific action of Ca effect depending on the cultivar. The interaction of Ca with other metabolites differentially present in each cultivar may underlie these effects; accordingly, previous studies showed that the combination of Ca and plant hormones such as jasmonic or abscisic acid greatly determines the redirecting of secondary metabolism toward the synthesis of specific compounds such as different types of viniferins (Martins et al., 2018, 2021b). The targeted action of Ca over specific polyphenols was evident in other metabolic classes, including anthocyanins (discussed above), flavonols, and flavan-3-ols. The large increase of the flavonols kaempferol-3-*O*-rutinoside, quercetin-3-*O*-glucuronide, and myricetin-hexoside 2 observed in cv. Loureiro was not reported previously in cv. Vinhão (Martins et al., 2020a). Flavonols are exclusively found in the grape berry skin and seeds, peaking at veraison stage of fruit development (Teixeira et al., 2013). Thus, the increase in their levels upon Ca treatment supports the delay in fruit maturation in cv. Loureiro, as discussed previously. In parallel, only epicatechin was affected in this cultivar, suggesting a minor influence of Ca over flavan-3-ols contrary to that observed in cv. Vinhão and cv. Gamay Fréaux var. Teinturier cell cultures where a general repression of the flavonoid pathway was reported (Martins et al., 2018, 2020a).

CONCLUSION

Results in the present study confirmed the postulated hypothesis, showing that vineyard Ca sprays induce precise metabolic rearrangements in cv. Loureiro berries that result in a substantial delay in fruit maturation. A specific integrated effect of Ca over biochemical and structural properties of cv. Loureiro berries is thus suggested: by inhibiting the action of polygalacturonases responsible for degradation of cell wall pectin and fruit softening, Ca prevents fruit growth and other processes associated with fruit maturation, leading to increased flavonol content and firmness, at the expense of fruit size and °Brix. This effect may be specific for white cultivars, a topic that deserves further investigation. The results may pave the way for the optimization of protocols of Ca treatments in the field aimed to prevent early fruit ripening in specific cultivars from wine regions most affected by climate change, possibly consisting of a good alternative to crop forcing. Additional benefits on the resistance to biotic and abiotic stresses and on shelf-life could also be expected, in accordance to previous studies (Romanazzi et al., 2012; Martins et al., 2021a).

DATA AVAILABILITY STATEMENT

The original contributions presented in the study are included in the article/**Supplementary Material**, further inquiries can be directed to the corresponding author.

AUTHOR CONTRIBUTIONS

VM and HG conceptualized the work. VM performed field trials, sample processing, firmness measurements, quantification of biochemical parameters, and gene expression analyses. AL and MU performed metabolomic analysis and data treatment. AT performed statistical analysis. HG and AL contributed with resources and funding acquisition. VM, HG, and AL wrote the manuscript. All authors edited and reviewed the manuscript, contributed to the article, and approved the submitted version.

FUNDING

This work was supported by the "Contrato-Programa" UIDB/04050/2020 funded by Portuguese national funds through the FCT IP. This work was also supported by FCT, CCDR-N (Norte Portugal Regional Coordination and Development Commission), European Funds (FEDER/POCI/COMPETE2020) through the project AgriFood XXI (NORTE-01-0145-FEDER-000041) and the research projects BerryPlastid (PTDC/BIA-FBT/28165/2017 and POCI-01-0145-FEDER-028165), and MitiVineDrought (PTDC/BIA-FBT/30341/2017 and POCI-01-0145-FEDER-030341). AT was supported by a postdoctoral researcher contract/position within the project "BerryPlastid". The Région-Centre Val de Loire (France) supported this work under the grant agreement to Projects CEPATLAS and VINODRONE to AL. This work also benefited from the networking activities within the European COST Action CA 17111 INTEGRAPE, the CoLAB VINES & WINES, and the CoLAB 4FOOD – Collaborative Laboratory for Innovation in the Food Industry.

ACKNOWLEDGMENTS

The authors thank Ana Garcia (CIIMAR, Portugal) for providing access to the experimental fields used in this study. The authors also acknowledge Senentxu Lanceros-Méndez and Pedro Costa (Department of Physics, University of Minho, Portugal) for providing access to the Shimadzu Autograph used in fruit firmness measurements.

SUPPLEMENTARY MATERIAL

The Supplementary Material for this article can be found online at: https://www.frontiersin.org/articles/10.3389/fpls.2021.742887/full#supplementary-material

Supplementary Figure 1 | Edaphoclimatic conditions of the vineyard located in the DOC region 'Vinhos Verdes' where field trials were conducted.

Supplementary Table 1 | Accession numbers and specific primers forward (F) and reverse (R) of sequences used in quantitative real-time PCR studies.

Supplementary Table 2 | Polyphenolic compounds quantified in mature grape berries from cv. Loureiro vines treated with Ca (+ Ca) or without treatment (− Ca).

REFERENCES

Alcaraz-López, C., Botía, M., Alcaraz, C. F., and Riquelme, F. (2005). Induction of fruit calcium assimilation and its influence on the quality of table grapes. *Span. J. Agric. Res.* 3, 335–343.

Aldon, D., Mbengue, M., Mazars, C., and Galaud, J. P. (2018). Calcium signalling in plant biotic interactions. *Int. J. Mol. Sci.* 19:665. doi: 10.3390/ijms19030665

Amiri, E. M., Fallahi, E., and Safari, G. (2009). Effects of preharvest calcium sprays on yield, quality and mineral nutrient concentrations of 'Asgari' table grape. *Int. J. Fruit Sci.* 9, 294–304. doi: 10.1080/15538360903241377

Andrés-Lacueva, C., Ibern-Gomez, M., Lamuela-Raventos, R. M., Buxaderas, S., and de la Torre-Boronat, M. C. (2002). Cinnamates and resveratrol content for sparkling wine characterization. *Am. J. Enol. Vitic.* 53, 147–150.

Arapitsas, P., Oliveira, J., and Mattivi, F. (2015). Do white grapes really exist? *Food Res. Int.* 69, 21–25. doi: 10.1016/j.foodres.2014.12.002

Barnavon, L., Doco, T., Terrier, N., Ageorges, A., Romieu, C., and Pellerin, P. (2001). Involvement of pectin methyl-esterase during the ripening of grape berries: partial cDNA isolation, transcript expression and changes in the degree of methyl-esterification of cell wall pectins. *Phytochemistry* 58, 693–701. doi: 10.1016/S0031-9422(01)00274-6

Billet, K., Delanoue, G., Arnault, I., Besseau, S., Oudin, A., Courdavault, V., et al. (2018a). Vineyard evaluation of stilbenoid-rich grape cane extracts against downy mildew: a large-scale study. *Pest Manag. Sci.* 75, 1252–1257. doi: 10.1002/ps.5237

Billet, K., Houillé, B., Besseau, S., Mélin, C., Oudin, A., Papon, N., et al. (2018b). Mechanical stress rapidly induces *E*-resveratrol and *E*-piceatannol biosynthesis in grape canes stored as a freshly-pruned byproduct. *Food Chem.* 240, 1022–1027. doi: 10.1016/j.foodchem.2017.07.105

Billet, K., Houillé, B., de Bernonville, T. D., Besseau, S., Oudin, A., Courdavault, V., et al. (2018c). Field-based metabolomics of *Vitis vinifera* L. stems provides new insights for genotype discrimination and polyphenol metabolism structuring. *Front. Plant Sci.* 9:798. doi: 10.3389/fpls.2018.00798

Bogs, J., Downey, M. O., Harvey, J. S., Ashton, A. R., Tanner, G. J., and Robinson, S. P. (2005). Proanthocyanidin synthesis and expression of genes encoding leucoanthocyanidin reductase and anthocyanidin reductase in developing grape berries and grapevine leaves. *Plant Physiol.* 139, 652–663. doi: 10.1104/pp.105.064238

Bonomelli, C., and Ruiz, R. (2010). Effects of foliar and soil calcium application on yield and quality of table grape cv. 'Thompson Seedless'. *J. Plant Nutr.* 33, 299–314. doi: 10.1080/01904160903470364

Boss, P. K., Davies, C., and Robinson, S. P. (1996). Expression of anthocyanin biosynthesis pathway genes in red and white grapes. *Plant Mol. Biol.* 32, 565–569. doi: 10.1007/BF00019111

Castellarin, S. D., Pfeiffer, A., Sivilotti, P., Degan, M., Peterlunger, E., and Di Gaspero, G. (2007). Transcriptional regulation of anthocyanin biosynthesis in ripening fruits of grapevine under seasonal water deficit. *Plant Cell Environ.* 30, 1381–1399. doi: 10.1111/j.1365-3040.2007.01716.x

Ciccarese, A., Stellacci, A. M., Gentilesco, G., and Rubino, P. (2013). Effectiveness of pre-and post-veraison calcium applications to control decay and maintain table grape fruit quality during storage. *Postharvest Biol. Tech.* 75, 135–141. doi: 10.1016/j.postharvbio.2012.08.010

Cilliers, J. J., and Singleton, V. L. (1990). Nonenzymic autoxidative reactions of caffeic acid in wine. *Am. J. Enol. Vitic.* 41, 84–86.

Coombe, B. G. (1995). Growth stages of the grapevine: adoption of a system for identifying grapevine growth stages. *Aust. J. Grape Wine Res.* 1, 104–110. doi: 10.1111/j.1755-0238.1995.tb00086.x

Correia, S., Queirós, F., Ribeiro, C., Vilela, A., Aires, A., Barros, A. I., et al. (2019). Effects of calcium and growth regulators on sweet cherry (*Prunus avium* L.) quality and sensory attributes at harvest. *Sci. Hortic.* 248, 231–240. doi: 10.1016/j.scienta.2019.01.024

Deytieux-Belleau, C., Vallet, A., Donèche, B., and Geny, L. (2008). Pectin methylesterase and polygalacturonase in the developing grape skin. *Plant Physiol. Biochem.* 46, 638–646. doi: 10.1016/j.plaphy.2008.04.008

Fu, W., Zhang, M., Zhang, P., Liu, Z., Dong, T., Zhang, S., et al. (2020). Transcriptional and metabolite analysis reveal a shift in fruit quality in response to calcium chloride treatment on "Kyoho" grapevine. *J. Food Sci. Technol.* 58, 2246–2257. doi: 10.1007/s13197-020-04735-5

Fukushima, E. O., Seki, H., Ohyama, K., Ono, E., Umemoto, N., Mizutani, M., et al. (2011). CYP716A subfamily members are multifunctional oxidases in triterpenoid biosynthesis. *Plant Cell Physiol.* 52, 2050–2061. doi: 10.1093/pcp/pcr146

González-Fontes, A., Navarro-Gochicoa, M. T., Ceacero, C. J., Herrera-Rodríguez, M. B., Camacho-Cristóbal, J. J., and Rexach, J. (2017). "Understanding calcium transport and signaling, and its use efficiency in vascular plants," in *Plant Macronutrient Use Efficiency–Molecular and Genomic Perspectives in Crop Plants*, eds M. A. Hossain, T. Kamiya, D. J. Burritt, L.-S. P. Tran, and T. Fujiwara (Cambridge, MA: Academic Press), 165–180.

Hocking, B., Tyerman, S. D., Burton, R. A., and Gilliham, M. (2016). Fruit calcium: transport and physiology. *Front. Plant Sci.* 7:569. doi: 10.3389/fpls.2016.00569

Jeong, S. T., Goto-Yamamoto, N., Kobayashi, S., and Esaka, M. J. P. S. (2004). Effects of plant hormones and shading on the accumulation of anthocyanins and the expression of anthocyanin biosynthetic genes in grape berry skins. *Plant Sci.* 167, 247–252. doi: 10.1016/j.plantsci.2004.03.021

Lampíř, L. (2013). Varietal differentiation of white wines on the basis of phenolic compounds profile. *Czech J. Food Sci.* 31, 172–179.

Lara, I., Belge, B., and Goulao, L. F. (2014). The fruit cuticle as a modulator of postharvest quality. *Postharvest Biol. Technol.* 87, 103–112. doi: 10.1016/j.postharvbio.2013.08.012

Manganaris, G. A., Vasilakakis, M., Diamantidis, G., and Mignani, I. (2007). The effect of postharvest calcium application on tissue calcium concentration, quality attributes, incidence of flesh browning and cell wall physicochemical aspects of peach fruits. *Food Chem.* 100, 1385–1392. doi: 10.1016/j.foodchem.2005.11.036

Martín-Diana, A. B., Rico, D., Barry-Ryan, C., Frías, J. M., Mulcahy, J., and Henehan, G. T. (2005). Comparison of calcium lactate with chlorine as a washing treatment for fresh-cut lettuce and carrots: quality and nutritional parameters. *J. Sci. Food Agric.* 85, 2260–2268. doi: 10.1002/jsfa.2254

Martín-Diana, A. B., Rico, D., Frias, J. M., Barat, J. M., Henehan, G. T. M., and Barry-Ryan, C. (2007). Calcium for extending the shelf life of fresh whole and minimally processed fruits and vegetables: a review. *Trends Food Sci. Technol.* 18, 210–218. doi: 10.1016/j.tifs.2006.11.027

Martins, V., Billet, K., Garcia, A., Lanoue, A., and Gerós, H. (2020a). Exogenous calcium deflects grape berry metabolism towards the production of more stilbenoids and less anthocyanins. *Food Chem.* 313:126123. doi: 10.1016/j.foodchem.2019.126123

Martins, V., Garcia, A., Alhinho, A. T., Costa, P., Lanceros-Méndez, S., Costa, M. M. R., et al. (2020b). Vineyard calcium sprays induce changes in grape berry skin, firmness, cell wall composition and expression of cell wall-related genes. *Plant Physiol. Biochem.* 150, 49–55. doi: 10.1016/j.plaphy.2020.02.033

Martins, V., Garcia, A., Costa, C., Sottomayor, M., and Gerós, H. (2018). Calcium- and hormone-driven regulation of secondary metabolism and cell wall enzymes in grape berry cells. *J. Plant Physiol.* 231, 57–67. doi: 10.1016/j.jplph.2018.08.011

Martins, V., López, R., Garcia, A., Teixeira, A., and Gerós, H. (2020c). Vineyard calcium sprays shift the volatile profile of young red wine produced by induced and spontaneous fermentation. *Food Res. Int.* 131:108983. doi: 10.1016/j.foodres.2020.108983

Martins, V., Soares, C., Spormann, S., Fidalgo, F., and Gerós, H. (2021a). Vineyard calcium sprays reduce the damage of postharvest grape berries by stimulating enzymatic antioxidant activity and pathogen defense genes, despite inhibiting phenolic synthesis. *Plant Physiol. Biochem.* 162, 48–55. doi: 10.1016/j.plaphy.2021.02.025

Martins, V., Unlubayir, M., Teixeira, A., Gerós, H., and Lanoue, A. (2021b). Calcium and methyl jasmonate cross-talk in the secondary metabolism of grape cells. *Plant Physiol. Biochem.* 165, 228–238. doi: 10.1016/j.plaphy.2021.05.034

Niu, S., Hao, F., Mo, H., Jiang, J., Wang, H., Liu, C., et al. (2017). Phenol profiles and antioxidant properties of white skinned grapes and their coloured genotypes during growth. *Biotechnol. Biotechnol. Equip.* 31, 58–67. doi: 10.1080/13102818.2016.1258329

Pelloux, J., Rusterucci, C., and Mellerowicz, E. J. (2007). New insights into pectin methylesterase structure and function. *Trends Plant Sci.* 12, 267–277. doi: 10.1016/j.tplants.2007.04.001

Reid, K. E., Olsson, N., Schlosser, J., Peng, F., and Lund, S. T. (2006). An optimized grapevine RNA isolation procedure and statistical determination of reference genes for real-time RT-PCR during berry development. *BMC Plant Biol.* 6:27. doi: 10.1186/1471-2229-6-27

Romanazzi, G., Lichter, A., Gabler, F. M., and Smilanick, J. L. (2012). Recent advances on the use of natural and safe alternatives to

conventional methods to control postharvest gray mold of table grapes. *Postharvest Biol. Technol.* 63, 141–147. doi: 10.1016/j.postharvbio.2011.06.013

Saftner, R. A., Buta, J. G., Conway, W. S., and Sams, C. E. (1997). Effect of surfactants on pressure infiltration of calcium chloride solutions into Golden Delicious' apples. *J. Am. Soc. Hortic. Sci.* 122, 386–391. doi: 10.21273/JASHS.122.3.386

Sampedro, J., and Cosgrove, D. J. (2005). The expansin superfamily. *Genome Biol.* 6:242. doi: 10.1186/gb-2005-6-12-242

Spare, P. D. (1964). A stable murexide reagent for the estimation of calcium in micro quantities of serum. *Clin. Chem.* 10, 726–729. doi: 10.1093/clinchem/10.8.726

Tavares, S., Vesentini, D., Fernandes, J. C., Ferreira, R. B., Laureano, O., Ricardo-Da-Silva, J. M., et al. (2013). *Vitis vinifera* secondary metabolism as affected by sulfate depletion: diagnosis through phenylpropanoid pathway genes and metabolites. *Plant Physiol. Biochem.* 66, 118–126. doi: 10.1016/j.plaphy.2013.01.022

Teixeira, A., Eiras-Dias, J., Castellarin, S. D., and Gerós, H. (2013). Berry phenolics of grapevine under challenging environments. *Int. J. Mol. Sci.* 14, 18711–18739. doi: 10.3390/ijms140918711

Vilanova, M., Ugliano, M., Varela, C., Siebert, T., Pretorius, I. S., and Henschke, P. A. (2007). Assimilable nitrogen utilisation and production of volatile and non-volatile compounds in chemically defined medium by *Saccharomyces cerevisiae* wine yeasts. *Appl. Microbiol. Biotechnol.* 77, 145–157. doi: 10.1007/s00253-007-1145-z

Wang, Y., Xie, X., and Long, L. E. (2014). The effect of postharvest calcium application in hydro-cooling water on tissue calcium content, biochemical changes, and quality attributes of sweet cherry fruit. *Food Chem.* 160, 22–30. doi: 10.1016/j.foodchem.2014.03.073

Yu, J., Zhu, M., Wang, M., Xu, Y., Chen, W., and Yang, G. (2020). Transcriptome analysis of calcium-induced accumulation of anthocyanins in grape skin. *Sci. Hortic.* 260:108871. doi: 10.1016/j.scienta.2019.108871

Conflict of Interest: The authors declare that the research was conducted in the absence of any commercial or financial relationships that could be construed as a potential conflict of interest.

Publisher's Note: All claims expressed in this article are solely those of the authors and do not necessarily represent those of their affiliated organizations, or those of the publisher, the editors and the reviewers. Any product that may be evaluated in this article, or claim that may be made by its manufacturer, is not guaranteed or endorsed by the publisher.

frontiers in Plant Science

ORIGINAL RESEARCH
published: 01 October 2021
doi: 10.3389/fpls.2021.739964

Exogenous Abscisic Acid Mediates Berry Quality Improvement by Altered Endogenous Plant Hormones Level in "Ruiduhongyu" Grapevine

Jiajia Li[1], Boyang Liu[1], Xiangyi Li[1], Dongmei Li[1], Jiayu Han[2], Ying Zhang[2], Chao Ma[1], Wenping Xu[1], Lei Wang[1]*, Songtao Jiu[1], Caixi Zhang[1] and Shiping Wang[1]*

[1] *Department of Plant Science, School of Agriculture and Biology, Shanghai Jiao Tong University, Shanghai, China,* [2] *Grape and Wine Institute, Guangxi Academy of Agricultural Sciences, Nanning, China*

Abscisic acid (ABA) plays a key role in fruit development and ripening in non-climacteric fruit. A variety of metabolites such as sugars, anthocyanins, fatty acids, and several antioxidants, which are regulated by various phytohormones, are important components of fruit quality in grape. Here, grape cultivar "*Ruiduhongyu*" was used to investigate the relationship between endogenous phytohormones and metabolites associated to grape berry quality under exogenous ABA treatment. 500 mg/L ABA significantly improved the appearance parameters and the content of many metabolites including sugar, anthocyanin, and other compounds. Exogenous ABA also increased the contents of ABA, auxin (IAA), and cytokinins (CTKs), and transcription level of ABA biosynthesis and signaling related genes in fruit. Furthermore, a series of genes involved in biosynthesis and the metabolite pathway of sugars, anthocyanins, and fatty acids were shown to be significantly up-regulated under 500 mg/L ABA treatment. In addition, Pearson correlation analysis demonstrated that there existed relatively strong cooperativities in the ABA/kinetin (KT)-appearance parameters, ABA/IAA/KT-sugars, ABA/indolepopionic acid (IPA)/zeatin riboside (ZR)-anthocyanins, and gibberellin 3 (GA_3)/methyl jasmonate (MeJA)-fatty acids, indicating that 13 kinds of endogenous phytohormones induced by ABA had different contributions to the accumulation of quality-related metabolites, while all of them were involved in regulating the overall improvement of grape fruit quality. These results laid a primary foundation for better understanding that exogenous ABA improves fruit quality by mediating the endogenous phytohormones level in grape.

Keywords: ABA, phytohormones, fruit quality, correlation analysis, grape

OPEN ACCESS

Edited by:
M. Teresa Sanchez-Ballesta, Instituto de Ciencia y Tecnología de Alimentos y Nutrición (ICTAN), Spain

Reviewed by:
Paula Muñoz, University of Barcelona, Spain
Xiaohong Kou, Tianjin University, China

****Correspondence:***
Xiangyi Li
lixiangyi@sjtu.edu.cn
Lei Wang
leiwang2016@sjtu.edu.cn

Specialty section:
This article was submitted to Plant Metabolism and Chemodiversity, a section of the journal Frontiers in Plant Science

Received: *12 July 2021*
Accepted: *31 August 2021*
Published: *01 October 2021*

Citation:
Li J, Liu B, Li X, Li D, Han J, Zhang Y, Ma C, Xu W, Wang L, Jiu S, Zhang C and Wang S (2021) Exogenous Abscisic Acid Mediates Berry Quality Improvement by Altered Endogenous Plant Hormones Level in "Ruiduhongyu" Grapevine. Front. Plant Sci. 12:739964. doi: 10.3389/fpls.2021.739964

INTRODUCTION

Grape (*Vitis vinifera* L.), one of the most important and oldest cultivated fruit crops, is originated from western Asia (El-Mashharawi et al., 2020). Due to the versatility of its fruit products (fresh eating and wine making) and good economic benefits, grape plantations are popular among orchardists and widely distributed around world (Reisch et al., 2012). The fruit quality is the fundamental factor determining processing method (juice and raisin making) and commodity value. Appearance quality including fruit shape, firmness, and coloring are an important part of fruit quality, in which anthocyanins are the main pigment substances determining the coloring

of table grapes and wines (De Orduna, 2010). A variety of metabolites are involved in the quality formation of grape fruit, in which sugars, organic acid, amino acids, and fatty acids (FAs) play a vital role in fruit flavor (Lado et al., 2018). Moreover, there are also a variety of nutrients in grape, such as flavonoids, L-ascorbic acid, polyphenol, and resveratrol, which could alleviate neuronal and cardiovascular disease due to their antioxidant activity (Liu et al., 2018; Shiraishi et al., 2018). It has been widely acknowledged that molecular breeding is an effective way to obtain new species with good fruit traits in woody perennial fruit crops (Töpfer et al., 2011). However, considering the contradictoriness between the long breeding cycle and urgent market demands, fast and effective improvement methods are a priority to researchers. In recent decades, many studies had demonstrated that using exogenous harmless substances could be a feasible strategy to significantly improve fruit quality, including exogenous plant hormones, plant growth regulators, amino acids, and antioxidants (Cai et al., 2014; Raza et al., 2014). For example, 400 mg/L exogenous ABA sprayed on grapevine at the veraison stage could promote the coloration of pericarp (Shahab et al., 2019), and 400 and 600 mg/L ABA treatment on grapevine significantly contributed to grape yield promotion (Mohamed et al., 2019).

Abscisic acid (ABA), as a vital plant hormone and signal molecule, plays a key role in reproductive organ development, stress response, and fruit ripening (Leng et al., 2018; Kou et al., 2021a). Its biosynthesis and signaling mechanism have been well studied in model plants. ABA biosynthesis generally has two pathways: C15 direct pathway and C40 indirect pathway. The former directly forms ABA through C15 farine pyrophosphate (FPP), the latter forms ABA indirectly through oxidative cleavage of carotenoids, which is the main pathway of ABA biosynthesis in higher plants (Seo and Koshiba, 2002). ABA signal transduction mainly contains a complex network of PYR/PYL/RCAR, ABA receptors, Clade A PP2Cs, and SnRK2s (Santiago et al., 2012). ASR peptide is confirmed to respond to ABA signal and plays an important role in regulating ABA signal transmission (Carrari et al., 2004). Many investigations have focused on the effects of ABA on the fruit development and ripening, especially in non-climacteric fruit species. It had been demonstrated that exogenous ABA treatment significantly enhanced the accumulation of sugars (Alferez et al., 2021), double NCED isozymes controlled ABA biosynthesis for ripening and senescent regulation in peach fruits (Wang et al., 2021). Furthermore, in climacteric fruit species, it had been suggested that overexpression of the abscisic acid β−glucosidase gene (*DkBG1*) altered fruit ripening in transgenic tomato (Liang et al., 2020). There were also some reports on the improvement of ABA on fruit quality and nutrient value in grapes, exogenous ABA spraying on grapevine contributed to anthocyanins, flavonoids, resveratrol, and other phenolics accumulation (Deis et al., 2011; Ju et al., 2016). Sugar accumulation determines the market value of table grapes (Liu et al., 2007), it had been reported that exogenous ABA could improve grape frost-resistance via increasing sugar content (Li et al., 2017), and ABA receptor VvSnRK1.1/VvSnRK1.2 interacting with WRKY22 transcription factor jointly regulated the accumulation of sugars in grapevine (Huang et al., 2021).

Plant hormones do not act in isolation in the process of plant growth, development, maturity, and senescence. On the contrary, they co-regulate a series of plant life activities in the complex network of phytohormones interaction (Fenn and Giovannoni, 2021; Li et al., 2021). Thus, to explore the crosstalk among endogenous plant hormones regulating fruit quality improvement seems to be meaningful. Previous study demonstrated that ABA and ethylene (ETH) co-regulated tomato ripening (Kou et al., 2021b), IAA and GA contributed to citrus fruit set and development (Bermejo et al., 2018). IAA and ETH interacted together to promote the production of carotenoid in tomato at the maturity stage (Cruz et al., 2018). ABA, JA, SA, and ETH jointly regulated abiotic stress defense response of apple fruits under photooxidation and heat stress (Torres et al., 2017). It had also been demonstrated that crosstalk between ABA and GA was regulated by ETH and sugar signals, which jointly regulated the increase of non-climacteric fruit sugars content (Alferez et al., 2021), in addition, IAA and ABA co-regulated sugar accumulation in pear at the late ripening stage (Lindo-García et al., 2020). Otherwise, interaction between ABA, ETH, and JA mediated the enrichment of anthocyanins in *Lycium* plants (Li G. et al., 2019). As previous studies stated, crosstalk among endogenous phytohormones could interact together to regulate fruit development and ripening, stress resistance enhancement, sugars, and anthocyanins accumulation, ultimately resulting in the prominent improvement of fruit quality.

The new table grape cultivar "*Ruiduhongyu*," with various advantageous traits containing high-yield, precocity, pink coloring, and muscat flavor is selected from the bud mutation of "*Ruiduxiangyu*" (*Jingxiu* × *Xiangfei*), becoming a new variety with potential development in China (Xu et al., 2014). While in southern China, such as Guangxi province, it is difficult to obtain grapes with brilliant color in the ripening stage due to high temperature. Meanwhile, as a new table grape variety, studies on the effect of exogenous ABA on "*Ruiduhongyu*" fruit quality are still lacking. In this study, the effect of exogenous ABA on berry enlargement, coloration, and interior quality were discussed, whether exogenous ABA mediated a series of biosyntheses of endogenous phytohormones to regulate grape berry size, pericarp coloration, sugars accumulation, flavor formation, and stress resistance improvement were investigated, and the potential correlation between endogenous phytohormones variation and fruit quality-related metabolites was cleared out. The purpose of this study was to provide references for improving fruit quality via cultivation techniques amelioration.

MATERIALS AND METHODS

Plant Material and Experiment Design

This research was established in a greenhouse in Grape and Wine Institute, Guangxi Academy of Agricultural Sciences (107°45′ E, 22°13′ N, NanNing, Guangxi, China) in 2020, using 5 years secondary *"Ruiduhongyu"* grape, a red bud mutation origin from *"Ruiduxiangyu" (Jingxiu* × *Xiangfei)* grape. Grapevines

in both control groups and treatment groups were used as shelter cultivation with the same water and fertilizer condition supplied. Three whole grapevines were sprayed with exogenous ABA (ABA concentration: 500 mg/L; Spraying volume: 2L) at the veraison stage on November 20th (DAA 35). Thirty grape berries of a uniform size were collected from each 500 mg/L ABA treatment group and the control group at 5 specific sampling dates: DAA 40, November 25th; DAA 45, November 30th; DAA 53, December 8th; DAA 69, December 24th; DAA 75, December 30th, DAA was indicated as days after anthesis. All samples were immediately mailed back to the laboratory in Shanghai Jiao Tong University (121°29′ W, 31°11′ N, Shanghai, China) and stored in a −80°C refrigerator for further experiments. After physiological parameters had been measured, grape berries were grinded in liquid nitrogen and then the powder was stored in a −80°C refrigerator, all tests were implemented for at least three biological duplications.

Physiological Parameters Analysis

Thirty berries in each sampling stage without visible damage were selected for berry weight, longitudinal and transverse diameters, total soluble solid (TSS) and titratable acid (TA) measurements. Berry weights were measured by analytical balance (Sartorius, German), longitudinal and transverse diameters were quantified by vernier caliper (Mitutoyo, TKY, Japan), TSS was measured by refractometer (OWELL, Hangchow, CHN) using 1 mL of grounded and fully squeezed grape juice, and represented as °Brix (Sánchez-Moreno et al., 2003). TA was measured by potentiometric titrator (HAINENG, SZ, CHN) and represented as g/L (Sánchez-Moreno et al., 2003). All tests were implemented for at least three technical duplicates.

Quality-Related Parameters Quantification

According to the previous methods, reducing sugar was measured using 3, 5-dinitrosalicylic acid method with a little adjustment (Bonilla et al., 1999). The specific extraction process was as follows, firstly, 1 g of accurately weighed freeze-dried powder and 25 mL of deionized water were added in a centrifuge tube. Then the solution continued reacting for 30 min in a constant temperature water bath (JingHong, SHH, CHIN) at 80°C. After two filtrations, the liquid volume was metered to 100 mL by deionized water and then fully mixed. Finally, 2 mL of reducing sugar extracting solution and 1.5 mL of 3, 5-dinitrosalicylic acid reagent were fully blending, then the absorbance value in each sample was analyzed by spectrophotometer under 540 nm wavelength and converted to "glucose equivalents" according to the calibration curve prepared with a d-(+)-glucose.

The quantification of soluble sugar was referred to the anthrone colorimetry assay with a little adjustment (Bonilla et al., 1999), 50 mg freeze-dried grape powder and 4 mL 80% ethanol was added in a 10 mL graduated centrifuge tube. Then, the sample was placed in a water bath at 80°C for 40 min, after centrifugating at 4,000 rpm for 10 min, the supernatant was collected. Next, the residue was added with 2 mL 80% ethanol and centrifugated at 4,000 rpm for 10 min again. Supernatant was incorporated and 10 mg of activated carbon was added, decolorized at 80°C for 30 min, then 80% ethanol was added and constant solution volume to 10 mL. One milliliter of filtrate was added with 5 mL of anthrone reagent, then fully mixed and boiled in a boiling water bath for 10 min. After the solution was cooled to the room temperature, its absorbance value was measured at 625 nm by spectrophotometer.

The extraction of polyphenol and soluble dietary fiber method was as follows (Gorinstein et al., 1999). Firstly, 1 g of dry sample was accurately weighed, then 80% methanol and 1% hydrochloric acid (solid-liquid ratio = 1:30) were added. Next, under ultrasonic extraction reacting at 45°C for 40 min, the supernatant was collected for polyphenol, anthocyanins, and flavonoid quantifications, and residue was collected for dietary fiber determination. Soluble dietary fiber was measured as follows, 0.4 M hydrochloric acid (solid-liquid ratio = 1:15) was added to the residue, after vigorously shaking, the solution was dried in 80°C oven to constant weight, dry weight was measured by analytical balance (Sartorius, German) and reported as g. Polyphenol was measured as follows, 3 mL of 0.2 M Folin-Ciocalteau reagent was added to 3 mL of 10 times diluted supernatant, then 2.4 mL of 0.7 M Sodium carbonate solution was added. After mixture had been reacting for 120 min under no light condition, its absorbance was determined under 760 nm wavelength. The content of polyphenol in each sample was calculated as gallic acid equivalents (GAE) and reported as mg/g.

The method for determination of flavonoid content was implemented by the vanillin colorimetric assay with the calibration standard of (+)-catechin hydrate (Price et al., 1978). Firstly, 0.2 mL of supernatant extracting solution and 60 μL of 5% sodium nitrite solution were mixed, after fully blending and reacting for 6 min, then 0.8 mL of 1 M sodium hydroxide solution and 3.88 mL of 50% ethanol solution were added in turn. Finally, after mixture had been standing for 15 min, its absorbance was determined under 510 nm wavelength. The flavonoid content was calculated as rutin equivalent per gram of sample.

Total anthocyanin content was determined by PH differential method (Porter et al., 1985), 2.5 mL of supernatant extracting solution was added to reach a constant volume of 10 mL using 0.025 M potassium chloride buffer (PH = 1.0) and 0.4 M sodium acetate buffer (PH = 4.5), then the absorbance of two kinds of solution were determined under 520 nm wavelength and 700 nm wavelength. The total anthocyanin content in each sample was reported as mg/g.

Soluble protein was measured according to Coomassie Bright Blue assay (Singleton and Rossi, 1965). 2.0 g of freeze-dried sample and 5 mL of deionized water were added to a centrifuge tube, then the homogenate was centrifuged under 12,000 rpm for 15 min at 4°C. Finally, 1 mL of collected supernatant and 5 mL of Coomassie Bright Blue solution were fully mixed. Finally, the mixture was determined the absorbance under 595 nm wavelength, the concentration of soluble protein in each sample was reported as mg/g.

The method for determination of L-ascorbic acid content was as follows (Bonilla et al., 1999), Firstly, 1 g of dry sample was taken

and 2 mL of 50 g/L TCA solution was added, after sufficiently dissolving, the volume was adjusted to 10 mL using 50 g/L TCA solution again. Finally, 1 mL of extracting solution was added to 1 mL of 50 g/L TCA solution, after fully blending, the solution absorbance was determined under 534 nm wavelength. The ascorbic acid content was calculated as ascorbic acid equivalent per gram of sample.

The extraction of resveratrol was as follows: 3 g of freeze-dried powder and 10 mL of anhydrous ethanol were added in a centrifuge tube, then placed under ultrasonic treatment for more than 30 min. The obtained liquor was filtered by 0.22 μm membrane and its absorbance was determined under 525 nm by spectrophotometer.

The methods for determination of malondialdehyde (MDA), proline (Pro), guaiacol peroxidase (POD), superoxide dismutase (SOD), catalase (CAT), ascorbate peroxidase (APX), glutathione (GSH), and DPPH free radical scavenging rate were referred to Nahakpam and Shah (2011) with a little adjustment, all tests were implemented with at least three technical duplicates. MDA measurement was as follows: 0.5 g of freshy fruit was taken, 2 mL of 10% TCA solution was added for grinding, and then 5 mL of TBA solution was added for mixing. After reacting in a boiling water bath for 10 min, the liquid was centrifuged at 3,000 rpm for 10 min, then solution absorbance was, respectively, measured at 532, 600, and 450 nm, and MDA content was reported as μmol/g. Pro measurement was as follows, 0.5 g of flesh tissue was weighed, after reacting in a boiling water bath for 10 min, 2 mL of glacial acetic acid and 2 mL of acidic hydrin were added. Next, after reacting in a boiling water bath for 30 min, 4 mL of toluene was added after cooling. After centrifugation (3,000 rpm, 5 min), the supernatant absorbance was measured at 520 nm and final concentration was reported as μg/g. POD, SOD, and CAT measurements were as follows: Firstly, 0.5 g of flesh fruit was weighed, a small amount of phosphoric acid (PBS) buffer (0.05 mol/L, PH = 7.8) was added and ground into homogenate, then the volume was kept to a constant of 9 mL with PBS buffer. After centrifugation (4°C at 3,000 rpm) for 10 min, the supernatant was stored at 4°C for further experiments. For POD detection, 3 mL of enzyme solution was added 56 μL of guaiacol, heated until the color faded, then cooled to room temperature. After adding 38 μL of 30% hydrogen peroxide, the POD activity was determined at 470 nm. For SOD detection, 2.5 mL of the reaction mixture (contained 130 mmol/L of Met, 750 μmol/L of NBT, and 100 μmol/L of EDTA-Na_2) was added 0.2 mL of 0.05 M phosphate buffer (pH = 7.8) in a tube, 0.2 mL of enzyme solution was added to another tube, and 0.3 mL of 20 μmol/L riboflavin solution was quickly added to each tube. After 15 min reaction, the absorbance was measured at 560 nm and SOD activity was reported as mmol/g FW. CAT detection was measured as follows: 0.2 mL of enzyme solution was added to 1.5 mL of 0.2 mol/L PBS buffer (pH 7.8), 1 mL of distilled water and 0.3 mL of 0.1 mol/L hydrogen peroxide were added, then absorbance was detected at 240 nm and CAT activity was reported as U/g FW/min. For APX detection, 1.8 mL of 50 mmol/L phosphate buffer (pH 7.0), 0.1 mL of 15 mmol/L AsA, 0.1 mL of enzyme solution, and 1 mL of 0.3 mmol/L H_2O_2 were added to the test tube. Then, the change of OD_{290} was measured within 3 min with no enzyme solution (instead of PBS solution) as blank, the APX activity was reported as U/g FW. For GSH detection, 0.5 g of fruit was weighed and 5 mL of 5% trichloroacetic acid was added. After centrifugation at 15,000 rpm for 10 min, the absorbance of the supernatant was determined at 412 nm, and the final content was reported as μmol/g. DPPH free radical scavenging rate quantification was as follows: 4 mL of enzyme solution and 4 mL of DPPH solution were fully mixed. Then, it was brought to a constant volume of 10 mL using anhydrous ethanol. After full mixing, the solution absorbance was measured at 517 nm and DPPH free radical scavenging rate was reported as %.

Endogenous Phytohormones Quantification

Endogenous phytohormones were extracted by known method with a little adjustment (Kojima et al., 2009), and detected by HPLC. The detection and quantification limits of target compounds by HPLC were shown in **Supplementary Table 2**. Firstly, 100 mg of freeze-dried powder was dissolved in the 1 mL of extracting solution (Methanol: Formic acid: ddH_2O = 15:1:4) and stored in −20°C refrigerator for one night. The solution was then centrifugated (4°C, 13,000 rpm/min) for 20 min twice, incorporated the supernatant, and filtered by CNWBOND HC-C18 SPE Cartridge (CNW, German). Then, after rotary evaporating (YARONG, SHH, CHN) at 42°C residue was redissolved in 5 mL of 1 M formic acid. The liquid was immediately transferred into Poly-Sery MCX SPE Cartridge (CNW, German), first eluted by 5 mL of 1 M formic acid then eluted by 5 mL of methanol. Finally, after rotary evaporating again at 42°C, residue was redissolved using 0.5 mL of extraction solution (Methanol: Isopropanol: Acetic acid = 20:79:1), and the liquid containing abscisic acid (ABA), auxin (IAA), indolebutyric acid (IBA), indolepopionic acid (IPA), salicylic acid (SA), gibberellin$_3$ (GA_3), jasmonic acid (JA), and methyl jasmonate (MeJA) was acquired. Next, 5 mL of 0.35 M ammonia and 5 mL of 0.35 M ammonia in 60% methanol were immediately added into the same Poly-Sery MCX SPE Cartridge (CNW, German) in turn, then after the filter liquor was evaporated at 60°C, the residue was added 0.5 mL of 5% acetonitrile. Liquid containing zeatin (ZT), zeatin riboside (ZR), N-6 isopentenyl adenine (ip), N-6 isopentenyl adenine nucleoside (ipR), and kinetin (KT) was obtained.

The detection of endogenous phytohormones was performed on a LC3000 Semi-preparation Isocratic HPLC System (CXTH, BJ, CHN). A UV-detector (CXTH, BJ, CHN) and Capecell PAK C18 column (4.6 mm × 100 mm, 1.8 μm) was installed, the flow rate was adjusted to 0.8 mL/min. The elution system was first set as follows: 0–4 min, 20% A, 80% B; 4–8 min, 50% A, 50% B; 8–20 min, 80% A, 20% B; 20–22 min, 80% A, 20% B; 22–22.2 min, 20% A, 80% B. Under this program, ABA, IAA, IBA, IPA, SA, GA_3, JA, and MeJA were, respectively, eluted in different retention times. Then, mobile phase A (0.06% acetic acid water) and mobile phase B (0.06% acetic acid-methanol) was changed, injection volume was still 20 μ, while flow rate was adjusted to 0.5 mL/min. The gradient program was set as follows: 0–8 min, 99% A-55% A; 8–14 min, 55% A-30% A; 14–16 min, 30% A-1% A; 16–24 min, 1% A-99% A. Under this program, ZT, ZR, ip, ipR, and KT were eluted in different retention times. UV wavelength

was 254 nm and the temperature of the chromatographic column was 40°C. All reagents of chromatography grade were purchase in ANPEL (SHH, CHN), liquid for HPLC detection was filtered through a 0.22 μm membrane.

Fatty Acids Measurement

The extraction of different FAs was implemented according to the following method (Song et al., 2019), powder stored in −80°C refrigerator was transferred to 4°C refrigerator to thaw, then 3 mL of grape juice and 3 mL of n-hexane were fully mixed. After the mixture was placed in the shaking table (TENSUC, SHH, CHN) under 300 rpm for 15 min, liquid supernatant was collected and methyl dodecanoate (0.4 mg/mL) was added immediately. After nitrogen blew (Organomation, United States) to 1 mL, the liquid was immediately methylated by known method. Firstly, the solution was added to 3 mL of 2% sodium hydroxide-methanol, then placed in a water bath at 85°C for 30 min. Next, 3 mL of 14% boron trifluoride-methanol solution was added, then placed in a water bath at 85°C for 30 min again. After the solution was cooled to room temperature, 1 mL of n-hexane was added and then shocked for 2 min, and left to stand for 1 h. Finally, 100 μ of supernatant was collected and brought to a constant volume of 1 mL using n-hexane, after extraction solution was filtered by 0.22 μm membrane and then detected in GC.

Then, J&W DB-WAX capillary column (30 mm × 0.25 mm, 0.25 μm) was installed in the GC system, inlet temperature was set to 250°C and the fluid intake was 1.0 μL, the split ratio was set to 20:1 and carrier gas was high-purity helium with a flow rate of 1.0 mL/min. The initial temperature was set to 180°C for 5 min, and then increased to 230°C at a rate of 3°C/min till the set temperature was reached.

Fructose, Sucrose, and Glucose Measurements

The extraction of fructose, sucrose, and glucose contents referred to the known method (Nowicka et al., 2019), and was detected by HPLC. Firstly, 3 mL of grape juice was centrifuged under 10,000 rpm/min for 15 min. Then in a centrifuge tube, 1 mL of supernatant and 9 mL of ultrapure water was added. Finally, mixture liquid was filtrated through 0.22 μm membrane and detected by HPLC.

The standard curve was drawn as follows: firstly, glucose, sucrose, and fructose standard products were diluted with ultra-pure water into 100 ng/mL mixed liquid as the mother liquor, then the mother liquor was diluted in a gradient. Finally, the obtained solution was detected by HPLC, the standard curves of glucose and fructose were drawn, respectively, with the sugar content as the abscissa and the peak area as the ordinate. The determination method of each sample was consistent with the standard liquid measurement and repeatedly measured 3 times, then the corresponding sugar content was converted according to the standard curve, and the mean value as well as the standard deviation was calculated.

Detection of sugar levels was performed on LC3000 Semi-preparation Isocratic HPLC System (CXTH, BJ, CHN), differential detector (KNAUER, GERMAN), and Amino column (250 mm × 4.6 mm, 5 μm) was installed, mobile phase was acetonitrile-water (75:25, with a small amount of ammonium hydroxide). The flow rate was 0.6 mL/min and the column temperature was 25°C.

Real-Time RNA-Seq Analysis

The extraction of total RNA was performed on RNA prep Pure Plant Plus Kit (TaKaRa, Dalian, China) using berries collected in all five sampling stages from both 500 mg/L ABA treatment group and the control group. The purity and integrality analyses were established on BIO-RADXR gel imaging analysis system (Bio-Rad, CA, United States). Referencing to the manufacturer's instructions, the PrimeScript™ RT reagent kit with gDNA Eraser (Perfect Real Time) (TaKaRa, Dalian, China) used 1 μg of total RNA extracted from berries, aiming to obtain the first strand of cDNA.

10 μL of final volume consisted of 1 μL of cDNA, 5 μL of TB Green® Fast qPCR Mix, 3 μL of ddH_2O and 1 μL of forward and reverse primers mixture. Then qRT-PCR was carried out on a CFX connect Real Time PCR Detection System (Bio-Rad, CA, United States). The sequences of all genes and transcription factors in this research were downloaded from EnsemblPlants[1] and National Center for Biotechnology Information website (NCBI, https://www.ncbi.nlm.nih.gov/. The specific primers (55 genes, 7 transcription factors and actin) were all designed by Primer Premier 5.0, the sequences and information of genes and transcription factors were listed in **Supplementary Table 1**. The qPCR system was performed using the following program: 95°C for 20 s, then followed by 39 cycles of 95°C for 15 s, finally, 55°C for 15 s and 60°C for 15 s. The ultimate relative expression levels of test genes were calculated by the $2^{-\Delta\Delta Ct}$ assay.

Statistical Analysis and Figure Drawing

SPSS 16.0 statistical software package (IBM, Armonk, NY, United States) was used for analyzing results, the data were expressed as the mean ± standard error (SE) of at least three independent replicates. an independent-sample *T*-test was applied to assess significant differences among treatments ($P < 0.05$). Pearson correlation analysis on the variation tendencies between phytohormones and quality-related parameters was also analyzed by SPSS 16.0 (IBM, Armonk, NY, United States) and TBtools (CAN, CHN). GraphPad Prism 9.0 (GraphPad Software Inc., San Diego, CA, United States) and Visio 2020 (Microsoft, SEA, United States) were used for drawing figures.

RESULTS AND DISCUSSION

The Effect of Exogenous Abscisic Acid on Fruit Quality

Physiological parameters in two treatment groups (control, 500 mg/L ABA) measured throughout different collected stages were shown in the **Figure 1B**. Under 500 mg/L ABA treatment, berry weight in the DAA 75 stage was significantly higher than

[1]http://plants.ensembl.org/info/about/index.html

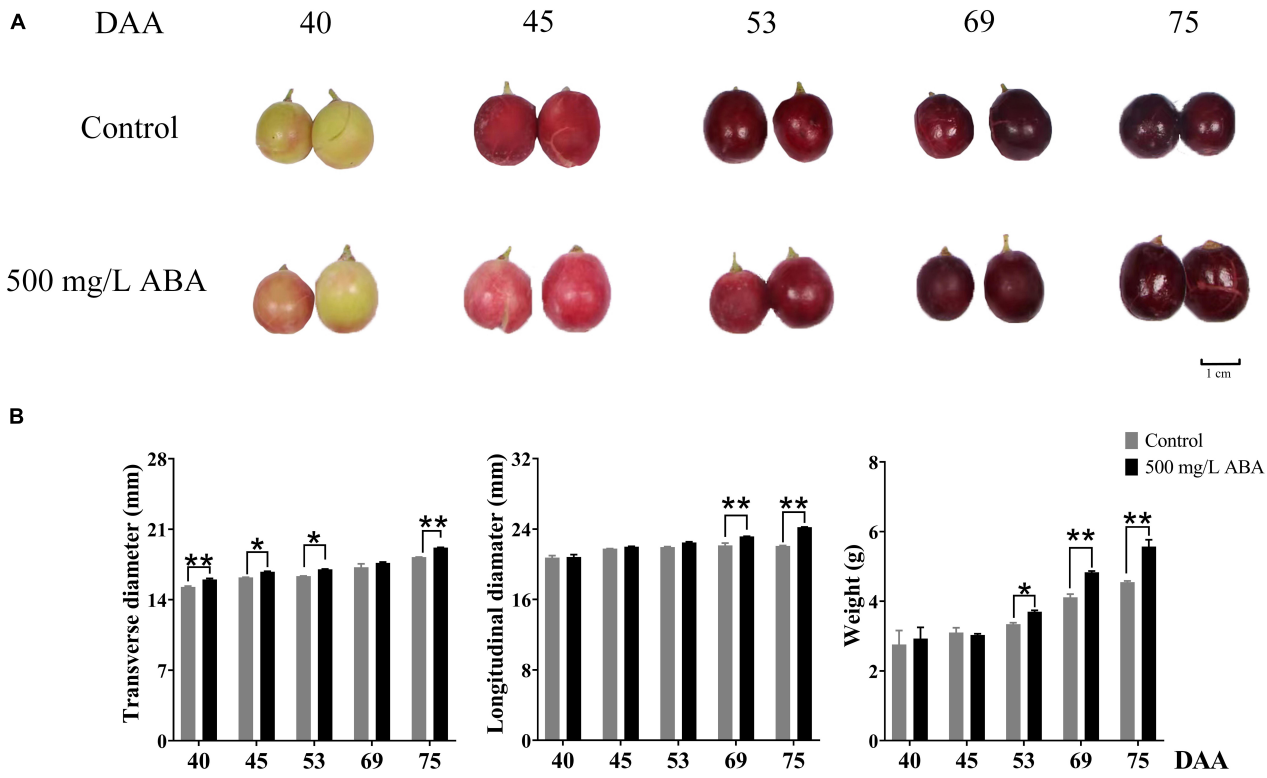

FIGURE 1 | Fruit phenotype and berry appearance parameters. **(A)** Berries collected in two treatment groups (control group and 500 mg/L ABA group) at five sampling stages. DAA 40, November 25th; DAA 45, November 30th; DAA 53, December 8th; DAA 69, December 24th; DAA 75, December 30th. **(B)** Appearance parameters in different sampling times, data from 500 mg/L ABA treatment were represented as a black column while data from control group were represented as a gray column. *Showed the comparatively significant differences with *T*-test ($p < 0.1$, $n = 3$) and **Showed the highly significant differences with *T*-test ($p < 0.05$, $n = 3$).

in the control group (an increasing of 22.4% over the control group), and in the DAA 69 stage the increase rate was 17.5%, berry longitudinal diameters in the DAA 69 and DAA 75 stages were significantly higher than in the control group (an increasing of 4.65 and 9.69% over the control group), while berry transverse diameters in the DAA 40 and DAA 75 stages were significantly higher than in the control group (an increasing of 4.85 and 5.71% over the control group).

In this study, we also investigated several interior quality parameters such as TSS, TA, soluble dietary fiber, soluble protein, and resveratrol contents. TSS was shown in the **Figure 2A**, ABA treatment could significantly increase its contents in the DAA 40, DAA 45, DAA 69, and DAA 75 stages compared to the control group, and the variation tendency was the same in the two groups, it kept rising in all five sampling stages, indicating that the sugar degree continuously increased with fruit ripening. Previous studies suggested that exogenous ABA could significantly increase TSS in "*Crimson Seedless*" grapevine, which was consistent with our study (Ferrara et al., 2013). Meanwhile, we found the differential of TSS levels between the control group and ABA treatment were more and more significant, indicating that exogenous ABA accelerated sugar accumulation in grape fruits mainly occurred in the late ripening period. TA contents decreased gradually with fruit ripening, in the ABA treatment group, its contents were significantly lower than in the control group during the last three sampling stages (**Figure 2B**). As for soluble dietary fiber contents, we discovered that ABA treatment significantly increased its contents in DAA 40 and DAA 53 stages while significantly decreasing its content in the DAA 69 stage compared with the control group. Interestingly, the variation tendencies in the two groups were the same, it went down first, then it rose and finally it reduced again (**Figure 2C**). Furthermore, **Figure 2D** demonstrated that in all five sampling stages, soluble protein contents were confirmed to significantly develop under ABA treatment compared with the control group. Resveratrol, one of the polyphenols, occupy a large amount in grape wine. As a preventive agent for tumor formation, it plays a vital role in the treatment of human cardiovascular and cerebrovascular diseases (Hasan and Bae, 2017). In this study, ABA treatment could significantly increase its concentrations in DAA 45, DAA 53, DAA 69, and DAA 75 stages compared with the control group, and the variation tendency kept increasing in all five sampling stages (**Figure 2E**).

MDA and Pro are indicators reflecting the degree of stress and ripening on plants (Huan et al., 2016), as shown in the **Supplementary Figures 2A,B**, MDA contents and Pro contents rose then dropped slightly. Their contents in ABA treatment group were significantly higher than in the control group

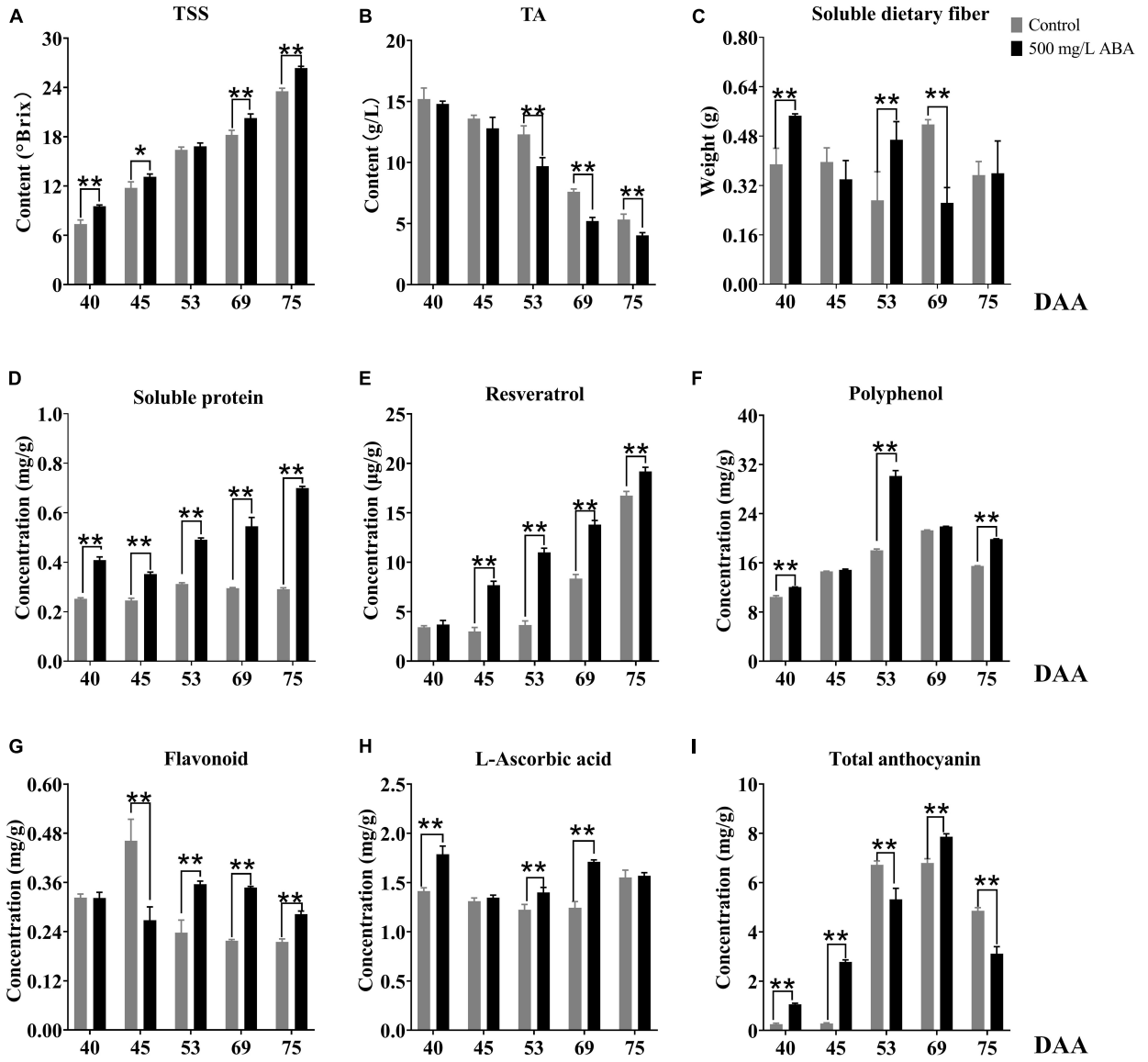

FIGURE 2 | Effect of exogenous ABA treatment on the variation tendency of different quality-related parameters in two treatment groups (control group and 500 mg/L ABA group) at five sampling stages. DAA 40, November 25th; DAA 45, November 30th; DAA 53, December 8th; DAA 69, December 24th; DAA 75, December 30th. **(A)** TSS. **(B)** TA. **(C)** Soluble dietary fiber contents. **(D)** Soluble protein contents. **(E)** Resveratrol contents. **(F)** Polyphenol contents. **(G)** Flavonoid contents. **(H)** L-ascorbic acid contents. **(I)** Total anthocyanin contents. Data from 500 mg/L ABA treatment were shown as a black column while data from control group were shown as a gray column. *Showed the comparatively significant differences with *T*-test ($p < 0.1$, $n = 3$) and **Showed the highly significant differences with *T*-test ($p < 0.05$, $n = 3$).

at DAA 40, 45, 69, 75 stages, indicating that abiotic stress degree and osmotic regulation increased with fruit ripening. The accumulation of a large amount of MDA and Pro would inevitably lead to changes in the contents of CAT, SOD, and POD in plants (Huan et al., 2016). As we expected, **Supplementary Figures 2C–E** had revealed the consistent variation trends, the activities of the three enzymes all peaked at DAA 53 or 69 stages and then decreased, and ABA treatment could activate their activity at DAA 40, 45, 53, and 75 stages. Interestingly, we found that exogenous ABA could accelerate the emergence of maximum POD value while slowing down the maximum CAT value. It is well-known that reactive oxygen species (ROS) is a general term for a class of chemically active molecules or ions with high oxidative activity, is also an important parameter reflecting the degree of stress faced by fruits (Decros et al., 2019). During fruit development and ripening, ROS content gradually increases and metabolites contributed to stress resistance are accumulated, stress resistance is also correspondingly improved (Giribaldi et al., 2010). ROS produced in plant cells could be eliminated by highly efficient antioxidation-related enzymes

(CAT, SOD, POD, APX), and in this process, several antioxidants (phenols, terpenes, thiol derivatives, vitamins, GSH) are enriched accordingly (Decros et al., 2019). Based our obtained results, we speculated that exogenous ABA could effectively eliminate ROS and MDA by regulating the activities of different antioxidant enzymes at different grapevine ripening stages. Another system for scavenging ROS in plants is ascorbate-glutathione cycle, in which APX plays the most important role (Decros et al., 2019). It had been reported that APX could improve the oxidative tolerance of plants and that the activity of GSH (a regulator that maintains cell homeostasis) was positively correlated with APX activity (Wei et al., 2017). In this study, we found that GSH content in both two treatment groups kept rising and under ABA treatment its contents were significant higher in all sampling stages (**Supplementary Figure 2F**). Moreover, exogenous ABA treatment could improve the activity of APX at all sampling stages and delayed the occurrence of APX peak value, its activity in ABA treatment group reached a maximum at the DAA 53 stage and then slowly declined (**Supplementary Figure 2G**). The above results demonstrated that GSH and APX increased synergistically at the early stage of fruit ripening and jointly enhanced the antioxidant metabolism process. In addition, DPPH is a very stable nitrogen-centered radical, its scavenging rate could also reflect abiotic stress degree and antioxidant capacity (Decros et al., 2019). Our study further found that the DPPH free radical scavenging rate was gradually increased in both treatment groups, and exogenous ABA treatment significantly increased its ratio at all five sampling stages (**Supplementary Figure 2H**). The changes of the above enzyme activities under ABA treatment were consistent with research in tomato (Tao et al., 2020), so we made a reasonable inference that during the ripening process of grapevine, plentiful oxidative metabolic reactions occurred and led to ROS, MDA, and DPPH accumulation, the damage of them to cells was reduced by Pro and several antioxidant enzymes, and exogenous ABA treatment contributed to the occurrence of these reactions.

As for antioxidants related to stress resistance, it had been reported that cold plasma treatment led to the accumulation of phenols in pitayas and regulated the ROS signal through the activation of phenylpropane metabolism (Li X. et al., 2019), and exogenous ABA significantly affected grape phenolic composition and contributed to the improvement of stress resistance (Deis et al., 2011). As the results show in **Figure 2F**, ABA treatment could significantly increase total polyphenol levels in DAA 40, DAA 53, and DAA 75 stages compared with the control group, the variation tendencies both rose first and then dropped down. Therefore, we deduced that exogenous ABA activated ROS signal and regulated the accumulation of polyphenol as the grape fruits ripened. Another vital antioxidant substance in grape is flavonoid, previous study highlighted that exogenous ABA treatment could significantly increase flavonoid content as well as expression levels of key genes revolved in its biosynthesis (Crizel et al., 2020). In our study, we found that ABA treatment could significantly enhance flavonoid concentrations in DAA 53, DAA 69, and DAA 75 stages compared with the control group (**Figure 2G**). In addition, it had been reported that ABA treatment significantly expedited the metabolism of L-ascorbic acid and improved strawberry antioxidant activity (Li et al., 2015), we found L-ascorbic acid concentrations under ABA treatment were significantly higher in DAA 40, DAA 53, and DAA 69 stages compared with the control group (**Figure 2H**). The variation tendencies in two groups first decreased and then rose, which was accordant with previous study revealing that L-ascorbic acid accumulated in the late grape ripening stage (Leng et al., 2017). Since UVC induced L-ascorbic acid and phenolic biosynthesis in cherry fruits via increasing mitochondrial activity and ROS (Rabelo et al., 2020), we deduced that exogenous ABA could amplify ROS signal and contributed to the accumulation of several antioxidants at the late grapevine ripening stage to reduce ROS damage to cells, thus delayed the decline of fruit quality due to postmaturity.

Figure 1A had well demonstrated that with fruit development and ripening, the color of grape pericarp constantly deepened, indicating the formation and accumulation of anthocyanins. ABA treatment could significantly increase total anthocyanins contents compared with the control group in the DAA 40, DAA 45, and DAA 69 **stages**. The variation tendency under ABA treatment was consistent with the control group, revealing that it first rose and then dropped down slightly (**Figure 2I**). Interestingly, we found that in DAA 53 stage anthocyanin content was significantly lower in the treatment group than in the control group (supposedly higher), and exogenous ABA treatment could delay the appearance of anthocyanin peak value. It had been reported that exogenous ABA could promote the postharvest color development of wine grape, and delayed the appearance of the maximum anthocyanin level (Berli et al., 2011). Thus, we deduced although anthocyanin content in the control group might be higher than the treatment group sometimes, the extremely significant effect of ABA on anthocyanins accumulation in late maturity stage was not affected. It had been reported that the long-term effect of ABA spraying on grape berry had been reported not only to influence anthocyanins content but also up-regulate expression levels of key genes in their biosynthesis pathway (Villalobos-González et al., 2016). Results in our study, shown in the **Supplementary Figure 1**, revealed that in DAA 69 stage under ABA treatment, the expression levels of *VvPAL* (*VIT_11s0016g01520*), *Vv4CL* (*VIT_16s0039g02040*), *VvCHI* (*VIT_13s0067g03820*), and *VvCHS* (*VIT_14s0068g00930*), which were upstream genes in anthocyanins biosynthesis pathway, were significantly up-regulated. Meanwhile, in DAA 40, 53, and 69 stages, the downstream genes in anthocyanins biosynthesis pathway of *VvF3H* (*VIT_04s0023g03370*), *VvF3'5'H* (*VIT_06s0009g02970*), *VvLAR* (*VIT_01s0011g02960*), *VvANR* (*VIT_00s0361g00040*), *Vv3GT* (*VIT_14s0006g03000*), and *Vv5GT* (*VIT_15s0021g00910*) were also up-regulated in the ABA treatment group compared with the control group, especially in the DAA 40 stage, the effect of exogenous ABA was significant. In addition, the expression of transcription factors of VvMYB5a (*VIT_08s0007g07230*), VvMYB14 (*VIT_07s0005g03340*), VvMYCa (*VIT_19s0014g05400*) regulating structural genes for anthocyanins biosynthesis increased under ABA treatment compared to the control group in the last four stages. Interestingly, most of downstream genes in anthocyanins

biosynthesis pathway were up-regulated in the DAA 53 stage, while the expression of key genes *VvFLS* (*VIT_18s0001g03430*) related to flavonoids biosynthesis was also increased. Therefore, based on the results that exogenous ABA treatment decreased the total anthocyanin content while increasing flavonoid content in DAA 53 stage, we speculated that exogenous ABA may have accelerated the production of flavonoids or other metabolites during this period. Previous studies had demonstrated that VvMYBA protein interacted with the promoter regions of *UFGT*, *LDOX*, and *CHS3* to mediate the biosynthesis of anthocyanins in grape pericarp (Poudel et al., 2021), PacMYBA interacted with several bHLH transcription factors to activate promoters of *PacDFR*, *PacANS*, and *PacUFGT* (Shen et al., 2014), MdWRKY40 interacted with MdMYB1 to promote anthocyanin biosynthesis, these two proteins were reported tightly in response to ABA signal (An et al., 2019). According to the above findings and our results, we deduced that exogenous ABA could promote the coloration of grape fruits in the late ripening stage, and transcription factors of MYB family could respond to exogenous ABA signals.

The Effect of Exogenous Abscisic Acid on Endogenous Abscisic Acid Biosynthesis, Catabolism, and Signal Transduction

To explore the effects of exogenous ABA treatment on endogenous ABA biosynthesis, catabolism, and signal transduction, endogenous ABA content was investigated and genes and transcription factors involved in ABA biosynthesis, catabolism, and signal transduction were quantified in all five sampling stages. Results in **Figure 3A** well revealed that ABA treatment could significantly increase ABA contents compared with the control group in all five sampling stages. The variation tendency of ABA content was going up all the time in both two treatment groups, substantiating that exogenous ABA treatment had a positive feedback effect on the biosynthesis of endogenous ABA in grape berry. ABA biosynthesis was regulated by *NCED1* and *BG1*, **Figure 3B** well demonstrated that the expression levels of *Vvertz1* (*VIT_02s0025g00240*), *VvNCED1* (*VIT_19s0093g00550*), *VvAAO3* (*VIT_11s0016g03490*), *VvABA3* (*VIT_17s0000g02290*), and *VvBG1* (*VIT_01s0011g00760*) under ABA treatment were significantly higher than in the control group at the DAA 53 stage, these genes were related to the biosynthesis of ABA, while *VvCYP707A* (*VIT_02s0087g00710*) and *VvUGTs* (*VIT_05s0094g01010*) were expressed at a low level in ABA treatment at DAA 40 and 69 stages, these genes contributed to ABA catabolic. Interestingly, the expression levels of *VvZEP* (*VIT_07s0031g00620*) were up-regulated in the ABA treatment group compared to the control group in all five sampling stages. ABA signal transduction also played a crucial role in ABA accumulation and degradation, results in the present study clearly revealed that at the DAA 40 and DAA 75 stages in the ABA treatment group, positive transcription factors of VvABI4 (*VIT_13s0067g01400*) and VvABI5 (*VIT_00s0357g00120*) were significantly up-regulated compared with the control group, while negative transcription factors of VvWRKY40 (*VIT_07s0005g01710*)

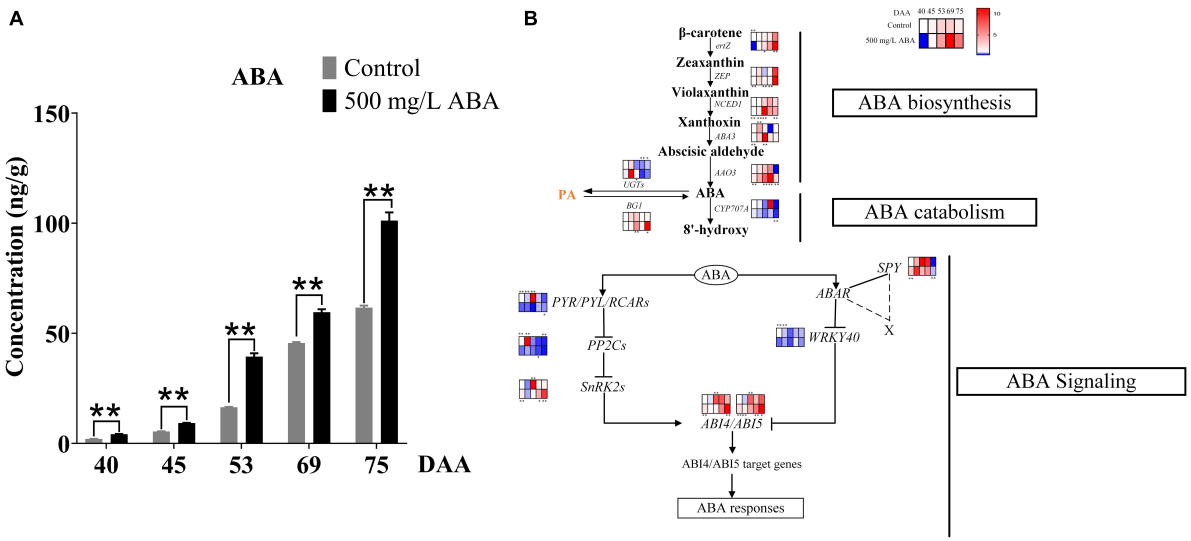

FIGURE 3 | Effect of exogenous ABA treatment on the variation tendency of endogenous ABA contents as well as expression levels of ABA biosynthetic, catabolic, and signaling genes in two treatment groups (control group and 500 mg/L ABA group) at five sampling stages. DAA 40, November 25th; DAA 45, November 30th; DAA 53, December 8th; DAA 69, December 24th; DAA 75, December 30th. **(A)** ABA contents. Data from 500 mg/L ABA treatment were shown as a black column while data from the control group were shown as a gray column. **(B)** Expression of genes and transcription factors involved in ABA biosynthesis, catabolic, and signal transduction Pathways. The relative expression changes in two treatment groups at other stages were relative to the control group (DAA 40) were represented as log2 fold change, key genes (*NCED1*, *ZEP*, *ertZ*, *CYP707A*, *ABA3*, *BG1*, *UGTs*, *AAO3*, *PP2C1*, *SnRK2*, *SPY*, *PYR*) and key transcription factors (WRKY40, ABI4, ABI5) expression levels were shown in the heatmap. heatmap. *Showed the comparatively significant differences with *T*-test ($p < 0.1$, $n = 3$) and **Showed the highly significant differences with *T*-test ($p < 0.05$, $n = 3$).

were down-regulated at four sampling stages except for the DAA 69 stage. Otherwise, in both two treatment groups, the expression of *VvSnRK2* (*VIT_05s0020g01580*) promoting ABA signal transduction were significantly increased at the last two sampling stages, while *VvPP2C* (*VIT_13s0067g01270*) inhibiting ABA signal transduction was significantly decreased at the DAA 40, 45, and 75 stages. Above results revealed that during the late stages of grape ripening in the ABA treatment group, most of the key genes in the ABA biosynthesis pathway were much up-regulated, ABA catabolic genes were down-regulated, and ABA signal transduction was enhanced.

The Effect of Exogenous Abscisic Acid on Diverse Endogenous Hormones Contents

It has been currently recognized that phytohormones play an important regulatory role in almost all plant growth and development processes, especially in regulating fleshy fruits quality improvement (Kumar et al., 2013). To obtain further investigation of variation trends of other phytohormones under exogenous ABA treatment, 12 kinds of phytohormones including IAA, SA, GA_3, JA, MeJA, IBA, IPA, ZT, ZR, ip, ipR, and KT contents in both two treatment groups were detected. The results sufficiently demonstrated that under ABA treatment, IAA concentrations were significantly enhanced in the DAA 40, DAA 45, and DAA 53 stages compared with the control group, the variation tendency in the ABA treatment group was going up all the time while the variation tendency in the control group first went up then decreased (**Figure 4A**). Exogenous ABA treatment indeed reduced the content of IAA as the development of peach fruit (Liu, 2019), while improving kiwi's ability to resist drought stress via increasing IAA content (Wang et al., 2011). Thus, a conjecture could be put forward that the biosynthesis of endogenous IAA could respond to exogenous ABA signal, exogenous ABA treatment had positive feedback effect on the endogenous IAA biosynthesis at early grape ripening stages, while this effect was not obvious at the later stage of fruit ripening. IBA and IPA are precursors in the IAA synthetic pathway, we found that IBA concentrations under ABA treatment were significantly higher than in the control group in all five sampling stages (**Figure 4B**), while IPA concentration under ABA treatment was only significantly higher than in the control group in the DAA 45 stage (**Figure 4C**). However, the variation tendencies of two hormones were opposite to the ABA variation tendency, two of them decreased gradually as the fruit ripened. Due to the fact that ABA, IBA, and IPA were antagonistic to each other and jointly regulated flowering (Pal, 2019), we inferred that ABA antagonism of IBA and IPA regulated fruit quality improvement. Furthermore, we found that ABA treatment could significantly increase GA_3 contents compared with the control group in the DAA 40, DAA 45, and DAA 75 stages (**Figure 4D**), which was consistent with previous studies indicating that ABA treatment could significantly increase GA contents in early sweet cherry development (Gutiérrez et al., 2021). SA concentration did not change significantly throughout the maturity and it was higher in grapevine at the early ripening stage (**Figure 4E**), the variation tendencies of GA_3 and SA were the same, first went up, then went down, and finally went up. The above results were related to previous studies, revealing endogenous ABA and SA co-regulated ABA signal transduction (Wang et al., 2015). Otherwise, both JA and MeJA concentrations under ABA treatment were higher than in the control group, but the change trends were showed distinctly opposite (**Figures 4F,G**), which was consistent with previous study confirming JA and MeJA were antagonistic in watermelon ripening (Kojima et al., 2021). The variation trends of JA and ABA in strawberry during ripening had been reported (Lee et al., 2020), while the change of MeJA under ABA treatment was not clear. Based on our results, we deduced that JA and MeJA came into play at different developmental stages of grapevine, and exogenous ABA positively regulated JA while negatively regulating MeJA.

Cytokinins (CTKs) generally synthesize in plant roots, have positive effects on promoting differentiation and growth of plant tissues, and play notable roles in regulating the development and sex differentiation of plants (Mok, 2019). In our study, KT concentration was higher under ABA treatment than in the control group at the DAA 75 stage, the variation trends were increasing all the time (**Figure 4H**). Under ABA treatment, ZT and ZR concentrations were significantly higher than the control group in the first four sampling stages (**Figures 4I,J**), while iP contents were significantly higher and ipR contents were conspicuously lower than in the control group in the last two sampling stages (**Figures 4K,L**). It had been reported that exogenous ABA could up-regulate the contents of ZT and ZR in the early ripening stage of sweet cherry (Gutiérrez et al., 2021), while other CTKs were not discussed. Therefore, we deduced that ZT and ipR regulated by exogenous ABA would accumulate at the veraison stage while ip, ZR, and KT regulated by exogenous ABA might accumulate at the maturity stage.

Exogenous IAA and ABA co-regulated the improvement of strawberry berry enlargement (Chen et al., 2016), these two phytohormones were closely related to the improvement of antioxidant activity in blueberry, while the improvement of fruit flavor was influenced by the increase of ABA and SA contents (Aires et al., 2017). In our study, we discovered that under exogenous ABA treatment and with grapevine ripening, berry enlargement was accompanied by the increase of endogenous IAA and KT contents, and the accumulation of ABA, SA, and ip was accordant with the enrichment of antioxidant substances at the late stage of fruit ripening. Thus, we legitimately inferred that exogenous ABA could affect the biosynthesis of endogenous phytohormones, fruit exterior quality improvement was regulated by endogenous IAA and KT, and stress resistance improvement was mediated by endogenous ABA, SA, and CTKs during grapevine developmental and ripening stages.

Exogenous Abscisic Acid Regulated Sugars Accumulation via Mediating Endogenous Hormones Biosynthesis

There were three main types of sugars in grapevine, including fructose, glucose, and sucrose (Liu et al., 2007). Due to

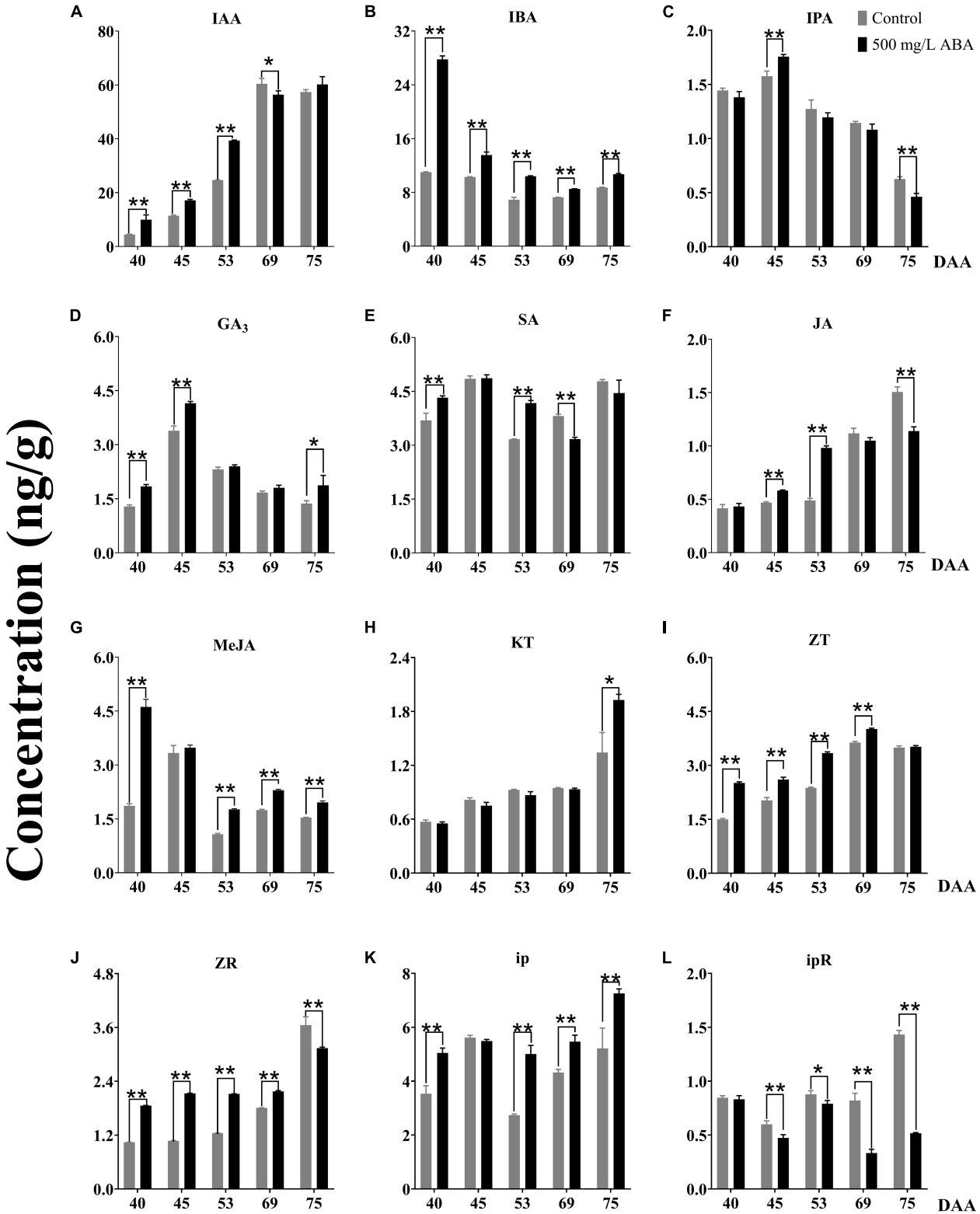

FIGURE 4 | Effect of exogenous ABA treatment on the variation tendency of different phytohormones contents in two treatment groups (control group and 500 mg/L ABA group) at five sampling stages. DAA 40, November 25th; DAA 45, November 30th; DAA 53, December 8th; DAA 69, December 24th; DAA 75, December 30th. **(A)** IAA concentrations. **(B)** IBA concentrations. **(C)** IPA concentrations. **(D)** GA_3 concentrations. **(E)** SA concentrations. **(F)** JA concentrations. **(G)** MeJA concentrations. **(H)** KT concentrations. **(I)** ZT concentrations. **(J)** ZR concentrations. **(K)** ip concentrations. **(L)** ipR concentrations. Data from 500 mg/L ABA treatment were shown as a black column while data from control group were shown as gray column. *Showed the comparatively significant differences with *T*-test ($p < 0.1$, $n = 3$) and **Showed the highly significant differences with *T*-test ($p < 0.05$, $n = 3$).

the low concentration sucrose has in the grape berry, only fructose and glucose in grape juice were quantified by HPLC in this research. As results show in **Figures 5A–D**, soluble sugar, reducing sugar, glucose, and fructose levels displayed the same variation tendency, they all kept rising in all 5 sampling stages, and ABA treatment significantly increased their levels in the DAA 40, DAA 53, DAA 69, and DAA 75 stages, which was accordant with previous study indicating that the maturity stage was a key period of sugar enrichment (Shen et al., 2017).

Crosstalk in the sugar and ABA signaling pathway had also been well studied, affirming that *VvSK1* and *VvHT1* could responded to ABA signal and regulated hexose transport and transmission (Lecourieux et al., 2010), grape hexokinase was involved in ABA regulation of sucrose synthase expression, indicating there existed crosstalk between ABA, hexose, and sucrose (Wang et al., 2017). Previous study also reported that FaSigE (a positive regulator of glucose catabolism) interacted with FaABAR (ABA signaling receptor) and actively regulated strawberry ripening (Zhang et al., 2017). In this study, the effects of exogenous ABA on glucose biosynthesis and catabolism were discussed at the transcriptional level (**Figure 5E**), revealing that under ABA treatment at DAA 69 and DAA 75 stages, the expression levels of genes involved in fructose catabolism including *VvALS* (*VIT_16s0022g01030*), *VvTK* (*VIT_17s0000g08560*), *VvPK*

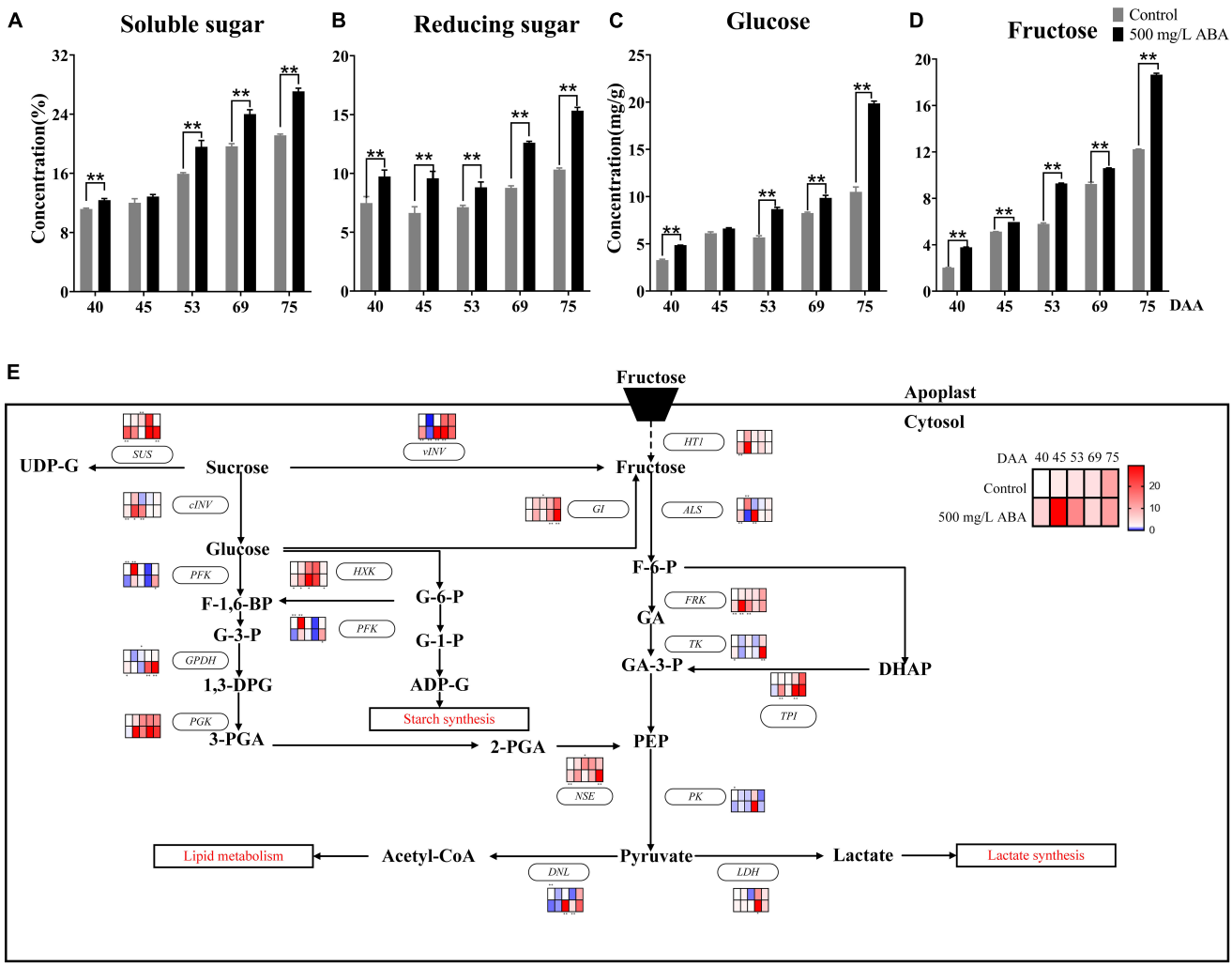

FIGURE 5 | Effect of exogenous ABA treatment on the variation tendency of different sugars contents as well as expression levels of sugars biosynthetic and catabolic genes in two treatment groups (control group and 500 mg/L ABA group) at five sampling stages. DAA 40, November 25th; DAA 45, November 30th; DAA 53, December 8th; DAA 69, December 24th; DAA 75, December 30th. **(A)** Soluble sugar levels. **(B)** Reducing sugar levels. **(C)** glucose levels. **(D)** fructose levels. Data from 500 mg/L ABA treatment were shown as black column while data from control group were shown as gray column. **(E)** Expression of genes involved in sugars biosynthesis and catabolic pathways. The relative expression changes in two treatment groups at other stages were relative to the control group (DAA 40) were represented as log2 fold change. The relative expression levels of key genes (*HT1*, *ALS*, *FRK*, *TK*, *PK*, *GI*, *vVIN*, *SUS*, *cINV*, *PGK*, *TPI*, *GPDH*, *NSE*, *DNL*, *LDH*, *PFK*, *HXK*) were shown as heatmap. *Showed the comparatively significant differences with *T*-test ($p < 0.1$, $n = 3$) and **Showed the highly significant differences with *T*-test ($p < 0.05$, $n = 3$).

(*VIT_08s0007g04170*), and *VvFRK* (*VIT_01s0011g00240*) were up-regulated, while genes participating in glucose catabolism including *VvPFK* (*VIT_14s0108g00540*), *VvGPDH* (*VIT_14s0219g00280*), *VvPGK* (*VIT_19s0085g00380*), *VvHXK* (*VIT_18s0001g14230*) were expressed higher than in the control group. Otherwise, compared with the control group, in the DAA 69 and 75 stages, *VvGI* (*VIT_18s0001g07280*) contributing to the conversion of glucose to fructose were expressed at significant higher level, while the expression of *VvHT1* (*VIT_00s0515g00050*) referred to be responsible for transporting hexose from apoplast to cytosol was increased in four sampling stages except for DAA 53 stage. Thus, it could be deduced that fructose was accumulated due to the continuous conversion of glucose and sucrose in the developmental stages of grapevine. Furthermore, we found that the expression of genes contributing to the conversion of sucrose to glucose and fructose including *VvvINV*, *VvcINV* (*VIT_06s0061g01520*) were all up-regulated under ABA treatment in all sampling stages. The above results attested that grape ripening was accompanied by a marked accumulation of sugars, and their biosynthesis and catabolism would respond to exogenous ABA signal.

It has been reported that IAA and SA might mediate sugar accumulation in tomato, which demonstrated there existed interaction between IAA, SA, and sugars (Malik and Lal, 2018). In this study, due to total sugar content in grape berry continuously increasing, SA content was higher in the early ripening period, while IAA and ABA content was higher in the late ripening period, thus we speculated that the sugar accumulation in the early stage of grape ripening was mainly regulated by endogenous SA, while the sugar accumulation in the late stage of grape ripening was mainly regulated by endogenous ABA and IAA, and the changes of these endogenous phytohormones were induced by exogenous ABA.

Exogenous Abscisic Acid Enriched Fatty Acids in Berry via Regulating Endogenous Hormones Biosynthesis

Lipids are important nutrients in plants and animals, which have crosstalk with the biosynthesis of many metabolites and play an important role in plant stress resistance and flavor formation (Liu et al., 2019). Although lipids play an important role in regulating quality improvement, the understanding of the effect of exogenous ABA on these substances in grape fruits and the variation trend of fatty acids ratio during fruit ripening is much lacking. To thoroughly make inquiry into different types of Fas proportion in both ABA treatment group and the control group, a total of nine Fas including butryic acid (C_4:0), undecanoic acid (C_{11}:0), tridecanoic acid (C_{13}:0), pentadecanoic acid (C_{15}:0), palmitic acid (C_{16}:0), stearic acid (C_{18}:0), linolelaidic acid (C_{18}:2n6t), *cis*-11,14,17-eicosatrienoic acid (C_{20}:3n3), and erucic acid (C_{22}:1n9) were measured in all five sampling stages. As shown in the **Figures 6Aa–i**, the variation tendency of butyric acid in two groups was same: first up, then down, and then up again, only at the DAA 40 and 75 stages was exogenous ABA significantly promoted in its production. Undecanoic acid proportion was relatively small, and none of the last four sampling stages were detected, leading to speculation that their contribution to fruit quality improvement was small. Moreover, palmitic acid was the main FAs in grapevine, which occupied the largest proportion in all five sampling stages, exogenous ABA treatment could significantly contribute to the increase of its proportion. And the proportion of tridecanoic acid was higher under ABA treatment than in the control group only in the DAA 40 stage, while in other stages had contrary results. Interestingly, the variation tendencies of pentadecanoic acid, stearic acid, and linolelaidic acid were consistent: first up, and then down, which indicated that they might accumulate in the early fruit ripening. Exogenous ABA could significantly promote pentadecanoic acid proportions in the last three sampling stages, while the stearic acid proportions under ABA treatment were significantly smaller than the control group in four stages except for the DAA 69 stage. Linolelaidic acid proportions accounting for the whole FAs under ABA treatment were larger than the control group in the DAA 40 and 53 stages, and other stage results showed inversely. Otherwise, *cis*-11,14,17-eicosatrienoic acid and erucic acid showed consistent variation tendencies: first down, and then up, indicating that they might accumulate in the late fruit ripening. We found that exogenous ABA treatment significantly inhibited *cis*-11,14,17-eicosatrienoic acid biosynthesis in the first three sampling stages while inhibiting erucic acid biosynthesis in all sampling stages. In summary, undecanoic acid, palmitic acid, stearic acid, and erucic acid occupied a large proportion in the early fruit ripening, while butyric acid, tridecanoic acid, pentadecanoic acid, linolelaidic acid, and *cis*-11,14,17-Eicosatrienoic acid would accumulate in the late fruit ripening, exogenous ABA had great effect on their proportion changes (With the exception of palmitic acid and pentadecanoic acid, most of the other effects are inhibitory). Due to the fact that FAs content in jujube fruits changed constantly during ripening and palmitic acid had the most obvious effect on the fruit flavor improvement (Fu et al., 2021). Thus, we concluded that exogenous ABA promoted the improvement of grape fruit flavor and nutritional value via promoting palmitic acid enrichment and regulating other FAs proportions.

Fas, as a key intermediate in the ABA, anthocyanins, sugars biosynthesis, and catabolism pathways, the change of its content will also affect the biosynthesis of several nutrients (Lafuente et al., 2021). It is necessary to explore the differential genes that exogenous ABA regulates FAs metabolism at the molecular level. As results in **Figure 6B** exhibited, in the last three sampling stages, the expression levels of *VvFAT* (*VIT_05s0094g00930*), *VvIAH1* (*VIT_10s0003g00960*), *VvFAS1* (*VIT_01s0011g06640*), *VvELO1* (*VIT_04s0023g01140*), *VvOLE1* (*VIT_14s0066g00700*), *VvADH1* (*VIT_18s0001g15410*), *VvARO10* (*VIT_03s0038g02120*), *VvPDC1* (*VIT_13s0067g00340*), *VvATF1* (*VIT_16s0039g00570*), and *VvEEB1* (*VIT_11s0016g01930*) were up-regulated under ABA treatment compared with the control group, these genes were responsible for FAs and other aromatic substances biosynthesis. At the DAA 40 stage, the expression levels of *VvACX2* (*VIT_00s0662g00010*), *VvPCK1* (*VIT_07s0205g00070*), and *VvMFP2* (*VIT_05s0077g02140*) were significantly

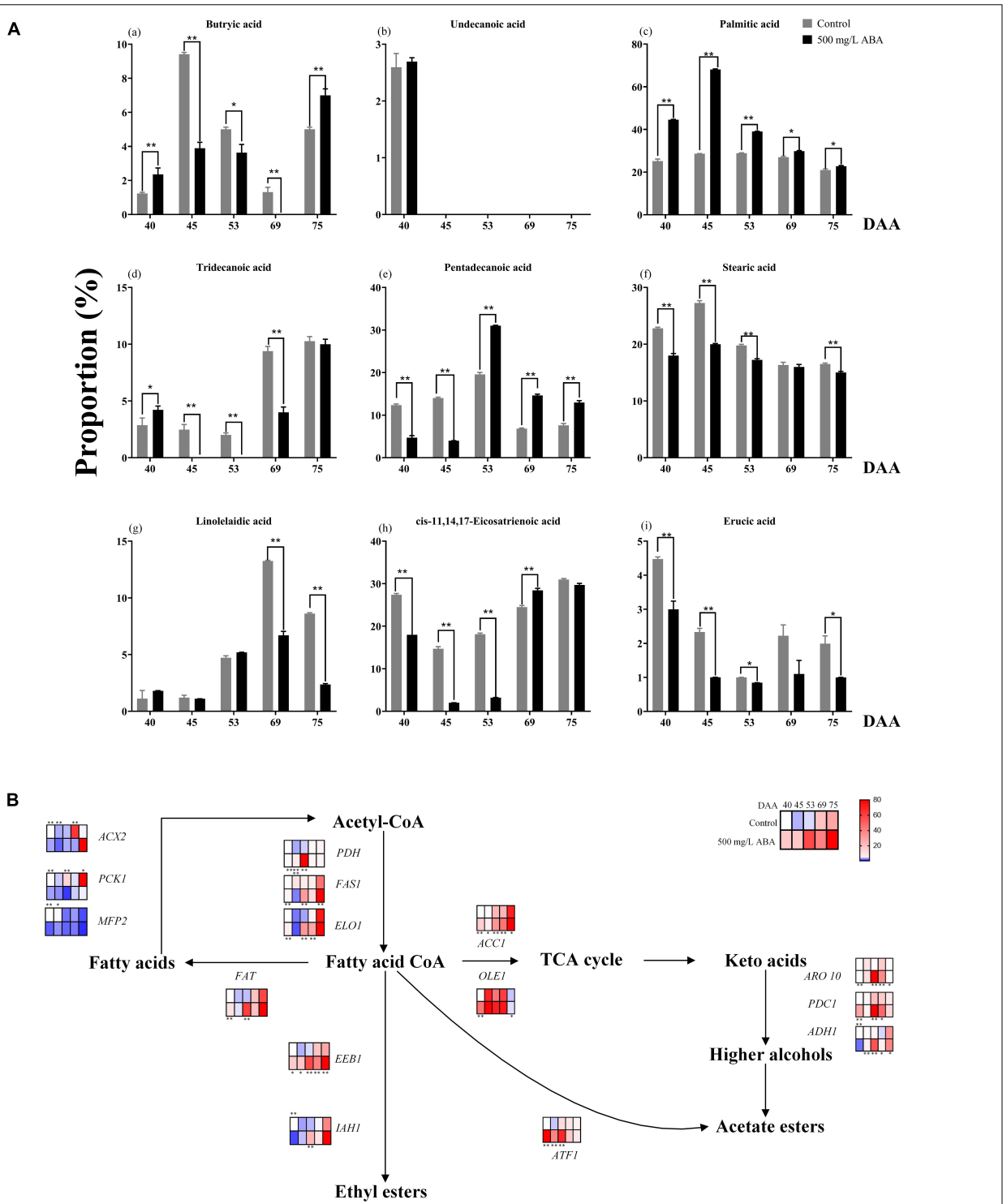

FIGURE 6 | Changes in the proportion of fatty acids as well as expression levels of fatty acids biosynthetic and catabolic genes in two treatment groups (control group and 500 mg/L ABA group) at five sampling stages. DAA 40, November 25th; DAA 45, November 30th; DAA 53, December 8th; DAA 69, December 24th; DAA 75, December 30th. **(A)** The proportions of fatty acids in grapevine at different sampling time. **(a)** Butryic acid. **(b)** Undecanoic acid. **(c)** Palmitic acid. **(d)** Tridecanoic acid. **(e)** Pentadecanoic acid. **(f)** Stearic acid. **(g)** Linolelaidic acid. **(h)** *cis*-11,14,17-Eicosatrienoic acid. **(i)** Erucic acid. **(B)** Expression of genes involved in fatty acids biosynthesis and catabolic pathways. The relative expression changes in two treatment groups at other stages were relative to the control group (DAA 40) were represented as log2 fold change. Key genes (*ACC1, PDH, FAS1, FAT, ELO1, IAH1, OLE1, ADH1, ARO10, PDC1, ACX2, PCK1, MFP2, ATF1, EEB1*) expression levels were shown as heat map. *Showed the comparatively significant differences with *T*-test ($p < 0.1$, $n = 3$) and **Showed the highly significant differences with *T*-test ($p < 0.05$, $n = 3$).

down-regulated in the ABA treatment group, these genes contributed to the catabolism of FAs. The above results indicated that exogenous ABA could have contributed to FAs accumulation and flavor improvement. Interestingly, under exogenous ABA treatment, the expression of *VvACC1* (*VIT_12s0059g01380*) was significantly increased in all sampling stages compared with the control group, indicating that plenty of fatty acid CoA entered the TCA cycle to participate in the formation of other important aromatic substances, and this process was regulated by exogenous ABA. Thus, we deduced that FAs accumulation would respond to exogenous ABA signal, however, the specific molecular mechanism of how it regulates the biosynthesis of quality-related metabolites in response to ABA signal remains to be further explored.

Plant hormones interaction plays an important role in the ripeness and lipids enrichment in fleshy fruits, GA and ABA interplayed in the regulation of fruit ripening in avocados (Vincent et al., 2020), and MYB41, MYB107, and MYC2 promoted ABA-mediated primary fatty alcohol accumulation in kiwi fruit by activating AchnFAR (Wei et al., 2020). In this study, GA_3 content was higher in the early stage of fruit ripening while ABA content was higher in the late ripening stage, accompanied by the continuous changes in the proportion of FAs and the accumulation of FAs. Consequently, it could be deduced that exogenous ABA mediated the accumulation of endogenous ABA and GA_3 at different developmental stages, thereby contributing to the enrichment of FAs.

Correlation Analysis of Different Endogenous Phytohormones and Quality-Related Parameters

IAA, GA, and CTK are the main regulators of fruit ripening (Chen et al., 2016). Berry enlargement and fruit ripening

FIGURE 7 | Correlation analysis of different phytohormones with appearance parameters, nutrients and flavor-related metabolites. The vertical row represented 13 phytohormones and the horizontal row represented 3 kinds of appearance parameters, 8 kinds of nutrients and 14 kinds of flavor-related metabolites. The size of the bubbles indicated the strength of the relational degree, with orange representing a positive correlation and green representing a negative correlation.

depends on IAA, CTKs, and GA, pericarp coloration of climactic and non-climactic fruits is controlled via ETH-dependent or ETH-independent manner (Kumar et al., 2013). Since the correlation between the changes of endogenous phytohormones regulated by exogenous ABA and the improvement of grape fruit quality has not been discussed, it is of great significance to explore the relationship between different endogenous phytohormones variation and berry enlargement, pericarp coloration, sugars accumulation, flavor formation, as well as stress resistance enhancement. To further validate our hypothesis, correlation analysis was carried out on the changes of 13 kinds of endogenous hormones and 25 kinds of quality-metabolites (**Figure 7**). The results revealed that under exogenous ABA treatment, the changes of ABA and KT were relatively associated with fruit appearance and quality improvement, the change of IAA was tightly correlated with sugars, anthocyanins, linolelaidic acid, and *cis*-11,14,17-eicosatrienoic acid accumulation. Meanwhile, we also found that the change of ip was closely related to berry enlargement, sugars accumulation, and antioxidant activity improvement. Meanwhile, the change of GA_3 had the greatest effect on the enrichment of FAs, including butyric acid, tridecanoic acid, palmitic acid, stearic acid, and *cis*-11,14,17-eicostrienoic acid. Therefore, we concluded that the endogenous biosynthesis of ABA, IAA, and CTKs regulated by exogenous ABA was most closely related to fruit quality improvement and stress resistance enhancement during grape fruit development and ripening.

CONCLUSION

To sum up, this research certified that exogenous ABA treatment had crucial effects on berry size, endogenous hormone contents variation, sugars formation, anthocyanins accumulation, and FAs enrichment. The correlation analysis of diverse phytohormones and quality-related parameters confirmed that ABA/KT was correlated with berry size, ABA/IAA/KT was correlated with sugar accumulation, ABA/IPA/ZR was correlated with anthocyanin accumulation, and GA3/MeJA was correlated with FAs enrichment. Thus, we deduced that endogenous hormones with different physiological functions could respond to exogenous ABA signal, although these phytohormones had different contributions to the improvement of fruit quality, they ultimately regulated the overall improvement of grape fruit quality. Therefore, spraying 500 mg/L ABA during the grapevine veraison stage was indeed an effective means to improve grape fruit quality, which is likely to have a broad prospect in future cultivation. However, further research on exploring the specific molecular mechanism of exogenous ABA regulating fruit quality improvement via inducing endogenous phytohormone biosynthesis should be carried out.

DATA AVAILABILITY STATEMENT

The original contributions presented in the study are included in the article/**Supplementary Material**, further inquiries can be directed to the corresponding author/s.

AUTHOR CONTRIBUTIONS

JL carried out all the experiments, data analyzations, manuscript writing, and figures drawing. BL provided the experimental methods and ideas, collected, grinded samples as well as reviewed the manuscript. DL collected the samples. JH and YZ provided experimental materials, CM, WX, SJ, CZ, and SW reviewed the manuscript. XL and LW designed the experiments, reviewed the manuscript, and supervised this study. All authors contributed to the article and approved the submitted version.

FUNDING

This work was supported by the project of developing agriculture by science and technology in Shanghai (2019-02-08-00-08-F01118), China Agriculture Research System of MOF and MARA.

ACKNOWLEDGMENTS

We sincerely thank the reviewers and editors for their careful reading and selfless help. Meanwhile, we also show gratitude to the people who helped with the successful establishment of this experiment.

SUPPLEMENTARY MATERIAL

The Supplementary Material for this article can be found online at: https://www.frontiersin.org/articles/10.3389/fpls.2021.739964/full#supplementary-material

Supplementary Figure 1 | Effect of exogenous ABA treatment on the expression levels of anthocyanin biosynthetic and catabolic genes in two treatment groups (control group and 500 mg/L ABA group) at 5 sampling stages. DAA 40, November 25th; DAA 45, November 30th; DAA 53, December 8th; DAA 69, December 24th; DAA 75, December 30th. **(A)** Expression of genes involved in anthocyanin biosynthesis pathway. The relative expression levels of key genes (*PAL*, *4CL*, *CHI*, *CHS*, *F3H*, *F3'5'H*, *FLS*, *DFR*, *LDOX*, *3GT*, *5GT*, *ANR*, *LAR*) were represented as heatmap. **(B)** Heatmap of key transcription factors (MYB5a, MYB5b, MYCa, MYB14) in anthocyanin biosynthesis pathway. The relative expression changes in two treatment groups at other stages were relative to the control group (DAA 40) were represented as log2 fold change. *Showed the comparatively significant differences with *T*-test ($p < 0.1$, $n = 3$) and **Showed the highly significant differences with *T*-test ($p < 0.05$, $n = 3$).

Supplementary Figure 2 | Effect of exogenous ABA treatment on stress-related parameters and antioxidant enzyme activity in two treatment groups (control group and 500 mg/L ABA group) at 5 sampling stages. DAA 40, November 25th; DAA 45, November 30th; DAA 53, December 8th; DAA 69, December 24th; DAA 75, December 30th. **(A)** MDA concentrations. **(B)** Pro concentrations. **(C)** POD activity. **(D)** CAT activity. **(E)** SOD activity. **(F)** GSH concentrations. **(G)** APX activity. **(H)** DPPH free radical scavenging rate. Data from 500 mg/L ABA treatment were shown as black column while data from control group were shown as gray column. *Showed the comparatively significant differences with *T*-test ($p < 0.1$, $n = 3$) and **Showed the highly significant differences with *T*-test ($p < 0$ .05, $n = 3$).

Supplementary Table 1 | Primers for qRT-PCR quantification. All primers were designed by Primer Premier 5.0.

Supplementary Table 2 | Detection and quantification limits of target compounds by HPLC.

REFERENCES

Aires, A., Carvalho, R., Matos, M., Carnide, V., Silva, A. P., and Gonçalves, B. (2017). Variation of chemical constituents, antioxidant activity, and endogenous plant hormones throughout different ripening stages of highbush blueberry (*Vaccinium corymbosum* L.) cultivars produced in centre of Portugal. *J. Food Biochem.* 41:e12414. doi: 10.1111/jfbc.12414

Alferez, F., de Carvalho, D. U., and Boakye, D. (2021). Interplay between abscisic acid and gibberellins, as related to ethylene and sugars, in regulating maturation of non-climacteric fruit. *Int. J. Mol. Sci.* 22:669. doi: 10.3390/ijms22020669

An, J. P., Zhang, X. W., You, C. X., Bi, S. Q., Wang, X. F., and Hao, Y. J. (2019). Md WRKY 40 promotes wounding-induced anthocyanin biosynthesis in association with Md MYB 1 and undergoes Md BT 2-mediated degradation. *New Phytol.* 224, 380–395. doi: 10.1111/nph.16008

Berli, F. J., Fanzone, M., Piccoli, P., and Bottini, R. (2011). Solar UV-B and ABA are involved in phenol metabolism of *Vitis vinifera* L. increasing biosynthesis of berry skin polyphenols. *J. Agric. Food Chem.* 59, 4874–4884. doi: 10.1021/jf200040z

Bermejo, A., Granero, B., Mesejo, C., Reig, C., Tejedo, V., Agustí, M., et al. (2018). Auxin and gibberellin interact in citrus fruit set. *J. Plant Growth Regul.* 37, 491–501. doi: 10.1007/s00344-017-9748-9

Bonilla, F., Mayen, M., Merida, J., and Medina, M. (1999). Extraction of phenolic compounds from red grape marc for use as food lipid antioxidants. *Food Chem.* 66, 209–215. doi: 10.1016/S0308-8146(99)00046-1

Cai, T., Xu, H., Peng, D., Yin, Y., Yang, W., Ni, Y., et al. (2014). Exogenous hormonal application improves grain yield of wheat by optimizing tiller productivity. *Field Crops Res.* 155, 172–183. doi: 10.1016/j.fcr.2013.09.008

Carrari, F., Fernie, A. R., and Iusem, N. D. (2004). Heard it through the grapevine? ABA and sugar cross-talk: the ASR story. *Trends Plant Sci.* 9, 57–59. doi: 10.1016/j.tplants.2003.12.004

Chen, J., Mao, L., Lu, W., Ying, T., and Luo, Z. (2016). Transcriptome profiling of postharvest strawberry fruit in response to exogenous auxin and abscisic acid. *Planta* 243, 183–197.

Crizel, R., Perin, E., Siebeneichler, T., Borowski, J., Messias, R., Rombaldi, C., et al. (2020). Abscisic acid and stress induced by salt: effect on the phenylpropanoid, L-ascorbic acid and abscisic acid metabolism of strawberry fruits. *Plant Physiol. Biochem.* 152, 211–220. doi: 10.1016/j.plaphy.2020.05.003

Cruz, A. B., Bianchetti, R. E., Alves, F. R. R., Purgatto, E., Peres, L. E. P., Rossi, M., et al. (2018). Light, ethylene and auxin signaling interaction regulates carotenoid biosynthesis during tomato fruit ripening. *Front. Plant Sci.* 9:1370. doi: 10.3389/fpls.2018.01370

De Orduna, R. M. (2010). Climate change associated effects on grape and wine quality and production. *Food Res. Int.* 43, 1844–1855. doi: 10.1016/j.foodres.2010.05.001

Decros, G., Baldet, P., Beauvoit, B., Stevens, R., Flandin, A., Colombié, S., et al. (2019). Get the balance right: ROS homeostasis and redox signalling in fruit. *Front. Plant Sci.* 10:1091. doi: 10.3389/fpls.2019.01091

Deis, L., Cavagnaro, B., Bottini, R., Wuilloud, R., and Silva, M. F. (2011). Water deficit and exogenous ABA significantly affect grape and wine phenolic composition under in field and in-vitro conditions. *Plant Growth Regul.* 65, 11–21. doi: 10.1007/s10725-011-9570-5

El-Mashharawi, H. Q., Abu-Naser, S. S., Alshawwa, I. A., and Elkahlout, M. (2020). Grape type classification using deep learning. *Int. J. Acad. Eng. Res. (IJAER)* 3:12.

Fenn, M. A., and Giovannoni, J. J. (2021). Phytohormones in fruit development and maturation. *Plant J.* 105, 446–458. doi: 10.1111/tpj.15112

Ferrara, G., Mazzeo, A., Matarrese, A. M. S., Pacucci, C., Pacifico, A., and Gambacorta, G. (2013). Application of abscisic acid (S-ABA) to 'crimson seedless' grape berries in a mediterranean climate: effects on color, chemical characteristics, catabolic profile, and S-ABA concentration. *J. Plant Growth Regul.* 32, 491–505. doi: 10.1007/s00344-012-9316-2

Fu, L., Yang, J., Shang, H., and Song, J. (2021). Changes of characteristic sugar, fatty acid, organic acid and amino acid in jujubes at different dry mature stages. *J. Food Compos. Anal.* 104:104104. doi: 10.1016/j.jfca.2021.104104

Giribaldi, M., Gény, L., Delrot, S., and Schubert, A. (2010). Proteomic analysis of the effects of ABA treatments on ripening *Vitis vinifera* berries. *J. Exp. Bot.* 61, 2447–2458. doi: 10.1093/jxb/erq079

Gorinstein, S., Zemser, M., Haruenkit, R., Chuthakorn, R., Grauer, F., Martin-Belloso, O., et al. (1999). Comparative content of total polyphenols and dietary fiber in tropical fruits and persimmon. *J. Nutr. Biochem.* 10, 367–371. doi: 10.1016/S0955-2863(99)00017-0

Gutiérrez, C., Figueroa, C. R., Turner, A., Munné-Bosch, S., Muñoz, P., Schreiber, L., et al. (2021). Abscisic acid applied to sweet cherry at fruit set increases amounts of cell wall and cuticular wax components at the ripe stage. *Sci. Hortic.* 283:110097. doi: 10.1016/j.scienta.2021.110097

Hasan, M., and Bae, H. (2017). An overview of stress-induced resveratrol synthesis in grapes: perspectives for resveratrol-enriched grape products. *Molecules* 22:294. doi: 10.3390/molecules22020294

Huan, C., Jiang, L., An, X., Yu, M., Xu, Y., Ma, R., et al. (2016). Potential role of reactive oxygen species and antioxidant genes in the regulation of peach fruit development and ripening. *Plant Physiol. Biochem.* 104, 294–303. doi: 10.1016/j.plaphy.2016.05.013

Huang, T., Yu, D., and Wang, X. (2021). VvWRKY22 transcription factor interacts with VvSnRK1. 1/VvSnRK1. 2 and regulates sugar accumulation in grape. *Biochem. Biophys. Res. Commun.* 554, 193–198. doi: 10.1016/j.bbrc.2021.03.092

Ju, Y., Liu, M., Zhao, H., Meng, J., and Fang, Y. (2016). Effect of exogenous abscisic acid and methyl jasmonate on anthocyanin composition, fatty acids, and volatile compounds of Cabernet Sauvignon (*Vitis vinifera* L.) grape berries. *Molecules* 21:1354. doi: 10.3390/molecules21101354

Kojima, K., Andou, D., and Ito, M. (2021). Plant hormone changes in growing small watermelon fruit. *Hortic. J.* 90, 202–208. doi: 10.2503/hortj.UTD-209

Kojima, M., Kamada-Nobusada, T., Komatsu, H., Takei, K., Kuroha, T., Mizutani, M., et al. (2009). Highly sensitive and high-throughput analysis of plant hormones using MS-probe modification and liquid chromatography–tandem mass spectrometry: an application for hormone profiling in Oryza sativa. *Plant Cell Physiol.* 50, 1201–1214. doi: 10.1093/pcp/pcp057

Kou, X., Yang, S., Chai, L., Wu, C., Zhou, J., Liu, Y., et al. (2021a). Abscisic acid and fruit ripening: multifaceted analysis of the effect of abscisic acid on fleshy fruit ripening. *Sci. Hortic.* 281:109999. doi: 10.1016/j.scienta.2021.109999

Kou, X., Zhou, J., Wu, C. E., Yang, S., Liu, Y., Chai, L., et al. (2021b). The interplay between ABA/ethylene and NAC TFs in tomato fruit ripening: a review. *Plant Mol. Biol.* 106, 223–238. doi: 10.1007/s11103-021-01128-w

Kumar, R., Khurana, A., and Sharma, A. K. (2013). Role of plant hormones and their interplay in development and ripening of fleshy fruits. *J. Exp. Bot.* 65, 4561–4575. doi: 10.1093/jxb/eru277

Lado, J., Gambetta, G., and Zacarias, L. (2018). Key determinants of citrus fruit quality: metabolites and main changes during maturation. *Sci. Hortic.* 233, 238–248. doi: 10.1016/j.scienta.2018.01.055

Lafuente, M. T., Ballester, A. R., Holland, N., Cerveró, J., and Romero, P. (2021). Interrelation between ABA and phospholipases D, C and A2 in early responses of citrus fruit to *Penicillium digitatum* infection. *Postharvest Biol. Technol.* 175:111475. doi: 10.1016/j.postharvbio.2021.111475

Lecourieux, F., Lecourieux, D., Vignault, C., and Delrot, S. (2010). A sugar-inducible protein kinase, VvSK1, regulates hexose transport and sugar accumulation in grapevine cells. *Plant Physiol.* 152, 1096–1106. doi: 10.1104/pp.109.149138

Lee, G. B., Lee, J. E., Lee, J. H., Lee, Y. J., Park, Y. H., Choi, Y. W., et al. (2020). Phytohormone profiles of 'Seolhyang'and 'Maehyang'strawberry fruits during ripening. *Hortic. Environ. Biotechnol.* 61, 229–239. doi: 10.1007/s13580-019-00213-w

Leng, F., Cao, J., Wang, S., Jiang, L., Li, X., and Sun, C. (2018). Transcriptomic analyses of root restriction effects on phytohormone content and signal transduction during grape berry development and ripening. *Int. J. Mol. Sci.* 19:2300. doi: 10.3390/ijms19082300

Leng, F., Tang, D., Lin, Q., Cao, J., Wu, D., Wang, S., et al. (2017). Transcriptomic analyses of ascorbic acid and carotenoid metabolites influenced by root restriction during grape berry development and ripening. *J. Agric. Food Chem.* 65, 2008–2016. doi: 10.1021/acs.jafc.6b05322

Li, D., Li, L., Luo, Z., Mou, W., Mao, L., and Ying, T. (2015). Comparative transcriptome analysis reveals the influence of abscisic acid on the metabolism of pigments, ascorbic acid and folic acid during strawberry fruit ripening. *PLoS One* 10:e0130037. doi: 10.1371/journal.pone.0130037

Li, G., Zhao, J., Qin, B., Yin, Y., An, W., Mu, Z., et al. (2019). ABA mediates development-dependent anthocyanin biosynthesis and fruit coloration in *Lycium* plants. *BMC Plant Biol.* 19:317. doi: 10.1186/s12870-019-1931-7

Li, S., Chen, K., and Grierson, D. (2021). Molecular and hormonal mechanisms regulating fleshy fruit ripening. *Cells* 10:1136. doi: 10.3390/cells10051136

Li, S., Zhao, L., Blakeslee, J., and Dami, I. (2017). "Exogenous abscisic acid increases freezing tolerance and induces sugar accumulation in grapevines," in *Proceedings of the 2017 ASHS Annual Conference*, Alexandria, VA: ASHS.

Li, X., Li, M., Ji, N., Jin, P., Zhang, J., Zheng, Y., et al. (2019). Cold plasma treatment induces phenolic accumulation and enhances antioxidant activity in fresh-cut pitaya (*Hylocereus undatus*) fruit. *LWT* 115:108447. doi: 10.1016/j.lwt.2019.108447

Liang, B., Zheng, Y., Wang, J., Zhang, W., Fu, Y., Kai, W., et al. (2020). Overexpression of the persimmon abscisic acid β-glucosidase gene (DkBG1) alters fruit ripening in transgenic tomato. *Plant J.* 102, 1220–1233. doi: 10.1111/tpj.14695

Lindo-García, V., Muñoz, P., Larrigaudière, C., Munné-Bosch, S., and Giné-Bordonaba, J. (2020). Interplay between hormones and assimilates during pear development and ripening and its relationship with the fruit postharvest behaviour. *Plant Sci.* 291:110339. doi: 10.1016/j.plantsci.2019.110339

Liu, H. F., Wu, B. H., Fan, P. G., Xu, H. Y., and Li, S. H. (2007). Inheritance of sugars and acids in berries of grape (*Vitis vinifera* L.). *Euphytica* 153, 99–107. doi: 10.1007/s10681-006-9246-9

Liu, N. (2019). Effects of IAA and ABA on the immature peach fruit development process. *Hortic. Plant J.* 5, 145–154. doi: 10.1016/j.hpj.2019.01.005

Liu, Q., Tang, G., Zhao, C., Feng, X., Xu, X., and Cao, S. (2018). Comparison of antioxidant activities of different grape varieties. *Molecules* 23:2432. doi: 10.3390/molecules23102432

Liu, X., Ma, D., Zhang, Z., Wang, S., Du, S., Deng, X., et al. (2019). Plant lipid remodeling in response to abiotic stresses. *Environ. Exp. Bot.* 165, 174–184. doi: 10.1016/j.envexpbot.2019.06.005

Malik, Z. A., and Lal, E. P. (2018). Effect of salicylic acid and indole acetic acid on growth, yield, lycopene and soluble sugar content of tomato (*Lycopersicum esculentum*) varieties under cadmium and salinity stressed environment. *Ann. Plant Soil Res.* 20, 396–400.

Mohamed, A. K. A., El-Salhy, A. M., Mostafa, R. A. A., El-Mahdy, M. T., and Hussein, A. S. (2019). Effect of exogenous abscisic acid (ABA), gibberellic acid (GA3) and cluster thinning on yield of some grape cultivars. *J. Plant Prod.* 10, 101–105. doi: 10.21608/jpp.2019.36239

Mok, M. C. (2019). "Cytokinins and plant development—an overview," in *Cytokinin: Chemistry, Activity and Function*, eds D. W. S. Mok and M. C. Mokeds (Boca Raton, FL: CRC Press), 155–166.

Nahakpam, S., and Shah, K. (2011). Expression of key antioxidant enzymes under combined effect of heat and cadmium toxicity in growing rice seedlings. *Plant Growth Regul.* 63, 23–35. doi: 10.1007/s10725-010-9508-3

Nowicka, P., Wojdyło, A., and Laskowski, P. (2019). Principal component analysis (PCA) of physicochemical compounds' content in different cultivars of peach fruits, including qualification and quantification of sugars and organic acids by HPLC. *Eur. Food Res. Technol.* 245, 929–938. doi: 10.1007/s00217-019-03233-z

Pal, S. L. (2019). Role of plant growth regulators in floriculture: an overview. *J. Pharmacogn. Phytochem.* 8, 789–796.

Porter, L. J., Hrstich, L. N., and Chan, B. G. (1985). The conversion of procyanidins and prodelphinidins to cyanidin and delphinidin. *Phytochemistry* 25, 223–230. doi: 10.1016/S0031-9422(00)94533-3

Poudel, P. R., Azuma, A., Kobayashi, S., Koyama, K., and Goto-Yamamoto, N. (2021). VvMYBAs induce expression of a series of anthocyanin biosynthetic pathway genes in red grapes (*Vitis vinifera* L.). *Sci. Hortic.* 283:110121. doi: 10.1016/j.scienta.2021.110121

Price, M. L., Van Scoyoc, S., and Butler, L. G. (1978). A critical evaluation of the vanillin reaction as an assay for tannin in sorghum grain. *J. Agric. Food Chem.* 26, 1214–1218. doi: 10.1021/jf60219a031

Rabelo, M. C., Bang, W. Y., Nair, V., Alves, R. E., Jacobo-Velázquez, D. A., Sreedharan, S., et al. (2020). UVC light modulates vitamin C and phenolic biosynthesis in acerola fruit: role of increased mitochondria activity and ROS production. *Sci. Rep.* 10, 1–14. doi: 10.1038/s41598-020-78948-1

Raza, M. A. S., Saleem, M. F., Shah, G. M., Khan, I. H., and Raza, A. (2014). Exogenous application of glycinebetaine and potassium for improving water relations and grain yield of wheat under drought. *J. Soil Sci. Plant Nutr.* 14, 348–364. doi: 10.4067/S0718-95162014005000028

Reisch, B. I., Owens, C. L., and Cousins, P. S. (2012). "Grape," in *Fruit Breeding*, eds M. L. Badenes and D. H. Byrne (New York, NY: Springer), 225–262. doi: 10.1007/978-1-4419-0763-9_7

Sánchez-Moreno, C., Plaza, L., de Ancos, B., and Cano, M. P. (2003). Quantitative bioactive compounds assessment and their relative contribution to the antioxidant capacity of commercial orange juices. *J. Sci. Food Agric.* 83, 430–439. doi: 10.1002/jsfa.1392

Santiago, J., Dupeux, F., Betz, K., Antoni, R., Gonzalez-Guzman, M., Rodriguez, L., et al. (2012). Structural insights into PYR/PYL/RCAR ABA receptors and PP2Cs. *Plant Sci.* 182, 3–11. doi: 10.1016/j.plantsci.2010.11.014

Seo, M., and Koshiba, T. (2002). Complex regulation of ABA biosynthesis in plants. *Trends Plant Sci.* 7, 41–48. doi: 10.1016/S1360-1385(01)02187-2

Shahab, M., Roberto, S. R., Ahmed, S., Colombo, R. C., Silvestre, J. P., Koyama, R., et al. (2019). Anthocyanin accumulation and color development of 'Benitaka'table grape subjected to exogenous abscisic acid application at different timings of ripening. *Agronomy* 9:164. doi: 10.3390/agronomy9040164

Shen, C., Wang, J., Jin, X., Liu, N., Fan, X., Dong, C., et al. (2017). Potassium enhances the sugar assimilation in leaves and fruit by regulating the expression of key genes involved in sugar metabolism of Asian pears. *Plant Growth Regul.* 83, 287–300. doi: 10.1007/s10725-017-0294-z

Shen, X., Zhao, K., Liu, L., Zhang, K., Yuan, H., Liao, X., et al. (2014). A role for PacMYBA in ABA-regulated anthocyanin biosynthesis in red-colored sweet cherry cv. Hong Deng (*Prunus avium* L.). *Plant Cell Physiol.* 55, 862–880. doi: 10.1093/pcp/pcu013

Shiraishi, M., Shinomiya, R., and Chijiwa, H. (2018). Variet al differences in polyphenol contents, antioxidant activities and their correlations in table grape cultivars bred in Japan. *Sci. Hortic.* 227, 272–277. doi: 10.1016/j.scienta.2017.09.032

Singleton, V. L., and Rossi, J. A. (1965). Colorimetry of total phenolics with phosphomolybdic-phosphotungstic acid reagents. *Am. J. Enol. Vitic.* 16, 144–158.

Song, J., Bi, J., Chen, Q., Wu, X., Lyu, Y., and Meng, X. (2019). Assessment of sugar content, fatty acids, free amino acids, and volatile profiles in jujube fruits at different ripening stages. *Food Chem.* 270, 344–352. doi: 10.1016/j.foodchem.2018.07.102

Tao, X., Wu, Q., Aalim, H., Li, L., Mao, L., Luo, Z., et al. (2020). Effects of exogenous abscisic acid on bioactive components and antioxidant capacity of postharvest tomato during ripening. *Molecules* 25:1346. doi: 10.3390/molecules25061346

Töpfer, R., Hausmann, L., and Eibach, R. (2011). "Molecular breeding," in *Genetics, Genomics And Breeding of Grapes*, eds A.-F. Adam-Blondon, J. M. Martínez-Zapater, and C. Kole (Boca Raton, FL: CRC Press), 160–185. doi: 10.1201/b10948

Torres, C. A., Sepúlveda, G., and Kahlaoui, B. (2017). Phytohormone interaction modulating fruit responses to photooxidative and heat stress on apple (*Malus domestica* Borkh.). *Front. Plant Sci.* 8:2129. doi: 10.3389/fpls.2017.02129

Villalobos-González, L., Peña-Neira, A., Ibáñez, F., and Pastenes, C. (2016). Long-term effects of abscisic acid (ABA) on the grape berry phenylpropanoid pathway: gene expression and metabolite content. *Plant Physiol. Biochem.* 105, 213–223. doi: 10.1016/j.plaphy.2016.04.012

Vincent, C., Mesa, T., and Munné-Bosch, S. (2020). Hormonal interplay in the regulation of fruit ripening and cold acclimation in avocados. *J. Plant Physiol.* 251:153225. doi: 10.1016/j.jplph.2020.153225

Wang, P., Lu, S., Zhang, X., Hyden, B., Qin, L., Liu, L., et al. (2021). Double NCED isozymes control ABA biosynthesis for ripening and senescent regulation in peach fruits. *Plant Sci.* 304:110739. doi: 10.1016/j.plantsci.2020.110739

Wang, X. Q., Zheng, L. L., Lin, H., Yu, F., Sun, L. H., and Li, L. M. (2017). Grape hexokinases are involved in the expression regulation of sucrose synthase-and cell wall invertase-encoding genes by glucose and ABA. *Plant Mol. Biol.* 94, 61–78.

Wang, X., Yang, B., Ren, C., Wang, H., Wang, J., and Dai, C. (2015). Involvement of abscisic acid and salicylic acid in signal cascade regulating bacterial endophyte-induced volatile oil biosynthesis in plantlets of *Atractylodes lancea*. *Physiol. Plant.* 153, 30–42. doi: 10.1111/ppl.12236

Wang, Y., Ma, F., Li, M., Liang, D., and Zou, J. (2011). Physiological responses of kiwifruit plants to exogenous ABA under drought conditions. *Plant Growth Regul.* 64, 63–74. doi: 10.1007/s10725-010-9537-y

Wei, X., Mao, L., Wei, X., Xia, M., and Xu, C. (2020). MYB41, MYB107, and MYC2 promote ABA-mediated primary fatty alcohol accumulation via activation of AchnFAR in wound suberization in kiwifruit. *Hortic. Res.* 7, 1–10. doi: 10.1038/s41438-020-0309-1

Wei, Y., Xu, F., and Shao, X. (2017). Changes in soluble sugar metabolism in loquat fruit during different cold storage. *J. Food Sci. Technol.* 54, 1043–1051. doi: 10.1007/s13197-017-2536-5

Xu, H., Zhang, G., Yan, A., and Sun, L. (2014). "Table grape breeding at the Beijing institute of forestry and pomology," in *Proceedings of the XI International Conference on Grapevine Breeding and Genetics*, Vol. 1082, Beijing, 43–46. doi: 10.17660/ActaHortic.2015.1082.3

Zhang, S., Hou, B., Chai, L., Yang, A., Yu, X., and Shen, Y. (2017). Sigma factor FaSigE positively regulates strawberry fruit ripening by ABA. *Plant Growth Regul.* 83, 417–427. doi: 10.1007/s10725-017-0308-x

Conflict of Interest: The authors declare that the research was conducted in the absence of any commercial or financial relationships that could be construed as a potential conflict of interest.

Publisher's Note: All claims expressed in this article are solely those of the authors and do not necessarily represent those of their affiliated organizations, or those of the publisher, the editors and the reviewers. Any product that may be evaluated in this article, or claim that may be made by its manufacturer, is not guaranteed or endorsed by the publisher.

frontiers in Plant Science

ORIGINAL RESEARCH
published: 06 October 2021
doi: 10.3389/fpls.2021.743993

Regulation of Tocopherol Biosynthesis During Fruit Maturation of Different *Citrus* Species

*Florencia Rey, Lorenzo Zacarias and María Jesús Rodrigo**

Departamento de Biotecnología de Alimentos, Instituto de Agroquímica y Tecnología de Alimentos, Consejo Superior de Investigaciones Científicas, Valencia, Spain

Tocopherols are plant-derived isoprenoids with vitamin E activity, which are involved in diverse physiological processes in plants. Although their biosynthesis has been extensively investigated in model plants, their synthesis in important fruit crops as *Citrus* has scarcely been studied. Therefore, the aim of this work was to initiate a physiological and molecular characterization of tocopherol synthesis and accumulation in *Citrus* fruits during maturation. For that purpose, we selected fruit of the four main commercial species: grapefruit (*Citrus paradisi*), lemon (*Citrus limon*), sweet orange (*Citrus sinensis*), and mandarin (*Citrus clementina*), and analyzed tocopherol content and the expression profile of 14 genes involved in tocopherol synthesis during fruit maturation in both the flavedo and pulp. The selected genes covered the pathways supplying the tocopherol precursors homogentisate (HGA) (*TAT1* and *HPPD*) and phytyl pyrophosphate (PPP) (*VTE5*, *VTE6*, *DXS1* and *2*, *GGPPS1* and *6*, and *GGDR*) and the tocopherol-core pathway (*VTE2*, *VTE3a*, *VTE3b*, *VTE1*, and *VTE4*). Tocopherols accumulated mainly as α- and γ-tocopherol, and α-tocopherol was the predominant form in both tissues. Moreover, differences were detected between tissues, among maturation stages and genotypes. Contents were higher in the flavedo than in the pulp during maturation, and while they increased in the flavedo they decreased or were maintained in the pulp. Among genotypes, mature fruit of lemon accumulated the highest tocopherol content in both the flavedo and the pulp, whereas mandarin fruit accumulated the lowest concentrations, and grapefruit and orange had intermediate levels. Higher concentrations in the flavedo were associated with a higher expression of all the genes evaluated, and different genes are suitable candidates to explain the temporal changes in each tissue: (1) in the flavedo, the increase in tocopherols was concomitant with the up-regulation of *TAT1* and *VTE4*, involved in the supply of HGA and the shift of γ- into α-tocopherol, respectively; and (2) in the pulp, changes paralleled the expression of *VTE6*, *DXS2*, and *GGDR*, which regulate PPP availability. Also, certain genes (i.e., *VTE6*, *DXS2*, and *GGDR*) were co-regulated and shared a similar pattern during maturation in both tissues, suggesting they are developmentally modulated.

Keywords: tocopherol, vitamin E, *Citrus*, fruit, ripening, tocopherol gene expression

OPEN ACCESS

Edited by:
Itay Maoz,
Agricultural Research Organization (ARO), Israel

Reviewed by:
Laura Perez Fons,
Royal Holloway, University of London, United Kingdom
Renata Szymańska,
AGH University of Science and Technology, Poland

***Correspondence:**
María Jesús Rodrigo
mjrodrigo@iata.csic.es

Specialty section:
This article was submitted to Plant Metabolism and Chemodiversity, a section of the journal Frontiers in Plant Science

Received: *19 July 2021*
Accepted: *17 September 2021*
Published: *06 October 2021*

Citation:
Rey F, Zacarias L and Rodrigo MJ (2021) Regulation of Tocopherol Biosynthesis During Fruit Maturation of Different Citrus Species. Front. Plant Sci. 12:743993. doi: 10.3389/fpls.2021.743993

INTRODUCTION

Tocopherols are lipid-soluble isoprenoids of the tocochromanol family which are mainly synthesized in photosynthetic organisms (Fritsche et al., 2017; Mène-Saffrané, 2017). Their chemical structure consists of a polar chromanol ring, originated from homogentisate (HGA), and a lipophilic isoprenoid side chain derived from a specific prenyl pyrophosphate donor. While HGA is the common precursor for all tocochromanols, the polyprenyl precursor varies according to the type of tocochromanol and is phytyl pyrophosphate (PPP) for tocopherol synthesis (Mène-Saffrané, 2017). Additionally, according to the position and degree of methylation of the chromanol ring, four natural subforms can exist: δ- (one methyl group), β- and γ- (two methyl groups), and α-tocopherol (three methyl groups). Tocopherols are of great importance because, together with tocotrienols, they are the only natural compounds exhibiting vitamin E activity in animal cells and are essential as dietary nutrients (Traber and Sies, 1996). In plants, tocopherols play diverse physiological functions, of which their role as antioxidants, either scavenging peroxyl radicals or quenching reactive oxygen species, is probable the most notable (Havaux et al., 2005; Mène-Saffrané et al., 2010). Nonetheless, other functions have been recently described for tocopherols in plants, including their involvement in photoassimilate transport, carbohydrate metabolism, cellular signaling and plant's response to biotic and abiotic stresses (Falk and Munné-Bosch, 2010; Muñoz and Munné-Bosch, 2019; Ma et al., 2020b).

The tocopherol biosynthesis pathway (**Figure 1**) has been well-characterized in the last decades, with all the vitamin E biosynthetic genes (VTE genes) encoding the enzymes catalyzing the core steps of tocopherol synthesis identified (Fritsche et al., 2017; Mène-Saffrané, 2017; Muñoz and Munné-Bosch, 2019). Tocopherol synthesis is initiated by the condensation of HGA with PPP, a reaction regulated by homogentisate phytyl transferase (HPT; *VTE2*) that results in the formation of 2-methyl-6-phytyl-1,4-benzoquinol (MPBQ) (Collakova and DellaPenna, 2001). After this step, the pathway can split into two branches depending on the subsequent reaction of MPBQ, leading toward the synthesis of δ- and β-tocopherol or γ- and α-tocopherol. Then, MPBQ can either be directly cyclized into δ-tocopherol, by the tocopherol cyclase (TC; *VTE1*), or it can be first methylated into 2,3-dimethyl-6-phytyl-1,4-benzoquinol (DMPBQ), by a MPBQ methyltransferase (MPBQ-MT; *VTE3*). The resulting product DMPBQ is then converted into γ-tocopherol by the same TC (*VTE1*) mentioned before. The final step of tocopherol synthesis is the methylation of δ- and γ-tocopherol into β- and α-tocopherol, respectively, which is catalyzed by the γ-tocopherol methyltransferase (γ-TMT; *VTE4*). These steps represent the tocopherol-core pathway, and of these enzymes only HPT (*VTE2*) is considered exclusive to tocopherol synthesis, while MPBQ-MT (*VTE3*), TC (*VTE1*), and γ-TMT (*VTE4*) are also involved in the synthesis of the other tocochromanols (Fritsche et al., 2017; Mène-Saffrané, 2017). *VTE2* has been reported to be a limiting step in tocopherol synthesis in seeds and leaves of Arabidopsis and other model plants (Savidge et al., 2002; Collakova and DellaPenna, 2003a). However, it does not seem to limit tocopherol synthesis in fruit of species such as tomato, olive, and mandarin (Quadrana et al., 2013; Georgiadou et al., 2019; Rey et al., 2021a), where *VTE3* appears to play a more important role regulating tocopherol content (Quadrana et al., 2013; Rey et al., 2021a).

Tocopherol content in plant cells is also highly dependent on the availability of the precursors HGA and PPP (Mène-Saffrané, 2017; Pellaud and Mène-Saffrané, 2017). In plants, the precursor HGA originates in a two-step reaction from the degradation of the amino acid L-tyrosine (L-Tyr) synthetized in the shikimate (SK) pathway. L-Tyr is converted into 4-hydroxyphenylpyruvate (HPP) by a tyrosine aminotransferase (TATs), and then transformed into HGA by a HPP dioxygenase (HPPD) (**Figure 1**). The loss of function of either *TAT* or *HPPD* in Arabidopsis has resulted in a reduction of tocopherol levels (Norris et al., 1998; Riewe et al., 2012), while the overexpression of these genes only modestly increased total tocopherols in leaves and seeds (Tsegaye et al., 2002; Karunanandaa et al., 2005). In fleshy fruit, such as tomato and mango, the role of *HPPD* in tocopherol accumulation has been reinforced, as higher accumulation of *HPPD* transcripts has been associated with genotypes containing high tocopherols levels (Quadrana et al., 2013; Singh et al., 2017). Recently, it has been shown that engineering the chorismate–tyrosine pathway in tomato fruit to produce HPP in combination with the overexpression of Arabidopsis *HPPD* resulted in a moderate increment in tocopherols (Burgos et al., 2021). The other precursor necessary for tocopherol synthesis, PPP, can be derived from geranylgeranyl pyrophosphate (GGPP), produced in the MEP pathway, or alternatively from the recycling of phytol formed in the degradation of chlorophylls (**Figure 1**). Two enzymes are involved in the supply of PPP *via* the recycling of phytol: phytol kinase (*VTE5*) and phytyl phosphate kinase (*VTE6*) (Valentin et al., 2006; vom Dorp et al., 2015). VTE5 appears to be a key enzyme regulating tocopherol content in fruits of tomato and olive, controlling the supply of PPP toward the tocopherol-core pathway (Georgiadou et al., 2015; Almeida et al., 2016). Nonetheless, in ripe tomato and mandarin fruits, tocopherol accumulation appears to be more influenced by the up-regulation of genes of the MEP pathway, such as *DXS* and *GGDR* (Quadrana et al., 2013; Almeida et al., 2015; Gramegna et al., 2019; Rey et al., 2021a). While the gene *DXS* regulates the influx into the MEP pathway, *GGDR* controls the final reduction of GGPP into PPP, and therefore its final availability for condensation with HGA (Estévez et al., 2001; Pellaud and Mène-Saffrané, 2017).

Tocopherol accumulation has been mainly studied in leaves and seeds, but they have also been detected in fruits, stems, roots, flowers, and other plant tissues (Horvath et al., 2006a). In general, α-tocopherol is the main form found in leaves, while γ-tocopherol is the predominant in seeds of most species (Horvath et al., 2006a). In fruits, α-tocopherol seems to be the main isoform accumulated (Chun et al., 2006; Horvath et al., 2006a), with variable contents depending on the species and through fruit ripening (Osuna-García et al., 1998; Almeida et al., 2011; Quadrana et al., 2013; Georgiadou et al., 2015, 2019). In recent years, great advances have been made into the regulation of tocopherol biosynthesis in fruit of different

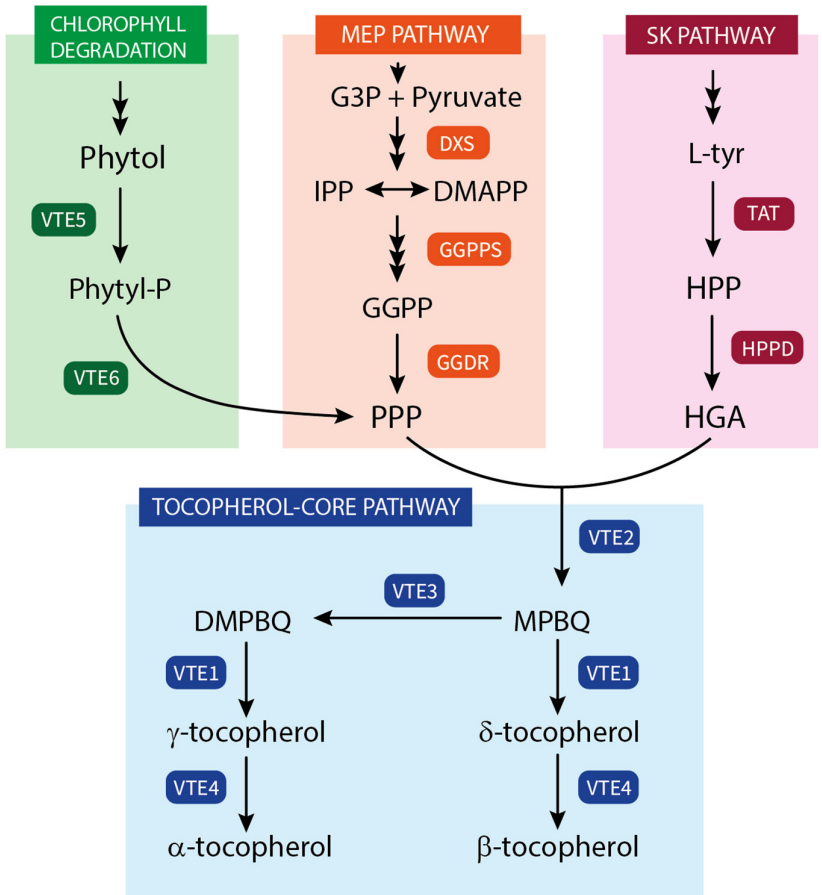

FIGURE 1 | Schematic representation of tocopherol biosynthetic pathway in plants. Phytyl-P, phytyl phosphate; G3P, glyceraldehyde 3-phosphate; IPP, isopentenyl diphosphate; DMAPP, dimethylallyl diphosphate; GGPP, geranylgeranyl diphosphate; PPP, phytyl pyrophosphate; L-Tyr, amino acid L-tyrosine; HPP, 4-hydroxyphenylpyruvate; HGA, homogentisate; MPBQ, 2-methyl-6-phytyl-1,4-benzoquinol; DMPBQ, 2,3-dimethyl-6-phytyl-1,4-benzoquinol; VTE5, phytol kinase; VTE6, phytyl-P kinase; DXS, 1-deoxy-D-xylulose-5-phosphate synthase; GGPPS, GGPP synthase; GGDR, GGPP reductase; TAT, tyrosine aminotransferase; HPPD, HPP dioxygenase; VTE2, homogentisate phytyltransferase (HPT); VTE3, MPBQ methyltransferase (MPBQ-MT); VTE1, tocopherol cyclase (TC); VTE4, tocopherol methyltransferase (γ-TMT).

species, such as tomato (Almeida et al., 2011, 2016; Quadrana et al., 2013; Gramegna et al., 2019; Burgos et al., 2021), pepper (Arango and Heise, 1998; Koch et al., 2002), olive (Georgiadou et al., 2015, 2016, 2019), and mango (Singh et al., 2017). These studies concluded that tocopherol accumulation in fruit is mainly transcriptionally regulated, and that tocopherol biosynthetic genes are modulated in a temporal manner, and also influenced by environmental factors (Almeida et al., 2011, 2020; Quadrana et al., 2013; Georgiadou et al., 2016, 2019; Singh et al., 2017; Gramegna et al., 2019).

Citrus is one of the world's most important fruit crops, being highly demanded for fresh consumption and juice processing (Spreen et al., 2020). This genus is characterized for its genotypic and phenotypic diversity (Wu et al., 2018), with a vast range of fruits with a different composition of nutrients and bioactive compounds (Rodrigo and Zacarías, 2006; Cano et al., 2008; Ma et al., 2020a). Current information about tocopherol contents in *Citrus* fruit is very limited. Tocopherols accumulate in the flavedo (external colored part of the peel) of mandarin, orange, lemon, grapefruit, and other less known species in the range of 65–130 $\mu g\ g^{-1}$, and mainly in the forms of α- and γ-tocopherol, with composition varying according to the specie (Assefa et al., 2017; Rey et al., 2021a,b). In the pulp, tocopherols have also been detected in fruit of mandarin, grapefruit, and orange in the form of α-tocopherol and at concentrations lower than in the flavedo (1.6–25 $\mu g\ g^{-1}$) (Chun et al., 2006; Cardeñosa et al., 2015). Recently, genes involved in the tocopherol-core pathway as well as genes regulating the supply of the precursors HGA and PPP have been identified in the *Citrus* genome. Analysis of their transcriptional profiling in the flavedo of mandarins and grapefruits in response to cold stress suggested candidate genes and mechanisms regulating tocopherol accumulation in each specie (Rey et al., 2021a,b). However, the temporal changes of tocopherols and the regulation of their synthesis during maturation of *Citrus* fruit have not been explored yet. Therefore, the aim of the present work was to perform a comparative study of tocopherol accumulation during on-tree fruit maturation in different *Citrus* genotypes belonging to the

main horticultural *Citrus* groups: orange, mandarin, lemon, and grapefruit. The relationship between tocopherol accumulation and the expression of tocopherol-biosynthetic genes in the flavedo and pulp of fruit from the selected species and ripening stages was also investigated.

MATERIALS AND METHODS

Plant Material

Fruit of four different genotypes belonging to the main horticultural groups of *Citrus* species: grapefruit (*Citrus paradisi* Macfad.) cv. 'Marsh', lemon [*Citrus limon* (L.) Burm. F] cv. 'Fino', sweet orange [*Citrus sinensis* (L.) Osbeck] cv. 'Washington Navel', and mandarin (*Citrus clementina* Hort. ex Tanaka) cv. 'Clemenules', were selected for this study. Trees were located in the Citrus Germplasm Bank at the Instituto Valenciano de Investigaciones Agrarias (IVIA) located in Moncada (Valencia, Spain; 39°35′22″N, 0°23′40″W; 55 m elevation above the sea level), and cultivated under standard agronomical conditions. Fruits were harvested from adult trees (more than 10 years old) grafted on Carrizo citrange rootstock [*C. sinensis* (L.) Osb. × *Poncirus trifoliata* (L.) Raf.], growing in a loamy-sand soil with drip irrigation. Fertilization, pruning, pest management, and other cultural conditions were performed according to the protocol established by IVIA for the Citrus Germplasm Bank. Fruits were harvested at four maturation stages: immature green (IG), mature green (MG), breaker (Br), and mature fruit (M), and the specific harvest dates for each genotype are detailed in **Supplementary Table 1**. For each genotype and sampling date three biological replicates of 10–15 fruits, collected randomly from the outside of the tree canopy of 2–3 trees, were used. Fruits were delivered to the laboratory and selected for color uniformity and free of any peel defect or damage, and the flavedo (external colored layer of fruit peel) and pulp (juice vesicles) were excised with a scalpel, frozen in liquid nitrogen and ground to a fine powder using an electric grinder with liquid nitrogen. Samples were stored at −80°C until analysis.

Tocopherol Extraction and Quantification

Tocopherol extraction of the flavedo and pulp, and quantification by HPLC coupled to fluorescence detector, was carried out following the procedure described in Rey et al. (2021a). In summary, flavedo and pulp material (200 and 500 mg, respectively) were extracted with methanol, Tris buffer (50 mM Tris pH 7.5) with 1 M NaCl, and dichloromethane in a mortar and pestle with sea sand as an abrasive. After vortex-mixing, samples were sonicated for 5 min and centrifuged for 10 min at 3000 × *g* and 4°C. The dichloromethane phase was recovered in a glass tube, and the methanol phase was re-extracted with dichloromethane. The pooled dichloromethane extracts were then dried under nitrogen gas and stored at −20°C until HPLC analysis. For quantification, dried extracts were re-suspended in ethyl acetate (500–700 μl) and a dilution (1:15 for flavedo extracts and 1:2 for pulps) was carried out. For analysis, 20 μl of the diluted extract were injected in a Waters HPLC system (Acquity® Arc™, Waters) coupled with a fluorescence detector (2475 FLR Detector, Waters). Tocopherol separation was done using a C30 column, 150 mm × 4.6 mm, 3 μm (YMC, Teknokroma, Spain), and a ternary gradient elution with methanol, water, and methyl *tert*-butyl ether at 1 ml min^{-1} flow (Rey et al., 2021a). Elution of tocopherols was monitored by fluorescence at an excitation wavelength of 296 nm and emission wavelength of 340 nm. Identification and quantification of the different tocopherols was achieved by comparison with the retention times and calibration curves for tocopherol standards (Sigma-Aldrich). All procedures were carried out on ice and under dim light to prevent photo-degradation. Total tocopherol content was calculated as the sum of the tocopherol isoforms, and concentrations are expressed as μg g of fresh weight (FW). Results are the mean of two biological replicates (mean ± SD).

RNA Extraction and cDNA Synthesis

Extraction of total RNA was different according to the fruit tissue. Total RNA was isolated from flavedo tissue using the RNeasy Plant Mini Kit (Qiagen), while the extraction from the pulp was done using the protocol described in Rodrigo et al. (2004). Once total RNA was isolated, DNA traces were removed by treating RNA with DNase I (DNA free, DNase treatment and removal, and Ambion) following the manufacturer's instructions. RNA concentration was later quantified by spectrophotometric analysis (NanoDrop, Thermo Fisher Scientific) and RNA quality was verified by agarose-gel electrophoresis with GoodView® Nucleic Acid Stain (SBS Genetech). For cDNA synthesis, 5 μg of total RNA were reverse-transcribed using the SuperScript III Reverse Transcriptase (Invitrogen) in a final volume of 20 μl, following the manufacturer's procedure.

Gene Expression Analysis by Quantitative Real-Time PCR

Gene expression was evaluated by quantitative real-time PCR in a LightCycler 480 instrument (Roche), using the LightCycler 480 SYBRGreen I Master kit (Roche) and following the manufacturer's instructions. Previously published oligonucleotides primers were used for the amplification of the following *C. sinensis* genes related to tocopherol synthesis: *DXS1*, *DXS2*, *GGPPS1*, *GGPPS6*, *GGDR*, *VTE5*, *VTE6*, *TAT1*, *HPPD*, *VTE2*, *VTE3a*, *VTE3b*, *VTE1*, and *VTE4* (Rey et al., 2021a). The primers sequences used for RT-qPCR analyses is listed in **Supplementary Table 2**. For all the genes analyzed, RT-qPCR conditions consisted of an initial pre-incubation at 95°C for 10 min, followed by 40 cycles of 10 s at 95°C for denaturation, 10 s at 59°C for annealing, and 10 s at 72°C for extension. For each amplification reaction 1 ml of 10 times diluted first-strand cDNA, containing approximately 100 ng of cDNA, was used. Specificity of the PCR reaction in the different *Citrus* species was assessed by the melting point analysis (Tm) after the amplification steps. For expression measurements, we used the LightCycler 480 Software release 1.5.0, version 1.5.0.39 (Roche) and calculated relative expression levels using the Relative Expression Software Tool (REST) (Pfaffl et al., 2002) with an external reference sample. The reference sample consisted of flavedo pool of a mix of cDNA from immature to mature fruit

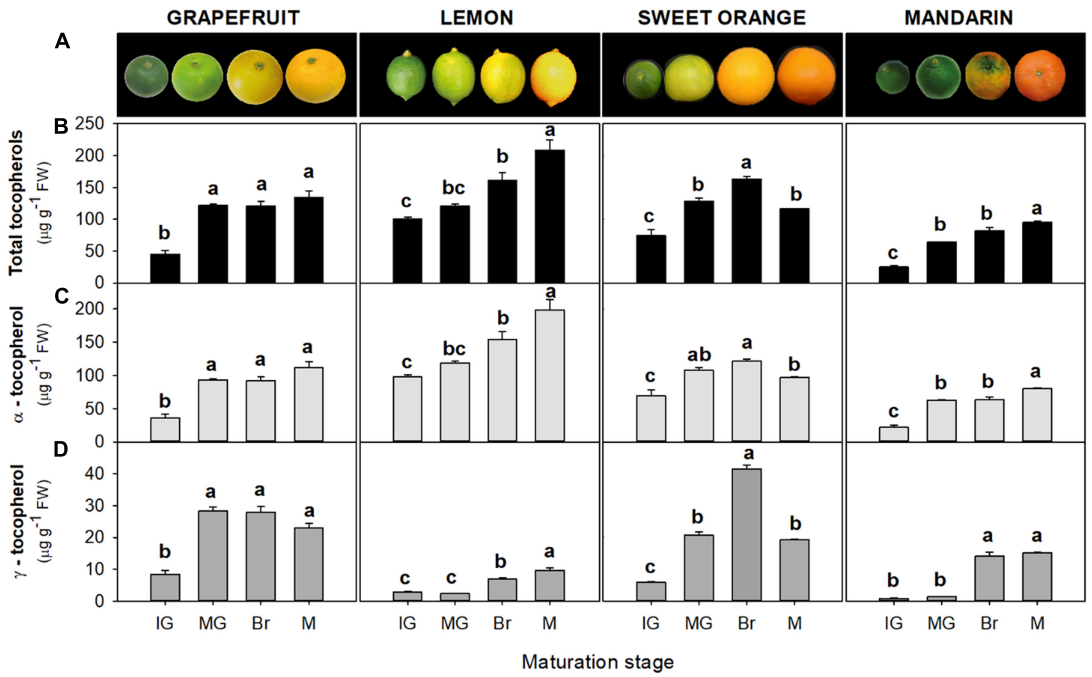

FIGURE 2 | Fruit external appearance **(A)** and total tocopherol **(B)**, α-tocopherol **(C)**, and γ-tocopherol content **(D)** in the flavedo during fruit maturation of grapefruit (*C. paradisi*), lemon (*C. limon*), sweet orange (*C. sinensis*), and mandarin (*C. clementine*). Contents are expressed as μg g^{-1} of fresh weight. The data are mean ± SE of at least two replicates (**Supplementary Table 9**). Maturation stages correspond to immature green (IG), mature green (MG), breaker (Br), and mature (M). Different letters indicate significant mean differences among maturation stages for each fruit specie (Tukey's test, $p \leq 0.05$).

of different *Citrus* species and cultivars, including those used in this work. The expression value obtained for each gene in the reference sample was set to 1, and it was used for the calculation of relative gene expression in all the flavedo and pulp samples analyzed in this work. Normalization was performed using *ACTIN* as a housekeeping gene (Alós et al., 2014; Zacarías-García et al., 2021). Results are the mean of three biological replicates (mean ± SE).

Correlation Matrix and Networks

To gain insight into possible common candidate genes regulating tocopherol accumulation in *Citrus* fruit, a correlation matrix and network was built independently for the flavedo and pulp, based on procedures described by Diretto et al. (2010). First, a Pearson's correlation analysis was carried out for each fruit tissue, taking into account all the metabolite (tocopherol contents) and expression data (relative gene expression levels). For each tissue, the input data for the calculation of correlation coefficients was the fold-change (log2 transformed) relative to the IG stage of grapefruit for all the variables, species, and maturation stages. The results were displayed as a matrix, in which each circle represents the correlation between the gene/metabolite in the column heading and the gene/metabolite in the row heading, with their size and color intensity being proportional to the absolute correlation coefficient. Correlation coefficients values are summarized in **Supplementary Tables 7**, **8**, where significant correlations are marked with an asterisk (p-value $\leq$ 0.05). Correlation analysis were carried in RStudio (version 1.3.1093, RStudio Team, PBC, Boston, MA, United States) using the function "*cormat*" and visualized using the function "*corrplot*" of the package "*ggplot2*." Subsequently, each correlation matrix was transformed into a correlation network to highlight the different connections between tocopherol contents and gene expression in the different tissues, and also possible co-regulation among genes. For the construction of the correlation networks only significant correlations were taken into account (p-value $\leq$ 0.05), and the networks were assembled manually using Cytoscape version 3.8.2 (National Institute of General Medical Sciences, Bethesda, MD, United States). The correlation network was displayed in a graph illustrating all-versus-all correlations (only significant) among the variables analyzed and it is composed of nodes, which represented tocopherol contents and gene expression levels, and edge lines which represented the links between those nodes. Positive correlations are represented in red and negative ones in blue, and color intensity is proportional to the absolute correlation coefficient.

Statistical Analyses

Tocopherol contents and relative gene expression data were subjected to a one-way analysis of variance (ANOVA) followed by the multiple comparison Tukey's test (significance level at $p \leq 0.05$), to determine significant mean differences. This analysis was carried to assessed differences among maturation stages for each specie, and additionally the same analysis was done to assess differences among species for a specific maturation stage.

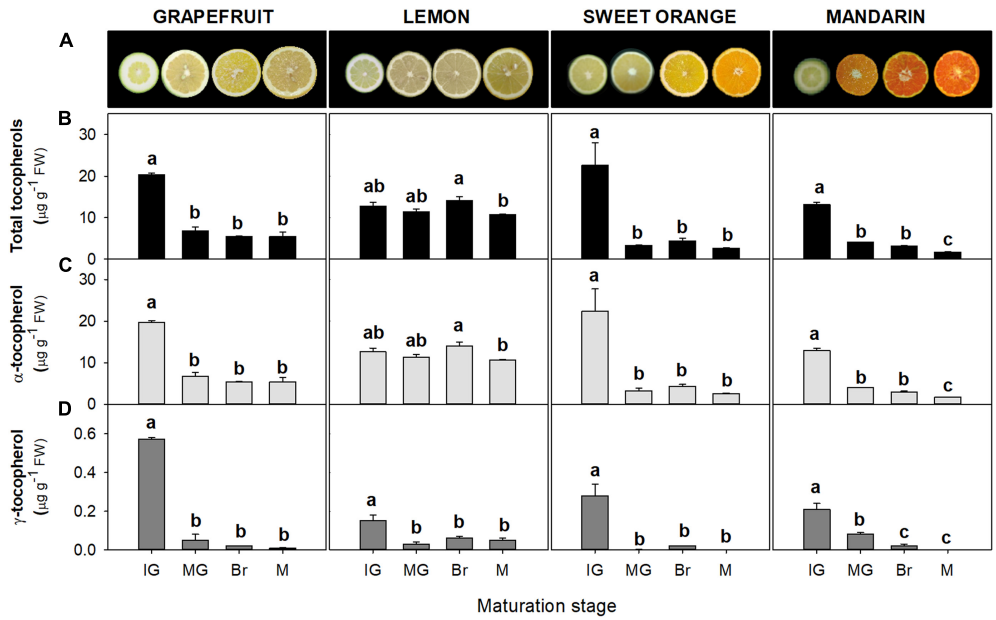

FIGURE 3 | Fruit internal appearance **(A)** and total tocopherol **(B)**, α-tocopherol **(C)**, and γ-tocopherol content **(D)** in the pulp during fruit maturation of grapefruit (*C. paradisi*), lemon (*C. limon*), sweet orange (*C. sinensis*), and mandarin (*C. clementine*). Contents are expressed as μg g^{-1} of fresh weight. The data are mean ± SE of at least two replicates (**Supplementary Table 10**). Maturation stages correspond to immature green (IG), mature green (MG), breaker (Br), and mature (M). Different letters indicate significant mean differences among maturation stages for each fruit specie (Tukey's test, $p \leq 0.05$).

The InfoStat software (version 2018, Grupo InfoStat, Córdoba, Argentina) was used for the statistical analyses.

RESULTS

Changes in Tocopherol Content During Fruit Maturation of Four *Citrus* Species: Grapefruit (*Citrus paradisi*), Lemon (*Citrus limon*), Sweet Orange (*Citrus sinensis*), and Mandarin (*Citrus clementine*) During Ripening

Tocopherols were detected in the flavedo and pulp of the four *Citrus* genotypes selected at the four successive stages of fruit maturation (**Figures 2**, **3**). The isoforms α- and γ-tocopherol were identified in all samples, while the presence of δ-tocopherol was only detected in a few samples at concentrations below 10 and 6 ng g^{-1} FW in the flavedo and pulp, respectively. α-Tocopherol was the predominant form in all species and stages, accounting on average for 85% of total tocopherols in the flavedo and 99% in the pulp. In the flavedo of all species, tocopherol content was higher than in the pulp and contents gradually increased with maturation (**Figure 2**). By contrast, total tocopherols in the pulp decreased sharply after the IG stage and, at the mature (M) stage, the content was between 3 and 8-times lower than in IG, with the exception of lemon where levels remained nearly constant during ripening (**Figure 3**). As a result, differences between tissues became greater during maturation, with contents being 2–7 times higher in the flavedo than in the pulp at the IG stage and more than 20–50 times higher at full maturity (M) (**Figures 2**, **3**).

Differences in tocopherol content in the flavedo and pulp were observed among genotypes (**Figures 2, 3** and **Supplementary Tables 3**, **4**). At the IG stage, total tocopherol contents (as the sum of α- and γ-tocopherol) were significantly higher in the flavedo of lemon (∼101 μg g^{-1} FW), followed by sweet orange (∼75 μg g^{-1} FW), and almost 2- and 4-times lower in the flavedo of grapefruit (∼45 μg g^{-1} FW) and mandarin (∼23 μg g^{-1} FW), respectively (**Figure 2** and **Supplementary Table 3**). During maturation, total tocopherols increased in the four species, but the magnitude of the increase varied among species (**Figure 2**). At the M stage, higher concentrations of tocopherols were detected in the flavedo of lemon (∼208 μg g^{-1} FW) than in grapefruit (∼134 μg g^{-1} FW), sweet orange (∼116 μg g^{-1} FW), and mandarin (∼95 μg g^{-1} FW) (**Supplementary Table 3**). In contrast to the other species, contents in sweet orange increased to a maximum at the breaker (Br) stage (∼160 μg g^{-1} FW) and then decreased toward M fruit (**Figure 2B**). Contents of α-tocopherol reflected the differences among species described for total tocopherol. In IG fruit, α-tocopherol levels ranged from 22 to 98 μg g^{-1} FW and increased to levels between 80 and 199 μg g^{-1} FW at the M stage, with lemon fruit accumulating the highest content (**Figure 2C** and **Supplementary Table 3**). γ-Tocopherol ranged from 0.75 to 8.4 μg g^{-1} FW at the IG stage, with lemon and mandarin accumulating the lowest content (<3 μg) (**Figure 2D** and **Supplementary Table 3**). This tocopherol isoform increased during maturation in the flavedo of all species, reaching maximum values at the Br or M stages, between 10 μg g^{-1} in lemon and 42 μg g^{-1} in sweet orange

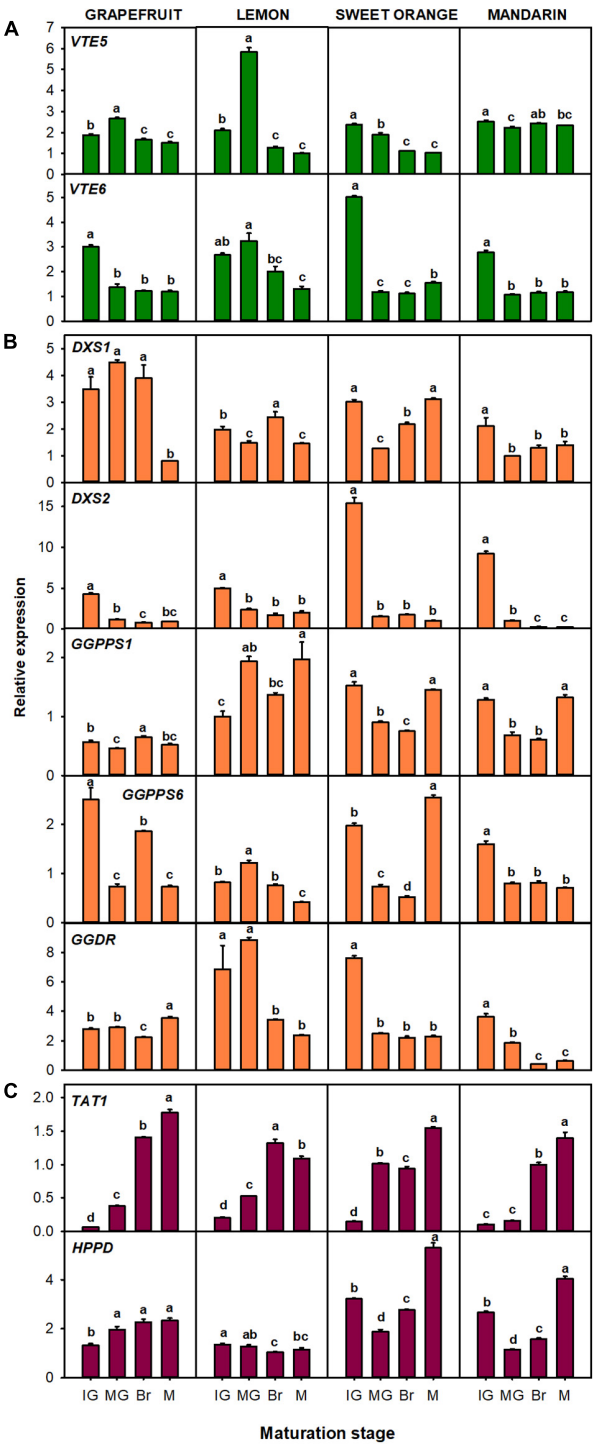

FIGURE 4 | Relative expression of genes involved in the synthesis of precursor PPP (phytyl pyrophosphate), through the recycling of free phytol **(A)** and MEP pathway **(B)**, and of precursor HGA (homogentisate) through the SK pathway **(C)**, in the flavedo during fruit maturation of grapefruit (*C. paradisi*), lemon (*C. limon*), sweet orange (*C. sinensis*), and mandarin (*C. clementine*). The genes analyzed were *VTE5* (phytol kinase), *VTE6* (phytyl-P kinase), *DXS1* and *DXS2* (1-deoxy-D-xylulose-5-phosphate synthase 1 and 2), *GGPPS1* and *GGPPS6* (geranylgeranyl pyrophosphate synthase 1 and 6), *GGDR* (geranylgeranyl diphosphate reductase), *TAT1* (tyrosine aminotransferase), and *HPPD* (4-hydroxyphenylpyruvate dioxygenase). Maturation stages correspond to immature green (IG), mature green (MG), breaker (Br), and mature (M). The data are mean ± SE of at least three replicates (**Supplementary Table 11**). Different letters indicate significant mean differences among maturation stages for each fruit specie (Tukey's test, $p \leq 0.05$).

(**Figure 2D**). It should be noticed that in all the ripening stages, the flavedo of lemon and mandarin showed lower concentrations of γ-tocopherol in comparison to sweet orange and grapefruit (**Figure 2D** and **Supplementary Table 3**).

The pulp of sweet orange, mandarin, and grapefruit showed the highest levels of total tocopherol at the IG stage (∼13–23 $\mu g\ g^{-1}$ FW), which decreased at the MG stage (more than fourfold) (**Figure 3**). In lemon, changes during ripening were minor and levels remained almost constant (∼11–14 $\mu g\ g^{-1}$ FW). In M fruit, the pulp of lemon accumulated the highest total contents, followed by grapefruit and lastly orange and mandarin (**Supplementary Table 4**). As in the flavedo, α-tocopherol contents reflected the main differences in total tocopherols among species and during maturation (**Figure 3C** and **Supplementary Table 4**). Contents in the pulp ranged from 13 to 22 $\mu g\ g^{-1}$ FW at IG stage, and 2 to 11 $\mu g\ g^{-1}$ FW at M fruit. The levels of γ-tocopherol in the pulp of the four species were below 1 $\mu g\ g^{-1}$ FW at IG stage and decreased during maturation in the four species (**Figure 3D**).

Expression Profile of Genes Involved in Tocopherol Synthesis in the Flavedo During Fruit Maturation of Four *Citrus* Species: Grapefruit (*Citrus paradisi*), Lemon (*Citrus limon*), Sweet Orange (*Citrus. sinensis*), and Mandarin (*Citrus clementine*)

The relative expression of genes related to tocopherol precursors production: *VTE5*, *VTE6*, *DXS1*, *DXS2*, *GGPPS1*, *GGPPS6*, *GGDR*, *TAT1*, and *HPPD* (**Figure 4**), and to the tocopherol-core pathway: *VTE2*, *VTE3a*, *VTE3b*, *VTE1*, and *VTE4* (**Figure 5**) were evaluated in the flavedo of the four selected *Citrus* species during fruit maturation. Changes in the expression of the genes involved in the synthesis of the precursor PPP, which includes genes involved in chlorophyll degradation (**Figures 1**, **4A**) and of the MEP pathway (**Figures 1**, **4B**) during fruit ripening, were in general gene- and specie-dependent, but tended to be down-regulated. Of the genes involved in the recycling of free phytol to form PPP (**Figure 4A**), a significant down-regulation of *VTE6* during fruit ripening (two- to threefold decrease) was detected in fruits of the four species. *VTE5* expression also decreased in the four species, although with a transient induction at the MG stage in lemon and grapefruit. Regarding genes of the MEP pathway (**Figure 4B**), a decrease in the expression of *DXS2* was detected during fruit ripening in the four species, and of *GGDR* in lemon, orange, and mandarin. In the flavedo of grapefruit, the expression decreased at Br stage but increased again at the M stage. No

clear common trend among the four species was found in the expression of *DXS1* and the two *GGPPS* paralogous during fruit maturation, although *DXS1* and *GGPPS6* tended to decrease in most species (**Figure 4B**). By contrast, the genes involved in the synthesis of the precursor HGA, *TAT1* and *HPPD*, were in general induced during maturation (**Figure 4C**). The expression of *TAT1* was significantly up-regulated in the four species, showing levels 6- to 28-fold higher at Br and M stages than at IG. The relative expression of *HPPD* gradually increased in grapefruit and at the last stage of maturation in sweet orange and mandarin, but decreased in lemon (**Figure 4C**).

Expression of the tocopherol-core pathway genes during maturation varied among species, but most of the genes were induced or maintained during ripening (**Figure 5**). The gene *VTE2*, which controls the condensation of PPP with HGA, was induced almost two-times in lemon at the Br stage, while it displayed a transient but significant down-regulation between the MG and Br stage in the other three genotypes. The two *VTE3* isoforms were significantly down-regulated in lemon and orange, although a transient increase at the MG stage was detected in lemon. In grapefruit *VTE3a* increased after the IG stage, while it decreased in mandarin's flavedo after the same stage. On the other hand, expression of *VTE3b* decreased in grapefruit, although with a peak at the MG stage, whereas it was induced at the M stage in mandarin fruit. The gene *VTE1* displayed an induction in grapefruit and mandarin (twofold increase), while its expression was maintained with transient variations at the MG and Br stage in sweet orange. In lemon, *VTE1* showed a similar pattern of expression to the *VTE3* isoforms, with a sharp and induction at the MG stage that decreased at later stages. Finally, *VTE4* displayed the most consistent expression pattern among the four species, with a significant up-regulation (two and three-times) during maturation.

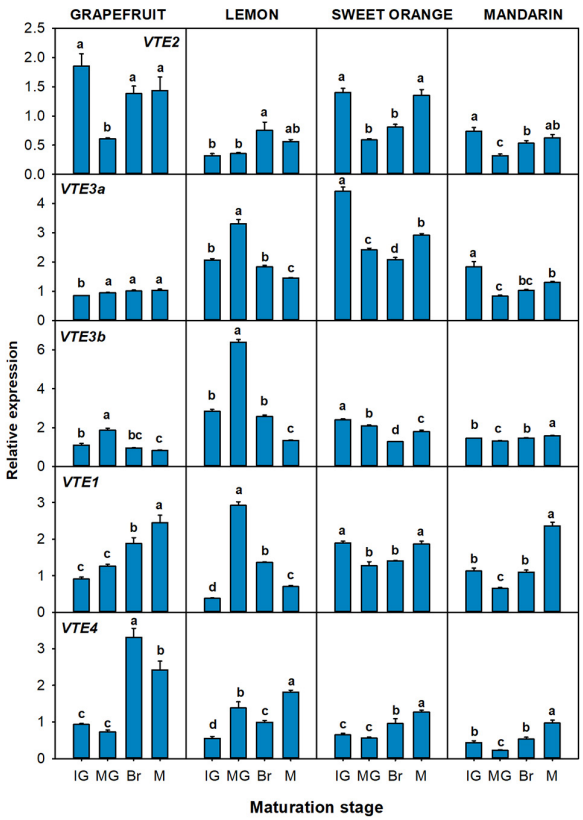

FIGURE 5 | Relative expression of genes of the tocopherol-core pathway in the flavedo during fruit maturation of grapefruit (*C. paradisi*), lemon (*C. limon*), sweet orange (*C. sinensis*), and mandarin (*C. clementine*). The genes analyzed were *VTE2* (HPT, homogentisate phytyl transferase), *VTE3a* and *VTE3b* (MPBQ-MT, 2-methyl-6-phytyl-1,4-benzoquinol methyltransferase a and b), *VTE1* (TC, tocopherol cyclase), and *VTE4* (γ-TMT, γ-tocopherol methyltransferase). Maturation stages correspond to immature green (IG), mature green (MG), breaker (Br), and mature (M). The data are mean ± SE of at least three replicates (**Supplementary Table 11**). Different letters indicate significant mean differences among maturation stages for each fruit specie (Tukey's test, $p \leq 0.05$).

Expression Profile of Genes Involved in Tocopherol Synthesis in the Pulp During Fruit Maturation of Four *Citrus* Species: Grapefruit (*Citrus paradisi*), Lemon (*Citrus limon*), Sweet Orange (*Citrus sinensis*), and Mandarin (*Citrus clementine*)

The relative expression of the genes related to the production of tocopherol precursors: *VTE5*, *VTE6*, *DXS1*, *DXS2*, *GGPPS1*, *GGPPS6*, *GGDR*, *TAT1*, and *HPPD* (**Figure 6**), and to the tocopherol-core pathway: *VTE2*, *VTE3a*, *VTE3b*, *VTE1*, and *VTE4* (**Figure 7**), were analyzed in the pulp of fruit from the selected genotypes. In general, temporal changes in the expression of genes involved in PPP synthesis in the pulp were dependent on the gene and specie, but similarities for certain genes were found. Concerning genes of chlorophyll degradation, *VTE5* transcripts were significantly up-regulated in lemon, orange, and mandarin during ripening and only transiently at the Br stage in grapefruit, while the expression of *VTE6* was significantly down-regulated in the pulp of the four species (**Figure 6A**). Of the MEP pathway genes, expression of *DXS1* was induced in sweet orange and mandarin (more than twofold) but remained relatively unaltered in grapefruit and lemon (only with transient decreases mid-ripening) (**Figure 6B**). Interestingly, expression of *DXS2* was induced in lemon but down-regulated in the pulp of the other *Citrus* species. Furthermore, while *GGPPS1* was significantly induced in the four species, the isoform *GGPPS6* was only induced in orange and down-regulated in the other species. The expression of *GGDR* decreased during maturation in the four species, but the reduction was more marked in sweet orange and mandarin than in the other species. On the other hand, the expression of both *TAT1* and *HPPD* genes, involved in HGA synthesis, was up-regulated during ripening in the pulp of the four citrus fruits.

In relation with the genes of the tocopherol-core pathway, no common expression trend among genotypes was detected (**Figure 7**). The gene *VTE2* was significantly down-regulated during fruit maturation in grapefruit, sweet orange, and

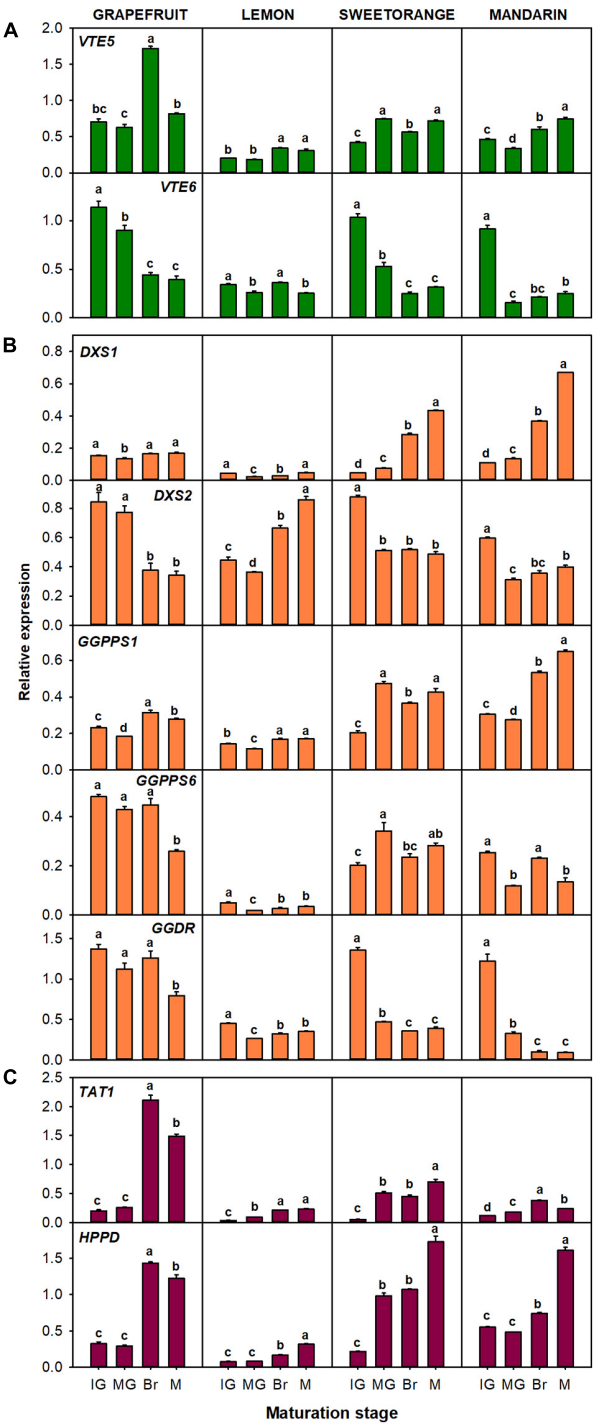

FIGURE 6 | Relative expression of genes involved in the synthesis of precursor PPP (phytyl pyrophosphate), through the recycling of free phytol **(A)** and MEP pathway **(B)**, and of precursor HGA (homogentisate) through the SK pathway **(C)**, in the pulp during fruit maturation of grapefruit (*C. paradisi*), lemon (*C. limon*), sweet orange (*C. sinensis*), and mandarin (*C. clementine*). The genes analyzed were *VTE5* (phytol kinase), *VTE6* (phytyl-P kinase), *DXS1* and *DXS2* (1-deoxy-D-xylulose-5-phosphate synthase 1 and 2), *GGPPS1* and *GGPPS6* (geranylgeranyl pyrophosphate synthase 1 and 6), *GGDR* (geranylgeranyl diphosphate reductase), *TAT1* (tyrosine aminotransferase), and *(Continued)*

FIGURE 6 | (Continued)
HPPD (4-hydroxyphenylpyruvate dioxygenase). Maturation stages correspond to immature green (IG), mature green (MG), breaker (Br), and mature (M). The data are mean ± SE of at least three replicates (**Supplementary Table 12**). Different letters indicate significant mean differences among maturation stages for each fruit specie (Tukey's test, $p \leq 0.05$).

mandarin, whereas no difference between the M and IG stages was detected in lemon. Moreover, the gene *VTE4* was significantly up-regulated during maturation in lemon, orange, and mandarin, but only transitionally at Br stage in grapefruit. In relation to the other genes, expression of *VTE3a* was induced in lemon while it remained almost unaltered in grapefruit and mandarin (with transient significant changes at the Br stage). A different pattern for the *VTE3b* isoform was detected in grapefruit, lemon, and mandarin, with its expression being down-regulated in grapefruit and relative constant in lemon and mandarin. In orange, both isoforms displayed the same expression pattern, with a significant increase at the MG stage that later decreased again. Expression of *VTE1* showed minor alterations in the pulp of grapefruit and sweet orange, but was significantly induced in lemon and mandarin.

Correlation and Network Analysis of Tocopherol Contents and Relative Expression of the Genes Involved in Tocopherol Synthesis in the Flavedo and Pulp During Fruit Maturation of Four *Citrus* Species: Grapefruit (*Citrus paradisi*), Lemon (*Citrus limon*), Sweet Orange (*Citrus sinensis*), and Mandarin (*Citrus clementine*)

To better understand the relationship between gene expression and the accumulation of tocopherols, a correlation matrix (**Figures 8A,C**) and network analysis (**Figures 8B,D**) were built independently for the flavedo and pulp, using data of the four species at the four maturation stages. The network analysis, in which only significant correlations were taken into account, revealed that tocopherols (total, α- and γ-forms) and all genes analyzed were present in both the flavedo and pulp networks, arranged in an interconnected group in each tissue (**Figure 8**). However, the number of interconnections in the networks was different between tissues, with a media of 3.76 edges in the flavedo and 8.82 in the pulp, and the number of negative links between metabolite nodes and the expression of genes was higher in the pulp than in the flavedo (**Figures 8B,D**).

In the flavedo, *VTE6* and *TAT1* were the most interconnected genes (6–7 edges), but *GGPPS6*, *VTE3a*, *VTE3b*, and *VTE4* also had links above the median (**Figure 8B**). Not surprisingly, α-tocopherol and γ-tocopherol showed a strong and positive relationship with total tocopherols, but the correlation between α- and γ-tocopherol was not significant (**Figures 8A,B**). Moreover, tocopherols were positively correlated with the genes *TAT1*, of the SK pathway, and *VTE4*, of the tocopherol

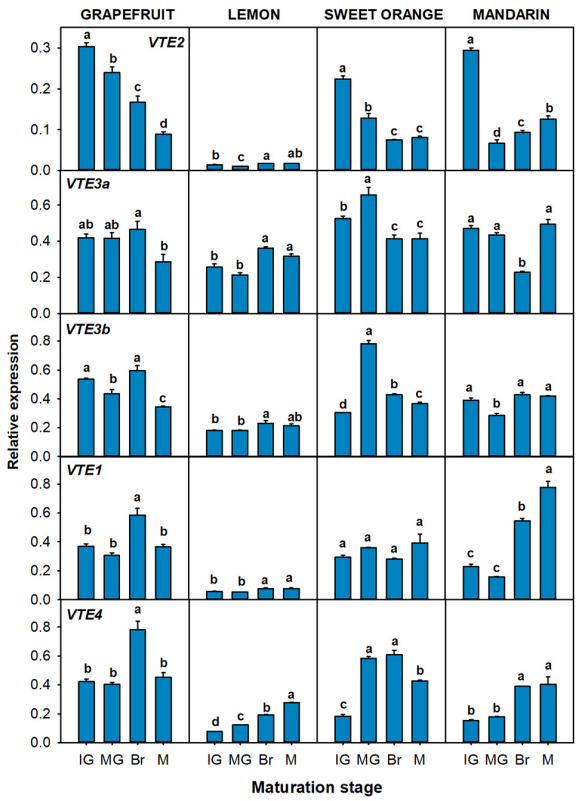

FIGURE 7 | Relative expression of genes of the tocopherol-core pathway in the pulp during fruit maturation of grapefruit (*C. paradisi*), lemon (*C. limon*), sweet orange (*C. sinensis*), and mandarin (*C. clementine*). The genes analyzed were *VTE2* (HPT, homogentisate phytyl transferase), *VTE3a* and *VTE3b* (MPBQ-MT, 2-methyl-6-phytyl-1,4-benzoquinol methyltransferase a and b), *VTE1* (TC, tocopherol cyclase), and *VTE4* (γ-TMT, γ-tocopherol methyltransferase). Maturation stages correspond to immature green (IG), mature green (MG), breaker (Br), and mature (M). The data are mean ± SE of at least three replicates (**Supplementary Table 12**). Different letters indicate significant mean differences among maturation stages for each fruit specie (Tukey's test, $p \leq 0.05$).

core pathway, suggesting that both *TAT1* and *VTE4* are key genes modulating tocopherol accumulation in the flavedo (**Figures 8A,B**). On the other hand, total tocopherols and α-tocopherol were negatively correlated with the gene *GGPPS6* of the MEP pathway, while γ-tocopherol displayed a negative correlation with the genes *VTE6* and *DXS2* (**Figures 8A,B**). Interestingly, the gene *VTE6* seemed highly connected to genes of the MEP pathway (*DXS2*, *GGDR*, and *GGPPS6*) and with both isoforms of *VTE3* (**Figure 8B**), suggesting that they are co-regulated in the flavedo during ripening.

In the pulp, 10 genes: *DXS1*, *GGPPS1*, *GGPPS6*, *VTE5*, *TAT1*, *HPPD*, *VTE2*, *VTE3b*, *VTE1*, and *VTE4*, showed a number of links above the median, being *GGPPS1*, *HPPD*, *VTE1*, *DXS1*, and *VTE4* the most interconnected genes (11–12 edges) (**Figures 8C,D**). A strong positive correlation was detected between α- and γ-tocopherol in the pulp (**Figures 8C,D**). The network analysis in the pulp also revealed a positive correlation of total and α-tocopherol with the genes *VTE6*, *DXS2*, and *GGDR* (**Figures 8C,D**). Tocopherols were negatively correlated with *GGPPS1* and *HPPD* and, in the case of total tocopherols and α-tocopherol, also with *DXS1*, *TAT1*, *VTE1*, and *VTE4* (**Figures 8C,D**). Similar to what was observed in the flavedo, a connection between *VTE6* and the genes *DXS2* and *GGDR* of the MEP pathway was detected. Furthermore, other genes were positively co-regulated in the pulp, including genes of the MEP pathway (*GGPPS6*, *GGPPS1*, and *DXS1*), involved in phytol recycling (*VTE5*), of the SK pathway (*HPPD* and *TAT1*) and of the tocopherol-core pathway (*VTE2*, *VTE3b*, *VTE1*, and *VTE4*).

DISCUSSION

Taking advantage of the genetic and phenotypical diversity of the genus *Citrus*, the aim of this work was to investigate the changes in tocopherol contents and their regulation during maturation of fruit of four *Citrus* species belonging to the main horticultural groups: grapefruit, lemon, sweet orange, and mandarin. Tocopherols were identified in all the selected *Citrus* species throughout maturation, with contents varying between tissues, maturation stages, and genotypes (**Figures 2, 3** and **Supplementary Tables 3**, **4**). The tocopherol profile was in agreement with previous reports, with α- and γ-tocopherol being the main forms detected in *Citrus* fruit (Assefa et al., 2017; Rey et al., 2021a,b). However, predominance of one form or another seems to be dependent on the *Citrus* specie, as similar or higher γ-tocopherol contents have been detected in less common Korean *Citrus* genotypes (Assefa et al., 2017). In fruit of other species, the prevalence of α- or γ-tocopherol is also specie-specific and, while α-tocopherol is the main form in tomato, pepper, mango, grape, olive, and avocado (Koch et al., 2002; Horvath et al., 2006b; Quadrana et al., 2013; Singh et al., 2017; Georgiadou et al., 2019; Vincent et al., 2020), γ-tocopherol accumulates at higher concentrations in zucchini and raspberry fruit (Carvalho et al., 2013; Rodov et al., 2020). In our experimental conditions, β-tocopherol was not detected, and δ-tocopherol was only identified in some samples but at levels below the limit of quantification, indicating that the δ-/β-tocopherol branch may not have a significant contribution to the tocopherol pool in citrus fruit.

Many physiological and metabolic processes are independently regulated in the flavedo and pulp of *Citrus* fruit (Tadeo et al., 2020), and this seems to be the case for tocopherol metabolism as contents were higher in the flavedo than the pulp (**Figures 2**, **3**). Similarly, higher concentrations of other bioactive compounds have been reported in the flavedo than in the pulp of citrus (Alquézar et al., 2008, 2013; Alós et al., 2014; Assefa et al., 2017). A possible explanation for this is that the direct exposure of the flavedo to environmental stresses could lead to a higher demand for antioxidants to cope with these adverse conditions. In relation to this, light could play a relevant role either as a stress factor or by its direct impact in the regulation of tocopherol biosynthesis. Tocopherols are involved in the photo-protection of plants (Spicher et al., 2017; Ma et al., 2020b), and increases in contents have been reported in response to high light stress (Collakova and DellaPenna, 2003b;

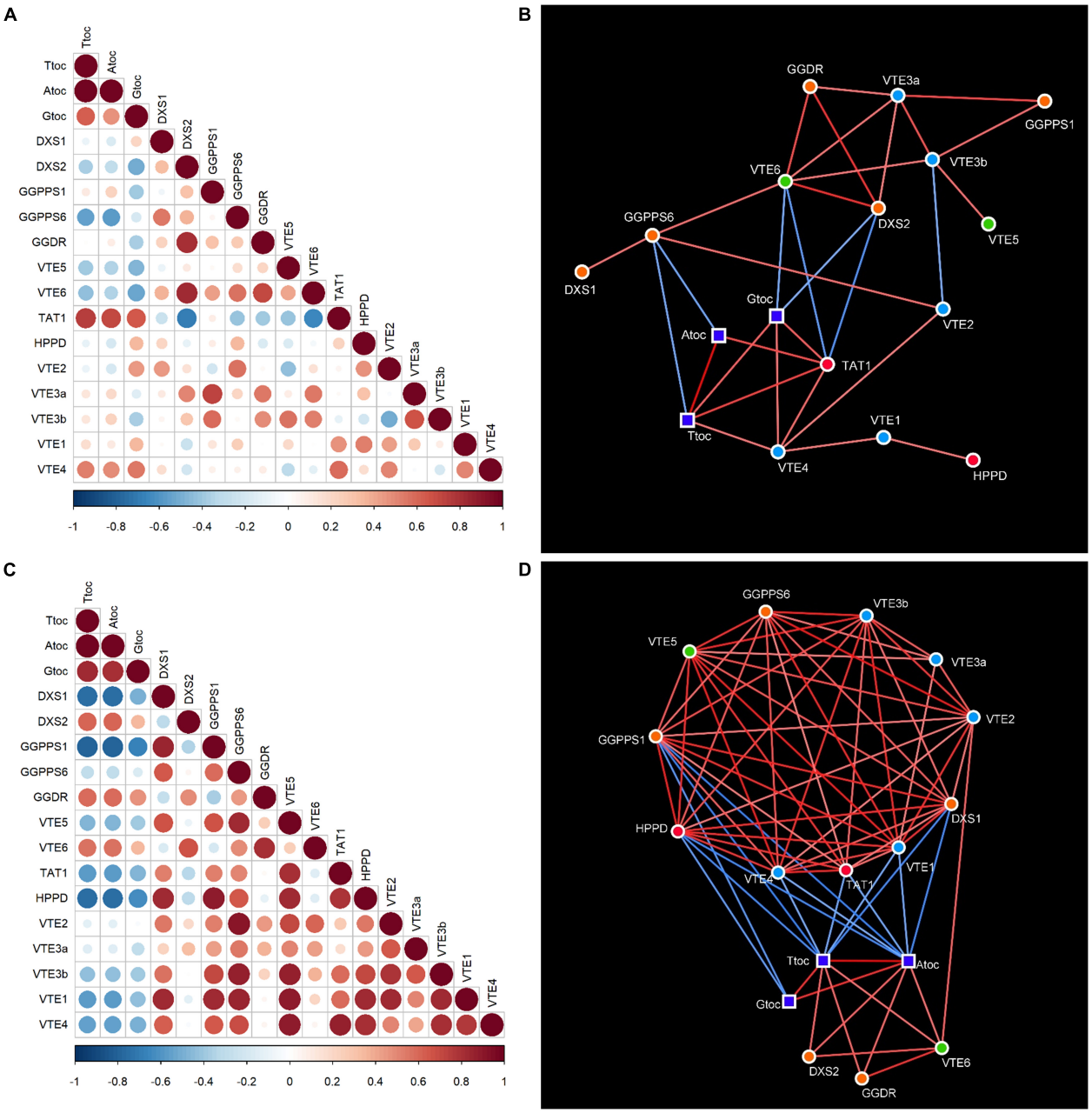

FIGURE 8 | Correlation matrices **(A,C)** and networks **(B,D)** of tocopherol contents and expression of genes involved in tocopherol synthesis in the flavedo **(A,B)** and pulp **(C,D)** during fruit maturation of grapefruit (*C. paradisi*), lemon (*C. limon*), sweet orange (*C. sinensis*), and mandarin (*C. clementine*). Positive and negative correlations in the matrices are shown in different shades of red and blue, respectively, with the size of the circle and color intensity indicating the magnitude of Pearson's correlation coefficient. In the correlation networks, square nodes represent tocopherol contents (Ttoc, total tocopherols; Atoc, α-tocopherol; Gtoc, γ-tocopherol) and circle nodes represent genes (green, genes involved in the recycling of phytol; orange, genes of the MEP pathway; red, genes of the SK pathway; and blue, genes of the tocopherol-core pathway). Lines joining the nodes represent correlations (edges); positive correlations are shown in red, while negative correlations are in blue, and the color intensity represents the strength of the correlation (absolute value of the Pearson's correlation coefficient). Only significant correlations (p-value ≤ 0.05) were taken into account for constructing the correlation networks. Values for the correlation coefficients and significances are detailed in **Supplementary Tables 7**, **8**, **13**, **14**.

Havaux et al., 2005). Furthermore, a positive role of light in the transcriptional regulation of certain tocopherol biosynthetic genes has been proposed in grapefruit (Rey et al., 2021b) and tomato (Gramegna et al., 2019).

The differences detected between fruit tissues were not only quantitative but also in the pattern of accumulation during maturation (**Figures 2**, **3**), suggesting that different mechanisms may operate in the regulation of tocopherol

synthesis in the flavedo and pulp of *Citrus* fruit. The differential accumulation of tocopherols between citrus fruit tissues may also be related to their chlorophyll contents, as an alternative source of PPP is through the recycling of free phytol formed during the degradation of chlorophylls (**Figure 1**; Valentin et al., 2006; Georgiadou et al., 2015; vom Dorp et al., 2015; Almeida et al., 2016). While chlorophyll content in the pulp of *Citrus* fruit is negligible or only detected in IG fruit, concentrations in the flavedo are high throughout development and decrease notably with the transition of chloroplasts to chromoplasts (Alquézar et al., 2008, 2013; Lado et al., 2015, 2019). Therefore, the higher concentration of chlorophylls in the flavedo at immature stages and their degradation as ripening progresses could lead to a higher availability of free phytol to form PPP, higher influx into the tocopherol-core pathway and an enhancement of tocopherol contents. Accumulation of tocopherols concomitantly with chlorophylls breakdown during color change has been also described in fruit of other species like pepper (Osuna-García et al., 1998; Koch et al., 2002) and olive (Georgiadou et al., 2016).

The transcriptional analysis of tocopherol genes revealed that differences in tocopherol concentrations between tissues were associated with a generalized higher expression in the flavedo than in the pulp (**Figures 4–7**), which reinforces the hypothesis of the differential regulation of tocopherols accumulation between tissues. Moreover, transcriptional patterns during fruit maturation and correlation analysis pointed specific candidate genes that may regulate tocopherol levels in each tissue (**Figures 4–8**). In the flavedo, *TAT1* and *VTE4* showed a significant positive correlation to total, α- and γ-tocopherol contents (**Figures 8A,B**) suggesting the importance of these genes in regulating tocopherol accumulation in this tissue. *TAT1* plays a major role in tocopherol synthesis by regulating HGA availability (Riewe et al., 2012), and an induction of this gene during senescence has been previously reported in Arabidopsis leaves, and associated with an increase in α- and γ-tocopherol content (Holländer-Czytko et al., 2005). On the other hand, the gene *VTE4*, which encodes for γ-TMT, plays a role in shaping tocopherol composition rather than increasing tocopherol contents (Bergmüller et al., 2003). Modifications in the expression of *VTE4* have been successful in increasing α-tocopherol but in detriment of γ-tocopherol contents, and thus not altering total contents (Bergmüller et al., 2003; Collakova and DellaPenna, 2003a; Maeda et al., 2006). Therefore, in the flavedo of citrus the combined up-regulation of *TAT1* and *VTE4* during maturation could indicate a higher influx into the tocopherol core-pathway, due to a higher availability of HGA, which afterward is mostly converted into α-tocopherol by the increase in downstream *VTE4*. Still, it is important to keep in mind that many substrates and enzymes involved in tocopherol synthesis also participate in other metabolic pathways, such as HGA, and therefore the possible channeling to other pathways should be considered. Additionally, other genes, such as *HPPD* or *GGPPS1*, were also induced during ripening in specific citrus species and may also contribute to the increase of tocopherols, although they were not significantly linked to tocopherol contents in the network analysis (**Figure 8B**).

The expression of most genes involved in the regulation of PPP production tended to decrease in the flavedo during maturation with no apparent effect on tocopherol contents (**Figures 2**, **4A,B**). Mutant plants of Arabidopsis in some of these genes (*vte6*, *dxs*, and *ggpps11*) have resulted in a reduction in tocopherol levels (Estévez et al., 2001; vom Dorp et al., 2015; Ruiz-Sola et al., 2016). Nonetheless, the expression of *GGPPS6*, the citrus orthologous gene of Arabidopsis *GGPPS11*, was significantly and negatively correlated with total and α-tocopherol levels, whereas *VTE6* and *DXS2* were negatively correlated with γ-tocopherol (**Figure 8B**). A down-regulation of *DXS* has been previously reported in the flavedo of grapefruit, orange, and mandarin linked to the onset of chlorophylls degradation at color break, rather than to the accumulation of other MEP-derived isoprenoids (Alós et al., 2006; Alquézar et al., 2008, 2013; Lado et al., 2015, 2019). Collectively, these results suggest that the supply of PPP by the recycling of free phytol or by *de novo* synthesis through the MEP pathway may not constrain tocopherol synthesis in the flavedo of *Citrus* during maturation.

In the pulp, most of the genes exhibited a similar expression tendency to that of the flavedo (**Figures 4–7**), although tocopherol concentrations were lower and followed contrasting temporal patterns (**Figures 2**, **3**). A similar pattern of expression among genotypes was detected in the pulp for the genes *TAT1*, *HPPD*, *VTE6*, *GGPPS1*, and *GGDR* (**Figure 6**), whereas changes in the expression of the other genes followed a distinct profile depending on the specie (**Figures 6**, **7**). Interestingly, *TAT1* was induced during maturation in the four species, similarly to the changes detected in the flavedo but opposite to the pattern of tocopherol accumulation in the pulp, and *HPPD* was induced in the pulp and in the flavedo of grapefruit, orange, and mandarin (**Figures 4C, 6C**). An induction of genes of the SK pathway (*TAT1* and *HPPD*) has also been observed with maturation in tomato and olive fruit but, as in the citrus pulp, did not mirror the changes in tocopherol contents (Quadrana et al., 2013; Georgiadou et al., 2015). This suggests that the up-regulation of these genes could be developmentally modulated and not necessarily associated to tocopherol contents in the pulp or in fleshy fruits. Since both *TAT1* and *HPPD* are involved in the synthesis of the precursor HGA, which is not specific of tocopherol synthesis, it is likely that their induction is related to the synthesis of other tocochromanols which also use HGA as a precursor (Szymańska and Kruk, 2010; Kruk et al., 2014; Burgos et al., 2021). In relation to the other genes involved in tocopherol synthesis, the decrease in tocopherol contents observed in the pulp of grapefruit, orange, and mandarin was synchronized with the down-regulation of the genes *VTE6*, *DXS2*, *GGDR*, and *VTE2* (**Figures 6**, **7**). These results suggest that transcriptional regulation of these genes play a role determining tocopherol content in the pulp, which was supported by the correlation network results (**Figures 8C,D**). These genes, in particular those involved in the supply of PPP, have been previously proposed as limiting steps in tocopherol accumulation in the flesh of tomato (Quadrana et al., 2013; Almeida et al., 2015). In the pulp of lemon, expression of these genes varied from the other species but still reflected the minor changes detected in tocopherol accumulation during ripening in this specie. In the pulp, genes *TAT1*, *HPPD*,

DXS1, *GGPPS1*, *VTE1*, and *VTE4* showed a negative correlation with total contents or a specific tocopherol form (**Figures 8C,D**). Then, in this tissue, the down-regulation of genes involved in regulating PPP availability (*VTE6*, *DXS2*, and *GGDR*) may constrain tocopherol synthesis, and the up-regulation of other genes of the SK pathway (*TAT1* and *HPPD*) and tocopherol-core pathway (*VTE1* and *VTE4*) is not enough to compensate this limitation.

The network analyses in the flavedo and pulp also revealed genes that are co-regulated in both tissues during fruit maturation but in the pulp a higher number of genes were co-regulated compared to flavedo (**Figures 8B,D**). The gene *VTE6* was positively linked to *DXS2* and *GGDR*, all involved in the supply of PPP in both tissues. Other genes that seemed to be co-expressed in both tissues were those of the SK pathway with the genes involved in the last steps of the tocopherol-core pathway (**Figure 8**).

Finally, the differences in the accumulation of tocopherols detected among genotypes in each tissue (**Figures 2**, **3**) were not clearly related to the expression of any gene (**Figures 4–7**; **Supplementary Tables 5, 6**), although some trends were observed in the flavedo. Focusing on differences in gene expression at early maturation stages, when differences among genotypes were already evident (**Supplementary Table 3**), a higher expression of *GGDR* and *VTE3b* was detected in the flavedo of lemon and orange than in the other genotypes (**Supplementary Table 5**), which could explain the higher contents in these two species. Higher expression of these genes has been previously reported in *Citrus* genotypes accumulating higher tocopherol concentrations (Rey et al., 2021a) and also in other fruit species as tomato (Quadrana et al., 2013; Gramegna et al., 2019).

CONCLUSION

This study addresses for the first time a comparative analysis of tocopherols accumulation and transcriptional regulation of their biosynthetic genes during fruit maturation of four *Citrus* species. Differences in tocopherol contents were detected between the flavedo and pulp, and also during maturation and genotypes. Concentration of tocopherols in the flavedo were between 2 and 50 times higher than in the pulp, and this was associated with higher expression levels in the flavedo of most genes involved in the precursors PPP and HGA synthesis, and the tocopherol core-pathway. Moreover, tocopherols increased in the flavedo with maturation while they tended to decrease in the pulp, and correlation and network analysis allow to suggest candidate genes regulating tocopherol accumulation in each tissue. In the flavedo, the increase in tocopherol contents mirrored a marked up-regulation of *TAT1* and *VTE4*, while contents in the pulp may be limited by the expression of *VTE6*, *DXS2*, and *GGDR*, regulating PPP availability. Furthermore, the genes *TAT1* and *VTE4*, *HPPD* and *VTE1*, and *VTE6* with *DXS2* and *GGDR*, were co-regulated and shared a similar pattern during maturation in both tissues, suggesting they are developmentally modulated. Finally, the differences among genotypes were not clearly correlated with the expression of specific genes, indicating the involvement of other regulatory mechanisms modulating differences among species.

DATA AVAILABILITY STATEMENT

The original contributions presented in the study are included in the article/**Supplementary Material**, further inquiries can be directed to the corresponding author.

AUTHOR CONTRIBUTIONS

MR and LZ: conceptualization, supervision, and funding acquisition. FR, MR, and LZ: methodology and writing – review. FR: experimental work, formal analysis, data curation, and writing – original draft preparation. All authors have read and agreed to the published version of the manuscript.

FUNDING

This work was funded by the research grant RTI2018-095131-B-I00 of the Ministry of Science and Innovation/Agencia Española de Investigación/FEDER (Spanish Government) and PROMETEO/2020/027 (Generalitat Valenciana). FR was the recipient of a Ph.D. scholarship (POS_EXT_2016_1_133720) from ANII (Uruguay). The authors acknowledge support of the publication fee by the CSIC Open Access Publication Support Initiative through its Unit of Information Resources for Research (URICI).

ACKNOWLEDGMENTS

The authors acknowledge the Citrus Germplasm Bank of Instituto Valenciano de Investigaciones Agrarias (IVIA, Generalitat Valenciana) for the provision of fruit. The excellent technical assistance of Mª C. Gurrea and I. Carbonell is gratefully acknowledged.

SUPPLEMENTARY MATERIAL

The Supplementary Material for this article can be found online at: https://www.frontiersin.org/articles/10.3389/fpls.2021.743993/full#supplementary-material

REFERENCES

Almeida, J., Asis, R., Molineri, V. N., Sestari, I., Lira, B. S., Carrari, F., et al. (2015). Fruits from ripening impaired, chlorophyll degraded and jasmonate insensitive tomato mutants have altered tocopherol content and composition. *Phytochemistry* 111, 72–83. doi: 10.1016/j.phytochem.2014.11.007

Almeida, J., Azevedo, M., da, S., Spicher, L., Glauser, G., vom Dorp, K., et al. (2016). Down-regulation of tomato PHYTOL KINASE strongly impairs tocopherol

biosynthesis and affects prenyllipid metabolism in an organ-specific manner. *J. Exp. Bot.* 67, 919–934. doi: 10.1093/jxb/erv504

Almeida, J., Perez-Fons, L., and Fraser, P. D. (2020). A transcriptomic, metabolomic and cellular approach to the physiological adaptation of tomato fruit to high temperature. *Plant. Cell Environ.* 2020:13854. doi: 10.1111/pce.13854

Almeida, J., Quadrana, L., Asis, R., Setta, N., deGodoy, F., Bermudez, L., et al. (2011). Genetic dissection of vitamin E biosynthesis in tomato. *J. Exp. Bot.* 62, 3781–3798. doi: 10.1093/jxb/err055

Alós, E., Cercos, M., Rodrigo, M. J., Zacarias, L., and Talon, M. (2006). Regulation of color break in citrus fruits. Changes in pigment profiling and gene expression induced by gibberellins and nitrate, two ripening retardants. *J. Agric. Food Chem.* 54, 4888–4895. doi: 10.1021/jf0606712

Alós, E., Rodrigo, M. J., and Zacarías, L. (2014). Differential transcriptional regulation of l-ascorbic acid content in peel and pulp of citrus fruits during development and maturation. *Planta* 239, 1113–1128. doi: 10.1007/s00425-014-2044-z

Alquézar, B., Rodrigo, M. J., Lado, J., and Zacarías, L. (2013). A comparative physiological and transcriptional study of carotenoid biosynthesis in white and red grapefruit (Citrus paradisi Macf.). *Tree Genet. Genomes* 9, 1257–1269. doi: 10.1007/s11295-013-0635-7

Alquézar, B., Rodrigo, M. J., and Zacarías, L. (2008). Regulation of carotenoid biosynthesis during fruit maturation in the red-fleshed orange mutant Cara Cara. *Phytochemistry* 69, 1997–2007. doi: 10.1016/j.phytochem.2008.04.020

Arango, Y., and Heise, K. P. (1998). Tocopherol synthesis from homogentisate in Capsicum anuum L. (yellow pepper) chromoplast membranes: evidence for tocopherol cyclase. *Biochem. J.* 336, 531–533. doi: 10.1042/bj3360531

Assefa, A. D., Saini, R. K., and Keum, Y.-S. (2017). Fatty acids, tocopherols, phenolic and antioxidant properties of six citrus fruit species: a comparative study. *J. Food Meas. Charact.* 11, 1665–1675. doi: 10.1007/s11694-017-9546-x

Bergmüller, E., Porfirova, S., and Dörmann, P. (2003). Characterization of an Arabidopsis mutant deficient in γ-tocopherol methyltransferase. *Plant Mol. Biol.* 52, 1181–1190. doi: 10.1023/B:PLAN.0000004307.62398.91

Burgos, E., Belen De Luca, M., Diouf, I., Haro, L. A., Albert, E., Sauvage, C., et al. (2021). Validated MAGIC and GWAS population mapping reveals the link between vitamin E content and natural variation in chorismate metabolism in tomato. *Plant J.* 105, 907–923. doi: 10.1111/tpj.15077

Cano, A., Medina, A., and Bermejo, A. (2008). Bioactive compounds in different citrus varieties. Discrimination among cultivars. *J. Food Compos. Anal.* 21, 377–381. doi: 10.1016/j.jfca.2008.03.005

Cardeñosa, V., Barreira, J., Barros, L., Arenas-Arenas, F., Moreno-Rojas, J., and Ferreira, I. (2015). Variety and harvesting season effects on antioxidant activity and vitamins content of citrus sinensis macfad. *Molecules* 20, 8287–8302. doi: 10.3390/molecules20058287

Carvalho, E., Fraser, P. D., and Martens, S. (2013). Carotenoids and tocopherols in yellow and red raspberries. *Food Chem.* 139, 744–752. doi: 10.1016/j.foodchem.2012.12.047

Chun, J., Lee, J., Ye, L., Exler, J., and Eitenmiller, R. R. (2006). Tocopherol and tocotrienol contents of raw and processed fruits and vegetables in the United States diet. *J. Food Compos. Anal.* 19, 196–204. doi: 10.1016/j.jfca.2005.08.001

Collakova, E., and DellaPenna, D. (2001). Isolation and Functional Analysis of Homogentisate Phytyltransferase from. *Society* 127, 1113–1124. doi: 10.1104/pp.010421.1

Collakova, E., and DellaPenna, D. (2003a). Homogentisate phytyltransferase activity is limiting for tocopherol biosynthesis in arabidopsis. *Plant Physiol.* 131, 632–642. doi: 10.1104/pp.015222

Collakova, E., and DellaPenna, D. (2003b). The role of homogentisate phytyltransferase and other tocopherol pathway enzymes in the regulation of tocopherol synthesis during abiotic stress. *Plant Physiol.* 133, 930–940. doi: 10.1104/pp.103.026138

Diretto, G., Al-Babili, S., Tavazza, R., Scossa, F., Papacchioli, V., Migliore, M., et al. (2010). Transcriptional-metabolic networks in β-carotene-enriched potato tubers: the long and winding road to the Golden phenotype. *Plant Physiol.* 154, 899–912. doi: 10.1104/pp.110.159368

Estévez, J. M., Cantero, A., Reindl, A., Reichler, S., and León, P. (2001). 1-Deoxy-d-xylulose-5-phosphate synthase, a limiting enzyme for plastidic isoprenoid biosynthesis in plants. *J. Biol. Chem.* 276, 22901–22909. doi: 10.1074/jbc.M100854200

Falk, J., and Munné-Bosch, S. (2010). Tocochromanol functions in plants: antioxidation and beyond. *J. Exp. Bot.* 61, 1549–1566. doi: 10.1093/jxb/erq030

Fritsche, S., Wang, X., and Jung, C. (2017). Recent advances in our understanding of tocopherol biosynthesis in plants: an overview of key genes. Functions, and Breeding of Vitamin E Improved Crops. *Antioxidants* 6:99. doi: 10.3390/antiox6040099

Georgiadou, E. C., Goulas, V., Ntourou, T., Manganaris, G. A., Kalaitzis, P., and Fotopoulos, V. (2016). Regulation of On-Tree Vitamin E biosynthesis in olive fruit during successive growing years: the impact of fruit development and environmental cues. *Front. Plant Sci.* 7:1656. doi: 10.3389/fpls.2016.01656

Georgiadou, E. C., Koubouris, G., Goulas, V., Sergentani, C., Nikoloudakis, N., Manganaris, G. A., et al. (2019). Genotype−dependent regulation of vitamin E biosynthesis in olive fruits as revealed through metabolic and transcriptional profiles. *Plant Biol.* 21, 604–614. doi: 10.1111/plb.12950

Georgiadou, E. C., Ntourou, T., Goulas, V., Manganaris, G. A., Kalaitzis, P., and Fotopoulos, V. (2015). Temporal analysis reveals a key role for VTE5 in vitamin E biosynthesis in olive fruit during on-tree development. *Front. Plant Sci.* 6:871. doi: 10.3389/fpls.2015.00871

Gramegna, G., Rosado, D., Sánchez Carranza, A. P., Cruz, A. B., Simon-Moya, M., Llorente, B., et al. (2019). PHYTOCHROME-INTERACTING FACTOR 3 mediates light-dependent induction of tocopherol biosynthesis during tomato fruit ripening. *Plant Cell Environ.* 42, 1328–1339. doi: 10.1111/pce.13467

Havaux, M., Eymery, F., Porfirova, S., Rey, P., and Dörmann, P. (2005). Vitamin E protects against photoinhibition and photooxidative stress in arabidopsis thaliana. *Plant Cell* 17, 3451–3469. doi: 10.1105/tpc.105.037036

Holländer-Czytko, H., Grabowski, J., Sandorf, I., Weckermann, K., and Weiler, E. W. (2005). Tocopherol content and activities of tyrosine aminotransferase and cystine lyase in Arabidopsis under stress conditions. *J. Plant Physiol.* 162, 767–770. doi: 10.1016/j.jplph.2005.04.019

Horvath, G., Wessjohann, L., Bigirimana, J., Jansen, M., Guisez, Y., Caubergs, R., et al. (2006a). Differential distribution of tocopherols and tocotrienols in photosynthetic and non-photosynthetic tissues. *Phytochemistry* 67, 1185–1195. doi: 10.1016/j.phytochem.2006.04.004

Horvath, G., Wessjohann, L., Bigirimana, J., Monica, H., Jansen, M., Guisez, Y., et al. (2006b). Accumulation of tocopherols and tocotrienols during seed development of grape (Vitis vinifera L. cv. Albert Lavallée). *Plant Physiol. Biochem.* 44, 724–731. doi: 10.1016/j.plaphy.2006.10.010

Karunanandaa, B., Qi, Q., Hao, M., Baszis, S. R., Jensen, P. K., Wong, Y. H., et al. (2005). Metabolically engineered oilseed crops with enhanced seed tocopherol. *Metab. Eng.* 7, 384–400. doi: 10.1016/j.ymben.2005.05.005

Koch, M., Arango, Y., Mock, H. P., and Heise, K. P. (2002). Factors influencing α-tocopherol synthesis in pepper fruits. *J. Plant Physiol.* 159, 1015–1019. doi: 10.1078/0176-1617-00746

Kruk, J., Szymańska, R., Cela, J., and Munne-Bosch, S. (2014). Plastochromanol-8: Fifty years of research. *Phytochemistry* 108, 9–16. doi: 10.1016/j.phytochem.2014.09.011

Lado, J., Alós, E., Manzi, M., Cronje, P. J. R., Gómez-Cadenas, A., Rodrigo, M. J., et al. (2019). Light regulation of carotenoid biosynthesis in the peel of mandarin and sweet orange fruits. *Front. Plant Sci.* 10:1288. doi: 10.3389/fpls.2019.01288

Lado, J., Cronje, P., Alquézar, B., Page, A., Manzi, M., Gómez-Cadenas, A., et al. (2015). Fruit shading enhances peel color, carotenes accumulation and chromoplast differentiation in red grapefruit. *Physiol. Plant.* 154, 469–484. doi: 10.1111/ppl.12332

Ma, G., Zhang, L., Sugiura, M., and Kato, M. (2020a). *Citrus and health in The Genus Citrus*. Amsterdam: Elsevier, 495–511. doi: 10.1016/B978-0-12-812163-4.00024-3

Ma, J., Qiu, D., Pang, Y., Gao, H., Wang, X., and Qin, Y. (2020b). Diverse roles of tocopherols in response to abiotic and biotic stresses and strategies for genetic biofortification in plants. *Mol. Breed.* 40:1097. doi: 10.1007/s11032-019-1097-x

Maeda, H., Song, W., Sage, T. L., and DellaPenna, D. (2006). Tocopherols Play a Crucial Role in Low-Temperature adaptation and phloem loading in arabidopsis. *Plant Cell* 18, 2710–2732. doi: 10.1105/tpc.105.039404

Mène-Saffrané, L. (2017). Vitamin E biosynthesis and its regulation in plants. *Antioxidants* 7:2. doi: 10.3390/antiox7010002

Mène-Saffrané, L., Jones, A. D., and DellaPenna, D. (2010). Plastochromanol-8 and tocopherols are essential lipid-soluble antioxidants during seed desiccation and quiescence in Arabidopsis. *Proc. Natl. Acad. Sci.* 107, 17815–17820. doi: 10.1073/pnas.1006971107

Muñoz, P., and Munné-Bosch, S. (2019). Vitamin E in Plants: Biosynthesis. Transport, and Function. *Trends Plant Sci.* 24, 1040–1051. doi: 10.1016/j.tplants.2019.08.006

Norris, S. R., Shen, X., and Della Penna, D. (1998). Complementation of the arabidopsis pds1 mutation with the gene encoding p -hydroxyphenylpyruvate dioxygenase. *Plant Physiol.* 117, 1317–1323. doi: 10.1104/pp.117.4.1317

Osuna-García, J. A., Wall, M. M., and Waddell, C. A. (1998). Endogenous levels of tocopherols and ascorbic acid during fruit ripening of new mexican-type chile (Capsicum annuum L.) Cultivars. *J. Agric. Food Chem.* 46, 5093–5096. doi: 10.1021/jf980588h

Pellaud, S., and Mène-Saffrané, L. (2017). Metabolic Origins and Transport of Vitamin E Biosynthetic Precursors. *Front. Plant Sci.* 8:1959. doi: 10.3389/fpls.2017.01959

Pfaffl, M. W., Horgan, G. W., and Dempfle, L. (2002). Relative expression software tool (REST) for group-wise comparison and statistical analysis of relative expression results in real-time PCR. *Nucleic Acids Res.* 30:e36. doi: 10.1093/nar/30.9.e36

Quadrana, L., Almeida, J., Otaiza, S. N., Duffy, T., da Silva, J. V. C., de Godoy, F., et al. (2013). Transcriptional regulation of tocopherol biosynthesis in tomato. *Plant Mol. Biol.* 81, 309–325. doi: 10.1007/s11103-012-0001-4

Rey, F., Rodrigo, M. J., Diretto, G., and Zacarías, L. (2021b). Effect of fruit shading and cold storage on tocopherol biosynthesis and its involvement in the susceptibility of Star Ruby grapefruit to chilling injury. *Food Chem. Mol. Sci.* 3:100037. doi: 10.1016/j.fochms.2021.100037

Rey, F., Rodrigo, M. J., and Zacarias, L. (2021a). Accumulation of tocopherols and transcriptional regulation of their biosynthesis during cold storage of mandarin fruit. *Postharvest Biol. Technol.* 180:111594. doi: 10.1016/j.postharvbio.2021.111594

Riewe, D., Koohi, M., Lisec, J., Pfeiffer, M., Lippmann, R., Schmeichel, J., et al. (2012). A tyrosine aminotransferase involved in tocopherol synthesis in Arabidopsis. *Plant J.* 71, 850–859. doi: 10.1111/j.1365-313X.2012.05035.x

Rodov, V., Paris, H. S., Friedman, H., Mihiret, M., Vinokur, Y., and Fennec, A. (2020). Chilling sensitivity of four near-isogenic fruit-color genotypes of summer squash (Cucurbita pepo. Cucurbitaceae) and its association with tocopherol content. *Postharvest Biol. Technol.* 168:111279. doi: 10.1016/j.postharvbio.2020.111279

Rodrigo, M. J., Marcos, J. F., and Zacarías, L. (2004). Biochemical and molecular analysis of carotenoid biosynthesis in flavedo of orange (Citrus sinensis L.) during fruit development and maturation. *J. Agric. Food Chem.* 52, 6724–6731. doi: 10.1021/jf049607f

Rodrigo, M. J., and Zacarías, L. (2006). *Horticultural and Quality Aspects of Citrus Fruits in Handbook of Fruits and Fruit Processing*. Hoboken: John Wiley & Sons, Ltd, 293–307. doi: 10.1002/9780470277737.ch18

Ruiz-Sola, M. A., Coman, D., Beck, G., Barja, M. V., Colinas, M., Graf, A., et al. (2016). Arabidopsis GERANYLGERANYL DIPHOSPHATE SYNTHASE 11 is a hub isozyme required for the production of most photosynthesis-related isoprenoids. *New Phytol.* 209, 252–264. doi: 10.1111/nph.13580

Savidge, B., Weiss, J. D., Wong, Y. H., Lassner, M. W., Mitsky, T. A., Shewmaker, C. K., et al. (2002). Isolation and Characterization of Homogentisate Phytyltransferase Genes from Synechocystis sp. PCC 6803 and Arabidopsis. *Plant Physiol.* 129, 321–332. doi: 10.1104/pp.010747

Singh, R. K., Chaurasia, A. K., Bari, R., and Sane, V. A. (2017). Tocopherol levels in different mango varieties correlate with MiHPPD expression and its over-expression elevates tocopherols in transgenic Arabidopsis and tomato.*3. Biotech* 7, 1–9. doi: 10.1007/s13205-017-0991-3

Spicher, L., Almeida, J., Gutbrod, K., Pipitone, R., Dörmann, P., Glauser, G., et al. (2017). Essential role for phytol kinase and tocopherol in tolerance to combined light and temperature stress in tomato. *J. Exp. Bot.* 68, 5845–5856. doi: 10.1093/jxb/erx356

Spreen, T. H., Gao, Z., Fernandes, W., and Zansler, M. L. (2020). "Chapter 23 - Global economics and marketing of citrus products," in *The Genus Citrus*, eds M. Talon, M. Caruso, and F. G. Gmitter (Sawston: Woodhead Publishing), 471–493. doi: 10.1016/B978-0-12-812163-4.00023-1

Szymańska, R., and Kruk, J. (2010). Plastoquinol is the main prenyllipid synthesized during acclimation to high light conditions in arabidopsis and is converted to plastochromanol by tocopherol cyclase. *Plant Cell Physiol.* 51, 537–545. doi: 10.1093/pcp/pcq017

Tadeo, F. R., Terol, J., Rodrigo, M. J., Licciardello, C., and Sadka, A. (2020). "Chapter 12 - Fruit growth and development," in *The Genus Citrus*, eds M. Talon, M. Caruso, and F. G. Gmitter (Sawston: Woodhead Publishing), 245–269. doi: 10.1016/B978-0-12-812163-4.00012-7

Traber, M. G., and Sies, H. (1996). Vitamin E in Humans: Demand and Delivery. *Annu. Rev. Nutr.* 16, 321–347. doi: 10.1146/annurev.nutr.16.1.321

Tsegaye, Y., Shintani, D. K., and DellaPenna, D. (2002). Overexpression of the enzyme p-hydroxyphenolpyruvate dioxygenase in Arabidopsis and its relation to tocopherol biosynthesis. *Plant Physiol. Biochem.* 40, 913–920. doi: 10.1016/S0981-9428(02)01461-4

Valentin, H. E., Lincoln, K., Moshiri, F., Jensen, P. K., Qi, Q., Venkatesh, T. V., et al. (2006). The Arabidopsis vitamin E pathway gene5-1 Mutant Reveals a Critical Role for Phytol Kinase in Seed Tocopherol Biosynthesis. *Plant Cell* 18, 212–224. doi: 10.1105/tpc.105.037077

Vincent, C., Mesa, T., and Munné-Bosch, S. (2020). Identification of a New Variety of Avocados *(Persea americana* Mill. CV. Bacon) with High vitamin e and impact of cold storage on tocochromanols composition. *Antioxidants* 9:403. doi: 10.3390/antiox9050403

vom Dorp, K., Holzl, G., Plohmann, C., Eisenhut, M., Abraham, M., Weber, A. P. M., et al. (2015). Remobilization of phytol from chlorophyll degradation is essential for tocopherol synthesis and growth of arabidopsis. *Plant Cell* 27:tc.15.00395. doi: 10.1105/tpc.15.00395

Wu, G. A., Terol, J., Ibanez, V., Lopez-Garcia, A., Perez-Roman, E., Borreda, C., et al. (2018). Genomics of the origin and evolution of Citrus. *Nature* 554, 311–316. doi: 10.1038/nature25447

Zacarías-García, J., Lux, P. E., Carle, R., Schweiggert, R. M., Steingass, C. B., Zacarias, L., et al. (2021). Characterization of the Pale Yellow Petal/Xanthophyll Esterase gene family in citrus as candidates for carotenoid esterification in fruits. *Food Chem.* 342:128322. doi: 10.1016/j.foodchem.2020.128322

Conflict of Interest: The authors declare that the research was conducted in the absence of any commercial or financial relationships that could be construed as a potential conflict of interest.

Publisher's Note: All claims expressed in this article are solely those of the authors and do not necessarily represent those of their affiliated organizations, or those of the publisher, the editors and the reviewers. Any product that may be evaluated in this article, or claim that may be made by its manufacturer, is not guaranteed or endorsed by the publisher.

frontiers in Plant Science

ORIGINAL RESEARCH
published: 08 October 2021
doi: 10.3389/fpls.2021.730692

Genome-Wide Characterization and Analysis of bHLH Transcription Factors Related to Anthocyanin Biosynthesis in Fig (*Ficus carica* L.)

Miaoyu Song[1], *Haomiao Wang*[1], *Zhe Wang*[1], *Hantang Huang*[1], *Shangwu Chen*[2] *and Huiqin Ma*[1,3]*

[1] College of Horticulture, China Agricultural University, Beijing, China, [2] College of Food Science and Nutritional Engineering, China Agricultural University, Beijing, China, [3] State Key Laboratory of Agrobiotechnology, China Agricultural University, Beijing, China

OPEN ACCESS

Edited by:
M. Teresa Sanchez-Ballesta, Instituto de Ciencia y Tecnología de Alimentos y Nutrición (ICTAN), Spain

Reviewed by:
Irene Romero, Consejo Superior de Investigaciones Científicas (CSIC), Spain
Yasuyuki Yamada, Kobe Pharmaceutical University, Japan
Ertugrul Filiz, Duzce University, Turkey

***Correspondence:**
Huiqin Ma
hqma@cau.edu.cn

Specialty section:
This article was submitted to Plant Metabolism and Chemodiversity, a section of the journal Frontiers in Plant Science

Received: 25 June 2021
Accepted: 03 September 2021
Published: 08 October 2021

Citation:
Song M, Wang H, Wang Z, Huang H, Chen S and Ma H (2021) Genome-Wide Characterization and Analysis of bHLH Transcription Factors Related to Anthocyanin Biosynthesis in Fig (Ficus carica L.). Front. Plant Sci. 12:730692. doi: 10.3389/fpls.2021.730692

The basic helix–loop–helix (bHLH) transcription factor family is the second largest transcription factor family in plants, and participates in various plant growth and development processes. A total of 118 bHLH genes were identified from fig (*Ficus carica* L.) by whole-genome database search. Phylogenetic analysis with *Arabidopsis* homologs divided them into 25 subfamilies. Most of the *bHLH*s in each subfamily shared a similar gene structure and conserved motifs. Seventy-two *bHLH*s were found expressed at fragments per kilobase per million mapped (FPKM) > 10 in the fig fruit; among them, 15 *bHLH*s from eight subfamilies had FPKM > 100 in at least one sample. *bHLH* subfamilies had different expression patterns in the female flower tissue and peel during fig fruit development. Comparing green and purple peel mutants, 13 bHLH genes had a significantly different (≥ 2-fold) expression. Light deprivation resulted in 68 significantly upregulated and 22 downregulated bHLH genes in the peel of the fruit. Sixteen bHLH genes in subfamily III were selected by three sets of transcriptomic data as candidate genes related to anthocyanin synthesis. Interaction network prediction and yeast two-hybrid screening verified the interaction between *FcbHLH42* and anthocyanin synthesis-related genes. The transient expression of *FcbHLH42* in tobacco led to an apparent anthocyanin accumulation. Our results confirm the first fig bHLH gene involved in fruit color development, laying the foundation for an in-depth functional study on other FcbHLH genes in fig fruit quality formation, and contributing to our understanding of the evolution of bHLH genes in other horticulturally important *Ficus* species.

Keywords: genome-wide, bHLH transcription factors, expression analysis, anthocyanin biosynthesis, *Ficus carica* L.

INTRODUCTION

Transcription factors are key regulatory elements in life processes (Yamasaki et al., 2013; Guo and Wang, 2017). To date, more than 60 transcription factor families have been found in plants. According to the number of lysine and arginine residues in the DNA-binding domain, transcription factors are divided into four categories: zinc finger (ZF) type,

helix–turn–helix (HLH), basic helix–loop–helix (bHLH), and basic leucine zipper (bZIP). The most commonly found transcription factors in higher plants are members of the WD40, MYB, WRKY, bHLH, and bZIP families (Kosugi and Ohashi, 2002).

The bHLH transcription factors, also called MYCs, form the second largest family of transcription factors in plants (Feller et al., 2011), with 162, 95, 167, and 152 bHLH genes identified in *Arabidopsis* (Bailey et al., 2003), grape (Wang et al., 2018), rice (Li et al., 2006), and tomato (Wang et al., 2015), respectively. The bHLH domain is approximately 60 amino acids long, containing a basic region and an HLH region. The basic region, located next to the N-terminus, contains the DNA *cis*-acting elements E-box (5'-CANNTG-3') and G-box (5'-CACGTG-3') that regulate gene expression, whereas the HLH region consists of two amphipathic α-helices linked by a loop that serve as the dimerization domain to promote protein interactions, producing homodimers or heterodimers (Massari and Murre, 2000). bHLHs can act as either repressors or activators of gene transcription and play important roles in various physiological processes, such as sexual maturation, metabolism, and development (Feller et al., 2011).

According to evolutionary relationships, the specificity of DNA binding and conservation of specific amino acids or domains (except the bHLH domain), members of the bHLH superfamily, have been assigned into subfamilies, or subgroups, by different researchers. The bHLH transcription factors in *Arabidopsis*, poplar, rice, moss, and algal genomes have been divided into 32 subfamilies (Carretero-Paulet et al., 2010). Members of subfamilies 9 and 27 are essential for the growth and development of terrestrial plants, and subfamilies 7, 18, 19, and 20 are unique to angiosperms. Members of subfamily 5 regulate flavonoid/anthocyanin metabolism, epidermal cell development, and trichome initiation. According to the classification of subgroups, 166 bHLH genes of the *Arabidopsis thaliana* genome are divided into 13 major subgroups (I–XIII). Genes in a particular major group contain a similar number of introns at conserved positions, the encoded proteins have similar predicted lengths, and the bHLH domain is in a similar position in the protein. Genes within each major group can be further divided into a total of 26 subgroups (Heim et al., 2003; Pires and Dolan, 2010). The 95 bHLH genes in grape (Wang et al., 2018), 167 bHLH genes in rice (Li et al., 2006), and 152 bHLH genes in tomato (Wang et al., 2015) are divided into second-level subgroups by this method.

Anthocyanin biosynthesis is achieved by structural genes in the anthocyanin-biosynthesis pathway (Allan et al., 2008). At the transcriptional level, it is mainly regulated by a series of transcription factors, especially members of the R2R3–MYB gene family. In *Arabidopsis*, R2R3–MYB PAP1 and PAP2 regulate anthocyanin biosynthesis (Zimmermann et al., 2004; Gonzalez et al., 2008). In flavonoid biosynthesis, bHLH proteins serve as cofactors of R2R3–MYB, together with WD40, making up the MYB-bHLH-WD40 (MBW) complex (Hichri et al., 2011a; Xie et al., 2012; Wang et al., 2020). Most bHLHs that are involved in anthocyanin biosynthesis belong to subgroup III, which is functionally conserved and has been shown to regulate plant defense and development (Bailey et al., 2003; Heim et al., 2003). In *Arabidopsis*, subgroup III fbHLHs are involved in both flavonoid biosynthesis and trichome formation. The members share a conserved amino acid, arginine, which is involved in protein interactions and normal functions (Ludwig et al., 1989; Zhao et al., 2012).

Since the identification of bHLH transcription factor *Lc* (leaf color) in corn (Ludwig et al., 1989), TT8, GL3, and EGL3 of subgroup IIIf have been found to interact with TTG1 (WD40 protein family) and MYB (Bailey et al., 2003; Heim et al., 2003) to form protein complexes that regulate flavonoid biosynthesis. Most plants have at least two bHLHs belonging to two distinct clades within subgroup IIIf (Heim et al., 2003; Feller et al., 2011). They are described as bHLH-1 (represented by *ZmR/ZmLc*, *AtGL3*, *AtEGL3*, *AtMYC1*, *PhJAF13*, and *AmDel*) and bHLH-2 (represented by *ZmIn*, *AtTT8*, *PhAN1*, and *VvMYC1*) (Albert et al., 2014). The bHLH-2 genes are essential for anthocyanin biosynthesis. The overexpression of R2R3–MYB PAP1 resulted in elevated transcript levels of *TT8* in *Arabidopsis* (Gonzalez et al., 2008). In petunia, *PhAN2* requires the bHLH cofactor *PhAN1* or *PhJAF13* to enhance the promoter activity of dihydroflavonol 4-reductase (*DFR*) (Spelt et al., 2000). The co-expression of *VvMYC1* and *VvMYBA1* in grape suspension cells led to anthocyanin accumulation (Hichri et al., 2011a). Previous transcriptome analysis of fig has suggested that *FcMYB114*, *FcCPC*, *FcMYB21*, and *FcMYB123* regulate anthocyanin biosynthesis (Wang et al., 2019; Li et al., 2020a), but that no anthocyanin-related fig bHLH has been identified. In addition, genes from bHLH subgroup III d + e have been shown to regulate the jasmonic acid (JA) signaling pathway, thereby enhancing plant defense capabilities and promoting anthocyanin biosynthesis (Xie et al., 2012). Low temperature promoted the expression of *MdbHLH3*, which increased anthocyanin accumulation and fruit coloring in apple (Xie et al., 2012; Yang et al., 2017).

The fig (*Ficus carica* L.), which originated from the Mediterranean coastal region, is one of the earliest cultivated fruit trees in the world. The fig fruit (syconia) demonstrates a typical double sigmoid growth curve with a rapid growth phase, a lag phase, and another rapid growth phase (Flaishman et al., 2008). Ripe figs with dark color and red flesh have a high anthocyanin content, are beneficial to health, have a great market potential. In a previous study, we confirmed that the coloring of cv. Purple-Peel was due to anthocyanin accumulation (Wang et al., 2017). However, the bHLH transcription factors involved in fig anthocyanin accumulation have not been revealed. In this study, a total of 118 FcbHLH genes were recruited by searching the whole-genome database of fig; physical and chemical properties, phylogeny, chromosome distribution, conserved motifs, and protein interactions were analyzed bioinformatically, and *bHLH* expression patterns in the fig fruit at different development stages and under different treatment conditions were revealed. *FcbHLH42* was selected for a functional study that proved its role in fig anthocyanin synthesis. The results lay the foundation for understanding the role of FcbHLHs further in fig anthocyanin and flavonoid biosynthesis.

MATERIALS AND METHODS

Plant Materials

The common fig cv. Purple-Peel from a commercial orchard in Weihai city, Shandong province, China (37°25′ N, 122°17′ E) was used. The fig trees were 7 years old with 3 m × 3 m spacing and standard cultivation. "Purple-Peel" is a bud mutation of "Green Peel," a main fig cultivar in China (Wang et al., 2017). Six stages of the main crop fruit were sampled for gene-expression analysis based on the characteristics of fruit development. The fruit samples were marked as stages 1–6: stage 1 represented phase I (the first rapid growth period), stages 2, 3, and 4 were the early, middle, and late stages of phase II (slow growth period), and stages 5 and 6 represented phase III (the second rapid growth period). In this study, following Wang et al. (2019), stages 4 and 5 fruits were termed young and mature, respectively. Sixty fruits were randomly selected at each stage, and 20 were used as the biological replicate. The peel and female flower tissue were separated onsite at the time of sampling. Fresh samples were quick-frozen with liquid nitrogen and stored at −80°C for subsequent experiments.

Identification and Annotation of FcbHLH Transcription Factors

The fig genome sequences of cvs. Horaishi and Dottato were downloaded from the National Center for Biotechnology Information (NCBI) (https://www.ncbi.nlm.nih.gov/genome/?Term=Ficus+carica) (Mori et al., 2017; Usai et al., 2020). The sequences were blasted (Evalue-5) using the hidden Markov model HMMER (v3.0) of Pfam (http://pfam.xfam.org/). Candidate genes containing the bHLH signature domain (PF00010) and with the most conserved amino acids in the bHLH region (Toledo-Ortiz et al., 2003) were screened further in the databases of Pfam, NCBI conserved domains (http://www.ncbi.nlm.nih.gov/Structure/cdd/wrpsb.cgi), and SMART (http://smart.emblheidelberg.de). Redundancies were removed. The bHLH family genes of *Arabidopsis thaliana* were downloaded from the Arabidopsis database (TAIR; https://www.arabidopsis.org/). The fig bHLH homologs were compared with *Arabidopsis* bHLHs by BLASTP with default parameters to obtain the annotation and grouping information. The FcbHLH and AtbHLH sequences were analyzed bioinformatically, and the physicochemical parameters of the proteins were calculated using ExPASy (http://www.expasy.ch/tools/pi_tool.html) (Guo et al., 2014).

Phylogeny and Multiple-Sequence Alignment of FcbHLH Genes

ClustalX version 2.0 with default parameters was used to perform multiple-sequence alignments of the predicted bHLHs of fig and *Arabidopsis* (Larkin et al., 2007; Guo and Wang, 2017). A phylogenetic tree of the bHLHs was constructed with MEGA6.0, using the neighbor-joining (NJ) method with parameters set as follows: mode "p-distance," gap setting "Complete Deletion," and calibration test parameter "Bootstrap = 1000" (Tamura et al., 2011).

Gene Structure and Protein Sequence Motif Analyses

The intron/exon structure map of the fig *bHLHs* was generated online using the Gene Structure Display Server (GSDS: http://gsds.gao-lab.org/). The conserved motifs were analyzed online using MEME4.11.2 (https://meme-suite.org/meme/tools/meme), with parameters set to: number of repetitions "any," highest motif number "20," motif length "6–200," and default values for the other parameters. The results were constructed with TBtools (Chen et al., 2020).

Chromosomal Location and Collinearity of bHLH Genes

The positions of *FcbHLHs* on the 13 fig chromosomes were determined by mapping bHLH gene sequences to fig chromosome survey sequences using BLAST programs. The Mapchart v2.2 software was used to display the precise gene-location results. The genome data of *Ficus hispida* and *Ficus microcarpa* were downloaded from the database of National Genomics Data Center (https://bigd.big.ac.cn/search/?dbId=gwh&q=PRJCA002187&page=1) (Zhang et al., 2020). The grape genome (*Vitis vinifera*) was also downloaded (https://data.jgi.doe.gov/refine-download/phytozome?organism=Vvinifera). An interspecies collinearity analysis of bHLHs between fig and *F. hispida*, *F. microcarpa*, *Arabidopsis* and grape was performed using MCscanX and TBtools (Tang et al., 2008; Chen et al., 2020). The final map was generated with Circos version 0.63 (http://circos.ca/). The non-synonymous replacement rate (Ka) and synonymous replacement rate (Ks) of the replicated gene pairs were calculated using KaKs_Calculator 2.0 (Wang et al., 2010), and environmental selection pressure was analyzed by Ka/Ks ratio.

Functional Verification of bHLH Proteins

The interaction network of 118 FcbHLH proteins was analyzed using the STRING protein interaction database (http://string-db.org/), with *Arabidopsis* selected for species parameters. E-value was set to 1e-4.

Yeast strain Y2HGold (Clontech, San Francisco, CA, United States) was used for the yeast two-hybrid (Y2H) assay. Competent cells were co-transformed with the bait vector pGBKT7-FaMYB10 without self-activation, and the pGADT7 plasmid with possible interaction genes. Diploids carrying both plasmids were created by mating on yeast peptone dextrose (YPD) (1% yeast extract, 2% peptone, 2% glucose, and 2% agar) followed by selection on SD/-Trp/-Leu, SD/-Trp/-Leu/-His, or SD/-Trp/-Leu/-Ade plates. Single colonies growing on the SD/-Trp/-Leu plates were picked and individually cultured in a 1-ml yeast peptone dextrose medium with adenine (YPDA) (1% yeast extract, 2% peptone, 2% glucose,0.04% adenine, and 2% agar) liquid medium at 30°C for 2 days. A 1-μl aliquot of the yeast solution was pipetted on X-α-gal-containing SD/-His/-Leu/-Trp + AbA*and SD/-Ade/-His/-Leu/-Trp + AbA* auxotrophic plates, and incubated at 30°C for 3 days. A single blue yeast colony indicated a positive interaction result.

Gene-Expression Analysis

Three fig fruit RNA-seq libraries established by our laboratory were re-mined. The first library contained data of the "Purple-Peel" fig fruit during development (NCBI Accession No. PRJNA723733). Briefly, syconia peel and the internal female flower tissue were collected at six stages of fruit development. The second library contained data of young and ripe "Purple-Peel" and the peel of its mutated mother cv. Green Peel fruit (NCBI Accession No. SRP114533) (Wang et al., 2017). The third library contained data of bagged and naturally grown "Purple-Peel" fruit (NCBI Accession No. PRJNA494945) (Wang et al., 2019). TBtools was used to analyze the expression patterns of FcbHLHs in each library, and significant differential expression was determined by $p < 0.05$ and $|\log2(\text{fold change})| \geq 1$.

A weighted gene co-expression network analysis (WGCNA) was performed to identify the modules of co-expressed genes (Langfelder and Horvath, 2008). Correlations of the co-expression relationships between *FcbHLH42* and other transcription factors were calculated according to their FPKM changes over the six stages of "Purple-Peel" fig development. The co-expression modules of *FcbHLH42* were visualized with Cytoscape 3.8.2. The thresholds for co-expression were set as correlation coefficient > 0.5 and $p < 0.001$.

The relative expression levels of *FcbHLH42*, strawberry (*Fa*)*MYB10*, *Nicotiana benthamiana* (*Nb*)*F3H*, *NbDFR*, *NbANS*, and *NbUFGT* in control and transient transgenic tobacco (*Nicotiana tabacum*) leaves were determined by quantitative reverse transcription (RT-q) PCR. The primer sequences are detailed in **Supplementary Table 8**. RNA extraction, DNA elimination, RNA quality check, and reverse transcription were carried out using the standard protocols of our laboratory (Wang et al., 2017). The RT-qPCR was carried out with ABI QuantStudio 6 Flex Real-Time PCR System (ABI, Waltham, MA, United Stated) using SYBR-Green Master Mix (Vazyme, Nanjing, China). The reaction program was: pre-denaturation at 94°C for 1 min, denaturation at 94°C for 15 s, annealing at 60°C for 30 s, and extension at 72°C for 1 min, for a total of 40 cycles. A relative quantification analysis with three replicates for each sample was performed as described in Zhai et al. (2021). Significance was analyzed with the SPSS 26.0 software.

Cloning of *FcbHLH42* and Transient Expression

Strawberry *MYB10* was shown to act synergistically with sweet cherry *bHLH* to promote anthocyanin synthesis, but neither was able to promote anthocyanin synthesis alone (Wang et al., 2019). We took *FaMYB10* as bait to verify the function of FcbHLHs. *FaMYB10* was obtained from the strawberry cDNA library, and *FcbHLH42*, *FcbHLH3*, *FcMYC2*, and *FcbHLH14* from the "Purple-Peel" fig cDNA library. The primers are shown in **Supplementary Table 8**. *FcbHLH42* was transiently expressed using the HyperTrans vector system (Albert et al., 2021). The constructs were transformed into a *Agrobacterium tumefaciens* strain GV3101, and a fresh single colony was picked and cultured overnight at 28°C, and then centrifuged at 4,200 × g for 15 min. The bacteria were resuspended in a 15-ml agroinfiltration solution (10 mM $MgCl_2$, 10 mM MES, pH 5.6) + 200 μM acetosyringone. *N. benthamiana* plants were grown in the greenhouse. The positive and negative controls, *FaMYB10*-expressing solution and *FcbHLH42*-expressing solution, respectively, were infiltrated into the back side of the leaves of 5-week-old tobacco (*N. tabacum*) plants (Sparkes et al., 2006). The leaves were photographed, and total anthocyanin content and gene expression were determined 7 days after the infiltration. Leaf tissue color was measured following Wang et al. (2019). Three biological replicates were used for the tests.

Color Measurement

For treatment and controls, 1 g tobacco leaf tissue was collected and added to a 10-ml color extraction solution (methanol:water 1:1, pH 2). After ultrasonic extraction with oscillation at 200 rev/min at 25°C for 10 min, the sample was centrifuged at 10,000 × g at 4°C for 10 min, and the supernatant was collected. The leaf tissue was washed twice, and the supernatants were combined. After filtration through a 0.45-μm membrane, anthocyanin content was determined by differential pH method. Three biological replicates were used. Significance was analyzed with the SPSS 26.0 software.

RESULTS

Genome-Wide Identification and Phylogenetic Analysis

A total of 118 bHLH genes were obtained from the published fig genome, and named *FcbHLH1* to *FcbHLH118* according to the equivalent classification for *Arabidopsis thaliana* (**Figure 1A**, and **Supplementary Table 1**). The predicted number of amino acids encoded by *FcbHLH*s ranged from 91 (*FcbHLH5*) to 892 (*FcbHLH56*), with an average of 356 amino acids per gene. The molecular masses of these proteins ranged from 10.25 (*FcbHLH5*) to 97.2 kD (*FcbHLH56*), and the isoelectric points were from 4.59 (*FcbHLH28*) to 11.53 (*FcbHLH111*), with 62.71% of them lower than 7, as predicted by ExPasy. This was similar to the isoelectric point pattern reported for the bHLH families of *Arabidopsis* (Bailey et al., 2003) and rice (Li et al., 2006). The hydrophilicity of the proteins ranged from −1.014 (*FcbHLH017*) to −0.014 (*FcbHLH053*), indicating that all FcbHLHs are hydrophilic. The instability index (II) ranged from 24.6 to 76.72, with only three indicated stable proteins (II < 40). The aliphatic index was between 50.08 and 102.86. Nuclear localization was predicted for most of the FcbHLHs, while cytoplasmic, chloroplastic, and mitochondrial matrix localization was predicted for a few of them. No signal peptide was found for any of the FcbHLHs by SignalP, demonstrating that they are non-secretory proteins.

To understand the evolutionary relationship of FcbHLH genes, a phylogenetic tree was constructed (**Figure 1A**). FcbHLHs were present in 25 of the 26 *Arabidopsis* bHLH subgroups; they were absent in subgroup II. Subgroups IX and X, both with 14 members, were the largest subgroups of FcbHLHs, while subgroups IIIf and IVd were the smallest, each with only a member. Fig and *Arabidopsis* had the same number of members in 12 subgroups, namely IIIa, IIIb, IIId + e, IVa, IVb, IVc, IVd, Va,

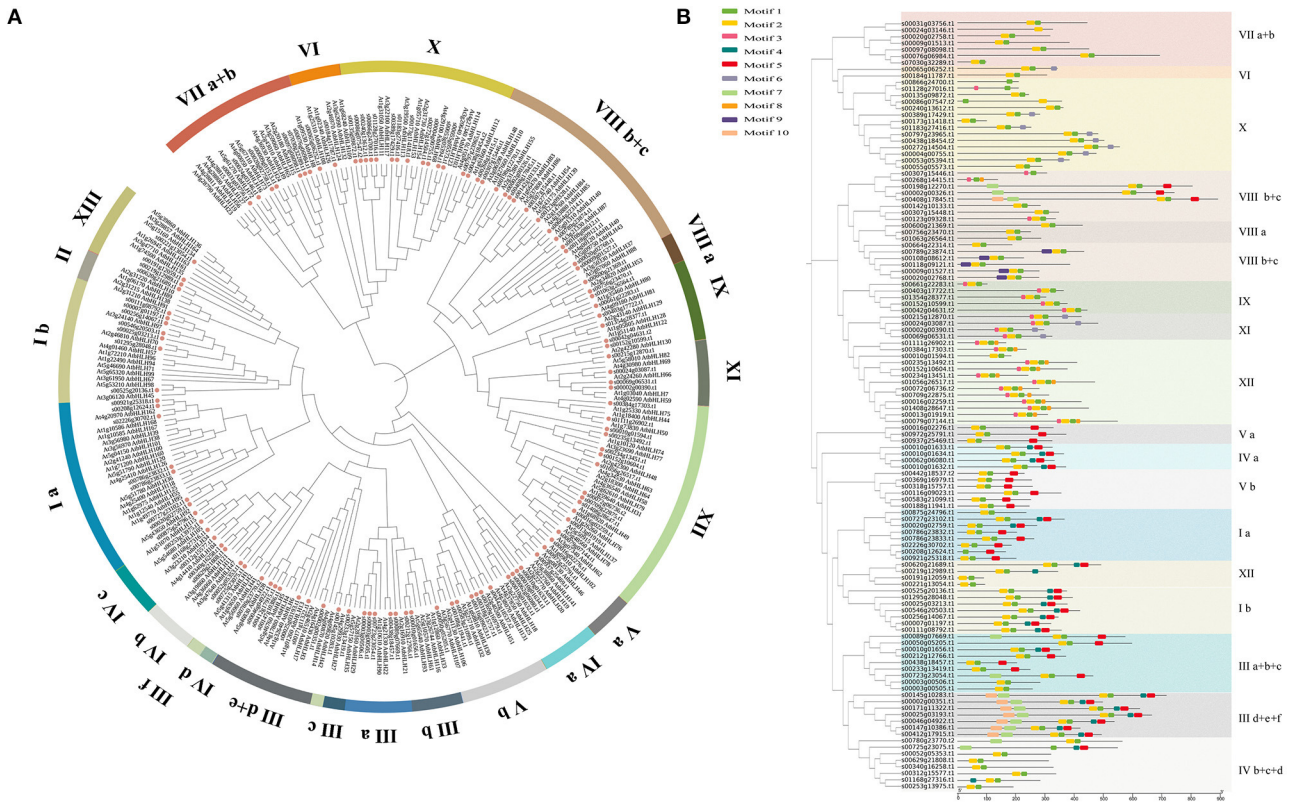

FIGURE 1 | Phylogenetic tree and conserved motif analysis of FcbHLHs. **(A)** The 25 subgroups are marked in different colors on the periphery of the circle. Pink dots indicate fig bHLH proteins. The phylogenetic tree was constructed using MEGA6, with bootstrap values based on 1,000 iterations. **(B)** Rootless neighbor-joining (NJ) phylogenetic tree of 118 full-length amino acid sequences of FcbHLH proteins. The 25 subgroups are marked with different background colors. Conserved motifs are represented by different colored boxes.

Vb, VIIIb + c, IX, and XI. The biggest numerical difference was found in subgroup Ia, with FcbHLH members being less than half of their *Arabidopsis* counterparts. FcbHLH had more members than *Arabidopsis* in subgroups IIIa, IVb, VIIIa, and X.

Sequence and Structure Analyses

Conserved motifs of FcbHLHs are shown in **Figure 1B**. Although the length of the FcbHLHs of different subfamilies varied greatly, the length and position of the conserved motifs were very similar. Motifs 1–10 are shown in different colors (**Figure 1B**), and the details of the 10 conserved motifs are shown in **Table 1** and **Supplementary Table 2**. The number of introns in the *FcbHLH*s ranged from 0 to 19 (**Supplementary Figure 1**). In some subfamilies, the structural pattern of all members was similar. For example, members of subgroup VIIIb had no introns, whereas members of subgroup Ia had two introns, and the corresponding positions of the introns were conserved.

The promoter region was obtained by searching the 2-kb sequence upstream of the translation initiation site of *FcbHLH*s from the fig genome (Mori et al., 2017; Usai et al., 2020). At least 16 *cis*-regulatory elements were predicted (**Supplementary Figure 1**). The elements participated in responses to abiotic stresses (light deprivation, drought, low temperatures, anaerobic conditions, defense, and stress), hormone responses (salicylic acid, gibberellin, methyl jasmonate, abscisic acid, and auxin), circadian rhythm regulation, and nutrition and development (meristem expression and endosperm expression) in all the FcbHLH genes. Light response and anaerobic-induced abiotic stress response regulatory elements, and MYB-binding sites were found in five *bHLH* (*FcbHLH8*, *FcbHLH24*, *FcbHLH83*, *FcbHLH46*, and *FcbHLH21*) promoters.

Expansion Patterns and Collinear Correlation

Large-fragment chromosome replication and tandem repeat are key means of gene family expansion. In our study, the 118 *FcbHLH*s were unevenly distributed among the chromosomes, with a maximum of 23 on chromosome 5 and a minimum of 3 on chromosome 13 (**Figure 2A**). It is generally believed that tandem replication occurs when the distance between genes is <100 kb, and 15 pairs of *FcbHLH*s were in that range (**Supplementary Table 3**). An intraspecific collinearity analysis showed that 11 pairs of *FcbHLH*s originated from fragment replication (**Figure 2B** and **Supplementary Table 4**). The results demonstrated that tandem replication and fragment replication were important events in the expansion of the FcbHLH gene

TABLE 1 | Sequences of 10 predicted motifs of FcbHLH proteins.

Motif	Best possible match	*E*-value	Width	Sites
1	K[TM]D[KT]AS[MI]L[DG][ED]A[IV]XY[VI]K[FE]LQRQ	2.0e-971	21	117
2	XSHSXAERRRRE[KR][IL][NS][ED]R[LFM]KAL [QR]SLVP[NG]XX	1.6e-1109	29	112
3	[KP]S[DV][YP][IC][HR]VRA[RK]RGQAT	1.6e-144	15	22
4	L[PA][DE][IV][ED]V[KRT][IV][VI][GDE]T[DEH][AV][LM][IL][RK][IV]Q[CS][PE][RK]	1.4e-72	21	23
5	[PQ]GLLLK[LI][MI]XAL[EQ]XL[GH]L[DE][VI][LV]HA[SN][IV][ST]T[FV][NG][GD]R	1.6e-126	29	39
6	C[DE][RS][AV][FK][EFL]A[RHQ][MS][HA]GIQT[LVI]VC[IV]P[MT][LP][ND]GV[VL]ELG[ST][TS]D[LS][IV]TE[DS][WL][SG]L[VL]Q	3e-60	41	8
7	[AP][KM]QDL[RQ]S[KR]GLCL[VM]P[IV]S[CL][TA]SA[VI]	7.4e-60	21	12
8	VEFLSMKL[AE][ATS][VA]N[PS]R[ML]	7.4e-54	15	13
9	[MIL][AG][AQ]M[KR]EM[IM][YF][RGK][IA]A[AV][MF][QR]P[VI][DHN][IL][DG][PL][EA][STI][ITV][KEPR][KPR]P[KR]R[RK]NV[RK]IS[DKT]	1.1e-48	36	5
10	[DE][DI][LV]TD[IT][ED]WF[YF][LT][MV]S[VM]T[RF][ST]F[PS]A[GE]SG[AL]PG[KR][AS]YSSGA[HY]VW[LV][TS]G[AN]	1.4e-46	40	6

family. The Ka/Ks values of all homologous FcbHLH gene pairs were <1 (**Supplementary Table 5**), suggesting negative selection.

The collinearity analysis identified 121 orthologs between *F. carica* and *F. hispida*, and 119 orthologs between *F. carica* and *F. microcarpa*, suggesting similar evolutionary distances between edible fig and the two evergreen *Ficus* species. There were two and seven isozymes between fig and *F. hispida* or *F. microcarpa*, respectively, indicating that evolution between fig and *F. hispida* tended to involve gene replication. Seventeen FcbHLH genes were not found to have a collinear relationship with either of the two other *Ficus* species, indicating possible unique bHLHs in the evolution of fig. A total 73 and 126 orthologous gene pairs were identified between fig and *Arabidopsis*, and between fig and grape, respectively (**Figure 2C**), indicating a closer homologous evolutionary relationship of the fig bHLH gene family with grape than with *Arabidopsis*. *FcbHLH40* (s00118g09121.t1) and *FcbHLH54* (s00307g15448.t1) only showed a collinear relationship with the two other *Ficus* species; both belonged to the VIIIb + c subgroup, indicating that this subgroup was relatively conserved in the evolution of *Ficus* plants. Detailed results of the analysis are shown in **Supplementary Table 6**.

Expression Pattern of *FcbHLH*s in Fruit

Among the 118 FcbHLH genes, 72 were at FPKM > 10 in at least a sample of the peel and female flower tissue at different stages of fig fruit development (**Figure 3**). Fifteen *FcbHLH*s from eight subfamilies demonstrated FPKM > 100, with subgroup XII leading the list with three members (*FcbHLH4*, *FcbHLH31*, and *FcbHLH75*). All three of these genes were upregulated along female flower development; in the peel they continued to increase until the fruit started ripening, at which point their expression decreased. Members of the same subgroup could have different expression patterns: in subgroup VIIIb + c; for example, *FcbHLH54* and *FcbHLH83* were expressed in the late stage of female flower and peel development, whereas *FcbHLH56*, *FcbHLH91*, *FcbHLH81*, and *FcbHLH116* were specifically expressed in the early stage of peel development, and *FcbHLH40* was highly expressed in the early and middle stages of female flower development. Members of subfamily IIId + e, such as *FcMYC2*, *FcbHLH96*, *FcbHLH31*, and *FcbHLH4*, which are closely related to the JA signaling pathway, were clearly repressed during female flower and peel development.

"Purple-Peel" and "Green Peel" are a pair of bud mutant cultivars with a different peel color at fruit ripening (**Figure 4A**). The expression pattern of *FcbHLH*s during fruit development was consistent in the two cultivars: 64 members showed the same expression trend, with 20 upregulated and 44 downregulated *FcbHLH*s during fruit development (**Figure 4B**). In the peel of the ripe fruit, 51 *FcbHLH*s were highly expressed in "Green Peel," but only 35 members were highly expressed in "Purple-Peel." *FcbHLH17* of subgroup IIId + e and *FcbHLH35* of subgroup IIIc were upregulated in "Purple-Peel" and downregulated in "Green Peel" during fruit ripening, with the expression level of *FcbHLH35* in ripening-stage "Purple-Peel" fruit peel being significantly higher than that in its "Green Peel" counterpart (2.11-fold). The differential expression of *FcbHLH* family members in this pair of cultivars supported their different secondary metabolite contents (Wang et al., 2017).

Anthocyanin synthesis in fig peel is light-dependent, whereas in the female flower tissue it is not (**Figure 4C**). For the bagged fruit, 68 and 22 *FcbHLH*s demonstrated upregulation and downregulation in the peel of the mature fruit, respectively, of which *FcbHLH98* of subgroup Ib was downregulated by 1.24-fold and showed an increment in the female flower. *FcbHLH42* of subgroup IIIf was downregulated by 0.82-fold after bagging and might be involved in the light-dependent anthocyanin-synthesis pathway in the peel (**Figure 4D**).

Interaction Network Prediction of bHLHs Involved in Anthocyanin Biosynthesis

Among the 118 *FcbHLH*s, 16 were assigned to subfamily III and their phylogenetic distance is shown in **Figure 5A**. Among the 16 genes, only *FcbHLH42*, encoding a bHLH-2 protein, was clustered in the IIIf subgroup, which also included *ZmLC1*, *AtbHLH42* (TT8), *AtMYC1*, and other bHLHs that have been confirmed to be related to anthocyanin synthesis. *FcbHLH42* was most closely related to apple (*Md*)*bHLH3* and *VvMYC1*.

FcbHLH42 expression was upregulated by 1.68- and 1.62-fold at stages F3 and F4, when female flower color is developing, and upregulated by 1.99-fold at stage P6 of peel coloring (**Figure 3**). "Purple-Peel" fruit bagging led to the 1.06-fold

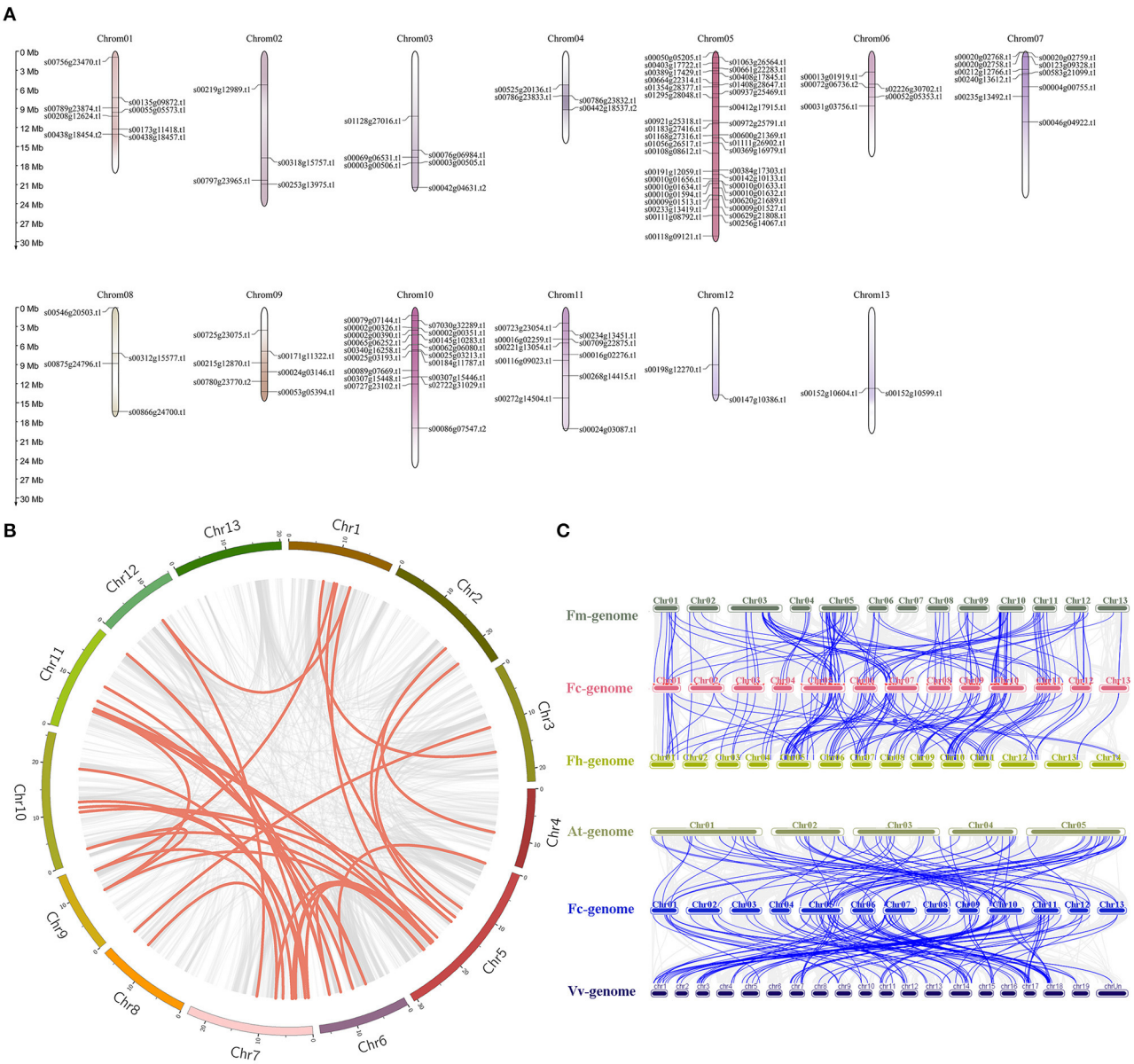

FIGURE 2 | Chromosomal locations and collinearity analysis of the FcbHLH gene family. **(A)** FcbHLH genes are marked on chromosomes; scale bar on the left indicates length of fig chromosome (Mb). **(B)** Collinearity analysis of FcbHLH genes; circle plot was created with the MCScanX tool. Identified collinear genes are linked by colored lines. **(C)** Collinearity relationship of bHLH genes among *Ficus carica* (Fc), *Ficus hispida* (Fh), *Ficus microcarpa* (Fm), *Arabidopsis thaliana* (At), and *Vitis vinifera* (Vv). Identified collinear genes are linked by blue lines.

repression of *FcbHLH42* compared with the control fruit. A relative expression analysis showed high synchronicity between *FcbHLH42* expression and the corresponding anthocyanin content in the female flower and peel of fig fruit. Moreover, in the peel of the ripening fruit, *FcbHLH42* was repressed in both "Purple-Peel" and "Green Peel" after bagging (**Figure 5B**).

The co-expression analysis is shown in **Supplementary Figure 4**. During the development of "Purple-Peel," MYBs (*FcCPC*, *FcMYB114*, *FcMYB5-1*, *FcMYB5-2*, etc.), WD40, and anthocyanin synthesis structural genes (*FcCHS*, *FcCHI*, *FcANS*, *FcUFGT1*, etc.), were strongly positively correlated with the expression of *FcbHLH42*. Specific co-expression combinations are listed in **Supplementary Table 9**.

Proteins with predicted interaction scores higher than 0.7 with FcbHLH42 are shown in **Figure 5C**. The red circles are R2R3–MYB genes, i.e., *TT1* (*MYB75*), *TT2*, *MYB5*, *MYB113*, *MYB114*, *MYB90*, *MYBL2*, and *TTG1* (*WD40*). The green circles represent key enzymes in the anthocyanin biosynthesis pathway, predicting that FcbHLH42 may be

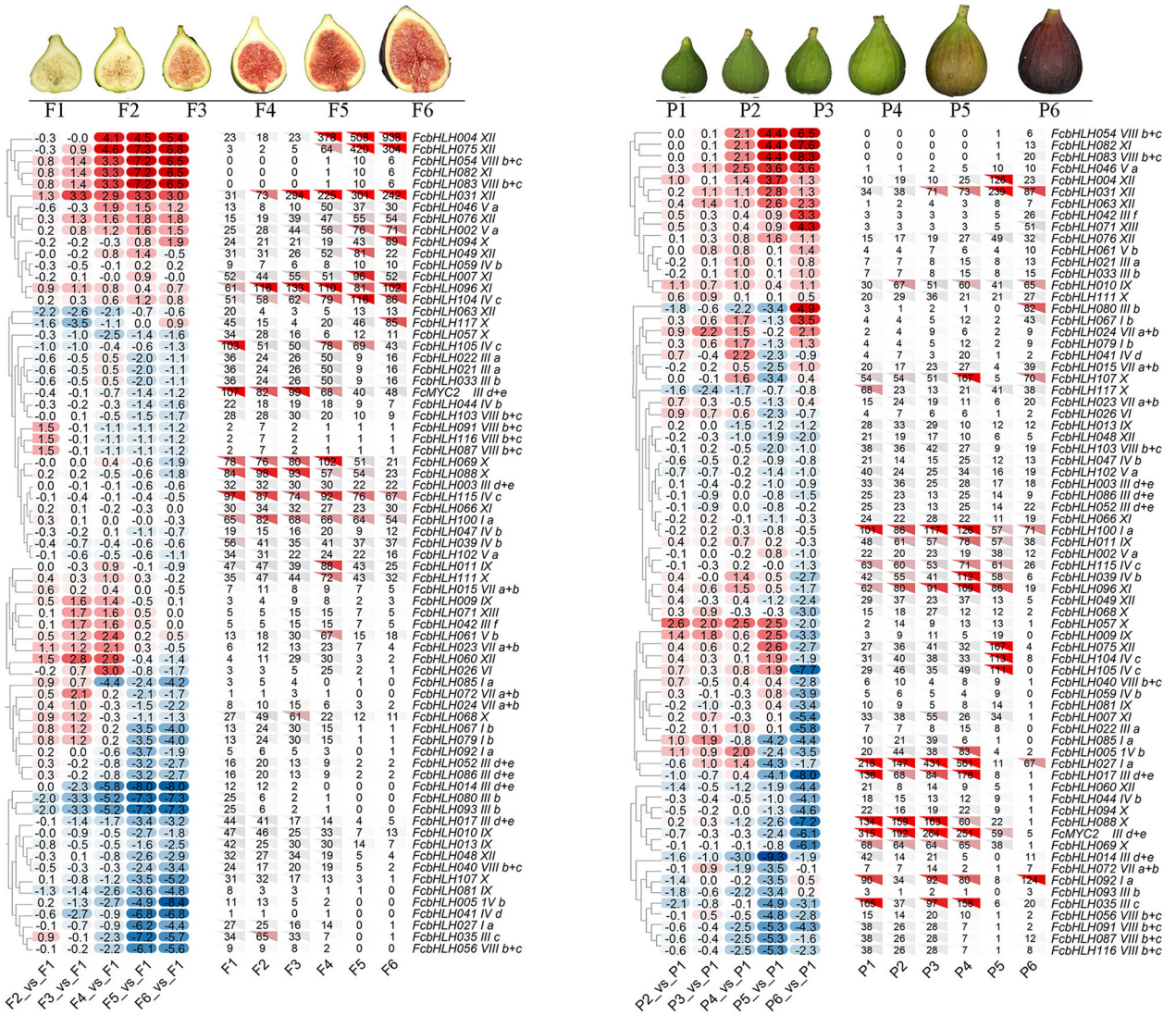

FIGURE 3 | Expression profile of FcbHLH genes in the female flower tissue and peel of fig fruit. Expression of FcbHLH genes is expressed by FPKM value and log_2FC. Hierarchical clustering method and average linkage method were used to construct the clustering tree. $Log_2FC > 0$ indicates upregulation, and $log_2FC < 0$ indicates downregulation. F1–F6 and P1–P6 represent the six stages of "Purple-Peel" female flower tissue and peel, respectively, during fig fruit development.

involved in the regulation and expression of DFR and LDOX (ANS).

FcbHLH3, *FcMYC2*, and *FcbHLH14* are clustered in subgroup IIId + e (**Figure 5A**). MYC2 is the core element of the COI1–JAZ–MYC2 complex that serves an important role in the JA signaling pathway in plants. The bHLHs in the IIId + e subgroup conservatively participate in the regulation of genes related to stress response and JA signaling. In our transcriptome data, *FcMYC2* was upregulated by 1.8-fold in the late-stage peel of the naturally grown fruit, whereas it was downregulated in the bagged fruit.

FcbHLH42 Promotes Anthocyanin Accumulation in Transgenic Tobacco by Interaction With MYB

A positive interaction between FaMYB10 andFcbHLH42 is shown by Y2H, along with weak interactions of FaMYB10 with FcbHLH3 and FcMYC2 (**Figure 6A**).The role of *FcbHLH42* in anthocyanin biosynthesis was analyzed further with transient transgenic technology using tobacco leaves. Leaves with combined overexpression of *FcbHLH42* and *FaMYB10* were purple, whereas those with the control *Agrobacterium* line-containing vector, or a single injection of *FaMYB10* or

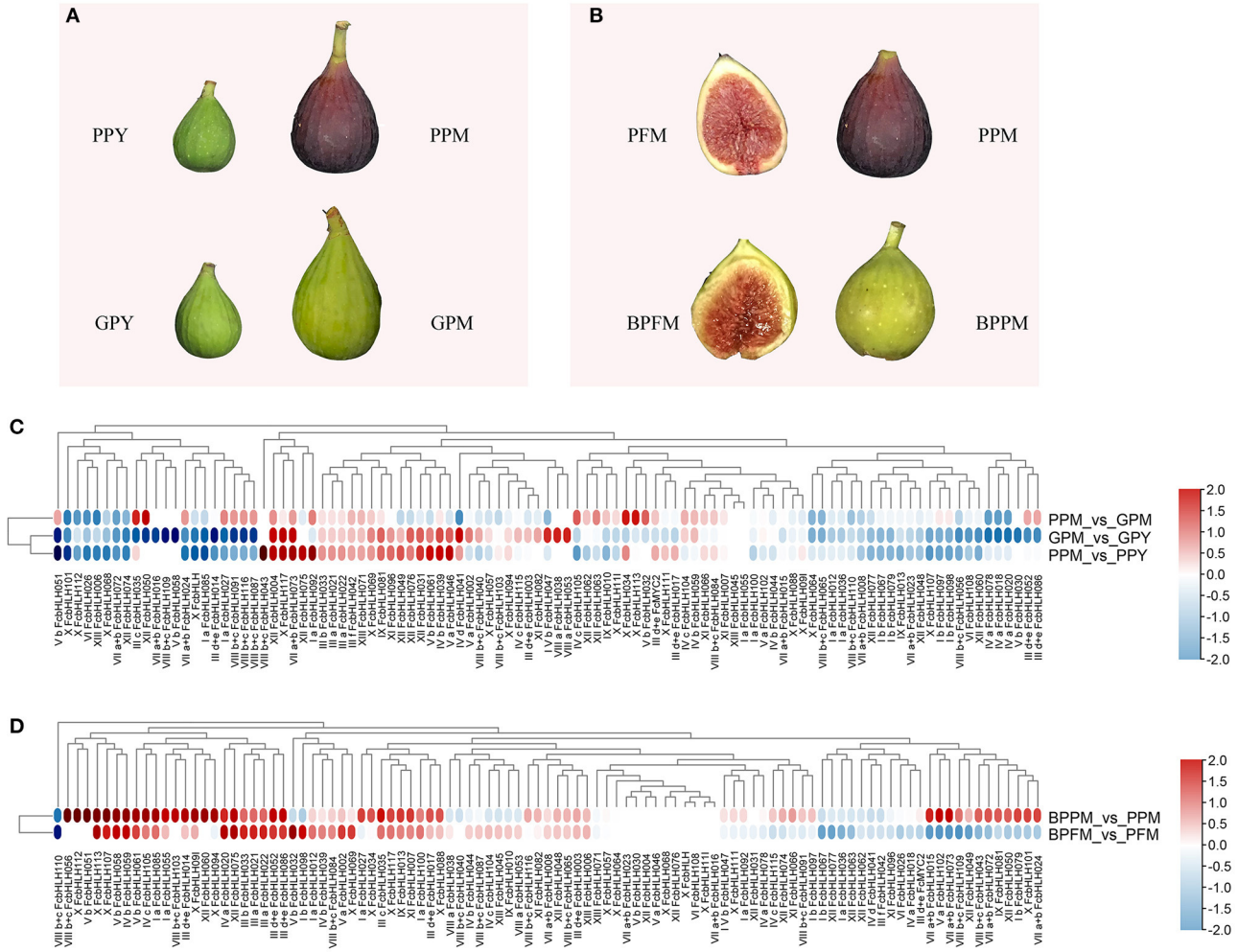

FIGURE 4 | Expression profiles of FcbHLH genes in different fig cultivars and under fruit-bagging treatment conditions. $Log_2FC > 0$ indicates upregulation, and $log_2FC < 0$ indicates downregulation. PPY and GPY represent the young-stage fruit peel of "Purple-Peel" and "Green Peel" cultivars, respectively; PPM and GPM represent the ripening-stage fruit peel of "Purple-Peel" and "Green Peel," respectively; PFM represents the ripening-stage female flower of "Purple-Peel"; BPFM and BPPM represent the ripening female flower and peel of "Purple-Peel" fruit, respectively, after bagging. **(A)** peel color of two fig cultivars. **(B)** the effect of fruit bagging on female flower and peel color. **(C)** expression comparison of FcbHLH genes. **(D)**, the effect of fruit bagging on the expression of FcbHLH genes.

FcbHLH42, were not (**Figure 6B**). The anthocyanin content following *FcbHLH42* + *FaMYB10* overexpression was also significantly higher than that of the control and the single transcription factor injections (**Figure 6C**). The transcription levels of four genes related to anthocyanin synthesis, i.e., *NbF3H*, *NbDFR*, *NbANS*, and *NbUFGT*, were all significantly increased in the *FcbHLH42* + *FaMYB10* combination. In the control group without color change, the expression levels of the four genes are low to undetectable (**Figures 6D–I**).

DISCUSSION

Gene Structure Provides Information on *FcbHLH* Evolutionary Relationships

The bHLH transcription factor family is the second largest family in plants and participates in various regulatory metabolic activities. Following the taxonomy of the *Arabidopsis* bHLH family, 118 FcbHLH genes were divided into 25 subgroups in this study, with most members in a particular subgroup bearing the same intron pattern and conserved motifs, suggesting the regulation of similar biofunctions (**Figure 1** and **Supplementary Table 1**).

The phylogenetic topology diagram revealed 10 highly conserved amino acid motifs in the 118 FcbHLHs. Signature Motifs 1 and 2 were found in almost all FcbHLH proteins and were always adjacent to each other, constituting the bHLH domain (**Figure 1B**). Most of the conserved motifs in a particular subgroup were similar, supporting the evolutionary classification of the FcbHLH gene family. The uniqueness and conservation of motifs in each subgroup indicate that the functions of the encoded bHLHs in that subgroup are stable, and that the specific

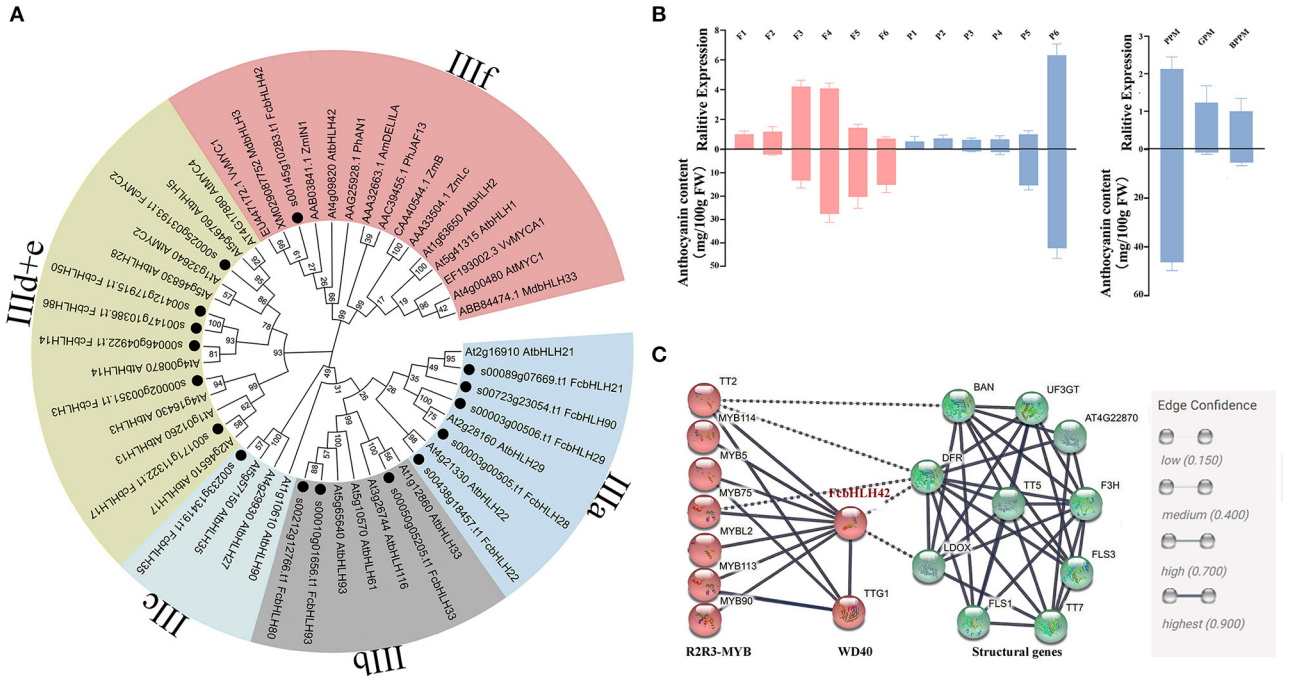

FIGURE 5 | Subgroup III FcbHLHs: phylogenetic tree analysis, expression profile, and interaction network of FcbHLH42. **(A)** NJ phylogenetic analysis of subgroup III FcbHLHs, AtbHLHs and bHLHs of other species. Different colors indicate different subgroups, and black dots indicate FcbHLHs. **(B)** Expression heat maps of 16 FcbHLH genes of subgroup III. After $\log_2$ conversion, $\log_2$FC > 0 indicates upregulation, and $\log_2$FC < 0 indicates downregulation. F1–F6 and P1–P6 represent the six stages of female flower and fruit peel development, respectively. GPY and GPM, peel of young and mature "Green-Peel" fruits, respectively. PPY and PPM, peel of young and mature "Purple-Peel" fruits, respectively. PFM, female flower of mature "Purple-Peel" fruit. BPPM and BPFM, peel and female flower of mature "Purple-Peel" fruits that were bagged at the young stage. **(C)** Interaction network of FcbHLH42 from the perspective of *Arabidopsis thaliana* homologous genes. Red represents transcription factors, and green represents key synthase genes.

motifs are pivotal in the implementation of the corresponding regulatory function.

The expansion of a gene family is mainly driven by gene duplication and subsequent diversification; tandem repeats and large-fragment replication are two major means of gene expansion (Vision et al., 2000). Tandem repeats refer to two adjacent genes on the same chromosome, and large-fragment replication events involve different chromosomes (McGowan et al., 2020). Chromosome localization indicates that FcbHLH genes are unevenly distributed (**Figure 2A**). It was speculated that 29 of the 118 FcbHLH genes had tandem repeat events, similar to the ratio reported for the potato (20 out of 124) (Wang et al., 2020) and tomato (14 out of 159) (Sun et al., 2015) bHLH families. The sequence of tandem replications was very similar in the conserved region, and their genetic relationship in the evolutionary tree was also very close. As a result, similar functions are expected.

bHLHs Expressed in Fig Fruit

The bHLH family plays a number of important regulatory roles in fruit-related growth and development, such as carpel, anther, and epidermal cell development, phytochrome signaling, flavonoid biosynthesis, and hormone signaling (Feller et al., 2011; Vanstraelen and Benkova, 2012). Our study revealed a universal expression of a large number of FcbHLHs in the fig fruit. Seventy-one *FcbHLH*s were transcribed in both female flower and peel, while 9 and 7 *FcbHLH*s demonstrated a peel- and female flower tissue-specific expression, respectively, suggesting important roles for bHLH family members in fig fruit development.

Among the 159 tomato bHLH genes, 11 displayed a tendency toward fruit-specific expression defined by >2-fold expression in fruit compared with other tissues. The bHLHs further showed a divergent expression during fruit development and ripening, and ethylene-responsive elements were found with the promoter of 7 bHLH genes (Sun et al., 2015). Three highly expressed *bHLH*s in the fig fruit, *FcbHLH4*, *FcbHLH31*, and *FcbHLH75*, all belonging to subgroup XII, were upregulated at fruit ripening. Subgroup XII has been shown to regulate brassinosteroid signaling, flower initiation, and cell elongation in other plants (Niu et al., 2017). The role of the highly expressed *FcbHLH*s needs to be further elucidated.

Basic helix–loop–helixes that have been suggested to regulate anthocyanin and proanthocyanin biosynthesis are often nominated according to their expression pattern and phylogenetic clustering. In the positively correlated co-expression network of *FcbHLH42* in subgroup IIIf, there were key structural genes for anthocyanin synthesis (*FcANS*, *FcUFGT*, etc.), and fig MYBs (*FcMYB114*, *FcMYB5*, etc.). The expression of grape *VvMYC1* has been reported to be correlated

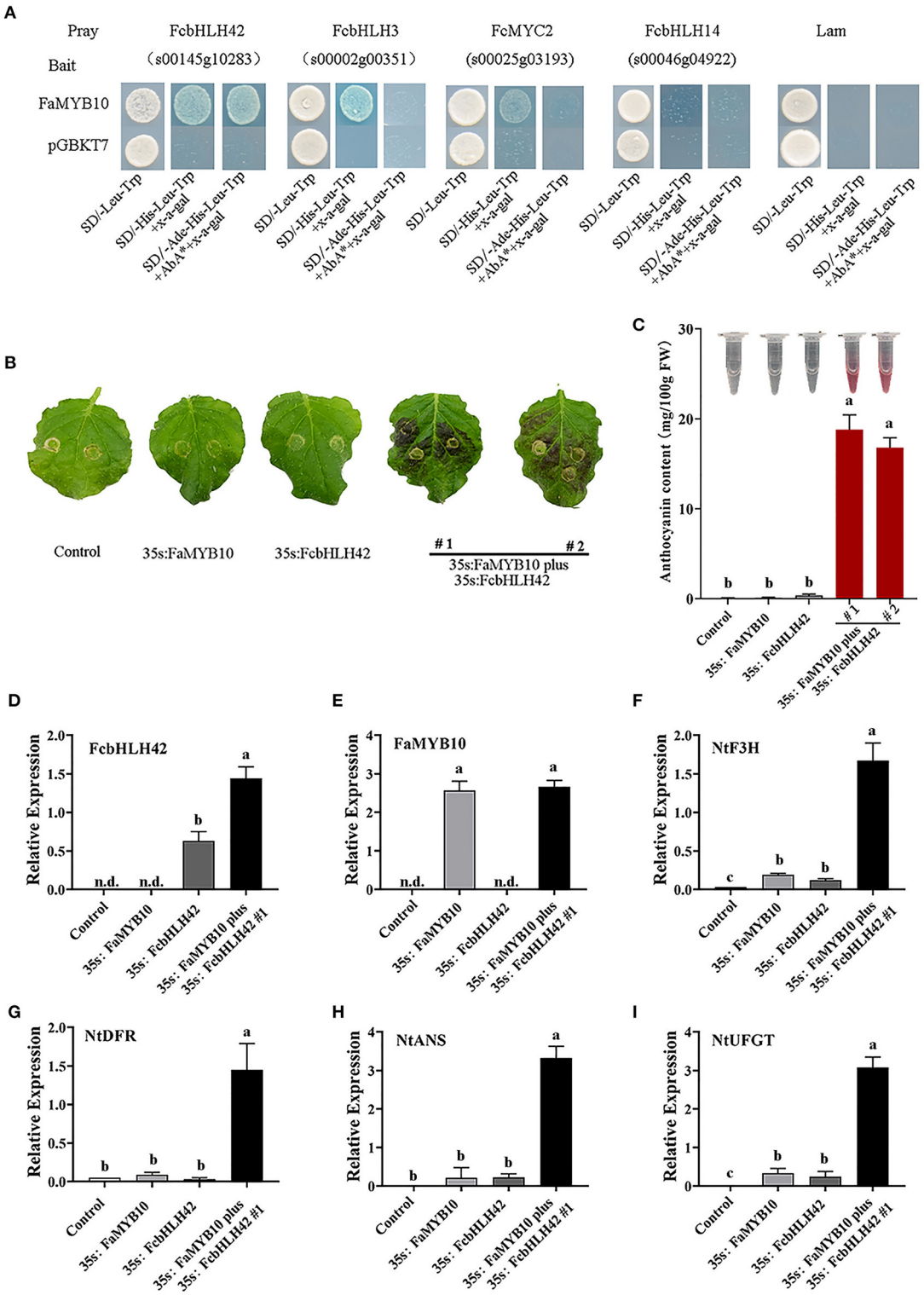

FIGURE 6 | Analysis of FcbHLH interactions with MYB by Y2H and transient overexpression of *FcbHLH42*. **(A)** Y2H tests for four FcbHLHs and FaMYB10 (R2R3–MYB). Interactions of FcbHLH42 (s00145g10283), FcbHLH3 (s00002g00351), FcMYC2 (s00023g03193), FcbHLH14 (s00046g04922), and FaMYB10. **(B)** Phenotype of tobacco leaves after infiltration. Tobacco (*N. benthamiana*) leaves were infiltrated with cDNA constructs corresponding to *FcbHLH42*, *FaMYB10*, and agroinfiltration solution (control). 35S: *FaMYB10* plus 35S: *FcbHLH42* #1 and #2 are two individual plants. **(C)** Color display after total anthocyanin extraction from the infiltrated tobacco leaves and the anthocyanin content in tobacco leaves after infiltration. **(D–I)** Expression of *FcbHLH*, *FaMYB10*, *NbF3H*, *NbDFR*, *NbANS*, and *NbUFGT* in the control, 35S:*FaMYB10*, 35S:*FcbHLH42,* and 35S:*FaMYB10* plus 35S: *FcbHLH42* #1 tobacco leaves after infiltration; n.d., not detected.

with the synthesis of anthocyanins and proanthocyanins in skin and seeds during berry development, suggesting that *VvMYC1* is involved in the regulation of anthocyanin and proanthocyanin synthesis in grapes. Similarly, the transient expression of *VvMYC1* and *VvMYBA1* induced anthocyanin synthesis in grapevine suspension cells (Hichri et al., 2010, 2011b). In blueberry, seven bHLH genes had differential expression patterns during fruit development (Zhao et al., 2019). Three jujube candidate bHLH genes, *ZjGL3a*, *ZjGL3b*, and *ZjTT8*, were suggested to be involved in anthocyanin biosynthesis and classified into subgroup III (Shi et al., 2019). Functional validation is required to confirm the specific role of these bHLHs.

FcbHLH Involvement in Fig Fruit Anthocyanin Biosynthesis

Only a few bHLH transcription factor genes, such as *VvMYC1*, *FvbHLH9*, *MdbHLH3*, and *MdbHLH33*, have been identified as being associated with anthocyanin biosynthesis in fleshy fruit (Espley et al., 2007; Hichri et al., 2011a; Li et al., 2020b). Our study revealed the first *bHLH* involved in fig fruit anthocyanin biosynthesis.

Previous studies have shown that bHLH genes of subgroup IIIf interact directly with anthocyanin biosynthesis. Previous reports have elucidated two functionally redundant *bHLH*s, *AmInc I* and *AmDel*, which directly regulate anthocyanin biosynthesis in *Antirrhinum majus* (Albert et al., 2021). In apple, *MdbHLH3* and *MdbHLH33* have been characterized in relation to anthocyanin biosynthesis (Xie et al., 2012). In figs, only *FcbHLH42* was assigned to subgroup IIIf. The selection of FcbHLH42 for a further study on its involvement in anthocyanin synthesis was also supported by its homologous clustering with confirmed anthocyanin biosynthesis-regulating *VvMYC1* and *MdbHLH3*, and the positive results from protein interaction and co-expression analyses. Although the function of *FcbHLH42* was confirmed by a series of experiments, including transient expression, in this study, further investigation could reveal other FcbHLHs that regulate anthocyanin biosynthesis in the fig fruit.

The FPKM values of *FcbHLH42* were 15 and 26 in the female flower tissue and peel during the stage of rapid anthocyanin content increase, but were not very high compared with those of the highly expressed FcbHLHs, or the FPKM values of the color development-regulating FcMYBs. *FcbHLH42* is a bHLH-2 gene. In addition to bHLH-2, bHLH-1 proteins could act in controlling anthocyanin biosynthesis (Zhang and Hulskamp, 2019). bHLH-1 and bHLH-2 transcription factors are suggested to function *via* distinct mechanisms (Pesch et al., 2015; Zhang et al., 2019).A previous transcriptome study has revealed that *FcMYB114*, *FcCPC*, *FcMYB21*, and *FcMYB123* might regulate anthocyanin biosynthesis in the fig fruit (Wang et al., 2019; Li et al., 2020a). WD40 and other MYB transcription factors are shown to be positively correlated with *FcbHLH42* in this study, which provides the basis for better analyses of various regulatory models of anthocyanin synthesis in figs. Moreover, our experiments showed that *FcbHLH3*, *FcMYC2*, and *FcbHLH14* are closely related to JAZ family members and have a predicted interaction with TT2/TTG1/MYB75 (**Supplementary Figure 3** and **Supplementary Table 7**). Their role in anthocyanin synthesis warrants a further study.

DATA AVAILABILITY STATEMENT

The datasets presented in this study can be found in online repositories. The names of the repository/repositories and accession number(s) can be found in the article/**Supplementary Material**.

AUTHOR CONTRIBUTIONS

MS and HM designed the experiments. MS and HW conducted the experiments. MS, HW, ZW, and HH analyzed the results and prepared the manuscript. HM and SC revised the manuscript. All authors read and approved the final manuscript.

FUNDING

This study was supported by the National Natural Science Foundation of China [31372007].

ACKNOWLEDGMENTS

We thank Professor George Lomonossoff from John Innes Centre for providing the HyperTrans vector system.

SUPPLEMENTARY MATERIAL

The Supplementary Material for this article can be found online at: https://www.frontiersin.org/articles/10.3389/fpls.2021.730692/full#supplementary-material

REFERENCES

Albert, N. W., Butelli, E., Moss, S. M. A., Piazza, P., Waite, C. N., Schwinn, K. E., et al. (2021). Discrete bHLH transcription factors play functionally overlapping roles in pigmentation patterning in flowers of Antirrhinum majus. *New Phytol.* 231, 849–863. doi: 10.1111/nph.17142

Albert, N. W., Davies, K. M., Lewis, D. H., Zhang, H., Montefiori, M., Brendolise, C., et al. (2014). A conserved network of transcriptional activators and repressors regulates anthocyanin pigmentation in eudicots. *Plant Cell* 26, 962–980. doi: 10.1105/tpc.113.122069

Allan, A. C., Hellens, R. P., and Laing, W. A. (2008). MYB transcription factors that colour our fruit. *Trends Plant Sci.* 13, 99–102. doi: 10.1016/j.tplants.2007.11.012

Bailey, P. C., Martin, C., Toledo-Ortiz, G., Quail, P. H., Huq, E., Heim, M. A., et al. (2003). Update on the basic helix-loop-helix transcription factor gene family in Arabidopsis thaliana. *Plant Cell* 15, 2497–2502. doi: 10.1105/tpc.151140

Carretero-Paulet, L., Galstyan, A., Roig-Villanova, I., Martinez-Garcia, J. F., Bilbao-Castro, J. R., and Robertson, D. L. (2010). Genome-wide classification and evolutionary analysis of the bHLH family of transcription factors in Arabidopsis, poplar, rice, moss, and algae. *Plant Physiol.* 153, 1398–1412. doi: 10.1104/pp.110.153593

Chen, C., Chen, H., Zhang, Y., Thomas, H. R., Frank, M. H., He, Y., et al. (2020). TBtools: An integrative toolkit developed for interactive analyses of big biological data. *Mol. Plant* 13, 1194–1202. doi: 10.1016/j.molp.2020.06.009

Espley, R. V., Hellens, R. P., Putterill, J., Stevenson, D. E., Kutty-Amma, S., and Allan, A. C. (2007). Red colouration in apple fruit is due to the activity of the MYB transcription factor, MdMYB10. *Plant J.* 49, 414–427. doi: 10.1111/j.1365-313X.2006.02964.x

Feller, A., Machemer, K., Braun, E. L., and Grotewold, E. (2011). Evolutionary and comparative analysis of MYB and bHLH plant transcription factors. *Plant J.* 66, 94–116. doi: 10.1111/j.1365-313X.2010.04459.x

Flaishman, M. A., Rodov, V., and Stover, E. (2008). The fig: botany, horticulture, and breeding. *Hort. Rev.* 34, 113–196. doi: 10.1002/9780470380147.ch2

Gonzalez, A., Zhao, M., Leavitt, J. M., and Lloyd, A. M. (2008). Regulation of the anthocyanin biosynthetic pathway by the TTG1/bHLH/Myb transcriptional complex in Arabidopsis seedlings. *Plant J.* 53, 814–827. doi: 10.1111/j.1365-313X.2007.03373.x

Guo, C., Guo, R., Xu, X., Gao, M., Li, X., Song, J., et al. (2014). Evolution and expression analysis of the grape (*Vitis vinifera* L.) WRKY gene family. *J. Exp. Bot.* 65, 1513–1528. doi: 10.1093/jxb/eru007

Guo, X. J., and Wang, J. R. (2017). Global identification, structural analysis and expression characterization of bHLH transcription factors in wheat. *BMC Plant Biol.* 17:90. doi: 10.1186/s12870-017-1038-y

Heim, M. A., Jakoby, M., Werber, M., Martin, C., Weisshaar, B., and Bailey, P. C. (2003). The basic helix-loop-helix transcription factor family in plants: a genome-wide study of protein structure and functional diversity. *Mol. Biol. Evol.* 20, 735–747. doi: 10.1093/molbev/msg088

Hichri, I., Barrieu, F., Bogs, J., Kappel, C., Delrot, S., and Lauvergeat, V. (2011a). Recent advances in the transcriptional regulation of the flavonoid biosynthetic pathway. *J. Exp. Bot.* 62, 2465–2483. doi: 10.1093/jxb/erq442

Hichri, I., Deluc, L., Barrieu, F., Bogs, J., Mahjoub, A., Regad, F., et al. (2011b). A single amino acid change within the R2 domain of the VvMYB5b transcription factor modulates affinity for protein partners and target promoters selectivity. *BMC Plant Biol.* 11:117. doi: 10.1186/1471-2229-11-117

Hichri, I., Heppel, S. C., Pillet, J., Leon, C., Czemmel, S., Delrot, S., et al. (2010). The basic helix-loop-helix transcription factor MYC1 is involved in the regulation of the flavonoid biosynthesis pathway in grapevine. *Mol. Plant* 3, 509–523. doi: 10.1093/mp/ssp118

Kosugi, S., and Ohashi, Y. (2002). DNA binding and dimerization specificity and potential targets for the TCP protein family. *Plant J.* 30, 337–348. doi: 10.1046/j.1365-313x.2002.01294.x

Langfelder, P., and Horvath, S. (2008). WGCNA: an R package for weighted correlation network analysis. *BMC Bioinformatics* 9:559. doi: 10.1186/1471-2105-9-559

Larkin, M. A., Blackshields, G., Brown, N. P., Chenna, R., McGettigan, P. A., McWilliam, H., et al. (2007). Clustal W and Clustal X version 2.0. *Bioinformatics* 23, 2947–2948. doi: 10.1093/bioinformatics/btm404

Li, J., An, Y., and Wang, L. (2020a). Transcriptomic analysis of *Ficus carica*peels with a focus on the key genes for anthocyanin biosynthesis. *Int. J. Mol. Sci.* 21:1245. doi: 10.3390/ijms21041245

Li, X., Duan, X., Jiang, H., Sun, Y., Tang, Y., Yuan, Z., et al. (2006). Genome-wide analysis of basic/helix-loop-helix transcription factor family in rice and Arabidopsis. *Plant Physiol.* 141, 1167–1184. doi: 10.1104/pp.106.080580

Li, Y., Xu, P., Chen, G., Wu, J., Liu, Z., and Lian, H. (2020b). FvbHLH9 functions as a positive regulator of anthocyanin biosynthesis by forming a HY5-bHLH9 transcription complex in strawberry fruits. *Plant Cell Physiol.* 61, 826–837. doi: 10.1093/pcp/pcaa010

Ludwig, S. R., Habera, L. F., Dellaporta, S. L., and Wessler, S. R. (1989). Lc, a member of the maize R gene family responsible for tissue-specific anthocyanin production, encodes a protein similar to transcriptional activators and contains the myc-homology region. *Proc. Natl. Acad. Sci. U.S.A.* 86, 7092–7096. doi: 10.1073/pnas.86.18.7092

Massari, M. E., and Murre, C. (2000). Helix-loop-helix proteins: regulators of transcription in eucaryotic organisms. *Mol. Cell. Biol.* 20, 429–440. doi: 10.1128/MCB.20.2.429-440.2000

McGowan, J., O'Hanlon, R., Owens, R. A., and Fitzpatrick, D. A. (2020). Comparative genomic and proteomic analyses of three widespread Phytophthora species: *Phytophthora chlamydospora*, *Phytophthora gonapodyides* and *Phytophthora pseudosyringae*. *Microorganisms* 8:653. doi: 10.3390/microorganisms8050653

Mori, K., Shirasawa, K., Nogata, H., Hirata, C., Tashiro, K., Habu, T., et al. (2017). Identification of RAN1 orthologue associated with sex determination through whole genome sequencing analysis in fig (*Ficus carica* L.). *Sci. Rep.* 7:41124. doi: 10.1038/srep41124

Niu, X., Guan, Y., Chen, S., and Li, H. (2017). Genome-wide analysis of basic helix-loop-helix (bHLH) transcription factors in Brachypodium distachyon. *BMC Genomics* 18:619. doi: 10.1186/s12864-017-4044-4

Pesch, M., Schultheiss, I., Klopffleisch, K., Uhrig, J. F., Koegl, M., Clemen, C. S., et al. (2015). TRANSPARENT TESTA GLABRA1 and GLABRA1 compete for binding to GLABRA3 in Arabidopsis. *Plant Physiol.* 168, 584–597. doi: 10.1104/pp.15.00328

Pires, N., and Dolan, L. (2010). Origin and diversification of basic-helix-loop-helix proteins in plants. *Mol. Biol. Evol.* 27, 862–874. doi: 10.1093/molbev/msp288

Shi, Q., Li, X., Du, J., and Li, X. (2019). Anthocyanin synthesis and the expression patterns of bHLH transcription factor family during development of the Chinese jujube fruit (*Ziziphus jujuba* Mill.). *Forests* 10:346. doi: 10.3390/f10040346

Sparkes, I. A., Runions, J., Kearns, A., and Hawes, C. (2006). Rapid, transient expression of fluorescent fusion proteins in tobacco plants and generation of stably transformed plants. *Nat. Protoc.* 1, 2019–2025. doi: 10.1038/nprot.2006.286

Spelt, C., Quattrocchio, F., Mol, J. N., and Koes, R. (2000). Anthocyanin1 of petunia encodes a basic helix-loop-helix protein that directly activates transcription of structural anthocyanin genes. *Plant Cell* 12, 1619–1631. doi: 10.1105/tpc.12.9.1619

Sun, H., Fan, H. J., and Ling, H. Q. (2015). Genome-wide identification and characterization of the bHLH gene family in tomato. *BMC Genomics* 16:9. doi: 10.1186/s12864-014-1209-2

Tamura, K., Peterson, D., Peterson, N., Stecher, G., Nei, M., and Kumar, S. (2011). MEGA5: molecular evolutionary genetics analysis using maximum likelihood, evolutionary distance, and maximum parsimony methods. *Mol. Biol. Evol.* 28, 2731–2739. doi: 10.1093/molbev/msr121

Tang, H., Wang, X., Bowers, J. E., Ming, R., Alam, M., and Paterson, A. H. (2008). Unraveling ancient hexaploidy through multiply-aligned angiosperm gene maps. *Genome Res.* 18, 1944–1954. doi: 10.1101/gr.080978.108

Toledo-Ortiz, G., Huq, E., and Quail, P. H. (2003). The Arabidopsis basic/helix-loop-helix transcription factor family. *Plant Cell* 15, 1749–1770. doi: 10.1105/tpc.013839

Usai, G., Mascagni, F., Giordani, T., Vangelisti, A., Bosi, E., Zuccolo, A., et al. (2020). Epigenetic patterns within the haplotype phased fig (*Ficus carica* L.) genome. *Plant J.* 102, 600–614. doi: 10.1111/tpj.14635

Vanstraelen, M., and Benkova, E. (2012). Hormonal interactions in the regulation of plant development. *Annu. Rev. Cell Dev. Biol.* 28, 463–487. doi: 10.1146/annurev-cellbio-101011-155741

Vision, T. J., Brown, D. G., and Tanksley, S. D. (2000). The origins of genomic duplications in Arabidopsis. *Science* 290, 2114–2117. doi: 10.1126/science.290.5499.2114

Wang, D., Zhang, Y., Zhang, Z., Zhu, J., and Yu, J. (2010). KaKs_Calculator 2.0: a toolkit incorporating gamma-series methods and sliding window strategies. *Genomics Proteomics Bioinformatics* 8, 77–80. doi: 10.1016/S1672-0229(10)60008-3

Wang, H., Zhang, H., Yang, Y., Li, M., Zhang, Y., Liu, J., et al. (2020). The control of red colour by a family of MYB transcription factors in octoploid strawberry (Fragaria x ananassa) fruits. *Plant Biotechnol. J.* 18, 1169–1184. doi: 10.1111/pbi.13282

Wang, J., Hu, Z., Zhao, T., Yang, Y., Chen, T., Yang, M., et al. (2015). Genome-wide analysis of bHLH transcription factor and involvement in the infection by yellow leaf curl virus in tomato (Solanum lycopersicum). *BMC Genomics* 16:39. doi: 10.1186/s12864-015-1249-2

Wang, R., Zhao, P., Kong, N., Lu, R., Pei, Y., Huang, C., et al. (2018). Genome-wide identification and characterization of the potato bHLH transcription factor family. *Genes* 9:54. doi: 10.3390/genes9010054

Wang, Z., Cui, Y., Vainstein, A., Chen, S., and Ma, H. (2017). Regulation of fig (*Ficus carica* L.) fruit color: metabolomic and transcriptomic

analyses of the flavonoid biosynthetic pathway. *Front. Plant Sci.* 8:1990. doi: 10.3389/fpls.2017.01990

Wang, Z., Song, M., Li, Y., Chen, S., and Ma, H. (2019). Differential color development and response to light deprivation of fig (*Ficus carica* L.) syconia peel and female flower tissues: transcriptome elucidation. *BMC Plant Biol.* 19:217. doi: 10.1186/s12870-019-1816-9

Xie, X. B., Li, S., Zhang, R. F., Zhao, J., Chen, Y. C., Zhao, Q., et al. (2012). The bHLH transcription factor MdbHLH3 promotes anthocyanin accumulation and fruit colouration in response to low temperature in apples. *Plant Cell Environ.* 35, 1884–1897. doi: 10.1111/j.1365-3040.2012.02523.x

Yamasaki, K., Kigawa, T., Seki, M., Shinozaki, K., and Yokoyama, S. (2013). DNA-binding domains of plant-specific transcription factors: structure, function, and evolution. *Trends Plant Sci.* 18, 267–276. doi: 10.1016/j.tplants.2012.09.001

Yang, J., Gao, M., Huang, L., Wang, Y., van Nocker, S., Wan, R., et al. (2017). Identification and expression analysis of the apple (Malus x domestica) basic helix-loop-helix transcription factor family. *Sci. Rep.* 7:28. doi: 10.1038/s41598-017-00040-y

Zhai, Y., Cui, Y., Song, M., Vainstein, A., Chen, S., and Ma, H. (2021). Papain-like cysteine protease gene family in fig (Ficus carica L.): genome-wide analysis and expression patterns. *Front. Plant Sci.* 12:e681801. doi: 10.3389/fpls.2021.681801

Zhang, B., Chopra, D., Schrader, A., and Hulskamp, M. (2019). Evolutionary comparison of competitive protein-complex formation of MYB, bHLH, and WDR proteins in plants. *J. Exp. Bot.* 70, 3197–3209. doi: 10.1093/jxb/erz155

Zhang, B., and Hulskamp, M. (2019). Evolutionary analysis of MBW function by phenotypic rescue in Arabidopsis thaliana. *Front. Plant Sci.* 10:375. doi: 10.3389/fpls.2019.00375

Zhang, X., Wang, G., Zhang, S., Chen, S., Wang, Y., Wen, P., et al. (2020). Genomes of the banyan tree and pollinator wasp provide insights into fig-wasp coevolution. *Cell* 183, 875–889.e817. doi: 10.1016/j.cell.2020.09.043

Zhao, H., Wang, X., Zhu, D., Cui, S., Li, X., Cao, Y., et al. (2012). A single amino acid substitution in IIIf subfamily of basic helix-loop-helix transcription factor AtMYC1 leads to trichome and root hair patterning defects by abolishing its interaction with partner proteins in Arabidopsis. *J. Biol. Chem.* 287, 14109–14121. doi: 10.1074/jbc.M111.280735

Zhao, M., Li, J., Zhu, L., Chang, P., Li, L., and Zhang, L. (2019). Identification and characterization of MYB-bHLH-WD40 regulatory complex members controlling anthocyanidin biosynthesis in blueberry fruits development. *Genes* 10:70496. doi: 10.3390/genes10070496

Zimmermann, I. M., Heim, M. A., Weisshaar, B., and Uhrig, J. F. (2004). Comprehensive identification of Arabidopsis thaliana MYB transcription factors interacting with R/B-like BHLH proteins. *Plant J.* 40, 22–34. doi: 10.1111/j.1365-313X.2004.02183.x

Conflict of Interest: The authors declare that the research was conducted in the absence of any commercial or financial relationships that could be construed as a potential conflict of interest.

Publisher's Note: All claims expressed in this article are solely those of the authors and do not necessarily represent those of their affiliated organizations, or those of the publisher, the editors and the reviewers. Any product that may be evaluated in this article, or claim that may be made by its manufacturer, is not guaranteed or endorsed by the publisher.

frontiers in Plant Science

ORIGINAL RESEARCH
published: 11 November 2021
doi: 10.3389/fpls.2021.763139

Alcohol Acyltransferase Is Involved in the Biosynthesis of C6 Esters in Apricot (*Prunus armeniaca* L.) Fruit

*Wanhai Zhou[1], Wenbin Kong[2], Can Yang[3], Ruizhang Feng[1] and Wanpeng Xi[3]**

[1] Key Lab of Aromatic Plant Resources Exploitation and Utilization in Sichuan Higher Education, Yibin University, Yibin, China, [2] China Chongqing Agricultural Technology Extension Station, Chongqing, China, [3] College of Horticulture and Landscape Architecture, Southwest University, Chongqing, China

Short-chain esters derived from fatty acid contribute to the characteristic flavor of apricot fruit, and the biosynthesis of these compounds in fruit is catalyzed by alcohol acyltransferase (AAT). In this work, we investigated the AAT gene family via genome-wide scanning, and three AAT loci were identified in different linkage groups (LGs), with PaAAT1 (PARG22907m01) in LG7, PaAAT2 (PARG15279m01) in LG4, and PaAAT3 (PARG22697m01) in LG6. Phylogenetic analysis showed that PaAAT1 belongs to clade 3, while PaAAT2 and PaAAT3 belong to clade 1 and clade 2, respectively. In contrast, the three AAT genes present different expression patterns. Only PaAAT1 exhibited distinct patterns of fruit-specific expression, and the expression of PaAAT1 sharply increased during fruit ripening, which is consistent with the abundance of C4–C6 esters such as (*E*)-2-hexenyl acetate and (*Z*)-3-hexenyl acetate. The transient overexpression of PaAAT1 in Katy (KT) apricot fruit resulted in a remarkable decrease in hexenol, (*E*)-2-hexenol, and (*Z*)-3-hexenol levels while significantly increasing the corresponding acetate production ($p < 0.01$). A substrate assay revealed that the PaAAT1 protein enzyme can produce hexenyl acetate, (*E*)-2-hexenyl acetate, and (*Z*)-3-hexenyl acetate when C6 alcohols are used as substrates for the reaction. Taken together, these results indicate that PaAAT1 plays a crucial role in the production of C6 esters in apricot fruit during ripening.

Keywords: ***Prunus armeniaca*** **L., alcohol acyltransferase, fruit aroma, ester, apricot**

OPEN ACCESS

Edited by:
M. Teresa Sanchez-Ballesta, Instituto de Ciencia y Tecnología de Alimentos y Nutrición (ICTAN), Spain

Reviewed by:
Joaquín J. Salas, Instituto de la Grasa (IG), Spain
Yasuyuki Yamada, Kobe Pharmaceutical University, Japan

****Correspondence:***
Wanpeng Xi
xwp1999@zju.edu.cn

Specialty section:
This article was submitted to Plant Metabolism and Chemodiversity, a section of the journal Frontiers in Plant Science

Received: *23 August 2021*
Accepted: *13 October 2021*
Published: *11 November 2021*

Citation:
Zhou W, Kong W, Yang C, Feng R and Xi W (2021) Alcohol Acyltransferase Is Involved in the Biosynthesis of C6 Esters in Apricot (Prunus armeniaca L.) Fruit. Front. Plant Sci. 12:763139. doi: 10.3389/fpls.2021.763139

INTRODUCTION

Apricot (*Prunus armeniaca* L.) is a widely cultivated temperate fruit tree species with fruit containing many phytochemicals that are nutritionally valuable components of the human diet (Aubert and Chanforan, 2007). The fruits are appreciated by consumers for their unique flavor, to which aroma volatiles make an important contribution, together with sugars and organic acids (Balbontín et al., 2010; Chen J. et al., 2020). More than 300 volatiles have been identified from apricot fruit, including aldehydes, alcohols, ketones, lactones, terpenes, and esters (Cumplido-Laso et al., 2012). Among them, C6 aldehydes and alcohols offer a green-note aroma,

while esters and lactones are responsible for fruity aromas. Esters such as (*E*)-2-hexenyl acetate and (*Z*)-3-hexenyl acetate are considered to be key odorants influencing the flavor quality of apricot fruit (D'Auria, 2006; Fu et al., 2017). Changes in aroma-related volatiles were previously reported during apricot fruit development and postharvest ripening (Gonzalez et al., 2009; Xi et al., 2016). Aldehydes tend to decline in the fruit while esters increase under post-harvest treatments (Cumplido-Laso et al., 2012; Galaz et al., 2013).

Volatile esters can be divided into two groups: straight-chain esters and branched-chain esters. In general, straight-chain esters are mainly synthesized via the fatty acid lipoxygenase (LOX), α-oxidation, and β-oxidation pathways (Schwab et al., 2008), while branched-chain esters are derived from the amino acid pathway. In the LOX pathway, unsaturated fatty acids, such as linoleic (18:2) and linolenic acid (18:3), are regio- and enantio-selectively deoxygenated by LOX and produce hydroperoxide isomers, which are subsequently cleaved by hydroperoxide lyase (HPL) to form hexanal and hexenal, respectively. The aldehydes can then be reduced to the corresponding C6 alcohols by alcohol dehydrogenase (ADH). Alcohol acyltransferase (AAT) catalyzes the final linkage of an acyl moiety and an alcohol to form esters and, thus, is directly responsible for the production of esters (Goff and Klee, 2006). The β-oxidation of saturated fatty acids is the primary biosynthetic process providing short-chain alcohols and acyl coenzyme A (CoA) for ester formation (Schwab et al., 2008). During the process, acyl CoAs can be reduced by acyl CoA reductase to aldehyde, which is continually reduced by ADH to alcohol. Finally, the alcohols can be used to produce esters by alcohol acyltransferase (AAT) (Bartley et al., 1985; Kruse et al., 2020; Liu et al., 2020). As for the amino acid pathway, amino acids such as L-isoleucine, L-leucine, L-valine, and L-methionine are the precursors of acyl-CoAs, involved in alcohol esterification reactions catalyzed by AATs to produce branched-chain esters (D'auria et al., 2007; Gonda et al., 2010; El Hadi et al., 2013). Therefore, alcohol acyltransferase enzymes catalyze the last decisive step in volatile ester formation in fruit (Schwab et al., 2008).

AATs from plant species belong to the BAHD superfamily of acyltransferases (ATs), which are important tailoring enzymes that contribute to the biosynthesis of several terpenoids, esters, alkaloids, and flavonoids (Kruse et al., 2020). BAHD-AT was named after the first four biochemically characterized ATs, namely benzylalcohol *O*-acetyltransferase (BEAT), anthocyanin O-hydroxycinnamoyltransferase (AHCTs), anthranilate N-hydroxycinnamoyl/benzoyltransferase (HCBT), and deacetylvindoline 4-*O*-acetyltransferase (DAT) (Bontpart et al., 2015). The proteins contain one 14–17 β-strand and one 13–17 α-helix domain connected to a crossover loop, and a solvent channel runs through the protein molecule. During the reaction, the donor binds to the front side, while the acceptor binds to the back side (Wang et al., 2021). Both of the most conserved motifs HXXXD and DFGWG are necessary for the catalytic function. HXXXD is exposed to the solvent channel and directly participates in the reaction. The catalytic His residue is accessible from both sides of the channel, while the Asp residue points away from the active site (Ma et al., 2005; Molina and Kosma, 2015). During the catalytic reaction process, the acyl acceptor and donor firstly approach the protein through the solvent channel and bind initially to the active site. Then, the basic His residue (H162) deprotonates the hydroxyl or amino group of the acceptor to form an oxyanion. Next, the oxyanion conducts a nucleophilic attack on the carbonyl carbon of the acyl donor to form a tetrahedral intermediate. Finally, the intermediate deprotonates to release a CoA-SH molecule and to form a new ester or amide (Walker et al., 2013). As for the functional protein, His-162 plays a key role in triggering the reaction, while Thr-384 and Trp-386 are vital for stabilizing the tetrahedral transition state through hydrogen bonds.

The products of AATs are mostly volatile esters, which are the main source of fruit flavors (Wang et al., 2021). During ripening of Korla fragrant pears, the production of hexyl acetate was induced and positively corelated with AAT enzyme activity and expression level of the AAT gene (Chen J. et al., 2020). A relatively high level of enzyme activity in apple fruit at harvest was observed to be accompanied by high levels of ester accumulation (Defilippi et al., 2005a). In peach, positive correlations between ester contents and AAT activity were also observed during low temperature storage plus shelf-life at 20°C (Xi et al., 2012). With increasing genome data of fruit trees, several AATs have been identified, and many AATs related to ester metabolism have been functionally characterized, such as in apple (Gonzalez et al., 2009), strawberry (Gonzalez-Agueero et al., 2009), melon (Guenther et al., 2011), papaya (Kader, 2008; Balbontín et al., 2010), and kiwifruit (Li et al., 2006). Although the role of the AAT protein in regulation of volatile ester content has been most extensively investigated in these fruits, no information is available on the function and regulation of enzymes in apricot. In our previous study, we observed that the AAT enzyme activities of apricot fruit are related to ester formation (Xi et al., 2016). However, the specific gene family member responsible for ester formation is still not identified in apricot, and the specific mechanism is poorly understood.

In the present study, we performed a genome-wide analysis of AAT family genes to identify to the specific gene impacting volatile esters in apricot fruit. PaAAT1 was ascertained as a new candidate gene through bioinformation and expression-pattern analysis. The function of cloning full-length cDNAs was verified by transient overexpression, and recombinant expression in *Escherichia coli* was used to assay the abilities of these proteins for different alcohol substrates. Ultimately, we demonstrated that PaAAT1 can function in the biosynthesis of C6 volatile esters and contribute to the aroma of apricot.

RESULTS

Gene Structures and Conserved Motifs in Apricot

Three members of the AAT gene family were obtained from the apricot genome. Three AAT loci were identified in different linkage groups (LGs). PaAAT1 (PARG22907m01) was located in LG7, PaAAT2 (PARG15279m01) was in LG4, and PaAAT3

(PARG22697m01) was in LG6 (**Figure 1A**). *Cis*-acting element analysis identified a total of 12 *cis*-acting elements from three promoters (**Figure 1B**). Most of the *cis*-elements found were involved in the light response (TCT-motif, ACE, AE-box, G-box, Box 4, GT1-motif, ACTC-motif, GATA-motif, MIRE, and TCCC-motif). Some *cis*-elements were identified to be involved in anaerobic induction (ARE), meristem expression (CAT-box), and endosperm-specific negative expression (AACA-motif). Others were found to participate in responses to temperature (LTR), stress (TC-rich), and phytohormones, including auxin (TGA-element, AuxRR-core), methyl jasmonate (CGTCA-motif, TGACG-motif), salicylic acid (TCA-element), abscisic acid (ABRE), gibberellin (TATC-box and P-box), and auxin (AuxRR-core and TGA-element). The DNAs of PaAAT1-3 contained different numbers of nucleotides, with two exons and one intron (**Figure 1B**). PaAAT1-3 encodes 447, 449, and 461 amino acids, with 49.905, 50.334, and 50.936 Da, respectively. Motif analysis showed that motif 2, motif 4, motif 5, motif 6, motif 7, and motif 8 were highly conserved among all proteins and that their relative positions were nearly fixed; motif 2 was found only in PaAAT1 (**Figure 1B**).

Phylogenetic Relationships and Conserved Domain Analysis

In order to analyze the potential function, a phylogenetic tree comprising 16 AAT sequences from seven species (**Supplementary Table 1**) was generated showing three main subfamilies (clade 1, 2, 3) based on sequence conservation (**Figure 2A**), establishing a correlation between phylogenesis and functional properties of the encoded proteins. The PaAAT2 protein is clustered in clade 1 with strawberry (FaAAT1 and FaAAT1), banana (BanAAT1), and closely to melon (CmAAT4). The PaAAT3 protein is grouped in the same subfamily with melon (CmAAT1, CmAAT2)

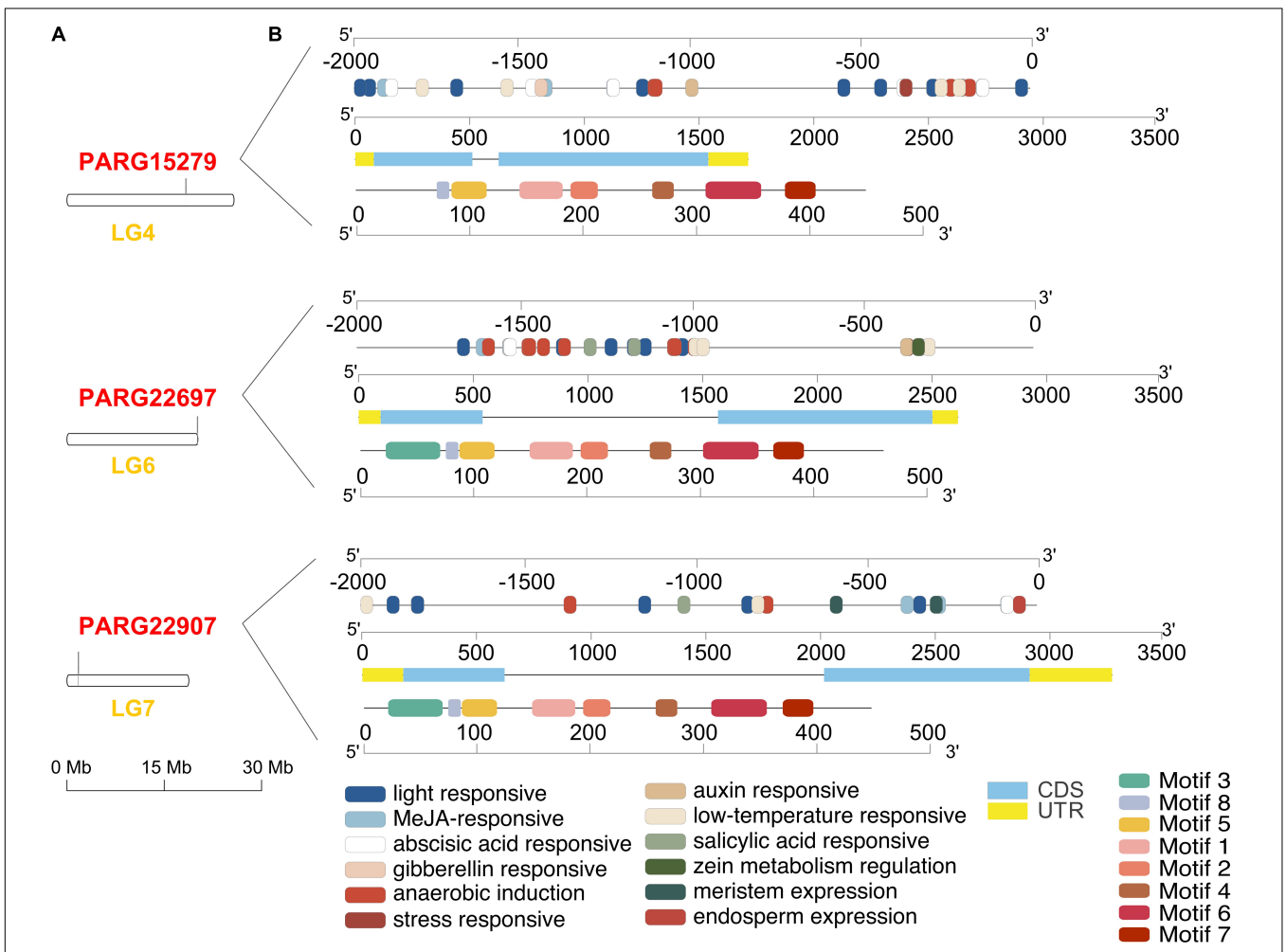

FIGURE 1 | Gene structure of alcohol acyltransferase in apricot. **(A)** Distribution of three AAT genes on the different linkage group (LG) of the apricot genome. **(B)** The upper section shows the *cis*-elements distributed in the promoters of apricot AAT genes, and the rectangles of different colors represent *cis*-elements with different functions. The middle section shows the untranslated 5′- and 3′-regions (UTR), pink boxes indicate coding sequence length (CDS), and black lines denote introns. The lower section provides the motif structure of the AAT genes.

and Clarkia breweri (CbBEBT), belonging to clade 2. The PaAAT1 protein is clustered in clade 3, similar to other AATs related to the synthesis of esters in peach (PpAAT1, PcAAT1), apple (MdAAT1, MdAAT2), and closely to PpAAT1. Multiple alignment of the three putative PaAATs and other characterized AAT genes from fruit or flower highlighted the conserved motif of PaAAT1-3 proteins containing an HXXXD motif in the middle of the protein and also another conserved motif DFGWD located at the carboxylic end of each protein.

Changes in Basic Quality Parameters and Volatile Esters During Fruit Ripening

To evaluate the status of fruit ripening, the fruit firmness, total soluble solids (TSS), and titratable acidity (TA) were determined during fruit development and ripening. As shown

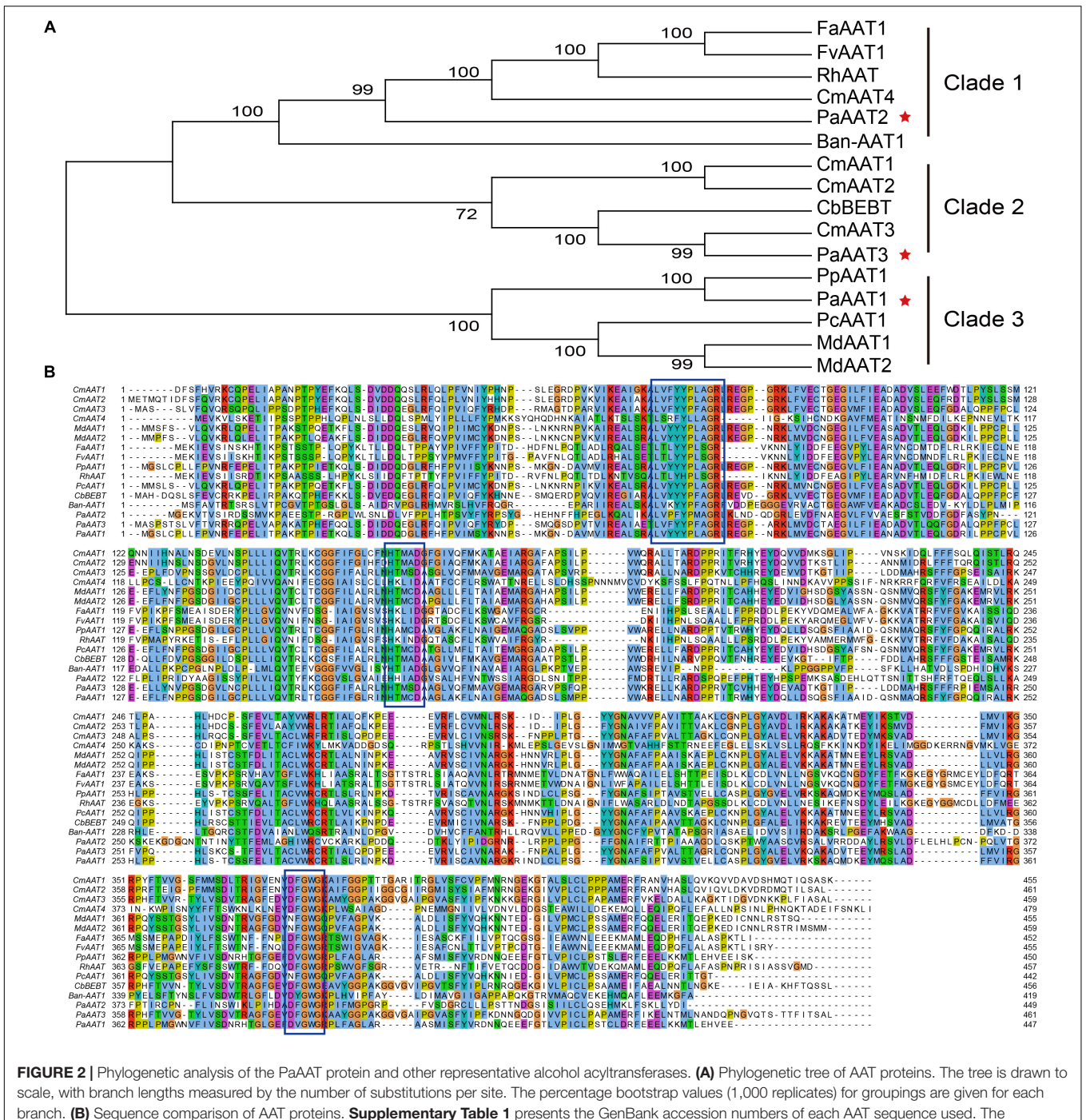

FIGURE 2 | Phylogenetic analysis of the PaAAT protein and other representative alcohol acyltransferases. **(A)** Phylogenetic tree of AAT proteins. The tree is drawn to scale, with branch lengths measured by the number of substitutions per site. The percentage bootstrap values (1,000 replicates) for groupings are given for each branch. **(B)** Sequence comparison of AAT proteins. **Supplementary Table 1** presents the GenBank accession numbers of each AAT sequence used. The five-pointed stars in **(A)** are the apricot AATs. The conserved motifs are framed in **(B)**.

in **Figure 3A**, the apricot fruit softened gradually from 42.2 to 4.3 N during ripening. Similarly, the TA content of tested fruit decreased significantly throughout the whole process ($p < 0.01$). Conversely, the TSS content of tested fruit increased to 17.1 ^{o}Brix during the ripening process. Based on the changes in firmness, TSS, and TA, the sampled fruit completely covered the whole development and ripening process. During the whole development, a total of 89 volatiles were detected in the tested fruit (**Figure 3B** and **Supplementary Figure 1**), and six esters were identified from the apricots: butyl acetate, 3-methylbutyl acetate, pentyl acetate, hexyl acetate, (*Z*)-3-hexenyl acetate, and (*E*)-2-hexenyl acetate (**Figure 3C**). The content of these six volatile esters in tested apricots increased remarkably during ripening ($p < 0.01$), especially hexyl acetate, (*Z*)-3-hexenyl acetate, and (*E*)-2-hexenyl acetate.

Changes in the Expression of PaAATs

To screen out the candidate genes involved in ester formation, the transcript levels of three *PaAATs* were detected during development and ripening using quantitative real-time PCR. The difference of transcript level was observed between the three PaAATs (**Figure 4**). A low transcript level was observed only for *PaAAT1* in the flower and fruitlet (**Figure 4A**). Even *PaAAT2* was not expressed in root and leave, and a low transcript level of *PaAAT2* was detected in the stem, flower and fruitlet, while *PaAAT3* was only expressed in the leave, flower, and fruitlet (**Figure 4A**). As for fruit, no transcript of *PaAAT1* was detected during early development, the expression of *PaAAT1* increased remarkably during fruit ripening ($p < 0.01$) (**Figure 4A**), and expression of *PaAAT2* and *PaAAT3* were kept at a low level throughout the whole developmental process (**Figure 4B**).

Transient Overexpression of PaAAT1 in "KT" Fruit

Transient overexpression analyses were performed with fruit peel before the turning stage to verify the functions of PaAAT1 related to volatile ester formation in apricot fruit. The expression of *PaAAT1* in agro-infiltrated fruit was analyzed by qRT-PCR on the third day after infiltration. We found that the transcript abundance of *PaAAT1* in PaAAT1-overexpressed fruit increased by 3.68–5.77-fold compared to the control fruit (**Figure 5A**). Compared with the control, higher chromatographic peaks of hexyl acetate (peak 4), (*Z*)-3-hexenyl acetate (peak 5), and (*E*)-2-hexenyl acetate (peak 6) were found in PaAAT1-overexpressed fruit, but no obvious significant chromatographic peaks of butyl

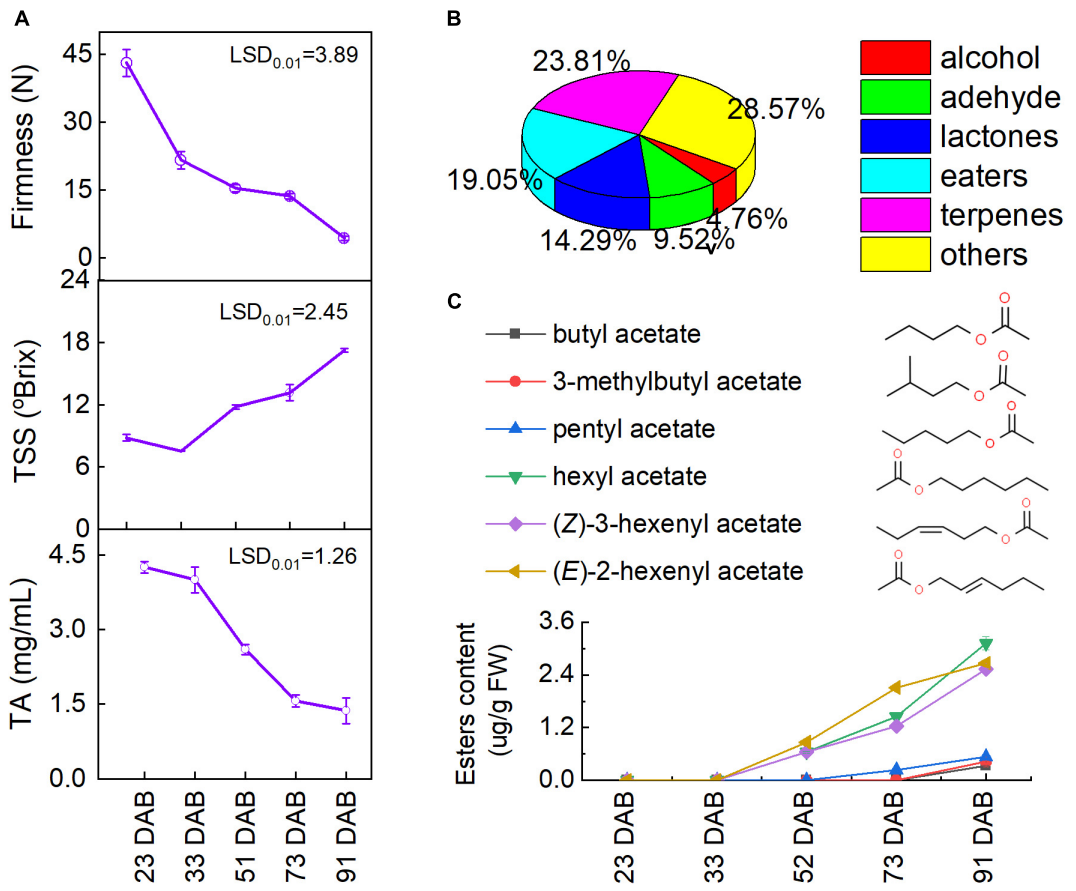

FIGURE 3 | Changes in volatile esters during fruit ripening: **(A)** fruit firmness, fruit weight, total soluble solids (TSS), and titratable acid (TA) contents; **(B)** ratio of all volatiles and **(C)** esters. LSD, least significant difference ($p < 0.01$).

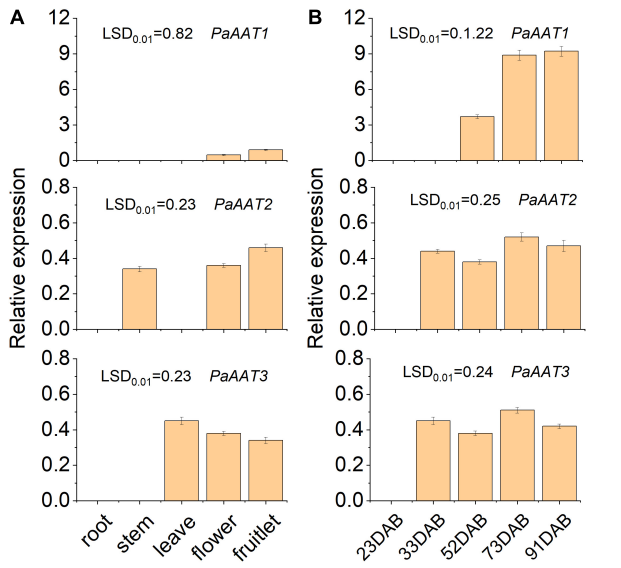

FIGURE 4 | Expression of three AATs in different tissues during apricot fruit ripening. **(A)** Expression of three AATs in different tissues. **(B)** Expression of three AATs in fruit during ripening. Error bars indicate the standard error from three biological replicates. LSD, least significant difference ($p < 0.01$).

acetate (peak 1), 3-methylbutyl acetate (peak 2), or pentyl acetate (peak 3) were found (**Figure 5B**). In the PaAAT1-overexpressed fruit, the butanol, 3-methybutanol, pentanol, hexenol, (*Z*)-3-hexenol, and (*E*)-2-hexenol contents significantly decreased ($p < 0.01$) (**Figure 5C**); on the contrary, the hexyl acetate, (*Z*)-3-hexenyl acetate, and (*E*)-2-hexenyl acetate contents significantly increased by 30, 56, and 18%, respectively, compared to the control ($p < 0.01$), while no significant content difference of butyl acetate, 3-methylbutyl acetate, or pentyl acetate were observed between PaAAT1-overexpressed fruit and the control fruit ($p < 0.01$) (**Figure 5C**).

In vitro Enzyme Properties and Activity of Recombinant PaAAT1

To test esterized activity of PaAAT1, a recombinant PaAAT1 protein purified from *E. coli* and *in vitro* experimentation was used to feed alcohol as substrate. Headspace solid-phase micro-extraction (HS-SPME) and gas chromatography (GC) were used to determine the products. A protein of about 50 kDa was obtained (**Figure 6A**). The recombinant PaAAT1 protein has the highest substrate affinity (Km) with (*E*)-2-hexenol (1.45 mM), followed by (Z)-3-hexenol (1.32 mM). The highest overall activity (Kcat/Km) was observed with hexyl acetate (**Figure 6B**). Six alcohols including butanol, 3-methybutanol, pentanol, hexenol, (*Z*)-3-hexenol, and (*E*)-2-hexenol were used as substrates for assays to assess PaAAT protein activity for producing corresponding ester. Low levels of esters were detected when butanol, 3-methybutanol, and pentanol were used as substrates for the reaction (**Figures 7A–C**). However, high corresponding peaks for hexyl acetate, (*Z*)-3-hexenyl acetate, and (*E*)-2-hexenyl acetate, eluting at 12.83, 14.24, and 15.06 min, respectively, were observed when hexenol, (*Z*)-3-hexenol, and (*E*)-2-hexenol were used as the substrate (**Figures 7D–F**).

DISCUSSION

Volatile esters play an important role in determining for flavor of a number of fruits, and are positive with consumer preference (Cao et al., 2019; Qian et al., 2019). Among them, short-chain esters that are derived fatty acids are the major class of volatile organic compounds (VOCs) contributing to the overall characteristic of ripe apricots (Livak and Schmittgen, 2001; Liu et al., 2019). However, considering the range of esters found in various fruit species, a wide variety of alcohol acyltransferases with various specificities are yet to be isolated, and little is known about the genes controlling ester biosynthesis in apricot fruit. The identification of an alcohol acyltransferase responsible for ester synthesis in apricot is a key step in understanding metabolic basis for regulatory aroma quality. Recently, the release of the genome facilitated the discovery of the key genes involved in the biosynthesis of these compounds in apricot. The present study was focused on identifying the AAT genes on a genome-wide scale, as well as characterizing their functions for volatile ester formation.

Plant BAHD-ATs constitute a large family of acyl CoA-utilizing enzymes, which contribute to the diversity of natural products, including small volatile esters and modified anthocyanins, as well as constitutive defense compounds and phytoalexins (Schwab et al., 2008; Peng et al., 2020). Most of these enzymes are *O*-acetyltransferases (*O*-ATs), and a few are N-acetyltransferases. *O*-ATs are further classified according to their acceptors: alcohols, flavonoids, quinic/shikimic acids, terpenoids, alkaloids, lipids, and sucrose (Wang et al., 2021). Many plant species genomes were published, and a number of BAHD-ATs have been identified. There are estimated to be about 88 genes encoding members of the BAHD family in *Arabidopsis* (Luo et al., 2007), and Oryza sativa contains more than 120 BAHD-ATs (Kumar et al., 2021). Xu et al. (2021) identified and characterized the expression of the 46 BAHD family genes during development, ripening, and stress response in banana (*Musa acuminata* Colla). A total of 717 BAHD-AT genes were identified from seven Rosaceae species, including the genomes of *Pyrus bretschneideri*, *Fragaria vesca*, *Malus domestica*, *Prunus avium*, *Pyrus communis*, *Prunus persica*, and *Rubus occidentalis*, producing final lists of 114, 89, 140, 124, 86, 81, and 68 putative BAHD genes (Liu et al., 2020). In the present study, based on conserved motif analysis, a total of 153 BAHD-AT genes were identified from the apricot genome (**Supplementary Table 2**). Recently, Wang et al. (2021) summarized biochemically characterized catalytic function and mechanisms of 141 ATs in plants. Among them, only 11 ATs can utilize benzoyl-containing alcohols or short/medium-chain alcohols as acyl acceptors. These results suggested that even the BAHD-AT family contains a large number of gene members in plants, and the members of this family have some unique roles. Only several AAT paralogs exist in many plant genomes, producing diverse ester volatiles associated with fruit flavor and flower aroma.

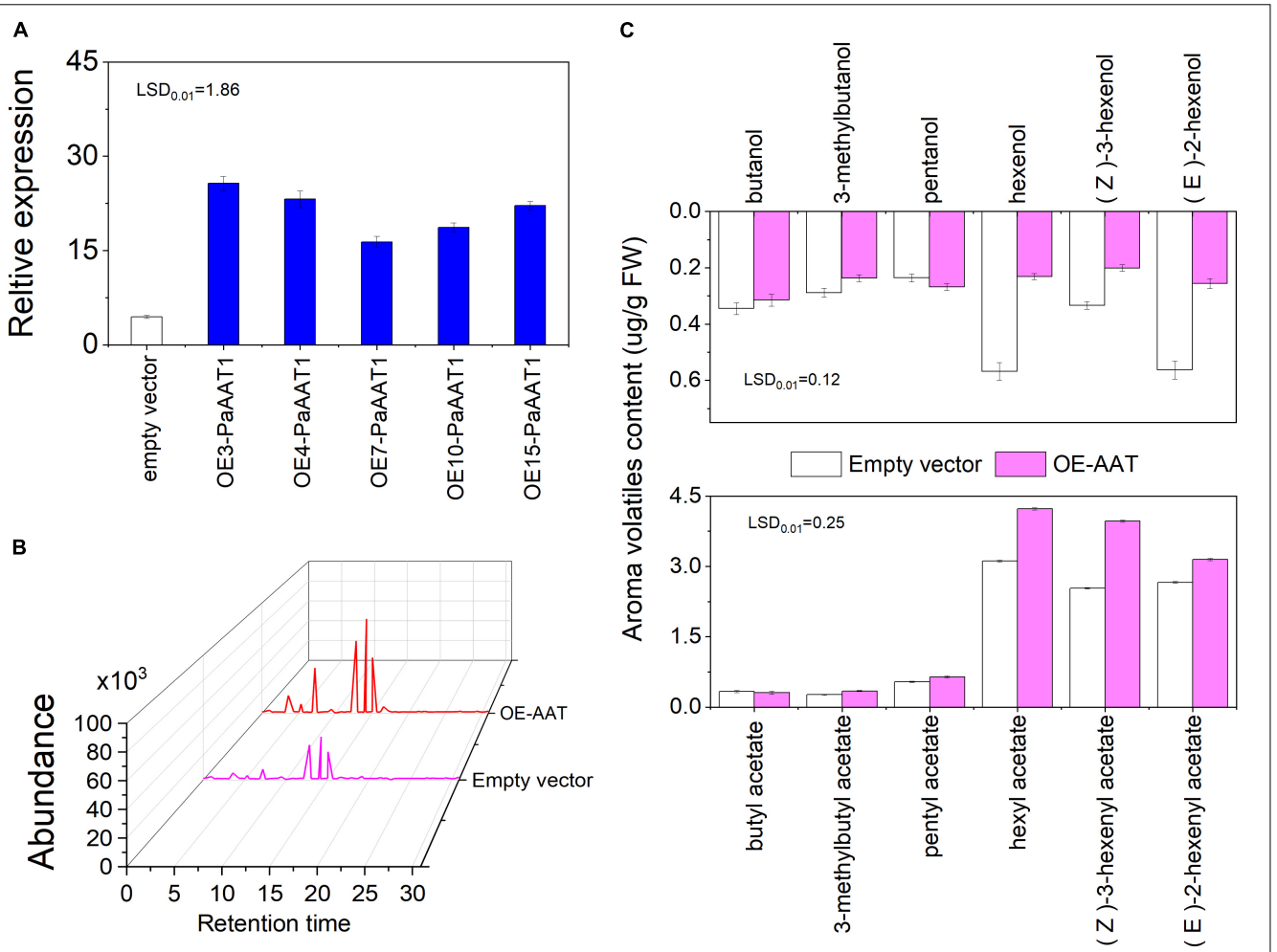

FIGURE 5 | Transient expression of PaAAT1 in KT fruit; **(A)** expression of PaAAT1 infiltrated with an empty vector and PaAAT1; **(B)** chromatogram of esters in peel infiltrated with an empty vector and PaAAT1; **(C)** volatile alcohols and esters emitted from the peel injected with an empty vector and PaAAT1. LSD, least significant difference ($p < 0.01$).

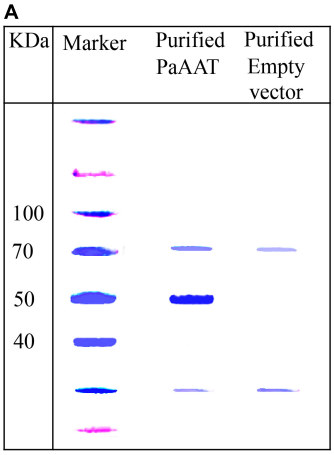

B

Substrate	K_m(mM)	K_{cat}(S^{-1})	K_{cat}/K_m
butanol	nd	nd	nd
3-methybutanol	nd	nd	nd
pentanol	nd	nd	nd
hexenol	0.82±0.11	78.19±2.13	95.35±3.23
(*E*)-2-hexenol	1.45±0.14	61.14±2.09	42.16±1.69
(*Z*)-3-hexenol	1.32±0.11	30.82±1.12	23.35±1.04

FIGURE 6 | The proteins purified from *E. coli* and its enzyme activity *in vitro*. **(A)** The SDS-PAGE analysis of recombinant PaAAT proteins purified from *E. coli*; **(B)** the kinetics of properties of PaAAT1 recombinant protein. Data are presented as the means ± SE. n.d. represents not detectable.

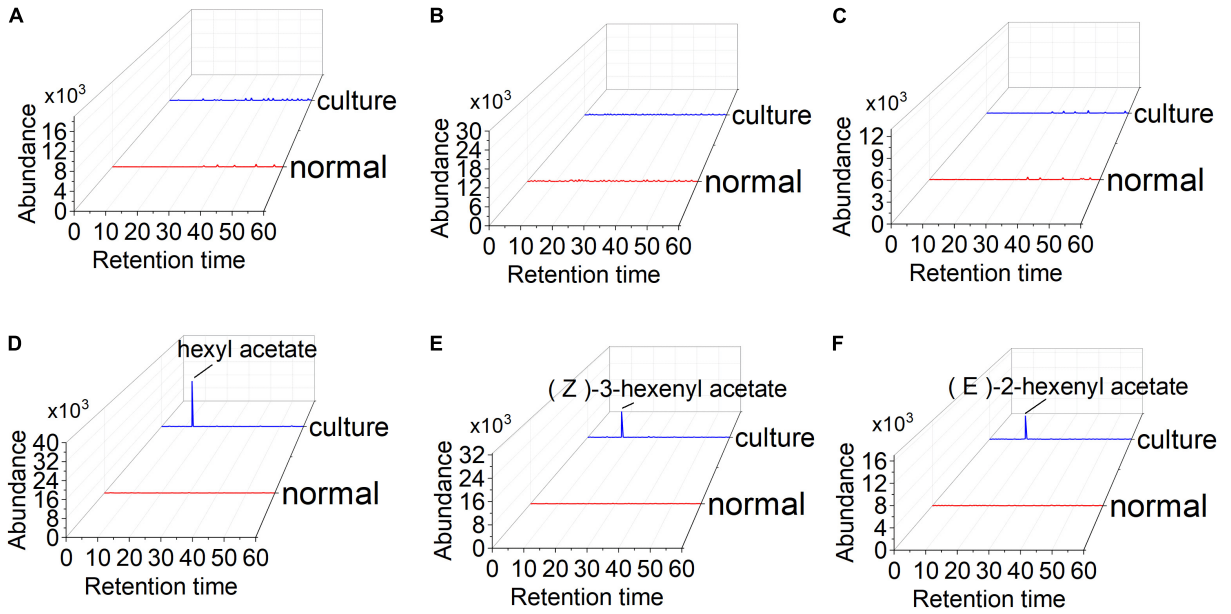

FIGURE 7 | Functional analysis of the PaAAT1 enzyme *in vitro*: **(A–F)** high pressure liquid chromatography (HPLC) analysis of the esters from the incubation of butanol, 3-methybutanol, pentanol, hexenol, (*E*)-2-hexenol, and (*Z*)-3-hexenol with the recombinant PaAAT1 protein. Culture represents PaAAT1 protein expressed in *Escherichia coli* added to the reaction system; normal means empty vector protein was added.

So far, many AAT genes expressed in fruit from this family have been earlier implicated in the biosynthesis of volatile esters (Goulet et al., 2015). The expression of *SlAAT1* substantially increases during ripening of the tomato fruit, in parallel with genes encoding other volatile-related enzymes, including SlCXE1 and lipoxygenase C (Goulet et al., 2012). Correlations between expression of flavor-related AAT genes and fruit ripening have also been established in other species including melon (El-Sharkawy et al., 2005), grape (Kalua and Boss, 2009), papaya (Balbontín et al., 2010), apple (Li et al., 2006), peach (Xi et al., 2012), *Fragaria ananassa*, and *Fragaria chiloensis* (Cumplido-Laso et al., 2012). However, of the five SlAAT genes, only SlAAT1 is highly expressed in the ripe fruit. In the present study, three PaAATs were identified from the apricot genome. To demonstrate the contribution of three PaAATs to ester production in apricot fruit, their expression levels were detected by qPCR. The results revealed that only *PaAAT1* was highly expressed in fruit. Simultaneously, the expression level of *PaAAT1* increased rapidly during the fruit ripening in parallel with volatile ester production. The expression pattern of *PaAAT1* was strongly linked with the accumulation of six esters, especially with the accumulation of hexyl acetate, (*Z*)-3-hexenyl acetate, and (*E*)-2-hexenyl acetate, which suggested that *PaAAT1* might play a vital role in the synthesis of esters in apricots.

Despite the low sequence homology found among the AAT genes identified to date, AAT proteins exhibited some common characteristics. All the fruit AAT genes identified to date encode proteins ranging from 419 to 479 amino acid residues, which corresponds to an average molecular weight of 48–55 kDa (Wang et al., 2021). The present study found that PaAAT1s are globular proteins with a size of 49.905 kDa, which is in good agreement with the molecular weight of the native AAT proteins purified in banana (40 kDa), strawberry (48 kDa), grape (50 kDa), and melon (50 kDa) (Hui et al., 2010). As for the complete protein, conserved motifs are generally the basis for recognition of homologous proteins across species boundaries. Most functionally characterized BAHD acyltransferases share two conserved motifs: a conserved HXXXD(G) motif and a less conserved DFGWG motif (D'Auria, 2006; Unno et al., 2007). For VlAMAT of the Concord grape cultivar, however, besides the basic motifs, another conserved LXXYYPXAGR motif existed near the N terminus of the sequence (75–84 residues). In the present study, PaAAT1 not only contained two common HTMCD (165–169 residues) in motif 1 and DVGWG (386–340 residues) conserved motifs in motif 7 but also contained the AAT-specific conserved motif LVYYYPLAGR (74–83 residues) in motif 8 (**Figures 1**, **2**). Even so, residue differences might significantly alter the catalytic activity of the AAT protein and dramatically affected the esterification reactions as reported for SAAT, VAAT, CmAAT1-4, and peach (D'Auria, 2006; Song et al., 2021). Based on this, we inferred that the difference of two conserved motifs HXXXD and LXXYYPXAGR for position X might be a main reason for the difference in esterification ability of PaAAT1-3.

Plants are diverse in volatile esters, and the diversity mainly depends on substrate specificities of their corresponding proteins. Similar to BAHD enzymes, most of the native and recombinant AAT proteins exhibit broad specificities of many substrates. In many fruits, different specificities of the multiple AAT proteins codified by the genes have been identified. In strawberry, FaAAT2 and FvAAT1 both influence the ester content of the fruit. FaAAT2 has been identified to be responsible for ester

biosynthesis in cultivated strawberry (*Fragaria* × *ananassa*); the enzyme had activity with C1–C8 straight-chain alcohols and aromatic alcohols in the presence of acetyl-CoA (Cumplido-Laso et al., 2012), whilst FvAAT function in wild strawberry (*Fragaria vesca*) and the FaAAT2 enzyme have a preference for C6–C10 aliphatic alcohols (Beekwilder et al., 2004). In apple (*Malus pumila*), at least two AAT enzymes are thought to produce ester volatiles (Souleyre et al., 2005; Li et al., 2006), and silencing AAT1 results in a strong decrease in some individual compound levels of propyl and butyl 2-methylbutanoate as well as propyl propanoate in ripe fruit (Souleyre et al., 2014; Yauk et al., 2017). Overexpressing MdAAT2 in transgenic tobacco leaves significantly increased the concentrations of methyl benzoate and methyl tetradecanoate, suggesting that MdAAT2 may use medium-chain fatty acyl CoA and benzoyl-CoA as acyl donors together with methanol acceptors as substrates (Li et al., 2008). Melon CmAAT1, CmAAT3, and CmAAT4 effectively account for the great diversity of esters formed in the fruit (El-Sharkawy et al., 2005; Galaz et al., 2013). As an aromatic alcohol AT, PhBPBT in *Petunia hybrida* displayed a broad spectrum for 13 acceptors, including: benzyl alcohol, 3-hydroxybenzyl alcohol, and 2-phenylethanol (Wang et al., 2021). PtSABT and PtBEBT from *Populus trichocarpa* catalyzed the formation of salicyl benzoate and benzyl benzoate with 75 and 70% conversion rates, respectively (Wang et al., 2021). All these examples illustrate the specificity in aroma production that each species can acquire while maintaining an overall ability to produce an array of esters. Peach PpAAT1 can produce esters and lactones by different acetyl (Song et al., 2021). In the present study, phylogenetic analysis revealed that PpAAT1 was close to PpAAT1, and overexpression PaAAT1 led to the remarkable content increase in hexyl acetate, (*Z*)-3-hexenyl acetate, and (*E*)-2-hexenyl acetate. Therefore, PpAAT1 might be the most important enzyme for volatile C6 ester biosynthesis in apricot fruit.

Previous work suggested that volatile esters or the expression of AAT genes is influenced by plant hormone treatment and specific transcription factors. The expression of genes from wild and cultivated strawberries (Aharoni et al., 2004), banana (Beekwilder et al., 2004), melon (El-Sharkawy et al., 2005), and grape (Wang and De Luca, 2005) is strongly induced during fruit ripening. Ethylene has proved to be a major regulator of the AAT activity in apple (Defilippi et al., 2005b; Schaffer et al., 2007), melon (Flores et al., 2002), kiwifruit (Zhang et al., 2009; Günther et al., 2015), pear (Li G. et al., 2014) and peach (Ortiz et al., 2010). Abscisic acid is also reported to be involved in aromatic ester biosynthesis related to ethylene in green apples (Wang et al., 2018). Salicylic acid and methyl jasmonate enhance ester regeneration in 1-MCP-treated apple fruit after long-term cold storage (Li et al., 2006). The expression of apple AAT (MdAAT2) is induced by salicylic acid (SA) in apple fruits and the MdAAT2 promoter's response to SA and ethylene in transgenic tobacco (Li P.-C. et al., 2014). Influence of methyl jasmonate (MeJA) on production of aroma-related esters in "Nanguo" pears was recently closely connected to ethylene biosynthesis and signal transduction (Yin et al., 2021). In the present study, an ABA, MeJA, and salicylic acid-response element (TCA) was found in the promoter of PaAATs (**Figure 1B**), suggesting that the three plant hormones might play a potential regulatory role in PaAAT expression and the ester biosynthesis pathway. At present, only few transcription factors have been found to regulate ester formation and AAT expression. In strawberry, overexpression of FveERF could activate the expression of the AAT gene and ester accumulation (Li et al., 2020), and volatile esters in postharvest strawberry were affected by the interaction of light and temperature (Fu et al., 2017). In the study, *cis*-elements of light response and temperature were found in the promoters of three PaAAT1s, suggesting that PaAAT1s are also involved in light and temperature regulation. These studies suggested that the ester metabolism was finely controlled by the complex network of environment factors, transcription factors, and AAT expression.

MATERIALS AND METHODS

Identification of Alcohol Acyltransferase Gene Family Members and Chromosomal Distribution

Sequences and annotations of the apricot (*Prunus armeniaca*) genome were obtained from Genome Database for Rosaceae (GDR).[1] We extracted the AATase domain (PF07247) from the Pfam database[2] to determine the AAT proteins using the HMMER 3.0 software (Finn et al., 2011). The *E*-value of the HMMER search results should be less than 0.001. Whether candidates could be the AAT gene family members was contingent on whether they had the conserved AAT domain, so Pfam[3] (Bateman et al., 2004), NCBI[4], or SMART[5] (Letunic et al., 2012) were required to examine the presence of the conserved AAT domain. All AAT genes were mapped to the chromosomes of apricot using TBtools (Chen C. et al., 2020).

Gene Structure Analysis and *Cis*-Element Prediction

The exon–intron structure of the AAT genes was obtained via the online tool Gene Structure Display Server (GSDS)[6]. MEME[7] was used to analyze the conserved motifs under the following parameters: motif site distribution with any number of repetitions and 20 as the maximum number of motifs. Other parameters used the default settings. The results were visualized using TBtools (Chen C. et al., 2020). The promoter sequences (2 kb upstream of the 5′ untranslated regions (UTR)) for all AAT genes were used for *cis*-element identification via submission to the PlantCARE database.[8] The molecular weight (MW) of

[1]https://www.rosaceae.org/

[2]http://pfam.xfam.org/

[3]http://pfam.xfam.org/search#tabview=tab1

[4]https://www.ncbi.nlm.nih.gov/Structure/cdd/wrpsb.cgi

[5]http://smart.embl-heidelberg.de/

[6]http://gsds.cbi.pku.edu.cn/

[7]http://meme-suite.org/tools/meme

[8]http://bioinformatics.psb.ugent.be/webtools/plantcare/html/

the AATs obtained was calculated using the ExPASy Compute pI/MW Program.[9]

Phylogenetic Analysis

The full-length apricot AAT protein sequences were obtained from the Genome Database for Rosaceae (see text footnote 1), and the amino acid sequences and accession numbers of AAT in strawberry, melon, banana, peach, Clrikia breweri, apple, papaya, and *P. communis*, as described (Yauk et al., 2017), were downloaded from GenBank.[10] The related sequence information is shown in **Supplementary Table 1**. The alignment of all sequences was performed with the MEGA version 10.1 software. The aligned result was used to construct a phylogenetic tree via the neighbor-joining (NJ) method with 1,000 bootstrap replicates. The results were visualized by the online tool iTOL[11] (Chen C. et al., 2020).

Plant Materials

The cultivar Katy apricot (KT) was grown in Liuchuan town, Jingyuan county, Bainyin, Gansu, China. "KT" apricot trees were planted in 2014 in rows in a north–south orientation, with a distance of 3-4 m between rows. Normal management and pest control were uniformly carried out according to local practices. Fifteen individual trees were marked; five trees were considered as one replicate, with a total of three biological replicates. Roots, leaves, and flowers were collected at the flowering phase. Fruits were harvested 23, 33, 51, 73, and 91 days after blossoming (DAB). After being transported to the laboratory on the day of picking, 90 fruits of uniform size and free of visible defects were collected at each stage between April 20th and August 10th; 20 fruits were used as one biological replicate. For each replicate, 10 of the 20 fruits were used to measure basic physiological indexes such as the firmness, total soluble solids (TSS), and titratable acidity (TA). After measuring the basic quality values, all materials were immediately frozen in liquid nitrogen and kept at −80°C until use.

Fruit Ripening Evaluation

A texture analyzer (TA-XT2i Plus, Stable Micro System, United Kingdom) fitted with a 7.9 mm diameter head was used to measure the fruit firmness according to the method of described by Xi et al. (2016). The rate of penetration was 1 mm s^{-1} with a final penetration depth of 10 mm. Two measurements were made on opposite sides at the equator of each fruit after the removal of a 1 mm-thick slice of skin. Ten fruits were considered one replicate, and three replicates were used for each sampling point. To determine the total soluble solids (TSS) values, three drops of juice from each slice were applied to an Atago PR-101α digital hand-held refractometer (ATAGO, Tokyo, Japan). The TSS value was read as the degree (°) Brix of the juice. Titratable acidity (TA) values were determined after the juice sample was diluted 100 times with pure water. The solution was transferred into a 250 mL beaker, which was placed over a magnetic stirrer to provide a continuous stirring of the sample solution. A pH meter probe was then immersed into the solution, and 0.1 N NaOH was added until the pH of the sample exceeded 8.1. TA was expressed in mg citric acid mL^{-1} pulp juice. All measurements were performed in triplicate.

Volatile Ester Analysis

Volatile esters were determined according to our previous method (Xi et al., 2012). Five grams of frozen flesh powder were homogenized with saturated NaCl solution and then incubated at 40°C for 30 min. Before the vials were sealed, 30 μL of 2-octanol (8.69 mg mL^{-1}) was added as an internal standard and stirred for 10 s with a vortex. For solid-phase microextraction (SPME) analysis, samples were equilibrated at 40°C for 30 min, and then volatile esters were extracted using a SPME needle with a 1 cm-long fiber coated with 65 μm divinylbenzene/carboxen/polydimethylsiloxane (DVB/CAR/PDMS) fibers (Supelco Co., Bellefonte PA, United States). The volatiles were subsequently desorbed over 5 min into the splitless injection port of the GC (Agilent 6890N equipped with a DB-WAX column, 0.32 mm, 30 m, 0.25 μm, J&W Scientific, Folsom CA, United States). The separation conditions were as follows: injector 230°C, initial oven temperature 34°C held for 2 min, increased by 0.033°C s^{-1} to 60°C, then increased by 0.083°C s^{-1} to 220°C and held for 2 min. Nitrogen was used as a carrier gas at 16.7 L s^{-1}. Volatiles were identified by comparison of retention times with those of authentic standards from Sigma-Aldrich, and their contents were quantified based on the standard curves of authentic compounds. Nitrogen was used as a carrier gas at a flow rate of 1 mL min^{-1}. Three biological replicates were used for each sample.

Real-Time Quantitative PCR Analysis

Total RNA was isolated and extracted from 1 g of fruit for each sample using a Tiangen reagent kit (Tiangen, Beijing, China). Contaminating genomic DNA was removed by RNase-free DNase I (Fermentas) treatment. The concentration of isolated total RNA was determined by the absorbance at 260 nm (A260) using a NanoDropND-3300 fluorospectrometer with Quant-iTRibo GreenRNA reagent (Invitrogen) following the instructions of the manufacturer, and the integrity was evaluated by electrophoresis on 1.0% agarose gels. The cDNA was synthesized from 3.0 μg of DNA-free RNA with RevertAid Premium reverse transcriptase (Fermentas) and oligo d(T)18 as primers followed the protocol of the manufacturer. Ribosomal RNA and actin gene expression were used as the normalization reference. Specific primers were designed using Primer5 (**Supplementary Table 3**). Gene expression levels were detected using an iQ5 instrument (Bio-Rad Laboratories, Inc., America) with a SYBR® Premix Ex Taq™ II Kit (TaKaRa Biotechnology (Dalian) Co, Ltd., China). The amplification program was as follows: 95°C for 1 min, followed by 40 cycles at 95°C for 20 s, 58°C for 20 s, and 72°C for 30 s. Each qRT-PCR analysis was performed in triplicate, and the mean value was used for the qRT-PCR analysis. The relative expression of the genes was calculated according to the $2^{-\Delta\Delta CT}$ method (Zhang et al., 2019).

[9]https://web.expasy.org/compute_pi/

[10]https://www.ncbi.nlm.nih.gov/

[11]https://itol.embl.de/index.shtml

Transient Overexpression in Apricot Fruit

The overexpression pMDC32 binary vector 49 was constructed according to the method described by Liu et al. (2019). The PaAAT1 coding sequence was amplified by PCR using the primers 5′ F: ATGGGTTCATTGTGCCCTCTA 3′ (forward) and 5′ CTCCTCGACATGCTCCAATGT 3′ (reverse) and cloned using a pCR8^{TM}/GW/TOPO TA cloning kit (Invitrogen). After the sequence was confirmed, the PCR product was inserted into the pMDC32 binary vector49 using Gateway LR Clonase II Enzyme mix (Invitrogen), thereby generating the overexpression vector, which was transformed into *Agrobacterium tumefaciens* GV3101. The transformed *A. tumefaciens* strain was cultured in a liquid MS medium to a final O.D. of 0.8. One mL of the suspension was then evenly injected into the "KT" fruit before the turning stage (51 days post anthesis). As a control, fruits were injected with *Agrobacterium tumefaciens* carrying an empty vector. Thirty fruits were injected with *A. tumefaciens* of PaAAT1 overexpression vector, and 10 were injected with the empty. Ester levels were measured 7–14 days after injection according to the abovementioned method. Three biological replicates were used for each sample.

In vitro PaAAT1 Enzyme Assay

The *in vitro* PaAAT1 protein expression and enzyme assay was performed according to the method described by a previous study (Cumplido-Laso et al., 2012). The full-length PaAAT1 cDNA from "KT" was amplified by RT-PCR and cloned into the bacterial expression vector pEXP5-CT/Topo (Invitrogen, California, United States) and was expressed in *Escherichia coli*. For recombinant PaAAT1 protein expression, 300 μL of transformed *E. coli* cells were cultured in fresh Luria–Bertani medium (300 mL) supplemented with ampicillin (μg/mL) at 37°C until OD600 = 0.6. The expression was induced with 1 mM isopropyl-b-D-thiogalactoside. After 12 h of growth at 16°C, cells were harvested by centrifugation, and the pellet was frozen for 15 min at −80°C. After suspension, the cells were sonicated on ice. The sonicated cells were centrifuged at 4°C and 20,000 × g for 20–30 min. The soluble protein fraction (supernatant) was incubated with GST-sepharose (Novogen) for at least 30 min at 4°C with continuous agitation and then centrifuged at 4°C and 800 × g for 3 min. The protein attached to the sepharose was washed and the sepharose-bound protein was released by incubating for 5 min in 200 μL of 1 × elution buffer at room temperature and centrifuged again at 800 × g for 5 min. The eluate was quantified by Bradford's method (Bradford, 1976) and analyzed by SDS-PAGE. The activity of recombinant semi-purified FaAAT2 protein was quantified by its ability to convert different alcohols and acyl-CoA substrates into the corresponding esters. PaAAT1 protein (2 μg) in 500 μL of total volume was used in the presence of 20 mM alcohol and 0.1 mM acyl-CoA in 50 mM TRIS-HCl buffer (pH 7.5) containing 10% (v/v) glycerol and 1 mM dithiothreitol (DTT). (*E*)-2-hexenol, (*Z*)-3-hexenol, hexenol, pentanol, 3-methybutanol, and butanol were used for the substrate test. Reactions were always initiated by adding semi-purified recombinant PaAAT1 protein and then incubated with continuous agitation at 30°C for 20 min. After incubation, 1 mM nonane was added as internal standard. The volatiles was extracted and analyzed with SPME-GC as described above. At least three biological replicates were performed for enzymatic assays.

CONCLUSION

In the study, three AAT genes were identified in the apricot genome. The gene structure and gene expression analysis indicated that *PpAAT1* is putatively associated with ester formation in apricots. The transient overexpression of PaAAT1 in apricot fruit resulted in a remarkable decrease in hexenol, (*E*)-2-hexenol, and (*Z*)-3-hexenol levels while significantly increasing the corresponding acetate production ($p < 0.01$). The substrate assay revealed that the PaAAT1 enzyme can produce hexenyl acetate, (*E*)-2-hexenyl acetate, and (*Z*)-3-hexenyl when C6 alcohols are used as substrates for the reaction. These results suggest that PpAAT1 is responsible for the biosynthesis of C6 esters in apricot during fruit ripening. However, the regulation mechanism of esters needs to be further explored in the future work.

DATA AVAILABILITY STATEMENT

The original contributions presented in the study are included in the article/**Supplementary Material**, further inquiries can be directed to the corresponding author/s.

AUTHOR CONTRIBUTIONS

WX conceptualized the experiments, reviewed, and edited the manuscript. WZ and WK performed the experiments. CY analyzed the data. WZ and RF prepared the manuscript. All authors contributed to the article and approved the submitted version.

FUNDING

This research was funded by the National Natural Science Foundation of China (No. 31872046) and Innovation Research team of Yibin University (Nos. 2017TD01 and 2018TD04).

ACKNOWLEDGMENTS

We thank Junhui Zhou (Department of Cell Biology and Molecular Genetics, University of Maryland) for comments on an earlier version of this manuscript.

SUPPLEMENTARY MATERIAL

The Supplementary Material for this article can be found online at: https://www.frontiersin.org/articles/10.3389/fpls.2021.763139/full#supplementary-material

REFERENCES

Aharoni, A., Giri, A. P., Verstappen, F. W., Bertea, C. M., Sevenier, R., Sun, Z., et al. (2004). Gain and loss of fruit flavor compounds produced by wild and cultivated strawberry species. *Plant Cell* 16, 3110–3131. doi: 10.1105/tpc.104.023895

Aubert, C., and Chanforan, C. (2007). Postharvest changes in physicochemical properties and volatile constituents of apricot (*Prunus armeniaca L.*). Characterization of 28 cultivars. *J. Am. Soc. Hortic. Sci.* 55, 3074–3082. doi: 10.1021/jf063476w

Balbontín, C., Gaete-Eastman, C., Fuentes, L., Figueroa, C. R., Herrera, R., Manriquez, D., et al. (2010). VpAAT1, a gene encoding an alcohol acyltransferase, is involved in ester biosynthesis during ripening of mountain papaya fruit. *J. Agric. Food Chem.* 58, 5114–5121. doi: 10.1021/jf904296c

Bartley, I. M., Stoker, P. G., Martin, A. D., Hatfield, S. G., and Knee, M. (1985). Synthesis of aroma compounds by apples supplied with alcohols and methyl esters of fatty acids. *J. Sci. Food Agric.* 36, 567–574. doi: 10.1002/jsfa.2740360708

Bateman, A., Coin, L., Durbin, R., Finn, R. D., Hollich, V., Griffiths-Jones, S., et al. (2004). The Pfam protein families database. *Nucleic Acids Res.* 32, D138–D141. doi: 10.1093/nar/gkh121

Beekwilder, J., Alvarez-Huerta, M., Neef, E., Verstappen, F. W., Bouwmeester, H. J., and Aharoni, A. (2004). Functional characterization of enzymes forming volatile esters from strawberry and banana. *Plant Physiol.* 135, 1865–1878. doi: 10.1104/pp.104.042580

Bontpart, T., Cheynier, V., Ageorges, A., and Terrier, N. (2015). BAHD or SCPL acyltransferase? What a dilemma for acylation in the world of plant phenolic compounds. *New Phytol.* 208, 695–707. doi: 10.1111/nph.13498

Bradford, M. M. (1976). A rapid and sensitive method for the quantitation of microgram quantities of protein utilizing the principle of protein-dye binding. *Anal. Biochem.* 72, 248–254. doi: 10.1016/0003-2697(76)90527-3

Cao, X., Xie, K., Duan, W., Zhu, Y., Liu, M., Chen, K., et al. (2019). Peach carboxylesterase PpCXE1 is associated with catabolism of volatile esters. *J. Agric. Food Chem.* 67, 5189–5196. doi: 10.1021/acs.jafc.9b01166

Chen, C., Chen, H., Zhang, Y., Thomas, H. R., Frank, M. H., He, Y., et al. (2020). TBtools: an integrative toolkit developed for interactive analyses of big biological data. *Mol. Plant.* 13, 1194–1202. doi: 10.1101/289660

Chen, J., Lü, J., He, Z., Zhang, F., Zhang, S., and Zhang, H. (2020). Investigations into the production of volatile compounds in Korla fragrant pears (*Pyrus sinkiangensis* Yu). *Food Chem.* 302:125337. doi: 10.1016/j.foodchem.2019.125337

Cumplido-Laso, G., Medina-Puche, L., Moyano, E., Hoffmann, T., Sinz, Q., Ring, L., et al. (2012). The fruit ripening-related gene FaAAT2 encodes an acyltransferase involved in strawberry aroma biogenesis. *J. Exp. Bot.* 63, 4275–4290. doi: 10.1093/jxb/ers120

D'Auria, J. C. (2006). Acyltransferases in plants: a good time to be BAHD. *Curr. Opin. Plant Biol.* 9, 331–340. doi: 10.1016/j.pbi.2006.03.016

D'auria, J. C., Pichersky, E., Schaub, A., Hansel, A., and Gershenzon, J. (2007). Characterization of a BAHD acyltransferase responsible for producing the green leaf volatile (*Z*)-3-hexen-1-yl acetate in *Arabidopsis thaliana*. *Plant J.* 49, 194–207. doi: 10.1111/j.1365-313X.2006.02946.x

Defilippi, B. G., Dandekar, A. M., and Kader, A. A. (2005a). Relationship of ethylene biosynthesis to volatile production, related enzymes, and precursor availability in apple peel and flesh tissues. *J. Agric. Food Chem.* 53, 3133–3141. doi: 10.1021/jf047892x

Defilippi, B. G., Kader, A. A., and Dandekar, A. M. (2005b). Apple aroma: alcohol acyltransferase, a rate limiting step for ester biosynthesis, is regulated by ethylene. *Plant Sci.* 168, 1199–1210. doi: 10.1016/j.plantsci.2004.12.018

El Hadi, M. A. M, Zhang, F.-J., Wu, F.-F., Zhou, C.-H., and Tao, J. (2013). Advances in fruit aroma volatile research. *Molecules* 18, 8200–8229. doi: 10.3390/molecules18078200

El-Sharkawy, I., Manríquez, D., Flores, F. B., Regad, F., Bouzayen, M., Latche, A., et al. (2005). Functional characterization of a melon alcohol acyl-transferase gene family involved in the biosynthesis of ester volatiles. Identification of the crucial role of a threonine residue for enzyme activity. *Plant Mol. Biol.* 59, 345–362. doi: 10.1007/s11103-005-8884-y

Finn, R. D., Clements, J., and Eddy, S. R. (2011). HMMER web server: interactive sequence similarity searching. *Nucleic Acids Res.* 39, W29–W37. doi: 10.1093/nar/gkr367

Flores, F., El Yahyaoui, F., De Billerbeck, G., Romojaro, F., Latche, A., Bouzayen, M., et al. (2002). Role of ethylene in the biosynthetic pathway of aliphatic ester aroma volatiles in *Charentais Cantaloupe* melons. *J. Exp. Bot.* 53, 201–206. doi: 10.1093/jexbot/53.367.201

Fu, X., Cheng, S., Zhang, Y., Du, B., Feng, C., Zhou, Y., et al. (2017). Differential responses of four biosynthetic pathways of aroma compounds in postharvest strawberry (*Fragaria x ananassa* Duch.) under interaction of light and temperature. *Food Chem.* 221, 356–364. doi: 10.1016/j.foodchem.2016.10.082

Galaz, S., Morales-Quintana, L., Alejandra Moya-Leon, M., and Herrera, R. (2013). Structural analysis of the alcohol acyltransferase protein family from *Cucumis melo* shows that enzyme activity depends on an essential solvent channel. *FEBS J.* 280, 1344–1357. doi: 10.1111/febs.12127

Goff, S. A., and Klee, H. J. (2006). Plant volatile compounds: sensory cues for health and nutritional value? *Science* 311, 815–819. doi: 10.1126/science.1112614

Gonda, I., Bar, E., Portnoy, V., Lev, S., Burger, J., Schaffer, A. A., et al. (2010). Branched-chain and aromatic amino acid catabolism into aroma volatiles in *Cucumis melo L.* fruit. *J. Exp. Bot.* 61, 1111–1123. doi: 10.1093/jxb/erp390

Gonzalez, M., Gaete-Eastman, C., Valdenegro, M., Figueroa, C. R., Fuentes, L., Herrera, R., et al. (2009). Aroma development during ripening of *Fragaria chiloensis* fruit and participation of an alcohol acyltransferase (FcAAT1) gene. *J. Am. Soc. Hortic. Sci.* 57, 9123–9132. doi: 10.1021/jf901693j

Gonzalez-Agueero, M., Troncoso, S., Gudenschwager, O., Campos-Vargas, R., Moya-Leon, M. A., and Defilippi, B. G. (2009). Differential expression levels of aroma-related genes during ripening of apricot (*Prunus armeniaca* L.). *Plant Physiol. Biochem.* 47, 435–440. doi: 10.1016/j.plaphy.2009.01.002

Goulet, C., Kamiyoshihara, Y., Lam, N. B., Richard, T., Taylor, M. G., Tieman, D. M., et al. (2015). Divergence in the enzymatic activities of a tomato and *Solanum pennellii* alcohol acyltransferase impacts fruit volatile ester composition. *Mol. Plant* 8, 153–162. doi: 10.1016/j.molp.2014.11.007

Goulet, C., Mageroy, M. H., Lam, N. B., Floystad, A., Tieman, D. M., and Klee, H. J. (2012). Role of an esterase in flavor volatile variation within the tomato clade. *Proc. Natl. Acad. Sci. U.S.A.* 109, 19009–19014. doi: 10.1073/pnas.1216515109

Guenther, C. S., Chervin, C., Marsh, K. B., Newcomb, R. D., and Souleyre, E. J. F. (2011). Characterisation of two alcohol acyltransferases from kiwifruit (*Actinidia spp.*) reveals distinct substrate preferences. *Phytochemistry* 72, 700–710. doi: 10.1016/j.phytochem.2011.02.026

Günther, C. S., Marsh, K. B., Winz, R. A., Harker, R. F., Wohlers, M. W., White, A., et al. (2015). The impact of cold storage and ethylene on volatile ester production and aroma perception in 'Hort16A'kiwifruit. *Food Chem.* 169, 5–12. doi: 10.1016/j.foodchem.2014.07.070

Hui, Y. H., Chen, F., Nollet, L. M., Guiné, R. P., Martín-Belloso, O., Mínguez-Mosquera, M. I., et al. (2010). *Handbook Of Fruit And Vegetable Flavors*. New York, NY: John Wiley and Sons, 129.

Kader, A. A. (2008). Flavor quality of fruits and vegetables. *J. Sci. Food Agric.* 88, 1863–1868. doi: 10.1002/jsfa.3293

Kalua, C. M., and Boss, P. K. (2009). Evolution of volatile compounds during the development of cabernet sauvignon grapes (*Vitis vinifera* L.). *J. Agric. Food Chem.* 57, 3818–3830. doi: 10.1021/jf803471n

Kruse, L. H., Weigle, A. T., Martínez-Gómez, J., Chobirko, J. D., Schaffer, J. E., Bennett, A. A., et al. (2020). Ancestral class-promiscuity as a driver of functional diversity in the BAHD acyltransferase family in plants. *bioRxiv* [Preprint]. doi: 10.1101/2020.11.18.385815

Kumar, G., Kumar, P., Kapoor, R., Lore, J. S., Bhatia, D., and Kumar, A. (2021). Characterization of evolutionarily distinct rice BAHD-Acyltransferases provides insight into their plausible role in rice susceptibility to *Rhizoctonia solani*. *Plant Genome* 14:e20140. doi: 10.1002/tpg2.20140

Letunic, I., Doerks, T., and Bork, P. (2012). SMART 7: recent updates to the protein domain annotation resource. *Nucleic Acids Res.* 40, D302–D305. doi: 10.1093/nar/gkr931

Li, D. P., Xu, Y. F., Xu, G. M., Gu, L. K., Li, D. Q., and Shu, H. R. (2006). Molecular cloning and expression of a gene encoding alcohol acyltransferase (MdAAT2) from apple. (cv. Golden Delicious). *Phytochemistry* 67, 658–667. doi: 10.1016/j.phytochem.2006.01.027

Li, D., Shen, J., Wu, T., Xu, Y., Zong, X., Li, D., et al. (2008). Overexpression of the apple alcohol acyltransferase gene alters the profile of volatile blends in transgenic tobacco leaves. *Physiol. Plant.* 134, 394–402. doi: 10.1111/j.1399-3054.2008.01152.x

Li, G., Jia, H., Li, J., Wang, Q., Zhang, M., and Teng, Y. (2014). Emission of volatile esters and transcription of ethylene-and aroma-related genes during ripening of 'Pingxiangli'pear fruit (*Pyrus ussuriensis* Maxim). *Sci. Hortic.* 170, 17–23. doi: 10.1016/j.scienta.2014.03.004

Li, P.-C., Yu, S.-W., Shen, J., Li, Q.-Q., Li, D.-P., Li, D.-Q., et al. (2014). The transcriptional response of apple alcohol acyltransferase (MdAAT2) to salicylic acid and ethylene is mediated through two apple MYB TFs in transgenic tobacco. *Plant Mol. Biol.* 85, 627–638. doi: 10.1007/s11103-014-0207-8

Li, Z., Wang, Z., Wang, K., Liu, Y., Hong, Y., Chen, C., et al. (2020). Co-expression network analysis uncovers key candidate genes related to the regulation of volatile esters accumulation in Woodland strawberry. *Planta* 252:55. doi: 10.1007/s00425-020-03462-7

Liu, B., Jiao, W., Wang, B., Shen, J., Zhao, H., and Jiang, W. (2019). Near freezing point storage compared with conventional low temperature storage on apricot fruit flavor quality (volatile, sugar, organic acid) promotion during storage and related shelf life. *Sci. Hortic.* 249, 100–109. doi: 10.1016/j.scienta.2019.01.048

Liu, C., Qiao, X., Li, Q., Zeng, W., Wei, S., Wang, X., et al. (2020). Genome-wide comparative analysis of the BAHD superfamily in seven Rosaceae species and expression analysis in pear (*Pyrus bretschneideri*). *BMC Plant Biol.* 20:14. doi: 10.1186/s12870-019-2230-z

Livak, K. J., and Schmittgen, T. D. (2001). Analysis of relative gene expression data using real-time quantitative PCR and the 2(T)(-Delta Delta C) method. *Methods* 25, 402–408. doi: 10.1006/meth.2001

Luo, J., Nishiyama, Y., Fuell, C., Taguchi, G., Elliott, K., Hill, L., et al. (2007). Convergent evolution in the BAHD family of acyltransferases: identification and characterization of anthocyanin acyltransferases from *Arabidopsis thaliana*. *Plant J.* 50, 678–695. doi: 10.1111/j.1365-313X.2007.03079.x

Ma, X., Koepke, J., Panjikar, S., Fritzsch, G. N., and StöCkigt, J. (2005). Crystal structure of vinorine synthase, the first representative of the BAHD superfamily. *J. Biol. Chem.* 280, 13576–13583. doi: 10.1074/jbc.M414508200

Molina, I., and Kosma, D. (2015). Role of HXXXD-motif/BAHD acyltransferases in the biosynthesis of extracellular lipids. *Plant Cell Rep.* 34, 587–601. doi: 10.1007/s00299-014-1721-5

Ortiz, A., Graell, J., López, M. L., Echeverría, G., and Lara, I. (2010). Volatile ester-synthesising capacity in 'Tardibelle'peach fruit in response to controlled atmosphere and 1-MCP treatment. *Food Chem.* 123, 698–704. doi: 10.1016/j.foodchem.2010.05.037

Peng, B., Xu, J., Cai, Z., Zhang, B., Yu, M., and Ma, R. (2020). Different roles of the five alcohol acyltransferases in peach fruit aroma development. *Plant Physiol. Biochem.* 145, 374–381. doi: 10.21273/jashs04951-20

Qian, X., Liu, Y., Zhang, G., Yan, A., Wang, H., Wang, X., et al. (2019). Alcohol acyltransferase gene and ester precursors differentiate composition of volatile esters in three interspecific hybrids of *Vitis labrusca*× *V*. Vinifera during berry development period. *Food Chem.* 295, 234–246. doi: 10.1016/j.foodchem.2019.05.104

Schaffer, R. J., Friel, E. N., Souleyre, E. J., Bolitho, K., Thodey, K., Ledger, S., et al. (2007). A genomics approach reveals that aroma production in apple is controlled by ethylene predominantly at the final step in each biosynthetic pathway. *Plant Physiol.* 144, 1899–1912. doi: 10.1104/pp.106.093765

Schwab, W., Davidovich-Rikanati, R., and Lewinsohn, E. (2008). Biosynthesis of plant-derived flavor compounds. *Plant J.* 54, 712–732. doi: 10.1111/j.1365-313x.2008.03446.x

Song, Z.-Z., Peng, B., Gu, Z.-X., Tang, M.-L., Li, B., Liang, M.-X., et al. (2021). Site-directed mutagenesis identified the key active site residues of alcohol acyltransferase PpAAT1 responsible for aroma biosynthesis in peach fruits. *Hortic. Res.* 8:32. doi: 10.1038/s41438-021-00461-x

Souleyre, E. J., Chagne, D., Chen, X., Tomes, S., Turner, R. M., Wang, M. Y., et al. (2014). The AAT 1 locus is critical for the biosynthesis of esters contributing to 'ripe apple'flavour in 'Royal Gala'and 'Granny Smith'apples. *Plant J.* 78, 903–915. doi: 10.1111/tpj.12518

Souleyre, E. J., Greenwood, D. R., Friel, E. N., Karunairetnam, S., and Newcomb, R. D. (2005). An alcohol acyltransferase from apple (cv. Royal Gala), MpAAT1, produces esters involved in apple fruit flavor. *FEBS J.* 272, 3132–3144. doi: 10.1111/j.1742-4658.2005.04732.x

Unno, H., Ichimaida, F., Suzuki, H., Takahashi, S., Tanaka, Y., Saito, A., et al. (2007). Structural and mutational studies of anthocyanin malonyltransferases establish the features of BAHD enzyme catalysis. *J. Biol. Chem.* 282, 15812–15822. doi: 10.1074/jbc.M700638200

Walker, A. M., Hayes, R. P., Youn, B., Vermerris, W., Sattler, S. E., and Kang, C. (2013). Elucidation of the structure and reaction mechanism of sorghum hydroxycinnamoyltransferase and its structural relationship to other coenzyme a-dependent transferases and synthases. *Plant Physiol.* 162, 640–651. doi: 10.1104/pp.113.217836

Wang, J., and De Luca, V. (2005). The biosynthesis and regulation of biosynthesis of concord grape fruit esters, including 'foxy'methylanthranilate. *Plant J.* 44, 606–619. doi: 10.1111/j.1365-313X.2005.02552.x

Wang, L., Chen, K., Zhang, M., Ye, M., and Qiao, X. (2021). Catalytic function, mechanism, and application of plant acyltransferases. *Crit. Rev. Biotechnol.* 41, 1–20. doi: 10.1080/07388551.2021.1931015

Wang, S., Saito, T., Ohkawa, K., Ohara, H., Suktawee, S., Ikeura, H., et al. (2018). Abscisic acid is involved in aromatic ester biosynthesis related with ethylene in green apples. *J. Plant Physiol.* 221, 85–93. doi: 10.1016/j.jplph.2017.12.007

Xi, W., Zhang, B., Shen, J., Sun, C., Xu, C., and Chen, K. (2012). Intermittent warming alleviated the loss of peach fruit aroma-related esters by regulation of AAT during cold storage. *Postharvest Biol. Technol.* 74, 42–48. doi: 10.1016/j.postharvbio.2012.07.003

Xi, W., Zheng, H., Zhang, Q., and Li, W. (2016). Profiling taste and aroma compound metabolism during apricot fruit development and ripening. *Int. J. Mol. Sci* 17:998. doi: 10.3390/ijms17070998

Xu, Y., Tie, W., Yan, Y., Xu, B., Liu, J., Li, M., et al. (2021). Identification and expression of the BAHD family during development, ripening, and stress response in banana. *Mol. Biol. Rep.* 48, 1127–1138. doi: 10.1007/s11033-020-06132-9

Yauk, Y. K., Souleyre, E. J., Matich, A. J., Chen, X., Wang, M. Y., Plunkett, B., et al. (2017). Alcohol acyltransferase 1 links two distinct volatile pathways that produce esters and phenylpropenes in apple fruit. *Plant J.* 91, 292–305. doi: 10.1111/tpj.13564

Yin, X. C., Ji, S. J., Cheng, S. C., Zhou, Q., Zhou, X., Luo, M. L., et al. (2021). Methyl jasmonate alleviates the reduced release of aroma-related esters in 'Nanguo'pears by regulating ethylene biosynthesis and signal transduction. *Int. J. Food Sci. Technol.* 56, 814–824. doi: 10.1111/ijfs.14725

Zhang, B., Yin, X.-R., Li, X., Yang, S.-L., Ferguson, I. B., and Chen, K.-S. (2009). Lipoxygenase gene expression in ripening kiwifruit in relation to ethylene and aroma production. *J. Agric. Food Chem.* 57, 2875–2881. doi: 10.1021/jf9000378

Zhang, Q., Feng, C., Li, W., Qu, Z., Zeng, M., and Xi, W. (2019). Transcriptional regulatory networks controlling taste and aroma quality of apricot (*Prunus armeniaca* L.) fruit during ripening. *BMC Genomics* 20:45. doi: 10.1186/s12864-019-5424-8

Conflict of Interest: The authors declare that the research was conducted in the absence of any commercial or financial relationships that could be construed as a potential conflict of interest.

Publisher's Note: All claims expressed in this article are solely those of the authors and do not necessarily represent those of their affiliated organizations, or those of the publisher, the editors and the reviewers. Any product that may be evaluated in this article, or claim that may be made by its manufacturer, is not guaranteed or endorsed by the publisher.

frontiers in Plant Science

ORIGINAL RESEARCH
published: 12 November 2021
doi: 10.3389/fpls.2021.757936

The Basic Helix-Loop-Helix Transcription Factor SmbHLH1 Represses Anthocyanin Biosynthesis in Eggplant

Zhaofei Duan[1†], Shiyu Tian[1†], Guobin Yang[1], Min Wei[1,2,3], Jing Li[1,3,4] and Fengjuan Yang[1,3,4*]*

[1]State Key Laboratory of Crop Biology, College of Horticulture Science and Engineering, Shandong Agricultural University, Shandong, China, [2]Scientific Observing and Experimental Station of Facility Agricultural Engineering (Huang-Huai-Hai Region), Ministry of Agriculture and Rural Affairs, Shandong, China, [3]Shandong Collaborative Innovation Center for Fruit and Vegetable Production With High Quality and Efficiency, Tai'an, China, [4]Key Laboratory of Biology and Genetic Improvement of Horticultural Crops in Huanghuai Region, Ministry of Agriculture and Rural Affairs, Shandong, China

OPEN ACCESS

Edited by:
Carlos R. Figueroa,
University of Talca, Chile

Reviewed by:
Sitakanta Pattanaik,
University of Kentucky, United States
Qiaomei Wang,
Zhejiang University, China

***Correspondence:**
Jing Li
lij19900525@163.com
Fengjuan Yang
beautyyfj@163.com

[†]These authors have contributed equally to this work

Specialty section:
This article was submitted to Plant Metabolism and Chemodiversity, a section of the journal Frontiers in Plant Science

Received: 13 August 2021
Accepted: 05 October 2021
Published: 12 November 2021

Citation:
Duan Z, Tian S, Yang G, Wei M, Li J and Yang F (2021) The Basic Helix-Loop-Helix Transcription Factor SmbHLH1 Represses Anthocyanin Biosynthesis in Eggplant. Front. Plant Sci. 12:757936. doi: 10.3389/fpls.2021.757936

Many basic helix-loop-helix transcription factors (TFs) have been reported to promote anthocyanin biosynthesis in numerous plant species, but little is known about bHLH TFs that inhibit anthocyanin accumulation. In this study, SmbHLH1 from *Solanum melongena* was identified as a negative regulator of anthocyanin biosynthesis. However, SmbHLH1 showed high identity with SmTT8, which acts as a SmMYB113-dependent positive regulator of anthocyanin-biosynthesis in plants. Overexpression of *SmbHLH1* in eggplant caused a dramatic decrease in anthocyanin accumulation. Only the amino acid sequences at the N and C termini of SmbHLH1 differed from the SmTT8 sequence. Expression analysis revealed that the expression pattern of *SmbHLH1* was opposite to that of anthocyanin accumulation. Yeast two-hybrid (Y2H) and bimolecular fluorescence complementation (BiFC) assays showed that SmbHLH1 could not interact with SmMYB113. Dual-luciferase assay demonstrated that SmbHLH1 directly repressed the expression of *SmDFR* and *SmANS*. Our results demonstrate that the biological function of *bHLH*s in anthocyanin biosynthesis may have evolved and provide new insight into the molecular functions of orthologous genes from different plant species.

Keywords: eggplant, anthocyanin biosynthesis, bHLH transcription factor, negative regulation, RNA-seq

INTRODUCTION

Anthocyanins are water-soluble pigments that are responsible for the red, purple, and blue colors of different organs in a wide range of plants (Mol et al., 1998; Koes et al., 2005; Allan et al., 2008). In addition to coloring flowers and fruits to attract pollinators and seed dispersers, anthocyanins can also protect plants from UV damage and promote resistance to low-temperature stress in plants (Ilk et al., 2015). Anthocyanins have been found to be the most powerful free radical scavengers in plants, and they have been used to lower blood pressure, improve vision, reduce inflammation, and prevent cancer (Konczak and Zhang, 2004; Tsuda, 2012).

Anthocyanins are an important branch of the flavonoid biosynthetic pathway and are formed in a stepwise series of enzymatic reactions catalyzed by chalcone synthase (CHS), chalcone

isomerase (CHI), flavanone-3-hydroxylase (F3H), flavonoid 3′-hydroxylase (F3′H), flavonoid 3′5′-hydroxylase (F3′5′H), dihydroflavonol 4-reductase (DFR), anthocyanidin synthase (ANS), and a 3-glucosyltransferase (3GT; Koes et al., 2005). These anthocyanin biosynthetic genes are transcriptionally regulated by a MYB-bHLH-WD40 (MBW) complex, the crucial role of which has been well-documented across many plants, such as *Arabidopsis*, apple, tomato, and so on (Xie et al., 2012; Tohge et al., 2017; Sun et al., 2020a). AcMYB123 and AcbHLH42, the *Actinidia chinensis* cv. Hongyang orthologs of *Arabidopsis* TT2 (MYB) and TT8 (bHLH), respectively, interact to activate the promoters of *AcANS* and *AcF3GT1* and elevate anthocyanin accumulation in *Actinidia arguta* cv. Baby star and transgenic *Arabidopsis thaliana* (Wang et al., 2019). In apple, MdbHLH3 interacts with MdMYB1, MdMYB9, and MdMYB11 to promote anthocyanin or proanthocyanidin (PA) accumulation (Xie et al., 2012; An et al., 2014).

The bHLH proteins are the second largest class of transcription factors (TFs) in plants; they can be divided into 26 subgroups (Pires and Dolan, 2010), and this classification can be extended to 32 subgroups if the "atypical" bHLHs are included (Carretero-Paulet et al., 2010). Compared with the 11–13 subgroups of the R2R3 MYBs (Li et al., 2012; He et al., 2016; Huang et al., 2018), bHLH family seems to have a more complex role in anthocyanin regulation. In general, the first 200 amino acids of the bHLH protein are involved in the interaction with the MYB partner, whereas the following 200 amino acids interact with the WD40 protein (Montefiori et al., 2015).

The G-box (5′-CACGTG-3′) or E-box (5′-CANNTG-3′) in gene promoter regions is recognized by bHLH family members (Atchley et al., 1999; Montefiori et al., 2015; Wang et al., 2018). Strikingly, the promoters of most flavonoid or anthocyanin biosynthetic genes contain G-box and E-box elements (Massari and Murre, 2000). Therefore, in addition to forming the MBW complex, bHLHs can also directly regulate anthocyanin biosynthesis. For example, MdbHLH3 can activate the expression of *MdMYB1*, *MdMYB9*, and *MdMYB11* to promote anthocyanin accumulation (Xie et al., 2012; An et al., 2014). TT8 is known to interact with MYB protein to enhance anthocyanin biosynthesis (Baudry et al., 2006; Li et al., 2016b; Wang et al., 2019). However, TT8 orthologs in different species may also perform different functions. Jia et al. (2021) found that *DcTT8* from *Dendrobium candidum* could directly activate the expression of *DcF3′H* and *DcUFGT* by binding to their promoters. Zhai et al. (2020) found that targeted mutations of *BnTT8* blocked PA-specific deposition, but elevated seed oil content and altered fatty acid (FA) composition in the seed coat of *Brassica napus*. In addition, bHLHs can also negatively regulate anthocyanin biosynthesis. To data, some *bHLH* genes have been reported as repressors of anthocyanin biosynthesis in plants, including IN1 from maize (Burr et al., 1996), *bHLH3*/*13*/14/17 from *Arabidopsis* (Song et al., 2013), *LcbHLH92* from *Leymus chinensis* (Zhao et al., 2018), and *CpbHLH1* from *Chimonanthus praecox* (Zhao et al., 2020), but the molecular mechanisms of their negative regulation have been little reported.

Eggplants (*Solanum melongena*) with purple peel are rich in anthocyanins and popular with consumers. They rank fourth in facility vegetable cultivation planting area. Noda et al. (2000) reported that eggplant extracts showed the most potent superoxide anion radical scavenging activity (SOD-like activity) of 16 common vegetables examined, highlighting the important role of anthocyanins in eggplant. Recently, research focused on the molecular mechanisms of anthocyanin biosynthesis in eggplant has increased (Jiang et al., 2016; Li et al., 2017, 2018; Moglia et al., 2020; Zhou et al., 2020), but gene functions have been verified primarily by ectopic expression in *Arabidopsis* or tobacco. The eggplant genome database was updated by Barchi et al. (2019), providing a valuable resource for the molecular breeding of new eggplant germplasm. Based on the updated eggplant genome, Moglia et al. (2020) functionally characterized the genes belonging to the MBW complex (*SmelANT1*, *SmelAN2*, *SmelJAF13*, and *SmelAN1*), and identified out an R3 MYB type repressor (*SmelMYBL1*) of anthocyanin biosynthesis.

Based on the two published eggplant genome databases (Hirakawa et al., 2014; Barchi et al., 2019), *SmbHLH1* (*Sme2.5_00592.1_g00005.1*) and *SmTT8* (*SMEL_009g326640.1*) were identified as two TT8 homologs. SmTT8 has been shown to interact with SmMYB75 to promote anthocyanin biosynthesis in eggplant (Shi et al., 2021). However, no studies on *SmbHLH1* have been reported. Hence, we overexpressed *SmbHLH1* in eggplant, and obtained two stable transformation lines, *SmbHLH1*-1 and *SmbHLH1*-2. The anthocyanin content was markedly reduced in both lines, indicating that *SmbHLH1* and *SmTT8* have different functions and molecular mechanisms in the regulation of anthocyanin biosynthesis in eggplant. We used biochemical experiments and transcriptomic analysis to investigate the molecular mechanism by which *SmbHLH1* regulates anthocyanin biosynthesis.

MATERIALS AND METHODS

Plant Materials and Growth Conditions

Six eggplant cultivars with different color and anthocyanin contents in the fruit and stem peels, named No. 44, No. 64, No. 76, No. 108, No. 109, and No. 133 (**Supplementary Figure S1**), were grown in the solar greenhouse of Shandong Agricultural University to perform phenotypic observations and collect experimental materials. No. 109 was used for genetic transformation.

Nicotiana benthamiana was grown in a phytotron under 25/16°C and 12/12 h day/night conditions. Plants with 5–6 leaves were used for bimolecular fluorescence complementation (BiFC), dual luciferase, and transient expression assays.

Anthocyanins Content Analysis

The anthocyanin content was measured with the methods described by Neff and Chory (1998).

Gene Isolation and Sequence Analysis

The full-length coding sequences (CDSs) of *SmbHLH1* and *SmTT8* were cloned by PCR amplification. The amino acid sequences of SmbHLH1 and SmTT8 were translated with DNAMAN 6.0

(Lynnon Biosoft, Quebec, Canada) based on the sequencing results. Multiple sequence alignments were performed using ClustalX (version 1.83) and DNAMAN 6.0. The MEGA 7.0 program was used to construct neighbor-joining phylogenetic trees with the following parameters: bootstrapping (1,000 replicates, random seed), Poisson model, and complete deletion (Kumar et al., 2016).

Subcellular Localization

The full-length CDS of *SmbHLH1* without the stop codon was inserted into the pHB:GFP vector. The fusion construct was transferred into *Agrobacterium tumefaciens* strain GV3101, and subcellular localization assays were performed as previously reported (Sparkes et al., 2006).

Yeast Two-Hybrid Assay

The full-length CDSs of *SmbHLH1* and *SmTT8* were inserted into the pGBKT7 vector as bait, and *SmMYB113* was fused to the pGADT7 vector as prey. The Y2H assays were performed as described in Zhou et al. (2020).

Bimolecular Fluorescence Complementation

The full-length CDSs of *SmbHLH1* and *SmTT8* without stop codons were inserted into the pXY104 vector, and *SmMYB113* with the stop codon was subcloned into the pXY106 vector. BiFC assays were performed as described by Li et al. (2016a).

Plasmid Construction and Plant Transformation

The full-length CDS of *SmbHLH1* was inserted into the pRI 101 vector with the 35S-CaMV promoter. The fusion vector was transferred into *Agrobacterium* strain LBA4404 and introduced into No. 109 by *Agrobacterium*-mediated cotyledon explant transformation based on an earlier report by Vasudevan et al. (2005) with minor modifications.

Dual Luciferase and Transient Expression Assays in *N. benthamiana* Leaves

The complete coding regions of *SmMYB113*, *SmbHLH1*, and *SmTT8* were inserted into the pHB vector, and the promoters of anthocyanin biosynthetic genes (*SmCHS*, *SmCHI*, *SmF3H*, *SmF3′H*, *SmF3′5′H*, *SmDFR*, *SmANS*, and *Sm3GT*) were amplified and cloned into pGreenII 0800-LUC vectors. The Dual-LUC assay was performed as previously reported (Hu et al., 2019). For the transient expression assays, 1/2×, 1×, and 2× pHB-*SmbHLH1* was co-infiltrated with pHB-*SmMYB113* or pHB-*SmMYB113* + pHB-*SmTT8*. The anthocyanin content was measured 4 days after infiltration with the methods described in Li et al. (2017).

Quantitative Reverse Transcription PCR

The fruit and stem peels of six eggplant cultivars and thetender stems close to the growing point of No.109 were collected, and total RNA was extracted from the samples using the TaKaRa MiniBEST Plant RNA Extraction Kit (TaKaRa, Otsu, Shiga, Japan) according to the manufacturer's instructions. Then 1 μg RNA was used for cDNA synthesis with the PrimeScript RT Reagent Kit with gDNA Eraser (TaKaRa). The quantitative rreverse ttranscription PCR (RT-qPCR) assay was performed according to the manufacturer's instructions of the SYBR Premix Ex Taq II Kit (TaKaRa) on the LightCycler 96 system (Roche, Basel, Switzerland). The *Actin* gene (GU984779.1) was used as an internal control gene. The relative expression levels of the amplified products were analyzed using the comparative CT method (Livak and Schmittgen, 2001).

RNA-Seq and Bioinformatics Analyses

Tender stems close to the growing point were collected from WT and two *SmbHLH1* transgenic eggplants for RNA-seq. RNA extraction, quality control, library construction, and high-throughput parallel sequencing were performed at the Beijing Genomics Institute (BGI) on the BGISEQ-500 sequencing platform. Bioinformatics analyses were performed as previously reported (Li et al., 2019).

Statistical Analysis

SPSS 17.0 (SPSS, Inc., Chicago, United States) was used to assess statistical significance by one-way ANOVA and Duncan's New Multiple Range test ($p \leq 0.05$).

RESULTS

Molecular Cloning and Characterization of TT8 Homologs in Eggplant

The CDSs of *SmbHLH1* and *SmTT8* were amplified based on the two published eggplant genome databases (Hirakawa et al., 2014; Barchi et al., 2019). After sequencing and alignment, we found that the *SmTT8* sequence showed some differences from the published sequence (*SMEL_009g326640.1*), whereas *SmbHLH1* was identical to *Sme2.5_00592.1_g00005.1* (**Supplementary Figure S2**). We then aligned the amino acid sequences of SmbHLH1 and SmTT8 (**Figure 1**) and found that only the regions at the N terminus (amino acids 1–158 and 188–193) and C terminus (amino acids 633–659) differed between SmbHLH1 and SmTT8.

A phylogenetic tree was constructed to analyze the relationships of SmbHLH1 and SmTT8 with all bHLH proteins from *Arabidopsis*, *Solanum lycopersicum*, *Malus* × *domestica*, *Vitis vinifera*, *Fragaria* × *ananassa*, *Petunia* × *hybrida*, *Prunus persica*, *Chimonanthus praecox*, and *Medicago truncatula* known to be involved in the anthocyanin biosynthesis pathway (**Supplementary Figure S3**; Li et al., 2017; Zhao et al., 2020). As shown in **Supplementary Figure S3**, SmbHLH1 and SmTT8 were placed in the same clade.

Different Expression Pattern of *SmbHLH1* and *SmTT8* in Eggplant

To analyze the relationship between *SmbHLH1* and *SmTT8*, the expression pattern of *SmbHLH1* and *SmTT8* were measured

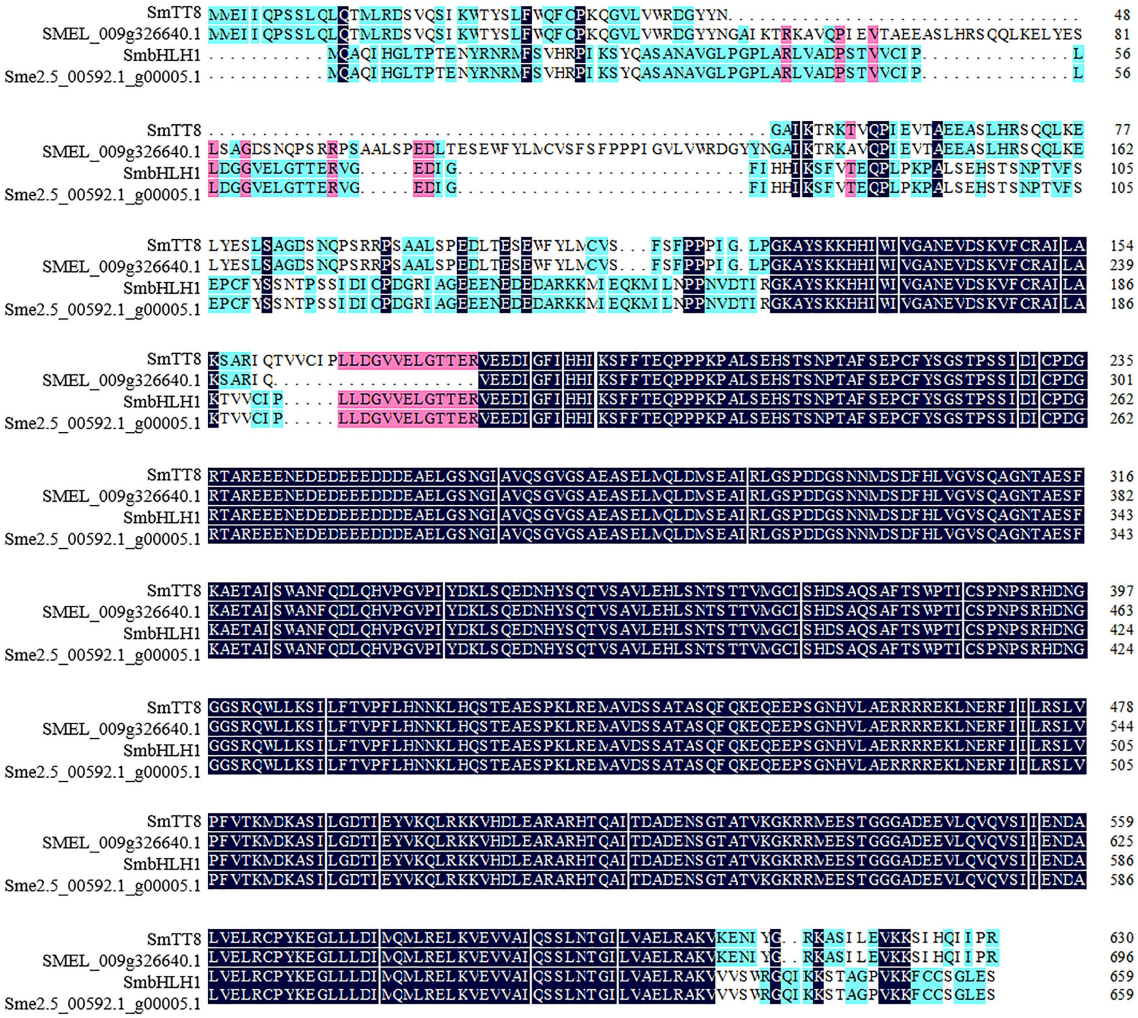

FIGURE 1 | Multiple sequence alignments of the amino acids of SmbHLH1 and SmTT8. SMEL_009g326640.1 and Sme2.5_00592.1_g00005.1 were both annotated as TT8 in the two published eggplant genome databases.

in the fruit and stem peels from six eggplant cultivars with different anthocyanin contents (**Figure 2A**; **Supplementary Figure S1**). The primers for RT-qPCR were designed from the 5′ termini, which differed between *SmbHLH1* and *SmTT8* (**Supplementary Table S1**). As shown in **Figure 2A** and **Supplementary Figure S1**, the anthocyanin content in the fruit peel was sorted as No. 76 > No. 64 > No. 44 > No. 108/ No. 109/No. 133, while No. 76/No. 109 > No. 44 > No. 64 > No. 108/No. 133 in the stem peel. The expression patterns of *SmTT8* in the fruit and stem peel were both consistent with anthocyanin contents (**Figure 2B**). However, the expression pattern of *SmbHLH1* was opposite with anthocyanin contents in both fruit and stem peel (**Figure 2C**). These results implied that the function of *SmbHLH1* may be different from that of *SmTT8*.

To confirm the subcellular location of *SmbHLH1*, the 35S::SmbHLH1-GFP fusion protein was constructed and transiently expressed in tobacco leaves. Compared with the positive control, SmbHLH1-GFP was predominately present in the cytosol and nucleus (**Figure 2D**).

Overexpression of *SmbHLH1* Inhibited Anthocyanin Accumulation in Eggplant

To characterize the function of *SmbHLH1* in eggplant, transient VIGS assay, CRISPR-Cas9 system, and overexpression system were all performed on all the six eggplant cultivars. However, the approaches to transform the eggplant with the transient VIGS assay and CRISPR-Cas9 system were failed. So we decided to transform the eggplant with 35S promoter-constructs to probe the overall function of the *SmbHLH1* gene. *SmbHLH1* was introduced into eggplant by *Agrobacterium*-mediated transformation. Only the eggplant cultivar No.109 differentiated two *SmbHLH1* overexpression transgenic lines (overexpressed by the 35S-CaMV promoter, named as *SmbHLH1*-1 and *SmbHLH1*-2), which would be used to probe the overall function of the *SmbHLH1*. Both of the two 35S::*SmbHLH1* transgenic eggplant lines showed increased *SmbHLH1* expression (**Figures 3A**,**B**). As shown in **Figure 3A**, the whole plant of the two 35S::*SmbHLH1* transgenic eggplant lines were greener than WT. Especially, the colors of stalks, sepals, and stem

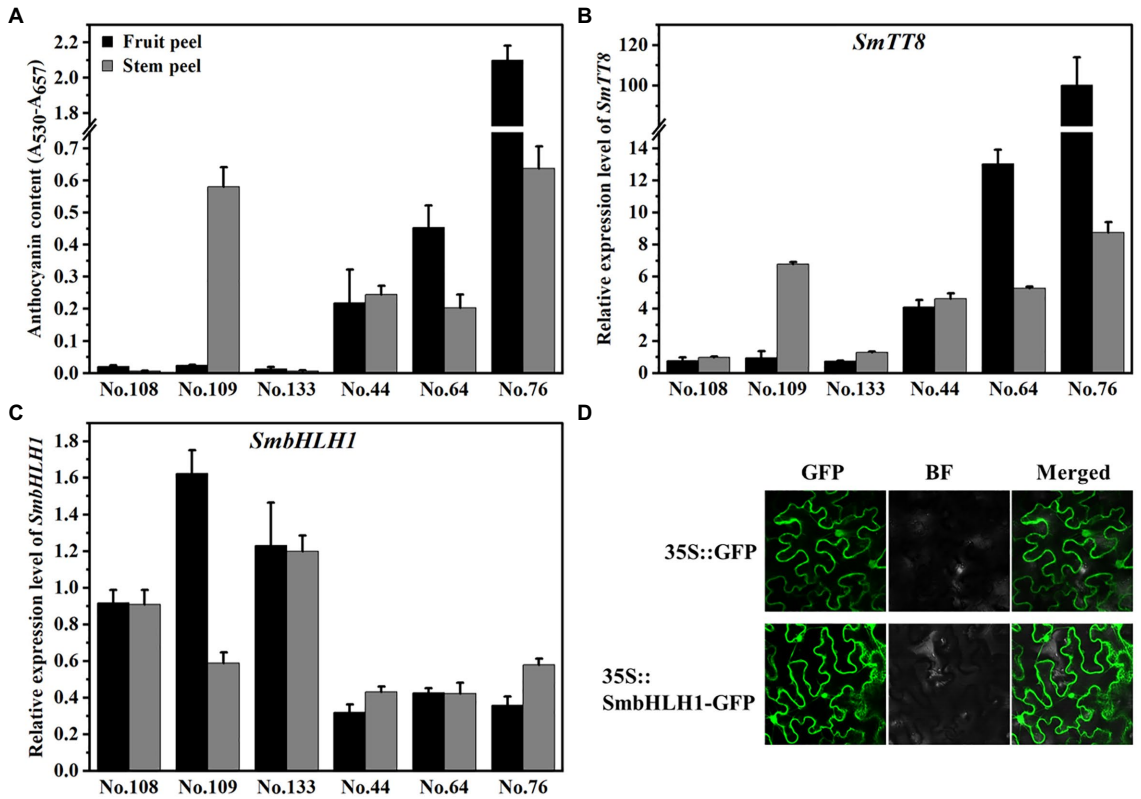

FIGURE 2 | Relationship of anthocyanin contents with the expression of *SmTT8* and *SmbHLH1*. **(A)** The anthocyanin contents in the fruit and stem peels of six eggplant cultivars; **(B,C)** The expression levels of *SmTT8* and *SmbHLH1* in the fruit and stem peels of six eggplant cultivars. Bars represent means ± SD of three biological replicates; and **(D)** Subcellular localization analysis of SmbHLH1.

peels were changed from purple to green, which could be accumulated anthocyanins in cultivar No.109. However, the fruit peels of cultivar No.109 was orange with little anthocyanins, no significant difference was found comparing with the two *35S*::*SmbHLH1* transgenic eggplant lines. Next, we evaluated the anthocyanin contents and the expression levels of anthocyanin biosynthetic genes (*SmCHS*, *SmCHI*, *SmF3H*, *SmF3′5′H*, *SmDFR*, and *SmANS*) in the stems peel. Anthocyanin contents and expression levels of anthocyanin biosynthetic genes were lower in stems peel of the two *SmbHLH1* transgenic lines than in WT stems (**Figures 3C**,**D**).

SmbHLH1 Could Not Interact With SmMYB113

We performed yeast two-hybrid (Y2H) assays to determine whether SmbHLH1 regulated anthocyanin biosynthesis through interaction with SmMYB113, which has been reported as a critical anthocyanin regulator and interacted with SmTT8 (Zhou et al., 2020). Positive β-gal activity was observed only in yeast that contained AD-SmMYB113 plus BD-SmTT8 grown on -T/−L/-H/−A screening medium but not in yeast that contained AD plus BD-SmbHLH1, AD plus BD-SmTT8, AD-SmMYB113 plus BD, or AD-SmMYB113 plus BD-SmbHLH1 (**Figure 4A**). These results indicated that SmbHLH1 could not interact with SmMYB113, whereas SmTT8 could.

Bimolecular fluorescence complementation assays were performed to further characterize the interaction between SmbHLH1/SmTT8 and SmMYB113 *in vivo*. As shown in **Figure 4B**, YFP fluorescence signals appeared only when YFP_C-SmMYB113 and YFP_N-SmTT8 were co-expressed. No fluorescence was detected in cells that contained combinations of YFP_C-SmMYB113 plus YFP_N-SmbHLH1 and other empty vector controls. In addition, we found that the interaction location of SmMYB113 and SmTT8 complexes was in the nucleus. These results confirmed that SmbHLH1 could not interact with SmMYB113 in plant cells, but SmTT8 could.

SmbHLH1 Is a Negative Transcription Regulator of *SmDFR* and *SmANS*

The *cis*-elements in the promoter sequences of six anthocyanin biosynthetic genes (*SmCHS*, *SmCHI*, *SmF3H*, *SmF3′5′H*, *SmDFR*, and *SmANS*) were analyzed, and E-box or G-box *cis*-elements recognized by bHLH family members were found in all six promoter sequences (**Supplementary Figure S4**). Then, we performed a dual-luciferase assay by infiltration of tobacco leaves to analyze whether SmbHLH1 can inhibit the transcription of the anthocyanin biosynthetic genes. As a result, we found that *SmDFR* and *SmANS* promoter activities were inhibited by SmbHLH1 (**Figure 5A**). Because SmMYB113 can bind directly to the *SmDFR* promoter and activate its expression

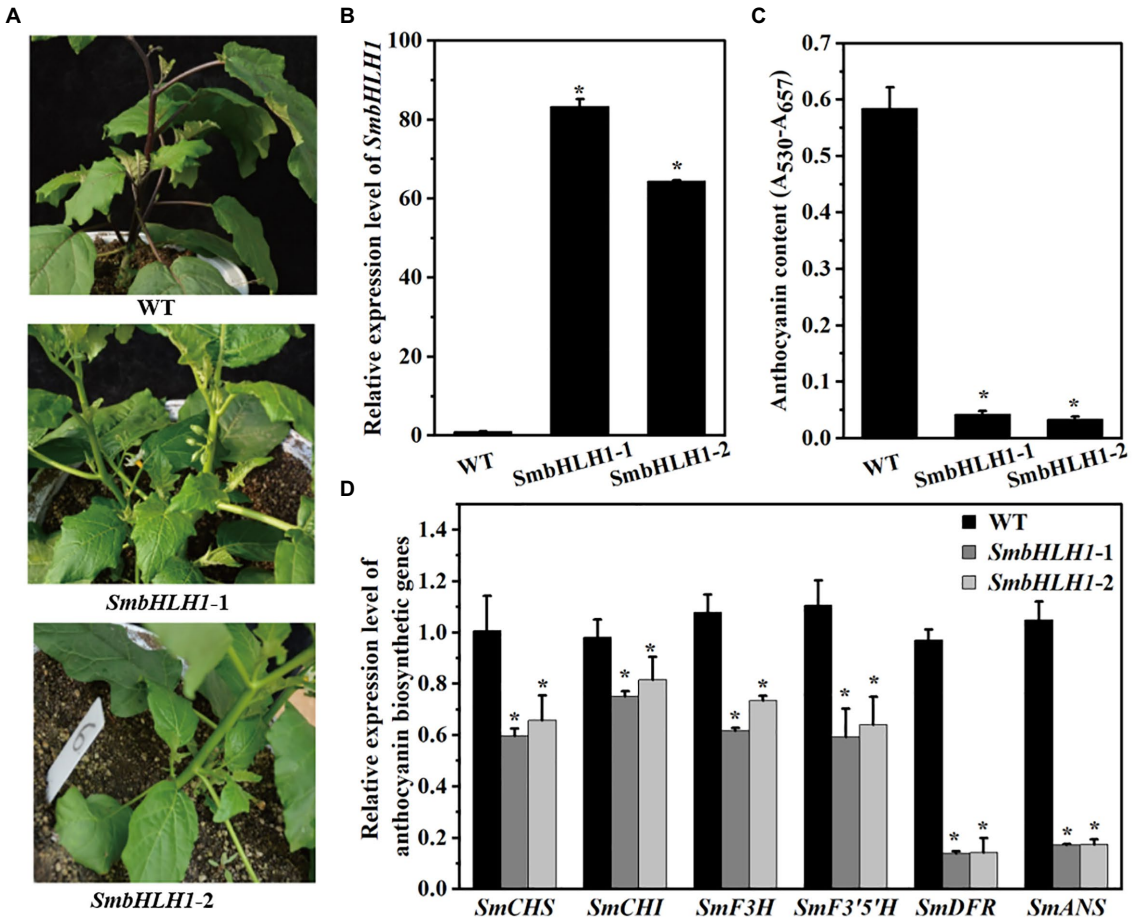

FIGURE 3 | *SmbHLH1* controls anthocyanin biosynthesis in the stem peels of eggplant (cultivar No. 109). **(A)** The phenotypes of WT and the two *SmbHLH1* transgenic lines (*SmbHLH*-1 and -2); **(B)** The relative expression level of *SmbHLH1* in the two 35S::*SmbHLH1* stem peels lines; **(C)** The anthocyanin content in the two 35S::*SmbHLH1* stem peels lines; and **(D)** The relative expression level of anthocyanin biosynthetic genes in stem peels of the two 35S::*SmbHLH1* lines. Values are means ± SD ($n = 3$). * represents significance at $p < 0.05$ comparing with wild-type (WT).

(Jiang et al., 2016), *SmMYB113* was co-infiltrated with *SmbHLH1*. As shown in **Figure 5B**, the inhibition of the *SmDFR* promoter activity by SmbHLH1 occurred in the presence of SmMYB113.

Another transient expression assay was carried out in tobacco leaves to explore the role of *SmbHLH1* in anthocyanin biosynthesis. *Agrobacterium tumefaciens* GV3101 strains containing the empty vector pHB, *SmbHLH1*, *SmTT8*, or *SmMYB113* were infiltrated or co-infiltrated into tobacco leaves. As shown in **Figure 5C**, pigmentation was evident after infiltration with *SmMYB113* alone and co-infiltration with *SmbHLH1* and *SmTT8*. Compared with the leaves infiltrated with *pHB* and *SmMYB113* alone, anthocyanin content decreased when SmbHLH1 was added but increased when SmTT8 was added. Next, different ratios of *SmbHLH1*:*SmMYB113* and *SmbHLH1*:*SmMYB113*:*SmTT8* were used to analyze the effect of SmbHLH1 on SmMYB113-induced anthocyanin biosynthesis (**Figures 5D,E**). We found that anthocyanin accumulation in infiltrated patches was negatively correlated with the dose of *SmbHLH1*. These results suggested that SmbHLH1 was a key negative regulator of anthocyanin accumulation in eggplant, directly inhibiting *SmDFR* and *SmANS* expression through a SmMYB113-independent pathway.

Overview of RNA-Seq Analysis

To explore how SmbHLH1 regulates gene expression at the whole-genome level, total RNA was extracted from stems of the WT and two *SmbHLH1* transgenic lines for RNA-seq analysis. A total of 29,840 genes or transcripts were obtained. Subsequently, we performed pairwise comparisons of transcript abundance to identify differentially expressed genes (DEGs) between the WT and transgenic lines based on an absolute fold change value of $|\log_2^{ratio}| \geq 0.5$ with $p < 0.001$. In total, 2,120 genes were differentially expressed in *SmbHLH1*-1 stems compared with the WT (933 up; 1,187 down), and 3,467 genes were differentially expressed in *SmbHLH1*-2 stems compared with the WT (1,811 up; 1,656 down; **Figure 6A**; **Supplementary Table S2**). Among these DEGs, only 126 genes were upregulated and 181 genes were downregulated simultaneously in both *SmbHLH1*-overexpressing lines compared with the WT (**Figure 6B**).

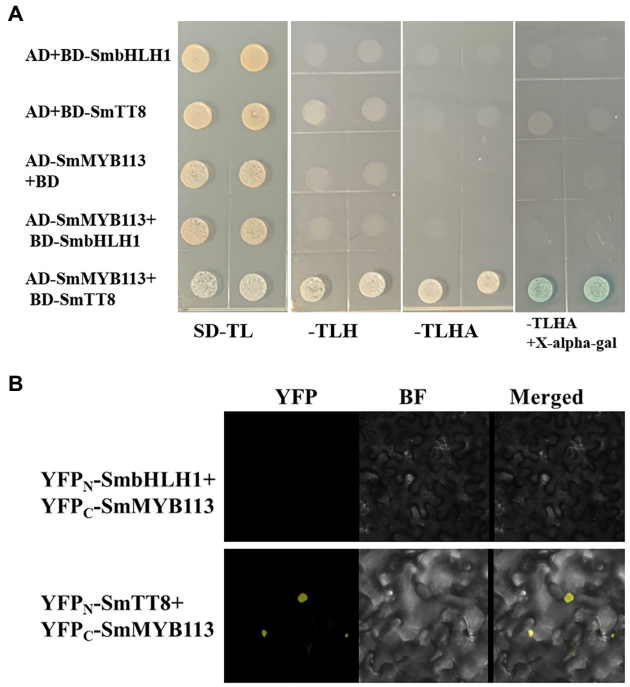

FIGURE 4 | SmbHLH1 could not specifically interact with SmMYB113 in both Y2H and bimolecular fluorescence complementation (BiFC) assays, while SmTT8 could. **(A)** The yeast cells of strain AH109 harboring the indicated plasmid combinations were grown in SD-TL (–Trp/–Leu), SD-TLH (–Trp/–Leu/-His), SD-TLHA (–Trp/–Leu/-His/–Ade) mediums, and SD-TLHA (–Trp/–Leu/-His/–Ade) with X-alpha-gal filter assay were indicated. **(B)** YFP fluorescent and bright-field images of *Nicotiana benthamiana* leaf cells infiltrated with a mixture of *Agrobacterium* suspensions harboring constructs encoding the indicated fusion proteins.

GO functional enrichment analysis was performed on the 126 upregulated and 181 downregulated genes shared by the two SmbHLH1 transgenic eggplant lines (**Figures 6C,D**). The 126 upregulated genes were enriched in 29 GO terms, and the 181 downregulated genes were enriched in 27 GO terms. In the "biological process" category, "cell proliferation" was enriched only in the downregulated genes, and "carbon utilization," "reproduction," and "reproductive process" were enriched only in the upregulated genes. In the "molecular function" category, "nutrient reservoir activity" was enriched only in the upregulated genes, and "structural molecule activity" was enriched only in the downregulated genes.

The Kyoto Encyclopedia of Genes and Genomes (KEGG) pathways of the 126 shared upregulated genes and the 181 shared downregulated genes were identified using a value of *p* less than 0.05 as the cut-off (**Table 1**). As shown in **Table 1**, the "carbon metabolism" and "starch and sucrose metabolism" pathways were enriched in the upregulated genes, and the "flavonoid biosynthesis" and "anthocyanin biosynthesis" pathways were enriched in the downregulated genes. These results suggest that SmbHLH1 inhibited anthocyanin biosynthesis but promoted carbon metabolism. We next examined glucose, fructose, and sucrose contents in stems, functional leaves, and expanding leaves. The two *SmbHLH1* transgenic eggplant lines showed significant increases in glucose, fructose, and sucrose content compared with the WT (**Supplementary Figure S5**). These results are consistent with the transcriptomic analysis.

TABLE 1 | Kyoto Encyclopedia of Genes and Genomes (KEGG) pathway enrichment analysis of common upregulated and downregulated genes in two SmbHLH1 transgenic eggplant stem peels lines vs. WT.

Upregulated genes	Downregulated genes
ko01100 Metabolic pathways (26)	ko01100 Metabolic pathways (31)
ko01110 Biosynthesis of secondary metabolites (15)	ko01110 Biosynthesis of secondary metabolites (19)
ko01200 Carbon metabolism (7)	ko00564 Glycerophospholipid metabolism (6)
ko:K00382 DLD; dihydrolipoamide dehydrogenase	ko04141 Protein processing in endoplasmic reticulum (5)
ko:K00873 PK; pyruvate kinase	ko00941 Flavonoid biosynthesis (5)
ko:K01602 rbcS; ribulose-bisphosphate carboxylase small chain	ko:K00475 F3H; Naringenin 3-dioxygenase
ko:K01913 AAE7; acetate/butyrate---CoA ligase	ko:K00660 CHS; Chalcone synthase (CHS)
ko:K02437 gcvH; glycine cleavage system H protein	ko:K05277 ANS; Anthocyanidin synthase
ko:K03841 FBP; fructose-1,6-bisphosphatase I	ko:K13065 E2.3.1.133; Shikimate O-hydroxycinnamoyl transferase
ko:K05605 HIBCH; 3-hydroxyisobutyryl-CoA hydrolase	ko:K13082 DFR; bifunctional dihydroflavonol 4-reductase (DFR)/ flavanone 4-reductase
ko04075 Plant hormone signal transduction (5)	ko04075 Plant hormone signal transduction (4)
ko04016 MAPK signaling pathway – plant (5)	ko00942 Anthocyanin biosynthesis (1)
ko04626 Plant-pathogen interaction (4)	ko:K12930 BZ1; Aanthocyanidin 3-O-glucosyltransferase
ko00630 Glyoxylate and dicarboxylate metabolism (4)	
ko00010 Glycolysis/Gluconeogenesis (4)	
ko00500 Starch and sucrose metabolism (2)	
ko:K01177 E3.2.1.2; beta-amylase	
ko:K01179 E3.2.1.4; endoglucanase	

DISCUSSION

The bHLH, R2R3-MYB, and WD repeat proteins can form a ternary MBW complex to modulate the expression of anthocyanin biosynthesis-related genes. Previous studies have revealed that several bHLH TFs, including AtTT8, AtGL3, AtEGL3, PhAN1, PhJAF13, GhMYC1, SlAN1, MdbHLH3, and PbbHLH2, interact with their respective MYB partners AtPAP1, AtTT2, PhAN2, GhMYB10, SlAN2, MdMYB1, and PbMYB9/10/10b to regulate anthocyanin or proanthocyanidin biosynthesis in *Arabidopsis*, *Petunia hybrida*, *Gerbera hybrida*, *S. lycopersicum*, *M. domestica*, and *Pyrus bretschneideri* (Elomaa et al., 2003; Koes et al., 2005; Ramsay and Glover, 2005; Xie et al., 2012; Sun et al., 2020a; Li et al., 2021b). Xie et al. (2012) reported that two regions (amino acids 1–24 and 186–228) at the *N* terminus of MdbHLH3 were crucial for the interaction between MdbHLH3 and

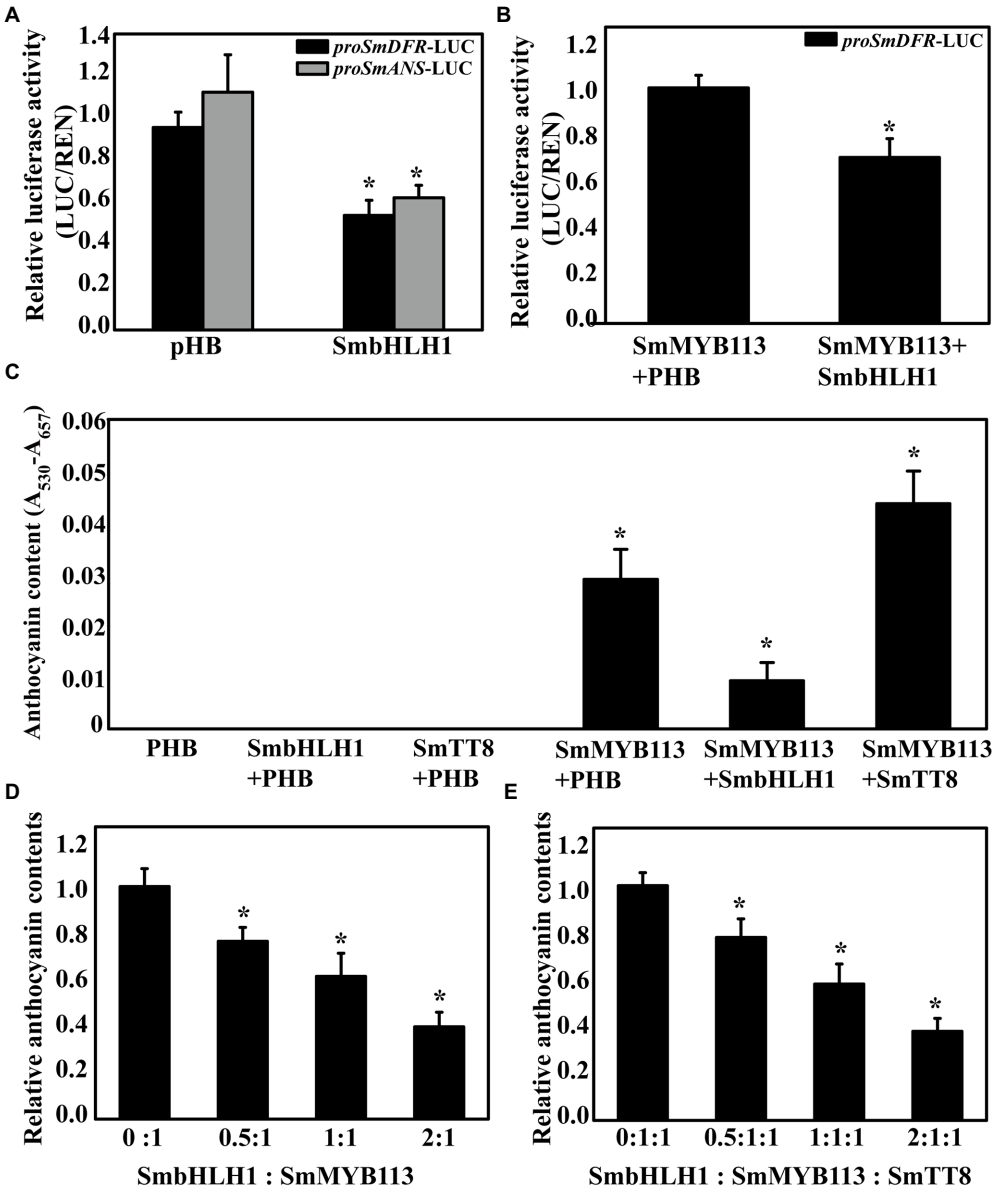

FIGURE 5 | Dual-luciferase and transient analysis of SmbHLH1 on anthocyanin accumulation. **(A)** Inhibition of the activity of the *SmDFR* and *SmANS* gene promoters by SmbHLH1 in transient expression assay in *N. benthamiana* leaves; **(B)** SmbHLH1 decreased the ratio of LUC/REN of the *SmDFR* promoter activated by SmMYB113; and **(C)** SmbHLH1 inhibited SmMYB113-induced anthocyanin accumulation while SmTT8 enhanced in *N. benthamiana* leaves. **(D,E)** The relative anthocyanin contents induced by different proportions of *SmbHLH1*:*SmMYB113* and *SmbHLH1*:*SmMYB113*:*SmTT8* in infiltrated regions. *Represents significance at $p < 0.05$ comparing with the control.

MdMYB1. In this study, we found that SmbHLH1, SmTT8, and MdbHLH3 were clustered into one clade by phylogenetic analysis (**Supplementary Figure S3**), and the *N* terminus (amino acids 1–158 and 188–193) and C terminus (amino acids 633–659) of SmbHLH1 differed significantly from those of SmTT8 (**Figure 1**). SmbHLH1 did not interact with SmMYB113 in both Y2H and BiFC assays (**Figure 4**), whereas SmTT8 did which was corresponding to the results reported by Moglia et al. (2020). These results suggested that the N-terminal portion of SmTT8 was crucial for its interaction with SmMYB113. Simultaneously, the pattern of *SmbHLH1* expression contrasted with those of *SmTT8* expression and anthocyanin accumulation (**Figure 2**). Previous studies have reported that the enhancement of anthocyanin biosynthesis by SmTT8 is dependent on SmMYB113 (Moglia et al., 2020; Zhou et al., 2020). However, we found that over-expression of *SmbHLH1* inhibited anthocyanin accumulation (**Figure 3**). Dual-luciferase assays revealed that SmbHLH1 directly repressed the expression of *SmDFR* and *SmANS* (**Figure 5**). Because the color of cultivar No.109 tissues was different, the phenotype changes of *35S*::*SmbHLH1* transgenic eggplant lines were different. For the tissues with anthocyanins accumulation were changed from purple to green, such as

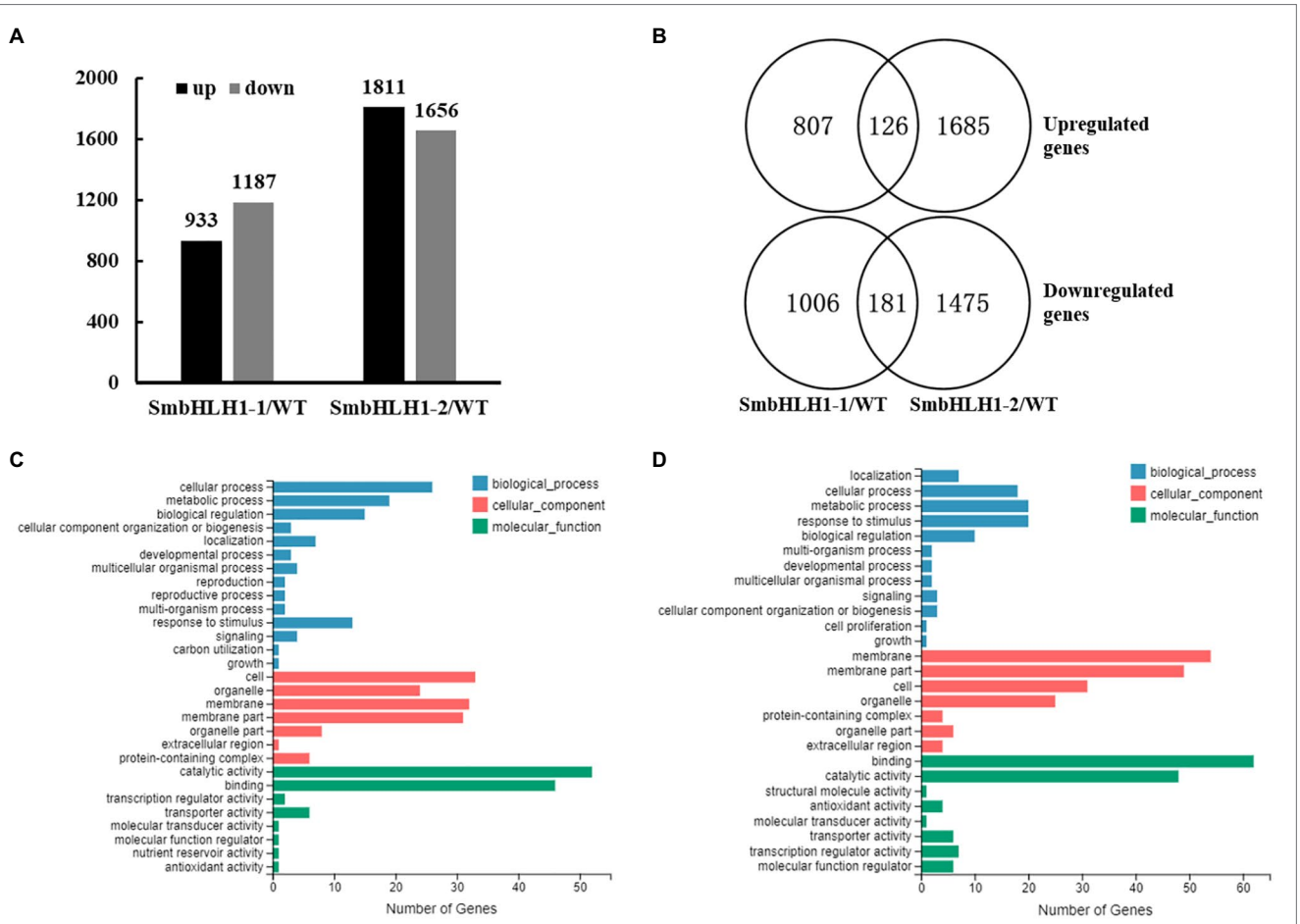

FIGURE 6 | Overview, Venn diagrams and GO enrichment analysis of up- or downregulated genes by SmbHLH1 in stems at a level $|\log_2^{ratio}| \geq 0.5$ with $p < 0.001$. **(A)** Number of upregulated and downregulated genes in the two *35S::SmbHLH1* stem peels lines vs. WT with RNA-seq. **(B)** Schematic of the Venn diagram analysis of common upregulated and downregulated genes [differentially expressed genes (DEGs)] in the two *35S::SmbHLH1* stem peels lines vs. WT. **(C,D)** GO functional enrichment analysis of common upregulated **(C)** and downregulated **(D)** genes.

stalks, sepals, and stem peels. However, no significant color change was found in the tissues with little anthocyanins content, such as the fruit peels. Taken all above, we could conclude that *SmbHLH1* was a repressor in anthocyanin biosynthesis. Moreover, the silencing of *SmbHLH1* in fruit peel tissue to verify the fruit can accumulate more anthocyanins is worthy in the future,

BHLH proteins are the second largest class of transcription factors in plants and can be divided into 26–32 subgroups (Carretero-Paulet et al., 2010; Pires and Dolan, 2010); they play important roles in stress tolerance, reproduction, and secondary metabolite biosynthesis (Sun et al., 2020b; Guo et al., 2021). It is worth noting that AtTT8, AtGL3, AtEGL1, and AtMYC1, which are positive regulator of anthocyanin biosynthesis, were placed into subgroup IIIf (Heim et al., 2003). However, *AtMYC1* orthologs in maize and *C. praecox*, as well as another bHLH TF from subgroup IVd, have been reported to negatively regulate anthocyanin biosynthesis (Burr et al., 1996; Zhao et al., 2018). Here, *SmTT8* and *SmbHLH1* are both eggplant orthologs of *AtTT8*, but they played opposite roles in anthocyanin biosynthesis. It is not uncommon for such homologous genes to exhibit different functions in the plant. For example, Li et al. (2021a) reported that the biological function of MS1 in pollen development differed in the evolution of Poaceae plants. The different biological functions of homologous genes probably result from differences in some amino acids. Taking all of our results into consideration, we speculate that the N-terminal front portion of SmbHLH1 may be the key to its role in anthocyanin biosynthesis.

RNA-seq analysis revealed that overexpression of *SmbHLH1* reduced the expression of anthocyanin biosynthetic genes while enhancing that of genes involved in carbon metabolism and starch and sucrose metabolism. Combined with another phenotype of the two *SmbHLH1* transgenic eggplant lines, which were greener than the WT due to increased chlorophyll content (**Figure 3**; **Supplementary Figure S4**), we speculated that more light was absorbed, resulting in significant increases in glucose, fructose, and sucrose content. Anthocyanin and chlorophyll are two major plant pigments. Anthocyanin can protect plants from UV light and oxidative damage, whereas

chlorophyll is essential for the conversion of light energy into stored chemical energy. Previous studies have reported that anthocyanin often accumulates in young leaves but degrades in mature leaves, which is beneficial for the gradual accumulation of chlorophyll in many plants (Oren-Shamir, 2009; Ren et al., 2019). On this basis, we speculate that the increased chlorophyll content may be directly regulated by *SmbHLH1* or caused by a decrease in anthocyanin, suggesting the existence of a much more complex molecular mechanism that is worthy of study in the future.

CONCLUSION

In the eggplant genome, we found that both SmbHLH1 and SmTT8 are homologs of TT8. Their amino acid sequences differed only at the N and C termini, but they had contrasting functions in anthocyanin biosynthesis. SmbHLH1 repressed the expression of *SmDFR* and *SmANS* and inhibited anthocyanin biosynthesis through SmMYB113-independent pathway. We identified *SmbHLH1* as a new target to silence to produce more anthocyanins in eggplant fruit peel. In addition, RNA-seq analysis revealed that genes involved in carbon metabolism and starch and sucrose metabolism were upregulated by overexpression of *SmbHLH1* in eggplant.

DATA AVAILABILITY STATEMENT

The datasets presented in this study can be found in online repositories. The names of the repository/repositories and accession number(s) can be found at: NCBI BioProject, PRJNA761256.

AUTHOR CONTRIBUTIONS

FY, JL, and MW designed the research. ZD, ST, JL, and GY performed experiments. JL and ZD analyzed data. JL wrote the manuscript. FY and JL read and modified the manuscript. All authors contributed to the article and approved the submitted version.

FUNDING

This work was supported by the National Natural Science Foundation of China (grant number: 31672169), Youth Project of Shandong Provincial Natural Science Foundation (grant number: ZR201911120670), Key Project of Shandong Provincial Natural Science Foundation (ZR2020KC039), and Special Project Protected Horticulture Advantage Team of Shandong Agricultural University 'Double First-Class' Science and Technology Team (grant number: SYL2017YSTD07).

ACKNOWLEDGMENTS

We are very grateful for the reviewers for their comments and suggestions, which is helpful for improving the quality of our manuscript.

SUPPLEMENTARY MATERIAL

The Supplementary Material for this article can be found online at: https://www.frontiersin.org/articles/10.3389/fpls.2021.757936/full#supplementary-material

REFERENCES

Allan, A. C., Hellens, R. P., and Laing, W. A. (2008). MYB transcription factors that colour our fruit. *Trends Plant Sci.* 13, 99–102. doi: 10.1016/j.tplants.2007.11.012

An, X.-H., Tian, Y., Chen, K.-Q., Liu, X.-J., Liu, D.-D., Xie, X.-B., et al. (2014). MdMYB9 and MdMYB11 are involved in the regulation of the ja-induced biosynthesis of anthocyanin and proanthocyanidin in apples. *Plant Cell Physiol.* 56, 650–662. doi: 10.1093/pcp/pcu205

Atchley, W. R., Terhalle, W., and Dress, A. (1999). Positional dependence, cliques, and predictive motifs in the bHLH protein domain. *J. Mol. Evol.* 48, 501–516. doi: 10.1007/PL00006494

Barchi, L., Pietrella, M., Venturini, L., Minio, A., Toppino, L., Acquadro, A., et al. (2019). A chromosome-anchored eggplant genome sequence reveals key events in *Solanaceae* evolution. *Sci. Rep.* 9:11769. doi: 10.1038/s41598-019-47985-w

Baudry, A., Caboche, M., and Lepiniec, L. (2006). TT8 controls its own expression in a feedback regulation involving TTG1 and homologous MYB and bHLH factors, allowing a strong and cell-specific accumulation of flavonoids in *Arabidopsis thaliana*. *Plant J.* 46, 768–779. doi: 10.1111/j.1365-313X.2006.02733.x

Burr, F. A., Burr, B., Scheffler, B. E., Blewitt, M., Wienand, U., and Matz, E. C. (1996). The maize repressor-like gene *intensifier1* shares homology with the *r1/b1* multigene family of transcription factors and exhibits missplicing. *Plant Cell* 8:1249. doi: 10.1105/tpc.8.8.1249

Carretero-Paulet, L., Galstyan, A., Roig-Villanova, I., Martínez-García, J. F., Bilbao-Castro, J. R., and Robertson, D. L. (2010). Genome-wide classification and evolutionary analysis of the bHLH family of transcription factors in *Arabidopsis*, poplar, rice, moss, and algae. *Plant Physiol.* 153, 1398–1412. doi: 10.1104/pp.110.153593

Elomaa, P., Uimari, A., Mehto, M., Albert, V. A., Laitinen, R. A., and Teeri, T. H. (2003). Activation of anthocyanin biosynthesis in Gerbera hybrida (Asteraceae) suggests conserved protein-protein and protein-promoter interactions between the anciently diverged monocots and eudicots. *Plant Physiol.* 133, 1831–1842. doi: 10.1104/pp.103.026039

Guo, J., Sun, B., He, H., Zhang, Y., Tian, H., and Wang, B. (2021). Current understanding of bHLH transcription factors in plant abiotic stress tolerance. *Int. J. Mol. Sci.* 22:4921. doi: 10.3390/ijms22094921

He, Q., Jones, D. C., Li, W., Xie, F., Ma, J., Sun, R., et al. (2016). Genome-wide identification of R2R3-MYB genes and expression analyses during abiotic stress in *Gossypium raimondii*. *Sci. Rep.* 6:22980. doi: 10.1038/srep22980

Heim, M. A., Jakoby, M., Werber, M., Martin, C., Weisshaar, B., and Bailey, P. C. (2003). The basic helix-loop-helix transcription factor family in plants: a genome-wide study of protein structure and functional diversity. *Mol. Biol. Evol.* 20, 735–747. doi: 10.1093/molbev/msg088

Hirakawa, H., Shirasawa, K., Miyatake, K., Nunome, T., Negoro, S., Ohyama, A., et al. (2014). Draft genome sequence of eggplant (*Solanum melongena* L.): the representative *solanum* species indigenous to the old world. *DNA Res.* 21, 649–660. doi: 10.1093/dnares/dsu027

Hu, D. G., Yu, J. Q., Han, P. L., Xie, X. B., Sun, C. H., Zhang, Q. Y., et al. (2019). The regulatory module MdPUB29-MdbHLH3 connects ethylene biosynthesis with fruit quality in apple. *New Phytol.* 221, 1966–1982. doi: 10.1111/nph.15511

Huang, J., Guo, Y., Sun, Q., Zeng, W., Li, J., Li, X., et al. (2018). Genome-wide identification of R2R3-MYB transcription factors regulating secondary cell wall thickening in cotton fiber development. *Plant Cell Physiol.* 60, 687–701. doi: 10.1093/pcp/pcy238

Ilk, N., Ding, J., Ihnatowicz, A., Koornneef, M., and Reymond, M. (2015). Natural variation for anthocyanin accumulation under high-light and low-temperature stress is attributable to the ENHANCER OF AG-4 2 (HUA2) locus in combination with production of anthocyanin pigmenT1 (PAP1) and PAP2. *New Phytol.* 206, 422–435. doi: 10.1111/nph.13177

Jia, N., Wang, J. J., Liu, J., Jiang, J., Sun, J., Yan, P., et al. (2021). DcTT8, a bHLH transcription factor, regulates anthocyanin biosynthesis in Dendrobium candidum. *Plant Physiol. Biochem.* 162, 603–612. doi: 10.1016/j.plaphy.2021.03.006

Jiang, M. M., Ren, L., Lian, H. L., Liu, Y., and Chen, H. Y. (2016). Novel insight into the mechanism underlying light-controlled anthocyanin accumulation in eggplant (*Solanum melongena* L.). *Plant Sci.* 249, 46–58. doi: 10.1016/j.plantsci.2016.04.001

Koes, R., Verweij, W., and Quattrocchio, F. (2005). Flavonoids: a colorful model for the regulation and evolution of biochemical pathways. *Trends Plant Sci.* 10, 236–242. doi: 10.1016/j.tplants.2005.03.002

Konczak, I., and Zhang, W. (2004). Anthocyanins-more than nature's colours. *J. Biomed. Biotechnol.* 2004, 239–240. doi: 10.1155/S1110724304407013

Kumar, S., Stecher, G., and Tamura, K. (2016). MEGA7: molecular evolutionary genetics analysis version 7.0 for bigger datasets. *Mol. Biol. Evol.* 33, 1870–1874. doi: 10.1093/molbev/msw054

Li, P., Chen, B., Zhang, G., Chen, L., Dong, Q., Wen, J., et al. (2016b). Regulation of anthocyanin and proanthocyanidin biosynthesis by Medicago truncatula bHLH transcription factor MtTT8. *New Phytol.* 210, 905–921. doi: 10.1111/nph.13816

Li, J., Gao, Z., Zhou, L., Li, L. Z., Zhang, J. H., Liu, Y., et al. (2019). Comparative transcriptome analysis reveals K^+ transporter gene contributing to salt tolerance in eggplant. *BMC Plant Biol.* 19:67. doi: 10.1186/s12870-019-1663-8

Li, J., He, Y. J., Zhou, L., Liu, Y., Jiang, M. M., Ren, L., et al. (2018). Transcriptome profiling of genes related to light-induced anthocyanin biosynthesis in eggplant (*Solanum melongena* L.) before purple color becomes evident. *BMC Genomics* 19:324. doi: 10.1186/S12864-018-4693-Y

Li, J., Jiang, M. M., Ren, L., Liu, Y., and Chen, H. Y. (2016a). Identification and characterization of CBL and CIPK gene families in eggplant (*Solanum melongen*a L.). *Mol. Gen. Genomics.* 291, 1769–1781. doi: 10.1007/s00438-016-1218-8

Li, J., Ren, L., Gao, Z., Jiang, M., Liu, Y., Zhou, L., et al. (2017). Combined transcriptomic and proteomic analysis constructs a new model for light-induced anthocyanin biosynthesis in eggplant (*Solanum melongena* L.). *Plant Cell Environ.* 40, 3069–3087. doi: 10.1111/pce.13074

Li, J., Wang, Z., Chang, Z., He, H., Tang, X., Ma, L., et al. (2021a). A functional characterization of TaMs1 orthologs in Poaceae plants. *Crop J.* doi: 10.1016/j.cj.2020.12.002 (in press).

Li, X., Xiang, F., Han, W., Qie, B., Zhai, R., Yang, C., et al. (2021b). The MIR-domain of PbbHLH2 is involved in regulation of the anthocyanin biosynthetic pathway in "red zaosu" (*pyrusbretschneideri* rehd.) pear fruit. *Int. J. Mol. Sci.* 22:3026. doi: 10.3390/ijms22063026

Li, Q., Zhang, C., Li, J., Wang, L., and Ren, Z. (2012). Genome-wide identification and characterization of R2R3MYB family in Cucumis sativus. *PLoS One* 7:e47576. doi: 10.1371/journal.pone.0047576

Livak, K. J., and Schmittgen, T. D. (2001). Analysis of relative gene expression data using real-time quantitative PCR and the 2(-Delta Delta C(T)) method. *Methods* 25, 402–408. doi: 10.1006/meth.2001.1262

Massari, M. E., and Murre, C. (2000). Helix-loop-helix proteins: regulators of transcription in eucaryotic organisms. *Mol. Cell. Biol.* 20, 429–440. doi: 10.1128/MCB.20.2.429-440.2000

Moglia, A., Florio, F. E., Iacopino, S., Guerrieri, A., Milani, A. M., Comino, C., et al. (2020). Identification of a new R3 MYB type repressor and functional characterization of the members of the MBW transcriptional complex involved in anthocyanin biosynthesis in eggplant (*S. melongena* L.). *PLoS One* 15:e0232986. doi: 10.1371/journal.pone.0232986

Mol, J., Grotewold, E., and Koes, R. (1998). How genes paint flowers and seeds. *Trends Plant Sci.* 3, 212–217. doi: 10.1016/S1360-1385(98)01242-4

Montefiori, M., Brendolise, C., Dare, A. P., Lin-Wang, K., Davies, K. M., Hellens, R. P., et al. (2015). In the *Solanaceae*, a hierarchy of bHLHs confer distinct target specificity to the anthocyanin regulatory complex. *J. Exp. Bot.* 66, 1427–1436. doi: 10.1093/jxb/eru494

Neff, M. M., and Chory, J. (1998). Genetic interactions between phytochrome A, phytochrome B, and cryptochrome 1 during *Arabidopsis* development. *Plant Physiol.* 118, 27–35. doi: 10.1104/pp.118.1.27

Noda, Y., Kneyuki, T., Igarashi, K., Mori, A., and Packer, L. (2000). Antioxidant activity of nasunin, an anthocyanin in eggplant peels. *Toxicology* 148, 119–123. doi: 10.1016/s0300-483x(00)00202-x

Oren-Shamir, M. (2009). Does anthocyanin degradation play a significant role in determining pigment concentration in plants? *Plant Sci.* 177, 310–316. doi: 10.1152/japplphysiol.00626.2005

Pires, N., and Dolan, L. (2010). Origin and diversification of basic-helix-loop-helix proteins in plants. *Mol. Biol. Evol.* 27, 862–874. doi: 10.1093/molbev/msp288

Ramsay, N. A., and Glover, B. J. (2005). MYB-bHLH-WD40 protein complex and the evolution of cellular diversity. *Trends Plant Sci.* 10, 63–70. doi: 10.1016/j.tplants.2004.12.011

Ren, J., Liu, Z., Chen, W., Xu, H., and Feng, H. (2019). Anthocyanin degrading and chlorophyll accumulation lead to the formation of bicolor leaf in *ornamental kale*. *Int. J. Mol. Sci.* 20:603. doi: 10.3390/ijms20030603

Shi, S. L., Liu, Y., He, Y. J., Li, L. Z., Li, D. L., and Chen, H. Y. (2021). R2R3-MYB transcription factor SmMYB75 promotes anthocyanin biosynthesis in eggplant (*Solanum melongena* L.). *Sci. Hortic.* 282:110020. doi: 10.1016/j.scienta.2021.110020

Song, S., Qi, T., Fan, M., Zhang, X., Gao, H., Huang, H., et al. (2013). The bHLH subgroup IIId factors negatively regulate jasmonate-mediated plant defense and development. *PLoS Genet.* 9:e1003653. doi: 10.1371/journal.pgen.1003653

Sparkes, I. A., Runions, J., Kearns, A., and Hawes, C. (2006). Rapid, transient expression of fluorescent fusion proteins in tobacco plants and generation of stably transformed plants. *Nat. Protoc.* 1, 2019–2025. doi: 10.1038/nprot.2006.286

Sun, C., Deng, L., Du, M., Zhao, J., Chen, Q., Huang, T., et al. (2020a). A transcriptional network promotes anthocyanin biosynthesis in tomato flesh. *Mol. Plant* 13, 42–58. doi: 10.1016/j.molp.2019.10.010

Sun, W., Jin, X., Ma, Z., Chen, H., and Liu, M. (2020b). Basic helix-loop-helix (bHLH) gene family in Tartary buckwheat (*Fagopyrum tataricum*): genome-wide identification, phylogeny, evolutionary expansion and expression analyses. *Int. J. Biol. Macromol.* 155, 1478–1490. doi: 10.1016/j.ijbiomac.2019.11.126

Tohge, T., de Souza, L. P., and Fernie, A. R. (2017). Current understanding of the pathways of flavonoid biosynthesis in model and crop plants. *J. Exp. Bot.* 68, 4013–4028. doi: 10.1093/jxb/erx177

Tsuda, T. (2012). Dietary anthocyanin-rich plants: biochemical basis and recent progress in health benefits studies. *Mol. Nutr. Food Res.* 56, 159–170. doi: 10.1002/mnfr.201100526

Vasudevan, S., Ponraj, K., Unni, S. C., Joy, N., and Radhakrishnan, E. K. (2005). Transformation and regeneration of *Solanum melongena* using *Agrobacterium tumefaciens*. *J. Plant Biol.* 32, 29–32. doi: 10.1007/BF00232129

Wang, P., Su, L., Gao, H., Jiang, X., Wu, X., Li, Y., et al. (2018). Genome-wide characterization of bHLH genes in grape and analysis of their potential relevance to abiotic stress tolerance and secondary metabolite biosynthesis. *Front. Plant Sci.* 9:64. doi: 10.3389/fpls.2018.00064

Wang, L., Tang, W., Hu, Y., Zhang, Y., Sun, J., Guo, X., et al. (2019). A MYB/bHLH complex regulates tissue-specific anthocyanin biosynthesis in the inner pericarp of red-centered kiwifruit Actinidia chinensis cv. Hongyang. *Plant J.* 99, 359–378. doi: 10.1111/tpj.14330

Xie, X. B., Li, S., Zhang, R. F., Zhao, J., Chen, Y. C., Zhao, Q., et al. (2012). The bHLH transcription factor MdbHLH3 promotes anthocyanin accumulation and fruit colouration in response to low temperature in apples. *Plant Cell Environ.* 35, 1884–1897. doi: 10.1111/j.1365-3040.2012.02523.x

Zhai, Y., Yu, K., Cai, S., Hu, L., Amoo, O., Xu, L., et al. (2020). Targeted mutagenesis of BnTT8 homologs controls yellow seed coat development for effective oil production in *Brassica napus* L. *Plant Biotechnol. J.* 18, 1153–1168. doi: 10.1111/pbi.13281

Zhao, P., Li, X., Jia, J., Yuan, G., Chen, S., Qi, D., et al. (2018). bHLH92 from sheepgrass acts as a negative regulator of anthocyanin/proanthocyandin

accumulation and influences seed dormancy. *J. Exp. Bot.* 70, 269–284. doi: 10.1093/jxb/ery335

Zhao, R., Song, X. X., Yang, N., Chen, L. Q., Xiang, L., Liu, X. Q., et al. (2020). Expression of the subgroup IIIf bHLH transcription factor CpbHLH1 from *Chimonanthus praecox* (L.) in transgenic model plants inhibits anthocyanin accumulation. *Plant Cell Rep.* 39, 891–907. doi: 10.1007/s00299-020-02537-9

Zhou, L., He, Y., Li, J., Liu, Y., and Chen, H. (2020). CBFs function in anthocyanin biosynthesis by interacting with MYB113 in eggplant (*Solanum melongena* L.). *Plant Cell Physiol.* 61, 416–426. doi: 10.1093/pcp/pcz209

Conflict of Interest: The authors declare that the research was conducted in the absence of any commercial or financial relationships that could be construed as a potential conflict of interest.

Publisher's Note: All claims expressed in this article are solely those of the authors and do not necessarily represent those of their affiliated organizations, or those of the publisher, the editors and the reviewers. Any product that may be evaluated in this article, or claim that may be made by its manufacturer, is not guaranteed or endorsed by the publisher.

frontiers in Plant Science

ORIGINAL RESEARCH
published: 02 December 2021
doi: 10.3389/fpls.2021.759968

Metabolic Profiling and Gene Expression Analysis Unveil Differences in Flavonoid and Lipid Metabolisms Between 'Huapi' Kumquat (*Fortunella crassifolia* Swingle) and Its Wild Type

*Qiaoli Ma[1], Yongwei Hu[1], Xinghua Dong[1], Gaofeng Zhou[2], Xiao Liu[3], Qingqing Gu[1] and Qingjiang Wei[1]**

[1] College of Agronomy, Jiangxi Agricultural University, Nanchang, China, [2] National Navel Orange Engineering Research Center, Gannan Normal University, Ganzhou, China, [3] School of Horticulture and Plant Protection, Yangzhou University, Yangzhou, China

OPEN ACCESS

Edited by:
Itay Maoz, Agricultural Research Organization (ARO), Israel

Reviewed by:
Qiang Xu, Huazhong Agricultural University, China
Xiaohong Kou, Tianjin University, China
Hongju Zhu, Zhengzhou Fruit Research Institute, Chinese Academy of Agricultural Sciences (CAAS), China

***Correspondence:**
Qingjiang Wei
qjwell@126.com

Specialty section:
This article was submitted to Plant Metabolism and Chemodiversity, a section of the journal Frontiers in Plant Science

Received: *17 August 2021*
Accepted: *14 October 2021*
Published: *02 December 2021*

Citation:
Ma Q, Hu Y, Dong X, Zhou G, Liu X, Gu Q and Wei Q (2021) Metabolic Profiling and Gene Expression Analysis Unveil Differences in Flavonoid and Lipid Metabolisms Between 'Huapi' Kumquat (Fortunella crassifolia Swingle) and Its Wild Type. Front. Plant Sci. 12:759968. doi: 10.3389/fpls.2021.759968

To elucidate the mechanism underlying special characteristic differences between a spontaneous seedling mutant 'Huapi' kumquat (HP) and its wild-type 'Rongan' kumquat (RA), the fruit quality, metabolic profiles, and gene expressions of the peel and flesh were comprehensively analyzed. Compared with RA, HP fruit has distinctive phenotypes such as glossy peel, light color, and few amounts of oil glands. Interestingly, HP also accumulated higher flavonoid (approximately 4.1-fold changes) than RA. Based on metabolomics analysis, we identified 201 differential compounds, including 65 flavonoids and 37 lipids. Most of the differential flavonoids were glycosylated by hexoside and accumulated higher contents in the peel but lower in the flesh of HP than those of RA fruit. For differential lipids, most of them belonged to lysophosphatidycholines (LysoPCs) and lysophosphatidylethanolamines (LysoPEs) and exhibited low abundance in both peel and flesh of HP fruit. In addition, structural genes associated with the flavonoid and lipid pathways were differentially regulated between the two kumquat varieties. Gene expression analysis also revealed the significant roles of *UDP-glycosyltransferase* (*UGT*) and *phospholipase* genes in flavonoid and glycerophospholipid metabolisms, respectively. These findings provide valuable information for interpreting the mutation mechanism of HP kumquat.

Keywords: metabolomics, flavonoids, lipids, kumquat fruit, gene expression

INTRODUCTION

Kumquat is of the genus *Fortunella* that is closely related to *Citrus* genus. Both belong to the true *Citrus* group of the Rutaceae family. As an important part of the most popular fruit crops of citrus, kumquat is widely distributed and cultivated in the world, particularly in southeast China. It is a favorite by consumers due to its good taste, small size, and being eaten raw without peeling. Besides its attractive organoleptic properties, kumquat is an excellent source of nutrients and phytochemicals, such as flavonoids, phenolic acids, carotenoids, vitamins, polysaccharides,

essential oil, lipids, and dietary fiber (Liu et al., 2019). Furthermore, it is an important herbal medicine in Chinese traditional medicine. Its dry roots, leaves, and fruits even have been commonly employed to treat traumatic injury, colds, and coughs (Rafiq et al., 2018). And in modern medicine, some bioactive compounds have been isolated from ripening or unripe fruit to study their pharmacological activities in immune defense, antioxidation, antimetabolic disorder, diabetes, cardiovascular diseases, psychiatric disorder, and cancer (Erlund, 2004; Aruoma et al., 2012). Hence, revealing the constitution and biosynthesis of functional compounds in kumquat fruit will benefit for citrus breeding to produce new resources of functional fruit.

Recently, more attentions have been paid to characterize the natural chemical profiles of citrus fruits (Wang et al., 2017). Flavonoids are a massive class of secondary metabolites in plants and are especially rich in citrus fruits with a more amount of total polyphenol and flavonoid than that of total carotenoids (Tan et al., 2016; Lou and Ho, 2017). Flavonoids are the part of fruit pigmentation and make fruit exhibit special taste, for instance, hesperidin, nobiletin, naringin, tangeretin, and neohesperidin for bitter taste in citrus, and dihydrochalcone for sweet taste (Ververidis et al., 2007). Based on differences in their chemical structures, flavonoids are mainly classified into several basic types, such as flavone, flavonol, flavanone, flavanonol, isoflavone, and isoflavanone (Ververidis et al., 2007). In citrus fruits, flavonoids are usually modified by different chemical groups, including *C*-glycosyl, *O*-glycosyl, -OCH_3, -OH, and -CH_3 (Zhang et al., 2012; Khan et al., 2014). And the flavonoids composition in flavedo, albedo, and juice vesicle tissues also showed a large-magnitude variation (Zhang et al., 2011), for example, polymethoxylated flavonoids (PMFs) preferentially accumulated in the flavedo (Wang et al., 2017).

However, little is known about total natural metabolites in kumquat fruits. Barreca et al. (2011) identified and quantified only 13 *C*- and *O*-glycosyl flavonoids in crude juice from kumquat fruits and first reported tvicenin-2, lucenin-2 4′-methyl ether, narirutin 4′-O-glucoside, acacetin 3,6-di-*C*-glucoside, and apigenin 8-*C*-neohesperidoside existing in kumquat juice. Tan et al. (2016) identified 12 compounds in ethanol extract of the whole kumquat fruit by using UPLC Q-TOF/MS, and five of these compounds were tentatively characterized in the four major cultivated *Fortunella* types with 3′,5′-di-*C*-glucopyranosylphloretin, acacetin 8-*C*-neohesperidoside, and acacetin 6-*C*-neohesperidoside as the dominant components. Lou and Ho (2017) reviewed all the flavonoids identified in kumquat and listed the 15 major flavonoids. Overall, the flavonoid profiles in kumquat fruit are limited till now. It is worth noting that based on HPLC-DAD-ESI-MA/MS, Wang et al. (2017) had identified 117 flavonoids in 62 *Citrus* germplasms from five citrus species, namely, sweet orange, mandarins, lemons, pummelos, and grapefruits, but excluded kumquat. This study guided us to identify the flavonoids existing in kumquat fruit.

Besides flavonoids, lipids are essential components of the edible part in kumquat fruits, which play a pivotal role in membrane structure and stability, time of storage, and organoleptic properties of the juices. There were 0.86 g lipids per 100 g edible portion of fresh kumquat, and phospholipids accounted for about 8–18% of the total lipids in different parts of citrus fruits (Kolesnik et al., 1989). Lysophosphatidylethanolamines (LysoPEs) and lysophosphatidycholines (LysoPCs) were the hydrolytic products of glycerophospholipids by PLA2 (Cowan, 2006), and they participated in regulating fruit quality formation and postharvest senescence (Amaro and Almeida, 2013). By using GC, Touns et al. (2011) had analyzed the lipid composition (mainly about fatty acids) of the oilseed in bitter orange and mandarin. But there were few reports of lipids profile in kumquat fruits to our limited knowledge. For the complex and diverse metabolites in citrus fruits, natural product identified in kumquat is very insignificant. Hence, using the existing advanced metabolomics technology, more kumquat metabolites can be isolated and identified, which may further enrich the product data resources of citrus fruits.

'Rongan' kumquat (*Fortunella crassifolia* Swingle, RA) is the main variety and has a long cultivation history in the Guangxi Zhuang Autonomous Region, China. 'Huapi' kumquat (HP), screened in the 1980s, is a spontaneous seedling mutant that originated from RA kumquat. Compared with the wild type, the mutant HP fruit has attractive traits such as glossy peel, fewer seeds, and less spicy flavor. We previously found that the contents of organic acid and soluble sugar and the expression levels of related genes exhibited large differences between HP and RA fruits (Wei et al., 2021). But the chemical material compositions associated with the morphological and quality differences of the two varieties are not fully understood. To illustrate the biochemical basis for its special traits, metabolic profiling of the peel and flesh derived from HP and RA fruits at the maturation stage was investigated based on a widely targeted metabolomics approach, and the expression patterns of genes related to compound differences were also comprehensively analyzed.

MATERIALS AND METHODS

Plant Materials

Fruits of RA and HP were harvested from 13-year-old trees growing on the same orchard (Rong'an County, Guangxi Zhuang Autonomous Region, China) under similar management conditions. For each variety, fruit samples were collected randomly from the peripheral canopy of at least three trees, with 40 representative fruits from each tree at 210 days after flowering (DAF). After collecting, the fruits were quickly transported to the laboratory in an ice-box. The peel and flesh were separated from each fruit, immediately frozen in liquid nitrogen, and stored at −80°C for further use.

Analysis of Phenotypic Characteristics and Determination of Flavonoids

Fresh coloration of fruit was determined by a CR-400 chromameter (Minolta, Japan) and described by the indexes of lightness (L*), green-red color value (a*), and blue-yellow value (b*). The citrus color index (CCI), a comprehensive indicator for color impression, was calculated as CCI = 1000 × a*/(L* × b*),

and it represents a degree of yellow/orange/reddish of fruit color. Ten fruits were used per replicate with three replicates for each variety. Two measurements were made at two symmetrical points at the equatorial region of each fruit.

Observation and calculation of oil morphology were performed using a light microscope (Olympus IX73, Tokyo, Japan). The fruit peel for scanning electron microscopy (SEM) was prepared as described by Liu et al. (2015). Then, the samples were observed and photographed under a scanning electron microscope (JSM-6390LV, JEOL, Japan). The total content of flavonoids was measured using the plant flavonoids test kit (Nanjing Jiancheng Bioengineering Research Institute, China). The flavonoid content was calculated by reading the absorbance at 502 nm using a spectrophotometer (Shimadzu UV-1800, Japan).

Metabolic Profiling

The peel and flesh samples acquired above were first freeze-dried and crushed using a mixer mill (MM 400, Retsch). Metabolite identification was carried out using a widely targeted metabolomics method by MetWare Biotechnology Co., Ltd (Wuhan, China) following their standard procedures. Three biological replicates were independently analyzed for each sample. To validate the technical reproducibility, the mixture of the sample extracts was serviced as a quality control sample and was added in the analytical pipeline. In total, 15 datasets, namely, three mixed quality control data (Mix01, 02, and 03) and 12 experimental sample data RA-Peel (RAP1, 2, and 3), RA-Flesh (RAF1, 2, and 3), HP-Peel (HPP1, 2, and 3), and HP-Flesh (HPF1, 2, and 3), were obtained. Mass spectrum signals were qualified and quantified according to the MetWare local database. Quantification of metabolites was carried out using a multiple reaction monitoring (MRM) method. Metabolites with a threshold of log2 (fold change) ≥ 2 or ≤ 0.5 and variable importance in project (VIP) ≥ 1 were considered as differential accumulation. Then, the differentially accumulated metabolites were mapped to the Kyoto Encyclopedia of Genes and Genomes (KEGG) database and used in the significant enrichment analysis and major enriched pathways. The differential metabolites were hierarchically clustered under the algorithm of Euclidean distance and complete linkage by MEV software (v 4.9.0).

Differential Gene Expression Analysis

To investigate the gene expression profiles, transcriptomic data generated from the peel and flesh of RA and HP fruits from 90, 150, and 210 DAF were downloaded from the NCBI Sequence Read Archive (SRA) database under the accession PRJNA658060 (Wei et al., 2021). Gene expression levels were calculated based on FPKM (fragments per kilobase of exon model per million mapped reads) using RSEM software. Significant difference thresholds [FDR (false discovery rate) ≤ 0.01 and $|\log2 \text{ (fold change)}| \geq 1$] were used to screen the differentially expressed genes (DEGs).

Statistical Analysis

All data were performed using SPSS Statistics (Chicago, IL, United States) and expressed as the mean $\pm$ standard error of triplicates. The differences between the means were evaluated using Student's *t*-test.

RESULTS

Fruit Characteristics of RA and HP Kumquats

Dynamic changes in fruit color of RA and HP kumquats were investigated during fruit development and maturation. Color indexes, including L*, a*, b*, and CCI, showed no difference between HP and RA during the development stage of 60∼150 DAF, but were significantly lower in HP compared to RA during the turning and maturation stage (150–180 DAF) (**Supplementary Figure 1**). The lower value of CCI in HP indicates a lighter orange/reddish external peel color than in RA fruit. This was in accordance with the color appearance of matured HP (yellow-orange) and RA (reddish-orange) fruit (**Figure 1A**). As an important type of flavor and pigments component, the total flavonoid content was also detected and compared between HP and RA. There was 17.71 mg/100 g^{-1} FW of flavonoids in HP, which was four times higher than that of RA fruit (4.33 mg/100 g^{-1} FW) (**Figure 1B**). Furthermore, HP fruit was seedless (**Figure 1A**) and has a higher single fruit weight (**Figure 1C**), lower pericarp thickness (**Figure 1D**), and fewer oil glands in the pericarp (**Figure 1E**), as well as thinner wax and cuticle (**Figure 1F**) than those of RA fruit. All these advanced characteristics make HP fruit more glossy and attractive than RA fruit.

Analysis of the Metabolomics Data Quality and Comparison of Metabolites Between Two Kumquat Varieties

To comprehensively investigate the biochemical mechanisms of the morphological differences between HP and RA kumquat, all metabolites in the peel and flesh were measured by LC-ESI-MS/MS system. The total ions current (TIC) and multi-peak detection plot (XIC) of metabolites in the MRM mode of a mixed-quality control samples are shown in **Supplementary Figure 2**. To further understand the overall metabolic variance among those samples, a PCA over the metabolic profiles of the 15 samples was conducted. The first two components of the PCA score plot represent 69.53% of the total variance: The explained values of PC1 and PC2 were 47.88% and 21.65%, respectively. In the PCA plot, any three replicated samples within a group were tightly clustered together, and samples from different varieties or tissues were separated from each other (**Figure 2A**). These PCA results indicated that mass data were good in repetition, and metabolites in different groups differed distinctively. Hierarchical cluster analysis of all detected metabolites in the 12 experimental samples showed that the three biological replicates of each group clustered together, which further confirmed the high reliability of these generated metabolite data (**Figure 2B**). Moreover, the two flesh groups of HP and RA were separated from the two peel groups, which was coordinated with the distribution of these four groups on PC1 of PCA.

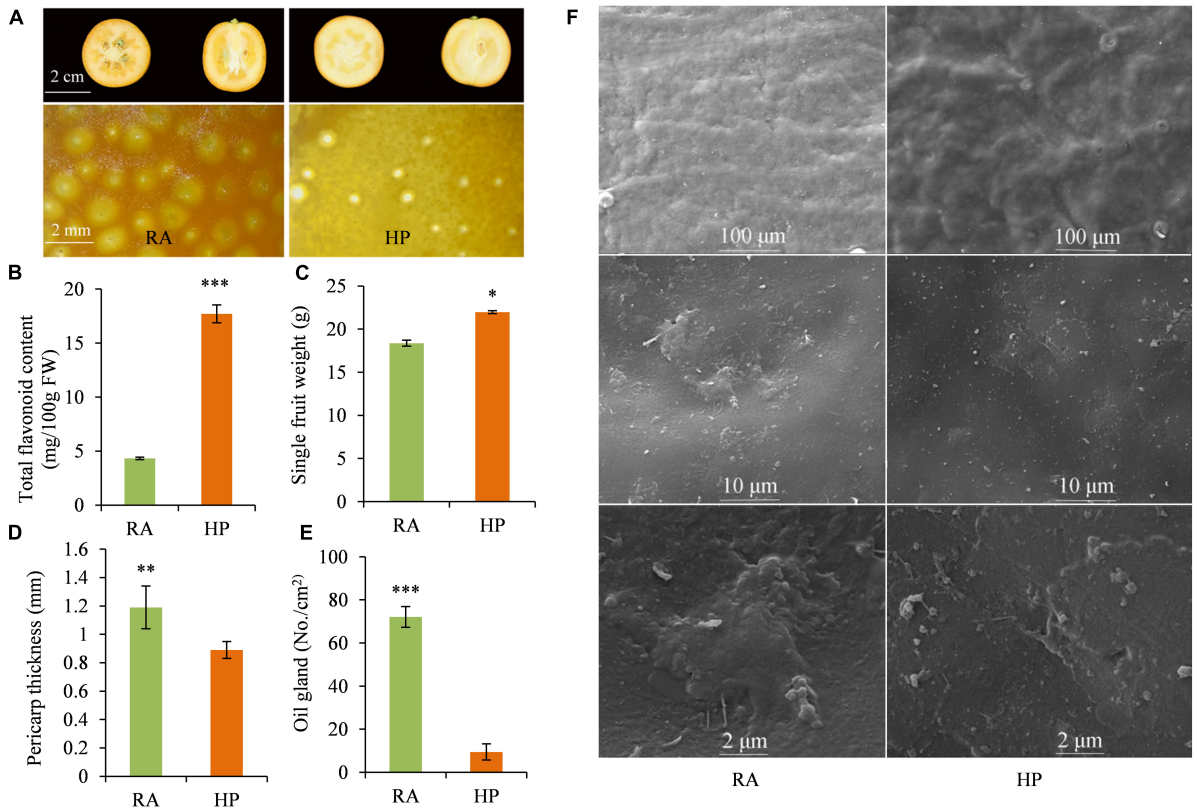

FIGURE 1 | Quality characteristics of RA and HP fruits. **(A)** Fruit photograph. **(B)** Total flavonoid content. **(C)** Single fruit weight. **(D)** Pericarp thickness. **(E)** Oil gland number. **(F)** Cuticle microscopic morphology. Asterisks indicate the significant difference between two verities (*$P < 0.05$, **$P < 0.01$, and ***$P < 0.001$).

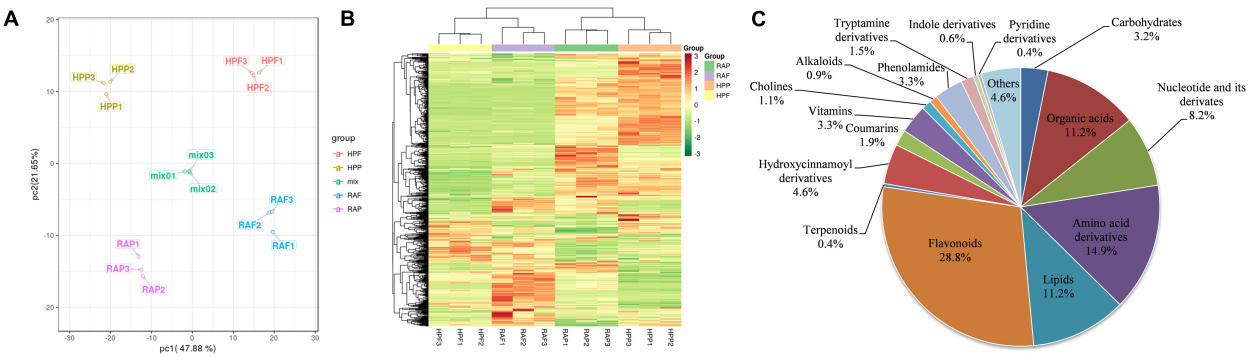

FIGURE 2 | Cluster analysis for all sample data. **(A)** Principal component analysis of the peel and flesh of two kumquat fruits and the mixed samples. **(B)** Hierarchical cluster analysis of all metabolites detected in the peel and flesh of RA and HP samples. Content of a metabolite was normalized by the range method. Each example is visualized in a single column, and each metabolite is represented by a single row. **(C)** Categories and proportion of all identified metabolites.

Mass spectrum signals were qualified and quantified based on the local metabolite database. In total, 538 metabolites were identified in the two kumquat fruits (**Supplementary Table 1**). Carbohydrates (3.2%), organic acids (11.2%), amino acids, and lipid-related substances (14.9% and 11.2%) in primary metabolites, as well as flavonoids (28.8%) and terpenoids (0.4%), and hydroxycinnamoyl derivatives (4.6%) in secondary metabolites, accounted for 66% of the detected metabolites. It is obvious that flavonoids are the most abundant components and account for about one-third of the total detected metabolites in matured kumquat fruits (**Figure 2C**).

There were 201 of the 538 metabolites exhibiting significantly different levels between the two kumquat varieties, with 151 metabolites differentially accumulating in the peel and 114 in the flesh, and 64 overlappings between the two tissues (**Figure 3A** and **Supplementary Table 2**). Among those differential metabolites,

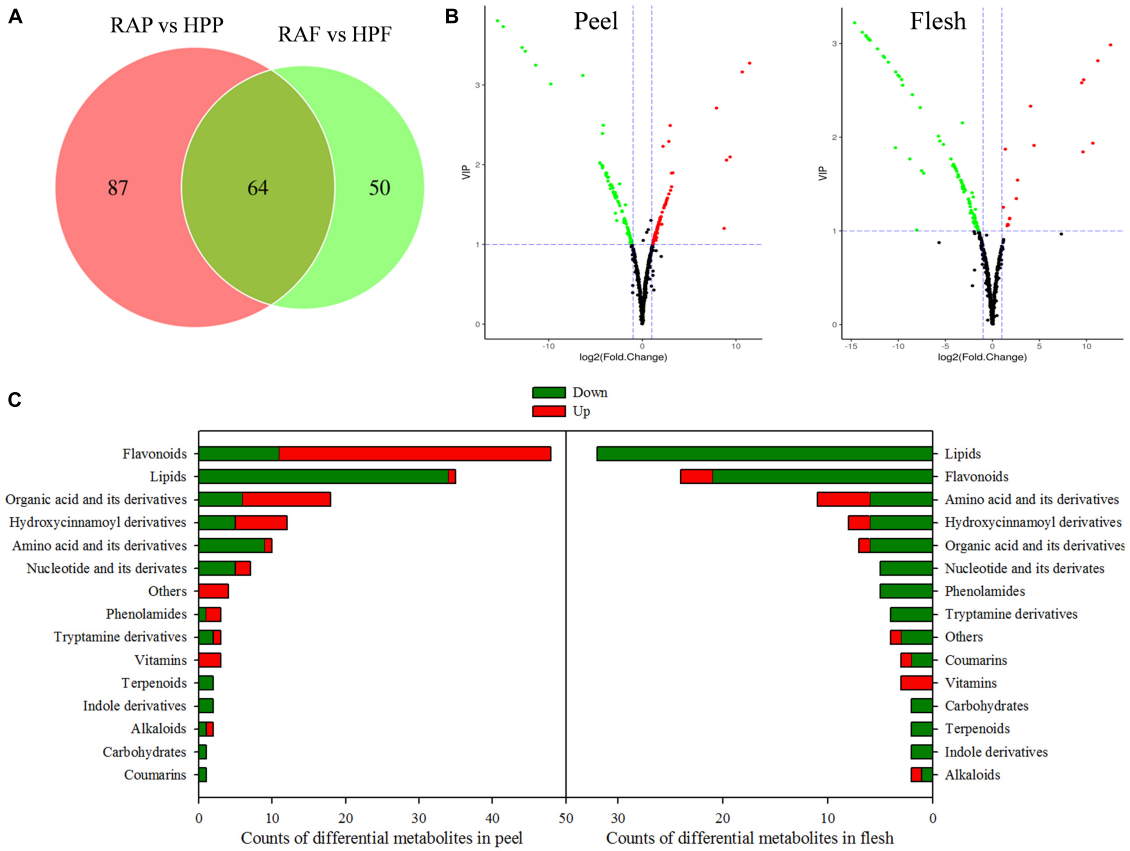

FIGURE 3 | Analysis of the differential metabolites in the peel and flesh of HP compared with RA. **(A)** Venn diagram of the differential metabolites. **(B)** Volcano plot of differential metabolites in the peel and flesh samples, respectively. Red scatter point indicates upregulated metabolite, whereas green scatter point indicates downregulated metabolite. **(C)** Functional categories and number of the differential metabolites.

71 metabolites were upregulated and 80 downregulated in the peel of HP compared to that of RA (**Figure 3B**). In the flesh, however, most of the differential metabolites (97 out of 114) were downregulated and only 17 metabolites were upregulated in HP (**Figure 3B**). According to the molecular structure and function, the differential metabolites were categorized into 15 categories (**Figure 3C**). In the peel, the top four categories were flavonoids (48), lipids (35), organic acids and their derivatives (18), and hydroxycinnamoyl derivatives (12). Similarly, lipids (32), flavonoids (24), amino acids and their derivatives (11), and hydroxycinnamoyl derivatives (8) were also on the top four categories in the flesh of two kumquat fruits (**Figure 3C**).

Kyoto Encyclopedia of Genes and Genomes Classification and Enrichment of the Differentially Accumulated Metabolites

To further identify the important metabolic pathways, KEGG classification analysis was performed. Of the 151 differential metabolites in HP peel, 58 were mapped into 62 KEGG pathways that were mainly responsible for the secondary metabolite biosynthesis pathways, such as flavonoid, phenylpropanoids, and alkaloids, and tryptophan metabolism (**Supplementary Figure 3A**). And of the 114 differential metabolites in HP flesh, 48 were mapped into 56 pathways that mainly were phenylpropanoids, flavonoid, tryptophan, and pyrimidine biosynthesis pathways (**Supplementary Figure 3B**). Enrichment analysis was further conducted to evaluate the importance of these pathways, and the top 20 pathways are shown in **Supplementary Figure 3**. There were five pathways significantly enriched in the peel, namely, (1) phenylalanine, tyrosine, and tryptophan biosynthesis; (2) stilbenoid, diarylheptanoid, and gingerol biosynthesis; (3) tryptophan metabolism; (4) staurosporine biosynthesis; and (5) anthocyanin biosynthesis (**Supplementary Figure 3C**). However, only the tryptophan metabolism pathway was significantly enriched in the flesh (**Supplementary Figure 3D**).

Differences of Flavonoid and Lipid Accumulation Between HP and RA Kumquats

Considering the wide variations of flavonoids and lipids in both peel and flesh in the two kumquat fruits, we conducted a detailed analysis of these two compounds. In the peel, most of

the differential flavonoids were glycosylated by hexoside, and the glycosides often occurred at 3-*O*, 5-*O*, 7-*O*, 6-*C*, and 8-*C*. Compared with RA, 37 out of the 48 flavonoids were upregulated in HP kumquat. According to the accumulation and change mode, the 48 differential flavonoids were classified into three clusters (**Figure 4A**). Metabolites in cluster I were the most abundant substances in the peel and their variation accounted for 79% of the total difference between HP and RA fruits. Among these metabolites, tricin 7-*O*-hexoside, *C*-hexosyl-apigenin *O*-pentoside, naringenin 7-*O*-neohesperidoside, chrysoeriol, and 6-*C*-hexosyl luteolin *O*-pentoside were highly accumulated in HP, whereas limocitrin *O*-hexoside, syringetin 3-*O*-hexoside, syringetin 7-*O*-hexoside, syringetin 5-*O*-hexoside, tangeretin, and nobiletin were highly accumulated in RA. There were 29 metabolites in cluster II, which both moderately accumulated in the peel and showed higher accumulation in HP. Eight metabolites in cluster III with trace accumulation in the peel were relatively highly accumulated in HP; among them, velutin *O*-glucuronic acid and isoliquiritigenin were only detected in HP. In contrast with the peel, most of these flavonoids (21 out of 24) were downregulated in the flesh of HP kumquat (**Figure 4B**). And they were clustered into two classes. Metabolites in cluster I were abundantly accumulated in both kumquat fruits: Tangeretin, selgin *O*-malonyl hexoside, isorhamnetin *O*-acetyl-hexoside, eriodictyol *C*-hexoside, neohesperidin, and methyl quercetin *O*-hexoside were particularly lower in HP than in RA. Metabolites in cluster II were tiny accumulated either in HP or in RA. Furthermore, only seven differential flavonoids overlapped between the peel and the flesh, namely, genistein 7-*O*-glucoside, limocitrin *O*-hexoside, syringetin, syringetin 3-*O*-hexoside, syringetin 5-*O*-hexoside, syringetin 7-*O*-hexoside, and tangeretin.

Lipids are an important constituent of plant cells. Almost all differential lipids were less in amount in HP than in RA (**Figures 4C,D**), and their distinction between the two kumquats was very similar among different tissues; 30 of 37 differential lipids were overlapped. The overlapped differential lipids belonged to either LysoPCs or LysoPEs, which were the hydrolytic products of glycerophospholipids catalyzed by several phospholipases. Furthermore, LysoPC 18:3, 18:2, 18:1, and 16:0 and LysoPE 18:1 and 16:0 are the main differential lipids between HP and RA fruits.

Differential Expression of Genes Related to Flavonoid and Lipid Metabolism

In order to clarify the molecular basis of the differences in flavonoid and lipid contents between HP and RA fruits, we further detected the expression of genes related to flavonoid and lipid metabolism by transcriptional sequencing. Transcriptomic data from the peel and flesh of the two kumquat fruits at three developmental stages showed that a total of 65 structural genes involved in flavonoid biosynthesis showed differential expression between HP and RA fruits. These genes included *PAL*, *C4H*, *4CL*, *CHS*, *CHI*, *F3H*, *F3'H*, *FLS*, *1,2-Rhat*, *UGT*, *DFR*, *ANS*, *UFGT*, and *LAR*. Specifically, the genes that related to early enzymatic reactions during phenylpropanoid pathway, including four *PAL* genes (sjg171720, sjg252410, sjg141140, and sjg170590), three *C4H* genes (sjg256270, sjg023860, and sjg303290), four *4CL* genes (sjg203960, sjg116210, sjg021810, and sjg114460), three *CHS* genes (sjg294150, sjg125680, and sjg125520), and one *CHI* gene (sjg280460), were generally upregulated in the peel of HP during fruit development, particularly at 90 DAF. In contrast, most of the above structural genes demonstrated low expression levels and were downregulated in the flesh of HP compared with RA fruit (**Figure 5**). Furthermore, nine genes encoding FLS also changed greatly, with four members (sjg143160, sjg125710, sjg143720, and sjg034020) showing upregulation in the peel, while all members showing downregulation in the flesh of HP compared with RA. In addition, six genes related to the anthocyanin biosynthesis pathway were identified and all of them exhibited downregulated expressions in both peel and flesh in HP fruit, with an exception of one *LAR* gene (sjg029150), which was specifically upregulated in HP peel and flesh at 90 DAF. Meanwhile, one *F3H* gene (sjg320640) was continuously downregulated in the peel and flesh, and one *F3'H* gene (sjg186480) was also downregulated in the flesh but upregulated in the peel. We also found that two *1,2-Rhat* genes were regulated, with one (sjg050250) being specifically upregulated and the other (sjg147470) downregulated in the peel, while both downregulated in the flesh (**Figure 5**). The UGTs catalyze the synthesis of galactosylated derivatives with various substrates, which is a key modifying enzyme in flavonoid metabolism. Here, a total of 24 *UGT* genes were identified and most of them were upregulated in both peel and flesh in HP fruit at all three developmental stages, particularly at 90 and 150 DAF (**Figure 5**). However, some exceptions were also observed. For instance, one *UGT* member (sjg237020) was continuously downregulated in both HP peel and flesh. In summary, a large number of genes involved in the flavonoid pathway were upregulated in the peel but downregulated in the flesh of HP fruit, which was consistent with the change of flavonoid content in different tissues of the mutant.

A total of 32 genes associated with glycerophospholipid metabolism were also screened out in the two kumquat fruits (**Figure 6**). Of these, six genes encoding GPAT were upregulated in the peel, while they were mostly downregulated in the flesh of HP compared with RA kumquat. The expressions of two *LPAAT* members were slightly downregulated but no significant difference was observed between the two kumquat fruits. The activities of PAP and DGK enzymes determined the interconversion of phosphatidic acid and diacylglycerol (DAG). There were one *PAP* gene (sjg173590) and two *DGK* genes (sjg256170 and sjg001480) showing downregulation in the peel and flesh of HP kumquat. The phosphotransferase CPT and EPT can catalyze DAG into phosphatidylcholine (PC) and phosphatidylethanolamine (PE), respectively. Here, three *EPT* genes were identified, namely, two (sjg235130 and sjg108670) upregulated and one (sjg030780) downregulated member in the peel of RA fruit. In the flesh, however, all three *EPT* members were downregulated (**Figure 6**). We also screened four *PLA2* genes, namely, two downregulated members (sjg166220 and sjg048850), one upregulated member (sjg270070), and one complex expression member (sjg245510) in the peel and flesh. However, all five *PLC* genes were downregulated in HP peel

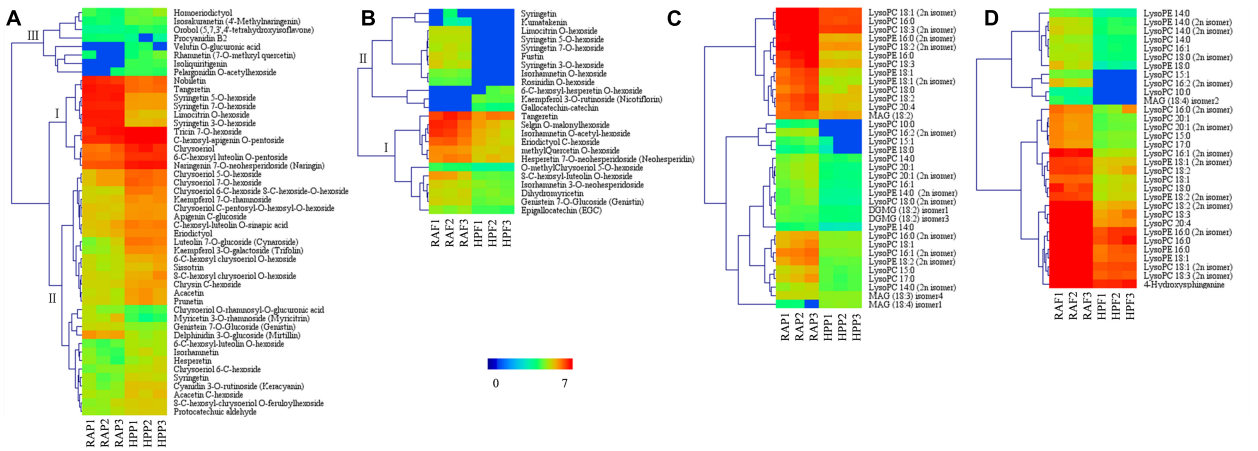

FIGURE 4 | Heat map visualization of the relative differences in flavonoids and lipids in the peel and flesh of HP compared with those of RA. **(A)** Flavonoids in the peel and **(B)** in the flesh. **(C)** Lipids in the peel and **(D)** in the flesh. The content of each metabolite was logarithm-normalized to complete linkage hierarchical clustering. Each column represents one sample, and each single row represents one metabolite. Red to dark blue indicates abundance changes from high to low.

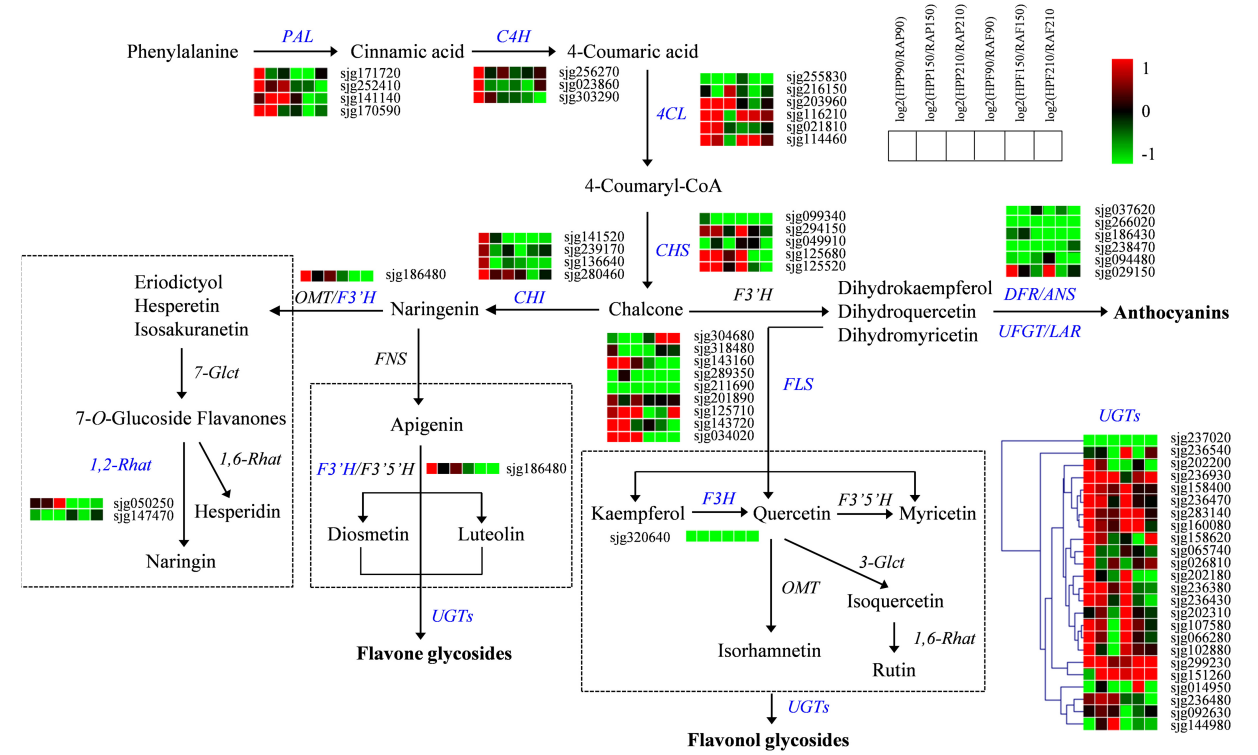

FIGURE 5 | Expression profiles of genes from the flavonoid biosynthesis pathway in the peel and flesh of kumquat fruits. The color scale from green (low) to red (high) represents the values of the log2 ratio (HP/RA) at 90, 150, and 210 DAF. The differentially expressed genes are highlighted in blue. PAL, phenylalanine ammonia-lyase; C4H, trans-cinnamate 4-monooxygenase; 4CL, 4-coumarate-CoA ligase; CHS, chalcone synthase; CHI, chalcone isomerase; 1,2-Rhat, 1,2-rhamnosyltransferase; F3′H, flavonoid 3′-monooxygenase; F3H, flavanone 3-dioxygenase; FLS, flavonol synthase; DFR, dihydroflavonol 4-reductase; ANS, anthocyanidin synthase; LAR, leucocyanidin reductase; UFGT, UDP-glucose flavonoid 3-O-glucosyltransferase; UGT, UDP-glycosyltransferase; 1,6-Rhat, 1,6-rhamnosyltransferase; 7-Glct, flavanone 7-O-glucosyltransferase; 3-Glct, anthocyanidin 3-O-glucosyltransferase; FNS, flavone synthase; F3′5′H, flavanoid 3′,5′-hydroxylase; OMT, O-methyltransferase.

compared with those in RA peel. In the flesh, three of these *PCL* genes (sjg030110, sjg018190, and sjg054490) were upregulated at 150 and 210 DAF. Regarding *PLD* genes, ten members were identified and their expression levels varied depending on developmental stage and fruit tissue. Of these, six *PLD* members (sjg026180, sjg036630, sjg218940, sjg312970, sjg275850,

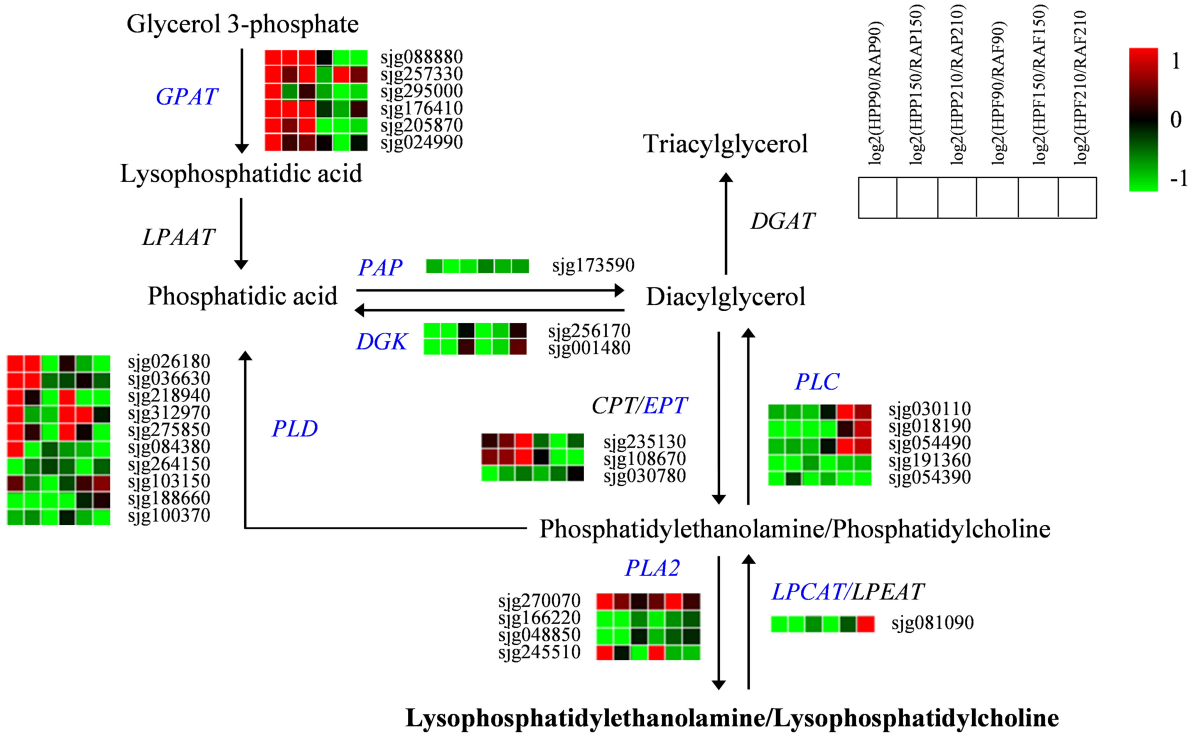

FIGURE 6 | Expression profiles of genes from the glycerophospholipid pathway in the peel and flesh of kumquat fruits. The color scale from green (low) to red (high) represents the values of the log2 ratio (HP/RA) at 90, 150, and 210 DAF. The differentially expressed genes are highlighted in blue. GPAT, glycerol-3-phosphate acyltransferase; LPAAT, Lysophosphatidic acid acyltransferase; PAP, phosphatidate phosphatase; DGK, diacylglycerol kinase; EPT, ethanolaminephosphotransferase; CPT, cholinephosphotransferase; PLA, phospholipase A; PLC, phospholipase C; PLD, phospholipase D; LPCAT, lysophosphatidylcholine acyltransferase; LPEAT, lysophosphatidylethanolamine acyltransferase; DGAT, diacylglycerol O-acyltransferase.

and sjg084380) displayed upregulated expression in the peel, and three members (sjg218940, sjg312970, and sjg275850) displayed upregulated expression in the flesh of HP at 90 and/or 150 DAF. Furthermore, one *LPCAT* gene was downregulated over most of the developmental stages but was upregulated in the flesh of HP fruit at 210 DAF (**Figure 6**).

DISCUSSION

The kumquat fruits are widely consumed fresh and have also been used in folk medicine in China (Tan et al., 2016). HP kumquat fruit has drawn increasing attention for its desirable traits, such as glossy peel. Given that the flavonoids play essential roles in determining citrus coloration, we measured the total flavonoid concentration and found it was over four times higher in HP than in RA fruit. Besides, the HP fruit peel was glossier and had less oil gland (**Figure 1**). Previous reports demonstrated that oil glands in the citrus peel are closely associated with the synthesis and accumulation of important secondary metabolites, such as monoterpenoids and sesquiterpenoids (Liu et al., 2019). Therefore, to further determine metabolite components and understand the morphological differences between the HP and its wild type, widely targeted metabolomics was used to identify the metabolites existing in the peel and flesh of kumquat fruits at the maturation stage. In total, 538 metabolites were identified in the two kumquat varieties. These metabolites were categorized into 17 substances in the secondary classification (**Figure 2C** and **Supplementary Table 1**). Among them, flavonoids and lipids were the top two differential metabolite classifications. Besides, hydroxycinnamoyl derivatives are the main differential secondary metabolites between the two kumquat varieties. For example, resveratrol and p-coumaraldehyde were highly expressed in RA fruit, but could not be detected in HP fruit (**Supplementary Table 1**). Taken together, our results suggested that the HP fruit exhibited a distinct pattern in metabolites accumulation, especially in flavonoids and lipids, and it could be a unique material for germplasm construction and citrus breeding.

Regulation of Flavonoid Metabolism

Flavonoids constitute a highly diverse family of secondary metabolites and contain about 8,000 known chemicals, which are generally responsible for the color change and flavor development in fruits (Winkel-Shirley, 2001; Ververidis et al., 2007; Khan et al., 2014). Our metabolomic analysis revealed that flavonoids were mostly upregulated in HP peel (**Figure 3C**), which was consistent with the result of total flavonoid determination (**Figure 1B**). Flavonoids and carotenoids are the two main pigments in citrus fruits. In general, carotenoids relate to various colors, whereas most flavonoids are colorless except for anthocyanins, which

produce "blood" color in blood oranges (Ververidis et al., 2007; Khan et al., 2014). Thus, we conclude that the high flavonoid accumulation in HP peel may contribute to its lighter color when compared with RA fruits. In the flesh, however, differentially accumulated flavonoids were mostly downregulated in HP, with little members in common with the peel. These results supported the finding that flavonoids composition in different tissues of citrus fruits showed a large magnitude variation among the flavedo, albedo, and juice vesicle tissues (Zhang et al., 2011). In addition, the compositions and quantities of flavonoids in kumquat fruit are rather different from other citrus species. It is reported that *O*-glycosylated flavonoids are rich in all fruit tissues from *Citrus* genus (Wang et al., 2017), whereas *C*-glycoside flavonoids are dominant phenolic compounds in kumquat fruit (Lou and Ho, 2017). However, herein metabolomic analysis uncovered that flavonoids are mostly in the form of *O*-glycosides in HP and RA kumquat fruits. In addition, the flavedo of *Citrus* genus widely contains PMFs, another kind of special flavonoid subclass, which have high oral bioavailability, antioxidant, and antibacterial activities (Zhang et al., 2012). In HP peel, several PMFs such as nobiletin (Cit305) and tangeretin (Cit367), which can cause lingering bitterness of citrus fruits, were identified and showed downregulation (**Figure 4A**). Another bitter substance, limonin, was also highly expressed but accumulated lower in the peel of HP than in the peel of RA (**Supplementary Table 1**). The low accumulation of these compounds could reduce the medicinal value of HP fruit but is an important reason for its pleasant taste.

Flavonoid biosynthesis is primarily regulated by phenylalanine, which is catalyzed by a series of genes involving the phenylpropanoid pathway, such as *PAL*, *C4H*, and *4CL*, and provides precursors for major phenolic metabolites biosynthesis in higher plants (Winkel-Shirley, 2001). Chen et al. (2021) reported that *PAL* and *4CL* are important genes in flavonoids accumulation in the yellow peel of cucumber. Our results suggested that at least four *PAL* and *4CL* genes and three *C4L* genes may be involved in the early reactions of flavonoids biosynthesis in HP peel. However, those genes showed downregulation during HP flesh development. In addition, *CHS* and *CHI* are also two key enzyme genes of intermediate flavonoid biosynthesis in plants. Previous studies reported that the expression level of *CHS* and *CHI* genes is closely associated with the content of flavonoids in citrus fruits (Moriguchi et al., 2001; Wang et al., 2010). Functional characterization of both genes was also conducted by Dong et al. (2001), who introduced *CHS* (*C2*) and *CHI* (*CHI1*) genes of maize into Arabidopsis mutants and found that the transgenic plants could accumulate flavonoids and anthocyanins. Similar results were obtained when a *Freesia hybrida CHS* gene (*FhCHS1*) was transformed into Arabidopsis *tt4* mutants (Sun et al., 2015). The upregulated expression of *CHS* and *CHI* members in HP peel was supported by their potential functions in the biosynthesis of anthocyanins and flavonoids (Tian et al., 2020).

Dihydroflavonols are kind of branching-point metabolites, which can be converted either by *DFR* in the first step for anthocyanin biosynthesis or by *FLS* to produce various flavonols and glycosidic derivatives (Erlund, 2004; Khan et al., 2014). Therefore, the downregulation of *DFR*, as well as other related genes including *ANS*, *LAR*, and *UFGT*, could limit anthocyanin synthesis in HP fruit. Meanwhile, the upregulation of *FLS* genes suggested their positive roles in flavonol accumulation in HP, particularly in the peel. Our results also implied that there is a competitive relationship between flavonol and anthocyanin biosynthesis in HP kumquat like in Arabidopsis (Gou et al., 2011), but different with tea plant, in which flavonoids were accompanied by anthocyanin (Shen et al., 2018). The HP fruit mainly accumulated *O*-glycosylated flavonoids, which are generated by activities of various UGTs (Osmani et al., 2010). At present, *UGTs* have been reported in many plant species (Caputi et al., 2012; Kumar et al., 2013). Recently, a *UGT* member from sweet orange (*CsUGT76F1*) was isolated, and its functions as flavonoid 7-O-glucosyltransferase and 7-O-rhamnosyltransferase were also established *in vivo* (Liu et al., 2018). As indicated in the present study, we screened out many *UGTs* that may contribute to glycosylated flavonoid accumulation in kumquat. Among them, three members (sjg158400, sjg283140, and sjg299230) increased their transcript abundance in all tested samples of HP fruit and likely played significant roles in flavonoid glycosylation (**Figure 5**). Further functional characterizations of these *UGTs* are essential for exploring their roles in the modification of biological activities and accumulation of flavonoids in the kumquat fruits.

Regulation of Lipid Metabolism

Lipid compounds are mainly categorized into eight subgroups, namely, fatty acyls, glycerolipids, polyketides, sphingolipids, prenol lipids, sterol lipids, saccharolipids, and glycerophospholipids (Liebisch et al., 2020). The citrus fruit is mostly composed of lipids belonging to fatty acids and glycerophospholipids (Kolesnik et al., 1989; Touns et al., 2011). Recently, studies on the glossy surface of the 'Newhall' navel orange mutant demonstrated that the decrease in aliphatic wax components such as aldehydes, alkanes, alcohols, and fatty acids was related to its glossy phenotype (Liu et al., 2015; He et al., 2019). Another study found that the plastid lipids (including monogalactosyldiacylglycerols, digalactosyldiacylglycerols, and lysophosphatidylglycerols) and the phospholipid precursors (including phosphatidic acids and DAGs) were highly accumulated in the glossy mutant (Wan et al., 2020). Although HP fruit possessed glossy peel, it showed a decrease in the lipids, particularly the LysoPCs and LysoPEs in the peel and flesh, compared with those in RA fruit. This could be partly ascribed to the few amount of oil glands observed in HP peel (**Figure 1E**). Previous studies reported that lipids are components or precursors of essential oils, which are mostly synthesized and accumulated in oil gland in citrus fruits (Voo et al., 2012; Liu et al., 2019). Lysophospholipids such as LysoPEs and LysoPCs are present only in trace amounts but they are involved in cell expansion, wound response, and freezing acclimation in plants (Cowan, 2006). Furthermore, several reports provide support for the roles of lysophospholipids in retarding leaf senescence and enhancing fruit shelf life (Hong et al., 2009). Thus, it is of great importance to investigate whether the decrease in LysoPCs and LysoPEs reduces the storage quality of HP fruit.

Lysophosphatidycholines and LysoPEs can be hydrolyzed from PCs and PEs, which are synthesized from glycerol 3-phosphate by the activation of a series of enzymes such as GPAT, LPAAT, PAP, DGK, CPT, and EPT (Cowan, 2006; Nakamura, 2017). Xu et al. (2021) reported that glycerophospholipid metabolism is responsible for the postharvest softening of pears, and the expressions of *GPAT1* (glycerol-3-phosphate acyltransferase), *CCT2* (cholinephosphate cytidylyltransferase 1), *LCAT3* (phospholipase A), *LCAT4* (lecithin-cholesterol acyltransferase), and *NPC1* (non-specific phospholipase C1) are significantly correlated with the contents of PE and PC. In the present study, different numbers of *GPAT*, *PAP*, *DGK*, and *EPT* genes were observed to be differentially regulated between HP and RA fruits, indicating their important roles in the glycerophospholipid metabolism of these two kumquats. The plant phospholipases hydrolyzed glycerophospholipids at different ester bonds. They can be grouped into phospholipase A (PLA1 and PLA2), phospholipase C, and phospholipase D depending on the cleaved site in the phospholipid molecule (Filkin et al., 2020). PLA2 hydrolyzes the sn-2 position of glycerophosphates and produces lysophospholipids (Nakamura, 2017), while lysophospholipid: acyl-COA acyltransferases (LPCAT/LPEAT) can acylate lysophospholipids and reduce its level (Jasieniecka-Gazarkiewicz et al., 2017). Thus, the downregulation of two *PLA2* and upregulation of one *LPCAT* in HP could be associated with the low accumulations of lysophospholipids, including LysoPEs and LysoPCs in the fruits. In addition to PLA, both PLC and PLD can hydrolyze the glycerophosphates, resulting in the generation of DAG and phosphatidic acid, respectively (Filkin et al., 2020). Therefore, the upregulation of *PLC* and *PLD* may accelerate the degradation of glycerophospholipid and limit supply for lysophospholipids synthesis and finally, responsible for the low concentrations of LysoPEs and LysoPCs in HP fruit. Collectively, the differences in lysophospholipid accumulations and related gene expressions suggested a possible change of the glycerophospholipid pathway in HP variety.

CONCLUSION

HP fruit displayed integrative differences in morphological and physiological features compared with RA fruit. These observed differences may be ascribed to the differential accumulation of metabolites, particularly the high glycosylated flavonoid and low lysophospholipid compounds in HP fruit. Furthermore, various genes involved in flavonoid and lipid metabolisms were differentially expressed. The upregulations of *PAL*, *C4H*, *4CL*, *CHS*, and particularly the *UGT* genes contributed to high flavonoid accumulations in HP fruit. On the other hand, expression levels of the lipid degradation-related genes, including *LPCAT*, *PLC*, and *PLD,* were also upregulated, resulting in low lysophospholipid accumulations in HP fruit. Together, our results reveal that the flavonoid and lipid pathways are regulated at the transcriptional levels, which provide comprehensive insights into the regulatory network of both components in kumquat fruits.

DATA AVAILABILITY STATEMENT

The datasets presented in this study can be found in online repositories. The names of the repository/repositories and accession number(s) can be found in the article/ **Supplementary Material**.

AUTHOR CONTRIBUTIONS

QW and QM designed the experiment. YH and XD performed the study. QW, QG, and QM drafted the manuscript. GZ and XL revised the manuscript. All authors read and approved the final version of this manuscript.

FUNDING

This work was supported by the National Natural Science Foundation of China (31501811 and 31460496) and the Natural Science Foundation of Jiangxi Province (20202BABL205005).

SUPPLEMENTARY MATERIAL

The Supplementary Material for this article can be found online at: https://www.frontiersin.org/articles/10.3389/fpls.2021.759968/full#supplementary-material

REFERENCES

Amaro, A. L., and Almeida, D. P. F. (2013). Lysophosphatidylethanolamine effects on horticultural commodities: a review. *Postharvest Biol. Technol.* 78, 92–102. doi: 10.1016/j.postharvbio.2012.12.011

Aruoma, O. I, Landes, B., Ramful-Baboolall, D., Bourdon, E., Neergheen-Bhujun, V., Wagner, K. H., et al. (2012). Functional benefits of citrus fruits in the management of diabetes. *Prev. Med.* 54, 12–16. doi: 10.1016/j.ypmed.2012.02.012

Barreca, D., Bellocco, E., Caristi, C., Leuzzi, U., and Gattuso, G. (2011). Kumquat (*Fortunella japonica* Swingle) juice: flavonoid distribution and antioxidant properties. *Food Res. Int.* 44, 2190–2197. doi: 10.1016/j.foodres.2010.11.031

Caputi, L., Malnoy, M., Goremykin, V., Nikiforova, S., and Martens, S. (2012). A genome-wide phylogenetic reconstruction of family 1 UDP-glycosyltransferases revealed the expansion of the family during the adaptation of plants to life on land. *Plant J.* 69, 1030–1042. doi: 10.1111/j.1365-313X.2011.04853.x

Chen, C., Zhou, G., Chen, J., Liu, X., Lu, X., Chen, H., et al. (2021). Integrated metabolome and transcriptome analysis unveils novel pathway involved in the formation of yellow peel in cucumber. *Int. J. Mol. Sci.* 22:1494. doi: 10.3390/ijms22031494

Cowan, A. K. (2006). Phospholipids as plant growth regulators. *Plant Growth Regul.* 48, 97–109. doi: 10.1007/s10725-005-5481-7

Dong, X. Y., Braun, E. L., and Grotewold, E. (2001). Functional conservation of plant secondary metabolic enzymes revealed by complementation of

Arabidopsis flavonoid mutants with Maize genes. *Plant Physiol.* 127, 46–57. doi: 10.2307/4280058

Erlund, I. (2004). Review of the flavonoids quercetin, hesperetin, and naringenin. Dietary sources, bioactivities, bioavailability, and epidemiology. *Nutr. Res.* 24, 851–874. doi: 10.1016/j.nutres.2004.07.005

Filkin, S. Y., Lipkin, A. V., and Fedorov, A. N. (2020). Phospholipase superfamily: structure, functions, and biotechnological applications. *Biochemistry Mosc.* 85, 177–195. doi: 10.1134/S0006297920140096

Gou, J., Felippes, F., Liu, C., Weigel, D., and Wang, J. (2011). Negative regulation of anthocyanin biosynthesis in *Arabidopsis* by a miR156-targeted SPL transcription factor. *Plant Cell* 23, 1512–1522. doi: 10.1105/tpc.111.084525

He, Y., Li, Z., Tan, F., Liu, H., Zhu, M., Yang, H., et al. (2019). Fatty acid metabolic flux and lipid peroxidation homeostasis maintain the biomembrane stability to improve citrus fruit storage performance. *Food Chem.* 292, 314–324. doi: 10.1016/j.foodchem.2019.04.009

Hong, J. H., Chung, G., and Cowan, A. K. (2009). Delayed leaf senescence by exogenous lyso-phosphatidylethanolamine: towards a mechanism of action. *Plant Physiol. Biochem.* 47, 526–534. doi: 10.1016/j.plaphy.2008.12.014

Jasieniecka-Gazarkiewicz, K., Lager, I., Carlsson, A. S., Gutbrod, K., Peisker, H., Dörmann, P., et al. (2017). Acyl-CoA: lysophosphatidylethanolamine acyltransferase activity regulates growth of *Arabidopsis*. *Plant Physiol.* 174, 986–998. doi: 10.1104/pp.17.00391

Khan, M. K., Zill, E. H., and Dangles, O. (2014). A comprehensive review on flavanones, the major citrus polyphenols. *J. Food Compos. Anal.* 33, 85–104. doi: 10.1016/j.jfca.2013.11.004

Kolesnik, A. A., Golubev, V. N., Meteshkin, Y. V., Sprinsyan, T. V., and Papunidze, G. R. (1989). Lipids of the fruit of *Citrus unshiu*. *Chem. Nat. Compd.* 25:7. doi: 10.1007/BF00597705

Kumar, R. J. S., Singh, S., Sonawane, P. D., Vishwakarma, R. K., and Khan, B. M. (2013). Functional characterization of a glucosyltransferase specific to flavonoid 7-O-glucosides from *Withania somnifera*. *Plant Mol. Biol. Rep.* 31, 1100–1108. doi: 10.1007/s11105-013-0573-4

Liebisch, G., Fahy, E., Aoki, J., Dennis, E. A., Durand, T., Ejsing, C. S., et al. (2020). Update on LIPID MAPS classification, nomenclature and shorthand notation for MS-derived lipid structures. *J. Lipid Res.* 61, 1539–1555.

Liu, D., Yang, L., Zheng, Q., Wang, Y., Wang, M., Zhuang, X., et al. (2015). Analysis of cuticular wax constituents and genes that contribute to the formation of 'glossy Newhall', a spontaneous bud mutant from the wild-type 'Newhall' navel orange. *Plant Mol. Biol.* 88, 573–590. doi: 10.1007/s11103-015-0343-9

Liu, X., Lin, C., Ma, X., Yan, T., Wang, J., and Zeng, M. (2018). Functional characterization of a flavonoid glycosyltransferase in sweet orange (*Citrus Sinensis*). *Front. Plant Sci.* 9:166. doi: 10.3389/fpls.2018.00166

Liu, X., Liu, B., Jiang, D., Zhu, S., Shen, W., Yu, X., et al. (2019). The accumulation and composition of essential oil in kumquat peel. *Sci. Hortic.* 252, 121–129. doi: 10.1016/j.scienta.2019.03.042

Lou, S. N., and Ho, C. T. (2017). Phenolic compounds and biological activities of small-size citrus: Kumquat and calamondin. *J. Food Drug. Anal.* 25, 162–175. doi: 10.1016/j.jfda.2016.10.024

Moriguchi, T., Kita, M., Tomono, Y., Endo-Inagaki, T., and Omura, M. (2001). Gene expression in flavonoid biosynthesis: correlation with flavonoid accumulation in developing citrus fruit. *Physiol. Plant.* 111, 66–74. doi: 10.1034/j.1399-3054.2001.1110109.x

Nakamura, Y. (2017). Plant phospholipid diversity: emerging functions in metabolism and protein-lipid interactions. *Trends Plant Sci.* 22, 1027–1040. doi: 10.1016/j.tplants.2017.09.002

Osmani, S. A., Bak, S., and Mller, B. L. (2010). Substrate specificity of plant UDP-dependent glycosyltransferases predicted from crystal structures and homology modeling. *Phytochemistry* 40, 325–347. doi: 10.1016/j.phytochem.2008.12.009

Rafiq, S., Kaul, R., Sofi, S. A., Bashir, N., Nazir, F., and Ahmad Nayik, G. (2018). Citrus peel as a source of functional ingredient: a review. *J. Saudi Soc. Agric. Sci.* 17, 351–358. doi: 10.1016/j.jssas.2016.07.006

Shen, J., Zou, Z., Zhang, X., Zhou, L., Wang, Y., Fang, W., et al. (2018). Metabolic analyses reveal different mechanisms of leaf color change in two purple-leaf tea plant (*Camellia sinensis* L.) cultivars. *Hortic. Res.* 5:7. doi: 10.1038/s41438-017-0010-1

Sun, W., Meng, X., Liang, L., Jiang, W., Huang, Y., He, J., et al. (2015). Molecular and biochemical analysis of chalcone synthase from Freesia hybrid in flavonoid biosynthetic pathway. *PLoS One* 10:e0119054. doi: 10.1016/j.gene.2017.09.002

Tan, S., Zhao, X., Yang, Y., Ke, Z., and Zhou, Z. (2016). Chemical profiling using Uplc Q-Tof/Ms and antioxidant activities of *Fortunella* fruits. *J. Food Sci.* 81, 1646–1653. doi: 10.1111/1750-3841.13352

Tian, R., Li, Q., Rao, S., Wang, A., Zhang, H., Wang, L., et al. (2020). Metabolic profiling and gene expression analysis provides insights into flavonoid and anthocyanin metabolism in poplar. *Tree Physiol.* 41, 1046–1064. doi: 10.1093/treephys/tpaa152

Touns, M. S., Moulehi, I., Ouerghemmi, I., Mejri, H., Wannes, W. A., Hamdaoui, G., et al. (2011). Changes in lipid composition and antioxidant capacity of bitter orange (*Citrus aurantium*. L) and mandarin (*Citrus reticulata*. Blanco) oilseeds on different stages of maturity. *J. Am. Oil Chem. Soc.* 88, 961–966. doi: 10.1007/s11746-010-1751-2

Ververidis, F., Trantas, E., Douglas, C., Vollmer, G., Kretzschmar, G., and Panopoulos, N. (2007). Biotechnology of flavonoids and other phenylpropanoid-derived natural products. Part I: chemical diversity, impacts on plant biology and human health. *Biotechnol. J.* 2, 1214–1234. doi: 10.1002/biot.200700084

Voo, S. S., Grimes, H. D., and Lange, B. M. (2012). Assessing the biosynthetic capabilities of secretory glands in *Citrus* peel. *Plant Physiol.* 159, 81–94. doi: 10.1104/pp.112.194233

Wan, H., Liu, H., Zhang, J., Lyu, Y., Li, Z., He, Y., et al. (2020). Lipidomic and transcriptomic analysis reveals reallocation of carbon flux from cuticular wax into plastid membrane lipids in a glossy "Newhall" navel orange mutant. *Hortic. Res.* 7:41. doi: 10.1038/s41438-020-0262-z

Wang, S., Yang, C., Tu, H., Zhou, J., Liu, X., Cheng, Y., et al. (2017). Characterization and metabolic diversity of flavonoids in citrus species. *Sci. Rep.* 7:10549. doi: 10.1038/s41598-017-10970-2

Wang, Y., Li, J., and Xia, R. (2010). Expression of chalcone synthase and chalcone isomerase genes and accumulation of corresponding flavonoids during fruit maturation of Guoqing No. 4 satsuma mandarin (*Citrus unshiu* Marcow). *Sci. Hortic.* 125, 110–116. doi: 10.1016/j.scienta.2010.02.001

Wei, Q., Ma, Q., Zhou, G., Liu, X., Ma, Z., and Gu, Q. (2021). Identification of genes associated with soluble sugar and organic acid accumulation in 'Huapi' kumquat (*Fortunella crassifolia* swingle) via transcriptome analysis. *J. Sci. Food. Agric.* 101, 4321–4331. doi: 10.1002/jsfa.11072

Winkel-Shirley, B. (2001). Flavonoid biosynthesis. a colorful model for genetics, biochemistry, cell biology, and biotechnology. *Plant Physiol.* 126, 485–493. doi: 10.1104/pp.126.2.485

Xu, J., Zhang, Y., Qi, D., Huo, H., Dong, X., Tian, L., et al. (2021). Metabolomic and transcriptomic analyses highlight the influence of lipid changes on the post-harvest softening of Pyrus ussurian max. 'Zaoshu Shanli'. *Genomics* 113, 919–926. doi: 10.1016/j.ygeno.2020.10.025

Zhang, J., Zhang, Q., Zhang, H., Ma, Q., Lu, J., and Qiao, Y. (2012). Characterization of polymethoxylated flavonoids (PMFs) in the peels of 'Shatangju' mandarin (*Citrus reticulata* Blanco) by online high-performance liquid chromatography coupled to photodiode array detection and electrospray tandem mass spectrometry. *J. Agric. Food Chem.* 60, 9023–9034.

Zhang, M., Duan, C., Zang, Y., Huang, Z., and Liu, G. (2011). The flavonoid composition of flavedo and juice from the pummelo cultivar (*Citrus grandis* (L.) Osbeck) and the grapefruit cultivar (*Citrus paradisi*) from China. *Food chem.* 129, 1530–1536. doi: 10.1016/j.foodchem.2011.05.136

Conflict of Interest: The authors declare that the research was conducted in the absence of any commercial or financial relationships that could be construed as a potential conflict of interest.

Publisher's Note: All claims expressed in this article are solely those of the authors and do not necessarily represent those of their affiliated organizations, or those of the publisher, the editors and the reviewers. Any product that may be evaluated in this article, or claim that may be made by its manufacturer, is not guaranteed or endorsed by the publisher.

frontiers in Plant Science

REVIEW
published: 27 January 2022
doi: 10.3389/fpls.2021.814138

Branched-Chain Volatiles in Fruit: A Molecular Perspective

*Lorenzo N. Bizzio[1,2], Denise Tieman[3] and Patricio R. Munoz[1,2]**

[1] Blueberry Breeding and Genomics Lab, Department of Horticultural Sciences, University of Florida, Gainesville, FL, United States, [2] Plant Molecular and Cellular Biology Program, University of Florida, Gainesville, FL, United States, [3] Department of Horticultural Sciences, University of Florida, Gainesville, FL, United States

Branched-chain volatiles (BCVs) constitute an important family of fruit volatile metabolites essential to the characteristic flavor and aroma profiles of many edible fruits. Yet in contrast to other groups of volatile organic compounds important to fruit flavor such as terpenoids, phenylpropanoids, and oxylipins, the molecular biology underlying BCV biosynthesis remains poorly understood. This lack of knowledge is a barrier to efforts aimed at obtaining a more comprehensive understanding of fruit flavor and aroma and the biology underlying these complex phenomena. In this review, we discuss the current state of knowledge regarding fruit BCV biosynthesis from the perspective of molecular biology. We survey the diversity of BCV compounds identified in edible fruits as well as explore various hypotheses concerning their biosynthesis. Insights from branched-chain precursor compound metabolism obtained from non-plant organisms and how they may apply to fruit BCV production are also considered, along with potential avenues for future research that might clarify unresolved questions regarding BCV metabolism in fruits.

Keywords: branched-chain, volatiles, fruit, aroma, flavor, biosynthesis, metabolism

OPEN ACCESS

Edited by:
Itay Maoz, Agricultural Research Organization (ARO), Israel

Reviewed by:
Jun Song, Agriculture and Agri-Food Canada (AAFC), Canada
Natasha Spadafora, University of Calabria, Italy

***Correspondence:**
Patricio R. Munoz
p.munoz@ufl.edu

Specialty section:
This article was submitted to Plant Metabolism and Chemodiversity, a section of the journal Frontiers in Plant Science

Received: *12 November 2021*
Accepted: *23 December 2021*
Published: *27 January 2022*

Citation:
Bizzio LN, Tieman D and Munoz PR (2022) Branched-Chain Volatiles in Fruit: A Molecular Perspective. Front. Plant Sci. 12:814138. doi: 10.3389/fpls.2021.814138

INTRODUCTION

Volatile organic compounds (VOCs) are essential components of fruit flavor, being necessary for human perception of the distinct flavors produced by the many different types of fruit found in nature (Noble, 1996; Goff and Klee, 2006; El Hadi et al., 2013; Plotto et al., 2017). The importance of VOCs to fruit flavor has prompted researchers to investigate the underlying biosynthetic pathways responsible for their formation. Great progress has been made in understanding the molecular basis of terpenoid (Cheng et al., 2007; Nagegowda, 2010; Tholl, 2015; Abbas et al., 2017), phenylpropanoid (Boatright et al., 2004; Qualley et al., 2012; Lackus et al., 2021), and oxylipin (Mosblech et al., 2009; Scala et al., 2013; Griffiths, 2015; Ameye et al., 2018) volatile biosynthesis in plants. However, much less is known about the molecular correlates underlying the production of branched-chain volatiles (BCVs), a family of compounds encompassing some VOCs that are notable contributors to the flavor of several important fruit crops.

Branched chain volatiles are defined as those volatile organic compounds that contain a branched-chain functional group structurally similar to those of the branched-chain amino acids-

valine, leucine, and isoleucine (**Figure 1**). Due to this structural similarity BCVs were theorized to derive from the metabolism of branched-chain amino acids (BCAAs), a hypothesis supported by numerous feeding experiments (Tressl and Drawert, 1973; Hansen and Poll, 1993; Rowan et al., 1996; Wyllie and Fellman, 2000; Pérez et al., 2002; Matich and Rowan, 2007; Gonda et al., 2010). Yet while thorough work has been done elucidating the biosynthesis and metabolism of branched-chain amino acids in plants (Singh and Shaner, 1995; Taylor et al., 2004; Binder et al., 2007; Binder, 2010; Xing and Last, 2017), the precise enzymatic mechanisms by which BCAA metabolism diverges into BCV biosynthesis remain relatively understudied. Furthermore, recent experimental evidence indicates that under certain circumstances BCV production may occur independently of normal BCAA metabolism (Sugimoto, 2011; Kochevenko et al., 2012; Sugimoto et al., 2021). A more complete understanding of BCV biosynthesis in plants would be of great importance to researchers working to better understand the molecular basis of fruit flavor, and in particular to those who desire to apply such knowledge to the development of novel fruit varieties with improved flavor traits.

This review seeks to collate and evaluate published research regarding the biosynthesis of branched chain volatiles in plants, with an emphasis on these processes as they might occur in fruit crops. While BCV biosynthesis has been touched upon in other reviews on the subject of plant volatiles (Dudareva et al., 2006, 2013; El Hadi et al., 2013), a comprehensive exploration of the state of current knowledge concerning the molecular basis of BCV biosynthesis in plants has yet to be published.

BRANCHED-CHAIN VOLATILES IN FRUITS

Branched-chain volatiles are ubiquitous components of fruit aroma volatile profiles. An examination of research literature concerning fruit volatile profiles found that 127 unique branched-chain volatile compounds were identified in 106 distinct types of edible fruit across 175 published studies (**Table 1**). A list of all BCVs reported for a particular fruit by these studies is given in **Supplementary Table 1**. These fruits include representatives from 22 individual taxonomic orders spanning monocots, eudicots, and magnoliids, suggesting that the production of branched-chain volatiles in fruit tissue is a characteristic with widespread evolutionary utility. It has been proposed that since many fruit volatiles are derived from nutritionally significant compounds, their production in fruit tissue might be a means of signaling nutritional value to seed-dispersing frugivores (Goff and Klee, 2006). Because animals are incapable of biosynthesizing branched-chain amino acids (Hou and Wu, 2018), volatile cues enabling the identification of food sources rich in these compounds could serve as powerful attractants to animal seed-dispersers. This may be one explanation for the ubiquity of branched-chain volatiles in fruits from plants across many divergent evolutionary lineages, though much more research is needed to firmly establish this hypothesis. Conversely BCVs may also find use as defense agents against herbivorous predators, an application associated with certain nitrogen-containing branched-chain VOCs (Irmisch et al., 2013, 2014).

An overwhelming majority of the branched-chain volatiles identified in fruits are classified as volatile esters. Out of the 127 distinct BCVs identified in **Table 1**, 108 are esters. Many of these are conjugate esters derived from a branched-chain structure attached to a compound from a completely different biosynthetic origin. In this way, branched-chain volatiles incorporating structures derived from terpenoid, phenylpropanoid, and oxylipin metabolism are formed- allowing for massive diversity in the number of possible volatiles containing a branched-chain structure. The remaining non-ester BCVs observed in **Table 1** include branched-chain alcohols, aldehydes, alkanes, and carboxylic acids. Several BCVs containing more unusual functional groups are also listed, including compounds with nitrile, nitrite, nitro, and thioester functional groups.

Branched-chain volatiles have been recognized as being crucially responsible for the distinctive flavor and aroma properties of many commercially important fruits such as apple, banana, melon, and pineapple, among others (Wyllie et al., 1995; Plotto, 1998; Dixon and Hewett, 2000; Boudhrioua et al., 2003; Tokitomo et al., 2005; Wendakoon et al., 2006). In terms of effect on human sensory perception it has been widely reported that branched-chain volatile esters tend to impart characteristic "fruity" aroma notes, while non-ester branched-chain volatiles induce a broader range of olfactory sensations (Schwab et al., 2008; Sugimoto, 2011; El Hadi et al., 2013; Lytra et al., 2014). Fruity aroma is a characteristic shared with several other non-branched-chain volatile compounds, particularly short- and medium- length straight-chain esters (Schwab et al., 2008; El Hadi et al., 2013). However, it has been observed that ester compounds containing the branched-chain moiety have significantly lower odor thresholds than the corresponding straight-chain counterparts (Takeoka et al., 1995), indicating that BCVs may be more potent stimulators of the "fruity" olfactory sensation. It is important to communicate that the "fruity" aroma notes imparted by BCVs are not always associated with positive consumer responses, and in some fruits are associated with decreased consumer ratings (Goulet et al., 2012).

CURRENT KNOWLEDGE REGARDING BRANCHED-CHAIN VOLATILE BIOSYNTHESIS

Because of the importance of branched-chain volatiles to the characteristic flavors of several important fruit crops much research has been done in trying to understand the general biosynthesis pathways that lead to BCV production, though this area remains relatively understudied when compared to the biosynthetic processes that produce other classes of important fruit volatiles such as terpenoids and oxylipins. The body of published experimental evidence regarding this topic points to four possible hypotheses regarding BCV biosynthesis (**Figure 2**),

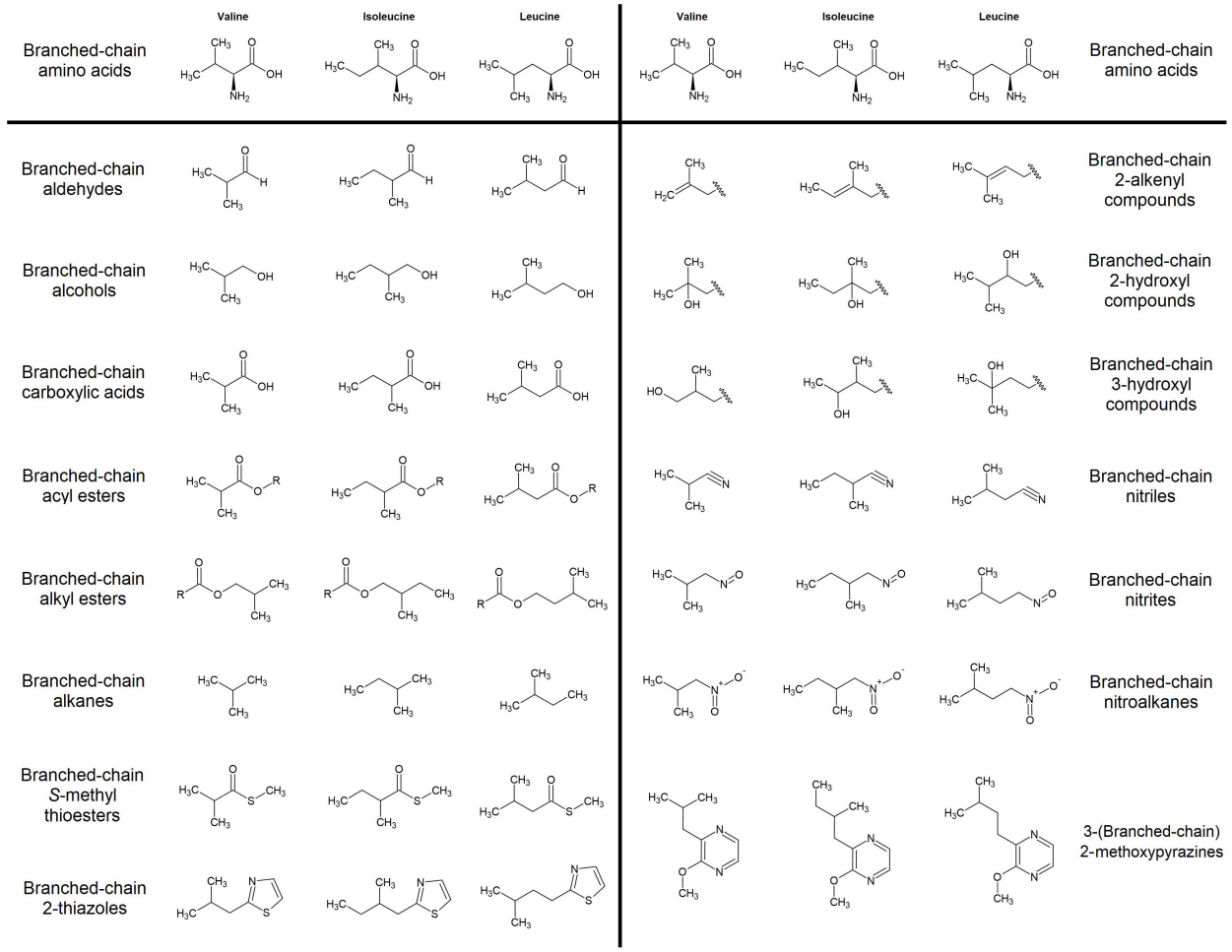

FIGURE 1 | Categories of branched-chain volatile compounds detected in edible fruits. At least one volatile from each family was reported in at least one of the 175 fruit volatile studies examined in this review (see **Supplementary Table 1**).

none of which are mutually exclusive with any of the others. These hypotheses are summarized below.

Mitochondrial Catabolism of Branched-Chain Amino Acids

The oldest and most studied of the four possibilities, this hypothesis posits that BCVs are generated through the catabolic degradation of BCAAs in mitochondria. It has long been known that plants possess the capability to break down excess BCAAs into the energy-rich metabolites acetyl-CoA and propionyl-CoA and that several of the key enzymes involved in this process are localized to mitochondria (Binder, 2010; Hildebrandt et al., 2015). An excellent overview of this pathway as hypothesized to occur in plants is provided in Binder (2010). Briefly, this process begins with the deamination of BCAAs by branched-chain aminotransferases (BCATs) followed by decarboxylation of the resulting branched-chain α-ketoacids (BCKAs) through the branched-chain α-ketoacid dehydrogenase complex (BCKDH). This results in the formation of various branched-chain acyl-CoAs (BCA-CoAs), which in turn are reduced at the α-carbon through the action of isovaleryl-CoA dehydrogenases or functionally similar enzymes. These reduced BCA-CoAs then undergo β-oxidation into acetyl-CoA and propionyl-CoA, though whether these later stages occur in mitochondria or in peroxisomes remains unresolved (Graham and Eastmond, 2002; Kaur et al., 2009).

Since numerous volatile esters are known to be biosynthesized in fruit tissue by alcohol acyltransferase (AAT) enzymes (Beekwilder et al., 2004; El-Sharkawy et al., 2005; Souleyre et al., 2005; Günther et al., 2011; Goulet et al., 2015) and because AATs require an alcohol and an acyl-CoA as substrates, the branched-chain acyl-CoAs produced by mitochondrial BCAA catabolism would naturally be considered likely candidates for conversion to volatile branched-chain acyl esters. Feeding and isotope labeling experiments conducted in apple, banana, and strawberry provide strong evidence that BCAAs can be directly converted to volatile branched-chain acyl esters in fruit tissue (Tressl and Drawert, 1973; Rowan et al., 1996; Wyllie and Fellman, 2000; Pérez et al., 2002). Furthermore, the detection

TABLE 1 | List of all branched-chain volatile compounds detected in 106 edible fruits across 175 published studies of fruit volatile content.

Compound name	CAS #	Molecular weight	Number of fruits identified in
Alcohols			
2-methyl-1-propanol	78-83-1	74.12	34
2-methyl-1-butanol	137-32-6	88.15	32
3-methyl-1-butanol	123-51-3	88.15	64
Aldehydes			
2-methylpropanal	78-84-2	72.11	12
2-methylbutanal	96-17-3	86.13	20
3-methylbutanal	590-86-3	86.13	31
Alkanes			
2-methylbutane	78-78-4	72.15	1
Carboxylic acids			
2-methylpropanoic acid	79-31-2	88.11	13
2-methylbut-2-enoic acid	13201-46-2	100.12	1
2-methylbutanoic acid	116-53-0	102.13	26
3-methylbutanoic acid	503-74-2	102.13	26
2-methyl-3-hydroxypropanoic acid	2068-83-9	104.1	1
Esters			
Methyl 2-methylprop-2-enoate	80-62-6	100.12	1
Methyl 2-methylpropanoate	547-63-7	102.13	4
Methyl 2-methylbut-2-enoate	6622-76-0	114.14	1
Methyl 3-methylbut-2-enoate	924-50-5	114.14	2
Ethyl 2-methylprop-2-enoate	97-63-2	114.14	1
2-methylpropyl acetate	110-19-0	116.16	29
Methyl 2-methylbutanoate	868-57-5	116.16	24
Methyl 3-methylbutanoate	556-24-1	116.16	13
Ethyl 2-methylpropanoate	97-62-1	116.16	29
Ethyl 2-methylbut-2-enoate	5837-78-5	128.17	12
Ethyl 3-methylbut-2-enoate	638-10-8	128.17	1
Propyl 2-methylprop-2-enoate	2210-28-8	128.17	1
2-methylpropyl propanoate	540-42-1	130.18	1
2-methylbutyl acetate	624-41-9	130.18	18
3-methylbutyl acetate	123-92-2	130.18	52
Ethyl 2-methylbutanoate	7452-79-1	130.18	49
Ethyl 3-methylbutanoate	108-64-5	130.18	27
Propyl 2-methylpropanoate	644-49-5	130.18	1
1-methylethyl 2-methylpropanoate	617-50-5	130.18	2
Methyl 2-hydroxy-2-methylbutanoate	32793-34-3	132.16	2
Methyl 2-hydroxy-3-methylbutanoate	17417-00-4	132.16	7
Methyl 3-hydroxy-3-methylbutanoate	6149-45-7	132.16	4
Propyl 2-methylbut-2-enoate	61692-83-9	142.2	1
2-methylpropyl butanoate	539-90-2	144.12	13
2-methylpropyl 2-methylpropanoate	97-85-8	144.21	4
2-methylbutyl propanoate	2438-20-2	144.21	2
3-methylbutyl propanoate	105-68-0	144.21	1
Propyl 2-methylbutanoate	37064-20-3	144.21	6
Propyl 3-methylbutanoate	557-00-6	144.21	5
Butyl 2-methylpropanoate	97-87-0	144.21	6
2-methylpropyl 2-hydroxypropanoate	585-24-0	146.18	1
Ethyl 2-hydroxy-2-methylbutanoate	77-70-3	146.18	2
Ethyl 2-hydroxy-3-methylbutanoate	2441-06-7	146.18	2
Ethyl 3-hydroxy-3-methylbutanoate	18267-36-2	146.18	4
2-methylpropyl 2-methylbut-2-enoate	7779-81-9	156.22	4
3-methylbut-3-enyl 2-methylpropanoate	76649-23-5	156.22	1
Butyl 2-methylbut-2-enoate	7785-66-2	156.23	2
2-methylpropyl 2-methylbutanoate	2445-67-2	158.24	3
2-methylpropyl 3-methylbutanoate	589-59-3	158.24	5
2-methylbutyl butanoate	51115-64-1	158.24	5
2-methylbutyl 2-methylpropanoate	2445-69-4	158.24	1
3-methylbutyl butanoate	106-27-4	158.24	14
3-methylbutyl 2-methylpropanoate	2050-01-3	158.24	6
Butyl 2-methylbutanoate	15706-73-7	158.24	8
Butyl 3-methylbutanoate	109-19-3	158.24	9
Pentyl 2-methylpropanoate	2445-72-9	158.24	4
3-methylbut-3-enyl 2-methylbut-2-enoate	83783-87-3	168.23	1
3-methylbut-3-enyl 3-methylbutanoate	54410-94-5	170.25	2
Hexyl 2-methylprop-2-enoate	142-09-6	170.25	1
Pentan-2-yl 3-methylbut-2-enoate	150462-84-3	170.25	1
(Z)-3-hexenyl 2-methylpropanoate	41519-23-7	170.25	6
2-methylpropyl hexanoate	105-79-3	172.26	10
2-methylbutyl 2-methylbutanoate	2445-78-5	172.26	2
2-methylbutyl 3-methylbutanoate	2445-77-4	172.26	3
3-methylbutyl pentanoate	2050-09-1	172.26	1
3-methylbutyl 2-methylbutanoate	27625-35-0	172.26	2
3-methylbutyl 3-methylbutanoate	659-70-1	172.26	6
Pentyl 2-methylbutanoate	68039-26-9	172.26	1
Pentyl 3-methylbutanoate	25415-62-7	172.26	2
Hexyl 2-methylpropanoate	2349-07-7	172.26	10
Pentan-2-yl 3-methylbutanoate	117421-34-8	172.27	1
2-methylpropyl benzoate	120-50-3	178.23	2
3-methylbutyl (E)-2-hexenoate	72928-34-8	184.28	1
Hexan-2-yl 3-methylbut-2-enoate	N/A	184.28	1
(E)-2-hexenyl 2-methylbutanoate	94089-01-7	184.28	1
(Z)-3-hexenyl 2-methylbutanoate	53398-85-9	184.28	4
(Z)-3-hexenyl 3-methylbutanoate	35154-45-1	184.28	4
2-methylbutyl hexanoate	2601-13-0	186.29	3
3-methylbutyl hexanoate	2198-61-0	186.29	16
Hexyl 2-methylbutanoate	10032-15-2	186.29	13
Hexyl 3-methylbutanoate	10032-13-0	186.29	11
Heptyl 2-methylpropanoate	2349-13-5	186.29	1
Benzyl 2-methylbut-2-enoate	37526-88-8	190.24	1
2-methylpropyl phenylacetate	102-13-6	192.25	1
2-methylbutyl benzoate	52513-03-8	192.25	1
3-methylbutyl benzoate	94-46-2	192.25	1
Benzyl 3-methylbutanoate	103-38-8	192.25	4
2-phenylethyl 2-methylpropanoate	103-48-0	192.25	2
(E)-4-hepten-2-yl 3-methylbutanoate	N/A	198.3	1

TABLE 1 | (Continued)

Compound name	CAS #	Molecular weight	Number of fruits identified in
(Z)-4-hepten-2-yl 3-methylbutanoate	N/A	198.3	1
2-methylpropyl octanoate	5461-06-3	200.32	4
Octyl 2-methylpropanoate	109-15-9	200.32	4
2-phenylethyl 2-methylbut-2-enoate	55719-85-2	204.26	1
2-phenylethyl 2-methylbutanoate	24817-51-4	206.28	1
2-phenylethyl 3-methylbutanoate	140-26-1	206.28	3
3-phenylpropyl 2-methylpropanoate	103-58-2	206.28	1
3-methylbutyl 2-aminobenzoate	28457-05-8	207.27	1
2-phenoxyethyl 2-methylpropanoate	103-60-6	208.26	2
(E)-4-octenyl 3-methylbutanoate	N/A	212.33	1
(Z)-4-octenyl 3-methylbutanoate	N/A	212.33	1
(Z)-5-octenyl 3-methylbutanoate	N/A	212.33	1
2-methylbutyl octanoate	67121-39-5	214.34	2
3-methylbutyl octanoate	2035-99-6	214.34	8
Octyl 2-methylbutanoate	29811-50-5	214.34	1
Octyl 3-methylbutanoate	7786-58-5	214.34	2
Cinnamyl 3-methylbutanoate	140-27-2	218.29	1
3-phenylpropyl 3-methylbutanoate	5452-07-3	220.31	1
Neryl 2-methylpropanoate	2345-24-6	224.34	2
2-methylpropyl decanoate	30673-38-2	228.37	1
Decyl 2-methylpropanoate	5454-22-8	228.37	1
Geranyl 3-methylbutanoate	109-20-6	238.37	2
(Z)-4-decenyl 3-methylbutanoate	N/A	240.38	1
3-methylbutyl decanoate	2306-91-4	242.4	2
2-methylpropyl dodecanoate	37811-72-6	256.42	1
3-methylbutyl dodecanoate	6309-51-9	270.45	1
2-methylpropyl hexadecanoate	110-34-9	312.54	1
3-methylbutyl hexadecanoate	81974-61-0	326.56	1
2-methylpropyl octadecanoate	646-13-9	340.58	1
Nitriles			
2-methylpropylnitrile	78-82-0	69.11	1
3-methylbutylnitrile	625-28-5	83.13	1
Nitrites			
3-methylbutylnitrite	110-46-3	117.15	1
Nitroalkanes			
3-methyl-1-nitrobutane	627-67-8	117.15	1
Pyrazines			
2-(2-methylpropyl)-3-methoxypyrazine	24683-00-9	166.22	6
Thiazoles			
2-(2-methylpropyl)-thiazole	18640-74-9	141.23	1
Thioesters			
S-methyl 3-methylbutanethioate	23747-45-7	132.22	1

Compounds are identified by both name and CAS registry number and are grouped according to the structural categories given in ***Figure 1****. An absence of a CAS registry number for a compound is indicated by "N/A." Within structural categories, compounds are listed in descending order according to molecular weight. Also provided is the number of distinct edible fruits each compound has been reported in by the sources cited throughout this. For a complete list of which branched-chain volatile compounds were detected in a given fruit along with the corresponding reporting studies, please refer to* ***Supplementary Table 1****.*

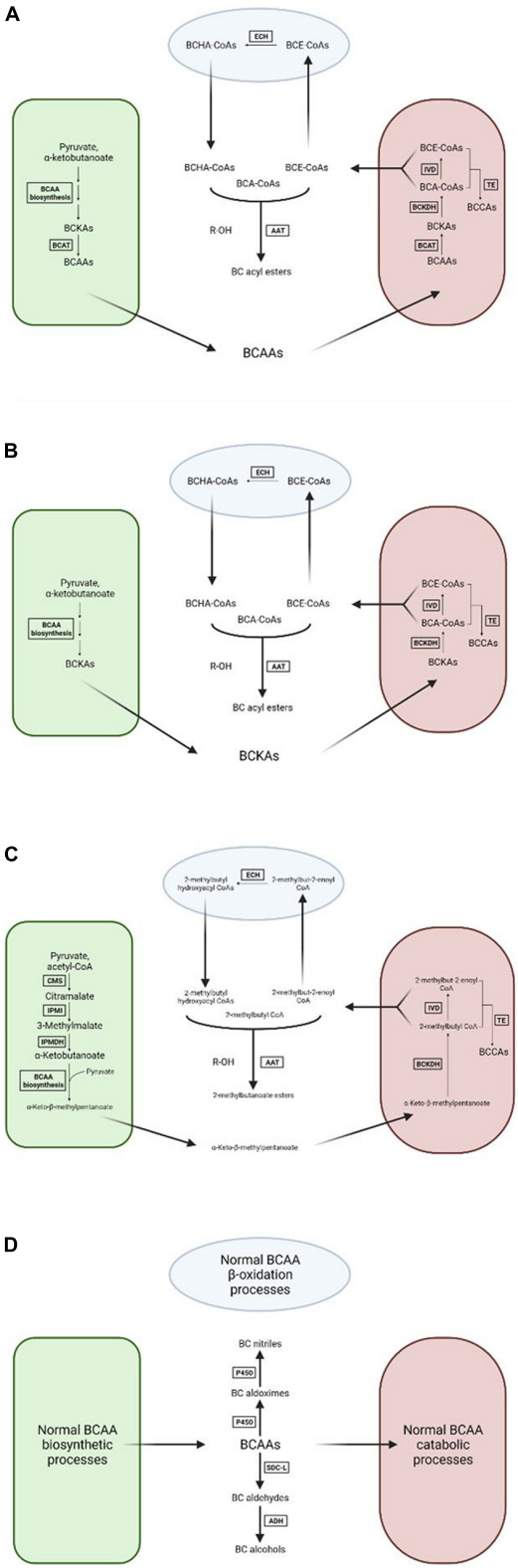

FIGURE 2 | Visual diagrams of the four hypotheses concerning branched-chain volatile biosynthesis in plant cells. **(A)** Mitochondrial

(Continued)

FIGURE 2 | catabolism of branched-chain amino acids. **(B)** *De novo* branched-chain α-ketoacid biosynthesis followed by mitochondrial catabolism. **(C)** Production of 2-methylbutyl volatiles by citramalate synthase. **(D)** Direct transformation of branched-chain amino acids. BCAA, branched-chain amino acid; BCKA, branched-chain α-ketoacid; BCAT, branched-chain amino acid aminotransferase; BCKDH, branched-chain α-ketoacid dehydrogenase complex; IVD, isovaleryl-CoA dehydrogenase; TE, thioesterase; ECH, enoyl-CoA hydratase; AAT, alcohol acyltransferase; CMS, citramalate synthase; IPMI, isopropylmalate isomerase; IPMDH, isopropylmalate dehydrogenase; P450, cytochrome P450 enzyme; SDC-L, serine-decarboxylase like enzyme; ADH, alcohol dehydrogenase. Green compartment represents the chloroplast, maroon compartment the mitochondrion, light blue compartment the peroxisome, and white background the cytosol. Arrows with faded ends indicate cross-membrane transport.

in several fruits of volatile branched-chain acyl esters with double bonds and hydroxyl groups in positions necessary for β-oxidation to proceed indicate that intermediaries of late-stage BCAA catabolism are actively incorporated into volatile fruit compounds. And it has also been demonstrated in hops that a mitochondrial thioesterase is capable of cleaving BCA-CoAs into branched-chain carboxylic acids (Xu et al., 2013), important aroma volatiles detected in many kinds of fruit (**Supplementary Table 1**). Notably, it was found that when apple and banana fruit tissue was fed with deuterium-labeled BCAAs, deuterated branched-chain carboxylic acid production was observed (Tressl and Drawert, 1973; Rowan et al., 1996). Taken together, these lines of evidence strongly support the hypothesis that fruit BCVs are formed through catabolic breakdown of BCAAs.

However, several difficulties remaining with this hypothesis indicate that it may not be generally applicable across all fruits. Evidence from tomato seems to show that BCAA catabolism may not be primarily responsible for the formation of BCVs in that fruit; when disks of tomato fruit tissue were fed elevated levels of BCAAs, no significant measurable increase in BCV quantity was detected as compared to control (Kochevenko et al., 2012). Furthermore, overexpression of tomato BCAT genes did not result in plants yielding fruits that produced increased levels of BCVs (Kochevenko et al., 2012). Since, BCAT enzymes catalyze the first step in BCAA catabolic breakdown, overexpression of the genes encoding these proteins should theoretically result in higher levels of BCAAs entering the degradation pathway which in turn should yield more substrates for conversion into greater amounts of BCVs- results not observed in the tomato BCAT overexpression experiments. Other difficulties with the BCAA catabolism hypothesis deal with the issue of cellular regulation of BCAA metabolism: since it is known that under ordinary conditions the biosynthesis of BCAAs is tightly regulated through feedback inhibition (Binder, 2010; Galili et al., 2016; Xing and Last, 2017), it must be explained how some fruits can overcome these regulatory barriers to produce the great amounts of BCAAs and corresponding breakdown products needed to support the biosynthesis of massive quantities of BCVs observed in these fruits. By itself, the BCAA catabolism hypothesis is incapable of accounting for this. These difficulties have led to the proposal and investigation of other hypotheses regarding possible alternate routes for BCV biosynthesis.

De novo Branched-Chain α-Ketoacid Biosynthesis Followed by Mitochondrial Catabolism

Based primarily off of research done in tomato, this hypothesis posits that BCAAs are not the main source of carbon used for biosynthesis of fruit BCVs but that instead it is branched-chain α-ketoacids that fill this role. In this hypothesis, the biosynthesis of BCAAs proceeds as normal up until the last step, where instead of conversion to BCAAs by BCAT enzymes branched-chain α-ketoacids produced so far are directly exported to the mitochondria for BCKDH-mediated catabolism into BCVs and associated precursors. This hypothesis has several explanatory advantages. For one, it explains the findings in tomato that feeding excess BCAAs to tomato fruit tissue does not result in elevated BCV volatile production, while feeding excess BCKAs does (Kochevenko et al., 2012). Another advantage is that this hypothesis manages to bypass BCAA-mediated feedback inhibition of upstream biosynthesis enzymes, though inhibition by non-BCAA precursors generated by this pathway may still occur depending on the sensitivities of these enzymes to those compounds.

Much more experimental evidence is needed to conclude whether or not this hypothesized pathway is involved in BCV biosynthesis in certain fruits. In particular, labeling experiments where deuterated BCKAs are fed to fruit tissue and deuterated BCVs are observed but not deuterated BCAAs would provide robust evidence for the validity of this hypothesis. Supporting evidence could include an observation that BCAT transcripts become drastically reduced in fruit tissue as compared to the other upstream BCAA biosynthesis enzymes. These *in vitro* assays would show that BCKAs do not cause feedback inhibition of the upstream biosynthesis enzyme isoforms present in fruit, or the discovery and characterization of a chloroplast transporter expressed in fruit tissue that preferentially exports BCKAs before they can be converted to BCAAs by chloroplastic BCATs.

It is important to note that this hypothesis may not be mutually exclusive with the BCAA catabolism hypothesis: it may be possible that fruit cells produce elevated levels of BCKAs while also simultaneously catabolizing BCAAs into volatiles. In fact, doing both might actually increase the quantity of carbon shunted into mitochondrial BCKDH-mediated volatile precursor production: catabolizing BCAAs would reduce inhibitory pressure on key BCAA biosynthesis enzymes which would then be free to produce greater quantities of BCKAs that would be directly used to support BCV production. Further investigation is needed to determine if such a scenario indeed occurs in fruit tissue in nature and if so, what quantifiable impact each pathway has on overall BCV production.

Production of 2-Methylbutyl Volatiles by Citramalate Synthase

Work in apple has revealed a third possible route for the biosynthesis of BCVs. Unlike the first two hypothesized pathways, this route does not involve the early steps of classical plant BCAA biosynthesis but instead relies on the enzyme citramalate synthase (CMS), an enzyme previously known to

be involved in BCAA biosynthesis only in bacteria (Sugimoto, 2011; Sugimoto et al., 2021). Briefly, in this pathway citramalate synthase condenses one molecule of pyruvate with one molecule of acetyl-CoA to form the dicarboxylic acid citramalate, a molecule of which is then converted to 3-methylmalate by the action of isopropylmalate isomerase (IPMI) enzymes. This compound is then acted upon by isopropylmalate dehydrogenase (IPMDH) enzymes to yield α-ketobutanoate, a known precursor of isoleucine biosynthesis via the established plant pathway. Biosynthesis to α-keto-β-methylpentanoate and isoleucine then proceeds along the conventional plant BCAA biosynthesis pathway. Direct experimental evidence for the activity of this pathway in apple has been obtained through the use of ^{13}C-labeled acetate feeding and *in vitro* biochemical characterization of CMS and IPMI enzymes expressed in apple fruit tissue (Sugimoto, 2011; Sugimoto et al., 2021). Supporting evidence in the form of measured increases in levels of citramalate and CMS transcripts as apple ripening progressed was also obtained in the same studies.

The primary explanatory advantage of this hypothesis is that it enables the production of massive quantities of 2-methylbutyl volatile compounds in fruit without being subject to the feedback inhibition that large concentrations of isoleucine exert on threonine deaminase (TD), an enzyme that catalyzes the first committed step in isoleucine biosynthesis (Sidorov et al., 1981; Singh and Shaner, 1995; Binder, 2010; Sugimoto et al., 2021). Furthermore, additional evidence in apple indicates that fruit CMS enzymes may also play a role in biosynthesizing straight-chain esters, a class of compound commonly found at high levels in several fruits including apple (Plotto, 1998; El Hadi et al., 2013; Liu et al., 2021; Sugimoto et al., 2021). Nevertheless, this hypothesis alone suffers from a serious limitation: it is unable to account for the high levels of 3-methylbutyl volatiles observed in several fruits as well as elevated levels of 2-methylpropyl volatiles observed in others. Therefore, other hypotheses must be deferred to when considering the biosynthetic mechanisms underlying the formation of 3-methylbutyl and 2-methylpropyl fruit volatiles. The fact that 3-methylbutyl and 2-methylpropyl compounds have been detected in apple alongside high levels of 2-methylbutyl volatiles (Qin et al., 2017; Liu et al., 2021) seems to indicate that at least two separate and distinct BCV biosynthesis pathways can be active at the same time in this fruit.

Direct Transformation of Branched-Chain Amino Acids

The last possible mechanism of BCV biosynthesis is direct conversion of BCAAs into volatile compounds or immediate precursors. Rather than undergoing several steps of degradation through the established BCAA catabolism process before being incorporated into BCVs, this hypothesis proposes that some volatiles are directly transformed through enzymatic action into BCVs or the immediate precursors of such. Evidence from alfalfa and chickpea indicates that plants form branched-chain aldehydes and alcohols through this pathway: in both species, cDNAs for serine decarboxylase-like (SDC-L) enzymes were found that when heterologously expressed in bacteria produced enzymes capable of directly forming branched-chain aldehydes from branched-chain amino acids (Torrens-Spence et al., 2014). Branched-chain alcohols could then be formed through the action of alcohol dehydrogenase (ADH) enzymes acting on these branched-chain aldehydes. Similarly, work done in poplar demonstrated that branched-chain nitrile volatiles can be biosynthesized from BCAAs through the action of two cytochrome P450 enzymes, one that converts BCAAs into branched-chain aldoximes and another that subsequently converts the branched-chain aldoximes into branched-chain nitriles (Irmisch et al., 2013, 2014). Presumably, this pathway may also be involved in the biosynthesis of other nitrogen-containing BCVs reported from various fruits as it does not involve the loss of the original amino acid's nitrogen atom but permits its refunctionalization into another chemical moiety. Indeed, evidence from grape indicates that branched-chain 2-methoxypyrazine volatiles are formed in just such a manner (Lei et al., 2019). Experiments involving feeding of ^{15}N-labeled BCAAs to tissue from fruits known to produce nitrogenous BCVs would be one way to empirically demonstrate such a role for this pathway. The biosynthesis of both types of branched-chain volatile compound have been shown to be accomplished without the involvement of the mitochondrial BCKDH enzyme complex, a key feature of the previous three hypotheses.

It is interesting to note that this pathway can theoretically provide a possible route for the biosynthesis of branched-chain acyl esters that also does not rely on the activity of the mitochondrial BCKDH complex (**Figure 3**). In this proposed route, branched-chain aldehydes are generated by a serine decarboxylase-like enzyme as per that characterized by Torrens-Spence et al. (2014). These branched-chain aldehydes would then be converted to branched-chain carboxylic acids by the action of aldehyde dehydrogenases (ALDHs), enzymes known to be found in the genomes of many plants (Brocker et al., 2013; Tola et al., 2021). The resulting branched-chain carboxylic acids could then be turns into the corresponding branched-chain acyl-CoAs by carboxyl-CoA ligases (CCLs), as was demonstrated to occur in hops (Xu et al., 2013). This route is fully compatible with existing data from feeding and labeling experiments that demonstrate the conversion of BCAAs into branched-chain acyl esters. In addition, given that neither of the known BCV-forming SDC-like enzymes are predicted to localize to mitochondria (Torrens-Spence et al., 2014) and that several plant ALDHs are known to be localized to the cytosol (Končitíková et al., 2015; Tola et al., 2021) along with CCLs shown to activate branched-chain substrates (Xu et al., 2013), this proposed pathway solves the difficulty of explaining how BCA-CoAs produced in the mitochondria can cross the mitochondrial membrane into the cytosol where plant AAT enzymes have been shown to be localized (Noichinda et al., 1999a; Zhang et al., 2019b). Furthermore, since prior research indicates that mitochondrial BCKDH-mediated BCAA catabolism is tightly regulated by a variety of factors in plants (Fujiki et al., 2001; Peng et al., 2015) a BCA-CoA production pathway not involving the BCKDH complex would not need to overcome in-built regulatory hurdles to generate large quantities of BCA-CoAs. Several difficulties are still apparent with this hypothetical route

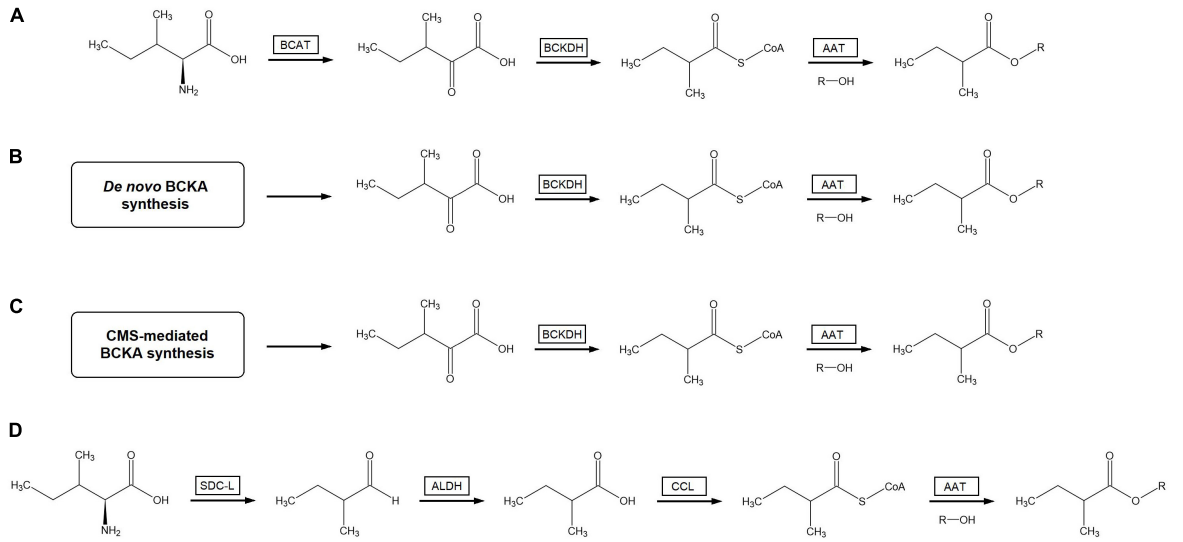

FIGURE 3 | Possible biosynthesis routes to volatile branched-chain acyl esters. **(A)** Mitochondrial BCAT- and BCKDH-mediated catabolism of free branched-chain amino acids to branched-chain acyl-CoAs followed by esterification with alcohols by AAT enzymes. **(B)** *De novo* chloroplast synthesis of branched-chain α-ketoacids followed by BCKDH-mediated catabolism to branched-chain acyl-CoAs and subsequent AAT-mediated esterification with alcohols. **(C)** CMS-initiated synthesis of α-keto-β-methylpentanoate followed by BCKDH-mediated catabolism to 2-methylbutyl acyl-CoA and subsequent AAT-mediated esterification with alcohols to form 2-methylbutanoate esters. **(D)** Branched-chain aldehyde synthesis from free branched-chain amino acids via SDC-L, followed by conversion of branched-chain aldehydes to branched-chain carboxylic acids through ALDH enzymes, followed by activation to branched-chain acyl-CoAs by CCL enzymes and subsequent condensation with alcohols via AAT to generate branched-chain acyl esters. The first, second, and fourth routes are capable of generating acyl esters with all three branched-chain structures, while the third route can only generate 2-methylbutanoate esters. The four pathways are illustrated yielding 2-methylbutanoate esters from appropriate precursors for ease of comparison. BCAT, branched-chain amino acid aminotransferase; BCKDH, branched-chain α-ketoacid dehydrogenase complex; AAT, alcohol acyltransferase; BCKA, branched-chain α-ketoacids; SDC-L, serine-decarboxylase like enzyme; ALDH, aldehyde dehydrogenase; CCL, carboxyl-CoA ligase.

to branched-chain acyl esters: the accumulation of high levels of aldehyde compounds is known to be toxic to cells, competition for aldehyde substrates with the ADH enzymes known to produce branched-chain alcohols, and the simple fact that no direct evidence of this alternate route has yet been empirically demonstrated. Experimental evidence such as deuterium-labeled branched-chain aldehydes yielding branched-chain acyl esters with deuterated acyl moieties or the characterization of fruit ALDH enzymes capable of forming branched-chain carboxylic acids from branched-chain aldehydes would go a long way to establish the viability of this proposed pathway to branched-chain acyl ester biosynthesis.

UNRESOLVED QUESTIONS CONCERNING BRANCHED-CHAIN VOLATILE BIOSYNTHESIS

Despite significant progress in understanding the molecular correlates of BCV biosynthesis in plants, much remains to be uncovered. In comparison, the metabolic bases of the biosynthesis of other important classes of fruit volatile such as the terpenoid, oxylipin, and phenylpropanoid families have been quite thoroughly characterized. For a similar level of understanding to be achieved for branched-chain volatiles, several important questions need to be resolved. A few of these unresolved questions regarding BCV biosynthesis most relevant to fruit volatile metabolism are explored below:

How Branched-Chain α-Ketoacid Dehydrogenase Complex-Mediated Branched-Chain Amino Acid Catabolism Is Regulated in Fruit Tissue

As has been discussed in previous sections of this review, branched-chain acyl esters have been shown to be among the most abundant BCVs detected in several important fruits and have also been demonstrated to be key components of many characteristic fruit flavors. The characterization of numerous fruit alcohol acyltransferase enzymes indicates that these volatiles are most likely formed through the condensation of alcohols with branched-chain acyl-CoAs (Beekwilder et al., 2004; El-Sharkawy et al., 2005; Souleyre et al., 2005; Günther et al., 2011). In three of the four hypotheses regarding BCV biosynthesis previously explored in this review, the mitochondrial BCKDH enzyme complex plays the critical role in generating the BCA-CoAs necessary for branched-chain acyl ester biosynthesis. Evidence in plants indicates that the activity of this complex is regulated by several factors (Fujiki et al., 2001; Peng et al., 2015), while work done on the far more studied mammalian BCKDH complex has identified several molecules that directly modulate BCKDH activity. These include a kinase which directly suppresses BCKDH activity and can itself be inhibited by

branched-chain α-ketoacids (Paxton and Harris, 1984; Harris et al., 1986, 1997), phosphatase enzymes that reverse the effects of the kinase and promote activity of the BCKDH complex (Lu et al., 2009; Zhou et al., 2012) and even BCA-CoAs themselves, which have been shown to suppress BCKDH activity *in vitro* (Parker and Randle, 1978).

The overall question relevant to researchers working in the field of fruit aroma volatile metabolism is what role if any do these BCKDH regulatory mechanisms play in the generation of branched-chain acyl esters? If regulatory mechanisms that directly or indirectly suppress BCKDH activity in plants are identified, how are they overcome in fruit tissues to produce the great quantities of BCA-CoAs needed to support large-scale branched-chain acyl ester biosynthesis as observed in fruits such as apple? If plant homologs of the mammalian BCKDH kinase and phosphatase enzymes are found, are their expression levels in fruit negatively or positively correlated with branched-chain acyl ester content? Are subunits of the plant BCKDH complex inhibited by high levels of BCA-CoAs as was demonstrated to occur in the mammalian complex (Parker and Randle, 1978)? The answers to these questions and related ones would shed great insight into an important aspect of fruit BCV production and may even offer potential avenues for altering the BCV content of fruits by manipulating or even bypassing the underlying regulatory mechanisms governing branched-chain acyl ester precursor biosynthesis.

What Biosynthetic Processes Form Sulfur-Containing Branched-Chain Volatiles

In this review's survey of 175 published studies of the volatile profiles of various fruits only two sulfur-containing BCVs, 2-(2-methylpropyl)-thiazole and *S*-methyl 3-methylbutanethioate, were found (**Table 1**). Compared with the 125 other branched-chain compounds reported, this would seem to indicate that sulfur-containing BCVs are of little importance to the study of fruit volatile metabolism. Nevertheless, the detection of one of these compounds [2-(2-methylpropyl)-thiazole] in the economically significant tomato fruit at concentrations far above the minimum odor threshold (Baldwin et al., 2000; Tieman et al., 2012) as well as the importance of sulfur-containing volatile compounds in general to the flavor of numerous tropical fruits (Engel, 1999; Cannon and Ho, 2018) justifies a closer look at the biosynthesis of sulfur-containing BCVs.

The compound 2-(2-methylpropyl)-thiazole, hereafter referred to as 2-isobutylthiazole, is a known enhancer of tomato flavor that finds frequent use in the preparation of artificial condiments (Kazeniac and Hall, 1972; Christiansen et al., 2011). It has been detected in ripe tomato fruits by several studies (Baldwin et al., 2000; Tikunov et al., 2005; Tieman et al., 2012). Very little is known about the biosynthesis of this compound (Paolo et al., 2018). Hierarchically clustered metabolite data from several tomato introgressed lines characterized for volatile content seems to indicate a branched-chain amino acid origin for this compound (Mathieu et al., 2009). It is the precise nature of how this biosynthetic process occurs that remains totally unknown. That plants possess the capacity to biosynthesize the thiazole moiety is well known from studies examining plant biosynthesis of thiamine (Belanger et al., 1995; Goyer, 2010). However, from a biochemistry perspective it is difficult to see how this established pathway could incorporate a branched-chain amino acid. It is far more likely that the biosynthesis of this volatile occurs via a novel mechanism that uses a leucine molecule as a starting point and source for the thiazole's nitrogen. Feeding ^{15}N-labeled leucine to portions of tomato fruit tissue and examining any generated 2-isobutylthiazole molecules for that radioisotope could confirm or refute that assertion. Far more difficult would be accounting for the sulfur component of the thiazole ring and the two carbons at the four- and five-positions. While experiments using radiolabeled cysteine or methionine could yield some insight into the thiazole ring's origin, ultimately it may be more feasible to use the abundant genetic resources available for tomato to track down potential biosynthesis enzymes using fine mapping of quantitative trait loci robustly associated with variable levels of this compound.

The other sulfur-containing BCV identified is the compound *S*-methyl 3-methylbutanethioate, isolated from cantaloupe (Beaulieu and Grimm, 2001). Several sulfur volatiles have been detected in the aroma profiles of ripe melons and are thought to

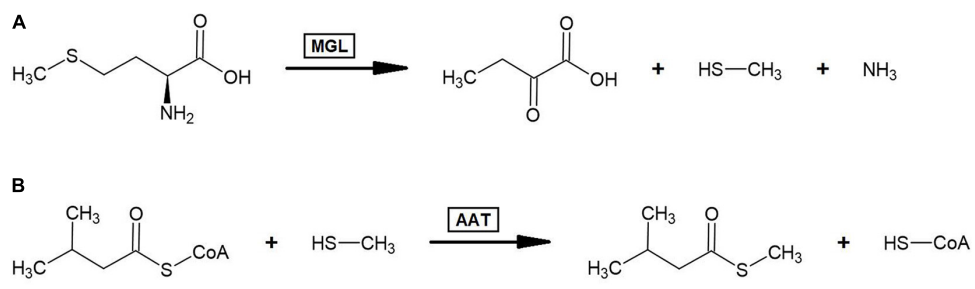

FIGURE 4 | Proposed biosynthesis pathway for *S*-methyl branched-chain thioester volatiles. **(A)** Breakdown of L-methionine to α-ketobutanoate, methanethiol, and ammonia by the action of L-methionine-γ–lyase (MGL). **(B)** Formation of *S*-methyl branched-chain thioesters via alcohol acyltransferase (AAT) mediated condensation of methanethiol with branched-chain acyl-CoAs. This panel illustrates this process occurring with 3-methylbutyl-CoA and yielding *S*-methyl 3-methylbutanethioate since that was the only *S*-methyl branched-chain thioester volatile identified across the 175 fruit volatile studies examined in this review; however, this process could theoretically yield *S*-methyl 2-methylpropanethioate and *S*-methyl 2-methylbutanethioate from 2-methylpropyl-CoA and 2-methylbutyl-CoA, respectively.

contribute to that fruit's characteristic aroma (Wyllie and Leach, 1992). Due to this, some investigation into the biosynthesis of sulfur volatiles in general in melon fruits has been conducted. Isotope feeding experiments conducted with $^{13}C_5$-L-methionine gave evidence that volatile *S*-methyl thioesters are formed through methionine catabolism (Gonda et al., 2013). This study found that the enzyme L-methionine-γ–lyase (MGL) was capable of cleaving radiolabeled methanethiol from L-methionine and that *S*-methyl thioesters incorporated a radiolabeled carbon at the methyl group. As it has been shown in strawberry that alcohol acyltransferase can catalyze the formation of straight-chain thioesters by condensing thioalcohols with acyl-CoAs (Noichinda et al., 1999b), it may be likely that branched-chain *S*-methyl thioesters in fruit arise from AAT-mediated condensation of branched-chain acyl-CoAs with methanethiol derived from the MGL-catalyzed cleavage of methionine (**Figure 4**). Empirically demonstrating if this process occurs in plants by incubating branched-chain volatile ester forming AAT enzymes with branched-chain acyl-CoAs and thioalcohols would answer an important question regarding the metabolism of volatile branched-chain sulfur compounds.

What Biosynthetic Processes Are Capable of Forming Branched-Chain Alkanes in Fruit

Only one branched-chain alkane volatile was reported from all of the literature examined, the compound being 2-methylbutane and its presence being reported in raspberry (Aprea et al., 2015). Because the presence of this compound was reported below the level required for reliable quantification and because other studies of raspberry aroma failed to detect its presence, it is unlikely that that this compound plays a role in raspberry aroma. Nevertheless, as small to medium size branched alkanes in general are important components of commercial gasoline the biosynthesis of 2-methylbutane in fruit may be of interest to workers researching ways to bioengineer plants capable of producing fuel hydrocarbons. It has been shown that some plants can produce alkanes through the decarbonylation of aldehydes (Cheesbrough and Kolattukudy, 1984; Dennis and Kolattukudy, 1991; Aarts et al., 1995; Schneider-Belhaddad and Kolattukudy, 2000). While this route has been demonstrated to operate primarily on long- and very-long chain fatty acid derivatives in plants (Bernard et al., 2012; Ni et al., 2018), it may be a viable biochemical route to short branched-chain alkanes especially since branched-chain aldehydes are commonly found in several different kinds of plant (**Supplementary Table 1**). Further research with an emphasis on short branched-chain substrates is needed to confirm if such a pathway is indeed responsible for branched-chain alkane volatile biosynthesis in plants.

CONCLUSION

While knowledge regarding the biochemical basis of branched-chain volatile metabolism in fruits has advanced significantly in recent years, it is still rather inadequate especially when compared to our detailed understanding of oxylipin, terpenoid, and phenylpropanoid volatile biosynthesis. Much more is known regarding the impact BCVs have on the flavor and aroma qualities of several edible fruits, yet this underlies the importance of obtaining a more thorough understanding of the molecular correlates underlying fruit BCV production. What has been published regarding this topic points to four general hypotheses concerning the mechanisms of BCV volatile biosynthesis in fruits, any or all of which might be operational *in vivo*. It is clear that properly elucidating which metabolic processes are responsible for fruit BCV biosynthesis will require a great deal of further experimental work, and it may very well be that the precise mechanisms vary from fruit to fruit.

Several questions regarding BCV metabolism remain unresolved, particularly those concerning the biosynthesis of more unusual compounds such as branched-chain alkanes and *S*-methyl thioesters. Furthermore, the regulation of important parts of several proposed BCV biosynthesis routes remains little known in plants. Whether well-studied regulatory mechanisms known to control similar pathways in mammals are also active in plants is a particularly relevant question, especially if bypassing these mechanisms presents a potential way to modulate BCV content in fruit tissue. Information gained on this aspect of BCV metabolism could prove quite useful to groups researching ways to improve the flavor of certain fruits by manipulating levels of important volatile compounds.

Ultimately, advancing our understanding of BCV metabolism represents a way to further our knowledge of the molecular basis of fruit flavor and aroma. The fact that important progress has been made should not detract from the fact that significant gaps remain regarding our understanding of how specifically these compounds are generated in fruits. Filling these gaps through rigorous experimental work will go a long way to making branched-chain volatiles as well understood as their oxylipin, terpenoid, and phenylpropanoid counterparts.

AUTHOR CONTRIBUTIONS

LB and PM conceived the idea to develop the manuscript. LB reviewed and wrote the original draft. DT and PM reviewed and helped to create the final version. All authors contributed to the article and approved the submitted version.

FUNDING

This research was funded by the Blueberry Breeding Program at University of Florida.

SUPPLEMENTARY MATERIAL

The Supplementary Material for this article can be found online at: https://www.frontiersin.org/articles/10.3389/fpls.2021.814138/full#supplementary-material

REFERENCES

Aarts, M. G., Keijzer, C. J., Stiekema, W. J., and Pereira, A. (1995). Molecular characterization of the Cer1 gene of arabidopsis involved in epicuticular wax biosynthesis and pollen fertility. *Plant Cell* 7, 2115–2127. doi: 10.1105/tpc.7.12.2115

Abbas, F., Ke, Y., Yu, R., Yue, Y., Amanullah, S., Jahangir, M. M., et al. (2017). Volatile terpenoids: multiple functions, biosynthesis, modulation and manipulation by genetic engineering. *Planta* 246, 803–816. doi: 10.1007/s00425-017-2749-x

Ağalar, H. G., Demirci, B., and Başer, K. H. C. (2014). The Volatile Compounds of Elderberries (*Sambucus nigra* L.). *Nat. Vol. Essent. Oils* 1, 51–54.

Alves, G. L., and Franco, M. R. B. (2003). Headspace gas chromatography-mass spectrometry of volatile compounds in murici (*Byrsonima crassifolia* l. Rich) *J. Chromatogr. A.* 985, 297–301. doi: 10.1016/S0021-9673(02)01398-5

Amanpour, A., Guclu, G., Kelebek, H., and Selli, S. (2019). Characterization of key aroma compounds in fresh and roasted terebinth fruits using aroma extract dilution analysis and GC–MS-Olfactometry. *Microchem. J.* 145, 96–104. doi: 10.1016/j.microc.2018.10.024

Ameye, M., Allmann, S., Verwaeren, J., Smagghe, G., Haesaert, G., Schuurink, R. C., et al. (2018). Green leaf volatile production by plants: a meta-analysis. *New Phytol.* 220, 666–683. doi: 10.1111/nph.14671

Amira, E. A., Guido, F., Behija, S. E., Manel, I., Nesrine, Z., Ali, F., et al. (2011). Chemical and aroma volatile compositions of date palm (*Phoenix dactylifera L.*) fruits at three maturation stages. *Food Chem.* 127, 1744–1754. doi: 10.1016/j.foodchem.2011.02.051

Aprea, E., Biasioli, F., and Gasperi, F. (2015). Volatile Compounds of Raspberry Fruit: From Analytical Methods to Biological Role and Sensory Impact. *Molecules* 20, 2445–2474. doi: 10.3390/molecules20022445

Arena, E., Campisi, S., Fallico, B., Lanza, M. C., and Maccarone, E. (2001). Aroma value of volatile compounds of prickly pear (*Opuntia ficus indica* (L.) Mill. Cactaceae). *Ital. J. Food Sci.* 13, 311–319.

Aubert, C., and Bourger, N. (2004). Investigation of Volatiles in Charentais Cantaloupe Melons (*Cucumis melo* Var. *cantalupensis*). Characterization of Aroma Constituents in Some Cultivars. *J. Agric. Food Chem.* 52, 4522–4528. doi: 10.1021/jf049777s

Augusto, F., Valente, A. L. P., dos Santos, Tada, E., and Ruvellino, S. R. (2000). Screening of Brazilian fruit aromas using solid-phase microextraction–gas chromatography–mass spectrometry. *J. Chromatogr. A.* 873, 117–127. doi: 10.1016/S0021-9673(99)01282-0

Baldwin, E. A., Scott, J. W., Shewmaker, C. K., and Schuch, W. (2000). Flavor trivia and tomato aroma: biochemistry and possible mechanisms for control of important aroma components. *HortScience* 35, 1013–1022. doi: 10.21273/HORTSCI.35.6.1013

Barrios Guio, J. C., Sinuco Leon, D. C., and Morales Perez, A. L. (2010). Compuestos volátiles libres y enlazados glicosídicamente en la pulpa de la uva Caimarona (*Pourouma cecropiifolia* Mart.). *Acta Amaz.* 40, 189–198. doi: 10.1590/S0044-59672010000100024

Beaulieu, J. C., and Grimm, C. C. (2001). Identification of Volatile Compounds in Cantaloupe at Various Developmental Stages Using Solid Phase Microextraction. *J. Agric. Food Chem.* 49, 1345–1352. doi: 10.1021/jf0005768

Beekwilder, J., Alvarez-Huerta, M., Neef, E., Verstappen, F. W. A., Bouwmeester, H. J., and Aharoni, A. (2004). Functional characterization of enzymes forming volatile esters from strawberry and banana. *Plant Physiol.* 135, 1865–1878. doi: 10.1104/pp.104.042580

Belanger, F. C., Leustek, T., Chu, B. Y., and Kriz, A. L. (1995). Evidence for the thiamine biosynthetic pathway in higher-plant plastids and its developmental regulation. *Plant Mol. Biol.* 29, 809–821. doi: 10.1007/bf00041170

Belgis, M. B., Wijaya, C. H., Apriyantono, A., Kusbiantoro, B., and Yuliana, N. D. (2017). Volatile and aroma characterization of several lai (*Durio kutejensis*) and durian (*Durio zibenthinus*) cultivars grown in Indonesia. *Sci Hortic.* 220, 291–298. doi: 10.1016/j.scienta.2017.03.041

Belo, R. F. C., Augusti, R., Lopes, P. S. N., and Junqueira, R. G. (2013). Characterization and classifcation of pequi trees (*Caryocar brasiliense* Camb.) based on the profle of volatile constituents using headspace solid-phase microextraction - gas chromatography - mass spectrometry and multivariate analysis. *Food Sci. Technol.* 33, 116–124. doi: 10.1590/S0101-20612013000500018

Bernard, A., Domerguem, F., Pascal, S., Jetter, R., Renne, C., Faure, J. D., et al. (2012). Reconstitution of plant alkane biosynthesis in yeast demonstrates that *Arabidopsis* ECERIFERSUM1 and ECERIFERUM3 are core components of a very-long-chain alkane synthesis complex. *Plant Cell* 24, 3106–3118. doi: 10.1105/tpc.112.099796

Besada, C., Sanchez, G., Gil, R., Granell, A., and Salvador, A. (2017). Volatile metabolite profiling reveals the changes in the volatile compounds of new spontaneously generated loquat cultivars. *Food Res. Int.* 100, 234–243. doi: 10.1016/j.foodres.2017.06.068

Binder, S. (2010). Branched-chain amino acid metabolism in *Arabidopsis thaliana*. *Arabidopsis Book* 8:e0137. doi: 10.1199/tab.0137

Binder, S., Knill, T., and Schuster, J. (2007). Branched-chain amino acid metabolism in higher plants. *Physiol. Plant.* 129, 68–78. doi: 10.1111/j.1399-3054.2006.00800.x

Boatright, J., Negre, F., Chen, X. L., Kish, C. M., Wood, B., Peel, G., et al. (2004). Understanding *in vivo* benzenoid metabolism in petunia petal tissue. *Plant Physiol.* 135, 1993–2011. doi: 10.1104/pp.104.045468

Borges, E. C., and Rezende, C. M. (2000). Main aroma constituents of genipap (*Genipa americana*) and bacuri (*Platonia sculenta*). *J. Essential Oil Res.* 12, 71–74. doi: 10.1080/10412905.2000.9712046

Boudhrioua, N., Giampaoli, P., and Bonazzi, C. (2003). Changes in aromatic components of banana during ripening and air-drying. *LWT* 36, 633–642. doi: 10.1016/S0023-6438(03)00083-5

Boulanger, R., and Crouzet, J. (2000). Free and bound flavour components of Amazonian fruits: 2. cupuaçu volatile compounds. *Flavour Fragr. J.* 15, 251–257. doi: 10.1002/1099-1026(200007/08)15:4<251::AID-FFJ905<3.0.CO;2-2

Boulanger, R., Chassagne, D., and Crouzet, J. (1999). Free and bound flavour components of amazonian fruits. 1: Bacuri. *Flavour Fragr. J.* 14, 303–311. doi: 10.1002/(SICI)1099-1026(199909/10)14:5<303::AID-FFJ834<3.0.CO;2-C

Brocker, C., Vasiliou, M., Carpenter, S., Carpenter, C., Zhang, Y., Wang, X., et al. (2013). Aldehyde dehydrogenase (ALDH) superfamily in plants: gene nomenclature and comparative genomics. *Planta* 237, 189–210. doi: 10.1007/s00425-012-1749-0

Cannon, R. J., and Ho, C. (2018). Volatile Sulfur Compounds in Tropical Fruits. *J. Food Drug Anal.* 26, 445–468. doi: 10.1016/j.jfda.2018.01.014

Carasek, E., and Pawliszyn, J. (2006). Screening of Tropical Fruit Volatile Compounds Using Solid-Phase Microextraction (SPME) Fibers and Internally Cooled SPME Fiber. *J. Agric. Food Chem.* 54, 8688–8696. doi: 10.1021/jf0613942

Ceva-Antunes, P. M. N., Bizzo, H. R., Alves, S. M., and Antunes, O. A. C. (2003). Analysis of volatile compounds of Taperebá (*Spondias mombin* L.) and Cajá (*Spondias mombin* L.) by simultaneous distillation and extraction (SDE) and solid phase microextraction (SPME). *J. Agric. Food Chem.* 51, 1387–1392. doi: 10.1021/jf025873m

Ceva-Antunes, P. M. N., Bizzo, H. R., Silva, A. S., Carvalho, C. P. S., and Antunes, O. A. C. (2006). Analysis of Volatile Composition of Siriguela (*Spondias Purpurea* L.) By Solid Phase Microextraction (SPME). *LWT-Food Sci. Technol.* 39, 436–442. doi: 10.1016/j.lwt.2005.02.007

Chai, Q., Liu, W., Wang, L., Yang, C., Wang, Y., Fang, J., et al. (2012). Volatiles of plums evaluated by HS-SPME with GC–MS at the germplasm level. *Food Chem.* 130, 432–440. doi: 10.1016/j.foodchem.2011.05.127

Cheesbrough, T. M., and Kolattukudy, P. E. (1984). Alkane biosynthesis by decarbonylation of aldehydes catalyzed by a particulate preparation from *Pisum sativum*. *Proc. Natl. Acad. Sci. U.S.A.* 81, 6613–6617. doi: 10.1073/pnas.81.21.6613

Chen, L., Zhang, X., Jin, Q., Yang, L., Li, J., and Chen, F. (2015). Free and Bound Volatile Chemicals in Mulberry (*Morus atropurpurea* Roxb.). *J. Food Sci.* 80, C975–C982. doi: 10.1111/1750-3841.12840

Chen, Q. Q., Song, J. X., Bi, J. F., Meng, X. J., and Wu, X. Y. (2018). Characterization of volatile profile from ten different varieties of Chinese jujubes by HS-SPME/GC–MS coupled with E-nose. *Food Res. Int.* 105, 605–615. doi: 10.1016/j.foodres.2017.11.054

Chen, X., Quek, S. W., Fedrizzi, B., and Kilmartin, P. A. (2020). Characterization of free and glycosidically bound volatile compounds from tamarillo (*Solanum betaceum* Cav.) with considerations on hydrolysis strategies and incubation time. *LWT* 124:109178. doi: 10.1016/j.lwt.2020.109178

Cheng, A.-X., Lou, Y.-G., Mao, Y.-B., Lu, S., Wang, L.-J., and Chen, X.-Y. (2007). Plant terpenoids: biosynthesis and ecological functions. *J. Integr. Plant Biol.* 49, 179–186. doi: 10.1111/j.1744-7909.2007.00395.x

Cheng, H., Chen, J., Li, X., Pan, J., Xue, S. J., Liu, D., et al. (2015). Differentiation of the volatile profiles of Chinese bayberry cultivars during storage by HS-SPME–GC/MS combined with principal component analysis. *Postharvest Biol. Technol.* 100, 59–72. doi: 10.1016/j.postharvbio.2014.09.003

Cheng, K., Peng, B., and Yuan, F. (2020). Volatile composition of eight blueberry cultivars and their relationship with sensory attributes. *Flavour Fragr. J.* 35, 443–453. doi: 10.1002/ffj.3583

Cheong, K. W., Tan, C. P., Mirhosseini, H., Hamid, N. S. A., Osman, A., and Basri, M. (2010). Equilibrium headspace analysis of volatile flavour compounds extracted from soursop (*Annona muricata*) using solid phase microextraction. *Food Res. Int.* 43, 1267–1276. doi: 10.1016/j.foodres.2010.03.001

Choi, J. Y., Lee, S. M., Lee, H. J., and Kim, Y.-S. (2018). Characterization of aroma-active compounds in Chinese quince (*Pseudocydonia sinensis* Schneid) by aroma dilution analyses. *Food Res. Int.* 105, 828–835. doi: 10.1016/j.foodres.2017.12.015

Christiansen, K. F., Olsen, E., Vegarud, G., Langsrud, T., Lea, P., Haugen, J. E., et al. (2011). Flavor release of the tomato flavor enhancer, 2-isobutylthiazole, from whey protein stabilized model dressings. *Food Sci. Technol. Int.* 17, 143–154. doi: 10.1177/1082013210381935

Conde-Martínez, N., Sinuco, D. C., and Osorio, C. (2014). Chemical studies on curuba (*Passiflora mollissima* (Kunth) L. H. Bailey) fruit flavour. *Food Chem.* 15, 356–363. doi: 10.1016/j.foodchem.2014.02.056

Corpas, E. J., Taborda, G., Tapasco, O. A., and Ortiz, A. (2016). Comparison between extraction methods to obtain volátiles from lulo (*Solatium quitoense*) pulp. *Rev. Colomb. Quim.* 45, 12–21. doi: 10.15446/rev.colomb.quim.v45n3.61359

Cozzolino, R., De Giulio, B., Petriccione, M., Martignetti, A., Malorni, L., Zampella, L., et al. (2020). Comparative analysis of volatile metabolites, quality and sensory attributes of *Actinidia Chinensis* fruit. *Food Chem.* 316:126340. doi: 10.1016/j.foodchem.2020.126340

da Rocha, R. F. J., da Silva, Araújo, I. M., de Freitas, S. M., dos Santos, and Garruti, D. (2017). Optimization of headspace solid phase micro-extraction of volatile compounds from papaya fruit assisted by GC–olfactometry. *J. Food Sci. Technol.* 54, 4042–4050. doi: 10.1007/s13197-017-2871-6

da Silva, A. P. G., Spricigo, P. C., Purgatto, E., de Alencar, S. M., and Jacomino, A. P. (2019a). Volatile Compounds Determined by SPME-GC, Bioactive Compounds, In Vitro Antioxidant Capacity and Physicochemical Characteristics of Four Native Fruits from South America. *Plant Foods Hum. Nutr.* 74, 358–363. doi: 10.1007/s11130-019-00745-7

da Silva, A. P. G., Spricigo, P. C., Purgatto, E., de Alencar, S. M., Sartori, A. P., and Jacomino, A. P. (2019b). Chemical composition, nutritional value and bioactive compounds in six uvaia accessions. *Food Chem.* 294, 547–556. doi: 10.1016/j.foodchem.2019.04.121

D'Agostino, M. F., Sanz, J., Sanz, M. L., Giuffrè, A. M., Sicari, V., and Soria, A. C. (2015). Optimization of a Solid-Phase Microextraction method for the Gas Chromatography–Mass Spectrometry analysis of blackberry (*Rubus ulmifolius* Schott) fruit volatiles. *Food Chem.* 178, 10–17. doi: 10.1016/j.foodchem.2015.01.010

de Araújo, F. F., de Paulo Farias, D., Neri-Numa, I. A., Dias-Audibert, F. L., Delafiori, J., de Souza, F. G., et al. (2021). Chemical characterization of *Eugenia stipitata*: A native fruit from the Amazon rich in nutrients and source of bioactive compounds. *Food Res. Int.* 139:109904. doi: 10.1016/j.foodres.2020.109904

de Santana, K. L., de Sousa Galvão, M., de Jesus, M. S., Nogueira, J. P., and Narain, N. (2017). HS-SPME optimization and extraction of volatile compounds from soursop (*Annona muricata* L.) pulp with emphasis on their characteristic impact compounds. *Ciênc. Tecnol. Aliment. Campinas* 37, 250–260. doi: 10.1590/1678-457X.20916

de Sousa Galvão, M., Narain, N., Madruga, M. S., and Santos, M. S. P. (2010). Volatile compounds in Umbu (*Spondias tuberosa* Arruda Câmara) fruits during maturation. *Acta Hortic.* 864, 509–517. doi: 10.17660/ActaHortic.2010.864.68

de Souza, M. P., Bataglion, G. A., da Silva, F. M. A., de Almeida, R. A., Paz, W. H. P., Nobre, T. A., et al. (2016). Phenolic and aroma compositions of pitomba fruit (*Talisia esculenta* Radlk.) assessed by LC–MS/MS and HS-SPME/GC–MS. *Food Res. Int.* 83, 87–94. doi: 10.1016/j.foodres.2016.01.031

Dennis, M. W., and Kolattukudy, P. E. (1991). Alkane biosynthesis by decarbonylation of aldehyde catalyzed by a microsomal preparation from *Botryococcus braunii*. *Arch. Biochem. Biophys.* 287, 268–275. doi: 10.1016/0003-9861(91)90478-2

Dixon, J., and Hewett, E. W. (2000). Factors affecting apple aroma/flavour volatile concentration: A Review. *N. Z. J. Crop Hortic. Sci.* 28, 155–173. doi: 10.1080/01140671.2000.9514136

Dong, J., Zhang, Y., Tang, X., Jin, W., and Han, Z. (2013). Differences in volatile ester composition between *Fragaria* × *ananassa* and *F. vesca* and implications for strawberry aroma patterns. *Sci. Hortic.* 150, 47–53. doi: 10.1016/j.scienta.2012.11.001

dos Santos, da Silva, M., Alves-Santos, A. M., dos Santos, I. D., Wagner, R., Naves, M. M. V., et al. (2020). A new population of pequi (*Caryocar* spp.) developed by Brazilian indigenous people has agro-industrial and nutraceutical advantages. *Eur. Food Res. Technol.* 246, 1715–1724. doi: 10.1007/s00217-020-03525-9

Du, X., Finn, C. E., and Qian, M. C. (2010). Volatile composition and odour-activity value of thornless 'Black Diamond' and 'Marion' blackberries. *Food Chem.* 119, 1127–1134. doi: 10.1016/j.foodchem.2009.08.024

Du, X., Plotto, A., Song, M., Olmstead, J., and Rouseff, R. (2011). Volatile Composition of Four Southern Highbush Blueberry Cultivars and Effect of Growing Location and Harvest Date. *J. Agric. Food Chem.* 59, 8347–8357. doi: 10.1021/jf201184m

Dudareva, N., Klempien, A., Muhlemann, J. K., and Kaplan, I. (2013). Biosynthesis, function and metabolic engineering of plant volatile organic compounds. *New Phytol.* 198, 16–32. doi: 10.1111/nph.12145

Dudareva, N., Negre, F., Nagegowda, D. A., and Orlova, I. (2006). Plant volatiles: recent advances and future perspectives. *Crit. Rev. Plant Sci.* 25, 417–440. doi: 10.1080/07352680600899973

El Hadi, M. A., Zhang, F. J., Wu, F. F., Zhou, C. H., and Tao, J. (2013). Advances in fruit aroma volatile research. *Molecules* 18, 8200–8229. doi: 10.3390/molecules18078200

Elizalde-González, M. P., and Segura-Rivera, E. J. (2018). Volatile compounds in different parts of the fruit *Psidium guajava* L. cv. "Media China" identified at distinct phenological stages using HS-SPME-GC-QTOF/MS. *Phytochem. Anal.* 29, 649–660. doi: 10.1002/pca.2778

El-Sharkawy, I., Manriquez, D., Flores, F. B., Regad, F., Bouzayen, M., Latché, A., et al. (2005). Functional characterization of a melon alcohol acyl-transferase gene family involved in the biosynthesis of ester volatiles. Identification of the crucial role of a threonine residue for enzyme activity. *Plant Mol. Biol.* 59, 345–362. doi: 10.1007/s11103-005-8884-y

Engel, K. H. (1999). "The Importance of Sulfur-Containing Compounds to Fruit Flavors," in *Flavor Chemistry*, eds R. Teranishi, E. L. Wick, and I. Hornstein (Boston, MA: Springer), 265–273. doi: 10.1007/978-1-4615-4693-1_23

Fang, H., Chen, J., Tian, Y., Liu, Y., Li, H., and Cheng, H. (2020). Chemometrics characterization of volatile changes in processed bayberry juice versus intact fruit during storage by headspace solid-phase micro-extraction combined with GC-MS. *J. Food Process. Preserv.* 44:e14444. doi: 10.1111/jfpp.14444

Faria, J. V., Valido, V. H., Weider, H. P., Paz, da Silva, F. M. A., de Souza, A. D. L., et al. (2021). Comparative evaluation of chemical composition and biological activities of tropical fruits consumed in Manaus, central Amazonia, Brazil. *Food Res. Int.* 139:109836. doi: 10.1016/j.foodres.2020.109836

Farneti, B., Khomenko, I., Grisenti, M., Ajelli, M., and Betta, E. (2017). Exploring Blueberry Aroma Complexity by Chromatographic and Direct-Injection Spectrometric Techniques. *Front. Plant Sci.* 8:617. doi: 10.3389/fpls.2017.00617

Feng, S., Huang, M. Y., Crane, J. H., and Wang, Y. (2018). Characterization of key aroma-active compounds in lychee (*Litchi chinensis* Sonn.). *J. Food Drug Anal.* 26, 497–503. doi: 10.1016/j.jfda.2017.07.013

Ferreira, D. D. F., Garruti, D. S., Barin, J. S., Cichoski, A. J., and Wagner, R. (2016). Characterization of odor-active compounds in gabiroba fruits (*Campomanesia xanthocarpa* O. Berg). *J. Food Qual.* 39, 90–97. doi: 10.3390/metabo10050197

Ferreira, L., Perestrelo, R., and Câmara, J. S. (2009). Comparative analysis of the volatile fraction from *Annona cherimola* Mill. cultivars by solid-phase microextraction and gas chromatography–quadrupole mass spectrometry detection. *Talanta* 77, 1087–1096. doi: 10.1016/j.talanta.2008.08.011

Fraga, S. R. G., and Rezende, C. M. (2001). The Aroma of Brazilian Ambarella Fruit (*Spondias cytherea* Sonnerat). *J. Essent. Oil Res.* 13, 252–255. doi: 10.1080/10412905.2001.9699686

Franco, M. R. B., and Shibamoto, T. (2000). Volatile Composition of Some Brazilian Fruits: Umbu-caja (*Spondias citherea*), Camu-camu (*Myrciaria*

dubia), Araça-boi (*Eugenia stipitata*), and Cupuaçu (*Theobroma grandiflorum*). *J. Agric. Food Chem.* 48, 1263–1265. doi: 10.1021/jf9900074

Fraternale, D., Ricci, D., Flamini, G., and Giomaro, G. (2011). Volatiles Profile of Red Apple from Marche Region (Italy). *Rec. Nat. Prod.* 5, 202–207.

Fredes, A., Sales, C., Barreda, M., Valcárcel, M., Roselló, S., and Beltrán, J. (2016). Quantification of prominent volatile compounds responsible for muskmelon and watermelon aroma by purge and trap extraction followed by gas chromatography–mass spectrometry determination. *Food Chem.* 190, 689–700. doi: 10.1016/j.foodchem.2015.06.011

Freitas, T. P., Taver, I. B., Spricigo, P. C., do Amaral, L. B., Purgatto, E., and Jacomino, A. P. (2020). Volatile Compounds and Physicochemical Quality of Four Jabuticabas (*Plinia* sp.). *Molecules* 25:4543. doi: 10.3390/molecules25194543

Fujiki, Y., Ito, M., Nishida, I., and Watanabe, A. (2001). Leucine and its keto acid enhance the coordinated expression of genes for branched-chain amino acid catabolism in *Arabidopsis* under sugar starvation. *FEBS Lett.* 499, 161–165. doi: 10.1016/s0014-5793(01)02536-4

Galili, G., Amir, R., and Fernie, A. R. (2016). The regulation of essential amino acid synthesis and accumulation in plants. *Annu. Rev. Plant Biol.* 67, 153–178. doi: 10.1105/tpc.17.00186

Gilbert, J. L., Guthart, M. J., Gezan, S. A., de Carvalho, M. P., Schwieterman, M. L., Colquhoun, T. A., et al. (2015). Identifying Breeding Priorities for Blueberry Flavor Using Biochemical, Sensory, and Genotype by Environment Analyses. *PLoS One* 10:e0138494. doi: 10.1371/journal.pone.0138494

Goff, S. A., and Klee, H. J. (2006). Plant volatile compounds: sensory cues for health and nutritional value? *Science* 311, 815–819. doi: 10.1126/science.1112614

Gonda, I., Bar, E., Portnoy, V., Lev, S., Burger, J., Schaffer, A. A., et al. (2010). Branched-chain and aromatic amino acid catabolism into aroma volatiles in *Cucumis melo* L. fruit. *J. Exp. Bot.* 61, 1111–1123. doi: 10.1093/jxb/erp390

Gonda, I., Lev, S., Bar, E., Sikron, N., Portnoy, V., Davidovich-Rikanati, R., et al. (2013). Catabolism of L-methionine in the formation of sulfur and other volatiles in melon (*Cucumis melo* L.) fruit. *Plant J.* 74, 458–472. doi: 10.1111/tpj.12149

Goulet, C., Kamiyoshihara, Y., Lam, N. B., Richard, T., Taylor, M. G., Tieman, D. M., et al. (2015). Divergence in the enzymatic activities of a Tomato and *Solanum pennellii* alcohol acyltransferase impacts fruit volatile ester composition. *Mol. Plant* 8, 153–162. doi: 10.1016/j.molp.2014.11.007

Goulet, C., Mageroy, M. H., Lam, N. B., Floystad, A., Tieman, D. M., and Klee, H. J. (2012). Role of an esterase in flavor volatile variation within the tomato clade. *Proc. Natl. Acad. Sci. U. S. A.* 109, 19009–19014. doi: 10.1073/pnas.1216515109

Goyer, A. (2010). Thiamine in plants: aspects of its metabolism and functions. *Phytochemistry* 71, 1615–1624. doi: 10.1016/j.phytochem.2010.06.022

Graham, I. A., and Eastmond, P. J. (2002). Pathways of straight and branched chain fatty acid catabolism in higher plants. *Prog. Lipid Res.* 41, 156–181. doi: 10.1016/S0163-7827(01)00022-4

Grande-Tovar, D. C., Johannes, D.-G., Puerta, L. F., Rodríguez, G. C., Sacchetti, G., Paparella, A., et al. (2019). Bioactive micro-constituents of ackee arilli (*Blighia sapida* K.D. Koenig). *An. Acad. Bras. Ciênc.* 91, 1–15. doi: 10.1590/0001-3765201920180140

Griffiths, G. (2015). Biosynthesis and analysis of plant oxylipins. *Free Radic. Res.* 49, 565–582. doi: 10.3109/10715762.2014.1000318

Grimm, J. E., and Steinhaus, M. (2019). Characterization of the Major Odor-Active Compounds in Jackfruit Pulp. *J. Agric. Food Chem.* 67, 5838–5846. doi: 10.1021/acs.jafc.9b01445

Grimm, J. E., and Steinhaus, M. (2020). Characterization of the Major Odorants in Cempedak—Differences to Jackfruit. *J. Agric. Food Chem.* 68, 258–266. doi: 10.1021/acs.jafc.9b06564

Güler, Z., and Gül, E. (2017). Volatile organic compounds in the aril juices and seeds from selected five pomegranate (*Punica granatum* L.) cultivars. *Int. J. Food Prop.* 20, 281–293. doi: 10.1080/10942912.2016.1155057

Günther, C. S., Chervin, C., Marsh, K. B., Newcomb, R. D., and Souleyre, E. J. F. (2011). Characterisation of two alcohol acyltransferases from kiwifruit (*Actinidia* spp.) reveals distinct substrate preferences. *Phytochemistry* 72, 700–710. doi: 10.1016/j.phytochem.2011.02.026

Hansen, K., and Poll, L. (1993). Conversion of L-isoleucine into 2-methylbut-2-enyl esters in apples. *LWT.* 26, 178–180. doi: 10.1006/fstl.1993.1036

Harb, J., Bisharat, R., and Streif, J. (2008). Changes in volatile constituents of blackcurrants (*Ribes nigrum* L. cv. 'Titania') following controlled atmosphere storage. *Postharvest Biol. Technol.* 47, 271–279. doi: 10.1016/j.postharvbio.2007.08.007

Harris, R. A., Hawes, J. W., Popov, K. M., Zhao, Y., Shimomura, Y., Sato, J., et al. (1997). Studies on the regulation of the mitochondrial α-ketoacid dehydrogenase complexes and their kinases. *Adv. Enzyme Regul.* 37, 271–293. doi: 10.1016/s0065-2571(96)00009-x

Harris, R. A., Paxton, R., Powell, S. M., Goodwin, G. W., Kuntz, M. J., and Han, A. C. (1986). Regulation of branched-chain alpha-ketoacid dehydrogenase complex by covalent modification. *Adv. Enz. Reg.* 25, 219–237. doi: 10.1016/0065-2571(86)90016-6

Hayaloglu, A. A., and Demir, N. (2016). Phenolic Compounds, Volatiles, and Sensory Characteristics of Twelve Sweet Cherry (*Prunus avium* L.) Cultivars Grown in Turkey. *J. Food Sci.* 81, C7–C18. doi: 10.1111/1750-3841.13175

Hildebrandt, T. M., Nunes Nesi, A., Araújo, W. L., and Braun, H.-P. (2015). Amino acid catabolism in plants. *Mol. Plant* 8, 1563–1579. doi: 10.1016/j.molp.2015.09.005

Hou, Y., and Wu, G. (2018). Nutritionally Essential Amino Acids. *Adv. Nutr.* 9, 849–851. doi: 10.1093/advances/nmy054

Irmisch, S., McCormick, A. C., Boeckler, G. A., Schmidt, A., Reichelt, M., Schneider, B., et al. (2013). Two herbivore-induced cytochrome P450 Enzymes CYP79D6 and CYP79D7 catalyze the formation of volatile aldoximes involved in poplar defense. *Plant Cell* 25, 4737–4754. doi: 10.1105/tpc.113.118265

Irmisch, S., McCormick, A. C., Günther, J., Schmidt, A., Boeckler, G. A., Gershenzon, J., et al. (2014). Herbivore-induced poplar cytochrome P450 enzymes of the CYP71 family convert aldoximes to nitriles which repel a generalist caterpillar. *Plant J.* 80, 1095–1107. doi: 10.1111/tpj.12711

Irwandi, J., Che Man, Y. B., Selamat, J., Ahmad, F., and Sugisawa, H. (2008). Retention of volatile components of durian fruit leather during processing and storage. *J. Food Process. Pres.* 32, 740–750. doi: 10.1111/j.1745-4549.2008.00211.x

Iwaoka, W., Hagi, Y., Umano, K., and Shibamoto, T. (1994). Volatile Chemicals Identified in Fresh and Cooked Breadfruit. *J. Agric. Food Chem.* 42, 975–976. doi: 10.1021/jf00040a026

Janzantti, N. S., and Monteiro, M. (2017). HS–GC–MS–O analysis and sensory acceptance of passion fruit during maturation. *J. Food Sci. Technol.* 54, 2594–2601. doi: 10.1007/s13197-017-2671-z

Jayarathna, P. L. I., Jayawardena, J. A. E. C., and Vanniarachchy, M. P. G. (2020). Identification of Physical, Chemical Properties and Flavor Profile of *Spondias dulcis* in Three Maturity Stages. *Int. J. Adv. Res. Sci. Eng.* 5, 208–211.

Joulain, D., Casazza, A., Laurent, R., Portier, D., Guillamon, N., Pandya, R., et al. (2004). Volatile Flavor Constituents of Fruits from Southern Africa: Mobola Plum (*Parinari curatellifolia*). *J. Agric. Food Chem.* 52, 2322–2325. doi: 10.1021/jf030702i

Jung, K. (2018). *Analysis and sensory evaluation of volatile constituents of blackcurrant (Ribes nigrum* L.) and redcurrant (*Ribes rubrum* L.) fruits. [PhD dissertation]. Munich: Technical University of Munich.

Kamatou, G. P. P., Viljoen, A. M., Özek, T., and Başer, K. H. C. (2008). Head-space volatiles of *Gethyllis afra* and *G. ciliaris* fruits ("kukumakranka"). *S. Afr. J. Bot.* 74, 768–770. doi: 10.1016/j.sajb.2008.07.002

Kang, W., Li, Y., Xu, Y., Jiang, W., and Tao, Y. (2012). Characterization of aroma compounds in Chinese bayberry (*Myrica rubra* Sieb. et Zucc.) by Gas Chromatography Mass Spectrometry (GC-MS) and Olfactometry (GC-O). *J. Food Sci.* 77, C1030–C1035. doi: 10.1111/j.1750-3841.2012.02747.x

Kaur, N., Reumann, S., and Hu, J. (2009). Peroxisome biogenesis and function. *Arabidopsis Book* 7:e0123. doi: 10.1199/tab.0123

Kazeniac, S. J., and Hall, R. M. (1972). *2-Alkylthiazoles as Tomato Product Enhancers. U.S. Patent No 3,660,112*. Washington, DC: U.S. Patent and Trademark Office.

Kochevenko, A., Araujo, W. L., Maloney, G. S., Tieman, D. M., Do, P. T., and Taylor, M. G. (2012). Catabolism of branched chain amino acids supports respiration but not volatile synthesis in tomato fruits. *Mol. Plant.* 5, 366–375. doi: 10.1093/mp/ssr108

Končitíková, R., Vigouroux, A., Kopečná, M., Andree, T., Bartoš, J., and Šebela, M. (2015). Role and structural characterization of plant aldehyde dehydrogenases from family 2 and family 7. *Biochem. J.* 468, 109–123. doi: 10.3390/genes12010051

Kozioł, M. J., and Macía, M. J. (1998). Chemical composition, nutritional evaluation, and economic prospects of *Spondias purpurea* (Anacardiaceae). *Econ. Botany* 52, 373–380. doi: 10.1007/BF02862067

Kraujalytė, V., Leitner, E., and Venskutonis, P. R. (2013). Characterization of *Aronia melanocarpa* Volatiles by Headspace-Solid-Phase Microextraction (HS-SPME), Simultaneous Distillation/Extraction (SDE), and Gas Chromatography-Olfactometry (GC-O) Methods. *J. Agric. Food Chem.* 61, 4728–4736. doi: 10.1021/jf400152x

Lackus, N. D., Schmidt, A., Gershenzon, J., and Köllner, T. G. (2021). A peroxisomal β-oxidative pathway contributes to the formation of C_6–C_1 aromatic volatiles in poplar. *Plant Physiol.* 186, 891–909. doi: 10.1093/plphys/kiab111

Lasekan, O., Khatib, A., Juhari, H., Patiram, P., and Lasekan, A. (2013). Headspace solid-phase microextraction gas chromatography-mass spectrometry determination of volatile compounds in different varieties of African star apple fruit (*Chrysophillum albidum*). *Food Chem.* 141, 2089–2097. doi: 10.1016/j.foodchem.2013.05.081

Leffingwell, J. C., Alford, E. D., and Leffingwell, D. (2015). Identification of the Volatile Constituents of Raw Pumpkin (*Cucurbita pepo* L.) by Dynamic Headspace Analyses. *Leffingwell Rep.* 7, 1–14.

Legua, P., Domenech, A., Martínez, J. J., Sánchez-Rodríguez, L., Hernández, F., Carbonell-Barrachina, A. A., et al. (2017). Bioactive and Volatile Compounds in Sweet Cherry Cultivars. *J. Food Nutr. Res.* 5, 844–851. doi: 10.12691/jfnr-5-11-8

Lei, Y., Xie, S., Chen, H., Guan, X., and Zhang, Z. (2019). Behavior of 3-isobutyl-2-methoxypyrazine biosynthesis related to proposed precursor and intermediate in wine grape. *Food Chem.* 277, 609–616. doi: 10.1016/j.foodchem.2018.10.121

Leite Neta, M. T. S., de Jesus, M. S., da Silva, J. L. A., Araujo, H. C. S., Sandes, R. D. D., Shanmugam, S., et al. (2019). Effect of spray drying on bioactive and volatile compounds in soursop (*Annona muricata*) fruit pulp. *Food Res. Int.* 124, 70–77. doi: 10.1016/j.foodres.2018.09.039

Li, C., Xin, M., Li, L., He, X., Yi, P., Tang, Y., et al. (2021). Characterization of the aromatic profile of purple passion fruit (*Passiflora edulis* Sims) during ripening by HS-SPME-GC/MS and RNA sequencing. *Food Chem.* 355:129685. doi: 10.1016/j.foodchem.2021.129685

Li, J.-X., Schieberle, P., and Steinhaus, M. (2012). Characterization of the major odor-active compounds in Thai durian (*Durio zibethinus* L. 'Monthong') by aroma extract dilution analysis and headspace gas chromatography–olfactometry. *J. Agric. Food Chem.* 60, 11253–11262. doi: 10.1021/jf303881k

Lim, S.-H., Nam, H., and Baek, H.-H. (2016). Aroma Characteristics of Acai Berry. *Korean J. Food Sci. Technol.* 48, 122–127. doi: 10.9721/KJFST.2016.48.2.122

Lindhorst, A. C., and Steinhaus, M. (2016). Aroma-active compounds in the fruit of the hardy kiwi (*Actinidia arguta*) cultivars Ananasnaya, Bojnice, and Dumbarton Oaks: differences to common kiwifruit (*Actinidia deliciosa* "Hayward"). *Eur. Food Res. Technol.* 242, 967–975. doi: 10.1007/s00217-015-2603-y

Liu, X., Hao, N., Feng, R., Meng, Z., Li, Y., and Zhao, Z. (2021). Transcriptome and metabolite profiling analyses provide insight into volatile compounds of the apple cultivar 'Ruixue' and its parents during fruit development. *BMC Plant Biol.* 21:231. doi: 10.1186/s12870-021-03032-3

Lu, G., Sun, H., She, P., Youn, J. Y., Warburton, S., Ping, P., et al. (2009). Protein phosphatase 2Cm is a critical regulator of branched-chain amino acid catabolism in mice and cultured cells. *J. Clin. Invest.* 119, 1678–1687. doi: 10.1172/jci38151

Lu, J., Li, H., Quan, J., An, W., Zhao, J., and Xi, W. (2017). Identification of characteristic aroma volatiles of Ningxia goji berries (*Lycium barbarum* L.) and their developmental changes. *Int. J. Food Prop.* 20, S214–S227. doi: 10.1080/10942912.2017.1295254

Lytra, G., Tempere, S., de Revel, G., and Barbe, J.-C. (2014). Distribution and Organoleptic Impact of Ethyl 2-Methylbutanoate Enantiomers in Wine. *J. Agric. Food Chem.* 62, 5005–5010. doi: 10.1021/jf500670z

Mahattanatawee, K., Goodner, K. L., and Baldwin, E. A. (2005). Volatile constituents and character impact compounds of selected Florida's tropical fruit. *Proc. Fla. State Hort. Soc.* 118, 414–418.

Maia, J. G. S., Andrade, E. H. A., and Silva, M. H. L. (2008). Aroma volatiles of pequi fruit (*Caryocar brasiliense* Camb.). *J. Food Compos. Anal.* 21, 574–576. doi: 10.1016/j.jfca.2008.05.006

Maia, J. G. S., Andrade, E. H. A., and Zoghbi, M. G. B. (2003). Volatiles from fruits *of Pouteria Pariry* (Ducke) Baehni and *P. caimito* (Ruiz and Pavon.) Rdlkl. *J. Essent. Oil-Bear. Plants* 6, 127–129. doi: 10.1080/0972-060x.2003.10643339

Maia, J. G. S., Andrade, E. H. A., and Zoghbi, M. G. B. (2004). Aroma volatiles from two fruit varieties of jackfruit (*Artocarpus heterophyllus* Lam.). *Food Chem.* 85, 195–197. doi: 10.1016/S0308-8146(03)00292-9

Majcher, M. A., Scheibe, M., and Jelén, H. H. (2020). Identification of Odor Active Compounds in *Physalis peruviana* L. *Molecules* 25:245. doi: 10.3390/molecules25020245

Márquez, C. J., Jimenez, A. M., Osorio, C., and Cartagena, J. R. (2011). Volatile compounds during ripening of Colombian soursop (*Annona muricata* L. cv. Elita). *Vitae* 18, 245–250.

Marsol-Vall, A., Kortesniemi, M., Karhu, S. T., Kallio, H., and Yang, B. (2018). Profiles of volatile compounds in blackcurrant (*Ribes nigrum*) cultivars with a special focus on the influence of growth latitude and weather conditions. *J. Agric. Food Chem.* 66, 7485–7495. doi: 10.1021/acs.jafc.8b02070

Martín, D. A., and Osorio, C. (2019). Identification of aroma-active volatile compounds in *Pouteria sapota* fruit by aroma extraction dilution analyses (AEDA). *Quím. Nova* 42, 1–4. doi: 10.21577/0100-4042.20170369

Mathieu, S., Cin, V. D., Fei, Z., Li, H., Bliss, P., Taylor, M. G., et al. (2009). Flavour compounds in tomato fruits: identification of loci and potential pathways affecting volatile composition. *J. Exp. Bot.* 60, 325–337. doi: 10.1093/jxb/ern294

Matich, A., and Rowan, D. (2007). Pathway analysis of branched-chain ester biosynthesis in apple using deuterium labeling and enantioselective gas chromatography–mass spectrometry. *J. Agric. Food Chem.* 55, 2727–2735. doi: 10.1021/jf063018n

Misran, A., Padmanabhan, P., Sullivan, J. A., Khanizadeh, S., and Paliyath, G. (2015). Composition of phenolics and volatiles in strawberry cultivars and influence of preharvest hexanal treatment on their profiles. *Can. J. Plant Sci.* 95, 115–126. doi: 10.4141/CJPS-2014-245

Mohd Ali, M., Hashim, N., Abd Aziz, S., and Lasekan, O. (2020). Pineapple (*Ananas comosus*): A comprehensive review of nutritional values, volatile compounds, health benefits, and potential food products. *Food Res. Int.* 137:109675. doi: 10.1016/j.foodres.2020.109675

Monteiro, S. S., Ribeiro, S. R., Soquetta, M. B., Pires, F. J., Wagner, R., and Rosa, C. S. (2018). Evaluation of the chemical, sensory and volatile composition of sapota-do-Solimões pulp at diferent ripening stages. *Food Res. Int.* 109, 159–167. doi: 10.1016/j.foodres.2018.04.033

Montero-Calderón, M., Rojas-Graü, M. A., and Martín-Belloso, O. (2010). Aroma Profile and Volatiles Odor Activity Along Gold Cultivar Pineapple Flesh. *J. Food Sci.* 75, S506–S512. doi: 10.1111/j.1750-3841.2010.01831.x

Mosblech, A., Feussner, I., and Heilmann, I. (2009). Oxylipins: structurally diverse metabolites from fatty acid oxidation. *Plant Physiol. Bioch.* 47, 511–517. doi: 10.1016/j.plaphy.2008.12.011

Nagegowda, D. A. (2010). Plant volatile terpenoid metabolism: biosynthetic genes, transcriptional regulation and subcellular compartmentation. *FEBS Lett.* 584, 2965–2973. doi: 10.1016/j.febslet.2010.05.045

Narain, N., Almeida, J. N., Galvão, M. S., Madruga, M. S., and Brito, E. S. (2004). Compostos voláteis dos frutos de maracujá (*Passiflora edulis* forma *Flavicarpa*) e de cajá (*Spondias mombin* L.) obtidos pela técnica de headspace dinâmico. *Ciênc. Tecnol. Aliment.* 24, 212–216. doi: 10.1590/S0101-20612004000200009

Narain, N., de Sousa Galvão, M., da, S., Ferreira, D., and Navarro, D. M. A. F. (2010). Identification of Volatile Compounds in Mangaba (*Hancornia speciosa* Gomes) Fruit – a Preliminary Study. *Acta Hortic.* 864, 289–294. doi: 10.17660/ActaHortic.2010.864.38

Ni, E., Zhou, L., Li, J., Jiang, D., Wang, Z., Zheng, S., et al. (2018). *OsCER1* plays a pivotal role in very-long-chain alkane biosynthesis and affects plastid development and programmed cell death of tapetum in rice (*Oryza sativa* L.). *Front. Plant Sci.* 9:1217. doi: 10.3389/fpls.2018.01217

Noble, A. C. (1996). Taste-aroma interactions. *Trends Food Sci. Technol.* 7, 439–444. doi: 10.1016/S0924-2244(96)10044-3

Nogueira, J. M. F., Fernandes, P. J. P., and Nascimento, A. M. D. (2003). Composition of Volatiles of Banana Cultivars from Madeira Island. *Phytochem. Anal.* 14, 87–90. doi: 10.1002/pca.691

Nogueira, J. P., Pires, de Siqueira, A. C., Dutra Sandes, R. D., de Sousa Galvão, M., Santos Leite, et al. (2018). An insight into key volatile compounds in acerola (*Malpighia emarginata* DC.) pulp based on their odour activity values

and chemometric evaluation. *Anal. Methods* 10, 5851–5866. doi: 10.1039/c8ay01427b

Noichinda, S., Ueda, Y., Imahori, Y., and Chachin, K. (1999a). Subcellular Localization of Alcohol Acetyltransferase in Strawberry Fruit. *Food Sci. Technol. Res* 5, 239–242. doi: 10.3136/fstr.5.239

Noichinda, S., Ueda, Y., Imahori, Y., and Chachin, K. (1999b). Thioester Production and Thioalcohol Specificity of Alcohol Acetyltransferase in Strawberry Fruit. *Food Sci. Technol. Res* 5, 99–103. doi: 10.3136/fstr.5.99

Oliveira, A. L., Lopes, R. B., Cabral, F. A., and Eberlin, M. N. (2006). Volatile compounds from pitanga fruit (*Eugenia uniflora* L.). *Food Chem.* 99, 1–5. doi: 10.1016/j.foodchem.2005.07.012

Oliveira, I., de Pinho, P. G., Malheiro, R., Baptista, P., and Pereira, J. A. (2011). Volatile profile of *Arbutus unedo* L. fruits through ripening stage. *Food Chem.* 128, 667–673. doi: 10.1016/j.foodchem.2011.03.084

Ong, B. T., Nazimah, S. A. H., Tan, C. P., Mirhosseini, H., Osman, A., Mat Hashim, D., et al. (2008). Analysis of volatile compounds in five jackfruit (*Artocarpus heterophyllus* L.) cultivars using solid-phase microextraction (SPME) and gas chromatography-time-of-flight mass spectrometry (GC-TOFMS). *J. Food Compos. Anal.* 21, 416–422. doi: 10.1016/j.jfca.2008.03.002

Ong, P. K., Acree, T. E., and Lavin, E. H. (1998). Characterization of volatiles in rambutan fruit (*Nephelium lappaceum* L.). *J. Agric. Food Chem.* 46, 611–615. doi: 10.1021/jf970665t

Ong, P. K., and Acree, T. E. (1998). Gas chromatography/olfactory analysis of lychee (*Litchi chinesis* Sonn.). *J. Agric. Food Chem.* 46, 2282–2286. doi: 10.1021/jf9801318

Osorio, C., Alarcon, M., Moreno, C., Bonilla, A., Barrios, J., Garzón, C., et al. (2006). Characterization of Odor-Active Volatiles in Champa (*Campomanesia lineatifolia* R. & P.). *J. Agric. Food Chem.* 54, 509–516. doi: 10.1021/jf052098c

Oz, A. T., Baktemur, G., Paydas Kargi, S., and Kafkas, E. (2016). Volatile Compounds of Strawberry Varieties. *Chem. Nat. Compd.* 52, 507–509. doi: 10.1007/s10600-016-1690-8

Paolo, D., Bianchi, G., Scalzo, R. L., Morelli, C. F., Rabuffetti, M., and Speranza, G. (2018). The Chemistry behind Tomato Quality. *Nat. Prod. Commun.* 13, 1225–1232. doi: 10.1177/1934578X1801300927

Parker, P. J., and Randle, P. J. (1978). Partial purification and properties of branched-chain 2-oxo acid dehydrogenase of ox liver. *Biochem. J.* 171, 751–757. doi: 10.1042/bj1710751

Parliament, T. H., and Smith, A. J. (1999). Volatile Components of *Amelanchier arborea* Nutt. (Shadberry) Fruit. *J. Essent. Oil Res.* 11, 606–608. doi: 10.1080/10412905.1999.9701222

Paxton, R., and Harris, R. A. (1984). Regulation of branched-chain α-ketoacid dehydrogenase kinase. *Arch. Biochem. Biophys.* 231, 48–57. doi: 10.1016/0003-9861(84)90361-8

Peng, C., Uygun, S., Shiu, S. H., and Last, R. L. (2015). The impact of the branched-chain ketoacid dehydrogenase complex on amino acid homeostasis in Arabidopsis. *Plant Physiol.* 169, 1807–1820. doi: 10.1104/pp.15.00461

Pérez, A. G., Olias, R., Luaces, P., and Sanz, C. (2002). Biosynthesis of Strawberry Aroma Compounds through Amino Acid Metabolism. *J. Agric. Food Chem.* 50, 4037–4042. doi: 10.1021/jf011465r

Pino, J. A. (2010). Volatile Compounds from Fruits of *Pouteria campechiana* (Kunth) Baehni. *J. Essent. Oil-Bear. Plants* 13, 326–330. doi: 10.1080/0972060X.2010.10643829

Pino, J. A. (2014). Odour-active compounds in papaya fruit cv. Red Maradol. *Food Chem.* 146, 120–126. doi: 10.1016/j.foodchem.2013.09.031

Pino, J. A., and Bent, L. (2013). Odour-active compounds in guava (*Psidium guajava* L. cv. Red Suprema). *J. Sci. Food Agric.* 93, 3114–3120. doi: 10.1002/jsfa.6153

Pino, J. A., and Marbot, R. (2001). Volatile Flavor Constituents of Acerola (*Malpighia emarginata* DC.) Fruit. *J. Agric. Food Chem.* 49, 5880–5882. doi: 10.1021/jf010270g

Pino, J. A., and Quijano, C. E. (2007). Volatile compounds of arazá fruit (*Eugenia stipitata* McVaught). *Rev. CENIC, Cienc. Quím.* 38, 363–366.

Pino, J. A., and Quijano, C. E. (2012). Study of the volatile compounds from plum (*Prunus domestica* L. cv. Horvin) and estimation of their contribution to the fruit aroma. *Ciênc. Tecnol. Aliment. Campinas* 32, 76–83. doi: 10.1590/S0101-20612012005000006

Pino, J. A., and Roncal, E. (2016). Characterisation of odour-active compounds in cherimoya (*Annona cherimola* Mill.) fruit. *Flavour Fragr. J.* 31, 143–148. doi: 10.1002/ffj.3292

Pino, J. A., Cuevas-Glory, L. F., Marbot, R., and Fuentes, V. (2008). Volatile compounds of grosella (*Phyllanthus acidus* [L.] Skeels) fruit. *Rev. CENIC, Cienc. Quím.* 39, 3–5.

Pino, J. A., Marbot, R., and Aguero, J. (2003a). Volatile components of sapodilla fruit (*Manilkara achras* L.). *J. Essent. Oil Res.* 15, 374–375. doi: 10.1080/10412905.2003.9698614

Pino, J. A., Marbot, R., and Vazquez, C. (2002). Characterization of volatiles in Loquat fruit (*Eriobotrya japonica* Lindl.). *Rev. CENIC, Cienc. Quím.* 33, 115–119.

Pino, J. A., Márquez, E., Quijano, C. E., and Castro, D. (2010). Volatile compounds in noni (*Morinda citrifolia* L.) at two ripening stages. *Ciênc. Tecnol. Aliment., Campinas* 30, 183–187. doi: 10.1590/S0101-20612010000100028

Pino, J. A., Mesa, J., Muñoz, Y., Pilar Marti, M., and Marbot, R. (2005). Volatile Components from Mango (*Mangifera indica* L.) Cultivars. *J. Agric. Food Chem.* 53, 2213–2223. doi: 10.1021/jf0402633

Pino, J., Marbot, R., Rosado, A., and Vazquez, C. (2003b). Volatile constituents of fruits of *Garcinia dulcis* Kurz. from Cuba. *Flavour Fragr. J.* 18, 271–274. doi: 10.1002/ffj.1187

Pintea, L., Dulf, F. V., Bunea, A., Socaci, S. A., Pop, E. A., Oprita, V.-A., et al. (2020). Carotenoids, Fatty Acids, and Volatile Compounds in Apricot Cultivars from Romania-A Chemometric Approach. *Antioxidants* 9:562. doi: 10.3390/antiox9070562

Pinto, A. B., Guedes, C. M., Moreira, R. T. A., and De Maria, C. A. B. (2006). Volatile constituent from headspace and aqueous solution of genipap (*Genipa americana*) fruit isolated by the solid-phase extraction method. *Flavour Fragr. J.* 21, 488–491. doi: 10.1002/ffj.1623

Plagemann, I, Krings, I, Berger, R. G., and Maróstica, M. R. Jr. (2012). Volatile constituents of jaboticaba (*Myrciaria jabuticaba* (Vell.) O. Berg) fruits. *J. Essent. Oil Res.* 24, 45–51. doi: 10.1080/10412905.2012.645651

Plotto, A. (1998). *Instrumental and sensory analysis of 'Gala' apple (Malus domestica*, Borkh) aroma. [PhD dissertation]. Corvallis (OR): Oregon State University.

Plotto, A., Bai, J., and Baldwin, E. (2017). "Fruits," in *Springer Handbook of Odor*, ed. A. Buettner (Switzerland: Springer International Publishing), 27–28.

Qian, M. C., and Wang, Y. (2005). Seasonal Variation of Volatile Composition and Odor Activity Value of'Marion'(*Rubus* spp. *hyb*) and 'Thornless Evergreen' (*R. laciniatus* L.) Blackberries. *J. Food Sci.* 70, C13–C20. doi: 10.1111/j.1365-2621.2005.tb09013.x

Qin, G., Tao, S., Cao, Y., Wu, J., Zhang, H., Huang, W., et al. (2012). Evaluation of the volatile profile of 33 *Pyrus ussuriensis* cultivars by HS-SPME with GC-MS. *Food Chem.* 134, 2367–2382. doi: 10.1016/j.foodchem.2012.04.053

Qin, L., Wei, Q.-P., Kang, W.-H., Zhang, Q., Sun, J., and Liu, S.-Z. (2017). Comparison of Volatile Compounds in 'Fuji' Apples in the Different Regions in China. *Food Sci. Technol.* 23, 79–89. doi: 10.3136/fstr.23.79

Qualley, A. V., Widhalm, J. R., Adebesin, F., Kish, C. M., and Dudareva, N. (2012). Completion of the core beta-oxidative pathway of benzoic acid biosynthesis in plants. *Proc. Natl. Acad. Sci. U.S.A.* 109, 16383–16388. doi: 10.1073/pnas.1211001109

Quijano, C. E., and Pino, J. A. (2006). Changes in volatile constituents during the ripening of cocona (*Solanum sessiliflorum* Dunal) fruit. *Rev. CENIC, Cienc. quím.* 37, 133–136.

Quijano, C. E., and Pino, J. A. (2007). Analysis of Volatile Compounds of camu-camu (*Myrciaria dubia* (HBK) Mcvaugh) Fruit Isolated by Different Methods. *J. Essent. Oil Res.* 19, 527–533. doi: 10.1080/10412905.2007.9699323

Quijano-Célis, C. E., Echeverri-Gil, D., Ruiz, Y., and Pino, J. A. (2013). Volatiles from *Syzygium paniculatum* Fruit. *Nat. Prod. Commun.* 8, 129–130. doi: 10.1177/1934578X1300800131

Ramadan, M. M., El-Ghorab, A. H., and Ghanem, K. Z. (2015). Volatile compounds, antioxidants, and anticancer activities of Cape gooseberry fruit (*Physalis peruviana* L.): An in-vitro study. *J. Arab Soc. Med. Res.* 10, 56–64. doi: 10.4103/1687-4293.175556

Rezende, C. M., and Fraga, S. R. G. (2003). Chemical and aroma determination of the pulp and seeds of murici (*Byrsonima crassifolia* L.). *J. Braz. Chem. Soc.* 14, 425–428. doi: 10.1590/S0103-50532003000300014

Rohloff, J., Nestby, R., Nes, A., and Martinussen, I. (2009). Volatile profiles of European blueberry: few major players, but complex aroma patterns. *Latv. J. Agron.* 12, 98–103.

Rowan, D. D., Lane, H. P., Allen, J. M., Fielder, S., and Hunt, M. B. (1996). Biosynthesis of 2-methylbutyl, 2-methyl-2-butenyl, and 2-methylbutanoate esters in red delicious and granny smith apples using deuterium-labeled substrates. *J. Agric. Food Chem.* 44, 3276–3285. doi: 10.1021/jf9508209

Ruse, K., Sabovics, M., Rakcejeva, T., Dukalska, L., Galoburda, R., and Berzina, L. (2012). The effect of drying conditions on the presence of volatile compounds in cranberries. *Int. J. Agric. Biosyst. Eng.* 6, 163–169. doi: 10.5281/zenodo.1086205

Russo, F., Caporaso, N., Paduano, A., and Sacchi, R. (2017). Characterisation of volatile compounds in Cilento (Italy) figs (*Ficus carica* L.) cv. Dottato as affected by the drying process. *Int. J. Food Prop.* 20, S1366–S1376. doi: 10.1080/10942912.2017.1344991

Sampaio, T. S., and Nogueira, P. C. L. (2006). Volatile components of mangaba fruit (*Hancornia speciosa* Gomes) at three stages of maturity. *Food Chem.* 95, 606–610. doi: 10.1016/j.foodchem.2005.01.038

Sanabria, G. G. R., Garcia, A. J. C., Lima, A. W. O., Alejandra, B.-M. M., and Narain, N. (2018). HS-SPME-GC-MS detection of volatile compounds in *Myrciaria jabuticaba* Fruit. *Sci. Agropecu.* 9, 319–327. doi: 10.17268/sci.agropecu.2018.03.03

Sánchez, G., Besada, C., Badenes, M. L., Monforte, A. J., and Granell, A. (2012). A Non-Targeted Approach Unravels the Volatile Network in Peach Fruit. *PLoS One* 7:e38992. doi: 10.1371/journal.pone.0038992

Santos, G. B. M., Dionísio, A. P., Magalhães, H. C. R., Abreu, F. A. P., Lira, S. M., Lima, A. C. V., et al. (2020). Effects of processing on the chemical, physicochemical, enzymatic, and volatile metabolic composition of pitaya (*Hylocereus polyrhizus* (F.A.C. Weber) Britton & Rose). *Food Res. Int.* 127, 108710–108711. doi: 10.1016/j.foodres.2019.108710

Scala, A., Allmann, S., Mirabella, R., Haring, M. A., and Schuurink, R. C. (2013). Green Leaf Volatiles: a plant's multifunctional weapon against herbivores and pathogens. *Int. J. Mol. Sci.* 14, 17781–17811. doi: 10.3390/ijms140917781

Scheuermann, E., Seguel, I., Montenegro, A., Bustos, R. O., Hormazabal, E., and Quiroz, A. (2008). Evolution of aroma compounds of murtilla fruits (*Ugni molinae* Turcz) during storage. *J. Sci. Food Agric.* 88, 485–492. doi: 10.1002/jsfa.3111

Schneider-Belhaddad, F., and Kolattukudy, P. E. (2000). Solubilization, partial purification, and characterization of a fatty aldehyde decarbonylase from a higher plant, *Pisum sativum*. *Arch. Biochem. Biophys.* 377, 341–349. doi: 10.1006/abbi.2000.1798

Schwab, W., Davidovich-Rikanati, R., and Lewinsohn, E. (2008). Biosynthesis of plant-derived flavor compounds. *Plant J.* 54, 712–732. doi: 10.1111/j.1365-313X.2008.03446.x

Shiota, H. (1993). New Esteric Components in the Volatiles of Banana Fruit (*Musa sapientum* L.). *J. Agric. Food Chem.* 41, 2056–2062. doi: 10.1021/jf00035a046

Shoko, T., Apostolides, Z., Monjerezi, and Saka, J. D. K. (2013). Volatile constituents of fruit pulp of *Strychnos cocculoides* (Baker) growing in Malawi using solid phase microextraction. *S. Afr. J. Bot.* 84, 11–12. doi: 10.1016/j.sajb.2012.09.001

Sidorov, V., Menczel, L., and Maliga, P. (1981). Isoleucine-requiring *Nicotiana* plant deficient in threonine deaminase. *Nature* 294, 87–88. doi: 10.1038/294087A0

Silva, M. R., Bueno, G. H., Araújo, R. L. B., Lacerda, I. C. A., Freitas, L. G., Morais, H. A., et al. (2019). Evaluation of the Influence of Extraction Conditions on the Isolation and Identification of Volatile Compounds from Cagaita (*Eugenia dysenterica*) Using HS-SPME/GC-MS. *J. Braz. Chem. Soc.* 30, 379–387. doi: 10.21577/0103-5053.20180187

Singh, B. K., and Shaner, D. L. (1995). Biosynthesis of branched chain amino acids: from test tube to field. *Plant Cell* 7, 935–944. doi: 10.2307/3870048

Sosa-Moguel, O., Pino, J. A., Sauri-Duch, E., and Cuevas-Glory, L. (2018). Characterization of odor-active compounds in three varieties of ciruela (*Spondias purpurea* L.) fruit. *Int. J. Food Prop.* 21, 1008–1016. doi: 10.1080/10942912.2018.1479858

Souleyre, E. J. F., Greenwood, D. R., Friel, E. N., Karunairetnam, S., and Newcomb, R. D. (2005). An alcohol acyl transferase from apple (cv. Royal Gala), MpAAT1, produces esters involved in apple fruit flavor. *FEBS J.* 272, 3132–3144. doi: 10.1111/j.1742-4658.2005.04732.x

Sugimoto, N. (2011). *Branched-Chain Ester Biosynthesis in Ripening Apple Fruit. [PhD dissertation]*. East Lansing (MI): Michigan State University.

Sugimoto, N., Engelgau, P., Jones, A. D., Song, J., and Beaudry, R. (2021). Citramalate synthase yields a biosynthetic pathway for isoleucine and straight- and branched-chain ester formation in ripening apple fruit. *Proc. Natl. Acad. Sci. U.S.A.* 118:e2009988118. doi: 10.1073/pnas.2009988118

Sun, S. Y., Jiang, W. G., and Zhao, Y. P. (2010). Characterization of the aroma-active compounds in five sweet cherry cultivars grown in Yantai (China). *Flavour Fragr. J.* 25, 206–213. doi: 10.1002/ffj.1994

Takeoka, G. R., Buttery, R. G., Turnbaugh, J. G., and Benson, M. (1995). Odor thresholds of various branched esters. *LWT* 28, 153–156. doi: 10.1016/S0023-6438(95)80028-X

Tateo, F., and Bononi, M. (2010). Headspace-SPME Analysis of Volatiles from Quince Whole Fruits. *J. Essent. Oil Res.* 22, 416–418. doi: 10.1080/10412905.2010.9700360

Taylor, N. L., Heazlewood, J. L., Day, D. A., and Millar, A. H. (2004). Lipoic Acid-Dependent oxidative catabolism of α-keto acids in mitochondria provides evidence for branched-chain amino acid catabolism in *Arabidopsis*. *Plant Physiol.* 134, 838–848. doi: 10.1104/pp.103.035675

Tholl, D. (2015). Biosynthesis and biological functions of terpenoids in plants. *Adv. Biochem. Eng. Biotechnol.* 148, 63–106. doi: 10.1007/10_2014_295

Tieman, D., Bliss, P., McIntyre, L. M., Blandon-Ubeda, A., Bies, D., Odabasi, A. Z., et al. (2012). The chemical interactions underlying tomato flavor preferences. *Curr. Biol.* 22, 1035–1039. doi: 10.1016/j.cub.2012.04.016

Tietel, Z., Porat, R., Weiss, K., and Ulrich, D. (2011). Identification of aroma-active compounds in fresh and stored 'Mor' mandarins. *Int. J. Food Sci. Technol.* 46, 2225–2231. doi: 10.1111/j.1365-2621.2011.02740.x

Tikunov, Y., Lommen, A., Ric de Vos, C. H., Verhoeven, H. A., Bino, R. J., Hall, R. D., et al. (2005). A novel approach for non-targeted data analysis for metabolomics: large-scale profiling of tomato fruit volatiles. *Plant. Physiol.* 139, 1125–1137. doi: 10.1104/pp.105.068130

Tokitomo, Y., Steinhaus, M., Bütner, A., and Schieberle, P. (2005). Odor-active constituents in fresh pineapple (*Ananas comosus* [L.] Merr.) by quantitative and sensory evaluation. *Biosci. Biotechnol. Biochem.* 69, 1323–1330. doi: 10.1271/bbb.69.1323

Tola, A. J., Jaballi, A., Germain, H., and Missihoun, T. D. (2021). Recent Development on Plant Aldehyde Dehydrogenase Enzymes and Their Functions in Plant Development and Stress Signaling. *Genes* 12:51. doi: 10.3390/genes12010051

Torrens-Spence, M. P., von Guggenberg, R., Lazear, M., Ding, H., and Li, J. (2014). Diverse functional evolution of serine decarboxylases: identification of two novel acetaldehyde synthases that uses hydrophobic amino acids as substrates. *BMC Plant Biol.* 14:247. doi: 10.1186/s12870-014-0247-x

Tressl, R., and Drawert, F. (1973). Biogenesis of banana volatiles. *J. Agric. Food Chem.* 21, 560–565. doi: 10.1021/jf60188a031

Uekane, T. M., Nicolotti, L., Griglione, A., Bizzo, H. R., Rubiolo, P., Bicchi, C., et al. (2017). Studies on the volatile fraction composition of three native Amazonian-Brazilian fruits: Murici (*Byrsonima crassifolia* L., Malpighiaceae), Bacuri (*Platonia insignis* M., Clusiaceae), and sapodilla (*Manilkara sapota* L., Sapotaceae). *Food Chem.* 219, 13–22. doi: 10.1016/j.foodchem.2016.09.098

Ulrich, D., Komes, D., Olbricht, K., and Hoberg, E. (2007). Diversity of aroma patterns in wild and cultivated *Fragaria* accessions. *Genet. Resour. Crop Evol.* 54, 1185–1196. doi: 10.1007/s10722-006-9009-4

Vendramini, A. L., and Trugo, L. C. (2000). Chemical composition of acerola fruit (*Malpighia punicifolia* L.) at three stages of maturity. *Food Chem.* 71, 195–198. doi: 10.1016/S0308-8146(00)00152-7

Viljanen, K., Heinio, R.-L., Juvonen, R., Kosso, T., and Puupponen-Pimia, R. (2014). Relation of sensory perception with chemical composition of bioprocessed lingonberry. *Food Chem.* 157, 148–156. doi: 10.1016/j.foodchem.2014.02.030

Viljoen, A. M., Kamatou, G. P. P., and Başer, K. H. C. (2008). Head-space volatiles of marula (*Sclerocarya birrea* subsp. *caffra*). *S. Afr. J. Bot.* 74, 325–326. doi: 10.1016/j.sajb.2007.10.005

Wall, M. M., Miller, S., and Siderhurst, M. S. (2018). Volatile changes in Hawaiian noni fruit, *Morinda citrifolia* L., during ripening and fermentation. *J. Sci. Food Agric.* 98, 3391–3399. doi: 10.1002/jsfa.8850

Wang, C., Zhang, W., Li, H., Mao, J., Guo, C., Ding, R., et al. (2019). Analysis of volatile compounds in pears by HS-SPME-GC×GC-TOFMS. *Molecules* 24:1795. doi: 10.3390/molecules24091795

Wendakoon, S. K., Ueda, Y., Imahori, Y., and Ishimaru, M. (2006). Effect of short-term anaerobic conditions on the production of volatiles, activity of alcohol acetyltransferase and other quality traits of ripened bananas. *J. Sci. Food Agric.* 86, 1475–1480. doi: 10.1002/jsfa.2518

Werkhoff, P., Güntert, M., Krammer, G., Sommer, H., and Kaulen, J. (1998). Vacuum Headspace Method in Aroma Research: Flavor Chemistry of Yellow Passion Fruits. *J. Agric. Food Chem.* 46, 1076–1093. doi: 10.1021/jf970655s

Wijaya, C. H., Ulrich, D., Lestari, R., Schippel, K., and Ebert, G. (2005). Identification of potent odorants in different cultivars of snake fruit [*Salacca zalacca* (Gaert.) Voss] using gas chromatography-olfactometry. *J. Agric. Food Chem.* 53, 1637–1641. doi: 10.1021/jf048950h

Wong, K. C., and Loi, H. K. (1996b). Volatile Constituents of *Bouea macrophylla* Griff. *Fruit. J. Essent. Oil Res.* 8, 99–100. doi: 10.1080/10942912.2016.1218892

Wong, K. C., Chee, S. G., and Er, C. C. (1996a). Volatile constituents of the fruits of *Muntingia calabura* L. *J. Essent. Oil Res.* 8, 423–426. doi: 10.1080/10412905.1996.9700655

Wong, K. C., Wong, S. N., Loi, H. K., and Lim, C. L. (1996c). Volatile constituents from the fruits of four edible Sapindaceae: Rambutan (*Nephelium lappaceum* L.), pulasan (*N. ramboutan-ake* (Labill.) Leenh.), longan (*Dimocarpus longan* Lour.), and mata kucing (*D. longan ssp. malesianus* Leenh.). *Flavour Fragr. J.* 11, 223–229. doi: 10.1002/(SICI)1099-1026(199607)11:4<223::AID-FFJ579<3.0.CO;2-B

Wong, K. C., Wong, S. W., Siew, S. S., and Tie, D. Y. (1994). Volatile Constituents of the Fruits of *Lansium domesticum* Correa (Duku and Langsat) and *Baccaurea motleyana* (Muell. Arg.) Muell. Arg. (Rambai). *Flavour Fragr. J.* 9, 319–324. doi: 10.1002/ffj.2730090608

Wu, Y., Duan, S., Zhao, L., Gao, Z., Luo, M., Song, S., et al. (2016). Aroma characterization based on aromatic series analysis in table grapes. *Sci. Rep.* 6:31116. doi: 10.1038/srep31116

Wu, Y., Pan, Q., Qu, W., and Duan, C. (2009). Comparison of volatile profiles of nine litchi (*Litchi chinensis* Sonn.) cultivars from Southern China. *J. Agric. Food Chem.* 57, 9676–9681. doi: 10.1021/jf902144c

Wyllie, S. G., and Fellman, J. K. (2000). Formation of volatile branched chain esters in bananas (*Musa sapientum* L.). *J. Agric. Food Chem.* 48, 3493–3496. doi: 10.1021/jf0001841

Wyllie, S. G., and Leach, D. N. (1992). Sulfur-containing compounds in the aroma volatiles of melons (*Cucumis melo*). *J. Agric. Food Chem.* 40, 253–256. doi: 10.1021/jf00014a017

Wyllie, S. G., Leach, D. N., Wang, Y., and Shewfelt, R. L. (1995). "Key aroma compounds in melons: Their development and cultivar dependence," in *Fruit Flavors: Biogenesis, Characterization, and Authentication*, eds R. L. Rouseff and M. M. Leahy (Washington, DC: American Chemical Society), 248–257. doi: 10.1021/bk-1995-0596.ch022

Xi, W., Zheng, H., Zhang, Q., and Li, W. (2016). Profiling Taste and Aroma Compound Metabolism during Apricot Fruit Development and Ripening. *Int. J. Mol. Sci.* 17:998. doi: 10.3390/ijms17070998

Xiao, Z., Wu, Q., Niu, Y., Wu, M., Zhu, J., Zhou, X., et al. (2017). Characterization of the key aroma compounds in five varieties of mandarins by gas chromatography-olfactometry, odor activity values, aroma recombination, and omission analysis. *J. Agric. Food Chem.* 65, 8392–8401. doi: 10.1021/acs.jafc.7b02703

Xing, A., and Last, R. L. (2017). A regulatory hierarchy of the Arabidopsis branched-chain amino acid metabolic network. *Plant Cell* 29, 1480–1499. doi: 10.1105/tpc.17.00186

Xu, H., Zhang, F., Liu, B., Huhman, D. V., Sumner, L. W., Dixon, R. A., et al. (2013). Characterization of the formation of branched short-chain fatty acid:CoAs for bitter acid biosynthesis in hop glandular trichomes. *Mol. Plant* 6, 1301–1317. doi: 10.1093/mp/sst004

Yang, C., Wang, Y., Wu, B., Fang, J., and Li, S. (2011). Volatile compounds evolution of three table grapes with different flavour during and after maturation. *Food Chem.* 128, 823–830. doi: 10.1016/j.foodchem.2010.11.029

Yang, L., Liu, J., Wang, X., Wang, X., Ren, F., Zhang, Q., et al. (2019). Characterization of Volatile Component Changes in Jujube Fruits during Cold Storage by Using Headspace-Gas Chromatography-Ion Mobility Spectrometry. *Molecules.* 24:3904. doi: 10.3390/molecules24213904

Yilmaztekin, M. (2014). Analysis of volatile components of cape gooseberry (*Physalis peruviana* L.) grown in Turkey by HS-SPME and GC-MS. *Sci. World J.* 2014:796097. doi: 10.1155/2014/796097

Zhang, C. Y., Zhang, Q., Zhong, C. H., and Guo, M. Q. (2016). Analysis of volatile compounds responsible for kiwifruit aroma by desiccated headspace gas chromatography-mass spectrometry. *J. Chromatogr. A.* 1440, 255–259. doi: 10.1016/j.chroma.2016.02.056

Zhang, C. Y., Zhang, Q., Zhong, C. H., and Guo, M. Q. (2019a). Volatile fingerprints and biomarkers of three representative kiwifruit cultivars obtained by headspace solid-phase microextraction gas chromatography mass spectrometry and chemometrics. *Food Chem.* 271, 211–215. doi: 10.1016/j.foodchem.2018.07.169

Zhang, T., Bao, F., Yang, Y., Hu, L., Ding, A., Wang, J., et al. (2019b). A comparative analysis of floral scent compounds in intraspecific cultivars of *Prunus mume* with different corolla colours. *Molecules* 25:145. doi: 10.3390/molecules25010145

Zhao, Y., Zhan, P., Tian, H.-L., Wang, P., Lu, C., Tian, P., et al. (2021). Insights into the Aroma Profile in Three Kiwifruit Varieties by HS-SPME-GC-MS and GC-IMS Coupled with DSA. *Food Anal. Methods* 14, 1033–1042. doi: 10.1007/s12161-020-01952-8

Zheng, L.-Y., Sun, G.-M., Liu, Y.-G., Lv, L.-L., Yang, W.-X., Zhao, W.-F., et al. (2012). Aroma Volatile Compounds from Two Fresh Pineapple Varieties in China. *Int. J. Mol. Sci.* 13, 7383–7392. doi: 10.3390/ijms13067383

Zhou, M., Lu, G., Gao, C., Wang, Y., and Sun, H. (2012). Tissue-specific and nutrient regulation of the branched-chain α-keto acid dehydrogenase phosphatase, protein phosphatase 2Cm (PP2Cm). *J. Biol. Chem.* 287, 23397–23406. doi: 10.1074/jbc.m112.351031

Zhu, J.-C., Chen, F., Wang, L.-Y., Niu, Y.-W., Chen, H.-X., Wang, H.-L., et al. (2016). Characterization of the Key Aroma Volatile Compounds in Cranberry (*Vaccinium Macrocarpon* Ait.) Using Gas Chromatography–Olfactometry (GC-O) and odor activity value (OAV). *J. Agric. Food Chem.* 64, 4990–4999. doi: 10.1021/acs.jafc.6b01150

Zhu, J.-C., Wang, L.-Y., Xiao, Z.-B., and Niu, Y.-W. (2018). Characterization of the key aroma compounds in mulberry fruits by application of gas chromatography–olfactometry (GC-O), odor activity value (OAV), gas chromatography-mass spectrometry (GC–MS) and flame photometric detection (FPD). *Food Chem.* 245, 775–785. doi: 10.1016/j.foodchem.2017.11.112

Zhu, X., Li, Q., Li, J., Luo, J., Chen, W., and Li, X. (2018). Comparative Study of Volatile Compounds in the Fruit of Two Banana Cultivars at Different Ripening Stages. *Molecules* 23:2456. doi: 10.3390/molecules23102456

Conflict of Interest: The authors declare that the research was conducted in the absence of any commercial or financial relationships that could be construed as a potential conflict of interest.

Publisher's Note: All claims expressed in this article are solely those of the authors and do not necessarily represent those of their affiliated organizations, or those of the publisher, the editors and the reviewers. Any product that may be evaluated in this article, or claim that may be made by its manufacturer, is not guaranteed or endorsed by the publisher.

frontiers in Plant Science

ORIGINAL RESEARCH
published: 27 January 2022
doi: 10.3389/fpls.2021.809558

Effect of the Seasonal Climatic Variations on the Accumulation of Fruit Volatiles in Four Grape Varieties Under the Double Cropping System

*Hao-Cheng Lu[1,2], Wei-Kai Chen[1,2], Yu Wang[1,2], Xian-Jin Bai[3], Guo Cheng[4], Chang-Qing Duan[1,2], Jun Wang[1,2] and Fei He[1,2]**

[1] Center for Viticulture and Enology, College of Food Science and Nutritional Engineering, China Agricultural University, Beijing, China, [2] Key Laboratory of Viticulture and Enology, Ministry of Agriculture and Rural Affairs, Beijing, China, [3] Guangxi Academy of Agricultural Sciences, Nanning, China, [4] Grape and Wine Research Institute, Guangxi Academy of Agricultural Sciences, Nanning, China

The double cropping system has been widely applied in many subtropical viticultural regions. In the 2-year study of 2014–2015, four grape varieties were selected to analyze their fruit volatile compounds in four consecutive seasons in the Guangxi region of South China, which had a typical subtropical humid monsoon climate. Results showed that berries of winter seasons had higher concentrations of terpenes, norisoprenoids, and C6/C9 compounds in "Riesling," "Victoria," and "Muscat Hamburg" grapes in both of the two vintages. However, in the "Cabernet Sauvignon" grapes, only the berries of the 2014 winter season had higher terpene concentrations, but lower norisoprenoid concentrations than those of the corresponding summer season. The Pearson correlation analysis showed the high temperature was the main climate factor that affected volatile compounds between the summer and winter seasons. Hexanal, γ-terpinene, terpinen-4-ol, *cis*-furan linalool oxide, and *trans*-pyran linalool oxide were all negatively correlated with the high-temperature hours in all of the four varieties. Transcriptome analysis showed that the upregulated *VviDXSs*, *VviPSYs*, and *VviCCDs* expressions might contribute to the accumulations of terpenes or norisoprenoids in the winter berries of these varieties. Our results provided insights into how climate parameters affected grape volatiles under the double cropping system, which might improve the understanding of the grape berries in response to the climate changes accompanied by extreme weather conditions in the future.

Keywords: climate factors, double cropping system, table grape, volatile compounds, wine grape

OPEN ACCESS

Edited by:
Itay Maoz, Agricultural Research Organization (ARO), Israel

Reviewed by:
Susana Río Segade, University of Turin, Italy
Pei Ge Fan, Institute of Botany, Chinese Academy of Sciences (CAS), China

***Correspondence:**
Fei He
wheyfey@cau.edu.cn

Specialty section:
This article was submitted to Plant Metabolism and Chemodiversity, a section of the journal Frontiers in Plant Science

Received: *05 November 2021*
Accepted: *20 December 2021*
Published: *27 January 2022*

Citation:
Lu H-C, Chen W-K, Wang Y, Bai X-J, Cheng G, Duan C-Q, Wang J and He F (2022) Effect of the Seasonal Climatic Variations on the Accumulation of Fruit Volatiles in Four Grape Varieties Under the Double Cropping System. Front. Plant Sci. 12:809558. doi: 10.3389/fpls.2021.809558

INTRODUCTION

The grape double cropping system has been applied widely in many subtropical regions (Favero et al., 2011; Chou and Li, 2014). The traditional single cropping system seems not applicable in these regions because of the excess heat resources and the heavy rainfall in the summer season. The excessive rainfall and temperature during the grape ripening period can easily cause insufficient fruit ripeness and fungal infections. Moreover, relatively high temperature in winter does not meet the low-temperature requirements of the grapes for their normal dormancy, which results in uneven bud bursts in the spring (Favero et al., 2011). However, if the dormant buds were forced out of dormancy early during the current season, the double cropping system could be achieved

(Chen et al., 2017). Even in winter, there was still adequate temperature and sunlight for the berry ripening in the subtropical viticulture regions, making the double cropping system more commercially adopted. There were two advantages of applying the double cropping system in these regions: (1) in the summer season, the grape berries could ripen earlier than the normal single cropping system, which could avoid the intense rainfall and heatwave as much as possible; and (2) in the winter season, cool climate and less rainfall usually led to better grape quality (Xu et al., 2011; Chen et al., 2017).

In the double cropping system, bud break was usually enforced between late January and mid-February in the northern hemisphere, resulting in the first bloom in early April and the first crop in June or July. Vines were then pruned and forced again around mid-August, resulting in the second bloom of the side shoots in mid-September and the second crop in mid-January of the following year (Chou and Li, 2014). Even in the one-crop-a-year culture system, berries composition could vary significantly in different vintages (Downey et al., 2006). In the double cropping system, the climate variations between the summer season and winter season were greater than the single cropping system, which led to great variations in grape qualities. The winter berries were usually considered more favorable for wine production than the summer berries. Junior et al. (2017) showed that the higher values of yield, cluster weight, and titratable acidity (TA) were observed during the summer growing season, whereas the higher values of soluble solids content and pH were observed during winter, which suggested that the grapes harvested during the winter show physicochemical characteristics more suitable than those observed during the summer crops for winemaking purposes in Brazil. However, the winter berries usually had lower cluster weights than the summer berries, thus leading to a lower yield in the winter season (Mitra et al., 2018). Some previous researches reported that the fruitfulness of the second crop of some cultivars, such as "Summer Black," was much worse in some subtropical areas (Guo et al., 2018). Some plant growth inhibitors, such as chlormequat chloride (CCC), were usually used to promote inflorescence induction to enhance fruitfulness.

For grape secondary metabolites, the phenolic compositions were the focus of many researchers in dissecting the variations between the summer and the winter berries in the double cropping system (Xu et al., 2011; Chen et al., 2017; Zhu et al., 2017; Cheng et al., 2019). Similar results were found by previous studies that phenolic compounds, including anthocyanins, flavonols, and flavan-3-ols, were significantly higher in the winter season berries than in the summer season berries. Chen et al. (2017) showed that winter season berries greatly triggered the expression of the upstream genes in the flavonoid pathway in a coordinated expression pattern. However, other secondary metabolites were little studied in the double-cropping system, such as volatile compounds.

Volatile compounds are critical secondary metabolites in grapes, which play an essential role in their sensory evaluations. Aromas derived from grapes mainly include norisoprenoids, terpenes, C6/C9 compounds, methoxypyrazines, etc. (Wang et al., 2020). Terpenes and norisoprenoids have low sensory thresholds and pleasant flavors (Fenoll et al., 2009). Grapes of the Muscat family usually have abundant terpenes, which contribute to their intense varietal flavors. Commonly identified terpenes in grapes include a rose oxide, geraniol, nerol, linalool, terpineol, and citronellol, which contribute to the typical rose and floral aroma (Fenoll et al., 2009). 1,1,6-Trimethyl-1,2-dihydronaphthalene (TDN), β-damascenone, and β-ionone are common C_{13}-norisoprenoids that contribute to fruity, violet, and petrol aromas to grapes and wines (Black et al., 2015). The abundant C6/C9 compounds in grapes contribute to a typical "green leaf" aroma, so they are also called green leaf volatiles (GLVs) (Kalua and Boss, 2010). The metabolic pathways of these volatile compounds are complicated, and many of them are still not quite clear until now. Mevalonic acid (MVA) and 2-methyl-D-erythritol-4-phosphate phosphate (MEP) pathway, carotenoid metabolism, and oxylipin pathway were the most investigated pathways, which could synthesize terpenes, norisoprenoids, and C6/C9 compounds, respectively (Kalua and Boss, 2009; Miziorko, 2010; Lashbrooke et al., 2013). The grape aromas were not only affected by the varieties and their development periods but also affected by the climate factors, such as temperature and light. In general, cluster exposure was beneficial for the accumulation of terpenes, whereas shading would reduce terpene concentrations (Bureau et al., 2000; Zhang et al., 2017). Grapes in cool-climate regions usually had higher C6 aldehyde concentrations, whereas warm-region grapes usually had higher terpene concentrations (Wen et al., 2015; Xu et al., 2015b). Rainfall and irrigation also affected the aroma accumulation in grapes. Regulated deficit irrigation during the berry development would promote the accumulation of terpenes (Savoi et al., 2016).

In a previous study, we investigated the variations of ripening progression and flavonoid metabolism in Cabernet Sauvignon (CS) and Riesling (R) grapes under the double cropping system (Chen et al., 2017). In the present study, the aroma characteristics in grapes under the double cropping system were furthermore investigated. Moreover, the two wine grape varieties, another two table grape varieties, Muscat Hamburg (MH) and Victoria (V), that occupied a good market in South China were also investigated. There were significant climate variations between the summer and winter seasons, and the corresponding aroma variations were also found in all of the four varieties under the double cropping system. This study helped us to understand better how climate parameters affected grape volatiles under the double cropping system, which might improve the understanding of the grape berries in response to the climate changes accompanied by extreme weather conditions in the future. Furthermore, the feasibility of applying a double-cropping system in viticulture in South China could be evaluated.

MATERIALS AND METHODS

Experiment Site and Double Cropping System

The 2-year (2014–2015) study was performed at Guangxi Academy of Agricultural Sciences located in South China (22°36′N–108°14′E, elevation 104 m). The climate belonged to a subtropical humid monsoon climate with abundant sunshine

and heat resources. Vines were trained to a Y-shaped training system with 2 × 4/5 shoots per meter and 1.0 m cordon above ground. Rain shelters were applied to all vines to prevent over-rainfall damage. Four varieties were investigated in this study: CS, R, MH, and V. CS and R grapevines were in the same vineyard, whereas MH and V grapes were in another. The distance between the two vineyards was within 1 km. The detailed information on the variety and phenological stages are shown in **Supplementary Tables 1**, **2**. Clusters were weighted at harvest, and estimated yield was obtained by multiplying the average cluster weight by the average cluster numbers per meter.

The double cropping system in the experiment site was described by Chen et al. (2017). Briefly, vines were pruned two times, and the grapes were harvested two times per year. In mid-February, 2.5–3.0% hydrogen cyanamide was used to accelerate the bud burst. Summer grapes were harvested around late July and early August, which was called the summer cropping cycle. Then vines were pruned and followed the same procedure in August to start the second season. Winter grapes were harvested in January, which was called the winter cropping cycle.

Berry Sampling and Meteorological Data Collection

Berries of all varieties were sampled four times in each growing season. Sampling time points were as follows: (1) pea-size (E-L 31), (2) onset of veraison (E-L 35), (3) veraison complement (E-L 36), and (4) harvest (E-L 38). There were three biological replicates for each variety. For each replicate, 300 berries were randomly sampled from about 50 vines, which were distributed in three adjacent rows. One hundred berries of which were used in the determination of the physicochemical parameters. The remaining berries were immediately frozen in liquid nitrogen and stored at −80°C for the subsequent metabolite and transcriptome analysis.

Meteorological data was acquired from the local climate monitoring station within 1 km away from the experiment site. Photosynthetically active radiation and temperature were recorded per hour. Accumulated rainfall was recorded per day. Growing degree days (base 10°C) was calculated from bloom to harvest according to Bindi et al. (1997).

Analysis of Grape Physicochemical Parameters

For each replicate, 100 berries were weighted and then manually squeezed. The must was centrifuged (8000 × *g*) to get clear juice. The total soluble solids (TSS) of the juice were determined with a digital pocket handheld refractometer (PAL-1, ATAGO CO., LTD., Tokyo, Japan). The juice pH was determined by a pH meter (Sartorius PB-10, Gottingen, Germany). TA was measured and expressed as tartaric acid equivalents (g/L) according to the National Standard of People's Republic of China (GB/T15038-2006).

Extraction of Grapes Volatile Compounds

The extraction of grapes volatile compounds was according to Lan et al. (2016). For each replicate, about 50 g of berries were de-seeded and mashed under liquid nitrogen. Then, the frozen samples with the addition of 1 g polyvinylpolypyrrolidone and 0.5 g D-gluconic acid lactone were ground into powder. The frozen powder was melted under 4°C for about 6 h and then centrifuged at 8000 × *g* to get the clear juice. For free volatile compounds, 5 ml grape juice was added in a 20-ml vial with 1 g NaCl and 10 μl 4-methyl-2-pentanol (internal standard). For bound volatile compounds, 2 ml of the clear grape juice sample was added to Cleanert® PEP-SPE resins (150 mg/6 mL, Bonna-Agela Technologies, Tianjin, China), which had been activated with 10 ml of methanol and 10 ml of water. Then, the resins were washed with 2 ml of water and 5 ml of dichloromethane to remove water-soluble compounds and free volatiles, respectively. The resins were eluted with 20 ml methanol afterward. The methanol extract was concentrated to dryness by a rotary evaporator under vacuum at 30°C and was redissolved in 10 ml of citrate/phosphate buffer solution (0.2 M, pH = 5). The enzymatic hydrolysis of glycosidic precursors was conducted at 40°C for 16 h by adding 100 μl AR 2000 (Rapidase, 100 g/L, DSM Food Specialties, France). The 5 ml of the above sample was added in a 20-ml vial with 1 g NaCl and 10 μl 4-methyl-2-pentanol (internal standard). Both free and bound samples were placed in a CTC-Combi PAL autosampler (CTC Analytics, Zwingen, Switzerland) equipped with a 2-cm DVB/CAR/PDMS 50/30 μm SPME fiber (Supelco Inc., Bellefonte, PA., United States) and agitated at 500 rpm for 30 min at 40°C. The SPME fiber was then inserted into the headspace to absorb aroma compounds at 40°C for 30 min and was instantly desorbed into the gas chromatography (GC) injector for 8 min to thermally desorb aroma compounds, and the injection temperature was set at 250°C.

Gas Chromatography–Mass Spectrometer Analysis of Volatile Compounds in Grapes

Both free-volatile and bound-form aroma compounds were extracted by headspace solid-phase microextraction (HS-SPME). Agilent 6890 GC coupled with Agilent 5973C mass spectrometer (MS) was used for the aroma determination. GC was equipped with an HP-INNOWAX capillary column (60 m × 0.25 mm, 0.25 μm, J&W Scientific, Folsom, CA, United States) to separate volatile compounds. The carrier gas was high purity helium with a flow rate of 1 ml/min. The oven program was set as follows: 50°C for 1 min, increased to 220°C at a rate of 3°C/min, and held at 220°C for 5 min. Identification and quantification of volatile compounds followed our research group method (Wang et al., 2019). Concentrations of volatile compounds were expressed as μg/L grape juice.

RNA Extraction and Transcriptome Sequencing

The berries of three development stages (E-L 35, 36, and 38) in 2014 were selected to determine the transcriptome sequencing. For each replicate, de-seeded 50 berries were ground into powder under liquid nitrogen protection. The following procedures had been described by Chen et al. (2017). Briefly, the sample total RNA was extracted by using a Spectrum Plant Total RNA Kit (Sigma-Aldrich, Carlsbad, CA, United States).

Transcriptome analysis was conducted on the Illumina HiSeq 2000 platform (Illumina, Inc., San Diego, CA, United States) with 50-bp single reads and aligned against the reference grapevine genome 12 × V2, allowing no more than two mismatches. Gene expression abundance was calculated using the fragments per kilobase per million reads (FPKM) method to eliminate the influence of variation in gene length and total reads numbers on gene expression calculation (Sun et al., 2015). The R package "DESeq2" was used to identify differentially expressed genes (DEGs), and the criteria were set as false discovery rate $\leq$ 0.05 and fold change $\geq$ 2. Gene Ontology (GO) and Kyoto Encyclopedia of Genes and Genomes (KEGG) enrichment analysis of DEGs was used to select candidate genes responsible for the differences in aroma compounds between seasons. The data have been deposited in the NCBI Gene Expression Omnibus (GEO) database and are accessible through GEO accession GSE103226 (CS and R grapes) and GSE168785 (V and MH grapes). Total reads and total mapped reads per sample are shown in **Supplementary Table 3**.

Statistical Analysis

The SPSS version 22.0 (SPSS Inc., United States) was used for all significance analysis at $p < 0.05$ (Duncan's multiple range test or *t*-test). The Pearson correlation analysis was performed in MataboAnalyst 4.0[1]. The figures were prepared by using GraphPad Prism 8.0.2 (GraphPad Software, San Diego, CA, United States), SIMCA 14.1 (Umetrics, Umea, Sweden), and R-3.6.1. Heatmap was prepared by using the "pheatmap" package in R. Principal component analysis (PCA) was performed in SIMCA 14.1 (Umetrics, Umea, Sweden).

RESULTS

Meteorological Data

Meteorological data in the year 2014 and 2015 were shown and discussed by Chen et al. (2017). The climate conditions of growing seasons in all varieties were further analyzed in this study (**Table 1**). CS and R grapes had a similar phenological stage in all growing seasons in 2014 and 2015. The MH and V grapes had a similar phenological stage in the winter seasons of 2014 and 2015. In the summer season of 2015, MH grapes were harvested 23 days later than V grapes. The summer season had higher mean daily temperature and more high-temperature hours than the winter season in all varieties, but the cumulative PAR and rainfall were not consistent in the years 2014 and 2015. For CS and R grapes, the winter season had less cumulative PAR but similar cumulative sunshine hours and rainfall than the summer season in 2014. In 2015, the summer season of CS and R grapes had more cumulative PAR, sunshine hours, and rainfall than the winter season. In 2014, the winter season of MH and V grapes had more cumulative PAR, sunshine hours, and rainfall than the summer season, while in 2015, the winter season of MH and V grapes had fewer cumulative PAR and sunshine hours. Furthermore, the summer season of MH had more rainfall than the winter season. The weather condition in 2010–2019 was analyzed to present the regular climate characteristics in Guangxi (**Supplementary Figure 1**). June, July, and August were the hottest months in the whole year with almost the most abundant rainfall, which was a typical subtropical humid monsoon climate. However, the rainfall and sunshine hours also had wide ranges in many months, which made a high intra- or interseasonal variability.

Grape Physicochemical Parameters

The physicochemical parameters of CS and R grapes were shown and discussed by Chen et al. (2017). In brief, the berries in the summer cropping showed a higher TSS at E-L 31 but showed an opposite result at E-L 38 in CS and R grapes. Berry weight increased along with the berry development, but the berry weight in the winter cropping was significantly lower than those of the summer cropping at E-L 35, 36, and 38 in CS and R grapes. The TSS, TA, pH, and 100 berries weight of MH and V grapes in different sampling times are shown in **Table 2**. In 2014, the winter season berries had higher TSS than the summer season berries during the development stages. V grapes reached only 12.8°Brix at harvest in the summer season of 2014, which was almost 8°Brix lower than their corresponding winter season berries. In 2015, there was no significant difference in TSS of MH berries between the summer and winter seasons during the development stages. For V grapes, the summer season grapes ripened faster than the winter season ones, although there was

[1]https://www.metaboanalyst.ca/

TABLE 1 | Meteorological data in 2014 and 2015 growing seasons.

Year	Season	Variety	GDD (°C)	Average daily temperature (°C)	High temperature (>35°C) hours	Cumulative PAR (10^3 μmol/m^2/s)	Cumulative sunshine hours (h)	Cumulative rainfall (mm)
2014	Summer	CS and R	2128.6	28.8	459	45.9	483.3	488.2
	Summer	MH and V	1588.9	28.7	351	33.9	312.2	226.5
	Winter	CS and R	1042.9	19.7	109	41.0	503.2	466.7
	Winter	MH and V	1123.2	19.3	89	38.4	506.3	503.5
2015	Summer	CS and R	2180.8	29.3	490	54.1	586.5	599.8
	Summer	V	1699.6	29.7	410	45.2	475.7	386.0
	Summer	MH	2238.8	29.7	516	56.5	627.1	599.8
	Winter	CS and R	1330.4	20.6	62	40.4	384.0	398.3
	Winter	MH and V	1207.0	20.3	45	39.2	379.1	378.4

GDD, growing degree days (based on 10°C); CS, Cabernet Sauvignon; R, Riesling; MH, Muscat Hamburg; V, Victoria; PAR, photosynthetically active radiation.

TABLE 2 | Physicochemical parameters of MH and V grapes grown under double cropping system in 2014 and 2015.

Parameters	Development stages	MH		Sig.	V		Sig.	MH		Sig.	V		Sig.
		2014 Summer	2014 Winter		2014 Summer	2014 Winter		2015 Summer	2015 Winter		2015 Summer	2015 Winter	
TSS (Brix)	E-L 31	3.7 ± 0.1	4.4 ± 0.6	ns	4.0 ± 0.2	3.7 ± 0.5	ns	5.5 ± 0.9	5.4 ± 0.6	ns	5.7 ± 0.3	4.6 ± 0.3	*
	E-L 35	8.3 ± 2.0	12.3 ± 0.2	*	9.1 ± 0.3	12.8 ± 1.3	*	8.0 ± 1.9	7.4 ± 0.2	ns	9.1 ± 0.3	6.5 ± 0.2	*
	E-L 36	17.4 ± 0.8	19.0 ± 0.9	ns	12.6 ± 0.4	18.3 ± 0.5	*	17.6 ± 1.1	16.4 ± 0.4	ns	15.4 ± 0.6	11.6 ± 0.6	*
	E-L 38	19.8 ± 1.3	22.0 ± 0.4	*	12.8 ± 0.8	20.7 ± 0.5	*	20.4 ± 0.8	20.9 ± 1.0	ns	15.6 ± 0.5	17.0 ± 0.5	*
TA (g/L)	E-L 31	27.3 ± 0.5	30.0 ± 3.3	ns	35.1 ± 1.1	28.3 ± 5.3	ns	33.3 ± 5.8	31.4 ± 1.3	ns	30.0 ± 1.5	24.4 ± 2.3	*
	E-L 35	11.8 ± 1.0	20.6 ± 1.7	*	6.8 ± 1.2	10.2 ± 1.2	*	27.6 ± 1.8	33.9 ± 0.2	*	6.8 ± 1.2	26.7 ± 1.8	*
	E-L 36	5.8 ± 0.3	12.0 ± 2.0	*	2.3 ± 0.0	6.7 ± 0.7	*	2.2 ± 0.1	10.4 ± 1.1	*	2.0 ± 0.4	6.1 ± 0.8	*
	E-L 38	3.7 ± 0.4	8.1 ± 0.3	*	1.8 ± 0.1	3.9 ± 0.2	*	1.8 ± 0.3	5.1 ± 0.2	*	1.4 ± 0.2	2.5 ± 0.3	*
pH	E-L 31	2.48 ± 0.04	2.41 ± 0.08	ns	2.41 ± 0.06	2.35 ± 0.05	ns	2.33 ± 0.01	2.40 ± 0.02	*	2.32 ± 0.03	2.26 ± 0.06	ns
	E-L 35	2.64 ± 0.25	2.60 ± 0.03	ns	3.14 ± 0.11	2.86 ± 0.05	*	2.50 ± 0.01	2.41 ± 0.01	*	3.14 ± 0.11	2.37 ± 0.03	*
	E-L 36	3.47 ± 0.03	3.18 ± 0.11	*	4.02 ± 0.09	3.35 ± 0.10	*	4.15 ± 0.03	2.99 ± 0.07	*	4.17 ± 0.08	3.17 ± 0.06	*
	E-L 38	3.85 ± 0.17	3.42 ± 0.08	*	4.12 ± 0.10	3.89 ± 0.09	*	4.34 ± 0.09	3.46 ± 0.12	*	4.36 ± 0.06	3.83 ± 0.08	*
100 berries weight (g)	E-L 31	124.9 ± 17.0	107.0 ± 8.9	ns	209.1 ± 9.9	153.1 ± 14.5	*	172.1 ± 2.4	169.9 ± 11.6	ns	180.4 ± 4.7	74.4 ± 5.0	*
	E-L 35	267.8 ± 17.9	155.0 ± 7.5	*	536.4 ± 7.3	309.2 ± 19.6	*	236.7 ± 16.6	205.4 ± 7.3	*	362.6 ± 45.5	251.4 ± 24.4	*
	E-L 36	320.2 ± 4.3	159.6 ± 10.8	*	723.4 ± 20.3	371.8 ± 27.0	*	378.2 ± 35.1	315.7 ± 9.3	*	792.8 ± 10.8	582.5 ± 30.9	*
	E-L 38	361.4 ± 8.8	265.8 ± 16.9	*	734.2 ± 137.3	408.6 ± 31.0	*	372.6 ± 14.3	357.3 ± 19.1	ns	786.1 ± 29.6	578.4 ± 60.7	*

MH, Muscat Hamburg; V, Victoria; TSS, total soluble solids; TA, titratable acidity; 2014 Summer, 2014 summer season; 2014 Winter, 2014 winter season; 2015 Summer, 2015 summer season; 2015 Winter, 2015 winter season. Values are reported as mean ± SD of three biological replicates. Sig., significance. Asterisk indicates there are significant differences between summer and winter season berries ($p < 0.05$, t-test). ns, not significant.

still higher TSS in winter season berries at harvest. MH and V berries had lower TA and higher pH in the summer season than the winter season. Similar to CS and R grapes, berry weight in the winter cropping was also lower than that in the summer season in MH and V grapes. Reduced berry weight in the winter cropping led to a lower yield than the summer cropping (**Supplementary Table 2**).

Grape Volatile Compounds

Totally, there were 173 free-form and 137 bound-form volatile compounds identified in the four grape varieties, and these compounds were sorted into seven groups: C6/C9 compounds, terpenes, norisoprenoids, alcohols, carbonyl compounds, esters, and others (**Supplementary Tables 4**, **5**). The PCA was used to identify the aroma profile variations between the mature grapes (E-L 38) under the double cropping system, as shown in **Figure 1**.

In CS grapes (**Figure 1A**), two principal components explained 69.2% of the total variance. PC1 (R2X[1]) discriminated the berries of 2014 from those of 2015 and accounted for 43.1% of the total variance. The loading plot showed that the CS berries of 2014 had more abundant aroma compounds than those of 2015. PC2 (R2X[2]) discriminated the winter berries from the summer berries and accounted for 26.1% of the total variance. The loading plot showed that the winter berries had abundant terpenes, and the summer berries had abundant norisoprenoids.

In R grapes (**Figure 1B**), two principal components explained 71.7% of the total variance. Similar to the CS grapes, the two principal components could discriminate berries of the four seasons from each other. The loading plot showed that the winter berries had more abundant aroma compounds than the summer berries, especially terpenes.

In V grapes (**Figure 1C**), two principal components explained 68.6% of the total variation. PC1 (R2X[1]) separated the berries of different seasons, accounted for 50.7% of the total variation. Vintage variation only occupied 17.9% of the total variation. The winter season berries had an abundant aroma profile than the summer season berries, and most terpenes and norisoprenoid concentrations were higher in the winter berries than those in the summer berries.

In MH grapes (**Figure 1D**), two principal components explained 76.8% of the total variation. Unlike the previous three varieties, the summer season berries of 2014 and 2015 could not be clearly discriminated by the PCA model. PC1 (R2X[1]) accounted for 53.3% of the total variation that could discriminate the winter season berries of 2015 from the berries of the two summer seasons. PC2 (R2X[2]) accounted for 23.5% of the total variation that could discriminate the winter season berries of 2014 from other seasons. The winter season berries of 2015 had the most abundant aroma compounds, especially terpenes, norisoprenoids, and C6/C9 compounds.

Total Concentrations of C6/C9 Compounds, Terpenes, and Norisoprenoids

To figure out how the grape-derived aromas changed during the development stages, the total concentrations of C6/C9 compounds, terpenes, and norisoprenoids were calculated, as shown in **Figure 2**.

The C6/C9 compounds were the most abundant aroma compounds in all the grapes. The accumulation trends of C6/C9 compounds were not consistent in the four growing

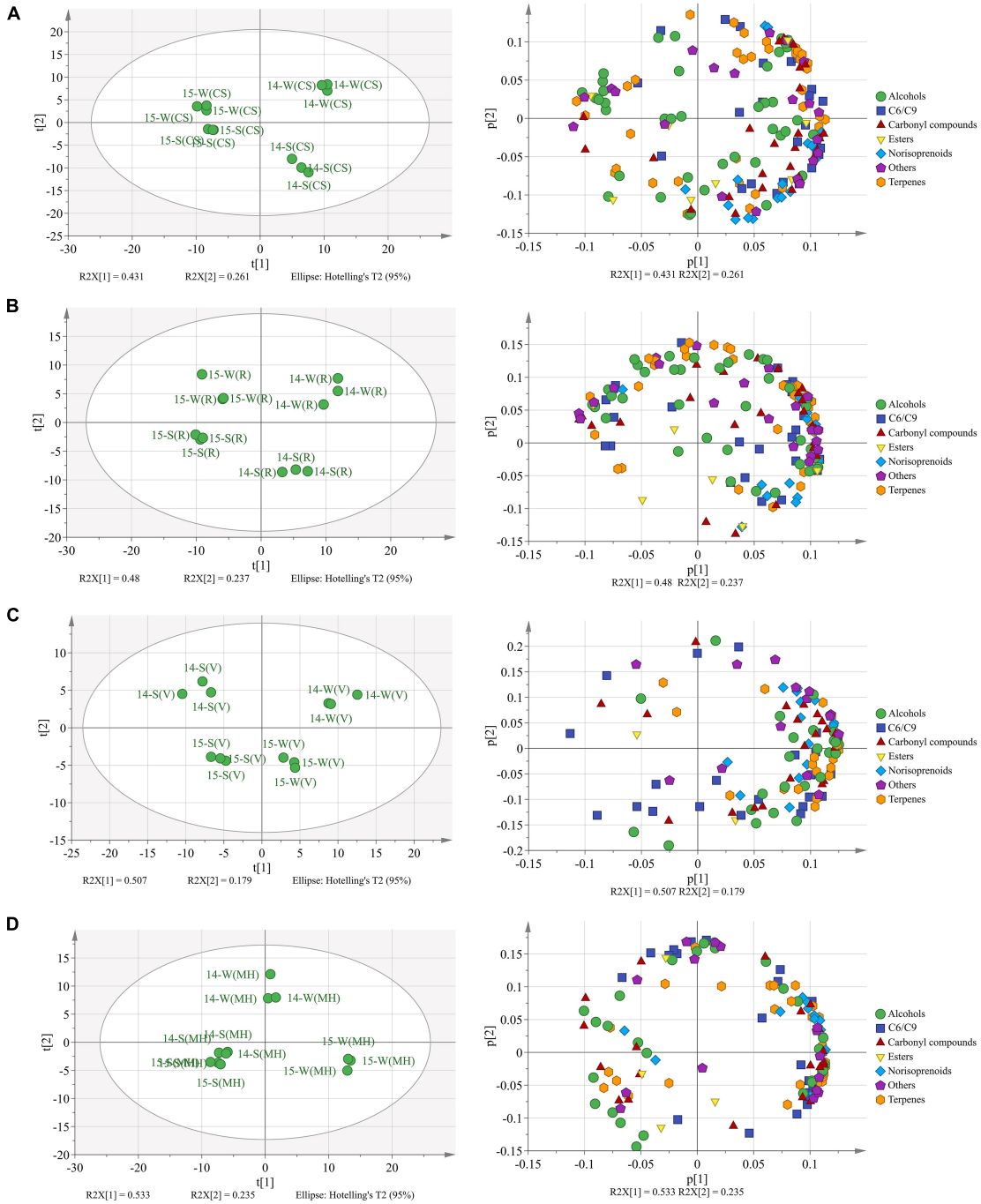

FIGURE 1 | The principal component analysis (PCA) based on the aroma compounds in Cabernet Sauvignon **(A)**, Riesling **(B)**, Victoria **(C)**, and Muscat Hamburg **(D)** grapes in 2014 and 2015. 14-S, 2014 summer season; 14-W, 2014 winter season; 15-S, 2015 summer season; 15-W, 2015 winter season.

seasons. In most seasons, C6/C9 compounds peaked at E-L 36 and then declined until the harvest, which was in agreement with the previous study (Wang et al., 2019). However, there were some seasons when the grapes of E-L 38 had the highest C6/C9 concentration, such as the winter season of V and MH grapes. In CS grapes, the berries of 2014 had higher C6/C9 compound concentrations than those of 2015. The significant difference between the summer and winter seasons in C6/C9 compound concentrations only occurred in the former development stages in 2014. However, in the other three varieties, the winter season berries had higher C6/C9 compound concentrations than those of the summer season within the same vintage in most development stages, especially at harvest.

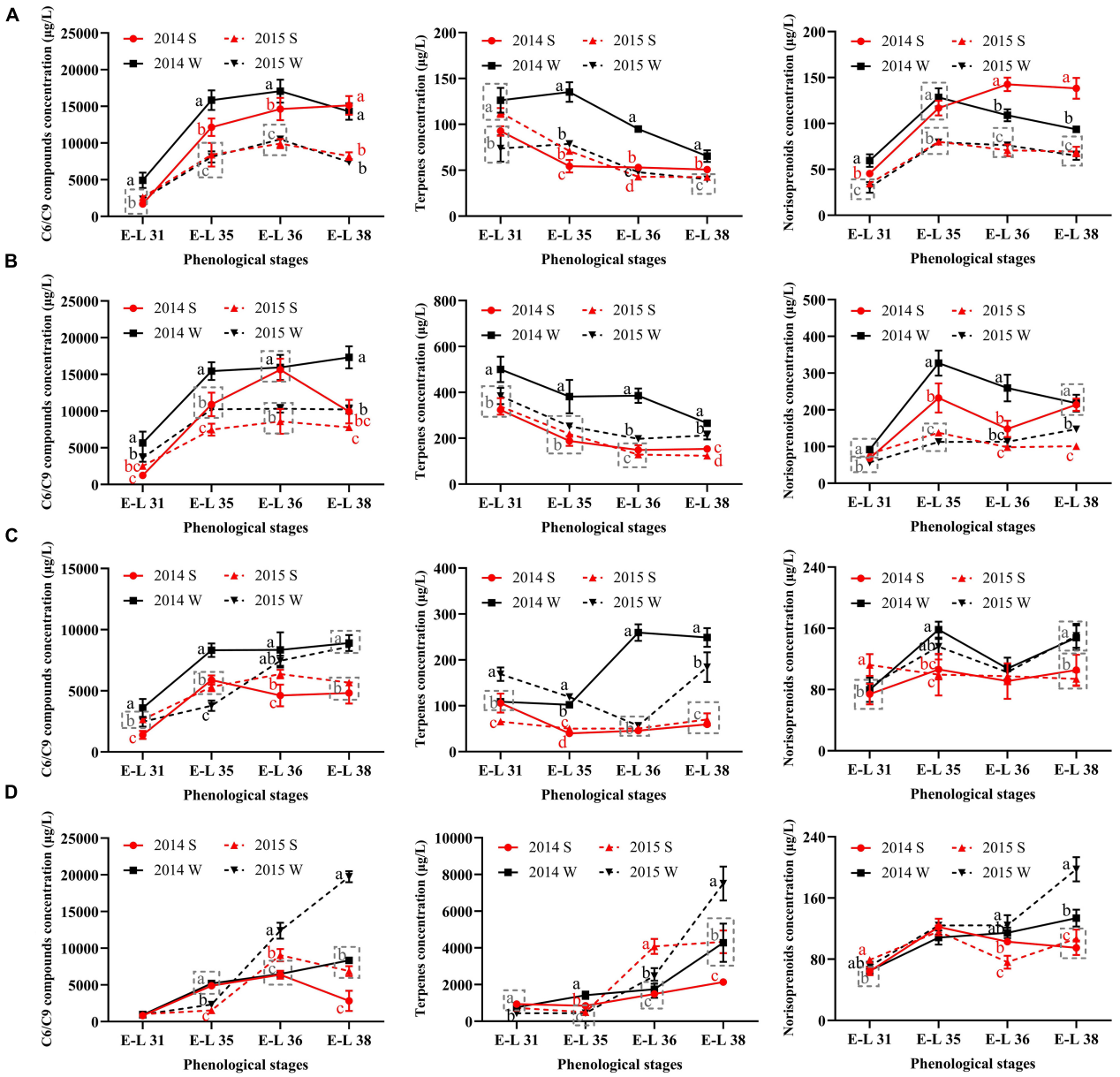

FIGURE 2 | The total concentrations of C6/C9 compounds, terpenes, and norisoprenoids in Cabernet Sauvignon **(A)**, Riesling **(B)**, Victoria **(C)**, and Muscat Hamburg **(D)** grapes in 2014 and 2015. 2014 S, 2014 summer season; 2014 W, 2014 winter season; 2015 S, 2015 summer season; 2015 W, 2015 winter season. Different letters indicate significant differences among seasons based on Duncan's multiple range test at $p < 0.05$.

For terpenes, MH grapes had the highest concentration among the four varieties, with at least 2000 μg/L at harvest. The other three varieties only had 50–400 μg/L terpenes at harvest, indicating that the grapes of the Muscat family usually had abundant terpenes (Fenoll et al., 2009). CS and R grapes had similar trends in terpenes accumulation. They had the highest total terpene concentrations at E-L 31, then declined until harvest. In MH grapes, the highest terpene concentration occurred at E-L 38. In V grapes, a significant increase of terpene only occurred in the 2014 winter season as grapes developed. However, in other seasons, the terpene concentration at harvest was slightly higher or have little difference than E-L 31 in V grapes.

For norisoprenoids, there were no consistent results in all varieties. In CS grapes, the summer season berries of 2014 had higher norisoprenoid concentration than those of the winter season in the same year, whereas no significant difference showed in the vintage of 2015. In R grapes, the significant differences between the summer and winter season berries occurred at E-L 35 and E-L 36 in 2014 and at E-L 38 in 2015. MH and V grapes had the same results in the two vintages, and the winter berries

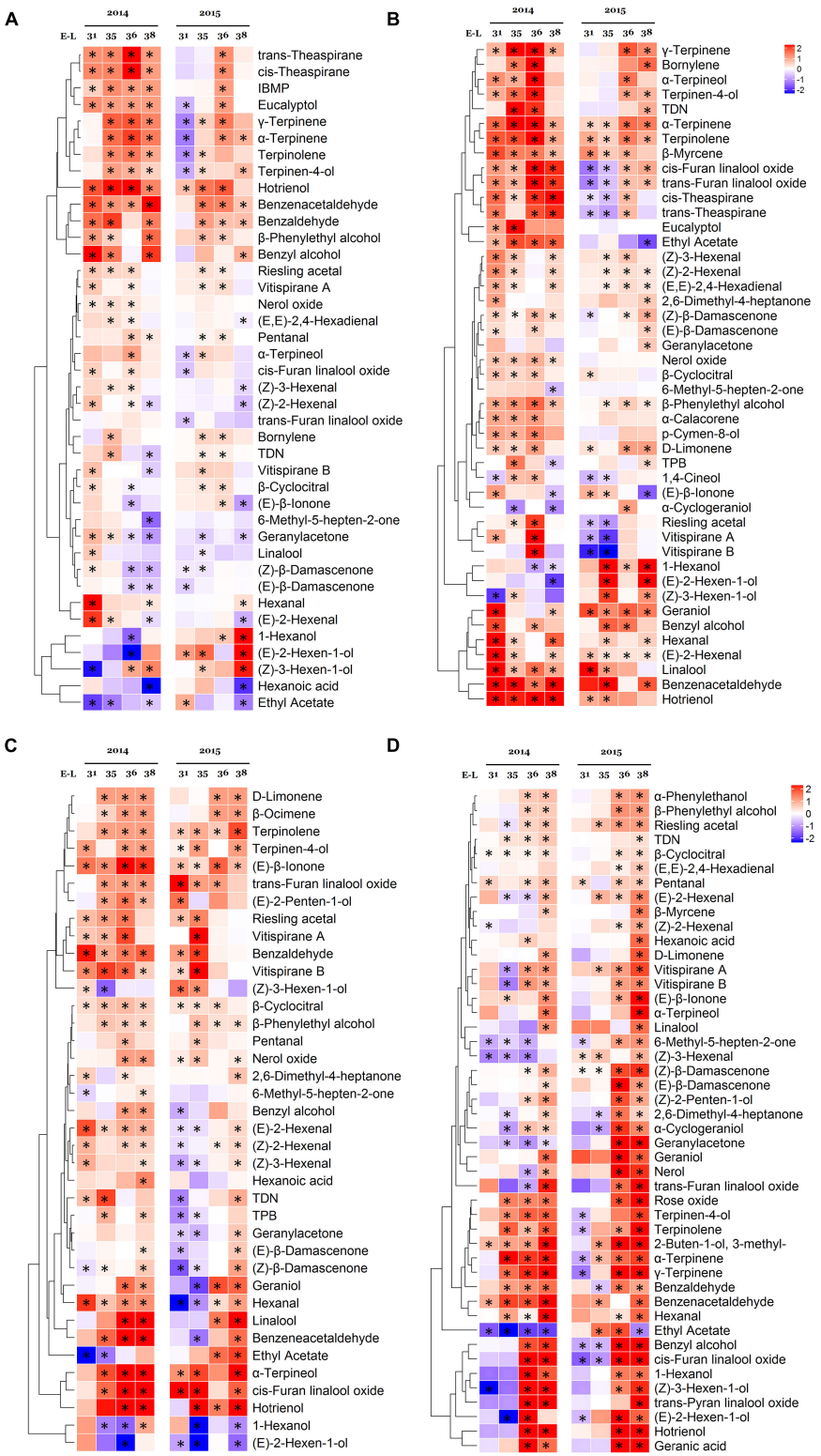

FIGURE 3 | Effect of the growing season on the free volatile compounds in Cabernet Sauvignon **(A)**, Riesling **(B)**, Victoria **(C)**, and Muscat Hamburg **(D)** grapes during fruit development in 2014 and 2015. Heatmaps show the $\log_2$ fold changes between seasons (winter season/summer season). Red block indicates higher aroma concentrations in the winter season berries. Blue block indicates lower aroma concentrations in the winter season berries. *Significant differences between the summer and winter season ($p < 0.05$, *t*-test). IBMP, 2-isobutyl-3-methoxypyrazine; TDN, 1,1,6-trimethyl-1,2-dihydronaphthalene; TPB, (*E*)-1-(2,3,6-trimethylphenyl)buta-1,3-diene.

had higher norisoprenoid concentrations than those of the summer season.

Variations of Volatile Compounds Between Growing Seasons

To figure out how the growing seasons affected the concentrations of individual volatile compounds, the key compounds were selected by using the *t*-test, which showed significant differences in at least one sampling point between seasons. The selected free volatile compounds are shown in **Figure 3**.

In CS grapes, many terpenes had higher concentrations in the winter season in several or a specific stage, especially in 2014. However, some norisoprenoids, such as (*E*)-β-ionone, 6-methyl-5-hepten-2-one, geranylacetone, (*Z*)-β-damascenone, and (*E*)-β-damascenone had lower concentrations in the winter season. β-Damascenone occupied the highest proportion in norisoprenoids of CS grapes (**Supplementary Table 4**). (*E*)-2-hexenal and hexanal were the main C6/C9 compounds with the highest concentrations (**Supplementary Table 4**). The winter berries had higher hexanal concentration but had lower (*E*)-2-hexenal than the summer berries at the harvest date.

In R grapes, most terpenes had higher concentrations in the winter season, such as γ-terpinene, α-terpinene, β-myrcene, terpinolene, geraniol, etc. In 2014, many terpenes only had higher concentrations before harvest in the winter season berries, but these differences disappeared at harvests, such as bornylene, α-terpineol, terpinen-4-ol, α-calacorene, and D-limonene. Although most norisoprenoids had higher concentrations in several stages, (*E*)-β-ionone was the only norisoprenoid with a higher concentration in the summer berries in both of the two vintages at harvest. TDN was well-known to contribute "petrol" aromas to "Riesling" wines (Sacks et al., 2012), and it had a higher concentration in the winter berries at harvest in 2015. Different from CS grapes, its winter season berries had high concentrations of both (*E*)-2-hexenal and hexanal.

In V grapes, most terpenes were also more abundant in the winter season berries, such as D-limonene, β-ocimene, terpinolene, terpinen-4-ol, linalool, α-terpineol, *cis*-furan linalool oxide, etc. For norisoprenoids, the winter season berries had a higher (*E*)-β-ionone concentration in all sampling times of 2014 and 2015. (*Z*)-β-damascenone and (*E*)-β-damascenone only showed higher concentrations in the winter season berries at harvest in 2014 and 2015. Similar to R grape, its (*E*)-2-hexenal and hexanal also had higher concentrations in the winter season berries at harvest.

In MH grapes, almost all of the selected compounds had higher concentrations in the winter season berries at E-L 38. Many of them did not show any difference in the early development, even were higher in the summer season berries at E-L 35 and E-L 36.

Except for terpenes, norisoprenoids, and C6/C9 compounds, some benzene derivatives were also had higher concentrations in the winter season berries in all varieties, such as benzaldehyde, benzeneacetaldehyde, benzyl alcohol, and β-phenylethyl alcohol. These compounds contribute roasted, honey, almond, fruity, and floral flavors to the grapes or their wines (Cai et al., 2014). High temperatures could enhance their biotransformation and degradation rate, whereas lower temperatures would increase their concentrations (Scafidi et al., 2013).

The selected bound volatile compounds are shown in **Supplementary Figure 2**. Compared to the free volatile compounds, there were fewer selected bound-form compounds with significant differences between seasons. In CS grapes, most of the selected compounds had no consistent trends in 2014 and 2015. Only 2,3-butanedione, *cis*-furan linalool oxide, and *trans*-furan linalool oxide showed higher concentrations in the winter season berries in serval stages over 2 years. In R and V grapes, most of the terpenes had higher concentrations in the winter season berries, which was in agreement with the free volatile results. However, in MH grapes, most of the selected compounds showed the opposite trends in 2014 and 2015.

Relationship Between Volatile Compounds and Climate Factors

As mentioned above, the summer seasons had more high-temperature hours than the winter seasons, but the accumulated PAR and rainfall were not consistent in the two vintages. Thus, the Pearson correlation analysis was used to figure out how climate factors affect the berries' volatile compounds at harvest. The highly correlated compounds ($|r^2| > 0.6$) in at least three varieties were selected, as shown in **Table 3**. Seventeen volatiles showed high correlations to the high-temperature hours, and most of them were negatively correlated. For C6/C9 compounds, hexanal was negatively correlated with the high temperatures in all of the four varieties. For terpenes, γ-terpinene, terpinen-4-ol, *cis*-furan linalool oxide (G), and *trans*-pyran linalool oxide (G) were all negatively correlated with high temperatures in all of the four varieties. Other terpenes, such as geraniol, were negatively correlated with high temperatures in R, MH, and V grapes, and geranial (G), nerol (G), geraniol (G), and *p*-cymene were negatively correlated with high temperatures in R and MH grapes. Different from the pronounced effects of high-temperature hours on aromas, fewer compounds highly correlated with PAR and rainfall were selected. Free- and bound-form *p*-menthan-8-ol concentrations were all positively correlated with accumulated whole season PAR. *trans*-Furan linalool oxide (G) was negatively correlated with accumulated whole season PAR in CS, R, and MH grapes. The rainfall correlated compounds had no consistent trends in four varieties.

Expression Profiles of Aroma Synthesis-Related Genes in the Grapes

2-Methyl-D-Erythritol-4-Phosphate Phosphate and Mevalonic Acid Pathway

Terpenes were derived from two common precursors: isopentenyl pyrophosphate (IPP) and its isomer dimethylallyl diphosphate (DMAPP), which were synthesized from two independent pathways: the plastidial MEP and the cytoplasmic MVA pathways, respectively (Wen et al., 2015). Carotenoids, the precursors of norisoprenoids, were also synthesized from the MEP pathway (Meng et al., 2020). The $\log_2$ fold

TABLE 3 | The Pearson correlation analysis between grape volatile compounds and climate factors.

Climate factor	Compound	Correlation			
		CS	R	MH	V
High-temperature hours	(*E,E*)-2,4-hexadienal	0.20	−0.65	−0.87*	−0.60
	(*E*)-2-hexen-1-ol	−0.62	0.15	0.68**	−0.69
	Hexanal	−0.43	−0.70	−0.91*	−0.87*
	γ-Terpinene	−0.46	−0.61	−0.91*	−0.96*
	Terpinen-4-ol	−0.67	−0.49	−0.95*	−0.87*
	Geraniol	0.45*	−0.75*	−0.84*	−0.79*
	1-Octen-3-ol	−0.30	−0.78*	−0.68	−0.79*
	Benzeneacetaldehyde	−0.58	−0.70	−0.78*	−0.92*
	cis-Furan linalool oxide (G)	−0.74	−0.96*	−0.84*	−0.73
	trans-Pyran linalool oxide (G)	−0.77*	−0.99*	−0.76*	−0.80*
	α-Ionene	0.64**	0.10	−0.73	−0.92*
	Geranylacetone	0.71**	0.05	−0.82*	−0.67
	Geranial (G)	–	−0.79*	−0.78*	0.81**
	Nerol (G)	0.21	−0.76*	−0.79*	0.82**
	Geraniol (G)	0.08	−0.90*	−0.81*	0.73**
	1-Heptanol (G)	0.12	−0.82*	−0.83*	0.62**
	p-Cymene (G)	–	−0.85*	−0.85*	0.73**
Accumulated whole-season PAR	*p*-Menthan-8-ol	0.65**	0.89**	–	0.86**
	trans-Furan linalool oxide (G)	−0.75*	−0.78*	−0.61	0.40
	p-Menthan-8-ol (G)	0.92**	0.92**	–	0.86**
	3-Buten-1-ol, 3-methyl-(G)	0.29	−0.83*	0.64**	0.86**
Accumulated whole-season rainfall	1-Octen-3-ol	−0.75*	−0.82*	0.45*	0.76**
	α-Terpineol (G)	−0.56	−0.78*	0.63**	0.63**
	trans-Pyran linalool oxide (G)	−0.70	−0.77*	0.12	0.64**
	Acetoin (G)	−0.87*	−0.07	−0.78*	0.72**

*CS, Cabernet Sauvignon; R, Riesling; MH, Muscat Hamburg; V, Victoria. (G), glycosidically bound form. –, not detected. **Significantly correlated at $p < 0.01$; *significantly correlated at $p < 0.05$.*

change was used to present the variations between the summer and winter season berries through MVA and MEP pathways (**Figure 4**).

In the MEP pathway, five *VviDXS* genes (VIT_200s0218g00110, VIT_204s0008g04970, VIT_205s0020 g02130, VIT_211s0052g01730, and VIT_211s0052g01780) were expressed differently in the berries of the winter and summer seasons in at least two varieties. Only the expression of *VviDXS2* (VIT_200s0218g00110) was downregulated in MH grapes, and other genes were all upregulated in several varieties in the winter season berries. *VviDXS3* (VIT_204s0008g04970) was the common upregulated expression gene in the winter season berries of all four varieties. *VviIPI* (VIT_204s0023g00600 and VIT_211s0206g00020) was responsible for the transformation between IPP and DMAPP, which had upregulated expression in R and V winter season berries. The mRNA levels of the GPPS small subunit might play a key role in regulating the formation of GPPS and thus affecting the monoterpene biosynthesis (Tholl et al., 2004). In the present study, *VviGPPS small subunit* (VIT_219s0090g00530) had higher expressions in MH grapes than other varieties and had low expression levels in CS and V grapes (**Supplementary Table 6**), which might be correlated with the monoterpene concentration variation among these varieties.

In the MVA pathway, there were also many genes significantly affected by the growing seasons. The expression of one *VviAACT* gene (VIT_218s0089g00590) was downregulated in the winter season berries of all four varieties. HMGR was the key enzyme of the MVA pathway. There were three *VviHMGR* genes (VIT_203s0038g04100, VIT_204s0044g01740, and VIT_218s0122g00610) differently expressed in the winter and summer season berries. Among them, VIT_204s0044g01740 was upregulated in R, V, and MH grapes. Terpene synthases (TPSs) were the final enzymes of the terpene biosynthetic pathway. *TPS-a*, *TPS-b*, and *TPS-g* were the main *VviTPS* genes with high expressions (Wen et al., 2015). In CS grapes, most selected *VviTPS* genes were downregulated in the winter season berries. Glycosyltransferases (GTs) could converse free terpenes into their corresponding glycoside bound forms, and three genes had been proved to have such character: *VviGT7*, *VviGT14*, and *VviGT15* (Bönisch et al., 2014). The downregulated expression of *VviGT7* and *VviGT14* were shown in all of the four varieties in the winter season berries.

Carotenoid Metabolism Pathway

As mentioned above, the MEP pathway also synthesized carotenoids, which were the precursors of norisoprenoids. The following pathway after synthesizing geranylgeranyl

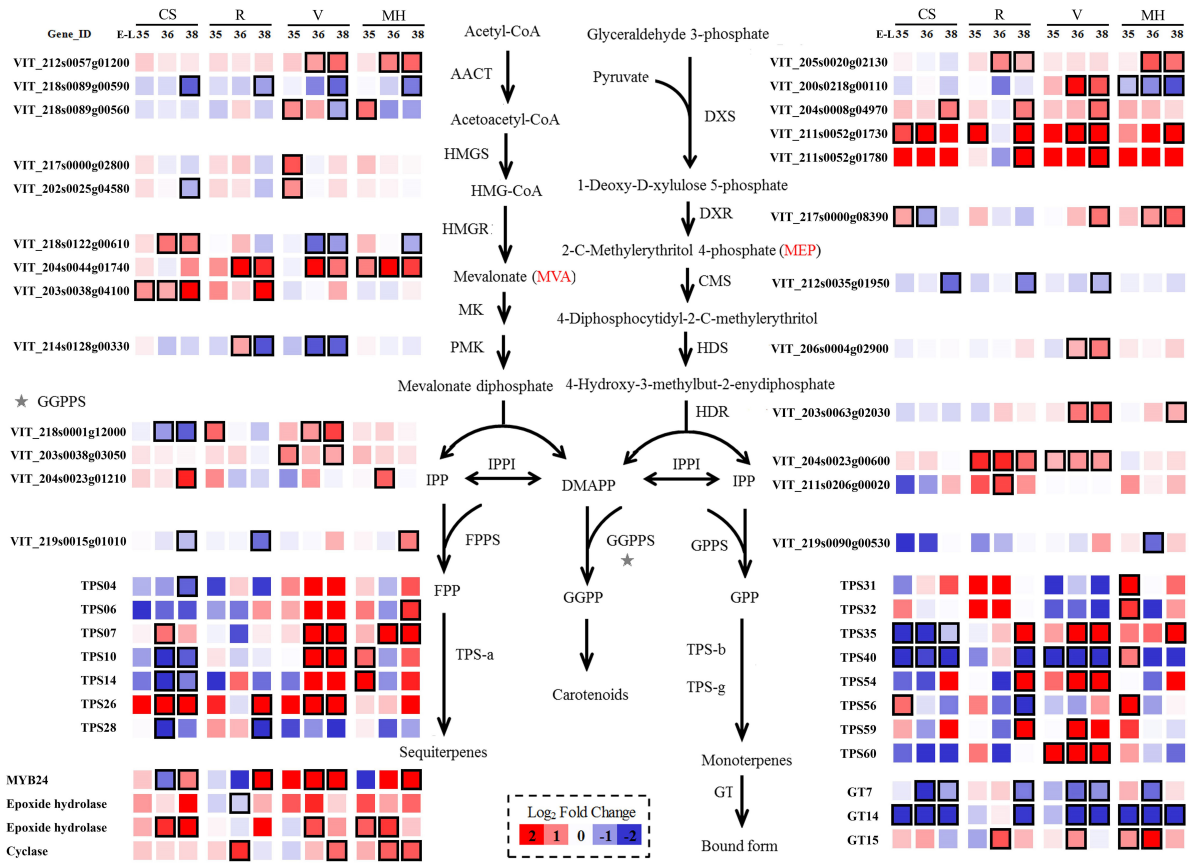

FIGURE 4 | Effect of the growing season on the expression profiles of MEP and MVA synthesis pathways during Cabernet Sauvignon, Riesling, Victoria, and Muscat Hamburg grapes development in 2014. Heatmaps show the $\log_2$ fold change between the seasons (winter season/summer season). Red block indicates higher gene expression in the winter season berries. Blue block indicates lower gene expression in the winter season berries. Boxes with bold margins indicate differently expressed genes between the summer and winter season berries. MEP, 2-methyl-D-erythritol-4-phosphate phosphate; MVA, mevalonic acid.

diphosphate (GGPP) was shown in **Supplementary Figure 3** and **Supplementary Table 7**. The condensation of two GGPPs by phytoene synthase (PSY) formed phytoene, the first carotenoid (Cazzonelli and Pogson, 2010). There were three identified *VviPSYs* genes (VIT_212s0028g00960, VIT_206s0004g00820, and VIT_204s0079g00680), which expressed differently between the berries of the summer and the winter season. *VviPSY3* (VIT_206s0004g00820) and *VviPSY2* (VIT_212s0028g00960) had higher expressions in the winter season berries and showed significant differences in several stages. Carotenoid cleavage dioxygenases (CCDs) were the key enzymes that catalyzed the generation of norisoprenoids (apocarotenoids) by cleaving the conjugate double bond of carotenoids (Meng et al., 2020). There were four *VviCCDs* selected in the present study, and most of them had higher expressions in the winter season berries, especially *VviCCD4a*. In CS grapes, *VviCCD4a* (VIT_202s0087g00910) had higher expressions at E-L 35 and E-L 38, whereas it was downregulated at the E-L 36 stage.

Oxylipin Pathway

The C6/C9 compounds, or GLVs, were short-chain alcohols, aldehydes, and esters formed through the oxylipin pathway (Hassan et al., 2015). The main enzymes in the oxylipin pathway included lipoxygenase (LOX), hydroperoxide lyase (HPL), and alcohol dehydrogenase (ADH). The selected genes were expressed differently in the oxylipin pathway between the summer and winter season berries are shown in **Supplementary Figure 4**. Compared with LOXs, *VviLOXA* (VIT_206s0004g01510) had high expression levels in the whole development stages of all the four varieties, which might play a key role in the LOX family (**Supplementary Table 8**; Podolyan et al., 2010; Xu et al., 2015a). The expression of *VviLOXA* was upregulated in the winter season berries of R, V, and MH grapes, whereas it was downregulated in the CS winter season berries. *VviHPL1* (VIT_212s0059g01060) had high expression levels in the development stages. It was reported that *VviHPL1* was also related to the accumulation of C6 compounds (Xu et al., 2015a). However, there were no consistent trends in all of the four varieties in the present study. ADH was responsible for the conversion of aldehydes to alcohols. About half of *VviADH* expressions were downregulated in the winter season berries in all of the four varieties, and others were upregulated. For C6 alcohols, only the MH winter season berries had higher (*E*)-2-hexen-1-ol and (*Z*)-3-hexen-1-ol concentrations than the

summer season berries in 2014 and 2015. The winter season berries of CS and R had higher (*E*)-2-hexen-1-ol concentrations than the summer season berries in 2015 and showed an opposite trend in 2014. The V winter season berries had a lower (*E*)-2-hexen-1-ol concentration than the summer season berries in both of the two vintages.

Relationship Between Volatile Compounds and Transcriptome Gene Expression

To figure out the relationship between volatile compounds and transcriptome gene expression, we selected the transcriptome genes involved in C6/C9, terpenes, and norisoprenoids synthesis pathway to calculate their correlation with the concentration of each corresponding category during berry development (E-L 35, E-L 36, and E-L 38). The highly correlated compounds (the Pearson correlation analysis, $|r^2| > 0.6$) in at least two varieties were selected, as shown in **Supplementary Table 9**. Only three genes involved in the oxylipin pathway showed high correlations to total C6/C9 compound concentration, and two of them were negatively correlated. The genes related to terpenes occupied the highest proportion in all selected genes, and 51 genes showed high correlations with total terpene concentration. Among them, five genes (VIT_211s0052g01730, VIT_203s0038g03050, VIT_202s0025g04864, VIT_202s0025g04880, and VIT_205 s0051g00670) were positively correlated with the total terpene concentration and six genes (VIT_215s0046g03550, VIT_215s0046g03590, VIT_215s0046g03600, VIT_215s0046 g03650, VIT_206s0004g02740, and VIT_214s0083g00770) were negatively correlated with high total terpene concentration in at least three varieties. The *VviDXS3* (VIT_211s0052g01730), which was upregulated in the winter berries in all varieties (**Figure 4**), was positively correlated with the berry terpene concentration in CS, V, and MH grapes. In the carotenoid metabolism pathway, only five genes were selected to have a high correlation with berry norisoprenoid concentration. Among them, two *VviCCDs* (VIT_213s0064g00810 and VIT_213s0064g00840) were positively correlated with the norisoprenoid concentration in R and V grapes, which was in agreement with the previous analysis. However, the two *VviCCDs* (VIT_213s0064g00810 and VIT_213s0064g00840) were upregulated in the winter berries in R and V grapes.

DISCUSSION

Effect of the Growing Season on Berries Physicochemical Parameter

The berries in the summer season usually had lower TSS than in the winter season under the double cropping system (Xu et al., 2011; Zhu et al., 2017), which was also confirmed in the present study. Severer high-temperature pressure and fewer sunshine hours in the 2014 summer season might inhibit TSS accumulation in the grapes. For MH and V grapes, there were 351 high-temperature hours in the 2014 summer season but only 89 h in the 2014 winter season. Although elevated temperature usually accelerated the sugar accumulation in the grape berries, scorching conditions would exceed the optimum photosynthetic temperature (Gutiérrez-Gamboa and Moreno, 2019). When the temperature exceeded 35°C, it would cause damage to the photosynthetic apparatus of the grapevines (Gutiérrez-Gamboa et al., 2021). However, in 2015, there was no significant difference in TSS in the MH berries between the summer and winter seasons during the developmental stages. This might be due to the sunshine hours in the winter season of MH grape, which were only 57% of the summer season and led to less carbon assimilation of vines. Fewer sunshine hours during the grape development in the 2015 winter season might slow down the TSS accumulation in the V grapes, which led to a slower ripening rate from the stages of E-L 31 to E-L 35 in the winter season berries.

Effect of the Growing Season on Berries Volatile Compounds

The winter season berries had higher terpene concentrations than those of the summer seasons in all of the four varieties. In general, most studies on the aromas and aroma precursors of fruity and floral nuances not only highlighted the benefit of the higher temperatures during berry ripening but also their negative effects on the fruit metabolism whenever they were excessively high (Pons et al., 2017). Grapes in warm regions were reported to have higher terpene concentrations than in hot regions (Lecourieux et al., 2017). The Pearson correlation analysis showed that γ-terpinene, terpinen-4-ol, *cis*-furan linalool oxide (G), and *trans*-pyran linalool oxide (G) were all negatively correlated with high temperatures in all of the four varieties in the present study. The elevated temperature (>35°C) would inhibit the accumulation of terpenes (Scafidi et al., 2013). Furthermore, terpene concentrations might be negatively correlated with the average daily maximum temperature during the ripening because of volatilization (Gutiérrez-Gamboa et al., 2021). In our study, the expression of *VviDXSs* was commonly upregulated in the winter season berries of all four varieties. Lecourieux et al. (2017) showed that the strong repression of the genes encoding the 1-deoxy-D-xylulose-5-phosphate synthase (VIT_05s0020g02130, VIT_09s0002g02050, VIT_11s0052g01730, and VIT_11s0052g01780) suggested that the volatile terpenoid biosynthesis might be decreased by high temperature. Similarly, Rienth et al. (2014) reported that high temperatures impaired the expression of 1-deoxy-D-xylulose-5-phosphate synthase transcripts (VIT_11s0052g01730 and VIT_11s0052g01780), which were required for the isopentenyl pyrophosphate (IPP) synthesis, the universal precursor for the biosynthesis of terpenes. The regression of high temperatures on the *VviDXSs* expression might be the reason for the lower terpene concentration in the summer season berries in the present study. There were also some gene expressions, such as *VviGTs*, that were downregulated in the winter season berries. The contents of many bound terpene substances are lower in winter than in the summer season (**Supplementary Table 5** and **Supplementary Figure 2**). The GTs were responsible for the synthesis of bound terpene substances as a GT, so to a certain extent, it could be speculated that the downregulation of *VvGTs* expression caused a decrease of bound terpene

substances in winter berries. Free- and bound-form *p*-menthan-8-ol concentrations were all positively correlated with the accumulation of PAR in the whole season. In general, previous studies reported that the increased light exposure was beneficial for the terpene accumulation, and the shading treatment led to lower monoterpenes levels in bunches (Bureau et al., 2000). In hot climates, the beneficial effect of increased synthesis of terpenes induced by light might be surpassed by the negative effect of the elevated berry temperature (Friedel et al., 2016). The rainfall correlated compounds had no consistent trends in all of the four varieties, and its effect might also be covered up by the high temperature effect.

The MH and V grapes had similar results in the two vintages, and the winter season berries had a higher norisoprenoid concentration than those of the summer season. Similar to the terpenes accumulation, high temperatures also inhibited the biosynthesis of norisoprenoids (Wang et al., 2020). Lecourieux et al. (2017) found that heat treatment would repress the expressions of the genes encoding the key enzymes in the carotenoid metabolism, which formed norisoprenoids. So in R, V, and MH grapes, the winter season berries had higher norisoprenoid concentrations than those of the summer seasons. Regarding the different results in CS grapes, different varieties had varied temperature, sunlight, or water requirements, leading to varying responses to the climate changes (Schultz, 2003; Parker et al., 2020). The CS grapes were reported as a late-ripening variety (Parker et al., 2013), which might require more temperature than the other three varieties. The winter seasons might not meet the temperature requirement for the norisoprenoids accumulation in CS grapes, which led to less norisoprenoid concentrations than in the summer seasons. Moreover, the variation between different vineyards might also contribute to the differences between CS and the other two table varieties. The east–west row orientation was believed to have the lowest sunlight interception in canopies among all vineyard orientations (Lu et al., 2021), which was also unfavorable for the norisoprenoid accumulation in CS grapes. In the present study, four *VviCCDs* were expressed differently in different growing seasons, and most of them had higher expressions in the winter season berries. Scherzinger and Al-Babili (2008) found that both cold (20°C) and heat stress (38°C) could increase the expression of the CCD genes. However, Meng et al. (2020) found the high temperature (37°C) repressed the activity of the *VvCCD4b* promoter. In the present study, the upregulated expression of most *VviCCDs* in the winter season berries might show that high temperatures were unfavorable for their expressions. However, in CS grapes, the winter season berries had lower norisoprenoid concentration than those in the summer season. Different expressions of *VviCCD1s* (VIT_213s0064g00840 and VIT_213s0064g00810) in CS grapes and other varieties might be the reason.

The accumulation trends of C6/C9 compounds were not consistent in the four growing seasons in the present study. In most seasons, C6/C9 compounds peaked at E-L 36 and then declined until the harvest. However, there were some seasons when the berries at E-L 38 had the highest C6/C9 concentrations, such as the winter seasons of V and MH grapes. Kalua and Boss (2010) found that CS grapes had the highest C6/C9 compound concentration at pre-harvest, whereas R grapes had the highest C6/C9 compound concentration at harvest. As the C6 compounds are derived from varietal precursors, they could hypothetically contribute to judging wine origin and affiliation (Oliveira et al., 2006). In the Pearson correlation analysis in this study, hexanal was negatively correlated with high temperatures in all of the four varieties. As reported, hexanal was derived from linoleic acid hydroperoxide through the LOX pathway (Oliveira et al., 2006). Podolyan et al. (2010) also reported that two recombinant LOXs had the maximum enzymatic activity at 25°C and lost about 40% of their maximal activity when the temperature exceeded 35°C. As for LOXs, the expression of *VviLOXA* was upregulated in the winter berries of R, V, and MH grapes, whereas it was downregulated in CS winter berries. R, V, and MH winter berries had higher C6/C9 concentrations than the summer berries, whereas there was no significant difference in CS grapes at harvest. The variations of *VviLOXA* expression in CS and other varieties might be the reason.

CONCLUSION

This research used metabolomics and transcriptomics to reveal the aroma variations in different grape varieties under the double cropping system. The winter berries had higher TSS content and TA than the summer berries. The lower berry weight in the winter season caused a decreased yield compared to those of the summer season. The winter berries had higher concentrations in many aroma categories than the summer berries, especially terpenes. Climate factor variations were the main reason for the quality variations in the summer and winter season berries. Among all of the climate factors, the temperature might be the dominant one, and its influence could cover up the effects of other factors. Different from other varieties, the CS winter berries had lower norisoprenoid concentrations than the summer berries, indicating that the responses to climate changes might be variety-dependent. The higher concentrations of terpenes and norisoprenoids in the winter berries of most varieties could be associated with the regulated expressions of *VviDXSs*, *VviPSYs*, and *VviCCDs* at the transcription level. The different climates in the summer and winter seasons provided us with a better understanding of how climate changes influenced the grapes' secondary metabolites. The season variation within a vintage under the double cropping system usually exceeded the effects of the vintage in the traditional viticulture regions, making our results more apparent.

DATA AVAILABILITY STATEMENT

The original contributions presented in the study are publicly available. This data can be found here: National Center for Biotechnology Information (NCBI) BioProject database under accession numbers GSE103226 and GSE168785.

AUTHOR CONTRIBUTIONS

FH, JW, and C-QD designed the experiments. W-KC and H-CL performed the experiments. H-CL analyzed the data and prepared the original draft. YW provided the statistical support. X-JB and GC provided the double cropping system vineyards. FH revised the manuscript. All authors approved the submitted version.

FUNDING

This research was supported by the China Agriculture Research System of MOF and MARA (CARS-29).

ACKNOWLEDGMENTS

The authors are grateful to the Grape and Wine Research Institute in the Guangxi Academy of Agricultural Sciences for field experiment and technical assistance.

SUPPLEMENTARY MATERIAL

The Supplementary Material for this article can be found online at: https://www.frontiersin.org/articles/10.3389/fpls.2021.809558/full#supplementary-material

REFERENCES

Bindi, M., Miglietta, F., Gozzini, B., Orlandini, S., and Seghi, L. (1997). A simple model for simulation of growth and development in grapevine (*Vitis vinifera* L.). *II Model Valid. Vitis.* 36, 73–76.

Black, C., Parker, M., Siebert, T., Capone, D., and Francis, I. (2015). Terpenoids and their role in wine flavour: recent advances. *Aust. J. Grape Wine Res.* 21, 582–600. doi: 10.1111/ajgw.12186

Bönisch, F., Frotscher, J., Stanitzek, S., Ruehl, E., Wüst, M., Bitz, O., et al. (2014). A UDP-glucose: monoterpenol glucosyltransferase adds to the chemical diversity of the grapevine metabolome. *Plant Physiol.* 165, 561–581. doi: 10.1104/pp.113.232470

Bureau, S. M., Razungles, A. J., and Baumes, R. L. (2000). The aroma of Muscat of Frontignan grapes: effect of the light environment of vine or bunch on volatiles and glycoconjugates. *J. Sci. Food Agric.* 80, 2012–2020. < 2012:AID-JSFA738 > 3.0.CO;2-X doi: 10.1002/1097-0010(200011)80:14

Cai, J., Zhu, B.-Q., Wang, Y.-H., Lu, L., Lan, Y.-B., Reeves, M. J., et al. (2014). Influence of pre-fermentation cold maceration treatment on aroma compounds of Cabernet Sauvignon wines fermented in different industrial scale fermenters. *Food Chem.* 154, 217–229. doi: 10.1016/j.foodchem.2014.01.003

Cazzonelli, C. I., and Pogson, B. J. (2010). Source to sink: regulation of carotenoid biosynthesis in plants. *Trends Plant Sci.* 15, 266–274. doi: 10.1016/j.tplants.2010.02.003

Chen, W.-K., Bai, X.-J., Cao, M.-M., Cheng, G., Cao, X.-J., Guo, R.-R., et al. (2017). Dissecting the variations of ripening progression and flavonoid metabolism in grape berries grown under double cropping system. *Front. Plant Sci.* 8:1912. doi: 10.3389/fpls.2017.01912

Cheng, G., Zhou, S. H., Zhang, J., Huang, X. Y., Bai, X. J., Xie, T. L., et al. (2019). Comparison of transcriptional expression patterns of phenols and carotenoids in 'Kyoho' grapes under a two-crop-a-year cultivation system. *PLoS One* 14:e0210322. doi: 10.1371/journal.pone.0210322

Chou, M.-Y., and Li, K.-T. (2014). Rootstock and seasonal variations affect anthocyanin accumulation and quality traits of 'Kyoho' grape berries in subtropical double cropping system. *Vitis* 53, 193–199.

Downey, M. O., Dokoozlian, N. K., and Krstic, M. P. (2006). Cultural practice and environmental impacts on the flavonoid composition of grapes and wine: a review of recent research. *Am. J. Enol. Viticult.* 57, 257–268.

Favero, A., Amorim, D., Mota, R., Soares, A. M., Souza, C., and Regina, M. (2011). Double-pruning of 'Syrah' grapevines: a management strategy to harvest wine grapes during the winter in the Brazilian Southeast. *Vitis* 50, 151–158.

Fenoll, J., Manso, A., Hellín, P., Ruiz, L., and Flores, P. (2009). Changes in the aromatic composition of the *Vitis vinifera* grape Muscat Hamburg during ripening. *Food Chem.* 114, 420–428. doi: 10.1016/j.foodchem.2008.09.060

Friedel, M., Frotscher, J., Nitsch, M., Hofmann, M., Bogs, J., Stoll, M., et al. (2016). Light promotes expression of monoterpene and flavonol metabolic genes and enhances flavour of winegrape berries (*Vitis vinifera* L. cv). *Aust. J. Grape Wine Res.* 22, 409–421. doi: 10.1111/ajgw.12229

Guo, R., Wang, B., Lin, L., Cheng, G., Zhou, S., Xie, S., et al. (2018). Evolutionary, interaction and expression analysis of floral meristem identity genes in inflorescence induction of the second crop in two-crop-a-year grape culture system. *J. Genet.* 97, 439–451. doi: 10.1007/s12041-018-0929-5

Gutiérrez-Gamboa, G., and Moreno, Y. (2019). Terroir and typicity of Carignan from Maule Valley (Chile): the resurgence of a minority variety. *OENO One* 53, 75–93. doi: 10.20870/oeno-one.2019.53.1.2348

Gutiérrez-Gamboa, G., Zheng, W., and de Toda, F. (2021). Current viticultural techniques to mitigate the effects of global warming on grape and wine quality: a comprehensive review. *Food Res. Int.* 139:109946. doi: 10.1016/j.foodres.2020.109946

Hassan, M., Zainal, Z., and Ismail, I. (2015). Green leaf volatiles: biosynthesis, biological functions and their applications in biotechnology. *Plant Biotechnol. J.* 13, 727–739. doi: 10.1111/pbi.12368

Junior, M. J. P., Hernandes, J. L., Bardin-Camparotto, L., and Blain, G. C. (2017). Plant parameters and must composition of 'Syrah' grapevine cultivated under sequential summer and winter growing seasons. *Bragantia* 76, 345–351. doi: 10.1590/1678-4499.146

Kalua, C., and Boss, P. (2009). Evolution of volatile compounds during the development of Cabernet Sauvignon grapes (*Vitis vinifera* L.). *J. Agric. Food Chem.* 57, 3818–3830. doi: 10.1021/jf803471n

Kalua, C. M., and Boss, P. K. (2010). Comparison of major volatile compounds from Riesling and Cabernet Sauvignon grapes (*Vitis vinifera* L.) from fruitset to harvest. *Aust. J. Grape Wine Res.* 16, 337–348. doi: 10.1111/j.1755-0238.2010.00096.x

Lan, Y.-B., Qian, X., Yang, Z.-J., Xiang, X.-F., Yang, W.-X., Liu, T., et al. (2016). Striking changes in volatile profiles at sub-zero temperatures during over-ripening of 'Beibinghong' grapes in Northeastern China. *Food Chem.* 212, 172–182. doi: 10.1021/jf001398l

Lashbrooke, J. G., Young, P. R., Dockrall, S. J., Vasanth, K., and Vivier, M. A. (2013). Functional characterisation of three members of the *Vitis vinifera* L. carotenoid cleavage dioxygenase gene family. *BMC Plant Biol.* 13:156. doi: 10.1186/1471-2229-13-156

Lecourieux, F., Kappel, C., Pieri, P., Charon, J., Pillet, J., Hilbert, G., et al. (2017). Dissecting the biochemical and transcriptomic effects of a locally applied heat treatment on developing Cabernet Sauvignon grape berries. *Front. Plant Sci.* 8:53. doi: 10.3389/fpls.2017.00053

Lu, H.-C., Gao, X.-T., Duan, C.-Q., Li, S.-D., Chen, W., and Wang, J. (2021). The effect of cluster position determined by vineyard row orientation on grape flavonoids and aroma profiles of *Vitis vinifera* L cv. Cabernet Sauvignon and Italian Riesling in the north foot of Tianshan Mountains. *S. Afr. J. Enol. Vitic.* 42, 44–55. doi: 10.21548/42-1-4308

Meng, N., Wei, Y., Gao, Y., Yu, K., Cheng, J., Li, X.-Y., et al. (2020). Characterization of transcriptional expression and regulation of carotenoid cleavage dioxygenase 4b in grapes. *Front. Plant Sci.* 11:483. doi: 10.3389/fpls.2020.00483

Mitra, S., Irshad, M., Debnath, B., Lu, X. C., Li, M., Dash, C. K., et al. (2018). Effect of vineyard soil variability on chlorophyll fluorescence, yield and quality of table grape as influenced by soil moisture grown under double cropping system in protected condition. *PeerJ* 6:e5592. doi: 10.7717/peerj.5592

Miziorko, H. (2010). Enzymes of the mevalonate pathway of isoprenoid biosynthesis. *Arch. Biochem. Biophys.* 505, 131–143. doi: 10.1016/j.abb.2010.09.028

Oliveira, J. M., Faria, M., Sá, F., Barros, F., and Araújo, I. M. (2006). C6-alcohols as varietal markers for assessment of wine origin. *Anal. Chim. Acta* 563, 300–309. doi: 10.1016/j.aca.2005.12.029

Parker, A., de Cortázar-Atauri, I. G., Chuine, I., Barbeau, G., Bois, B., Boursiquot, J.-M., et al. (2013). Classification of varieties for their timing of flowering and veraison using a modelling approach: A case study for the grapevine species *Vitis vinifera* L. *Agric. For. Meteorol.* 180, 249–264. doi: 10.1016/j.agrformet.2020.107902

Parker, A. K., de Cortázar-Atauri, I., Gény, L., Spring, J.-L., Destrac, A., Schultz, H., et al. (2020). Temperature-based grapevine sugar ripeness modelling for a wide range of *Vitis vinifera* L. cultivars. *Agric. For. Meteorol.* 28:107902. doi: 10.1016/j.agrformet.2013.06.005

Podolyan, A., White, J., Jordan, B., and Winefield, C. (2010). Identification of the lipoxygenase gene family from *Vitis vinifera* and biochemical characterisation of two 13-lipoxygenases expressed in grape berries of Sauvignon Blanc. *Funct. Plant Biol.* 37, 767–784. doi: 10.1071/FP09271

Pons, A., Allamy, L., Schüttler, A., Rauhut, D., Thibon, C., and Darriet, P. (2017). What is the expected impact of climate change on wine aroma compounds and their precursors in grape? *OENO One* 51, 141–146. doi: 10.20870/oeno-one.2016.0.0.1868

Rienth, M., Torregrosa, L., Luchaire, N., Chatbanyong, R., Lecourieux, D., Kelly, M. T., et al. (2014). Day and night heat stress trigger different transcriptomic responses in green and ripening grapevine (*Vitis vinifera*) fruit. *BMC Plant Biol.* 14:108. doi: 10.1186/1471-2229-14-108

Sacks, G. L., Gates, M. J., Ferry, F. X., Lavin, E. H., Kurtz, A. J., and Acree, T. E. (2012). Sensory threshold of 1,1,6-trimethyl-1,2-dihydronaphthalene (TDN) and concentrations in young Riesling and non-Riesling wines. *J. Agric. Food Chem.* 60, 2998–3004. doi: 10.1021/jf205203b

Savoi, S., Wong, D. C. J., Arapitsas, P., Miculan, M., Bucchetti, B., Peterlunger, E., et al. (2016). Transcriptome and metabolite profiling reveals that prolonged drought modulates the phenylpropanoid and terpenoid pathway in white grapes (*Vitis vinifera* L.). *BMC Plant Biol.* 16:67. doi: 10.1186/s12870-016-0760-1

Scafidi, P., Pisciotta, A., Patti, D., Tamborra, P., Di Lorenzo, R., and Barbagallo, M. G. (2013). Effect of artificial shading on the tannin accumulation and aromatic composition of the Grillo cultivar (*Vitis vinifera* L.). *BMC Plant Biol.* 13:175. doi: 10.1186/1471-2229-13-175

Scherzinger, D., and Al-Babili, S. (2008). *In vitro* characterization of a carotenoid cleavage dioxygenase from *Nostoc* sp. *Mol. Microbiol.* 69, 231–244. doi: 10.1111/j.1365-2958.2008.06282.x

Schultz, H. R. (2003). Differences in hydraulic architecture account for near-isohydric and anisohydric behaviour of two field-grown *Vitis vinifera* L. cultivars during drought. *Plant Cell Environ.* 26, 1393–1405. doi: 10.1046/j.1365-3040.2003.01064.x

Sun, R.-Z., He, F., Lan, Y.-B., Xing, R.-R., Liu, R., Pan, Q.-H., et al. (2015). Transcriptome comparison of Cabernet Sauvignon grape berries from two regions with distinct climate. *J. Plant Physiol.* 178, 43–54. doi: 10.1016/j.jplph.2015.01.012

Tholl, D., Kish, C. M., Orlova, I., Sherman, D., Gershenzon, J., Pichersky, E., et al. (2004). Formation of monoterpenes in *Antirrhinum majus* and *Clarkia breweri* flowers involves heterodimeric geranyl diphosphate synthases. *Plant Cell* 16, 977–992. doi: 10.1105/tpc.020156

Wang, Y., He, Y.-N., He, L., He, F., Chen, W., Duan, C.-Q., et al. (2019). Changes in global aroma profiles of Cabernet Sauvignon in response to cluster thinning. *Food Res. Int.* 122, 56–65. doi: 10.1016/j.foodres.2019.03.061

Wang, Y., Li, H.-Q., Gao, X.-T., Lu, H.-C., Peng, W.-T., Chen, W., et al. (2020). Influence of attenuated reflected solar radiation from the vineyard floor on volatile compounds in Cabernet Sauvignon grapes and wines of the north foot of Mt. *Tianshan Food Res. Int.* 137:109688. doi: 10.1016/j.foodres.2020.109688

Wen, Y.-Q., Zhong, G.-Y., Gao, Y., Lan, Y.-B., Duan, C.-Q., and Pan, Q.-H. (2015). Using the combined analysis of transcripts and metabolites to propose key genes for differential terpene accumulation across two regions. *BMC Plant Biol.* 15:240. doi: 10.1186/s12870-015-0631-1

Xu, C., Zhang, Y., Zhu, L., Huang, Y., and Lu, J. (2011). Influence of growing season on phenolic compounds and antioxidant properties of grape berries from vines grown in subtropical climate. *J. Agric. Food Chem.* 59, 1078–1086. doi: 10.1021/jf104157z

Xu, X.-Q., Cheng, G., Duan, L.-L., Jiang, R., Pan, Q.-H., Duan, C.-Q., et al. (2015a). Effect of training systems on fatty acids and their derived volatiles in Cabernet Sauvignon grapes and wines of the north foot of Mt. *Tianshan. Food Chem.* 181, 198–206. doi: 10.1016/j.foodchem.2015.02.082

Xu, X.-Q., Liu, B., Zhu, B.-Q., Lan, Y.-B., Gao, Y., Wang, D., et al. (2015b). Differences in volatile profiles of Cabernet Sauvignon grapes grown in two distinct regions of China and their responses to weather conditions. *Plant Physiol. Bioch.* 89, 123–133. doi: 10.1016/j.plaphy.2015.02.020

Zhang, E., Chai, F., Zhang, H., Li, S., Liang, Z., and Fan, P. (2017). Effects of sunlight exclusion on the profiles of monoterpene biosynthesis and accumulation in grape exocarp and mesocarp. *Food Chem.* 237, 379–389. doi: 10.1016/j.foodchem.2017.05.127

Zhu, L., Huang, Y., Zhang, Y., Xu, C., Lu, J., and Wang, Y. (2017). The growing season impacts the accumulation and composition of flavonoids in grape skins in two-crop-a-year viticulture. *J. Food Sci. Technol.* 54, 2861–2870. doi: 10.1007/s13197-017-2724-3

Conflict of Interest: The authors declare that the research was conducted in the absence of any commercial or financial relationships that could be construed as a potential conflict of interest.

Publisher's Note: All claims expressed in this article are solely those of the authors and do not necessarily represent those of their affiliated organizations, or those of the publisher, the editors and the reviewers. Any product that may be evaluated in this article, or claim that may be made by its manufacturer, is not guaranteed or endorsed by the publisher.

frontiers in Plant Science

ORIGINAL RESEARCH
published: 02 March 2022
doi: 10.3389/fpls.2022.826780

Functional Characterization of a Flavone Synthase That Participates in a Kumquat Flavone Metabolon

Shulin Tian[1,2], Yuyan Yang[1,2], Tao Wu[1], Chuan Luo[1], Xin Li[1], Xijuan Zhao[1,2], Wanpeng Xi[1,2], Xiaogang Liu[1,2] and Ming Zeng[1,2]**

[1] College of Horticulture and Landscape Architecture, Southwest University, Chongqing, China, [2] Key Laboratory of Horticulture Science for Southern Mountainous Regions, Ministry of Education, Chongqing, China

Flavones predominantly accumulate as *O*- and *C*-glycosides in kumquat plants. Two catalytic mechanisms of flavone synthase II (FNSII) support the biosynthesis of glycosyl flavones, one involving flavanone 2-hydroxylase (which generates 2-hydroxyflavanones for *C*-glycosylation) and another involving the direct catalysis of flavanones to flavones for *O*-glycosylation. However, FNSII has not yet been characterized in kumquats. In this study, we identified two kumquat *FNSII* genes (*FcFNSII-1* and *FcFNSII-2*), based on transcriptome and bioinformatics analysis. Data from *in vivo* and *in vitro* assays showed that FcFNSII-2 directly synthesized apigenin and acacetin from naringenin and isosakuranetin, respectively, whereas *FcFNSII-1* showed no detectable catalytic activities with flavanones. In agreement, transient overexpression of *FcFNSII-2* in kumquat peels significantly enhanced the transcription of structural genes of the flavonoid-biosynthesis pathway and the accumulation of several *O*-glycosyl flavones. Moreover, studying the subcellular localizations of FcFNSII-1 and FcFNSII-2 demonstrated that N-terminal membrane-spanning domains were necessary to ensure endoplasmic reticulum localization and anchoring. Protein–protein interaction analyses, using the split-ubiquitin yeast two-hybrid system and bimolecular fluorescence-complementation assays, revealed that FcFNSII-2 interacted with chalcone synthase 1, chalcone synthase 2, and chalcone isomerase-like proteins. The results provide strong evidence that FcFNSII-2 serves as a nucleation site for an *O*-glycosyl flavone metabolon that channels flavanones for *O*-glycosyl flavone biosynthesis in kumquat fruits. They have implications for guiding genetic engineering efforts aimed at enhancing the composition of bioactive flavonoids in kumquat fruits.

Keywords: kumquat plants, flavonoids, flavone synthase, protein–protein interaction, metabolon

OPEN ACCESS

Edited by:
M. Teresa Sanchez-Ballesta, Institute of Food Science, Technology and Nutrition (CSIC), Spain

Reviewed by:
Goro Taguchi, Shinshu University, Japan
Sumit Ghosh, Central Institute of Medicinal and Aromatic Plants (CSIR), India

****Correspondence:***
Xiaogang Liu
liu16853@swu.edu.cn
Ming Zeng
zengming@swu.edu.cn;
zengming2017swu@163.com

Specialty section:
This article was submitted to Plant Metabolism and Chemodiversity, a section of the journal Frontiers in Plant Science

Received: *01 December 2021*
Accepted: *07 February 2022*
Published: *02 March 2022*

Citation:
Tian S, Yang Y, Wu T, Luo C, Li X, Zhao X, Xi W, Liu X and Zeng M (2022) Functional Characterization of a Flavone Synthase That Participates in a Kumquat Flavone Metabolon. Front. Plant Sci. 13:826780. doi: 10.3389/fpls.2022.826780

INTRODUCTION

Flavones, one of the largest subclasses of flavonoids, perform various physiological roles in plants, such as participating in responses to biotic and abiotic stresses (Morimoto et al., 1998; Du et al., 2010a,b; Kong et al., 2010; Jiang et al., 2016; Righini et al., 2019). In addition, these metabolites contribute to the internal and external qualities of fruits, herbs, and vegetables by improving their appearance, taste, and nutritional value. Kumquats look like miniature oranges, are consumed worldwide, and contain diverse and abundant bioactive flavonoids. Kumquat extract possesses several health-promoting effects, and these effects are associated with the compositions and

quantities of these flavonoids (Sadek et al., 2009; Barreca et al., 2014; Lou et al., 2015; Nagahama et al., 2015). In contrast to the many other fruits that tend to biosynthesize anthocyanins and flavonols, kumquats and other citrus fruits predominantly accumulate large amounts of flavanones and flavone derivatives (Montanari et al., 1998; Lou et al., 2015; Butelli et al., 2017; Wang Y. et al., 2017; Zhao et al., 2020).

Flavonoid biosynthesis in higher plants initiates from the stepwise condensation of *p*-coumaroyl-coenzyme A (CoA) with three malonyl-CoAs in a reaction catalyzed by chalcone synthase (CHS). This is followed by chalcone cyclization into naringenin by chalcone isomerase (CHI) (Winkel-Shirley, 2001). Flavanone naringenin is a biochemical precursor used for the biosynthesis of many subclasses of flavonoids such as flavonols, anthocyanins, and flavones. The biosynthesis of flavones from flavanones in higher plants is catalyzed by two distinct flavone synthases (FNSs), FNSI and FNSII; FNSII is phylogenetically more widespread than FNSI (Jiang et al., 2016). FNSI, is a member of the Fe^{2+}/2-oxoglutarate-dependent dioxygenase (2-OGDD) family; it directly generates flavones from flavanones. Early research suggested that FNSI enzymes only occurred in the Apiaceae family (Gebhardt et al., 2005, 2007). Later, FNSI enzymes were identified in rice (Lee et al., 2008), *Arabidopsis*, and maize (Falcone Ferreyra et al., 2015), indicating that FNSI is more widely distributed (Jiang et al., 2016). All the functionally characterized FNSII enzymes are derived from the CYP93G subfamily in monocots and from the CYP93B subfamily in dicots. Similar to FNSI enzymes, most FNSII enzymes catalyze the direct conversion of flavanones into flavones through C2,C3-*cis*-desaturation (Martens and Mithofer, 2005). Interestingly, licorice CYP93B1 (Akashi et al., 1998), maize CYP93G5 (Morohashi et al., 2012), *Medicago truncatula* CYP93B10/11 (Zhang et al., 2007), rice CYP92G2 (Du et al., 2010a), and sorghum CYP93G3 (Du et al., 2010b) function as flavanone 2-hydroxylases (F2Hs) by catalyzing the conversion of flavanones into 2-hydroxyflavanones for *C*-glycosylation.

Except for trace amounts of polymethoxylated flavones (PMFs), kumquat flavones predominantly exist as *C*- or *O*-glycosides (Lou et al., 2016; Lou and Ho, 2017; **Figure 1**): *O*-glycosides such as rhoifolin (RHO) and fortunellin (FOR) and *C*-glucosides such as isovitexin, vitexin, vicenin-2 (VIC), 8-*C*-neohesperidosyl apigenin (APN), and margaritene (MAR). The sugar moieties of the *C*-glycosides are directly linked to the basic flavonoid skeleton through their respective carbon atoms. In *O*-glycosides, the sugar moieties are bonded to the hydroxyl groups of flavonoid aglycones. *C*-glycosylation can occur before the formation of the flavone backbone, whereas *O*-glycosylation usually occurs after backbone formation (Martens and Mithofer, 2005; Wu et al., 2016; Wang X. et al., 2017). A kumquat *C*-glycosyltransferase (CGT) utilizes 2-hydroxyflavanones, rather than flavones, as sugar acceptors and produces the corresponding *C*-glucosides (Ito et al., 2017). Therefore, FNSII enzymes might operate through multiple catalytic mechanisms.

The enzymes necessary for flavonoid biosynthesis could form flavonoid metabolons (ordered protein complexes), which are believed to occur in diverse plant species (Hrazdina and Wagner, 1985; Winkel, 2004; Nakayama et al., 2019). Specific protein–protein interactions could regulate the biosynthetic efficiency and spatiotemporal distributions of flavonoids. Metabolons are anchored to the endoplasmic reticulum (ER) membrane; therefore, ER-resident P450 enzymes could serve as anchors for metabolons. The formation of flavonoid metabolons on ER-resident P450 occurs in multiple plants, including rice (Shih et al., 2008), snapdragon, torenia (Fujino et al., 2018), and soybean (Mameda et al., 2018). In soybean roots, 2-hydroxyisoflavanone synthase (a P450 enzyme) can interact with chalcone reductase (CHR) and CHS to form a flavonoid metabolon, in which GmCHR5 is located near CHS to reduce the transit time of the CHR substrate from CHS to CHR (Mameda et al., 2018). In snapdragon and torenia plants, enzymes involved in late-stage anthocyanin biosynthesis interact with FNSII, although FNSII activity was not necessary for anthocyanin biosynthesis (Fujino et al., 2018). Therefore, ER-bound P450s (such as FNSII) are posited as components of flavonoid metabolons.

Considering that FNSII (also including F2H) are the only P450 enzymes involved in the biosynthetic pathway for *O*/*C*-glycosyl flavones in kumquat fruits (**Figure 1**), we hypothesized that they likely play roles in anchoring dynamic flavone metabolons to the ER. According to our model, specific protein–protein interactions modulate the diversity in terms of the accumulation patterns and chemical structures of flavone derivatives. However, no FNSII enzymes have been characterized in kumquat plants; this has limited further study on the regulatory and biosynthetic mechanisms of flavones and their derivatives. Therefore, in this study, we isolated 2 *FNSII* genes (*FcFNSII-1* and *FcFNSII-2*) through RNA-seq analysis. The results of *in vivo*, *in vitro*, and *in planta* experiments indicate that *FcFNSII-2* directly converted flavanones into corresponding flavones, whereas *FcFNSII-1* had no detectable catalytic activity against flavanones. Both *FcFNSII-1* and *FcFNSII-2* localized to the ER; however, only the latter interacted with upstream enzymes in the flavonoid-biosynthesis pathway. These findings imply that FcFNSII-2 might serve as a nucleation site for flavone-metabolon formation, mediating the biosynthesis of *O*-glycosyl flavone and its derivatives in kumquats.

MATERIALS AND METHODS

Plant Materials

"Huapi" kumquat trees (*Fortunella crassifolia*) were grown at the Citrus Research Institute (Chongqing, China). The flowers, young leaves, and young shoots were collected in the spring, and the fruits were collected at different growth stages, including 30, 90, and 150 days after full blooming (DAB). The samples were immediately frozen in liquid nitrogen and stored at −80°C until use.

Isolation and Bioinformatics Analysis of FNSIIs

Total RNA from the fruit peels, flowers, young leaves, and young shoots of "Huapi" trees were extracted using the MiniBEST Plant RNA Extraction Kit (TaKaRa Bio). cDNA was synthesized

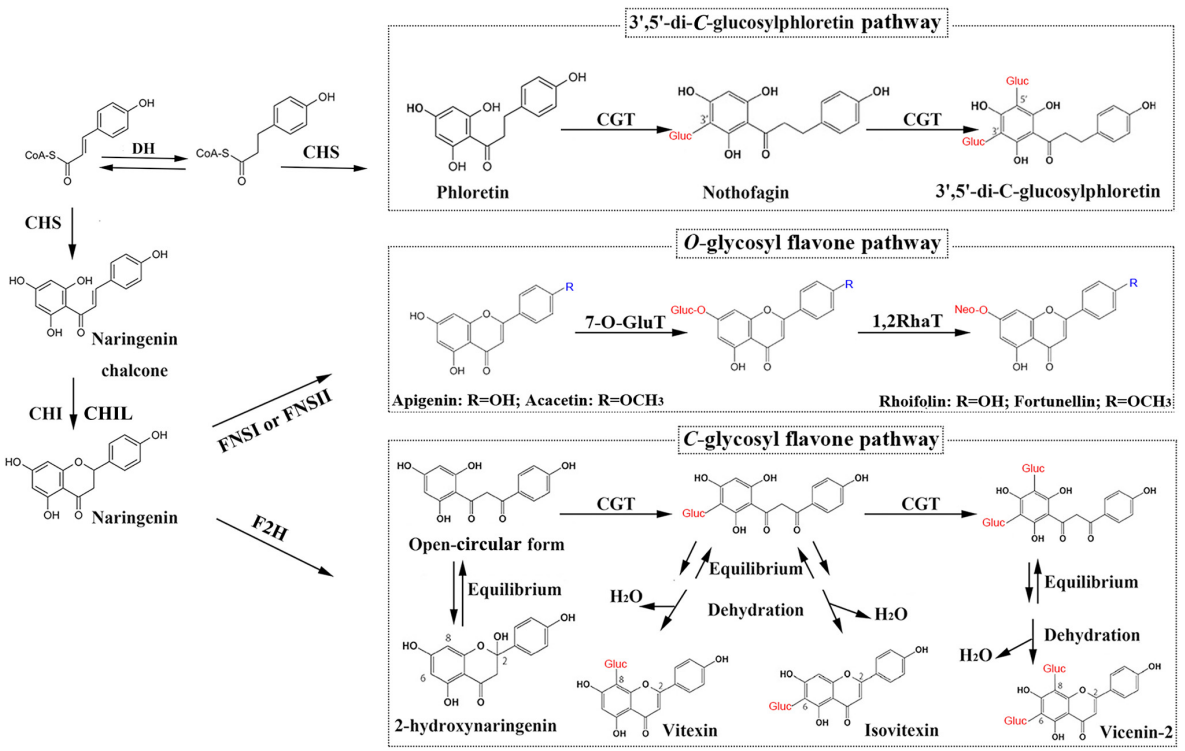

FIGURE 1 | Glycosyl flavone-biosynthesis pathways in kumquat plants. DH, dehydrogenase; CHS, chalcone synthase; CHI, chalcone isomerase; CHIL, chalcone isomerase-like; FNSI, flavone synthase I; FNSII, flavone synthase II; F2H, flavanone 2-hydroxylase; 7-*O*-GluT, flavonoid 7-*O*-glucosyltransferase; 1,2RhaT, 1,2-rhamnosyltransferase; CGT, *C*-glycosyltransferase.

for reverse transcription-polymerase chain reaction (RT-PCR) analyses using the PrimeScript^{TM} Double Strand cDNA Synthesis Kit (TaKaRa Bio). Subsequently, the open-reading frames (ORFs) of different *FcFNSII*s were cloned using PCR and gene-specific primers (**Supplementary Table 1**). A phylogenetic tree of the deduced amino acid (AA) sequences was constructed using the MEGA 6.0 program (Tamura et al., 2013), using the neighbor-joining method.

Quantitative Reverse Transcription-Polymerase Chain Reaction Analysis

Following cDNA synthesis, quantitative PCR was performed using the TB Green® Fast qPCR Mix (TaKaRa, Beijing, China) on a LightCycler 480 real-time system (Roche, Basel, Switzerland). The PCR mix (10 μL) contained 5 μL of 2 × TB Green *Premix Ex Taq* II (Tli RNaseH Plus), 50 ng of cDNA, and 0.4 μM of each primer (**Supplementary Table 1**). The reaction conditions were: 95°C for 30 s, followed by 35 cycles at 95°C for 5 s, 56–58°C for 10 s, and 72°C for 25 s. *Actin* was used as the internal reference gene for normalizing the Quantitative PCR data. The relative transcript levels were calculated using the $2^{-\Delta\Delta Ct}$ method. Three biological replicates were analyzed for each gene. The sequences of the primers are included in **Supplementary Table 1**.

Yeast Expression of Recombinant Proteins and Enzyme Assays

Yeast expression and *in vivo* yeast assays was performed according to previous studies (Lam et al., 2014; Wu et al., 2016; Righini et al., 2019), with several minor modifications. The ORF of each *FcFNSII*s were ligated directly into the yeast expression vector, pESC-HIS (to replace the FLAG epitope) and expressed under the control of the GAL10 promoter. Unless otherwise specified, all recombinant vectors were constructed following a seamless cloning strategy (ClonExpress Ultra One Step Cloning Kit, Vazyme, China). All recombinant plastids and the empty vector (negative control) were separately introduced into the *Saccharomyces cerevisiae* strain WAT11. Briefly, yeast cultures were grown overnight at 30°C in liquid synthetic dextrose minimal medium lacking histidine; they were collected through centrifugation and diluted to an optical density (at 600 nm: OD_{600}) of 1.0 in induction medium (synthetic galactose minimal medium). After inducing protein expression for 6 h, the substrate naringenin or isosakuranetin was added to a final concentration of 0.2 mM. Prior to addition, the flavanone substrates were dissolved in dimethyl sulfoxide (DMSO). After a 24 h incubation, the reactions were terminated by extraction with ethyl acetate, evaporated under nitrogen gas, and dissolved in 200 μL of 80% methanol for ultra-high performance liquid chromatography-quadrupole time-of-flight mass spectrometry (UPLC-Q-TOF-MS) analysis.

Yeast microsomes were extracted from the transformed cells, as described previously (Lam et al., 2014; Wu et al., 2016). The microsomal proteins were quantified using the Bradford Protein Assay (TransGen Biotech, Beijing, China). The enzyme activities were assayed at 30°C for 1 h in 100 mM Tris/HCl buffer (pH 7.0) containing 200 μg of microsome protein, 1 mM NADPH, 1 mM diethyl dithiocarbamate, 1 mM dithiothreitol, and appropriate amounts of substrate dissolved in DMSO. Optimal reactions were tested with the substrate naringenin (200 μM) at varying temperatures (20–70°C, 5°C increments) and pH values (5.0–9.0, 0.5 increments). The pH values were controlled using different buffers, such as acidic sodium citrate buffer (pH 5.0–6.5) and Tris/HCl buffer (pH 7.0–9.0). Different concentrations of the substrates, naringenin and isosakuranetin (0.2, 0.4, 0.8, 1.6, 3.2, 6.4, 12.8, 25.6, and 50 μM) were used to determine the kinetic parameters. Km and Vmax values were obtained using the Michaelis–Menten kinetics equation and non-linear regression analysis with GraphPad Prism 9 (GraphPad Software, La Jolla, CA, United States).

Transient Overexpression Assay in Kumquat Peel Tissue

The transient overexpression assay was performed, as described previously (Wang F. et al., 2017; Gong et al., 2021; Zhao et al., 2021), with minor modifications. The ORF of each *FcFNSII* gene was inserted into the pBI121 vector using a seamless cloning strategy to generate the constructs. All constructs and the empty vector were separately introduced into the *Agrobacterium* strain, EHA105. The EHA105 strain was cultivated in liquid LB medium at 28°C; the cells were collected through centrifugation, and diluted to an OD_{600} of 0.8 in infiltration medium containing 0.05 M MES, 2 mM Na_3PO_4, 0.5% D-glucose, and 0.1 mM acetosyringone. The suspensions were injected into the peels of kumquat fruits (150 DAB). The injected fruits were maintained in the dark for 24 h and then under a long photoperiod (16 h light and 8 h dark) for 4 days. Flavonoid components were extracted, as described previously (Liu et al., 2018, 2020).

Flavonoid Extraction and Ultra-High Performance Liquid Chromatography-Quadrupole Time-of-Flight-Mass Spectrometry Conditions

Filtered samples from enzyme assays and tissue sample extracts were separated on an ACQUITY UPLC BEH C18 column (2.1 × 100 mm, 1.7 μm, United Kingdom) connected to an ACQUITY UPLC I-Class PLUS System (Waters, Milford, MA). The mobile phases, consisting of 0.01% formic acid solution (A) and methanol (B) were used at a flow rate of 0.4 $mL{\cdot}min^{-1}$, with the following gradient program: 0–0.6 min, 90–80% A; 0.6–5 min, 80–30% A; 5–7 min, 30–10% A; and 7–8 min, 10–90% A. A photodiode-array detector was used to scan from 240 nm to 400 nm. A Xevo G2-S Q-TOF instrument (Waters MS Technologies, Manchester, United Kingdom) was used with an ESI source that was set from a mass: charge (m/z) ratio of 100–1,000. Data were collected in real time (scan time, 0.5 s; interval, 15 s) and processed using Waters UNIFI 1.7 software.

Subcellular-Localization Assay

The full-length ORFs of *FcFNSII*s and their partial segments were used for subcellular-localization assays. These sequences (which lacked a stop codon) were separately ligated into the pBWA(V)HS-GLosgfp vector (BioRun, Wuhan, China) in frame with the 5′ end of the coding sequence of green fluorescent protein (GFP) to create different fusion constructs (i.e., 35S::FcFNSII-1/2-GFP, 35S::nFcFNSII-1/2-GFP, and 35S::delFcFNSII-1/2-GFP). The red fluorescent protein (RFP) gene was fused with the ER localization sequence (MKTNLFLFLFLIFSLLLSLSSAEF) and used as an ER-localization marker. The fusion constructs were co-transformed into tobacco leaves (*Nicotiana benthamiana*), along with the ER-localization marker, through *Agrobacteria*-mediated infiltration. Following transformation, the tobacco leaves were maintained at 25°C under a long photoperiod (16 h light and 8 h dark) for at least 48 h. The fluorescence signals were detected using an LSM 700 confocal microscope (Zeiss).

Protein–Protein Interaction Assays

A split-ubiquitin yeast two-hybrid system (SU-YTH) in the DUAL membrane Kit 3 (Dualsystems Biotech, Zurich, Switzerland) was employed to test the potential interactions between FcFNSIIs and the upstream enzymes (i.e., FcCHS1, FcCHS2, FcCHI, and FcCHIL) in the flavonoid pathway. The interactions were assessed, as previously described (Waki et al., 2016; Fujino et al., 2018). Briefly, the ORF of FcFNSII-1 or FcFNSII-2 (without a translation-termination codon) was inserted into the *Sfi*I sites of the pBT3-SUC vector to express a recombinant protein with an N-terminal SUC peptide and a C-terminal Cub-LexA-VP16 protein, i.e., SUC-FcFNSII-1-Cub-LexA-VP16 or SUC-FcFNSII-2-Cub-LexA-VP16. The SUC peptide is a 19-residue signal peptide of yeast invertase (Suc2p). Cub-LexA-VP16 is a chimeric protein between the C-terminus of ubiquitin (Cub) and an artificial transcription factor (LexA-VP16). For upstream enzymes (referred to as X) involved in the flavonoid pathway, each of their ORFs was ligated into the *Sfi*I sites of the pPR3-N vector to generate recombinant proteins with a mutated N-terminal half of ubiquitin (NubG), i.e., NubG-X.

NMY51 yeast cells (Weidi Biotech, Shanghai, China) were transformed with one of the following pairs of plasmids (pBT3-SUC-FcFNSII-1/2-Cub-LexA-VP16 and pPR3-NubG-X; pBT3-SUC-FcFNSII-1/2-Cub-LexA-VP16 and pOst1-NubI as a positive control; pBT3-SUC-FcFNSII-1/2-Cub-LexA-VP16 and pPR3-NubG as a negative control). pOst1-NubI expresses a fusion protein comprising the yeast resident ER protein Ost1 and the wild-type N-terminal half of yeast ubiquitin (NubI). The transformed yeast cells were grown on synthetic dropout (SD) agar medium lacking tryptophan and leucine (SD/-WL), transferred to liquid SD/-WL medium, and cultured with agitation at 220 rotations/min for 12–16 h at 30°C. The cells were collected through centrifugation and diluted in ddH_2O to an

OD_{600} of 1.0. Five microliters of the yeast suspension, with five-fold serial dilutions in ddH_2O, were grown on SD/-WL, SD/-WL lacking histidine (SD/-WLH), SD/-WLH lacking adenine (SD/-WLHAde), or SD/-WLHAde containing 1 mM 3-aminotriazole (SD/-WLHAde + AT). The cells were maintained at 30°C for approximately 3–4 days.

Bimolecular Fluorescence Complementation Assay

For bimolecular fluorescence complementation assay (BiFC) analysis (Walter et al., 2004; Huang et al., 2015), the ORF of *FcFNSII-2* was cloned into the pSPYNE-35S vector (MiaoLing Plasmid Sharing Platform, Wuhan, China), containing the N-terminal sequence of yellow fluorescent protein (nYFP, AAs 1–174) to create the 35S::FcFNSII-2-nYFP fusion construct. In addition, each of three cytoplasmic flavonoid enzymes was recombined into the destination vector pSPYCE-35S (MiaoLing Plasmid Sharing Platform, Wuhan, China) containing the C-terminus of YFP (cYFP, AAs 175–239; i.e., 35S::FcCHS1/2/FcCHIL-cYFP). Tobacco leaves were co-infiltrated with an EHA105 strain harboring fusions containing the nYFP and cYFP fragments (Sparkes et al., 2006). YFP fluorescence was detected after 48 h to study subcellular localization.

Accession Numbers

Sequence data for FcFNSII-1 (accession number sjg260860.1) and FcFNSII-2 (sjg260830.1) can be found at CPBD[1].

RESULTS

Identification and Sequence Analysis of Flavone Synthase II Homologs

TBLASTN (*E*-value < $1e^{-5}$), using functionally characterized FNSIIs or F2Hs as queries against *Fortunella hindsii* genome[1] and transcriptome (Zhu et al., 2019), identified many candidate genes. The AA sequence identity between the candidates and functionally characterized FSNIIs and F2Hs was low; therefore, it was difficult to identify the genuine F2Hs or FNSIIs among the candidates. We used transcriptome co-expression analyses to screen target genes. Based on transcriptome analysis of "Hongkong" kumquat (*F. hindsii*), generated from 13 different tissues from five organs (Zhu et al., 2019), two *FNSII* homologs were identified. Their expression was positively correlated with the expression levels of upstream genes in the flavonoid-biosynthesis pathway, such as *CHS1*, *CHS2*, *CHI*, and chalcone isomerase-like (*CHIL*) (Pearson's correlation coefficient; between *FcFNSII-1* and flavonoid biosynthetic genes was >0.7 and between *FcFNSII-2* and flavonoid biosynthetic genes >0.6) (**Figure 2A**). The ORFs of the two *FNSII* homologs (*FcFNSII-1* and *FcFNSII-2*) were cloned through RT-PCR-based amplification from "Huapi" kumquat, a close relative of the "Hongkong" kumquat cultivar. The ORFs of *FcFNSII-1* and *FcFNSII-2* were 1542 and 1557 base pairs in length, encoding 513 and 518 amino acids with molecular weights (MWs) of 58.31 and 58.48 kDa, respectively. Sequence alignment revealed that both the FcFNSII-1 and FcFNSII-2 proteins harbor signature P450 motifs, such as a heme-binding motif and a Pro hinge region (**Supplementary Figure 1**). The phylogenetic analysis revealed that the proteins could be divided into two major groups (FSNIIs and F2Hs; **Figure 2B**). FcFNSII-1 and FcFNSII-2 clustered with members of the FNSII clade, which commonly catalyze the direct conversion of flavanones to flavones.

We analyzed the correlations between the accumulation of flavone derivatives and the expression patterns of *FcFNSII-1* and *FcFNSII-2* in different tissues including flowers, young leaves, young shoots, and fruit peels at 30, 90, and 150 DAB. Five flavone derivatives could be quantified in the different tissues of "Huapi" kumquats, including two *O*-glycosyl flavones (RHO and FOR) (**Supplementary Figures 2A, 3**) and three *C*-glycosyl flavones (APN, VIC, and MAR) (**Supplementary Figures 2B, 3**). The contents of *O*-glycosyl flavones in the peels at 30 DAB were higher than those in the other tissues and stages; *C*-glycosyl flavones showed preferential accumulation in flowers and in young leaves. Quantitative PCR was used to compare the spatiotemporal expression patterns of *FcFNSII*s (**Supplementary Figure 2C**) with the spatiotemporal-accumulation patterns of different flavone derivatives. The *FcFNSII-1* and *FcFNSII-2* transcripts were preferentially expressed in peels of fruits at 30 DAB, where the levels of *O*-glycosyl flavones were relatively high.

In vivo and *vitro* Enzyme-Activity Assays for FcFNSIIs

To examine the catalytic functions of both the *FcFNSII* genes, the ORF of each sequence was subcloned into the pESC-HIS vector and transformed into the WAT11 yeast strain. WAT11 cells express an *Arabidopsis* ATR1 P450 reductase that provides reducing equivalents to plant P450s, such as the FNSII enzymes. The transformed yeast cultures were incubated with naringenin or isosakuranetin. These two flavanones are the predominant precursors for the biosynthesis of flavone derivatives, such as RHO, FOR, isovitexin, vitexin, VIC, and MAR that are naturally present in kumquat fruits (**Figure 1**). After incubation for 24 h, yeast cells expressing *FcFNSII-2* metabolized naringenin and isosakuranetin to apigenin and acacetin, respectively (**Figures 3A,B**), whereas *FcFNSII-1* showed no detectable catalytic activities against naringenin and isosakuranetin. Control cells harboring the empty vector did not produce any detectable apigenin and acacetin. The reaction products were detected using UPLC-Q-TOF-MS; their retention times and mass-fragmentation patterns were compared with those of authentic standards.

To gain further insight into the enzymatic properties of FcFNSII-2, microsomes were extracted from the transformed yeast cells and assayed for their enzymatic activities on flavanone substrates in Tris/HCl buffer supplemented with NADPH (which supplied reducing equivalents for P450). After incubation for 1 h, the reaction products were extracted and analyzed using UPLC-Q-TOF-MS. Changing the pH or temperature strongly

[1]http://citrus.hzau.edu.cn/index.php/

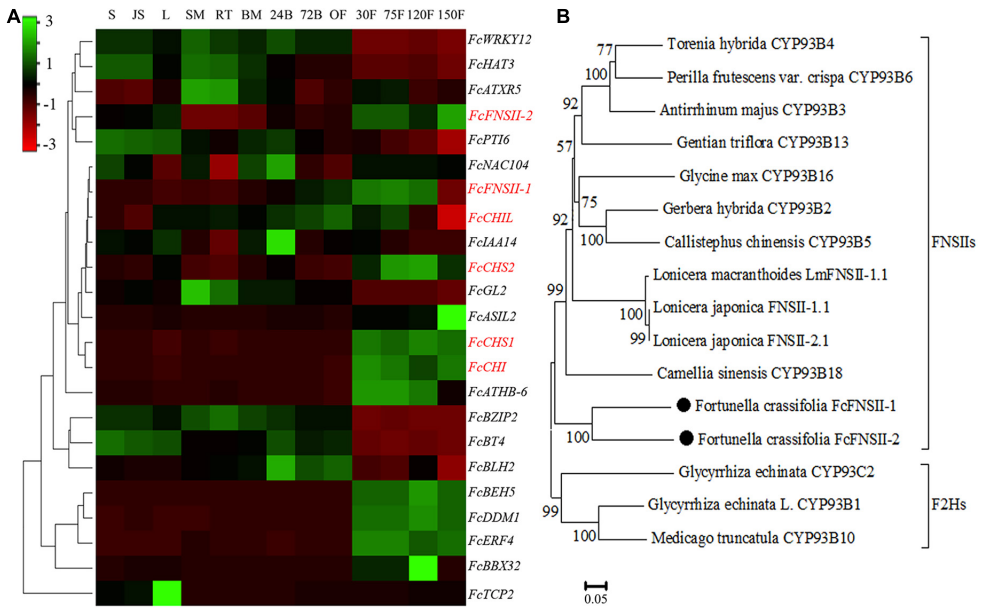

FIGURE 2 | Identification of potential *FNSII* genes. **(A)** Heat map of the expression patterns of flavonoid biosynthesis-related genes using transcriptome data from 13 tissues of five organs. The color scale in the upper left corner represents $\log_2$-transformed counts normalized to the fragments per kilobase of transcript per million mapped reads. S, seed; JS, seedling; L, leaf; SM, stem; RT, root; BM, bud meristem; 24B, 24-h flower bud; 72B, 72-h flower bud; OF, opened flower; 30F, 30-day fruitlet; 75F, 75-day fruitlet; 120F, yellow-mature fruit (about 120 days); 150F, red-mature fruit (about 150 days). **(B)** A phylogenetic tree of FcFNSII-1, FcFNSII-2, and other functionally characterized FSNIIs and F2Hs was constructed using the neighbor-joining method with MEGA 6.0. The numbers at the nodes represent the bootstrap values from 1,000 replicates.

affected the activities of the recombinant enzymes; they exhibited maximum activity at pH 7.0∼7.5 and a temperature of 30∼35°C (**Supplementary Figure 4**). Under these optimized conditions, the kinetic parameters of FcFNSII-2 were determined. The Km and Vmax for naringenin were 3.77 μM and 12.33 fkat mg^{-1}, and those for isosakuranetin were 2.10 μM and 9.63 fkat mg^{-1}, respectively (**Figure 3C**). The relatively higher Vmax: Km ratio for isosakuranetin suggested that it was slightly more preferred than naringenin as an *in vitro* substrate for FcFNSII-2.

In planta Enzyme Assays of Recombinant FcFNSIIs

To further understand the metabolic functions of *FcFNSII*s *in planta*, we transiently overexpressed them in the peels of kumquat fruits at 150 DAB (**Figure 4A**), as done previously with success in citrus plants (Wang F. et al., 2017; Gong et al., 2021; Zhao et al., 2021). Gene-transcript levels at the injected sites were determined using quantitative PCR (**Figure 4B**). Compared to that in the control, the transcript levels of *FcFNSII-1* and *FcFNSII-2* were significantly higher at the corresponding injection sites. *FcFNSII-2* overexpression significantly enhanced the expression of *FcCHS1*, *FcCHS2*, *FcCHI*, and *FcCHIL* genes; however, *FcFNSII-1* overexpression did not significant affect the expression of these flavonoid-related genes. *CHS*, *CHI*, and *CHIL* are key enzymes in the early biosynthetic pathway of flavonoids, and their expression levels are closely related to flavonoid accumulation.

To confirm the flavonoid accumulation-enhancing function of *FcFNSII*s in kumquats, the main flavonoids were analyzed and quantified using UPLC-Q-TOF-MS at the injected sites. The three flavonoids, 3′,5′-di-*C*-β-glucopyranosylphloretin (DCGP), RHO, and FOR, showed differential accumulation between the control and pBI121-FcFNSII-2 vector-injected sites (**Figure 4C** and **Supplementary Figure 3**). The amounts of DCGP decreased significantly at the pBI121-FcFNSII-2 injected sites; however, those of RHO and FOR increased significantly. These changes were associated with the elevated levels of *FcFNSII-2* and other flavonoid-related genes. *FcFNSII-1* overexpression did not influence the flavonoid contents, as expected. Taken together, the results of *in vivo*, *in vitro*, and *in planta* experiments demonstrated that *FcFNSII-2* can directly convert flavanones into the corresponding flavones.

Subcellular Localization

The two FcFNSIIs were predicted to harbor an N-terminal membrane-spanning domain (NMSD) spanning AAs 1–27 (**Supplementary Figure 5**), which anchors the P450s to the ER. The subcellular localizations of FcFNSII-1 and FcFNSII-2 were investigated by overexpressing C-terminally tagged GFP fusion proteins (FcFNSII-1-GFP and FcFNSII-2-GFP) to avoid interference with the NMSD. In tobacco leaf epidermal cells, the fluorescent signals of the fusion proteins were in the pattern of a network, which is consistent with the fluorescent signals specific to the ER (red color; **Figure 5**), suggesting that both FcFNSII-1 and FcFNSII-2 are localized to the

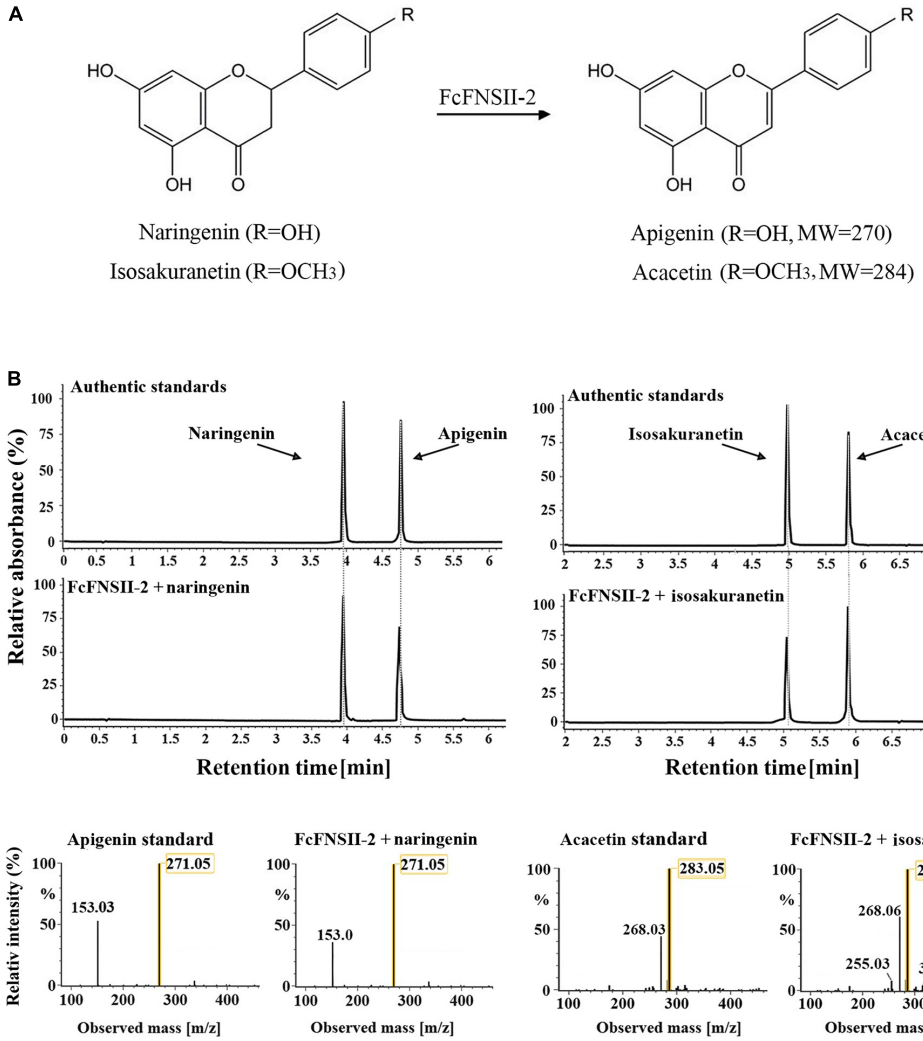

C

	Substrate	*Km* (μM)	*Vmax* (fkat mg^{-1})	*Vmax*/*Km*
FcFNSII-2	Naringenin	3.77 (0.46)	12.33 (0.98)	3.27 (0.27)
	Isosakuranetin	2.10 (0.33)	9.63 (0.46)	4.58 (0.39)

FcFNSII-2 activities were assayed under optimized conditions. The data shown are presented as the means of triplicate experiments, and standard error (SE) values are shown in the parentheses.

FIGURE 3 | UPLC-Q-TOF-MS analysis of the reaction products of FcFNSIIs, as determined by performing *in vivo* enzyme-activity assays. **(A)** The schematic diagram represents the catalytic mechanism of FcFNSII-2. **(B)** *In vivo* enzymatic assays performed with recombinant FcFNSII-2. The assays were conducted using naringenin and isosakuranetin as substrates. The mass spectra of apigenin and acacetin standards and the reaction products produced by incubation with FcFNSII-2. **(C)** *In vitro* kinetic parameters of recombinant FcFNSII-2 were determined using yeast microsome extracts.

ER, consistent with the localization of P450s. To examine whether this NMSD actually targeted FcFNSIIs to the ER, the NMSDs were expressed as GFP-labeled fusions (nFcFNSII-1-GFP and nFcFNSII-2-GFP); the localization pattern was consistent with the previously observed pattern. When FcFNSII-1 and FcFNSII-2 lacking the predicted NMSD were expressed as GFP-labeled fusions (delFcFNSII-1-GFP and delFcFNSII-2-GFP), the previously observed localization pattern was disrupted (**Figure 5**). Collectively, these results indicate that the predicted NMSD was necessary and essential for ER localization.

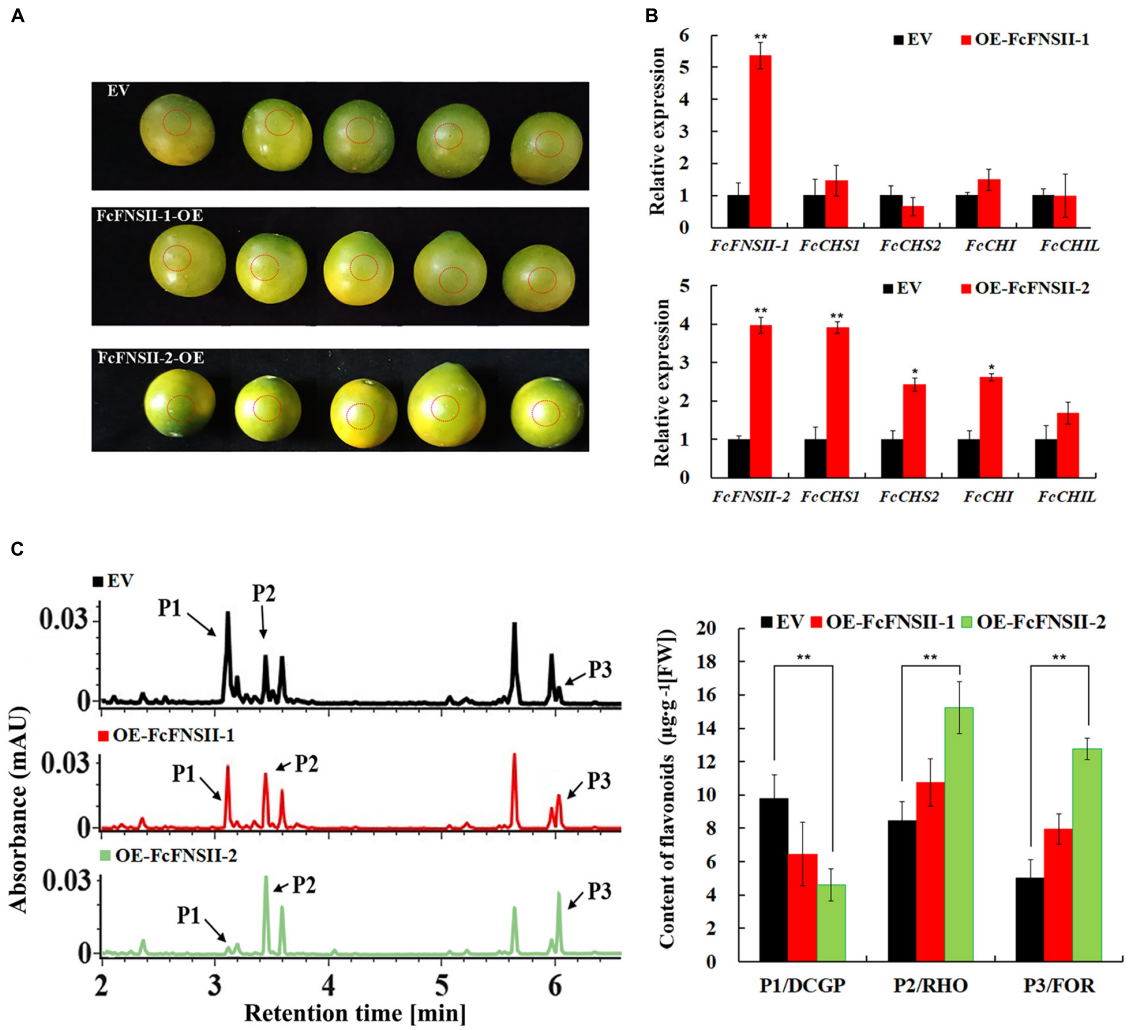

FIGURE 4 | Transient over-expression of *FcFNSII*s in kumquat peels. **(A)** Harvested mature green fruits were infiltrated with pBI121 [empty vector (EV)] and pBI121-*FcFNSII*s (OE) in a climate-controlled chamber. The injection sites were circled by red dotted lines, where the peels were used to analyze gene-expression levels and flavonoid contents. **(B)** Expression of *FcFNSII*s and flavonoid biosynthesis-related genes in kumquat peels at 5 days after injection. **(C)** Measurements of flavonoids in kumquat peels at 5 days after injection. RHO, rhoifolin; FOR, fortunellin; DCGP, 3′,5′-di-C-β-glucopyranosylphloretin; FW, fresh weight. The data are presented as mean ± SE of five independent replicates. Asterisks indicate significant differences (*$P < 0.05$; **$P < 0.01$).

Involvement of FcFNSIIs in the Flavone Metabolon

The flavonoid-synthesizing enzymes in plants associate with the cytoplasmic surface of the ER to form metabolons, which is commonly mediated by ER-bound P450 (Shih et al., 2008; Waki et al., 2016; Fujino et al., 2018; Mameda et al., 2018). To examine whether FcFNSIIs interact with the upstream enzymes in the flavonoid pathway to form a complex, interactions between FcFNSII-1/FcFNSII-2 and CHS1, CHS2, CHI, and CHIL were analyzed using SUYTH. Considering that FcFNSII enzymes contain an NMSD that locates them to the ER membrane, we designed SUC FcFNSII-Cub-LexA-VP16 constructs to ensure the NMSDs of both P450 proteins could be anchored to membranes. The yeast-growth results indicated that FcFNSII-2 interacted with FcCHS1, FcCHS2, and CHIL. No appreciable yeast growth was observed when interactions between FcFNSII-2 and CHI enzymes were assayed (**Figure 6**). In addition, no apparent interaction occurred between FcFNSII-1 and these enzymes (**Supplementary Figure 6**).

The binary protein-protein interactions between FcFNSII-2 and FcCHS1, FcCHS2, or FcCHIL were further examined *in planta* using BiFC assays. FcFNSII-2 was fused to the N-terminal end of a split YFP fragment (FcFNSII-2-nYFP) to preserve the ER-anchoring capacity, and other three enzymes were separately linked with a C-terminal split YFP fragment (FcCHS1-cYFP, FcCHS2-cYFP, or FcCHIL-cYFP). When FcFNSII-2-nYFP was transiently co-expressed with FcCHS1-cYFP, FcCHS2-cYFP, or FcCHIL-cYFP in tobacco leaf epidermal cells, the transformed cells generated yellow

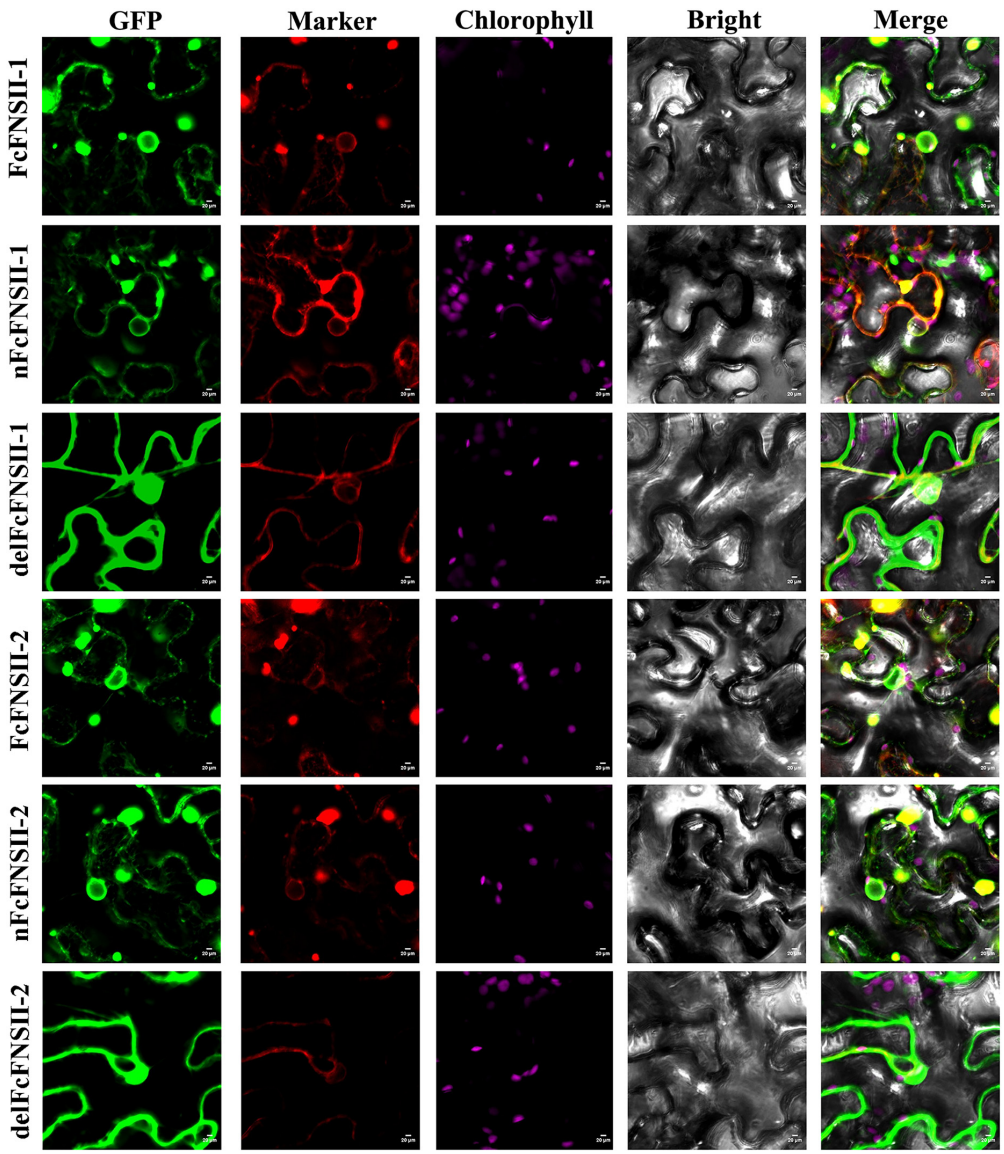

FIGURE 5 | Subcellular localization of FcFNSIIs. Tobacco cells were transformed with vectors expressing different fusion constructs (FcFNSII-1-GFP, nFcFNSII-1-GFP, FcFNSII-2-GFP, or nFcFNSII-2-GFP) in combination with an ER-GFP marker. nFcFNSII-1-GFP and nFcFNSII-2-GFP comprise the first 27 residues of FcFNSII-1 and FcFNSII-2 fused to GFP, respectively. Co-localization of the fluorescent signals is apparent in the merged images, indicating that FcFNSII-1 and FcFNSII-2 localized to the ER. When tobacco leaves were transformed with delFcFNSII-1 (the remaining part of FcFNSII-1, AAs 28–513) fused to GFP or delFcFNSII-2 (AAs 28–518)-GFP in combination with a nucleocytosolic marker, fluorescent signals were detected in both the nucleus and the cytoplasm. Scale bars = 20 mm.

fluorescence signals (**Figure 7**), indicating that FcFNSII-2 interacted with FcCHS1, FcCHS2, and FcCHIL *in planta*.

DISCUSSION

The stepwise catalytic reactions of CHS and CHI drive carbon flow from the phenylpropanoid pathway toward the flavanone-biosynthesis pathways; these drive the formation of different subclasses of flavonoids. Functional loss of *Ruby* gene (which encodes a MYB transcription factor) caused by a single-nucleotide insertion that resulted in a frame-shift mutation abolished anthocyanin biosynthesis in kumquat plants (Butelli et al., 2017; Huang et al., 2018). Therefore, flavone-derived metabolites are one of the predominant flavonoids synthesized in kumquats. Flavone biosynthesis from flavanones was catalyzed by either FNSI or FNSII, which resulted in a C2–C3 double bond in the C-ring (Martens and Mithofer, 2005; Lee et al., 2008; Han et al., 2014; Lam et al., 2017).

Here, we investigated the activities of two kumquat FNSII homologs by transiently overexpressing the recombinant

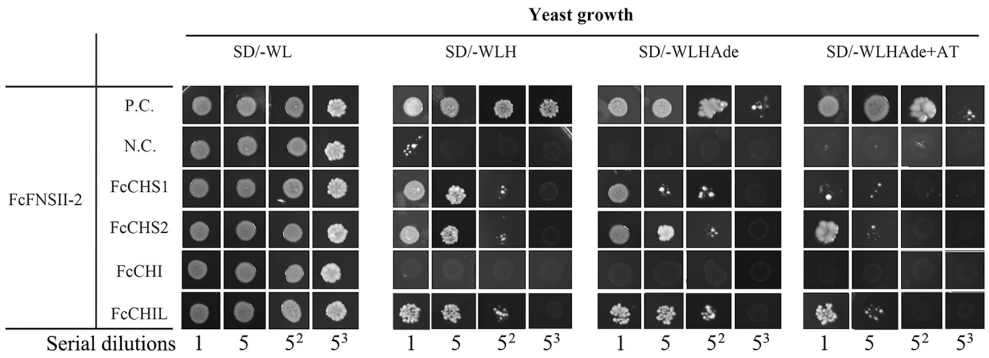

FIGURE 6 | Interactions between FcFNSII-2 and upstream enzymes in the flavonoid pathway were assayed using a split-ubiquitin system. Yeast cells co-expressing SUC-FcFNSII-2-Cub-LexAVP16 with NubG fused to FcCHS1, FcCHS2, FcCHI, or FcCHIL. P.C. and N.C. refer to the positive control and negative control, respectively. For interactions between FcFNSII-1 and upstream enzymes, see **Supplementary Figure 6**.

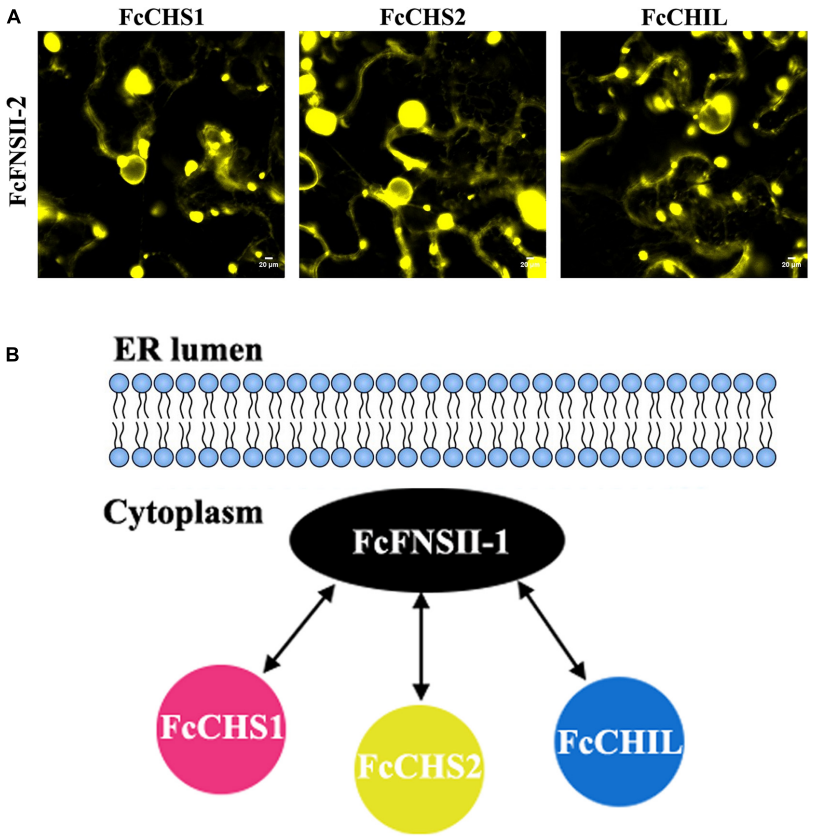

FIGURE 7 | Detecting binary interactions between FcFNSII-2 and FcCHS1, FcCHS2, or FcCHIL by performing BiFC assays. **(A)** FcFNSII-2-nYFP was co-expressed with FcCHS1-cYFP, FcCHS2-cYFP, or FcCHIL-cYFP in tobacco leaf cells. Scale bars = 20 μm. **(B)** A suggested model of protein–protein interactions between FcFNSII-2 and FcCHS1, FcCHS2, or FcCHIL. FcFNSII-2 serves as a component of the kumquat flavone metabolon. Scale bars = 20 μm.

enzymes in kumquat peels and performing enzyme assays (**Figures 3**, **4**). The catalytic activity of FcFNSII-2 was similar to that of gentian and soybean FNSII; it was capable of directly producing flavones from flavanones in yeast assays. FcFNSII-1 did not lead to flavone accumulation. Consistently, overexpressing *FcFNSII-2* in kumquats enhanced accumulation of the *O*-glycosyl flavones, RHO and FOR, which are naturally present in kumquat fruits. In licorice, flavones are synthesized from 2-hydroxyflavanones generated by GeFNSII, which functions as an F2H (Akashi et al., 1998). However, this catalytic activity could not be assigned to FcFNSII-2 due to the lack of 2-hydroxyflavanones accumulation, both *in vivo* and *in vitro*.

Further studies are required to determine the involvement of *FcFNSII-1* in flavonoid biosynthesis. In addition, prior to functional characterization, the expression of FcFNSII-1 in yeast and plants should be verified. The success of P450 expression depends on factors such as the expression vectors, posttranslational modifications, compatibility with the host, and coupling efficiency with CPR.

Most flavones in kumquat fruits are predominantly present as *C*- or *O*-glycosides. Flavone *O*-glycosylation occurs after the flavone backbones are generated by FNSI and/or FNSII. To synthesize *C*-glycosyl flavones, flavanones are first converted into 2-hydroxyflavanones by F2Hs, the open-circular forms of which are subsequently *C*-glycosylated by CGTs, followed by dehydration to generate the corresponding *C*-glycosyl flavones (Brazier-Hicks et al., 2009; Du et al., 2010b; Falcone Ferreyra et al., 2013; Ito et al., 2017). Thus, two catalytic mechanisms for FNSII enzymes might exist in kumquat plants. F2H (CYP93G2) and FNSII (CYP93G1) enzymes are present in rice (Du et al., 2010a; Lam et al., 2014). The former channels flavanones to 2-hydroxyflavanones, which is a substrate for *C*-glycosylation by OsCGT (Brazier-Hicks et al., 2009; Du et al., 2010a). The latter converts flavanones to flavones for the biosynthesis of different tricin *O*-linked conjugates. CYP93G1 and CYP93G2 are key branch-point enzymes that compete for channeling flavanone substrates to flavones or 2-hydroxyflavanones, respectively. In this study, we observed such competition; the transient *FcFNSII-2* overexpression significantly elevated the levels of *O*-glycosyl flavones (RHO and FOR) and reduced the level of flavonoid *C*-glycoside (DCGP) (**Figure 4**). An intriguing question elicited by our findings is why DCGP has a significant reduction, but not *C*-glycosyl flavones. We speculated that the DCGP content is much higher than that of *C*-glycosyl flavones in kumquat peels. Consequently, When *FcFNSII-2* was overexpressed, the change in the amount of DCGP was easily discernable. However, owing to the low basal levels of *C*-glycosyl flavones, the changes in their levels were not obvious.

By expressing fusion constructs in tobacco leaf epidermis cells, we demonstrated that FcFNSII-1 and FcFNSII-2 were anchored to the ER (**Figure 5**). Several P450s involved in flavonoid biosynthesis play roles in lodging their respective metabolons to the cytoplasmic surface of the ER (Waki et al., 2016; Fujino et al., 2018; Mameda et al., 2018). In rice, protein–protein interaction analyses revealed that CHS1 interacted with flavonoid 3′-hydroxylase, flavanone 3-hydroxylase, dihydroflavonol 4-reductase, and anthocyanidin synthase 1, functioning as a platform for generating a flavonoid metabolon (Shih et al., 2008). This metabolon could be anchored to the ER via the ER-bound flavonoid 3′-hydroxylase. Soybean isoflavonoids are biosynthesized through the formation of dynamic metabolons anchored to the ER *via* two P450s, i.e., cinnamate 4-hydroxylase and 2-hydroxyisoflavanone synthase (Fliegmann et al., 2010; Dastmalchi et al., 2016; Waki et al., 2016; Mameda et al., 2018). Additionally, in snapdragon and torenia plants, ER-bound FNSII is a component of flavonoid metabolons (Fujino et al., 2018).

The protein–protein interaction studies (based on the SUYTH system and BiFC assays, **Figures 6, 7A** and **Supplementary Figure 6**) demonstrated that ER-bound FcFNSII-2 was a component of the flavone metabolon and that it closely interacted with three upstream enzymes in flavonoid pathways, i.e., FcCHS1, FcCHS2, and FcCHIL (**Figure 7B**). Additionally, considering that FcFNSII-2 was preferentially expressed in young fruit peels (**Supplementary Figure 2C**), we speculate that this ER-bound metabolon likely plays a key role in biosynthesizing fruit-specific *O*-glycosyl flavones.

CONCLUSION

We characterized a kumquat type II FNS (FcFNSII-2) that catalyzes the direct conversion of flavanones to flavones. *In vivo* and *vitro* assays showed that it could directly synthesize apigenin and acacetin from naringenin and isosakuranetin, respectively. Moreover, transient *FcFNSII-2* overexpression enhanced the transcription of structural genes in the flavonoid-biosynthesis pathway and drove the accumulation of different *O*-glycosyl flavones that are naturally present in kumquats. Subcellular-localization analyses and protein–protein interaction assays revealed that FcFNSII-2 was anchored to the ER and that it interacted with CHS1, CHS2, and CHIL. Our results provide strong evidence that FcFNSII-2 serves as a nucleation site for the *O*-glycosyl flavone metabolon that channels flavanones toward the biosynthesis of *O*-glycosyl flavones in kumquat fruits. These results would be useful for engineering the pathway to improve the composition of bioactive flavonoids in kumquat fruits.

DATA AVAILABILITY STATEMENT

The datasets presented in this study can be found in online repositories. The names of the repository/repositories and accession number(s) can be found in the article/**Supplementary Material**.

AUTHOR CONTRIBUTIONS

XGL and MZ designed the study. XGL, ST, and WX wrote the manuscript. ST, YY, CL, and XL performed the experiments. ST, YY, and XZ contributed to analyzing the results. All authors reviewed the manuscript.

FUNDING

This work was supported by the National Natural Science Foundation of China (grant number 31600235), Earmarked Fund for Modern Agro-Industry Technology Research System (grant number nycytx-29-34), and Natural Science Foundation Project of China SWU (grant number SWU116016).

ACKNOWLEDGMENTS

We would like to thank Editage (www.editage.cn) for English language editing.

SUPPLEMENTARY MATERIAL

The Supplementary Material for this article can be found online at: https://www.frontiersin.org/articles/10.3389/fpls.2022.826780/full#supplementary-material

Supplementary Figure 1 | AA sequence alignment of FcFNSIIs with FNSII from other plants, comprising GhCYP93B2 of *Gerbera hybrida* (NCBI accession number AF156976), ThCYP93B4 of *Torenia hybrida* (AB028152), CsCYP93B18 of *Camellia sinensis* (FJ169499.1), LmFNSII-1.1 of *Lonicera macranthoides* (KU127580), LjFNSII-1.1 and LjFNSII-2.1 of *Lonicera japonica* (KU127576 and KU127578, respectively). The conserved motifs among P450s are boxed, including a region proline-rich membrane hinge (L/S/PPPS/G/TP), an I-helix (T/A/GAG/ATDTS/TA/S), a K-helix consensus sequence (KES/A/T/IL/FR), the PE/HRF consensus sequence, and a heme-binding domain (PFGS/TGRRG/A/SCPG).

Supplementary Figure 2 | *O*/*C*-glycosyl flavone contents and *FcFNSII*-expression levels in kumquats. **(A)** Contents of *O*-glycosyl flavones in different kumquat tissues. RHO, rhoifolin; FOR, fortunellin; **(B)** Contents of *C*-glycosyl flavones in different kumquat tissues. VIC, vicenin-2; APN, 8-*C*-neohesperidosyl apigenin; MAR, margaritene; FW, fresh weight. **(C)** The expression levels of *FcFNSII-1* and *FcFNSII-2* were calculated via the $2^{-\Delta\Delta Ct}$ method. FL, flowers; YL, young leaves; YS, young shoots; 30P, peels of fruits at 30 DAB; 90P, peels of fruits at 90 DAB; 150P, peels of fruits at 150 DAB. The data are presented as the mean ± SE of three independent replicates. Asterisks indicate significant differences (**$P < 0.01$).

Supplementary Figure 3 | Structure of key flavonoids in kumquat plants. DCGP, 3′,5′-di-*C*-β-glucopyranosylphloretin; APN, 8-*C*-neohesperidosyl apigenin; MAR, margaritene (8-*C*-neohesperidosyl acacetin); VIC, vicenin-2 (6,8-di-*C*-glucosylapigenin); RHO, rhoifolin (7-*O*-neohesperidosyl apigenin); FOR, fortunellin (7-*O*-neohesperidosyl acacetin).

Supplementary Figure 4 | Effects of pH and temperature on the enzyme activities of FcFNSII-2 proteins. **(A)** Effects of pH on enzyme activities at 30°C for 1 h. Relative activities are presented as a percentage of the activity measured at pH 7.0 (100%). **(B)** Effects of temperature on enzyme activities at a pH of 7.0 for 1 h. Relative activities as a percentage of the activity measured at 30°C. The data are presented as the mean ± SE of three independent replicates.

Supplementary Figure 5 | Detection of the NMSD of FcFNSII-1 and FcFNSII-2. Probabilities were calculated using the TMHMM server (TMHMM – 2.0 – Services – DTU Health Tech). The NMSDs of both FcFNSII-1 and FcFNSII-2 were predicted to be 26 AAs long.

Supplementary Figure 6 | Interactions between FcFNSII-1 and upstream enzymes in the flavonoid pathway were assayed with a split-ubiquitin system. Yeast cells co-expressing SUC- FcFNSII-1-Cub-LexAVP16 with NubG-fused FcCHS1, FcCHS2, FcCHI, or FcCHIL.

REFERENCES

Akashi, T., Aoki, T., and Ayabe, S. (1998). Identification of a cytochrome P450 cDNA encoding (2S)-flavanone 2-hydroxylase of licorice (*Glycyrrhiza echinata L.; Fabaceae*) which represents licodione synthase and flavone synthase II. *FEBS Lett.* 431, 287–290. doi: 10.1016/s0014-5793(98)00781-9

Barreca, D., Bellocco, E., Lagana, G., Ginestra, G., and Bisignano, C. (2014). Biochemical and antimicrobial activity of phloretin and its glycosilated derivatives present in apple and kumquat. *Food Chem.* 160, 292–297. doi: 10.1016/j.foodchem.2014.03.118

Brazier-Hicks, M., Evans, K. M., Gershater, M. C., Puschmann, H., Steel, P. G., and Edwards, R. (2009). The C-glycosylation of flavonoids in cereals. *J. Biol. Chem.* 284, 17926–17934.

Butelli, E., Garcia-Lor, A., Licciardello, C., Las Casas, G., Hill, L., Recupero, G. R., et al. (2017). Changes in anthocyanin production during domestication of citrus. *Plant Physiol.* 173, 2225–2242. doi: 10.1104/pp.16.01701

Dastmalchi, M., Bernards, M. A., and Dhaubhadel, S. (2016). Twin anchors of the soybean isoflavonoid metabolon: evidence for tethering of the complex to the endoplasmic reticulum by IFS and C4H. *Plant J.* 85, 689–706. doi: 10.1111/tpj.13137

Du, Y., Chu, H., Chu, I. K., and Lo, C. (2010a). CYP93G2 is a flavanone 2-hydroxylase required for C-glycosylflavone biosynthesis in rice. *Plant Physiol.* 154, 324–333. doi: 10.1104/pp.110.161042

Du, Y., Chu, H., Wang, M., Chu, I. K., and Lo, C. (2010b). Identification of flavone phytoalexins and a pathogen-inducible flavone synthase II gene (SbFNSII) in sorghum. *J. Exp. Bot.* 61, 983–994. doi: 10.1093/jxb/erp364

Falcone Ferreyra, M. L., Emiliani, J., Rodriguez, E. J., Campos-Bermudez, V. A., Grotewold, E., and Casati, P. (2015). The identification of maize and arabidopsis Type I flavone synthases links flavones with hormones and biotic interactions. *Plant Physiol.* 169, 1090–1107. doi: 10.1104/pp.15.00515

Falcone Ferreyra, M. L., Rodriguez, E., Casas, M. I., Labadie, G., Grotewold, E., and Casati, P. (2013). Identification of a bifunctional maize C- and O-glucosyltransferase. *J. Biol. Chem.* 288, 31678–31688. doi: 10.1074/jbc.M113.510040

Fliegmann, J., Furtwangler, K., Malterer, G., Cantarello, C., Schuler, G., Ebel, J., et al. (2010). Flavone synthase II (CYP93B16) from soybean *(Glycine max L.)*. *Phytochemistry* 71, 508–514. doi: 10.1016/j.phytochem.2010.01.007

Fujino, N., Tenma, N., Waki, T., Ito, K., Komatsuzaki, Y., Sugiyama, K., et al. (2018). Physical interactions among flavonoid enzymes in snapdragon and torenia reveal the diversity in the flavonoid metabolon organization of different plant species. *Plant J.* 94, 372–392. doi: 10.1111/tpj.13864

Gebhardt, Y. H., Witte, S., Steuber, H., Matern, U., and Martens, S. (2007). Evolution of flavone synthase I from parsley flavanone 3beta-hydroxylase by site-directed mutagenesis. *Plant Physiol.* 144, 1442–1454. doi: 10.1104/pp.107.098392

Gebhardt, Y., Witte, S., Forkmann, G., Lukacin, R., Matern, U., and Martens, S. (2005). Molecular evolution of flavonoid dioxygenases in the family *Apiaceae*. *Phytochemistry* 66, 1273–1284. doi: 10.1016/j.phytochem.2005.03.030

Gong, J., Zeng, Y., Meng, Q., Guan, Y., Li, C., Yang, H., et al. (2021). Red light-induced kumquat fruit coloration is attributable to increased carotenoid metabolism regulated by FcrNAC22. *J. Exp. Bot.* 72, 6274–6290. doi: 10.1093/jxb/erab283

Han, X. J., Wu, Y. F., Gao, S., Yu, H. N., Xu, R. X., Lou, H. X., et al. (2014). Functional characterization of a *Plagiochasma appendiculatum* flavone synthase I showing flavanone 2-hydroxylase activity. *FEBS Lett.* 588, 2307–2314. doi: 10.1016/j.febslet.2014.05.023

Hrazdina, G., and Wagner, G. J. (1985). Metabolic pathways as enzyme complexes: evidence for the synthesis of phenylpropanoids and flavonoids on membrane associated enzyme complexes. *Arch. Biochem. Biophys.* 237, 88–100. doi: 10.1016/0003-9861(85)90257-7

Huang, D., Wang, X., Tang, Z., Yuan, Y., Xu, Y., He, J., et al. (2018). Subfunctionalization of the Ruby2-Ruby1 gene cluster during the domestication of citrus. *Nat. Plants* 4, 930–941. doi: 10.1038/s41477-018-0287-6

Huang, X. S., Zhang, Q., Zhu, D., Fu, X., Wang, M., Zhang, Q., et al. (2015). ICE1 of Poncirus trifoliata functions in cold tolerance by modulating polyamine levels through interacting with arginine decarboxylase. *J. Exp. Bot.* 66, 3259–3274. doi: 10.1093/jxb/erv138

Ito, T., Fujimoto, S., Suito, F., Shimosaka, M., and Taguchi, G. (2017). C-Glycosyltransferases catalyzing the formation of di-C-glucosyl flavonoids in citrus plants. *Plant J.* 91, 187–198. doi: 10.1111/tpj.13555

Jiang, N., Doseff, A. I., and Grotewold, E. (2016). Flavones: from biosynthesis to health benefits. *Plants* 5:27. doi: 10.3390/plants5020027

Kong, C. H., Xu, X. H., Zhang, M., and Zhang, S. Z. (2010). Allelochemical tricin in rice hull and its aurone isomer against rice seedling rot disease. *Pest Manag. Sci.* 66, 1018–1024. doi: 10.1002/ps.1976

Lam, P. Y., Tobimatsu, Y., Takeda, Y., Suzuki, S., Yamamura, M., Umezawa, T., et al. (2017). Disrupting flavone synthase II alters lignin and improves biomass digestibility. *Plant Physiol.* 174, 972–985. doi: 10.1104/pp.16.01973

Lam, P. Y., Zhu, F. Y., Chan, W. L., Liu, H., and Lo, C. (2014). Cytochrome P450 93G1 is a flavone synthase II that channels flavanones to the biosynthesis of

tricin o-linked conjugates in rice. *Plant Physiol.* 165, 1315–1327. doi: 10.1104/pp.114.239723

Lee, Y. J., Kim, J. H., Kim, B. G., Lim, Y., and Ahn, J. H. (2008). Characterization of flavone synthase I from rice. *BMB Rep.* 41, 68–71. doi: 10.5483/bmbrep.2008.41.1.068

Liu, X., Lin, C., Ma, X., Tan, Y., Wang, J., and Zeng, M. (2018). Functional characterization of a flavonoid glycosyltransferase in sweet orange (*Citrus sinensis*). *Front. Plant. Sci.* 9:166. doi: 10.3389/fpls.2018.00166

Liu, X., Zhao, C., Gong, Q., Wang, Y., Cao, J., Li, X., et al. (2020). Characterization of a caffeoyl-CoA O-methyltransferase-like enzyme involved in biosynthesis of polymethoxylated flavones in *Citrus reticulata*. *J. Exp. Bot.* 71, 3066–3079. doi: 10.1093/jxb/eraa083

Lou, S. N., and Ho, C. T. (2017). Phenolic compounds and biological activities of small-size citrus: kumquat and calamondin. *J. Food Drug Anal.* 25, 162–175. doi: 10.1016/j.jfda.2016.10.024

Lou, S. N., Lai, Y. C., Hsu, Y. S., and Ho, C. T. (2016). Phenolic content, antioxidant activity and effective compounds of kumquat extracted by different solvents. *Food Chem.* 197, 1–6. doi: 10.1016/j.foodchem.2015.10.096

Lou, S. N., Lai, Y. C., Huang, J. D., Ho, C. T., Ferng, L. H., and Chang, Y. C. (2015). Drying effect on flavonoid composition and antioxidant activity of immature kumquat. *Food Chem.* 171, 356–363. doi: 10.1016/j.foodchem.2014.08.119

Mameda, R., Waki, T., Kawai, Y., Takahashi, S., and Nakayama, T. (2018). Involvement of chalcone reductase in the soybean isoflavone metabolon: identification of GmCHR5, which interacts with 2-hydroxyisoflavanone synthase. *Plant J.* 96, 56–74. doi: 10.1111/tpj.14014

Martens, S., and Mithofer, A. (2005). Flavones and flavone synthases. *Phytochemistry* 66, 2399–2407. doi: 10.1016/j.phytochem.2005.07.013

Montanari, A., Chen, J., and Widmer, W. (1998). Citrus flavonoids: a review of past biological activity against disease. Discovery of new flavonoids from Dancy tangerine cold pressed peel oil solids and leaves. *Adv. Exp. Med. Biol.* 439, 103–116.

Morimoto, S., Tateishi, N., Matsuda, T., Tanaka, H., Taura, F., Furuya, N., et al. (1998). Novel hydrogen peroxide metabolism in suspension cells of Scutellaria baicalensis Georgi. *J. Biol. Chem.* 273, 12606–12611. doi: 10.1074/jbc.273.20.12606

Morohashi, K., Casas, M. I., Falcone Ferreyra, M. L., Falcone Ferreyra, L., Mejia-Guerra, M. K., Pourcel, L., et al. (2012). A genome-wide regulatory framework identifies maize pericarp color1 controlled genes. *Plant Cell* 24, 2745–2764. doi: 10.1105/tpc.112.098004

Nagahama, K., Eto, N., Shimojo, T., Kondoh, T., Nakahara, K., Sakakibara, Y., et al. (2015). Effect of kumquat (*Fortunella crassifolia*) pericarp on natural killer cell activity in vitro and in vivo. *Biosci. Biotechnol. Biochem.* 79, 1327–1336. doi: 10.1080/09168451.2015.1025033

Nakayama, T., Takahashi, S., and Waki, T. (2019). Formation of flavonoid metabolons: functional significance of protein-protein interactions and impact on flavonoid chemodiversity. *Front. Plant Sci.* 10:821. doi: 10.3389/fpls.2019.00821

Righini, S., Rodriguez, E. J., Berosich, C., Grotewold, E., Casati, P., and Falcone Ferreyra, M. L. (2019). Apigenin produced by maize flavone synthase I and II protects plants against UV-B-induced damage. *Plant Cell Environ.* 42, 495–508. doi: 10.1111/pce.13428

Sadek, E. S., Makris, D. P., and Kefalas, P. (2009). Polyphenolic composition and antioxidant characteristics of kumquat (*Fortunella margarita*) peel fractions. *Plant Foods Hum. Nutr.* 64, 297–302. doi: 10.1007/s11130-009-0140-1

Shih, C. H., Chu, H., Tang, L. K., Sakamoto, W., Maekawa, M., Chu, I. K., et al. (2008). Functional characterization of key structural genes in rice flavonoid biosynthesis. *Planta* 228, 1043–1054. doi: 10.1007/s00425-008-0806-1

Sparkes, I. A., Runions, J., Kearns, A., and Hawes, C. (2006). Rapid, transient expression of fluorescent fusion proteins in tobacco plants and generation of stably transformed plants. *Nat. Protoc.* 1, 2019–2025. doi: 10.1038/nprot.2006.286

Tamura, K., Stecher, G., Peterson, D., Filipski, A., and Kumar, S. (2013). MEGA6: molecular evolutionary genetics analysis version 6.0. *Mol. Biol. Evol.* 30, 2725–2729. doi: 10.1093/molbev/mst197

Waki, T., Yoo, D., Fujino, N., Mameda, R., Denessiouk, K., Yamashita, S., et al. (2016). Identification of protein-protein interactions of isoflavonoid biosynthetic enzymes with 2-hydroxyisoflavanone synthase in *soybean (Glycine max (L.) Merr.)*. *Biochem. Biophys. Res. Commun.* 469, 546–551. doi: 10.1016/j.bbrc.2015.12.038

Walter, M., Chaban, C., Schutze, K., Batistic, O., Weckermann, K., Nake, C., et al. (2004). Visualization of protein interactions in living plant cells using bimolecular fluorescence complementation. *Plant J.* 40, 428–438. doi: 10.1111/j.1365-313X.2004.02219.x

Wang, F., Wang, M., Liu, X., Xu, Y., Zhu, S., Shen, W., et al. (2017). Identification of putative genes involved in limonoids biosynthesis in citrus by comparative transcriptomic analysis. *Front. Plant Sci.* 8:782. doi: 10.3389/fpls.2017.00782

Wang, X., Li, C., Zhou, C., Li, J., and Zhang, Y. (2017). Molecular characterization of the C-glucosylation for puerarin biosynthesis in *Pueraria lobata*. *Plant J.* 90, 535–546. doi: 10.1111/tpj.13510

Wang, Y., Qian, J., Cao, J., Wang, D., Liu, C., Yang, R., et al. (2017). Antioxidant capacity, anticancer ability and flavonoids composition of 35 Citrus (*Citrus reticulata Blanco*) varieties. *Molecules* 22:1114. doi: 10.3390/molecules22071114

Winkel, B. S. (2004). Metabolic channeling in plants. *Annu. Rev. Plant Biol.* 55, 85–107. doi: 10.1146/annurev.arplant.55.031903.141714

Winkel-Shirley, B. (2001). It takes a garden. How work on diverse plant species has contributed to an understanding of flavonoid metabolism. *Plant Physiol.* 127, 1399–1404.

Wu, J., Wang, X. C., Liu, Y., Du, H., Shu, Q. Y., Su, S., et al. (2016). Flavone synthases from *Lonicera japonica* and L. macranthoides reveal differential flavone accumulation. *Sci. Rep.* 6:19245. doi: 10.1038/srep19245

Zhang, J., Subramanian, S., Zhang, Y., and Yu, O. (2007). Flavone synthases from Medicago truncatula are flavanone-2-hydroxylases and are important for nodulation. *Plant Physiol.* 144, 741–751. doi: 10.1104/pp.106.095018

Zhao, C., Liu, X., Gong, Q., Cao, J., Shen, W., Yin, X., et al. (2021). Three AP2/ERF family members modulate flavonoid synthesis by regulating type IV chalcone isomerase in citrus. *Plant Biotechnol. J.* 19, 671–688. doi: 10.1111/pbi.13494

Zhao, C. Y., Wang, F., Lian, Y. H., Xiao, H., and Zheng, J. K. (2020). Biosynthesis of citrus flavonoids and their health effects. *Crit. Rev. Food Sci.* 60, 566–583. doi: 10.1080/10408398.2018.1544885

Zhu, C., Zheng, X., Huang, Y., Ye, J., Chen, P., Zhang, C., et al. (2019). Genome sequencing and CRISPR/Cas9 gene editing of an early flowering Mini-Citrus (*Fortunella hindsii*). *Plant Biotechnol. J.* 17, 2199–2210. doi: 10.1111/pbi.13132

Conflict of Interest: The authors declare that the research was conducted in the absence of any commercial or financial relationships that could be construed as a potential conflict of interest.

Publisher's Note: All claims expressed in this article are solely those of the authors and do not necessarily represent those of their affiliated organizations, or those of the publisher, the editors and the reviewers. Any product that may be evaluated in this article, or claim that may be made by its manufacturer, is not guaranteed or endorsed by the publisher.

frontiers in Plant Science

ORIGINAL RESEARCH
published: 08 March 2022
doi: 10.3389/fpls.2022.847268

The Effect of Topo-Climate Variation on the Secondary Metabolism of Berries in White Grapevine Varieties (*Vitis vinifera*)

*Kelem Gashu[1], Chao Song[1], Arvind Kumar Dubey[1], Tania Acuña[2], Moshe Sagi[2], Nurit Agam[3], Amnon Bustan[4] and Aaron Fait[2]**

[1] Albert Katz International School for Desert Studies, Jacob Blaustein Institutes for Desert Research, Ben-Gurion University of the Negev, Beersheba, Israel, [2] Albert Katz Department of Dryland Biotechnologies, French Associates Institute for Agriculture and Biotechnology of Drylands, Jacob Blaustein Institutes for Desert Research, Ben-Gurion University of the Negev, Beersheba, Israel, [3] Wyler Department of Dryland Agriculture, French Associates Institute for Agriculture and Biotechnology of Drylands, Jacob Blaustein Institutes for Desert Research, Ben-Gurion University of the Negev, Beersheba, Israel, [4] Ramat Negev Desert Agro-Research Center, Ramat Negev Works Ltd., Halutza, Israel

Exploiting consistent differences in radiation and average air temperature between two experimental vineyards (Ramat Negev, RN and Mitzpe Ramon, MR), we examined the impact of climate variations on total carotenoids, redox status, and phenylpropanoid metabolism in the berries of 10 white wine grapevine (*Vitis vinifera*) cultivars across three consecutive seasons (2017–2019). The differences in carotenoid and phenylpropanoid contents between sites were seasonal and varietal dependent. However, the warmer RN site was generally associated with higher H_2O_2 levels and carotenoid degradation, and lower flavonol contents than the cooler MR site. Enhanced carotenoid degradation was positively correlated with radiation and daily degree days, leading to a greater drop in content from véraison to harvest in Colombard, Sauvignon Blanc, and Semillon berries. Analyses of berry H_2O_2 and phenylpropanoids suggested differences between cultivars in the links between H_2O_2 and flavonol contents. Generally, however, grapes with higher H_2O_2 content seem to have lower flavonol contents. Correlative network analyses revealed that phenylpropanoids at the warmer RN site are tightly linked to the radiation and temperature regimes during fruit ripening, indicating potentially harmful effect of warmer climates on berry quality. Specifically, flavan-3-ols were negatively correlated with radiation at RN. Principal component analysis showed that Muscat Blanc, Riesling, Semillon, and Sauvignon Blanc were the most site sensitive cultivars. Our results suggest that grapevine biodiversity is likely the key to withstand global warming hazards.

Keywords: phenylpropanoid metabolism, carotenoid degradation, metabolite profiling, oxidative stress, high temperature

OPEN ACCESS

Edited by:
M. Teresa Sanchez-Ballesta, Institute of Food Science, Technology and Nutrition, Spanish National Research Council (CSIC), Spain

Reviewed by:
Ivana Tomaz, University of Zagreb, Croatia
Pablo Carbonell-Bejerano, Max Planck Institute for Developmental Biology, Max Planck Society, Germany

****Correspondence:***
Aaron Fait
fait@bgu.ac.il

Specialty section:
This article was submitted to Plant Metabolism and Chemodiversity, a section of the journal Frontiers in Plant Science

Received: *01 January 2022*
Accepted: *09 February 2022*
Published: *08 March 2022*

Citation:
Gashu K, Song C, Dubey AK, Acuña T, Sagi M, Agam N, Bustan A and Fait A (2022) The Effect of Topo-Climate Variation on the Secondary Metabolism of Berries in White Grapevine Varieties (Vitis vinifera). Front. Plant Sci. 13:847268. doi: 10.3389/fpls.2022.847268

Abbreviations: Myr-3-glr, Myricetin-3-*O*-glucuronide; Myr-3-glu, Myricetin-3-*O*-glucoside; Narin-ch-glu, *Naringenin*-chalcone-4-*O*-glucoside; Quer-3-glr, Quercetin-3-*O*-glucuronide; Quer-3-glu, Quercetin-3-*O*-glucoside; Quer-3-gal, Quercetin-3-*O*-galactoside; Kaempferol-3-glu, Kaempferol-3-*O*-glucoside; Kaempferol-3-glr, Kaempferol-3-*O*-glucuronide; Kaempferol-3-gal, Kaempferol-3-*O*-galactoside; Isorhamnetin-3-glu, Isorhamnetin-3-*O*-glucoside; D-viniferin, delta viniferin; hydroxybenzoic hex, hydroxybenzoic hexoside; Coumaric acid hex, Coumaric acid hexoside; Ferulic acid hex, Ferulic acid hex hexoside; TC, total carotenoid; Chl, Chlorophyll; ROS, reactive oxygen species; Asc, Ascorbate; Hs, accumulated heat stress degree hours; Relx, relaxation degree hours; DDD, daily degree days; MR, Mitzpe Ramon; RN, Ramat Negev; Chenin B, Chenin Blanc; Gewurzt, Gewurztraminer; Muscat A, Muscat of Alexandria; Muscat B, Muscat Blanc; Pinot G, Pinot Gris; Sauvignon B, Sauvignon Blanc.

INTRODUCTION

By the end of the 21st century, mean global air temperature is expected to rise between 1.5 and 2°C in most of the world's wine-growing regions (Ullah et al., 2020). Consequently, the longstanding relationship between geography and viticulture will be disrupted, necessitating changes to the wine industry (Wolkovich et al., 2018). A recent study showed that a 2°C rise in air temperature could result in a 24–56% loss of the viticultural area within current wine-growing regions (Morales-Castilla et al., 2020), the consequences of which are yet unknown. As elevated temperature has been reported to affect fruit chemical compounds, the essential components of wine quality, such projected air temperature change may impact the production of high-quality wine. In light of this, a recent extensive study that assessed the phenological diversity among wine cultivars in response to a consistent difference of 1.5°C, indicated that the genetic diversity of grapevines is the key to adapting viticulture to warmer climates/periods (Gashu et al., 2020).

As fruits transpire only sparingly, their ability to regulate surface temperature is limited, thus they commonly experience sunburn, dehydration, photo-oxidative damage, berry shriveling, and metabolite disorders when exposed to elevated air temperatures or excessive solar irradiance (Greer and Weston, 2010; Krasnow et al., 2010; Reshef et al., 2019; Rustioni et al., 2020). Upon such environmental stress, fruits use complex mechanisms to maintain their development and protect themselves from damaging processes. These mechanisms include osmotic adjustments and the accumulation of UV protectants and the free radical scavengers, ascorbate (Asc), glutathione (GSH), pyridine nucleotides, carotenoids, and phenylpropanoids (Weisshaar and Jenkinst, 1998; Baumes et al., 2002; Winkel-Shirley, 2002; Kamffer et al., 2010; Foyer and Noctor, 2011; Noctor et al., 2012; Decros et al., 2019; Karniel et al., 2020). Nevertheless, the balance between oxidant and antioxidant chemical production in fruit can be disrupted in a harsh environment, leading to cellular damage due to the overproduction of reactive oxygen species (ROS; Gill and Tuteja, 2010; Decros et al., 2019), with a consequent negative effect on fruit metabolism and commercial quality.

In wine grapes, phenylpropanoids and carotenoids (precursors of C_{13} norisoprenoids), in addition to their antioxidant properties, are of particular interest as precursors of aroma, astringency, bitterness, and other mouth-feel properties in wine (Baumes et al., 2002; Downey et al., 2006; Cohen et al., 2008; Teixeira et al., 2013). Their levels in developing fruit are regulated by environmental conditions, developmental stage, and cultivar characteristics (Oliveira et al., 2004; Young et al., 2015; Joubert et al., 2016; Reshef et al., 2018).

Air temperature affects the metabolism of grapevine fruit (Cohen et al., 2008; Del-Castillo-Alonso et al., 2016; Gouot et al., 2019b; Yan et al., 2020). The impact of temperature on phenylpropanoids has already been studied in several wine grape cultivars (Cohen et al., 2008; Pastore et al., 2017; Gaiotti et al., 2018). For example, high temperatures have been found to reduce the concentrations of flavonols and anthocyanins (Pastore et al., 2017) and increase carotenoid content (Chen et al., 2017). Radiation and temperature have also been reported to affect the diurnal change of berry primary and secondary metabolites (Reshef et al., 2017, 2018, 2019); radiation was shown to trigger phenylpropanoid biosynthesis, whereas high temperature was shown to accelerate their degradation (Tarara et al., 2008; Azuma et al., 2012). Similarly, bunch exposure to direct sunlight has been shown to inhibit carotenoid gene expression and even accelerate carotenoid degradation (He et al., 2020). In contrast, elevated temperature has been shown to increase berry carotenoid concentration (Marais et al., 1991; Chen et al., 2017). These lines of evidence suggest that a substantial knowledge gap exists regarding carotenoid metabolism in response to air temperature in grapevine.

The primary objective of the present study was to examine the modulating effect of environment × cultivar interactions on berry secondary metabolism, carotenoid metabolism, and berry redox status (H_2O_2), under field conditions in warm, arid regions. In a recent study on grapevine (Gashu et al., 2020), we observed that white cultivars had an earlier and shorter ripening phase, partially avoiding the summer heat, in contrast to red cultivars in the same region. These results raised the possible importance of the duration of the ripening phase in determining fruit quality. In the current study, we chose the same 10 white cultivars to address the following question: does the air temperature/radiation regime during fruit ripening significantly alter berry phenylpropanoids and carotenoids? Accordingly, we used spectrophotometry and mass spectrometry (MS) to examine (i) the relationships of berry phenylpropanoids and carotenoids with climate indices, and (ii) the association between berry H_2O_2 and phenylpropanoids. We discuss the developmental changes in grape metabolic profiles and relate them to climate indices through network analyses.

MATERIALS AND METHODS

Experimental Layout

The experiments were conducted over three consecutive seasons, from 2017 to 2019, in two vineyards 53 km apart in the Negev Highlands in Israel: the Mitzpe Ramon (MR) vineyard (30°38′48.6″N 34°47′24.5″E, 850 m asl) and the Ramat Negev (RN) vineyard at the Desert Agro-Research Center (30°58′43.4″N 34°42′31.6″E, 300 m asl). Average annual precipitation is 105 mm and 80 mm at MR and RN, respectively, occurring only in the winter (typically November through April), with considerable inter-annual fluctuations. Both vineyards shared the same experimental setup, comprising 10 white wine cultivars (Chardonnay, Chenin Blanc, Colombard, Gewurztraminer, Muscat Blanc, Muscat of Alexandria, Pinot Gris, Sauvignon Blanc, Riesling, and Semillon), grafted onto 140 RU rootstock; both vineyards were planted in 2012 in a randomized block design with four replicates of 8–9 vines each. The soils at both sites are sandy loam.

In all cultivars, yield was directed to about 5 kg vine^{-1}. This was achieved through winter pruning to about 32 fruit-buds per vine, followed by thinning of excess fruiting shoots toward bloom, and further thinning of excess bunches when the actual

clusters' number and size were clear. Final yield adjustments took place where necessary, soon after véraison. Subsequently, the fruit yield usually ranged from 4.2 to 5.8 kg vine^{-1}, with very few exclusions, and with minimum influences on fruit quality. Employing the vertical shoot positioning, canopy size was leveled throughout the vineyard using the following methods: (i) at the vegetative phase, shoots' length was consistently confined by topping to about 2.2 m above ground; (ii) most of the blind shoots were removed; and (iii) when berries reached pea-size among most of the cultivars, deficit irrigation was practiced to avoid further shoot growth and branching. The experimental layout and meteorological data measurement have been briefly described elsewhere (Gashu et al., 2020).

Daily degree days (DDD) were calculated following Jones et al. (2010); the sum of DDD from véraison to harvest was computed for each cultivar to assess the DDD effect on fruit quality parameters, as follows:

$$\mathrm{DDD} = \sum_{\mathrm{H}arvest}^{\mathrm{V}eraison} \max\left[\left(\frac{[\mathrm{T}max + Tmin]}{2}\right) - 10, 0\right] \quad (1)$$

where *Tmax* is the daily maximum air temperature and *Tmin* is the daily minimum air temperature.

To evaluate the effect of maximum and minimum air temperatures on fruit metabolism, we introduced accumulated degree hours indices expressing heat stress (Hs) and relaxation (Relx). Hs and Relx were calculated for each cultivar from véraison to harvest at which the hourly air temperatures were higher than 30°C and lower than 20°C, respectively.

$$Hs = \Sigma_{Harvest}^{Veraison}\ max[(Temp - 30), 0] \quad (2)$$

$$Relx = \Sigma_{Harvest}^{Veraison}\ max\left[(20 - Temp), 0\right] \quad (3)$$

where *Temp* is hourly air temperature.

Berry Sampling and Metabolite Extraction

During each season, berries were sampled for metabolite extraction and berry indices at véraison and harvest. At véraison, each cultivar was sampled when berries reached approximately 50% softening (estimated weekly in eight tagged representative clusters per replicate). Only softened berries were sampled. The range of sampling dates varied from 1 to 7 days at MR and 1 to 14 days at RN. Toward harvest, berries were sampled from each cultivar approaching the 20 ± 1 °Brix level, with sampling date varied from 7 to 14 days at MR and up to 21 days at RN depending on the season. To minimize the effect of circadian rhythm, berries were sampled at 09:00. Samples were collected from four biological replicates at each location from each cultivar. In each sampling, at least 30 berries per replicate were pooled from five different vines in each block on the east side of the vine (six berries per vine were sampled from the top, middle, and bottom of the bunch), and immediately snap-frozen in liquid nitrogen. Berries were peeled while still frozen, by carefully separating the skin from the pulp, and the seeds were removed. The skin was kept at −80°C until further analysis.

Grape skin samples were lyophilized and ground under liquid nitrogen using a Retsch-mill (Retsch, Haan, Germany) with pre-chilled holders and grinding beads. For metabolite extraction, 40 mg of frozen skin powder were weighed and extracted in a 1-mL pre-cooled methanol:chloroform:water extraction solution (2.5:1:1 v/v) with ampicillin (1 mg mL^{-1} in water) and corticosterone (1 mg mL^{-1} in methanol) as internal standards (Hochberg et al., 2013; Degu et al., 2014). Skin extracts were filtered (0.22 μm Millipore, Burlington, MA, United States) and transferred to glass vials for analysis using ultra-performance liquid chromatography coupled to a quadrupole time-of-flight mass spectrometer (UPLC QTOF-MS; Waters, Burlington, MA, United States) operating in negative and positive ion modes.

Liquid Chromatography-Mass Spectrometry Conditions

Chromatographic separation was performed using an Acquity UPLC BEH C_{18} column (100 mm × 2.1 mm, 1.7 μm) (Waters MS Technology, Manchester, United Kingdom) maintained at 40°C. The autosampler was maintained at 10°C. Leucine encephalin, at a concentration of 0.4 ng L^{-1}, was used for lock mass calibration, in 50/50 acetonitrile /H_2O with 0.1% v/v formic acid. The mobile phase was adjusted from 95% water, 5% acetonitrile, 0.1% formic acid (phase A) to 0.1% formic acid in acetonitrile (phase B), with the gradient transitioning from 100 to 60% phase A (0–8 min), 60–0% phase A (1 min), a gradual return to 100% phase A (3.5 min), and conditioning at 100–60% phase A (2.5 min), with a total run time of 15 min. The MS conditions were exactly as described previously by Hochberg et al. (2013). Briefly, the MS conditions were set as follows: Capillary voltage +3.0 keV; sampling cone voltage 27 V; extraction cone voltage 4 V; source temperature: 120°C; desolvation temperature: 300°C; cone gas flow: 50 L h^{-1}; desolvation gas flow: 650 L h^{-1}; collision energy: 6 eV, and for MS/MS spectra, collision energies were set from 25 to 50 eV; the scan range was set at 50–1,500 m/z; and the dynamic range enhancement mode was off.

Liquid Chromatography-Mass Spectrometry Data Processing and Annotation

MassLynx^{TM} version 4.1 (Waters) was used for system control and data acquisition. Metabolites were annotated based on fragmentation patterns searched against those in the ChemSpider metabolite database[1], and the consistency of their retention times with those of identified metabolites was compared with the data in the scientific literature. A targeted metabolite profiling approach was used, and 36 metabolites were annotated uniquely in both negative (29 metabolites) and positive (seven metabolites) ion modes. The metabolite data generated by liquid chromatography-mass spectrometry (LC-MS) comprised unique mass intensity (mass-to-charge ratio) values (height) for each annotated compound. To minimize differences due to separate injection periods, we ran a bulked extraction of all samples (pool) four times in each batch as a reference throughout the

[1]http://www.chemspider.com/

injection sets, to enclose all metabolic variability of the different cultivars. The raw data for each metabolite in each batch were then normalized by dividing each value by the mean of the pool in the corresponding data file generated from each chromatogram.

Spectrophotometric Assays for Hydrogen Peroxide, Glutathione, Ascorbic Acid (Ascorbate), Total Carotenoid, and Chlorophyll Measurements

A modified method of Noctor et al. (2016), was employed to measure H_2O_2 content in the berry. Eight to ten berries were sectioned while still frozen, and seeds were removed. The skin and pulp fractions were manually crushed with a mortar and pestle under liquid nitrogen. For H_2O_2 extraction, 100 mg of frozen powder were weighed and extracted in 2-mL of 1 M perchloric acid ($HClO_4$) containing polyvinylpyrrolidone (5%). The samples were then centrifuged for 10 min at 14,000 RPM (microcentrifuge 5417R) at 4°C. The supernatant was neutralized with 5 M potassium carbonate (K_2CO_3) in the presence of 50 μL of 0.3 mM P-buffer (composed of monobasic dihydrogen phosphate and dibasic monohydrogen phosphate) and centrifuged for 1 min at 14,000 RPM, and the supernatant was decanted into new tubes. The supernatants were mixed in a reaction mixture comprising of 8.5 mM 4-aminoantipyrine (APP), 3.4 mM sodium 3,5-dichloro-2-hydroxybenzenesulfonate (BHS), 45 U mL^{-1} horseradish peroxidase (HRP) in 2 mL of 50 mM tris buffer (pH 7.5). Briefly, 40-μl samples of the supernatant were mixed with tris:APP:BHS:HRP (5:1:1:1 v/v) on a microplate (Epoch BioTek Instruments Inc., Burlington, MA, United States, and later Tecan Infinite® M200, Tecan Austria GmbH, Salzburg, Austria). After 30 min of mixing the supernatant samples with the reaction mixture the H_2O_2 was measured spectrophotometrically at 510 nm, and then quantified using a standard calibration curve.

For total carotenoid and chlorophyll extraction, 20 mg of skin powder were weighed and extracted in 0.5 mL of 99% ethanol and stored in a dark room for 48 h at 4°C. Carotenoids and chlorophyll contents were determined spectrophotometrically at 470, 649, and 665 nm, respectively, in 200-μl samples of supernatant. The values obtained at the three wavelengths were used to calculate total carotenoid and chlorophyll content as described by Wintermans and De Mots (1965).

Since H_2O_2 measurements were consistent across the seasons, the 2018 samples were used for evaluating the other major redox buffers such as glutathione and Asc to explore the redox adjustment in white grapevine fruits. The samples were analyzed in bulks of the four replicates × cultivar × location. The method of Tietze (1969) was employed with minor modification to measure glutathione content in the berry skin tissue. For sample processing, 15 mg of lyophilized frozen skin powder were weighed and extracted in 1 mL of 1 M $HClO_4$, and the reduced (GSH) and oxidized (GSSG) glutathione were measured as described by Oshanova et al. (2021). The Asc level in the berry skin tissue was measured as described by Jagota and Dani (1982). Briefly, 10 mg of lyophilized frozen skin powder were weighed and extracted in 800 μl of 10% trichloroacetic acid. The samples were then vortexed and centrifuged for 20 min at 14,000 RPM (microcentrifuge 5417R) at 4°C, and the supernatant was decanted into new tubes. The supernatants (400 μl) were mixed in a reaction mixture comprised of 1.6 mL DDw, and 200 μl of 10 fold diluted folin reagent. After 10 min of mixing the supernatant samples with the reaction mixture, Asc was measured spectrophotometrically at 760 nm, and then quantified using a standard calibration curve.

Statistical Analyses

All statistical analyses were performed on log-transformed data using "R" version 3.6.0 (R Development Core Team, 2017). A three-way factorial analysis was used to assess the effects of cultivar (C), location (L), and growing season (Y), and the interactions between them, using the built-in *aov* function. The differences between locations for each cultivar were tested using the *Wilcox.test* function. Histograms were created using the *hist* function in the "ggplot2" package. Clustered heatmaps were created using *ComplexHeatmap* (Gu et al., 2016). Clustering of samples was calculated by Euclidean distances and the Ward.D2 clustering method in the functions *get_dist* and *hclust*, and the built-in "dendextend" and "factoextra" packages (Galili, 2015). Correlation-based network analyses were performed using the MetScape application and the NetworkAnalyzer tool, available in Cytoscape version 3.7.2. All correlation analyses and preparation for network visualizations were generated in "R" using the built-in cor function with the "Pearson" algorithm. Correlations were incorporated into the network if they were statistically significant ($p < 0.05$) and their correlation coefficient (r) was higher than 0.3 or lower than −0.3. Principal component analyses (PCA) were plotted using MetaboAnalyst version 4.0 (Chong et al., 2018) and JMP® version 13 (SAS Institute Inc., Cary, NC, United States, 1989–2007). The norm of reactions that represents phenotypic changes (*y*-axis) due to environmental changes (*x*-axis), was calculated using linear regression models for each trait computing the slope. The slope represents phenotypic plasticity.

RESULTS

Climatic Conditions in the Vineyards

The two experimental vineyards differed in their meteorological conditions (Gashu et al., 2020). On average, the RN vineyard experienced higher average, maximum and minimum air temperatures, despite the slightly lower incoming solar radiation. In addition, consistent 1.3-MJ m^{-2} day^{-1} difference in incoming solar radiation and 1.5°C difference in the daily mean temperature between the locations were maintained during all three seasons. Meteorological conditions between sites have been briefly described elsewhere (Gashu et al., 2020).

The Differences Between Locations in Total Carotenoid Content Were Predominantly Affected by the Climate × Season Interaction

Cultivar (C), location (L), and seasonal (Y) factors contributed significantly to the measured differences in carotenoid content,

while the non-significant contributions of location at harvest, and the C × L interaction at véraison were exceptions (**Supplementary Table 1**).

Testing each season independently revealed significant effects of cultivar and location in each season, except for ripe berries in 2017 and véraison berries in 2018, which were not affected by location (**Supplementary Table 1**). At véraison, the mean total carotenoid content ranged from 58 to 102 mg g^{-1} DW, with considerable variation among cultivars, locations, and seasons (**Figure 1A** and **Supplementary Table 1**). It was generally significantly higher at RN than MR in both 2017 and 2019 seasons, whereas in 2018, location had no effect (**Figure 1A** and **Supplementary Table 1**). Comparing seasons, the highest average total carotenoid content (92.8 mg g^{-1} DW) was measured in 2019. Among cultivars, Gewürztraminer (in 2019) displayed the highest carotenoid level (130.8 mg g^{-1} DW) at the warmer RN site across all seasons. In contrast, the lowest (43.4 mg g^{-1} DW) carotenoid level was measured in Semillon berries at MR in 2017 (**Supplementary Table 1**).

At harvest, the average carotenoid content across all cultivars ranged from 43.1 to 56.2 mg g^{-1} DW, with 2018 and 2019 seasons showing the greatest differences between locations (**Figure 1B** and **Supplementary Table 1**). In 2017, the carotenoid content was predominantly affected by cultivars, while in other years, it was significantly affected by location, being higher at MR than RN in 2018, but higher at RN than MR in 2019. Both the lowest (27.2 mg g^{-1} DW in 2017) and the highest (75.1 mg g^{-1} DW in 2019) carotenoid levels were measured at the warmer RN site for the Colombard and Pinot Gris cultivars, respectively (**Supplementary Table 1**).

The Level of Carotenoid Degradation Is Dependent on the Topo-Climatic Differences Between Locations During Fruit Ripening

The average total carotenoid degradation, measured as the difference between véraison and harvest across all cultivars, varied significantly between locations, being consistently higher at RN (**Figure 1C**). The difference between locations was greater in the 2017 season. In the 2018 and 2019 seasons, the difference between locations was not significant (**Figure 1C**). Comparing seasons at MR, the mean total carotenoid degradation across all cultivars was 1.8 fold and 2.4-fold greater, in 2018 and 2019, respectively, than in 2017. In contrast, at RN, the inter-seasonal variation in carotenoid degradation was not significant.

In addition, degradation was also cultivar-dependent, with significant variation measured between locations for many cultivars in the 2017 and 2019 seasons (**Figures 1D,F**). The highest values were displayed at RN, in 2017, by Chenin Blanc, Gewürztraminer, Chardonnay, Colombard, and Pinot Gris (36.0–65.7 mg g^{-1} DW) (**Figure 1D**). Interestingly, only Pinot Gris showed a similar trend in 2018 (**Figure 1E**). In 2019, Muscat of Alexandria, Riesling, Gewürztraminer, and Colombard exhibited significantly higher degradation (47.4–73.5 mg g^{-1} DW) at RN than at MR. Sauvignon Blanc at RN was an exception among the cultivars, showing the lowest degradation in 2019 (**Figure 1F**).

The sums of daily degree days (DDD) and radiation from véraison to harvest were correlated against total carotenoid degradation (**Figures 2A–J**). The results showed that an increase in either DDD or radiation was associated with greater carotenoid degradation (**Figures 2K,L**), and the relationship was cultivar-dependent. A significant correlation with DDD was found in Chardonnay, Colombard, Muscat of Alexandria, Sauvignon Blanc, Semillon, and Riesling (**Figures 2A–F**). Sauvignon Blanc displayed the strongest correlation ($p < 0.0001$, $R^2 = 0.73$) (**Figure 2D**). Similarly, an increase in the cumulative radiative flux was significantly associated with carotenoid degradation ($p < 0.05$), but the relationship was generally weaker (**Figure 2L**). Nevertheless, degradation in Sauvignon Blanc and Semillon exhibited a significant correlation with radiation ($R^2 = 0.56$ and 0.71, respectively, $p < 0.0001$) (**Figures 2I,J**). Colombard, Sauvignon Blanc, and Semillon were affected by both DDD and radiation. In Gewürztraminer, Muscat Blanc and Pinot Gris, carotenoid degradation was not significantly correlated with either factor (**Supplementary Table 2**).

Cultivar-Specific Response of Phenylpropanoid Metabolism to Climate Differences

Thirty-four secondary metabolites and four amino acids were identified in the skin of 10 different white wine grapevine cultivars at véraison and harvest. To explore the overall variability of skin phenylpropanoid accumulation in each location, UPLC-QTOF MS-generated metabolite profiles were plotted in a principal component analysis (PCA). The analysis revealed a cultivar-specific response to location, particularly at véraison. At RN, the separation between varieties was better resolved on PC1 and PC2 (**Figures 3A–D**). For example, Colombard, Riesling, and Sauvignon Blanc at véraison clustered together and were separated from other cultivars due to relatively lower levels of taxifolin (dihydroquercetin), astilbin, and naringenin chalcone-4-*O*-glucoside (naringenin ch-4-glu) at this time point (**Figure 3C** and **Supplementary Figure 1**). However, these cultivars were well separated from each other later at harvest (**Figure 3D**).

In contrast, the MR vineyard was characterized by greater variability at harvest (**Figures 3A,B**). At this time point, the PCA of the metabolic data showed that cultivars separated along PC1 and PC2 due to the contribution of astilbin, taxifolin, and naringenin-4-glu, myricetin and its aglycone, and stilbenes (**Figure 3B** and **Supplementary Figure 1**). Taxifolin, astilbin, and naringenin ch-4-glu accumulated to relatively higher levels mainly in Chardonnay, Chenin Blanc, Gewürztraminer, and Semillon (**Supplementary Figures 1A,B**), regardless of location.

The analysis also emphasized commonalities between the two experimental vineyards. At harvest, for example, in both locations, Colombard and Pinot Gris were grouped away from the other cultivars (**Figures 3B,D**), mainly because of stilbenes in the former and of myricetin and its conjugated forms in the latter (**Supplementary Figure 1B**).

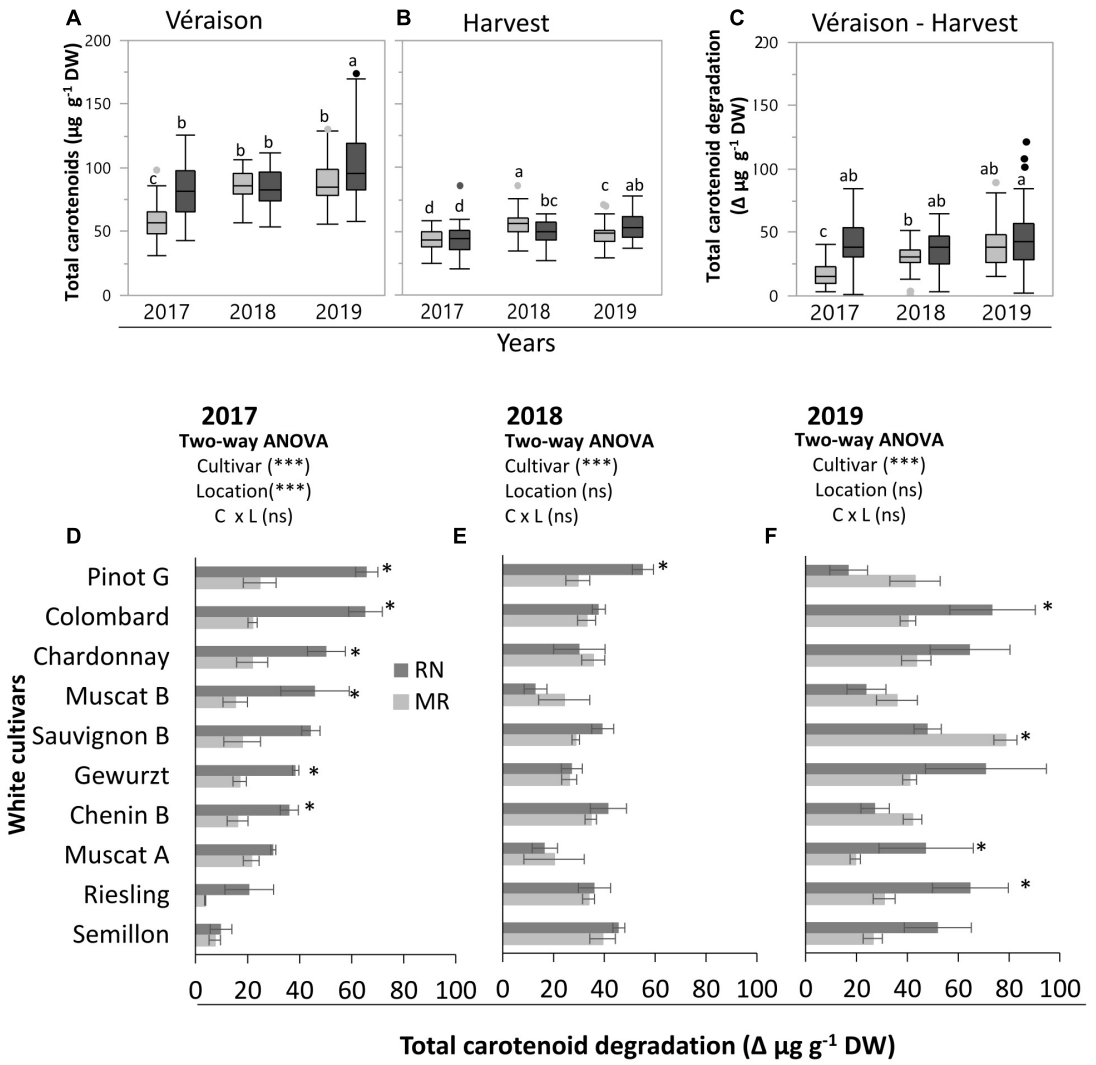

FIGURE 1 | Total carotenoid content at véraison **(A)** and harvest **(B)**, and its degradation **(C–F)** (measured as the difference between véraison and harvest) in white skin berries at the Mitzpe Ramon (MR) and Ramat Negev (RN) vineyards during 2017–2019. Box plots show the difference in the mean of all cultivars (n = 4 replicates × 10 cultivars) between locations in each season (see **Supplementary Table 1**). Gray and black colors indicate cultivars grown at Mitzpe Ramon and Ramat Negev, respectively. Different lowercase letters indicate significant differences in cultivar means between locations. The bar graphs **(D–F)** show the effect of location and cultivar on carotenoid degradation in the 2017, 2018, and 2019 seasons. Error bars are standard error (n = 4). Bar plots followed by * indicate significant differences between locations ($P < 0.05$) within the same cultivar based on a non-parametric t-test. *** indicates significant effects ($P < 0.0001$) of the main factors in each season based on a two-way ANOVA. C, cultivar; L, location; ns, not significant.

Cultivar-Specific Differences in Skin Phenylpropanoids Reflect the Cultivar × Environment Interaction in Response to the Climate Differences Between Locations

Cultivar, location, season, and their interaction all had a significant impact on berry phenology and primary metabolism (Gashu et al., 2020). In a similar manner, skin phenylpropanoids at both véraison and harvest were significantly affected by cultivar, location, season, and their interactions (**Supplementary Tables 3**, **4**). A hierarchical clustering (HCL)-based heatmap visualization of the fold changes (MR/RN) in metabolite level (**Figure 4**) shows the cultivar-related differences between locations; however, there was a seasonal element, as indicated by the significant L × Y interaction (**Supplementary Tables 3**, **4**).

At véraison, the HCL heatmap analysis on the fold change data produced three main metabolite clusters depending on the degree of differences between locations (**Figure 4A**). The first cluster (cluster 1) included metabolites that markedly accumulated at RN, e.g., flavan-3-ols, the phenolic acids, caftaric acid, hydroxybenzoic hexoside, p-coumaric and coutaric acid, and the stilbene, D-viniferin. Clusters 2 and 3 included mainly flavonols, flavanonols, naringenin ch-4-glu, other stilbenes and amino acids, all highly accumulated at MR. Exceptions among

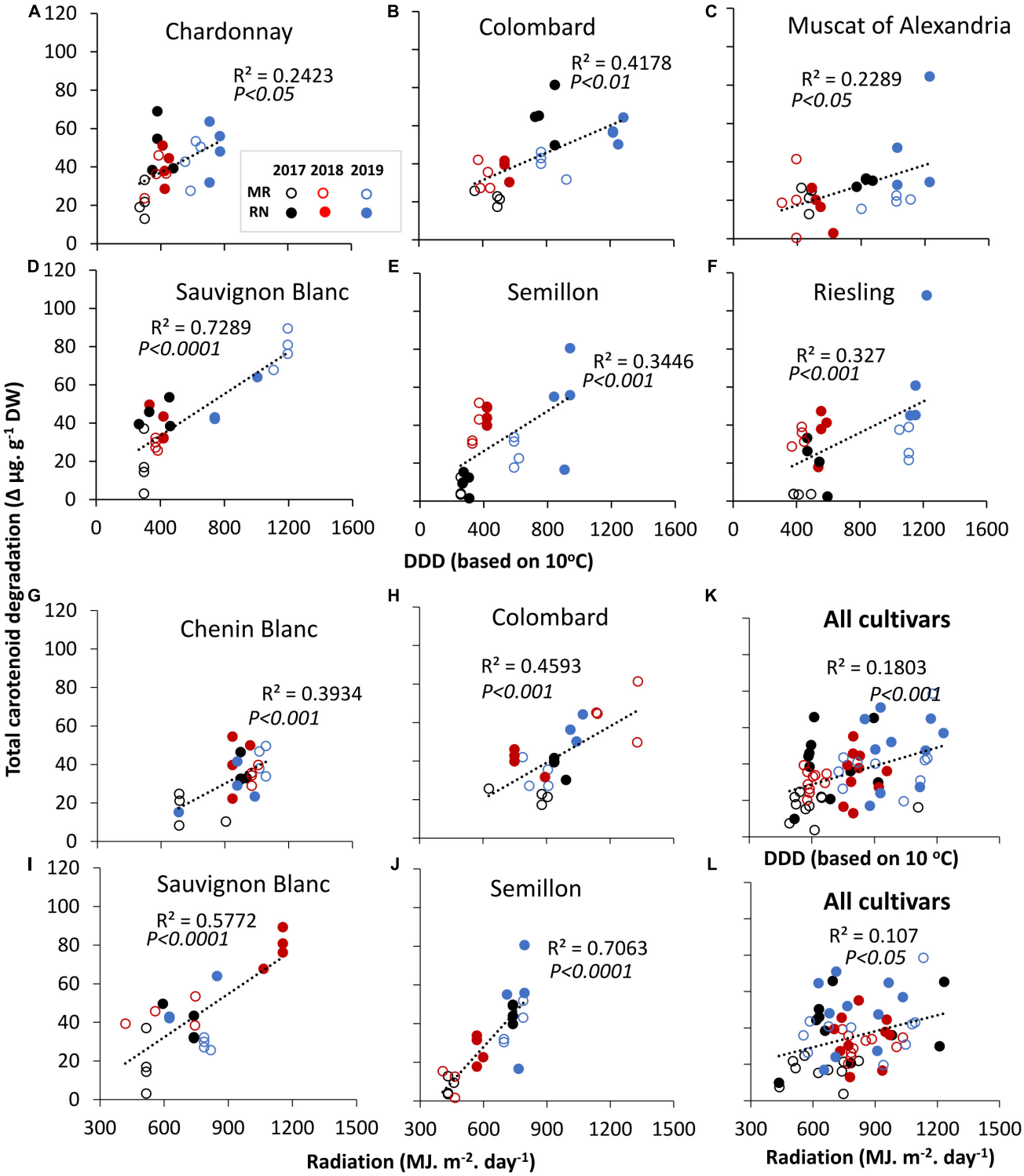

FIGURE 2 | Linear correlation of total carotenoid degradation against accumulated daily degree days (DDD) **(A–F)** and daily summed radiation **(G–J)** that were calculated from véraison to harvest in white cultivars grown at Mitzpe Ramon (MR) and Ramat Negev (RN) during 2017–2019. **(K,L)** Represent correlations of total carotenoid degradation across all cultivars (n = 4 replicates × 10 cultivars × 2 locations × 3 seasons) with DDD and radiation, respectively. In each season, data are values of four biological replicates. Only significant correlations are shown. Circles denote the MR (open) and RN (closed) vineyards. Colors indicate cultivars grown in 2017 (black), 2018 (red), and 2019 (blue). See **Supplementary Table 2**.

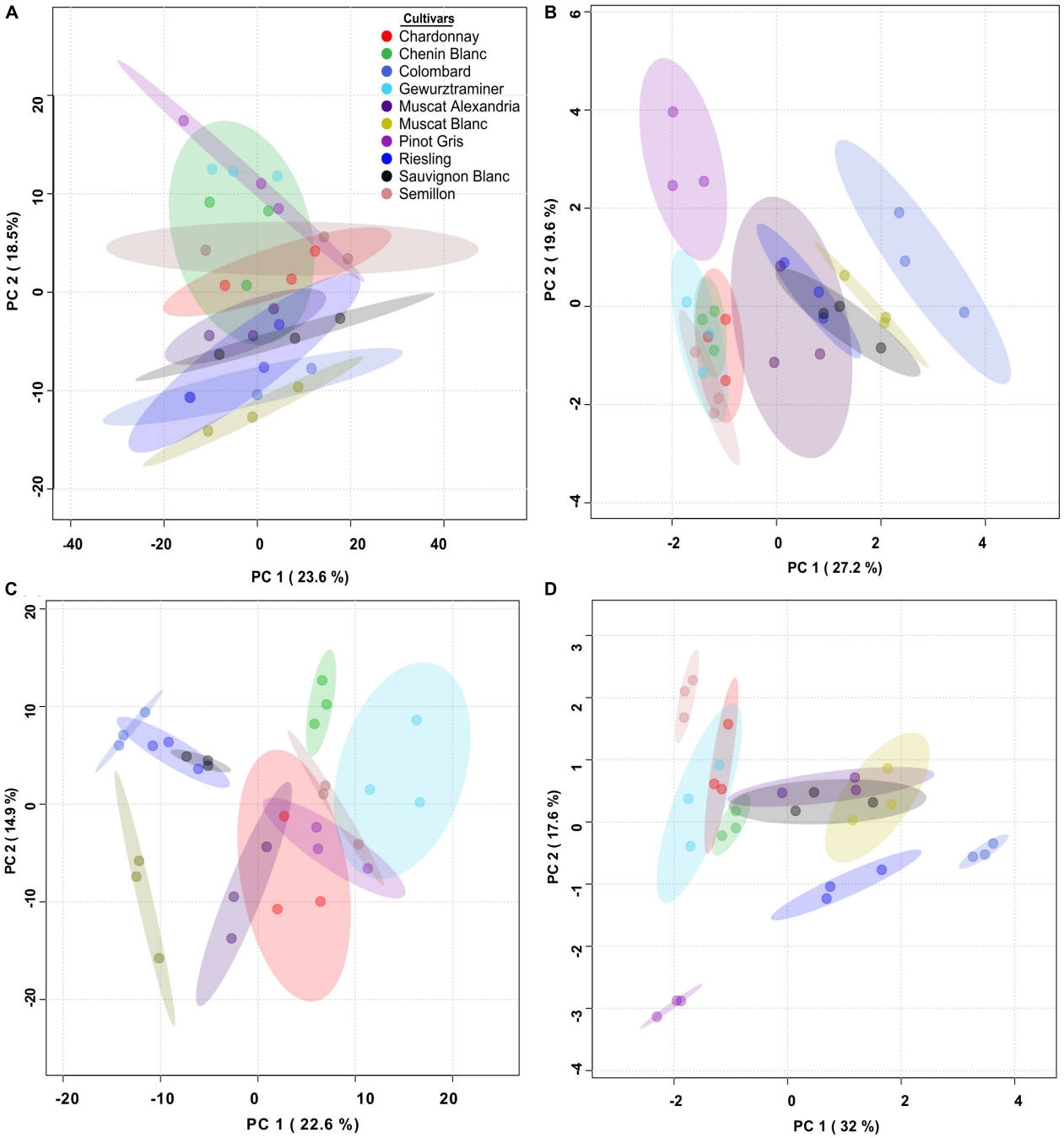

FIGURE 3 | Overview of the differences between cultivars in skin phenylpropanoids at véraison (left) and harvest (right) grown at the Mitzpe Ramon **(A,B)** and Ramat Negev **(C,D)** vineyards during 2017–2019. Principal component analyses (PCAs) were plotted using mean values of four biological replicates (n = 4) in each season. PCAs for véraison samples were generated using pareto-scaled data. PCAs for harvest samples were plotted using log-transformed and pareto-scaled data. Samples are colored by cultivar names.

flavonols (cluster 3) were the lower levels of kaempferol and its aglycones, rutin, and quercetin-3-galactoside in Semillon, Colombard, Sauvignon Blanc, and Pinot Gris at MR (2019) (**Figure 4A** and **Supplementary Figure 2A**). The relative abundance of naringenin ch-4-glu in these cultivars was also lower at MR than at RN in 2019.

At harvest, differences between locations were also evident, particularly in flavonols (**Figure 4B**). Cluster 1 included flavan-3-ols, amino acids, some phenolic acids, and stilbenes, which exhibited only minor differences between locations with very few exceptions among cultivars, e.g., a higher content of stilbenes in Sauvignon Blanc at MR in 2017, while Riesling

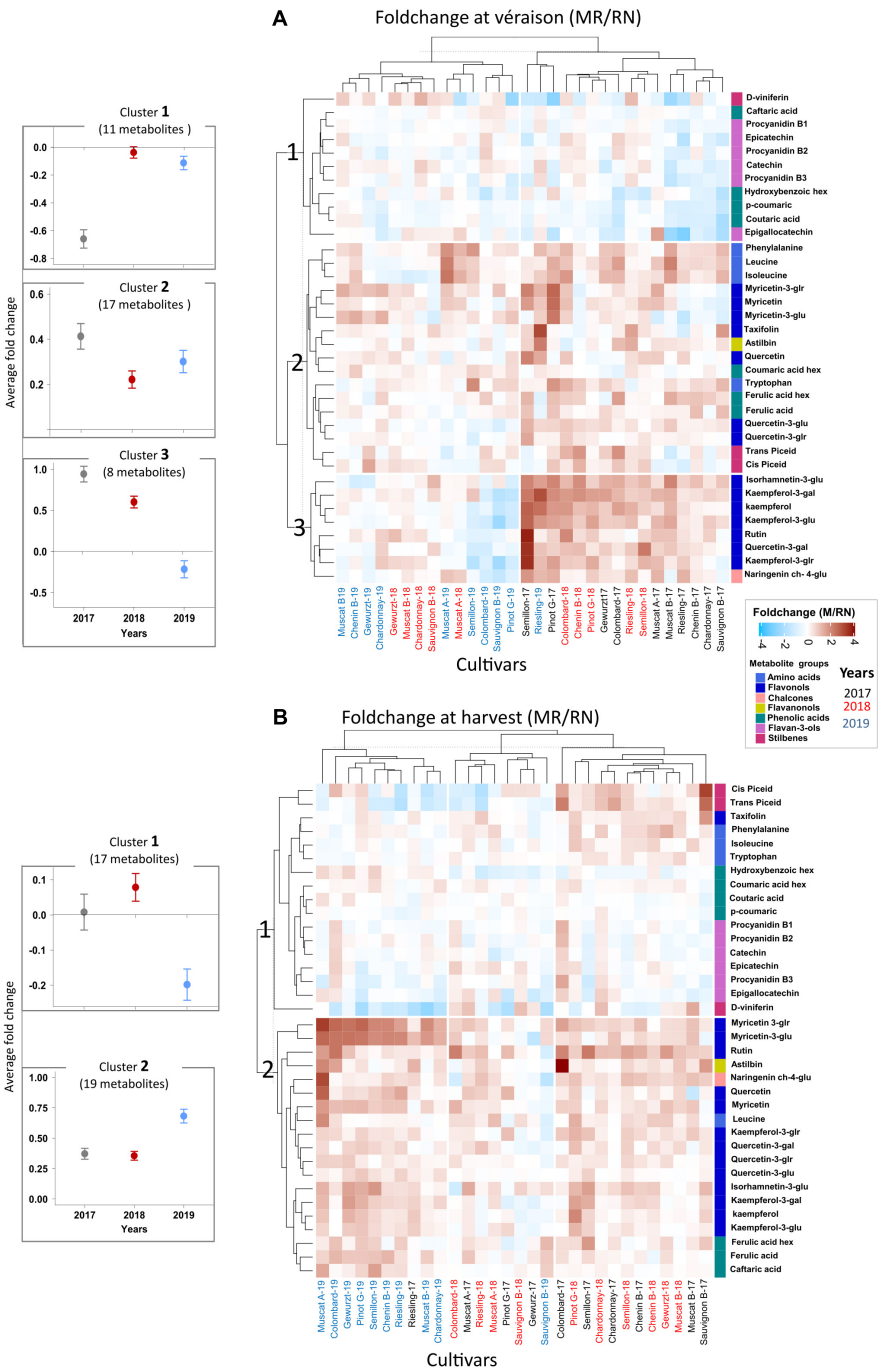

FIGURE 4 | The variability in skin phenylpropanoids at véraison **(A)** and harvest **(B)** between locations during 2017–2019, expressed as the foldchange of average response values [Mitzpe Ramon (MR)/Ramat Negev (RN)]. The mean value of each metabolite (n = 4 biological replicates) for each cultivar in each location and season was calculated separately. Then, the MR values were divided by the RN values and transformed by log2. The heatmap was generated using the log2-transformed data. Euclidean distance was used for hierarchical clustering dendrogram. Cultivar names are denoted by vintage abbreviations (17, 18, 19). Colored cultivar names indicate samples collected in 2017 (black), 2018 (red), and 2019 (blue). Colored rectangles represent metabolite increases at MR (red) and RN (blue). A mirror heatmap of significance values is presented in **Supplementary Figure 2**. The dot plots (left) indicate the average foldchange (±SE) of metabolites in each representative cluster in the 2017, 2018, and 2019 seasons.

had significantly higher stilbenes at the warmer RN site in the 2018 and 2019 seasons. Cluster 2 included metabolites with a remarkably higher content at MR, mainly flavonols and flavanonols. Results indicate that a strong C × Y interaction affected the metabolite profiles in each location (**Figure 4B** and **Supplementary Table 4**). For example, the astilbin foldchange

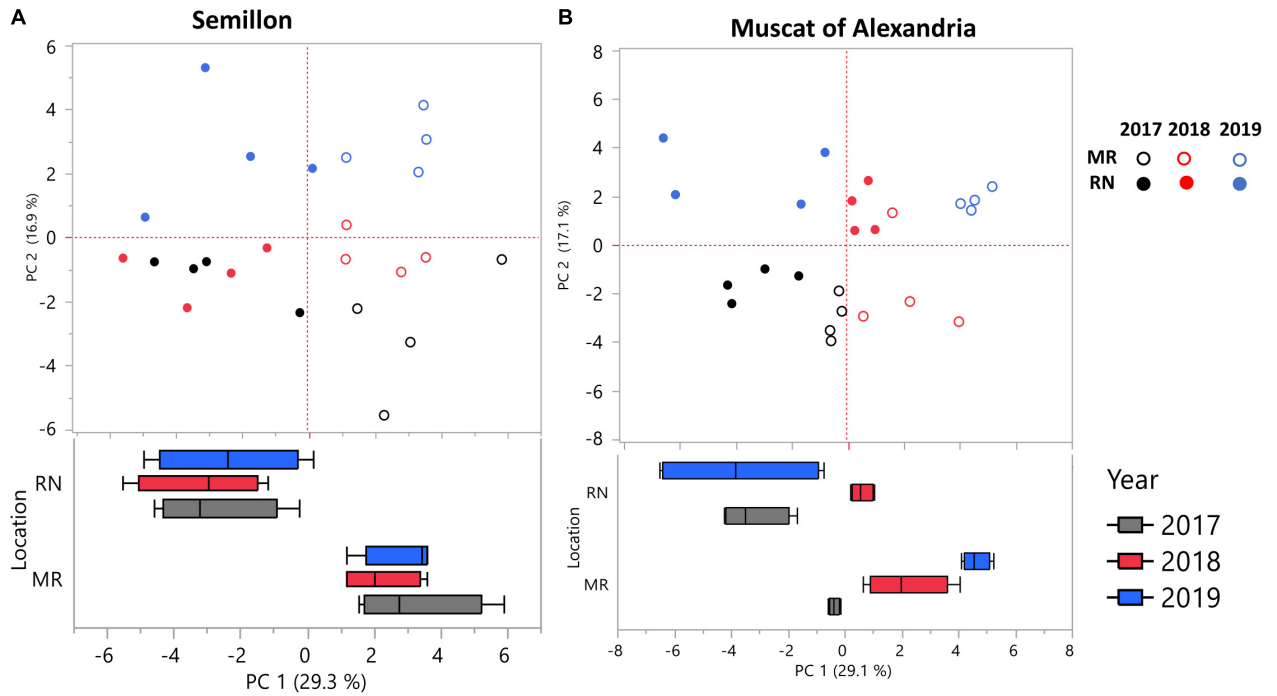

FIGURE 5 | Principal component analysis (PCA) of skin phenylpropanoids at harvest for cultivars affected by location (L) and season (Y) **(A)**, and their interaction **(B)**. **(A)** PCA performed on skin phenylpropanoids of the Semillon cultivar shows that samples are significantly separated by their location, i.e., Ramat Negev (RN) or Mitzpe Ramon (MR). **(B)** PCA performed on skin phenylpropanoids of the Muscat of Alexandria cultivar shows that sample separations are significantly influenced by the L × Y interaction. Data were scaled to the median of each metabolite, and the value of four biological replicates (n = 4) in each season and location were used to plot the PCs. The PCA was first plotted for each cultivar, and a two-way ANOVA model was performed using PCA scores for each cultivar separately. The analysis resulted in the identification of two subsets of cultivars; (i) cultivars affected by location and seasons, and (ii) cultivars affected by L × Y interactions. Only one representative cultivar, **(A,B)** from each group is depicted. Box plots were generated using the first PC scores.

between locations in Colombard (in 2017) was 4-fold greater than in Chardonnay, Gewürztraminer, and Pinot Gris in this year (**Figure 4B** and **Supplementary Figure 2B**). In contrast, only a minor location effect was observed for the phenylpropanoid metabolism of Sauvignon Blanc (in 2019 and 2018) and Gewürztraminer (in 2017).

The change in skin phenylpropanoids from véraison to harvest considerably differed between locations; however, it was season-dependent (**Supplementary Figure 3**). Generally, higher degradation was measured at the warmer RN site, e.g., flavan-3-ols, rutin, quercetin-3-glucuronide and kaempferol-3-glucuronide among flavonols, and caftaric acid, p-coumaric, coutaric acid, and coumaric acid hexoside; nonetheless, the seasonal effect was considerable. The higher pace of reduction from véraison to harvest in leucine in Colombard, Sauvignon Blanc, and Muscat of Alexandria at both locations was an exception among amino acids (**Supplementary Figure 3**), which may possibly affect their aromatic components.

In an effort to identify cultivars that are sensitive to topo-climatic variation, PCs were analyzed and plotted for each cultivar separately, using phenylpropanoid harvest data from 2017, 2018, and 2019. A two-way ANOVA was performed using PCA scores for each cultivar. The analysis resulted in two cultivar groups (**Figures 5A,B**, **Supplementary Table 5**): (i) location sensitive cultivars: Muscat Blanc, Riesling, Semillon and Sauvignon Blanc, and (ii) cultivars affected by the L × Y interaction: Chardonnay, Chenin Blanc, Gewürztraminer, Colombard, Muscat of Alexandria, and Pinot Gris.

To understand the cultivar versus environmental contribution to the observed metabolite changes, we calculated the norm of reaction for all traits (**Supplementary Figure 4**). In the norm of reaction plot, the slope represents phenotypic plasticity; thus, the higher the slope, the greater the phenotypic plasticity of a particular genotype for a particular trait in response to the environment. Among metabolites, myricetin-3-glucuronide exhibited the steepest slope (**Supplementary Figures 4A,B**), indicating that the differences between MR and RN sites were largely attributed to environmental variation.

A 1.5°C Warmer Topo-Climate Imposes Higher Oxidative Stress on Grapevine Cultivars, but Is Differentiated by Genotype

A statistical analysis of H_2O_2 in berries revealed significant effects of cultivar, location, season, and the C × L and C × Y interactions (**Supplementary Table 4**). In seasons 2017 and 2018, the cultivar mean of H_2O_2 was greater at RN than at MR (**Figure 6C**). Here, cultivars such as Sauvignon Blanc, Muscat of Alexandria, and Semillon, exhibited significant differences between locations

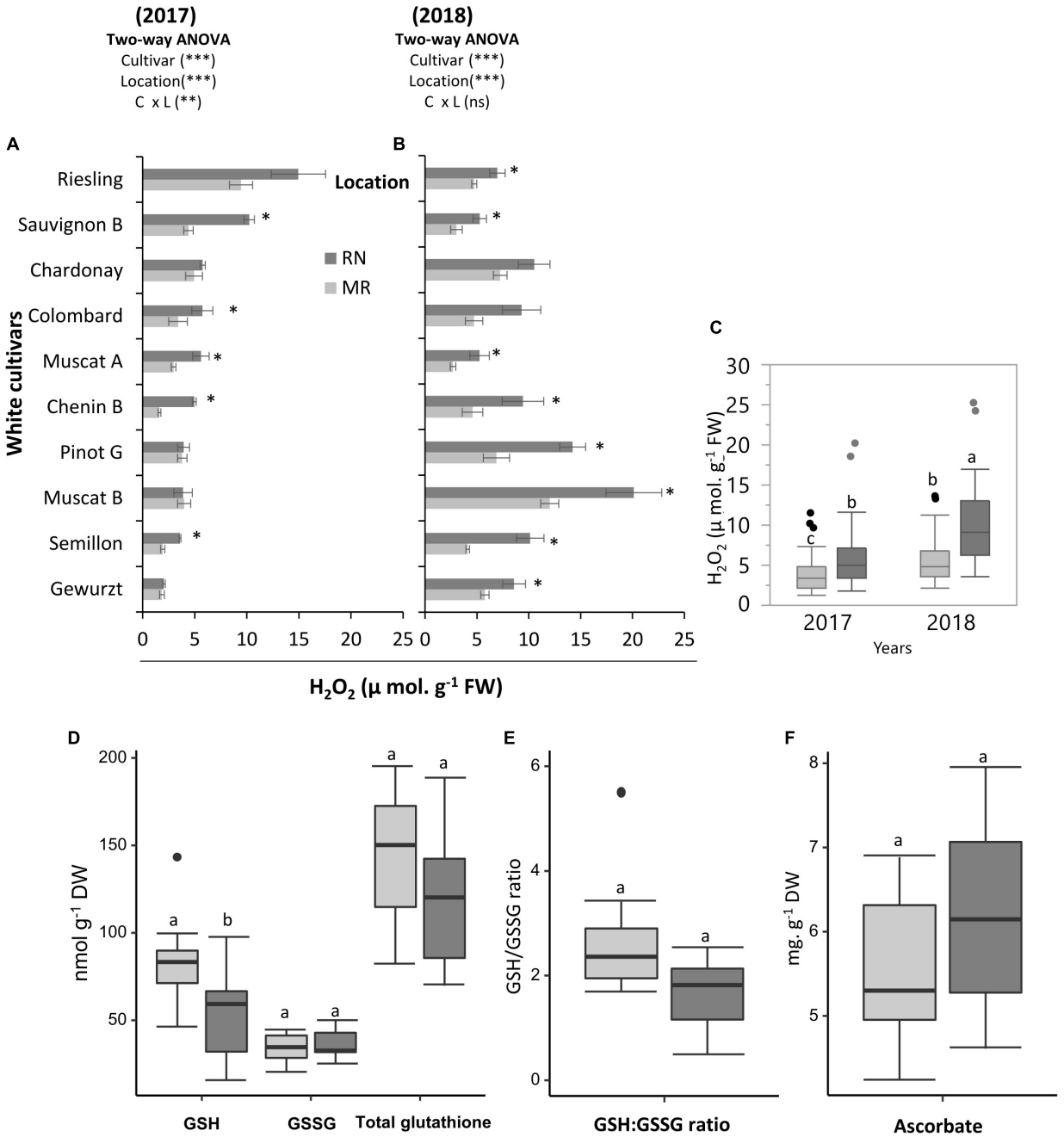

FIGURE 6 | Cultivar and environmental effect on H_2O_2 and major redox buffers in ripe white berries. H_2O_2 content measured on ripe white berries grown at the Mitzpe Ramon (MR) and Ramat Negev (RN) vineyards in 2017 **(A)** and 2018 **(B)**. Error bars are standard error ($n = 4$). Bar plots followed by * indicate significant differences between locations ($P < 0.05$) within the same cultivar based on a non-parametric t-test. $^{**}P < 0.01$, $^{***}P < 0.001$ indicates Significant effects of the main factors in each season based on a two-way ANOVA. The box plot **(C)** shows the difference in the mean H_2O_2 content of all cultivars ($n = 4$ replicates × 10 cultivars) between locations in the 2017 and 2018 seasons. **(D)** The differences in the mean glutathione content and GSH to GSSG ratio **(E)** of all cultivars (n = bulked replicate × 10 cultivars) between locations in the 2018 season. **(F)** The differences in the mean ascorbic acid content of all cultivars (n = bulked replicate × 10 cultivars) between locations in the 2018 season. Different lowercase letters in box plots indicate significant differences in cultivar means between locations. Gray and black colors indicate cultivars grown at Mitzpe Ramon and Ramat Negev, respectively.

in H_2O_2 content in both seasons (**Figures 6A,B**). In addition, the cultivar factor significantly affected ($P < 0.05$) H_2O_2, with accumulation greater in Riesling (14.9 µ mol. g^{-1} FW) and Sauvignon Blanc (10.2 µ mol. g^{-1} FW) berries in 2017, and Muscat Blanc (20.1 µ mol. g^{-1} FW) and Pinot Gris (14.2 µ mol. g^{-1} FW) in 2018 at RN. The lowest H_2O_2 content was

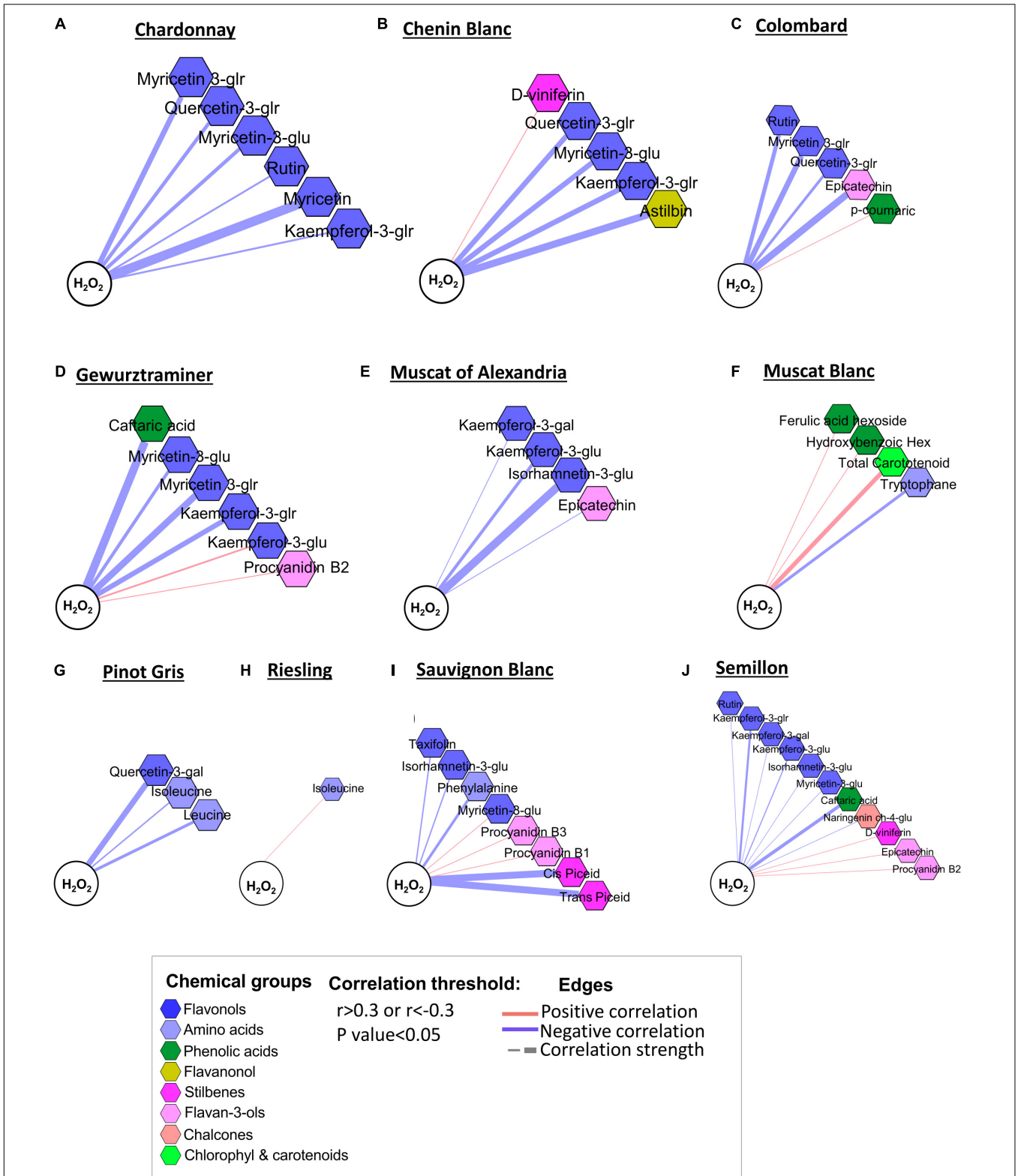

FIGURE 7 | Network visualization of correlations between H_2O_2 and skin phenylpropanoids measured in 10 white grapevine cultivars **(A–J)** in 2017 and 2018. Metabolites are color-coded according to the chemical groups. The correlation analysis was performed using four biological replicates at the Mitzpe Ramon (MR) and Ramat Negev (RN) vineyards in each season; only significant correlations are presented. Positive correlations are shown as red edges, and negative correlations as blue edges. Correlations were based on Pearson's method.

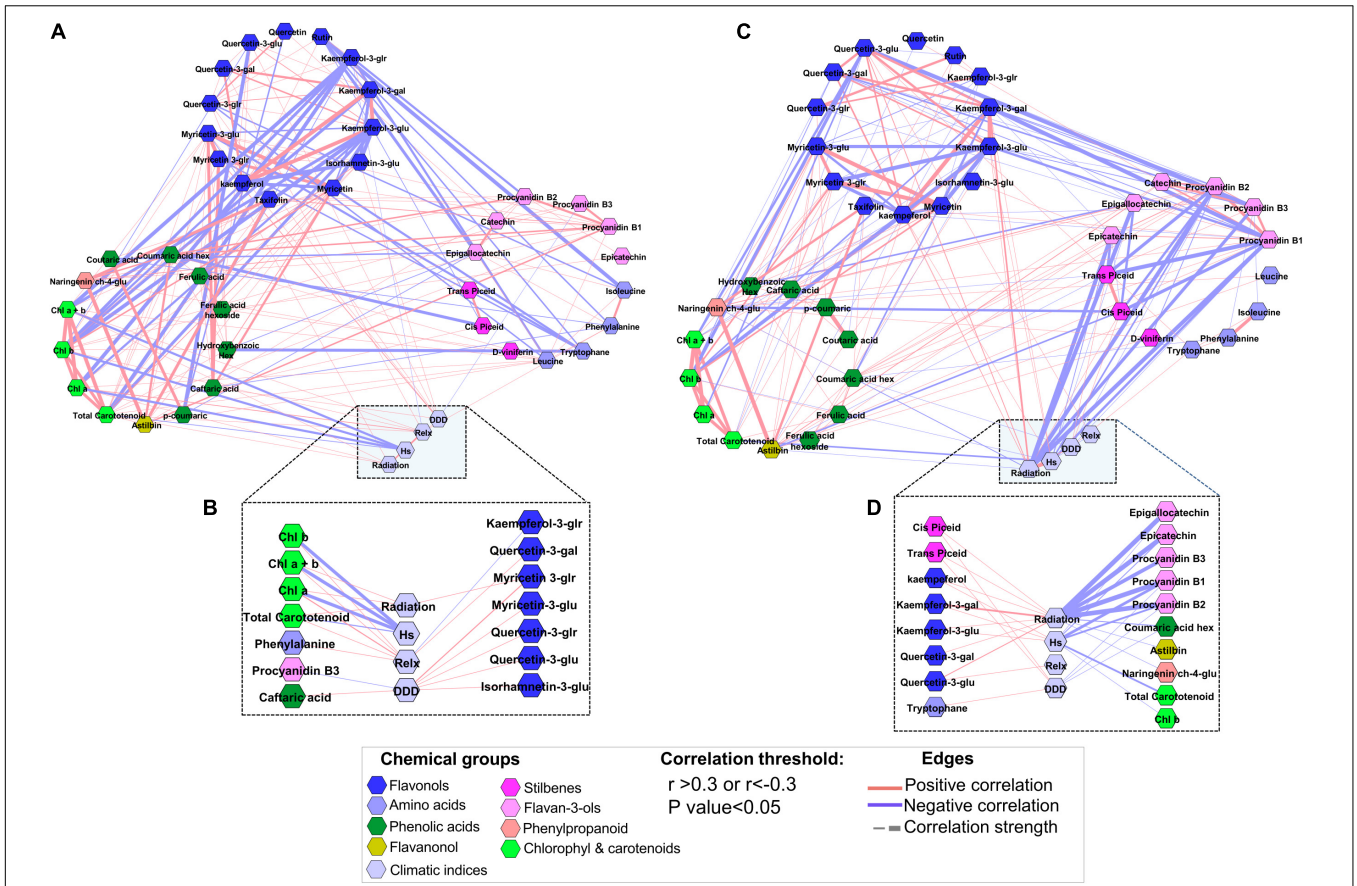

FIGURE 8 | Network visualization of skin phenylpropanoid metabolites as analyzed from ripe white grapevine berries grown at the Mitzpe Ramon (MR) **(A)** and Ramat Negev (RN) **(C)** vineyards during 2017–2019. **(B,D)** Show metabolites significantly correlated with environmental factors (Hs, Relx, and radiation) at MR and RN, respectively. Metabolites are color-coded and clustered according to the chemical groups. Correlation analyses were performed using the mean value of four biological replicates of each cultivar in the 2017, 2018, and 2019 seasons at MR and RN separately; only significant correlations are presented. Positive correlations are shown as red edges, and negative correlations as blue edges. Correlations were based on Pearson's method. Hs, heat stress degree hours; Relx, relaxation degree hours.

measured at the MR vineyard for Chenin Blanc, Semillon, and Gewürztraminer (**Figures 6A,B**).

Since the H_2O_2 content was consistent across seasons, the 2018 samples were used for evaluation of glutathione and Asc in order to get a better picture of the redox adjustment in the fruits. The cultivar mean of GSH was greater at cooler MR than at warmer RN (**Figure 6D**). Cultivars such as Chenin Blanc, Colombard, and Semillon, exhibited higher GSH content at MR than at RN (**Supplementary Figure 5**). In addition, cultivars displayed great variability in GSH content at each site, with the lowest GSH content measured for Chenin Blanc (46.1 and 15.9 nmol g^{-1} DW in MR and RN, respectively) at both sites, whilst the highest content was measured for Semillon (143.3 nmol g^{-1} DW) at MR and Sauvignon (97.3 nmol g^{-1} DW) at RN (**Supplementary Figure 5**). The GSSG content in grape berry skin ranged from 20.1 to 50.3 nmol g^{-1} DW (**Supplementary Figure 5**) but the overall effect of location was not significant (**Figure 6D**). Relatively high GSH:GSSG ratio was observed at the cooler MR, a difference which was mainly attributed to higher GSH content at MR (**Figure 6E**). The GSH:GSSG ratio varied from 1.7 to 5.5 at MR, and from 0.5 to 2.5 at warmer RN (**Supplementary Figure 5**). In addition, 61% (at RN) to 71% (at MR) of the total glutathione in the skin tissue was in the reduced form. In spite of considerable variability between cultivars, Asc content was not affected by location (**Figure 6F**). The Asc content varied from 3.3 to 8.3 mg g DW^{-1}, with the highest value measured for Chenin Blanc and lowest for Chardonnay and Semillon depending on location (**Supplementary Figure 5**).

Flavonols Are Strongly Associated With the Oxidative Status (H_2O_2) of the Berries

The oxidative status of the berries was correlated with the level of skin phenylpropanoids (p-value < 0.05 and $r > 0.3$ or $r < -0.3$), but this relationship was cultivar-specific (**Figures 7A–J**). An increase in the H_2O_2 level in Chardonnay, Chenin Blanc, Colombard, Gewürztraminer, Muscat of Alexandria, Sauvignon Blanc, and Semillon was associated with a lower content of flavonols, mainly glucuronide and glucoside (**Figures 7A–D**). The positive correlations of kaempferol-3-glucuronide and myricetin-3-glucoside with H_2O_2 in Gewürztraminer and

Sauvignon Blanc, respectively, were exceptions among the flavonols (**Figure 7D**). Amino acids, such as tryptophan, leucine, and isoleucine, were negatively correlated with H_2O_2 in Muscat Blanc, Pinot Gris, Riesling, and Sauvignon Blanc, suggesting that at the warmer RN site, higher oxidative stress may lead to the degradation of important volatile precursors. In contrast, flavan-3-ols were generally positively correlated with H_2O_2. Among stilbenes, D-viniferin was positively associated with H_2O_2 in Chenin Blanc and Semillon (**Figures 7B,J**). In contrast, *cis*- and *trans*-piceid displayed strong negative correlations with H_2O_2 in Sauvignon Blanc (**Figure 7I**). Muscat of Alexandria, Muscat Blanc, Pinot Gris, and Riesling (**Figures 7E–H**) showed relatively loose metabolic relations with H_2O_2 compared to Sauvignon Blanc and Semillon (**Figures 7I,J**).

Network Analysis Reveals the Differences Between Vineyards Within the Metabolite-to-Environmental Factor Correlation

To further investigate the relationship of metabolites with temperature and radiation during ripening, a correlation-based network analysis was performed using the metabolite profiles at harvest for RN and MR samples separately. The results showed that the MR network was characterized by a slightly smaller number of edges (180) and a lower network density (0.19) than RN (194 and 0.21 edges and density, respectively) (**Supplementary Table 6**). With the threshold level set at p-value < 0.05 and $r > 0.3$ or $r < -0.3$, metabolite-to-metabolite and metabolite-to-environmental factor correlations were location-specific (**Figure 8**). Amino acids at MR were negatively correlated with flavonols (**Figure 8A**). Similarly, kaempferol and its aglycone were negatively correlated with carotenoid and chlorophyll pigments. It is noteworthy that only phenylalanine, among the amino acids, and procyanidin B3, among the flavan-3-ols, were correlated with climatic factors (**Figure 8B**). Flavonols were positively correlated with accumulated DDD. Chlorophyll and carotenoid pigments were positively correlated with accumulated relaxation degree hours (Relx) and negatively correlated with heat stress degree hours (Hs) (**Figure 8B**).

In contrast to the MR network, in the RN network, amino acids were not correlated with flavonols, but with astilbin and naringenin ch-4-glu (**Figure 8C**). A single positive correlation of tryptophan with quercetin-3-glr was an exception. The correlations of chlorophyll and carotenoid pigments with Relx were not significant (**Figure 8D**). Another significant difference between the two networks stemmed from flavan-3-ols, which were negatively correlated with kaempferol aglycones and quercetin-3-glu in the RN network, but not in the MR network. Of all metabolites correlated with environmental factors, flavan-3-ols showed a robust negative correlation with radiation ($r < 0.5$), while flavonols were positively correlated with radiation and accumulated heat load (Hs) (**Figure 8D**). Network analyses revealed that skin phenylpropanoids at the warmer RN site are tightly linked to the radiation and temperature regimes during fruit ripening, suggesting that the warmer region could experience a greater decline in berry quality, and potentially in wine quality, than the cooler region.

DISCUSSION

Carotenoids are considered to be important ROS quenchers (Ramel et al., 2012). Taking this into account and considering their importance in aroma development, an acute knowledge gap exists regarding carotenoid metabolism in response to temperature in grapevine. For instance, it was found that grapes with a high carotenoid content are produced in warmer regions (Marais et al., 1991; Chen et al., 2017). We show that differences between the warmer RN site and the cooler MR site were strongly dependent on genotype, developmental stage, and seasonal variations (**Figure 1** and **Supplementary Table 1**). In line with what has been previously shown in this study, the mean carotenoid content of véraison berries was more pronounced at the warmer RN site in the 2017 and 2019 seasons. Likewise, the average carotenoid content of ripe berries was higher at RN than at MR in 2019; however, in 2018 it was higher at MR than at RN.

Carotenoids are synthesized from the first stage of fruit formation until véraison, and are degraded during ripening (Chen et al., 2017) to produce C_{13}-norisoprenoid and other compounds (Baumes et al., 2002; Crupi et al., 2010). Young et al. (2015) found that a high carotenoid content at early stages was positively correlated with the volatile norisoprenoid level at later stages in light-exposed berries. However, exposing berries to direct sunlight was reported to reduce carotenoid content in the Bairrada and Vinho Verde region, Portugal (Oliveira et al., 2004). Our results indicate that: (i) overall, greater carotenoid degradation occurs at slightly higher temperatures (**Figure 1**), (ii) degradation is cultivar–specific, and (iii) it was positively correlated with the accumulated DDD and radiation from véraison to harvest, suggesting a synergistic effect of radiation and temperature on carotenoid degradation. Notably, the degradation of carotenoids in Gewürztraminer, Muscat Blanc, and Pinot Gris was not correlated with either factor, suggesting that the enzymatic apparatus responsible for carotenoid cleavage and regulatory genes may differ substantially among cultivars.

Plants, in general, produce ROS when exposed to environmental stresses (Carvalho et al., 2015; Xi et al., 2017). In grape berries, an oxidative burst occurs immediately after véraison due to the rapid accumulation of H_2O_2, resulting in a hastened fruit ripening process (Pilati et al., 2007, 2014; Xi et al., 2017). In our study, however, despite considerable differences between cultivars and seasons, the overall H_2O_2 content among cultivars tended to be higher at the warmer RN site and was associated with extended fruit ripening (Gashu et al., 2020), possibly a con-cause of oxidative stress severity. In addition, higher H_2O_2 content at the warmer RN site was accompanied by lower GSH content, which may explain why berries at the warmer site experienced high oxidative stress. In contrast, greater than 70% of the total glutathione in the grape berry skin tissue at the cooler MR was in the reduced form, which is an indication of better redox buffer (Foyer and Noctor, 2011).

Our results are in contrast to Suklje et al. (2012), who found no increment of GSH content in Sauvignon Blanc grape juice in response to bunch exposure to direct sunlight. However, we believe that the climate component for each location played a role in the difference between the two studies. In other plant species, however, leaf glutathione increased in response to higher radiation, but was generally less responsive than ascorbate (Foyer and Noctor, 2011). Considering that there is no direct evidence showing that GSH can be synthesized in the berry (Kritzinger et al., 2013), lower GSH content at the warmer RN site could be attributed to a slower influx of GSH from source leaves to sink berries under elevated temperatures. A more detailed analysis of the interplay between leaf-photosynthesis and source-sink translocation under different temperature regimes is required to gain conclusive evidence on the regulatory mechanisms driving the redox machinery in grape berries.

In contrast to GSH, Asc content was not affected by location though its content was cultivar-dependent. In a recent study (Gashu et al., 2020), tartaric acid content, a product of Asc catabolism, was significantly higher in véraison berries at the warmer site. It is possible that high temperature could hasten Asc catabolism in the berries toward tartaric acid. Contrasting observations were reported in Shiraz grape berries, where the conversion of Asc to tartrate was shown not to be light-sensitive (Melino et al., 2011).

In different plant species, elevated temperature led to ROS overproduction, resulting in altered cellular metabolism and increased lipid peroxidation (Huan et al., 2016; Hasanuzzaman et al., 2016). Our results indicated that amino acids, flavonols, and stilbenes were inversely correlated with H_2O_2 content, suggesting that higher H_2O_2 content in the fruit could have led to degradation of important volatile precursors and might impair other important phenylpropanoid metabolites. This trend was characterized by considerable variability among cultivars. For instance, Pinot Gris and Riesling were more chemically resilient than Sauvignon Blanc and Semillon, indicating that cultivar diversity could be vital for high quality grape production in arid regions or in a future warmer climate scenario.

Elevated temperature is often reported to reduce anthocyanin accumulation in grapes (Cohen et al., 2008; Pastore et al., 2017; Arrizabalaga et al., 2018; Yan et al., 2020). In contrast, low night temperature (10–11°C) at véraison has been shown to enhance anthocyanin accumulation (Gaiotti et al., 2018). While much of the research on the effects of temperature has been dedicated to enhancing anthocyanin accumulation in red berries, its effect on white skin berry metabolites remains poorly understood. Our analyses show that phenylpropanoids in white skin berries were strongly influenced by cultivar, location, and season, where the warmer site was generally associated with lower phenylpropanoids. The analysis of the norm of reaction revealed (**Supplementary Figure 4A**) that the observed variance in metabolite content was trait-specific, i.e., for some metabolites such as myricetin and its aglycone the observed difference was due to the interaction between cultivar and environment, while for others, e.g., *trans*-piceid, the observed variance was specific to the variety.

In a previous study, prolonged pre-véraison and post-véraison intervals led to a higher risk of exposing clusters to recurrent heatwaves, which can lead to an imbalanced accumulation of precursors for aroma and other quality-related compounds in the fruit (Gashu et al., 2020). In support of this occurrence, we showed a diminished content of the amino acid phenylalanine (a precursor of phenylpropanoids), as well as tryptophan, leucine and isoleucine (precursors of aroma volatiles) in véraison berries at the warmer site. At harvest, results were similar, that is cultivar- and season-specific. These results are in contrast with other studies showing increased amino acid accumulation in the fruit in response to elevated temperature (Torres et al., 2017; Gouot et al., 2019a). Further research is needed to unravel the effect of temperature shifts on polyphenols and their precursors in the central metabolism, possibly by combining metabolite profiling and gene expression analysis.

Phenolic acids play important roles both in defense by protecting plants against biotic stress and as free radical scavengers when fruits are exposed to abiotic stresses (Proestos et al., 2006; Lafay and Gil-Izquierdo, 2008; Mandal et al., 2010; Teixeira et al., 2013). It has been reported that their synthesis, from the first stage of fruit formation until véraison, and their reduction in concentration, with an increase in ripeness (Teixeira et al., 2013), may conceal the influence of temperature on their content at harvest (Del-Castillo-Alonso et al., 2016). In line with what was shown by these studies, phenolic acids did not exhibit a strong correlation with climatic variables in the current study; however, significant differences between locations were found in both véraison and harvest berries, with the latter being more varietal-dependent.

Flavonols are ROS scavengers and UV-B screeners, and act as extreme temperature protectants when fruits are exposed to environmental constraints (Weisshaar and Jenkinst, 1998; Winkel-Shirley, 2002). The literature is inconsistent with respect to the impact of temperature on flavonol accumulation. For example, heat treatment from véraison to harvest reduced flavonol concentration in potted Sangiovese berries (Pastore et al., 2017), while in another study, high temperatures (28/18°C day/night) increased flavonol accumulation in Tempranillo berries (Torres et al., 2017). In the present study, flavonols and flavanonols generally decreased in RN berries both at véraison and harvest (**Figure 4**), suggesting a considerable metabolic response to arid environments, with increasing fruit susceptibility to oxidative stress in warmer regions.

Flavan-3-ols protect against biotic and abiotic stresses while contributing to fruit bitterness and astringency (Bogs et al., 2005; Ullah et al., 2017; Reshef et al., 2018). Despite their importance, little is known about environmental effects on their rate of production. Heat treatment after fruit set has been shown to significantly increase skin flavan-3-ol subunits, and subsequently, skin tannins, in Shiraz berries (Gouot et al., 2019a). In contrast, cold treatment from fruit set to véraison has been reported to increase epigallocatechin in Merlot berries (Cohen et al., 2012). This discrepancy can be explained by cultivar metabolic diversity. In the present study, significant variability between cultivars

was measured; while RN-véraison berries had a generally higher flavan-3-ol content than MR-véraison berries, a greater reduction of these compounds was monitored from véraison to harvest at RN than at MR, resulting in smaller overall differences between locations at harvest. In addition, network analysis revealed that flavan-3-ols were inversely correlated with accumulated radiation and heat load during ripening (**Figure 8B**), likely contributing to the observed pattern of change in flavan-3-ols.

UV light treatment has been reported to trigger stilbene accumulation (Douillet-Breuil et al., 1999; Adrian et al., 2000). However, other studies have not found a significant difference in stilbene accumulation between sites (Dal Santo et al., 2016). In the present study, stilbenes (*cis*- and *trans*-piceid) were significantly lower in the RN berries, particularly at véraison, but were characterized by a cultivar × season interaction. Taken together, these lines of evidence emphasize the significant potential of cultivar plasticity to withstand elevated temperature and heat-induced oxidative processes.

CONCLUSION

This detailed 3-year study on the oxidative status and carotenoid and phenylpropanoid contents of berries in 10 white grape cultivars provide evidence of the fundamental role of cultivar diversity in the production of high quality grapes in arid regions. Here, we showed that both radiation and temperature regimes during fruit ripening synergistically affect carotenoid and phenylpropanoid contents. However, the effect was seasonal and varietal dependent, and the differences in carotenoid and phenylpropanoid contents between sites were not always associated with differences in the length of fruit ripening phases. As a result, careful cultivar selection and strategies for controlled cluster microclimatic conditions must be considered in warm climates. Further research is required to unravel the biodiversity of the regulatory processes modulating carotenoid and phenylpropanoid degradation in *Vitis vinifera.*

DATA AVAILABILITY STATEMENT

The original contributions presented in the study are included in the article/**Supplementary Material**, further inquiries can be directed to the corresponding author.

AUTHOR CONTRIBUTIONS

AB and AF conceived and planned the study. KG, TA, CS, and AB collected the berry samples in the field. TA did carotenoid extraction. AD measured glutathione content. KG prepared the berry samples for extraction, performed the sample extraction and data analysis and analysis using the GC-MS device, and wrote the body of the manuscript with AF and AB. All authors reviewed and approved the manuscript.

FUNDING

This project was partially supported by the Chief Scientist Fund of the Israeli Ministry of Agriculture and the Israeli Wine Grapevine Board.

ACKNOWLEDGMENTS

We would like to thank Destayehu Semaneh, CS, Alon Shlisser, Dong Shuo, Khadijah Ayarnah, Yaara Zohar, Noam Reshef, Moses Kwame, Mais Dzhafarov, Angelica Shapiro, TA, Maria Dolores, Millena Oliveira, and BichThao Nguyen for their support in the field and lab.

SUPPLEMENTARY MATERIAL

The Supplementary Material for this article can be found online at: https://www.frontiersin.org/articles/10.3389/fpls.2022.847268/full#supplementary-material

REFERENCES

Adrian, M., Jeandet, P., Douillet-Breuil, A. C., Tesson, L., and Bessis, R. (2000). Stilbene content of mature *Vitis vinifera* berries in response to UV-C elicitation. *J. Agric. Food Chem.* 48, 6103–6105. doi: 10.1021/jf0009910

Arrizabalaga, M., Morales, F., Oyarzun, M., Delrot, S., Gomès, E., Irigoyen, J. J., et al. (2018). Tempranillo clones differ in the response of berry sugar and anthocyanin accumulation to elevated temperature. *Plant Sci.* 267, 74–83. doi: 10.1016/j.jplph.2020.153226

Azuma, A., Yakushiji, H., Koshita, Y., and Kobayashi, S. (2012). Flavonoid biosynthesis-related genes in grape skin are differentially regulated by temperature and light conditions. *Planta* 236, 1067–1080. doi: 10.1007/s00425-012-1650-x

Baumes, R., Wirth, J., Bureau, S., Gunata, Y., and Razungles, A. (2002). Biogeneration of C13-norisoprenoid compounds: experiments supportive for an apo-carotenoid pathway in grapevines. *Anal. Chim. Acta* 458, 3–14. doi: 10.1016/S0003-2670(01)01589-6

Bogs, J., Downey, M. O., Harvey, J. S., Ashton, A. R., Tanner, G. J., and Robinson, S. P. (2005). Proanthocyanidin synthesis and expression of genes encoding leucoanthocyanidin reductase and anthocyanidin reductase in developing grape berries and grapevine leaves. *Plant Physiol.* 139, 652–663. doi: 10.1104/pp.105.064238

Carvalho, L. C., Vidigal, P., and Amâncio, S. (2015). Oxidative stress homeostasis in grapevine (*Vitis vinifera* L.). *Front. Environ. Sci.* 3:20. doi: 10.3389/fenvs.2015.00020

Chen, W. K., Yu, K. J., Liu, B., Lan, Y. B., Sun, R. Z., Li, Q., et al. (2017). Comparison of transcriptional expression patterns of carotenoid metabolism in 'Cabernet Sauvignon' grapes from two regions with distinct climate. *J. Plant Physiol.* 213, 75–86. doi: 10.1016/j.jplph.2017.03.001

Chong, J., Soufan, O., Li, C., Caraus, I., Li, S., Bourque, G., et al. (2018). MetaboAnalyst 4.0: towards more transparent and integrative metabolomics analysis. *Nucleic Acids Res.* 46, W486–W494. doi: 10.1093/nar/gky310

Cohen, S. D., Tarara, J. M., and Kennedy, J. A. (2008). Assessing the impact of temperature on grape phenolic metabolism. *Anal. Chim. Acta* 621, 57–67. doi: 10.1016/j.aca.2007.11.029

Cohen, S. D., Tarara, J. M., Gambetta, G. A., Matthews, M. A., and Kennedy, J. A. (2012). Impact of diurnal temperature variation on grape berry development,

proanthocyanidin accumulation, and the expression of flavonoid pathway genes. *J. Exp. Bot.* 63, 2655–2665. doi: 10.1093/jxb/err449

Crupi, P., Coletta, A., and Antonacci, D. (2010). Analysis of carotenoids in grapes to predict norisoprenoid varietal aroma of wines from apulia. *J. Agric. Food Chem.* 58, 9647–9656. doi: 10.1021/jf100564v

Dal Santo, S., Fasoli, M., Negri, S., D'incà, E., Vicenzi, N., Guzzo, F., et al. (2016). Plasticity of the berry ripening program in a white grape variety. *Front. Plant Sci.* 7:970. doi: 10.3389/fpls.2016.00970

Decros, G., Baldet, P., Beauvoit, B., Stevens, R., Flandin, A., Colombie, S., et al. (2019). Get the balance right: ROS homeostasis and redox signalling in fruit. *Front. Plant Sci.* 10:1091. doi: 10.3389/fpls.2019.01091

Degu, A., Hochberg, U., Sikron, N., Venturini, L., Buson, G., Ghan, R., et al. (2014). Metabolite and transcript profiling of berry skin during fruit development elucidates differential regulation between Cabernet Sauvignon and Shiraz cultivars at branching points in the polyphenol pathway. *BMC Plant Biolol.* 14:188. doi: 10.1186/s12870-014-0188-4

Del-Castillo-Alonso, M. Á, Castagna, A., Csepregi, K., Hideg, É, Jakab, G., Jansen, M. A. K., et al. (2016). Environmental factors correlated with the metabolite profile of *Vitis vinifera* cv. Pinot noir berry skins along a european latitudinal gradient. *J. Agric. Food Chem.* 64, 8722–8734. doi: 10.1021/acs.jafc.6b03272

Douillet-Breuil, A. C., Jeandet, P., Adrian, M., and Bessis, R. (1999). Changes in the phytoalexin content of various *Vitis* spp. in response to ultraviolet C elicitation. *J. Agric. Food Chem.* 47, 4456–4461. doi: 10.1021/jf9900478

Downey, M. O., Dokoozlian, N. K., and Krstic, M. P. (2006). Cultural practice and environmental impacts on the flavonoid composition of grapes and wine: a review of recent research. *Am. J. Enol. Viticulture* 57, 257–268.

Foyer, C. H., and Noctor, G. (2011). Ascorbate and glutathione: the heart of the redox hub. *Plant Physiol.* 155, 2–18. doi: 10.1104/pp.110.167569

Gaiotti, F., Pastore, C., Filippetti, I., Lovat, L., Belfiore, N., and Tomasi, D. (2018). Low night temperature at veraison enhances the accumulation of anthocyanins in Corvina grapes (*Vitis Vinifera* L.). *Sci. Rep.* 8, 1–13. doi: 10.1038/s41598-018-26921-4

Galili, T. (2015). dendextend: an R package for visualizing, adjusting and comparing trees of hierarchical clustering. *Bioinformatics* 31, 3718–3720. doi: 10.1093/bioinformatics/btv428

Gashu, K., Persi, N. S., Drori, E., Harcavi, E., Agam, N., and Fait, A. (2020). Temperature shift between vineyards modulates berry phenology and primary metabolism in a varietal collection of wine grapevine. *Front. Plant Sci.* 11:588739. doi: 10.3389/fpls.2020.588739

Gill, S. S., and Tuteja, N. (2010). Reactive oxygen species and antioxidant machinery in abiotic stress tolerance in crop plants. *Plant Physiol. Biochem.* 48, 909–930. doi: 10.1016/j.plaphy.2010.08.016

Gouot, J. C., Smith, J. P., Holzapfel, B. P., and Barril, C. (2019a). Impact of short temperature exposure of *Vitis vinifera* L. cv. Shiraz grapevine bunches on berry development, primary metabolism and tannin accumulation. *Environ. Exp. Bot.* 168:103866. doi: 10.1016/j.envexpbot.2019.103866

Gouot, J. C., Smith, J. P., Holzapfel, B. P., Walker, A. R., and Barril, C. (2019b). Grape berry flavonoids: a review of their biochemical responses to high and extreme high temperatures . *J. Exp. Bot.* 70, 397–423. doi: 10.1093/jxb/ery392

Greer, D. H., and Weston, C. (2010). Heat stress affects flowering, berry growth, sugar accumulation and photosynthesis of *Vitis vinifera* cv. Semillon grapevines grown in a controlled environment. *Funct. Plant Biol.* 37, 206–214. doi: 10.1071/FP09209

Gu, Z., Eils, R., and Schlesner, M. (2016). Complex heatmaps reveal patterns and correlations in multidimensional genomic data. *Bioinformatics* 32, 2847–2849. doi: 10.1093/bioinformatics/btw313

Hasanuzzaman, M., Bhuyan, M. H. M. B., Zulfiqar, F., Raza, A., Mohsin, S. M., Mahmud, J. A., et al. (2020). Reactive oxygen species and antioxidant defense in plants under abiotic stress: revisiting the crucial role of a universal defense regulator. *Antioxidants* 9, 681. doi: 10.3390/antiox9080681

He, L., Xu, X. Q., Wang, Y., Chen, W. K., Sun, R. Z., Cheng, G., et al. (2020). Modulation of volatile compound metabolome and transcriptome in grape berries exposed to sunlight under dry-hot climate. *BMC Plant Biol.* 20:59. doi: 10.1186/s12870-020-2268-y

Hochberg, U., Degu, A., Toubiana, D., Gendler, T., Nikoloski, Z., Rachmilevitch, S., et al. (2013). Metabolite profiling and network analysis reveal coordinated changes in grapevine water stress response. *BMC Plant Biol.* 13:184. doi: 10.1186/1471-2229-13-184

Huan, C., Jiang, L., An, X., Yu, M., Xu, Y., Ma, R., et al. (2016). Potential role of reactive oxygen species and antioxidant genes in the regulation of peach fruit development and ripening. *Plant Physiol. Biochem.* 104, 294–303. doi: 10.1016/j.plaphy.2016.05.013

Jagota, S., and Dani, H. (1982). A new colorimetric technique for the estimation of vitamin C using Folin phenol reagent. *Anal. Biochem.* 127, 178–182.

Jones, G. V., Duff, A. A., Hall, A., and Myers, J. W. (2010). Spatial analysis of climate in winegrape growing regions in the western United States. *Am. J. Enol. Viticulture* 61, 313–326.

Joubert, C., Young, P. R., Eyéghé-Bickong, H. A., and Vivier, M. A. (2016). Field-grown grapevine berries use carotenoids and the associated xanthophyll cycles to acclimate to UV exposure differentially in high and low light (Shade) conditions. *Front. Plant Sci.* 7:786. doi: 10.3389/fpls.2016.00786

Kamffer, Z., Bindon, K. A., and Oberholster, A. (2010). Optimization of a method for the extraction and quantification of carotenoids and chlorophylls during ripening in grape berries (*Vitis vinifera* cv. Merlot). *J. Agric. Food Chem.* 58, 6578–6586. doi: 10.1021/jf1004308

Karniel, U., Koch, A., Zamir, D., and Hirschberg, J. (2020). Development of zeaxanthin-rich tomato fruit through genetic manipulations of carotenoid biosynthesis. *Plant Biotechnol. J.* 18, 2292–2303. doi: 10.1111/pbi.13387

Krasnow, M. N., Matthews, M. A., Smith, R. J., Benz, J., Weber, E., and Shackel, K. A. (2010). Distinctive symptoms differentiate four common types of berry shrivel disorder in grape. *Calif. Agric.* 64, 155–159. doi: 10.3733/ca.v064n03p155

Kritzinger, E. C., Bauer, F. F., and du Toit, W. J. (2013). Role of glutathione in winemaking: a review. *J. Agric. Food Chem.* 61, 269–277. doi: 10.1021/jf303665z

Lafay, S., and Gil-Izquierdo, A. (2008). Bioavailability of phenolic acids. *Phytochem. Rev.* 7, 301–311. doi: 10.1007/s11101-007-9077-x

Mandal, S. M., Chakraborty, D., and Dey, S. (2010). Phenolic acids act as signaling molecules in plant-microbe symbioses. *Plant Signal. Behav.* 5, 359–368. doi: 10.4161/psb.5.4.10871

Marais, J., van Wyk, C. J., and Rapp, A. (1991). Carotenoid levels in maturing grapes as affected by climatic regions, sunlight and shade. *South African J. Enol. Viticulture* 12, 64–69.

Melino, V. J., Hayes, M. A., Soole, K. L., and Ford, C. M. (2011). The role of light in the regulation of ascorbate metabolism during berry development in the cultivated grapevine *Vitis vinifera* L. *J. Sci. Food Agric.* 91, 1712–1721. doi: 10.1002/jsfa.4376

Morales-Castilla, I., de Cortázar-Atauri, I. G., Cook, B. I., Lacombe, T., Parker, A., van Leeuwen, C., et al. (2020). Diversity buffers winegrowing regions from climate change losses. *Proc. Natl. Acad. Sci. U.S.A.* 117, 2864–2869. doi: 10.1073/pnas.1906731117

Noctor, G., Mhamdi, A., and Foyer, C. H. (2016). Oxidative stress and antioxidative systems: recipes for successful data collection and interpretation. *Plant Cell Environ.* 39, 1140–1160. doi: 10.1111/pce.12726

Noctor, G., Mhamdi, A., Chaouch, S., Han, Y., Neukermans, J., Marquez-Garcia, B., et al. (2012). Glutathione in plants: an integrated overview. *Plant Cell Environ.* 35, 454–484. doi: 10.1111/j.1365-3040.2011.02400.x

Oliveira, C., Ferreira, A. C., Costa, P., Guerra, J., and De Pinho, P. G. (2004). Effect of some viticultural parameters on the grape carotenoid profile. *J. Agric. Food Chem.* 52, 4178–4184. doi: 10.1021/jf0498766

Oshanova, D., Kurmanbayeva, A., Bekturova, A., Soltabayeva, A., Nurbekova, Z., Standing, D., et al. (2021). Level of sulfite oxidase activity affects sulfur and carbon metabolism in *Arabidopsis*. *Front. Plant Sci.* 12:690830. doi: 10.3389/fpls.2021.690830

Pastore, C., Santo, S. D., Zenoni, S., Movahed, N., Allegro, G., Valentini, G., et al. (2017). Whole plant temperature manipulation affects flavonoid metabolism and the transcriptome of grapevine berries. *Front. Plant Sci.* 8:929. doi: 10.3389/fpls.2017.00929

Pilati, S., Brazzale, D., Guella, G., Milli, A., Ruberti, C., Biasioli, F., et al. (2014). The onset of grapevine berry ripening is characterized by ROS accumulation and lipoxygenase-mediated membrane peroxidation in the skin. *BMC Plant Biolol.* 14:87. doi: 10.1186/1471-2229-14-87

Pilati, S., Perazzolli, M., Malossini, A., Cestaro, A., Demattè, L., Fontana, P., et al. (2007). Genome-wide transcriptional analysis of grapevine berry ripening reveals a set of genes similarly modulated during three seasons and the occurrence of an oxidative burst at vèraison. *BMC Genomics* 8:428. doi: 10.1186/1471-2164-8-428

Proestos, C., Boziaris, I. S., Nychas, G. J. E., and Komaitis, M. (2006). Analysis of flavonoids and phenolic acids in Greek aromatic plants: investigation of their antioxidant capacity and antimicrobial activity. *Food Chem.* 95, 664–671. doi: 10.1016/j.foodchem.2005.01.049

R Development Core Team (2017). *R: A Language and Environment for Statistical Computing*. Vienna: R Foundation for Statistical Computing.

Ramel, F., Birtic, S., Ginies, C., Soubigou-Taconnat, L., Triantaphylides, C., and Havaux, M. (2012). Carotenoid oxidation products are stress signals that mediate gene responses to singlet oxygen in plants. *Proc. Natl. Acad. Sci. U.S.A.* 109, 5535–5540. doi: 10.1073/pnas.1115982109

Reshef, N., Agam, N., and Fait, A. (2018). Grape berry acclimation to excessive solar irradiance leads to repartitioning between major flavonoid groups. *J. Agric. Food Chem.* 66, 3624–3636. doi: 10.1021/acs.jafc.7b04881

Reshef, N., Fait, A., and Agam, N. (2019). Grape berry position affects the diurnal dynamics of its metabolic profile. *Plant Cell Environ.* 42, 1897–1912. doi: 10.1111/pce.13522

Reshef, N., Walbaum, N., Agam, N., and Fait, A. (2017). Sunlight modulates fruit metabolic profile and shapes the spatial pattern of compound accumulation within the grape cluster. *Front. Plant Sci.* 8:70. doi: 10.3389/fpls.2017.00070

Rustioni, L., Fracassetti, D., Prinsi, B., Geuna, F., Ancelotti, A., Fauda, V., et al. (2020). Oxidations in white grape (*Vitis vinifera* L.) skins: comparison between ripening process and photooxidative sunburn symptoms. *Plant Physiol. Biochem.* 150, 270–278. doi: 10.1016/j.plaphy.2020.03.003

Suklje, K., Lisjak, K., Cesnik, H. B., Janes, L., Du Toit, W., Coetzee, Z., et al. (2012). Classification of grape berries according to diameter and total soluble solids to study the effect of light and temperature on methoxypyrazine, glutathione, and hydroxycinnamate evolution during ripening of Sauvignon blanc (*Vitis vinifera* L.). *J. Agric. Food Chem.* 60, 9454–9461. doi: 10.1021/jf3020766

Tarara, J. M., Lee, J., Spayd, S. E., and Scagel, C. F. (2008). Berry temperature and solar radiation alter acylation, proportion, and concentration of anthocyanin in Merlot grapes. *Am. J. Enol. Viticulture* 59, 235–247.

Teixeira, A., Eiras-Dias, J., Castellarin, S. D., and Gerós, H. (2013). Berry phenolics of grapevine under challenging environments. *Int. J. Mol. Sci.* 14, 18711–18739. doi: 10.3390/ijms140918711

Tietze, F. (1969). Enzymic method for quantitative determination of nanogram amounts of total and oxidized glutathione: applications to mammalian blood and other tissues. *Anal. Biochem.* 27, 502–522.

Torres, N., Hilbert, G., Luquin, J., Goicoechea, N., and Antolín, M. C. (2017). Flavonoid and amino acid profiling on *Vitis vinifera* L. cv Tempranillo subjected to deficit irrigation under elevated temperatures. *J. Food Compos. Anal.* 62, 51–62. doi: 10.1016/j.jfca.2017.05.001

Ullah, C., Unsicker, S. B., Fellenberg, C., Constabel, C. P., Schmidt, A., Gershenzon, J., et al. (2017). Flavan-3-ols are an effective chemical defense against rust infection. *Plant Physiol.* 175, 1560–1578. doi: 10.1104/pp.17.00842

Ullah, S., You, Q., Zhang, Y., Bhatti, A. S., Ullah, W., Hagan, D. F. T., et al. (2020). Evaluation of CMIP5 models and projected changes in temperatures over South Asia under global warming of 1.5 oC, 2 oC, and 3 oC. *Atmos. Res.* 246:105122. doi: 10.1016/j.atmosres.2020.105122

Weisshaar, B., and Jenkinst, G. I. (1998). Phenylpropanoid biosynthesis and its regulation. *Curr. Opin. Plant Biol.* 1, 251–257. doi: 10.1016/S1369-5266(98)80113-1

Winkel-Shirley, B. (2002). Biosynthesis of flavonoids and effects of stress. *Curr. Opin. Plant Biol.* 5, 218–223. doi: 10.1016/S1369-5266(02)00256-X

Wintermans, J. F. G. M., and De Mots, A. (1965). Spectrophotometric characteristics of chlorophylls a and b and their phenophytins in ethanol. *Biochim. Biophys. Acta BBA Biophys. Including Photosynth.* 109, 448–453. doi: 10.1016/0926-6585(65)90170-6

Wolkovich, E. M., García De Cortázar-Atauri, I., Morales-Castilla, I., Nicholas, K. A., and Lacombe, T. (2018). From Pinot to Xinomavro in the world's future wine-growing regions. *Nat. Clim. Change* 8, 29–37. doi: 10.1038/s41558-017-0016-6

Xi, F. F., Guo, L. L., Yu, Y. H., Wang, Y., Li, Q., Zhao, H. L., et al. (2017). Comparison of reactive oxygen species metabolism during grape berry development between 'Kyoho' and its early ripening bud mutant 'Fengzao.'. *Plant Physiol. Biochem.* 118, 634–642. doi: 10.1016/j.plaphy.2017.08.007

Yan, Y., Song, C., Falginella, L., and Castellarin, S. D. (2020). Day temperature has a stronger effect than night temperature on anthocyanin and flavonol accumulation in 'Merlot' (*Vitis vinifera* L.) grapes during ripening. *Front. Plant Sci.* 11:1095. doi: 10.3389/fpls.2020.01095

Young, P., Eyeghe-Bickong, H. A., du Plessis, K., Alexandersson, E., Jacobson, D. A., Coetzee, Z. A., et al. (2015). Grapevine plasticity in response to an altered microclimate: sauvignon Blanc modulates specific metabolites in response to increased berry exposure. *Plant Physiol.* 170, 1235–1254. doi: 10.1104/pp.15.01775

Conflict of Interest: AB was employed by Ramat Negev Works Ltd.

The remaining authors declare that the research was conducted in the absence of any commercial or financial relationships that could be construed as a potential conflict of interest.

Publisher's Note: All claims expressed in this article are solely those of the authors and do not necessarily represent those of their affiliated organizations, or those of the publisher, the editors and the reviewers. Any product that may be evaluated in this article, or claim that may be made by its manufacturer, is not guaranteed or endorsed by the publisher.

frontiers in Plant Science

ORIGINAL RESEARCH
published: 10 March 2022
doi: 10.3389/fpls.2022.782159

Rapid Prediction of Fig Phenolic Acids and Flavonoids Using Mid-Infrared Spectroscopy Combined With Partial Least Square Regression

Lahcen Hssaini, Rachid Razouk and Yassine Bouslihim*

National Institute of Agricultural Research (INRA), Rabat, Morocco

Mid-infrared spectroscopy using Fourier transform infrared (FTIR) with attenuated total reflectance (ATR) correction was coupled with partial least square regression (PLSR) for the prediction of phenolic acids and flavonoids in fig (peel and pulp) identified with high-performance liquid chromatography-diode array detector (HPLC-DAD), with regards to their partitioning between peel and pulp. HPLC-DAD was used to quantify the phenolic compounds (PCs). The FTIR spectra were collected between 4,000 and 450 cm^{-1} and the data in the wavenumber range of 1.175–940 cm^{-1}, where the deformations of O-H, C-O, C-H, and C=C corresponded to flavanol and phenols, were used for the establishment of PLSR models. Nine PLSR models were constructed for peel samples, while six were built for pulp extracts. The results showed a high-throughput accuracy of such an approach to predict the PCs in the powder samples. Significant differences were detected between the models built for the two fruit parts. Thus, for both peel and pulp extracts, the coefficient of determination (R^2) ranged from 0.92 to 0.99 and between 0.85 and 0.95 for calibration and cross-validation, respectively, along with a root mean square error (RMSE) values in the range of 0.46–0.9 and 0.23–2.05, respectively. Residual predictive deviation (RPD) values were generally satisfactory, where cyanidin-3,5-diglucoside and cyanidin-3-O-rutinoside had the higher level (RPD $>$ 2.5). Similar differences were observed based on the distribution revealed by partial least squares discriminant analysis (PLS-DA), which showed a remarkable overlapping in the distribution of the samples, which was intense in the pulp extracts. This study suggests the use of FTIR-ATR as a rapid and accurate method for PCs assessment in fresh fig.

Keywords: FTIR-ATR, partial least square regression (PLSR), *Ficus carica* L., phenols, HPLC-DAD

OPEN ACCESS

Edited by:
M. Teresa Sanchez-Ballesta, Institute of Science and Technology of Food and Nutrition (CSIC), Spain

Reviewed by:
Diding Suhandy, Lampung University, Indonesia
Zineelabidine Bakher, Hassan Premier University, Morocco

****Correspondence:***
Lahcen Hssaini
hssaiini@gmail.com

Specialty section:
This article was submitted to Plant Metabolism and Chemodiversity, a section of the journal Frontiers in Plant Science

Received: *23 September 2021*
Accepted: *04 February 2022*
Published: *10 March 2022*

Citation:
Hssaini L, Razouk R and Bouslihim Y (2022) Rapid Prediction of Fig Phenolic Acids and Flavonoids Using Mid-Infrared Spectroscopy Combined With Partial Least Square Regression. Front. Plant Sci. 13:782159. doi: 10.3389/fpls.2022.782159

INTRODUCTION

The rapidly growing interest in functional foods, particularly underutilized fruits and beverages is based on their uniqueness as natural bioactive resources, necessary to enhance the human health and well-being. Worldwide, large species are not fully assessed for their nutritional components and biologically active compounds involved in consumer health promotion so far. Although the

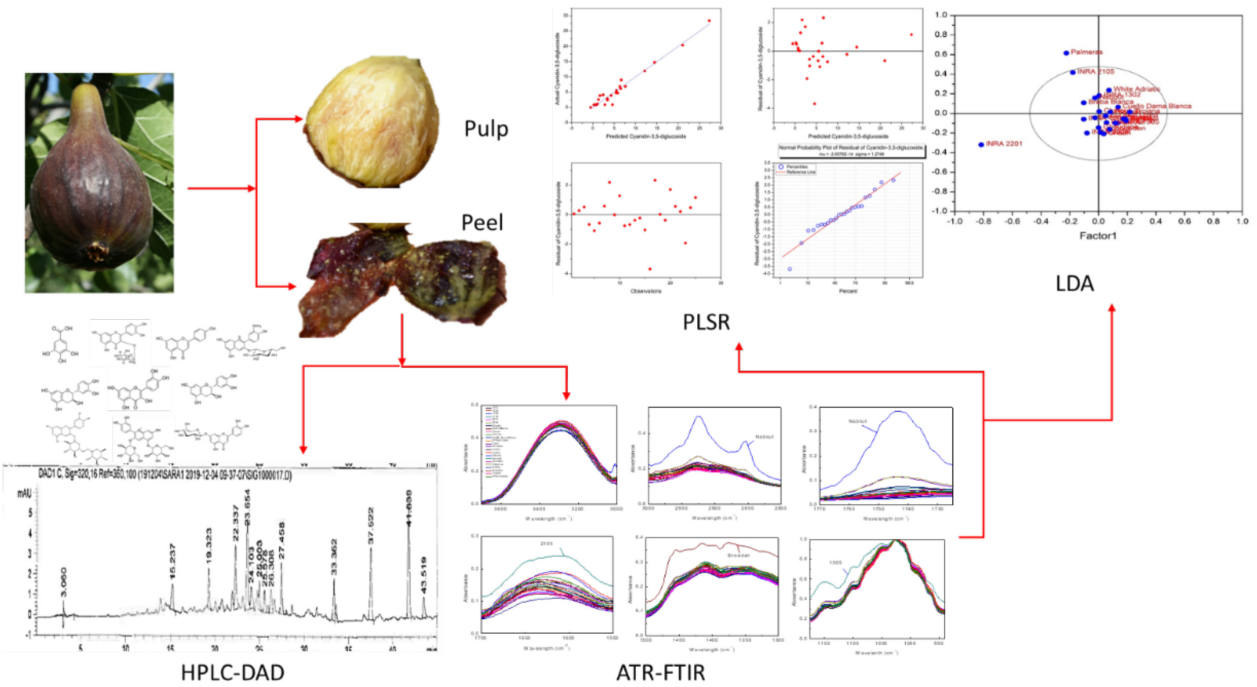

GRAPHICAL ABSTRACT | Scheme diagram showing the research methodology and analytical approaches.

naturally occurring phenotypic, chemotypic, and ecotypic diversity of most of these species is still scarcely screened, it is evident that they present an invaluable potential source of bioactive compounds directly associated with the prevention of coronary diseases. Particular attention should be devoted to the investigation of these species' bioactive compounds, mainly their secondary metabolites, since they not only present the main quality indicators of new cultivars but are also important in chemotaxonomy (Česoniene et al., 2009). Phenolic acids and flavonoids are among the most chemically heterogeneous groups of secondary metabolites synthetized by plants. Screening of these bioactive molecules has gained the most interest during these decades, since it helps in recognizing new raw materials for food, nutraceutical, and cosmetic industries. Figs are an emblematic food of the Middle Eastern and North African diets and constitute an important source of phenolic compounds (PCs) which contribute significantly to their taste, color, astringent flavors, and aroma (Vinson et al., 1998; Kamiloglu and Capanoglu, 2013; Haytowitz et al., 2018; Arvaniti et al., 2019). Anthocyanins, particularly cyanidin-3-rutinoside; flavanols, mainly quercetin-rutinoside; phenolic, such as chlorogenic acid; and flavones, such as luteolin and apigenin-rutinoside, were reported as the major PCs isolated from fresh figs (Vallejo et al., 2012; Viuda-martos et al., 2015; Harzallah et al., 2016).

For high quantification accuracy of these compounds, high performance liquid chromatography (HPLC), with diode array detector (DAD) or even coupled with mass spectroscopy (MS), are among the frequently used conventional techniques (Nadeem and Zeb, 2018). However, these methods are time-consuming, expensive, and require laborious work and a large number of solvents, some of which are hazardous (Koch et al., 2014). Therefore, accurate, rapid, with minimal sample preparation, and low-cost technologies are highly required. Fourier transform infrared (FTIR) spectroscopy presents all these features and therefore, has become among promising spectroscopic technologies, widespread in the analysis of main food components. This technology is highly sensitive, providing different levels of molecular information regarding primary and secondary metabolite structures (Bouyanfif et al., 2019). It measures predominantly molecular vibration and determines its intensity by the dipole moment change during the vibrational mode and provides a specific infrared spectrum, which is the biochemical fingerprint that provides information about molecular composition (Nadeem and Zeb, 2018). Earlier studies showed that the FTIR spectroscopy provided satisfactory results with high-throughput screening framework of numerous biomolecules in several food samples mainly fruits, vegetables, or beverages, e.g., biosynthesis of silver nanoparticles in figs (Jacob et al., 2017), Sudanese honey (Tahir et al., 2017), discrimination of bovine, porcine and fish gelatins (Cebi et al., 2016), fatty acid changes in *Caenorhabditis elegans* (Bouyanfif et al., 2019), mini kiwi (Baranowska-Wójcik and Szwajgier, 2019), red bell pepper (Prabakaran et al., 2017). Therefore, FTIR spectroscopy has emerged as a potential alternative for highly rapid metabolic fingerprinting technique, which can be applied in conjunction with an attenuated total reflection (ATR) correction procedure (Mamera et al., 2020). However, FTIR provides complex spectra, which consists of many related variables (wavenumber) per sample, making its visual analysis very difficult. Hence, the

chemometric and data mining approaches are usually applied to simplify or dimensionally reduce the dataset to fewer independent parameters, with a minimal loss of total variance, thereby making human interpretation easier (Lu et al., 2011). Achieving reproducible results, spectra dimensionality reduction and high fingerprinting throughput acquisition requires a rigorous use of chemometric models capable of associating the numerous spectral intensities from multiple calibration samples to identify chemical fingerprints within samples by removing potential outliers and determining the principal components capturing the high amount of total variance within the dataset (Mamera et al., 2020). The most commonly used multivariate calibrations is partial least squares (PLS), which is an appropriate method for predistortion when highly collinearity is present within the dataset.

One generally agreed, the chemometrics of multivariate adjustments may be used efficiently to identify the relationships between the actual concentration of targeted compounds, as determined by conventional methods, such as HPLC-DAD and predicted amounts using the mid infrared spectroscopy (FTIR spectroscopy in this case) (Tejamukti et al., 2020). Partial least squares regression (PLSR) is a versatile discriminant method, that has been well documented (Brereton and Lloyd, 2014; Mehmood and Ahmed, 2016; Lee and Jemain, 2019). Mathematically, the PLS model has a similar approach to PCA to project high dimensional data into a series of linear subspaces of the explanatory variables (Lee and Jemain, 2019). However, the PLS model assumes a supervised learning process instead of an unsupervised learning approach in the PCA model (Yang and Yang, 2003). The application of FTIR spectroscopy and HPLC combined with multivariate calibration for analysis was reported over several biological raw materials, showing a very significant prediction accuracy, such as honey (Anjos et al., 2015; Tahir et al., 2017), virgin olive oil (Hirri et al., 2016), Mangosteen (Tejamukti et al., 2020), grape, carob and mulberry (Yaman and Velioglu, 2019), coffee beans (Liang et al., 2016), salvia seeds (Tulukcu et al., 2019), and kakadu plum powders (Cozzolino et al., 2021).

Being the third worldwide fig producer, Morocco recognizes this fruit as a principal component of the local people diet. Despite hosting a wide range diversity of this species, local figs remain poorly screened for their biochemical fingerprints linked to its nutritional quality, mainly because of the classic methods used so far are often costly. In this context, the application of rapid, efficient, and the sampling cost approach, with approved prediction accuracy, is of utmost required. In this study, we aimed at screening twenty-five fig cultivars using HPLC-DAD and attenuated total reflectance Fourier transform infrared (ATR–FTIR) coupled with PLS. This study was designed to assess the fig peels and pulps of sampled cultivars separately to evaluate the throughput resolution of PCs prediction through the abovementioned design over the two fruits parts. It also attempts to determine which part of the fruit provides the most relevant discrimination among cultivars. This is the first attempt to predict the amounts of phenolic acids and flavonoids through modeling a colossal FTIR-ATR spectral dataset of fig peels and pulps in Morocco. Building those models for eventual confirmation through time, will immensely contribute to manage the wide range of fig diversity hosted in Moroccan agroecosystems, as a first screening stage with time saving and satisfactory precision level. This study will serve as a useful reference for researchers, food and nutraceutical industries, helping to efficiently and rapidly assess these key fingerprints.

MATERIALS AND METHODS

Plant Material and Experimental Design

Figs of an *ex situ* collection were randomly harvested at their complete ripening stage. The collection is composed of 16 local and 9 exotic varieties which have been planted in 2005 in the experimental station of the National Institute for Agricultural Research of Meknes (INRA) in the Northern Morocco. The collection is conducted in a complete randomized block on ferritic soil. These cultivars were chosen based on our previous studies on 135 cultivars under the same conditions and experimental design, which were screened for their chemotypic (Hssaini et al., 2019) and morphotypic (Hssaini et al., 2020a) diversity besides the combination of both (Hssaini et al., 2020b). The findings of the aforementioned studies revealed highly significant variability, where the cultivars herein investigated captured a high level of total variance and underwent further analysis. **Table 1** shows the fig cultivar herein investigated, their geographical origin, ripening period, and growing conditions along with their respective codes. Figs were considered fully ripened when they were easily separated from the twig and when the receptacle turned to reddish-purple coloration.

Samples Preparation

Immediately after harvesting, the fruits were manually peeled using a sharp stainless knife and both peels and pulp inclosing seeds were sliced, frozen under −80°C for 48 h and then lyophilized at a pressure of 0.250 mbar and temperature for −55°C for 48 h (Alpha 1-2 LD_{plus} lyophilizer, Christ, Osterode, Germany). Hereto, triplicate lots of fig fruits from each genotype were grounded to a powder using an IKA A11 Basic Grinder (St. Louis, MO) at room temperature. The samples were then packaged in polyethylene terephthalate (PET) bags (size: 17 cm × 12 cm L/W; permeability: 50–100 and 245.83–408.64 cm^3 $\mu m/m^2$ h atm for O_2 and CO_2, respectively; permeability to water vapor: 16.25–21.25 g $\mu m/m^2$ h) and vacuum sealed and then, kept refrigerated at 4°C until FTIR-ATR and HPLC-DAD fingerprinting.

Fourier Transform Infrare Spectroscopy

Fourier transform infrared spectra of fig peels and pulps powders were collected between 4,000 and 450 cm^{-1} at a resolution of 4 cm^{-1} on Perkin–Elmer Fourier transform infrared spectrometer (Perkin Elmer, Waltham, MA, United States). At room temperature, each sample was scanned three times in distinct randomly mass (50 mg) of the sample. For each FTIR spectrum, three scans were averaged and IR spectrum corresponded to the accumulation of 128 scans. The germanium crystal was in contact with the sample after applying a pressure setting at a maximum of 1,700 kg/cm^2 to ensure uniform

TABLE 1 | Cultivars geographical origins, harvest time, and monthly meteorological data from August to early September 2018 in Northern Morocco, Meknes (Ain-Taoujdate experimental station -INRA).

	Cultivars	Code	Geographical origin	August						September	
				[1–5]	[6–10]	[11–15]	[16–20]	[21–25]	[26–30]	[31–4]	[5–9]
Local	El Quoti Lbied	G13	Morocco								
	Nabout	G18									
	Fassi	G14									
	Noukali	G19									
	Ghoudan	G15									
	Chetoui	G11									
	Bioudie	G7									
	Chaari	G10									
	Ournaksi	G20									
	INRA 1305	G3									
	INRA 2105	G4									
	INRA 1302	G2									
	INRA 2201	G5									
	INRA 2304	G6									
	INRA 1301	G1									
Introduced	Snowden	G23	United States								
	White Adriatic	G25	Italy								
	Kadota	G17	Italy								
	Troiana	G24	Italy								
	Cuello Dama Blanca	G12	Spain								
	Breval Blanca	G9	Spain								
	Palmeras	G21	Spain								
	Herida	G16	Spain								
	Breba Blanca	G8	Spain								
Total rainfall (mm)				0	0	0	0	0	26.4	0	0
Average temperature (°c)				25.84	28.5	27.56	29.24	29.44	23.64	25.6	25.42
Average solar radiation (W/m^2)				169.29	208.74	243.83	238.28	185.35	123.5	270.21	271.38
Soil type				Sandy clay loam with an average organic matter of 1% [0–30 cm soil layer]							
Soil pH				7.2							

Climatic data collected from meteorological station installed next to the orchard.

distribution of the sample across the crystal and to achieve a high-resolution of the acquired IR spectra (Szakonyi and Zelkó, 2012). Prior to sample measurements, a background spectrum was collected from an empty germanium crystal surface and automatically subtracted from the spectra of the sample. The crystal cell was cleaned between spectral collections using ethyl alcohol and warm water and dried with absorbent paper. The standard normal variate (SNV) and multiplicative scattering correction (MSC) were first carried out to correct multiplicative interferences (Tahir et al., 2017). Then, the raw FTIR spectra were corrected by the extended ATR correction procedure using Essential FTIR software (version 3.50.183) (angle of incidence = 45 degrees; number of ATR reflection = 1; mean refractive index of sample = 1.5; maximum interaction = 50; 1.8 mm crystal surface). The most important feature of ATR is the evanescent field, which occurs during the reflection of IR light at the interface of a material with a high refractive index (ATR crystal) and a material with a low refractive index (sample) (de Nardo et al., 2009). The full spectra of fig samples indicate the presence of some regions corresponding to the sample fingerprints of which integrated areas were measured using Essential FTIR software.

Determination of Phenolic Compounds

Extraction Method

For each sample, 1 g of peel and pulp powder were separately mixed with 10 ml of methanol:water (80:20, v/v). The mixture was sonicated using an ultra-sonicator UP 400St Hielscher's (400 W, 24 kHz) and then macerated for 60 min at 4°C. Afterward, it was centrifuged for 10 min, 8,000 g at 4°C (Eppendorf Centrifuge 5804, Eppendorf, Hamburg, Germany) and the supernatant was collected and the sediment was mixed with 10 ml of acetone:water (70:30, v/v). The same steps (sonication, maceration, and centrifugation) were repeated three times, and the supernatants were mixed together and then evaporated using a rotary evaporator (Büchi R-205, Switzerland) under a speed of 1,500 rpm and reduced pressure, at 40°C. Then, 5 ml of methanol was added to the residue, and the mixture was well shaken in a

TABLE 2 | Descriptive analysis and multivariate ANOVA of all studied variables over fig peels and pulps.

Variables		Mini	Max	Mean	*SD*	Dominance	ANOVA p-value
Peel							
Gallic acid		0	11.29	0.54	2.24	2	< 0.001
(+)-Catechin		0	24.06	5.89	5.95	24	< 0.001
(−)-Epicatechin		2.61	55.44	17.31	12.89	25	< 0.001
Chlorogenic acid		0	10.67	3.03	2.94	24	< 0.001
Quercetin-3-O-rutinoside		5.3	147.42	58.46	38.66	25	< 0.001
Quercetin-3-O-glucoside		2.52	35.58	11.48	7.76	25	< 0.001
Luteolin-7-O-glucoside		0	18.24	6.75	4.87	22	< 0.001
Quercetin		0	59.61	4.49	12.48	15	< 0.001
Apigenin		0	4.91	0.41	1.04	5	< 0.001
Cyanidin-3,5-diglucoside		0	495.76	48.58	109.91	16	< 0.001
Cyanidin-3-O-rutinoside		0	478.9	46.78	105.29	15	< 0.001
Pelargonidin-3-O-rutinoside		0	12.67	0.67	2.58	2	< 0.001
Pulp							
Gallic acid		nd	nd	nd	Nd	nd	–
(+)-Catechin		0	6.65	1.47	1.4	19	< 0.001
(−)-Epicatechin		1.25	19.06	5.23	4.03	25	< 0.001
Chlorogenic acid		0	4.84	0.77	1.09	19	< 0.001
Quercetin-3-O-rutinoside		0	26.85	1.89	5.16	17	< 0.001
Quercetin-3-O-glucoside		0	4.05	0.44	0.95	6	< 0.001
Luteolin-7-O-glucoside		0	4.5	0.21	0.89	2	< 0.001
Quercetin		nd	nd	nd	Nd	nd	–
Apigenin		nd	nd	nd	Nd	nd	–
Cyanidin-3,5-diglucoside		0	28.45	5.82	6.68	24	< 0.001
Cyanidin-3-O-rutinoside		0.94	34.43	9.01	8.67	25	< 0.001
Pelargonidin-3-O-rutinoside		nd	nd	nd	Nd	nd	–
Effect	**Wilks Lambda's value**	**F**	**Hypothesis df**	**Error df**			**Significance**
Variety	0	477.23	560	1376.367			0
Fruit part	0	496075.72	20	79			0
Variety * Fruit part	0	464.37	440	1242.807			0

nd, not detected; df, degree of liberty; F, refers to Fisher statistic; Sig., signification; Cyan, cyanidin; cy-3-r, Cyanidin-3-rutinoside; dominance, denotes the number of samples, where the phenolic compound was identified.

Vortex for 2 min. The samples were filtered through a Sep-Pak (c-18) to remove the sugar content and then were stored at −20°C until further use.

Phenolic Compounds Assessment

Polyphenolic profiles of both peel and pulp fruits were determined by HPLC as described by Genskowsky et al. (2016). Briefly, a volume of 20 μl of each sample was injected into a Hewlett-Packard HPLC series 1200 instrument equipped with C18 column (Mediterranea sea 18, 25 cm × 0.4 cm, 5 cm particle size) from Teknokroma (Barcelona, Spain). Polyphenolic acids and flavonoids were assessed in standard and sample solutions, using a gradient elution at 1 ml/min. The mobile phases consisted of formic acid in water (1:99, v/v) as solvent A and acetonitrile as solvent B. The chromatograms were recorded at 280, 320, 360, and 520 nm. A quantitative analysis of PCs was carried out by reference to authentic standards: gallic acid, (+)-catechin, (−)-epicatechin, chlorogenic acid, quercetin-3-O-rutinoside, quercetin-3-O-glucoside, luteolin-7-O-glucoside, quercetin, apigenin, cyanidin-3,5-diglucoside, cyanidin-3-O-rutinoside, and pelargonidin-3-O-rutinoside (Extrasynthese, Genay, France). Their identification was carried out by comparing the UV absorption spectra and retention times of each of them with those of pure standards injected under the same conditions. Each sample was assessed in triplicate and the results were expressed as μg/g of the dry weight (dw).

The linearity of the method above described was evaluated by analyzing the herein used standard solutions at different concentrations. An average correlation coefficient of 0.987 was obtained through calibration curves for all the standards. Afterward, the recovery test was performed by spiking samples at different concentrations with known amounts of each standard. Spiked and unspiked extracts were then analyzed in triplicate. With regards to the complexity of the samples, satisfactory recovery levels were obtained (86–98%) alongside low standard error values within a narrow range of variation (0.07–1.23%).

Data Processing

Prior to statistical analysis, data were tested for normality and homogeneity. Afterward, one-way ANOVA was performed using SPSS software V 22 to test significant differences among the samples ($p < 0.05$) in both peels and pulps. The principal

component model was performed to detect any spectral outliers in the FTIR-ATR data prior to build a prediction model using PLSR. Interference and overlapping in the obtained spectra may be overcome by using a powerful multicomponent method, such as PLSR (Hirri et al., 2016). Therefore, PLSR was used for building predictive models between the FTIR-ATR spectra and HPLC-DAD reference data for both fig peel and the pulp using OriginPro software v 9 (OriginLab Corporation Inc.). The optimum numbers of factor to be extracted were decided based on the model with minimum root mean predicted residual sum of squares (PRESS) by jack-knifing within a cross-model validation framework to inspect the predictive capability of all calibration models. Jack-knifing is a cross validation procedure that relies on uncertainty tests of the regression coefficients to test the significance of the model parameters (Karaman et al., 2013). The samples were randomly divided into two subsets. One of them was used to develop a model (calibration set = 20 samples) and the second one was used to validate the robustness of the built model (prediction set = 5 samples). According to Goodhue et al. (2006) and Sarstedt et al. (2017), PLSR can be applied efficiently on a small sample size particularly when models are complex. Besides, many previous studies have performed a PLS regression model on smaller sample size with satisfactory results (Tenenhaus et al., 2005; Zheng et al., 2017). The accuracy of PLSR models

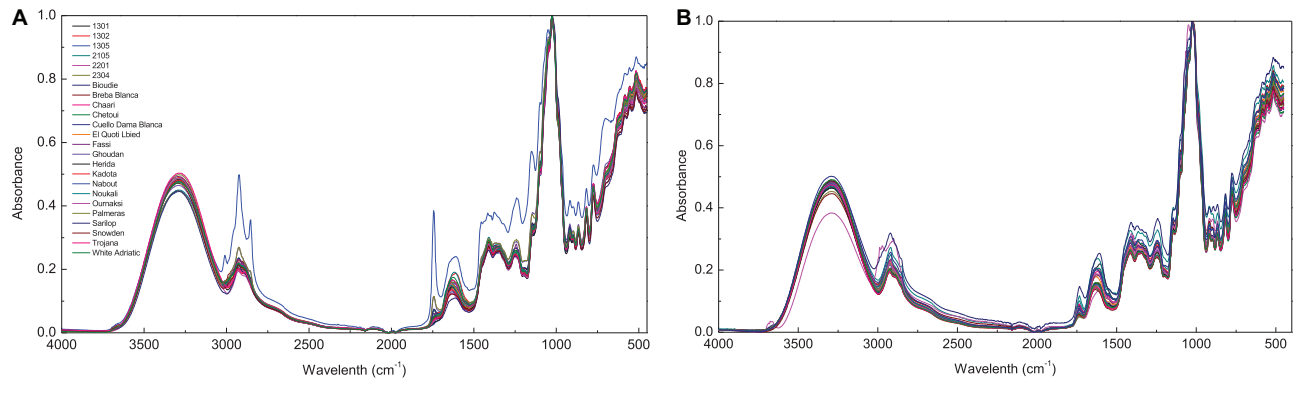

FIGURE 1 | Spectra of different fig cultivars. FTIR spectra with absorbance value 450–4,000 cm^{-1} (before data pre-processing); **(A)**, Fig pulp spectra; **(B)**, fig peels.

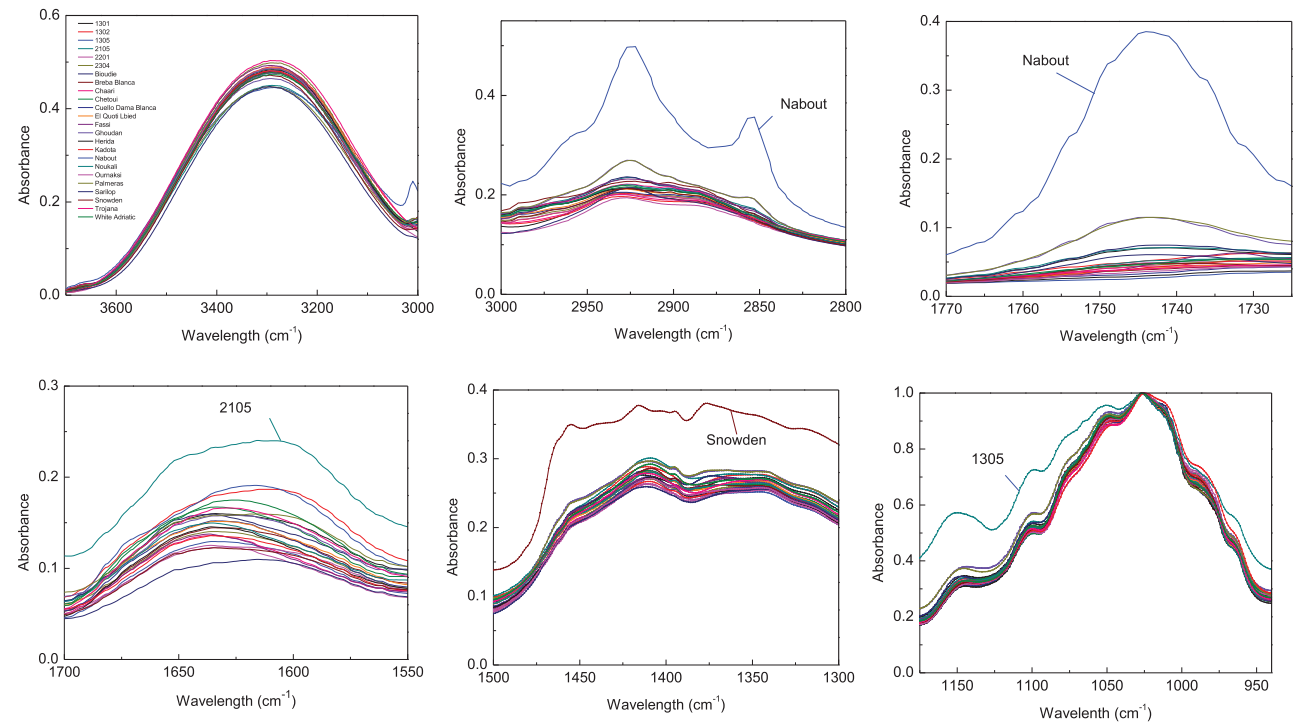

FIGURE 2 | Integrated ATR spectra of the major wavenumbers in pulp samples. Each sample IR represent the mean of 3 spectra, which correspond each to the accumulation of 128 scans using a nominal resolution of 4 cm^{-1}.

was assessed in the terms of root mean square error (RMSE), the correlation coefficient (R^2) between actual and predicted values along with the residual predictive deviation (RPD), which is calculated as the ratio of the SD of the dependent data to RMSE (Cozzolino et al., 2021). PLSR models were performed using the FTIR-ATR data within the vibration region of 1,175–940 cm^{-1}.

RESULTS AND DISCUSSION

Phenolic Profile

Table 2 shows the descriptive statistics (average, range, and SD) along with the ANOVA for the concentration of phenolic fractions in the fig peel and pulp of investigated cultivars. High performance chromatography analysis identified several PCs belonging to phenolic acids (hydroxycinnamic acid and hydroxybenzoic acid derivatives) and flavonoids (flavonols, flavones, and anthocyanidins). Eight PCs were identified over the pulp samples, mainly (+)-catechin, (−)-epicatechin, chlorogenic acid, quercetin-3-O-rutinoside, quercetin-3-O-glucoside, luteolin-7-O-glucoside, cyanidin-3,5-diglucoside, and cyanidin-3-O-rutinoside. On the other hand, twelve PCs were isolated: gallic acid, (+)-catechin, (−)-epicatechin, chlorogenic acid, quercetin-3-O-rutinoside, quercetin-3-O-glucoside, luteolin-7-O-glucoside, quercetin, apigenin, cyanidin-3,5-diglucoside, cyanidin-3-O-rutinoside, and pelargonidine-3-O-rutinoside. These compounds displayed highly significant differences across cultivars following both fruits parts ($p < 0.001$) (**Table 2**). Among all sampled fruits, the PCs concentrations were higher in peels compared with pulps extracts. Anthocyanins, particularly cyanidin-3,5-diglucoside and cyanidin-3-O-rutinoside, were predominant in peel extracts, of which the average concentrations were 75.902 ± 18.76 and 77.972 ± 18.95 μg/g dw, respectively. Regarding flavonols, only (−)-epicatechin, quercetin-3-O-rutinoside, and quercetin-3-O-glucoside were identified. Gallic acid and pelargonidin-3-O-rutinoside were only detected in two cultivars "Chetoui" and "Nabout," with the respective levels of 8.363 ± 1.88 and 6.731 ± 2.019 μg/g dw. These results agree with those reported in previous research (Vallejo et al., 2012; Hirri et al., 2016; Cozzolino et al., 2021). Only one sample ('1301') has displayed the highest levels in almost all identified compounds, especially (−)-epicatechin, quercetin-3-O-rutinoside, quercetin-3-O-glucoside, cyanidine-3,5-diglucoside, and cyanidine-3-O-rutinoside, where the average concentrations were 54.66, 141.08, 35.48, 494.08, and 478.66 μg/g dw, respectively. Similarly, the Spanish variety "Cuello Dama Blanca" combined the highest levels of chlorogenic acid, luteolin-7-O-glucoside, quercetin, and apigenin with 8.76, 17.9, 59.52, and 4.84 μg/g dw, respectively.

In pulps extracts, (−)-epicatechin and cyanidin-3-O-rutinoside were the major compounds, which were identified in all samples at high levels:1.25–19.06 and 0.94–34.43 μg/g dw, respectively. Cyanidin-3,5-diglucoside were the third predominant compound that ranged from 0.81 to 28.45 μg/g dw, with a mean of 6.06 ± 6.71 μg/g dw, followed by (+)-catechin and chlorogenic acid (1.93 ± 1.29 and 1.01 ± 1.16 μg/g dw, respectively). However, luteolin-7-O-glucoside was detected in

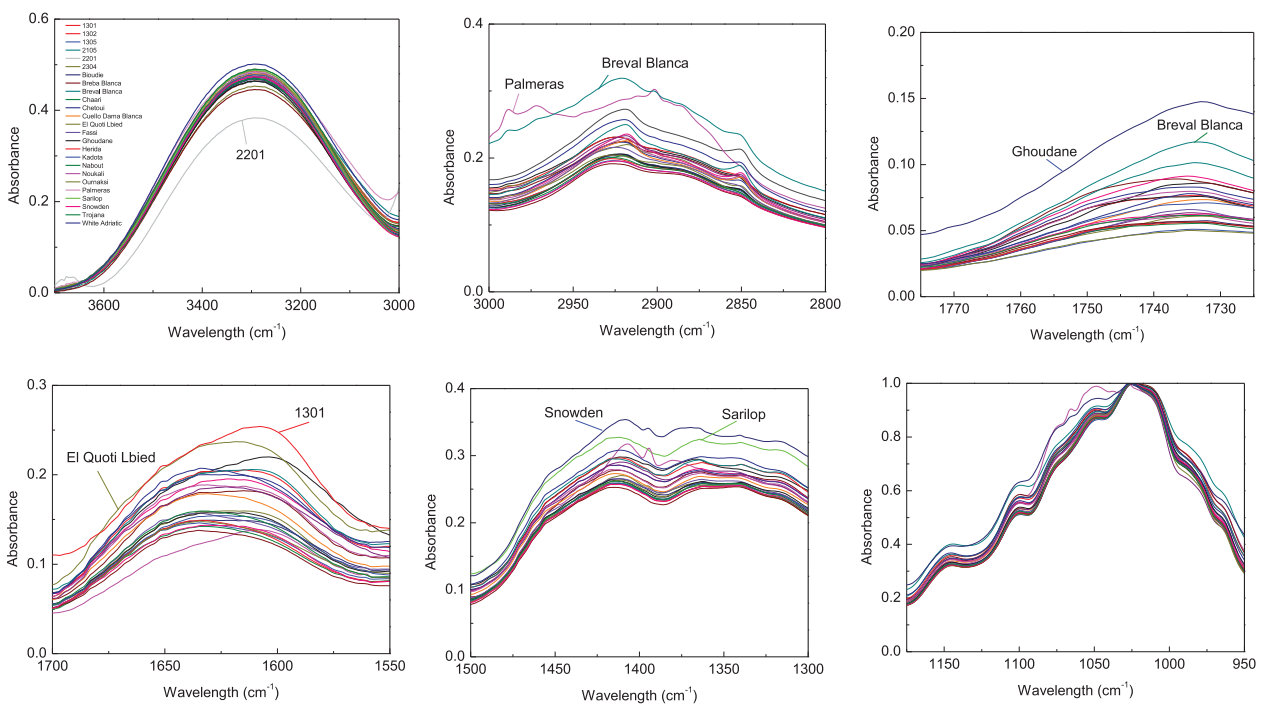

FIGURE 3 | Integrated ATR spectra of the major wavenumbers in peels samples. Each sample IR represent the mean of 3 spectra, which correspond each to the accumulation of 128 scans using a nominal resolution of 4 cm^{-1}.

only two cultivars, "Chetoui" and "Palmeras," with the following average concentrations: 0.75 ± 0.35 and 4.47 ± 0.04 μg/g dw, respectively. These results are, generally in agreement with those of Del Caro and Piga (del Caro and Piga, 2008), who used the same method on the Italian varieties "Mattalona" and "San Pietro." These levels, mainly of (+)-Catechin, cyanidin-3-O-rutinoside, and luteolin-7-O-glucoside, are much higher compared with bananas, pears, and apples, however, similar to black grapes (Rothwell et al., 2013). Contrary to our findings, Palmeira et al. (2019) reported that rutin (quercetin-3-O-rutinoside) was the predominant PC in fig peel. In our samples, cyanidine-3,5-diglucoside and cyanidine-3-O-rutinoside were apparently predominant.

Fourier Transform Infrare-Attenuated Total Reflectance Spectral Features

Fourier transform infrared spectra of fig peel and pulp samples are shown in **Figure 1**. The bands observed between 4,000 and 450 cm^{-1} displayed six fingerprints around the following absorption regions: 3,700–3,000, 3,000–2,800, 1,775–1,725, 1,700–1,550, 1,500–1,300, and 1,175–940 cm^{-1} (**Figure 1**). The first region is most likely assigned to fibers, which are highly present in fresh figs. The broadband in this region is probably due to the O-H stretching vibrations arising from hydrogen bonding in cellulose. The absorbance at the region 3,000–2,800 cm^{-1} is most likely assigned to C-H, O-H, and NH3, which may be referred to carbohydrates, carboxylic acids, free amino acids, and phenolics (Schwanninger et al., 2004; Baranowska-Wójcik and Szwajgier, 2019; Palmeira et al., 2019). It is noteworthy that this band was divided into two peaks at 2,925 and 2,855 cm^{-1} (Bouafif et al., 2008). The first one is probably related to C-H stretching of a lipid's methylene group. While the peak raised approximately at 2,855 cm^{-1} is possibly due to C-H stretching (symmetric) of CH_2 from lipid acyl chains.

The peak at 1,775–1,725 cm^{-1} was associated to ester carbonyl band stretching (C=O). This vibration region is within the range of 1,800–1,700 cm^{-1}, which is most probably correlated to the elongation of C=O of the ester type carboxylic (Oh et al., 2005; Bouafif et al., 2008). In case of the pulp samples, this vibration is most likely linked to the lipids contained in the fruit seeds (Vongsvivut et al., 2013). However, in the previous study by Terpugov et al. (2016) the peak was attributed to proteins. The vibration in the region of 1,700–1,550 cm^{-1} is typically originated to stretching band of carbonyl groups C=O and C=C (Tahir et al., 2017). The vibration bands in the region of 1,500–1,300 cm^{-1} corresponds to phosphodiester groups. This band is probably a result of several weak peaks that could not be differentiated among investigated samples. According to previous studies, this absorption band usually includes, among others, a vibration around 1,392 cm^{-1} that is most likely assigned to carbohydrates, fatty acids, or amino acids side chain (Vongsvivut et al., 2013), the 1,315 cm^{-1} vibration is associated with CH_2 rocking (Schwanninger et al., 2004), and a vibration approximately at 1,155 cm^{-1}, which is a result of C–O stretching (Vongsvivut et al., 2013). Finally, the vibrations in the regions 940–1,175 cm^{-1} marks a very strong and sharp peak, which is probably assigned to C–OH group as well as the stretches C–C and C–O in the carbohydrate structure and C–O in the phenol. In this region, quercetin-3-O-rutinoside was reported to record the highest vibration intensity around the wavenumber of 1,149 cm^{-1} (Paczkowska et al., 2015). It is noteworthy that this compound was found to be the major PC in all samples particularly in peel extracts (**Table 2**). The vibration at 1,149 cm^{-1} was assigned to C-C-H bending in benzene and dihydroxyphenyl aromatic rings (Paczkowska et al., 2015).

Since the entire spectra of screened samples present a high overlapping level, the abovementioned major vibration range was plotted separately in **Figures 2**, **3** for both pulp and peel extracts, respectively. For pulp extracts, the bands around 1,775–1,725, and 3,000–2,855 cm^{-1} were remarkably clear for the variety "Nabout," which recorded the highest absorbance intensity. In the bands corresponding to proteins (1,700–1,550 cm^{-1}), organic acids (1,500–1,300 cm^{-1}), and phenols

TABLE 3 | Calibration and cross-validation results of multivariate models developed by using attenuated total reflectance Fourier transform infrared (ATR-FTIR) spectra in the regions of 1,175–940 cm^{-1} in both fig peel and pulp.

Phenolic compounds (μg g^{-1})	Peel extracts							Pulp extracts						
	LV	R^2-Cal	R^2-Val	RMSE-Cal	RMSE-Val	RPD-Cal	RPD-Val	LV	R^2-Cal	R^2-Val	RMSE-Cal	RMSE-Val	RPD-Cal	RPD-Val
((+)-Catechin)	5	0.97	0,76	0.73	2.49	2.38	1.86	8	0.85	0.81	0.9	1.9	2,52	2.23
(−)-Epicatechin	5	0.95	0.84	0.9	1.14	2.14	2.24	7	0.94	0.7	0.9	1.05	2.72	1.75
Chlorogenic acid	6	0.92	0.89	0.91	0.12	3.47	2.56	6	0.91	0.84	0.5	2.05	2.47	2.03
Quercetin-3-O-rutinoside	7	0.95	0.83	1.05	1.04	2,95	2.44	6	0.98	0,87	0.46	1.21	3.21	2.36
Quercetin-3-O-glucoside	7	0.87	0.74	0.97	1.21	3.72	2.3	–	–	–	–	–	–	–
Quercetin	6	0.99	0.83	0.82	1.09	2.44	2.62	–	–	–	–	–	–	–
Cyanidin-3,5-diglucoside	6	0.99	0.75	0.07	1.83	4.47	2.15	8	0.95	0.81	0.5	1.08	4.13	2.49
Cyanidin-3-O-rutinoside	8	0.96	0.86	0.04	1.54	3.84	2.43	7	0.96	0.88	0.6	0.23	4.21	2.67

R^2-Cal, coefficient of determination of calibration; RMSE-Cal, root mean square error of cross-validation.
R^2-Val, coefficient of determination of validation; RMSE-Val, root mean square error of cross-validation.
LV, latent variable (orthogonal factors that provide maximum correlation with dependent variable).
RPD-Cal, residual predictive deviation of calibration; RPD-Val: residual predictive deviation of cross-validation.

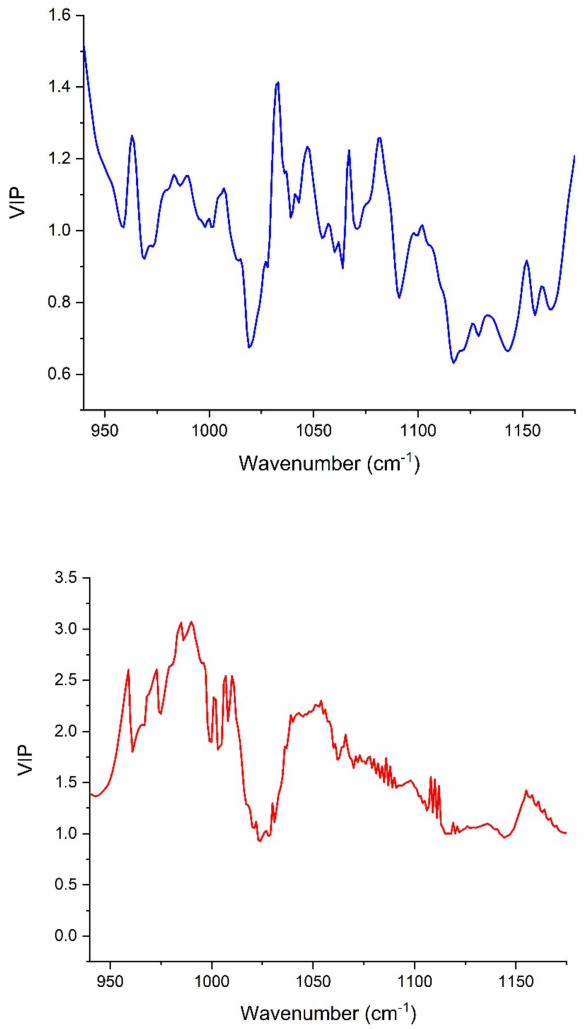

FIGURE 4 | Variables importance in projection (VIP) plot showing the contribution of each wavenumber in the PLSR model total variance for both peel (blue) and pulp (red).

(1,175–940 cm^{-1}), the higher absorptions and integrated areas were recorded by "2201," "Snowden," and "1305," respectively. These cultivars have combined, as previously mentioned, the promising levels of PCs, mainly (+)-catechin, quercetin-3-O-rutinoside, and quercetin-3-O-glucoside (**Table 2**). This makes sense, since these compounds record high vibration intensity at the wavenumber around 1,034 cm^{-1}, which is mainly attributed to C–O stretching between mannopyranosyl and glucopyranosyl aromatic rings (Robb et al., 2002; Paczkowska et al., 2015).

Regarding peels extracts (**Figure 2**), the cultivars 'Palmeras' and 'Breval Blanca' revealed the highest absorption in the region of 3,000–2,800 cm^{-1}. 'Breval Blanca' and 'Ghoudane' showed the highest absorption at the ester vibration region (1,775–1,725 cm^{-1}), whereas, the cultivars '1301' and 'EL Quoti Lbied' had the highest vibration in the proteins' region (1,700–1550 cm^{-1}). The vibration at the region of 1,500–1,300 cm^{-1} was superior in 'Snowden' compared with the other cultivars. In the phenols' region (1,175–940 cm^{-1}) 'Chaari' had the highest vibration intensity. Obviously, some dissimilarities between the both fingerprinting techniques are due to the fact that phenolics compounds revealed by HPLC-DAD could not totally explain the pattern yielded by FTIR fingerprinting between peel and pulp (Harvey et al., 2009).

Results of Partial Least Squares Regression Models

Partial least square is a particular method because it can construct predictive models with highly collinear, noisy, and numerous factors, and also at once model several targeted variables (Wold et al., 2001). The robust model must combine a high R^2, low RMSE, and a minimum number of latent variables (LVs), if at all possible less than ten (Liang et al., 2016; **Table 3**).

Partial least square regression models were built using the FTIR-ATR spectra set both in jack-knifing cross-validation and prediction set. These models were performed using IR data in the vibration region of 1,175–940 cm^{-1}, corresponding to the C–OH group and the stretches C–O in the phenol structure. Within this region, the vibration band 1,540–1,175 cm^{-1} corresponds to flavanol and phenol (deformations of O–H, C–O, C–H, and C=C) (Masek et al., 2014; Nickless et al., 2014). It is noteworthy that gallic acid and pelargonidin-3-O-rutinoside were not involved in the PLSR for peel samples since these compounds were detected only in few cultivars. Similarly, quercetin-3-o-rutinoside and luteolin-7-o-glucoside were scarcely detected and then excluded in PLSR analysis.

The number of LVs revealed by the models oscillated between 5 and 8 for the peel samples, whereas it was in the range of 6–8 in the pulp samples. Most of the number of LVs obtained by models built using pulp extracts were smaller than nine, henceforth demonstrating that the constructed models were not overfitting the data (the data used in observations fitting based on the learning set might not be practical to fit new observations) (Notions, 2010). In **Figure 4**, we see the contribution [variables importance in projection (VIP)] of each wavenumber within the wavenumber range of 1,175 and 940 cm^{-1} where the samples were scanned using the FTIR-ATR. The high value of VIP score indicates a great contribution to the model building. For peel samples, in order of importance, the following wavenumbers 940, 1,030, 1,081, 936, and 1,067 cm^{-1} had the highest VIP scores (> 1.2) and therefore, the main contribution to the built model total variance. Thus, the bands at 940 and 936 cm^{-1} are most likely assigned to C–C and C–O vibration (Movasaghi et al., 2018), while the peak at 1,030 cm^{-1} is attributed to C–O vibration (Paluszkiewicz and Kwiatek, 2001). At 1,081 cm^{-1}, the peak is probably assigned to the ring stretching mixed strongly with CH in-plane bending (Chiang et al., 1999). The absorbance at 1,067 cm^{-1} is assigned to (C=O)–O– stretching, which is most likely an ester spectral peak (Armenta et al., 2005; Dong et al., 2013). On the other hand, the main loading for pulp samples were observed around the following wavenumbers 536, 541, 509, 524, 558, and 561 cm^{-1}, which are most likely originated from strong deformation of C-C-C and C-C-O. These bands displayed the greatest VIP scores (>2.5) indicating a highest

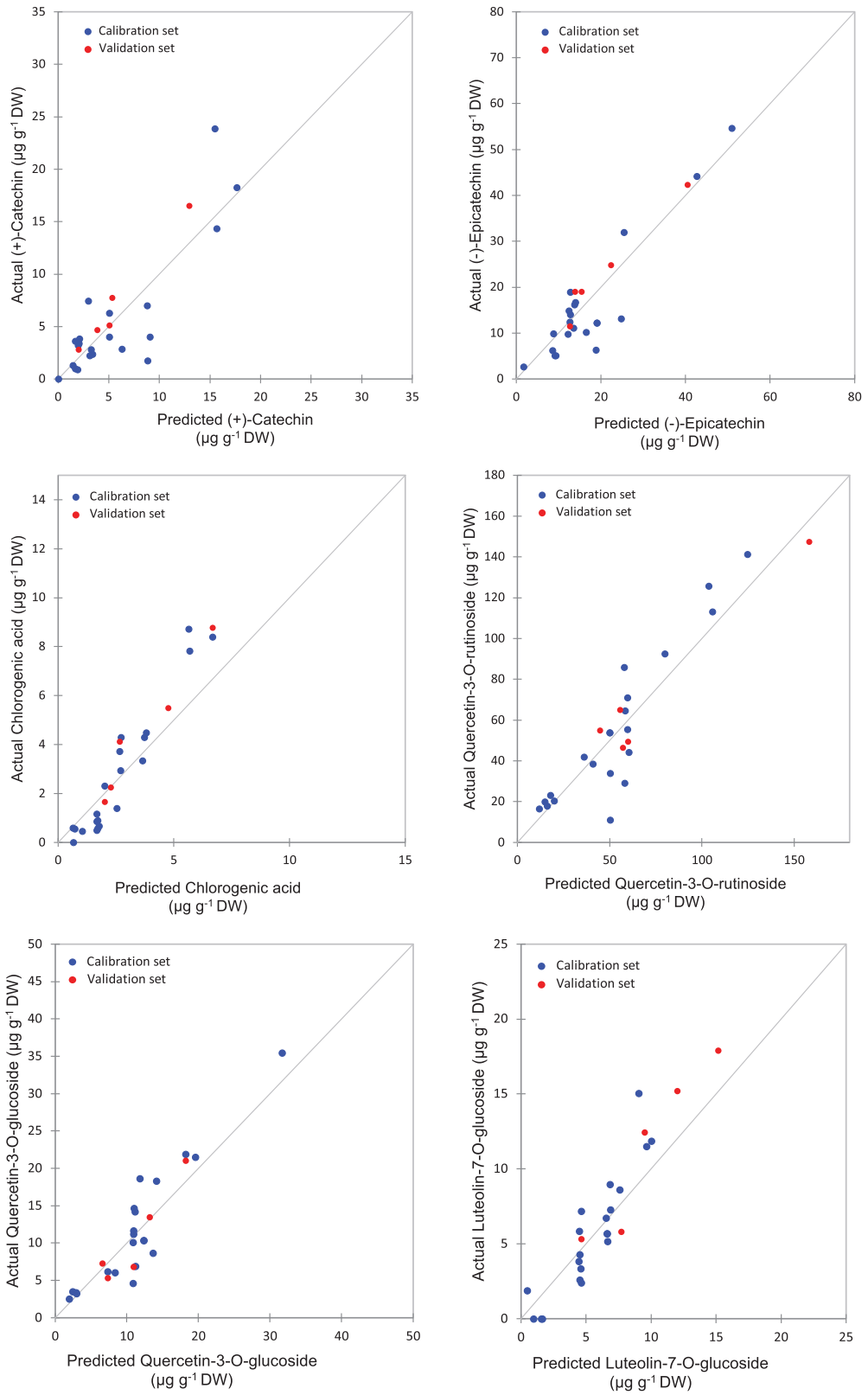

FIGURE 5 | (Continued)

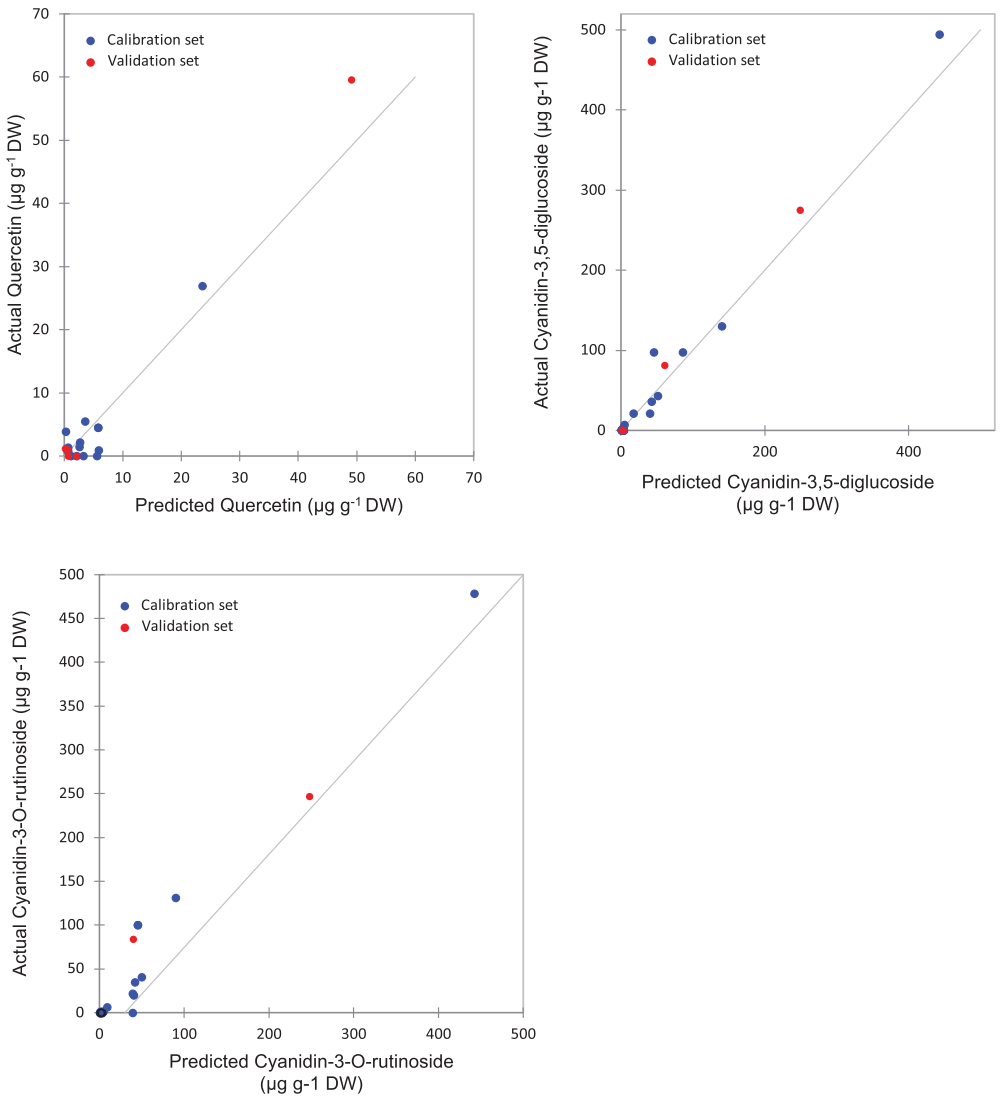

FIGURE 5 | Correlation plots for the prediction of phenolic compounds in the peel samples using PLSR based on the FT-IR spectra.

contribution to the model total variance. It should be noted that the VIP scores were much greater for the model built based on the pulp extracts compared with the peel samples prediction model (**Figure 4**).

Partial least square regression models statistics showed various levels of accuracy depending on targeted variables (PCs) and their partitioning in both fruit parts (peel and pulp). For peel samples, a good calibration model was achieved. Thus, the statistics displayed a coefficient of determination (R^2-Cal) ranging between 0.87 and 0.99, along with root mean square error (RMSE-Cal) values in the range of 0.73 and 1.05. Similarly, the R^2 for cross-validation was important for all PCs and was oscillating between 0.75 and 0.89 coupled with relatively low RMSE that was in the range of 0.12 and 2.49.

The highest levels of prediction were particularly observed for chlorogenic acid (R^2-Val = 0.86, RMSE-Val = 0.12), followed by (−)-epicatechin (R^2-Val = 0.84, RMSE-Val = 1.14) (**Table 3**). Scatter plots for the reference (*y*-axis) vs. predicted values (*x*-axis) for phenolic acids and flavonoids over the peel powders using FTIR-ATR spectroscopy shown in **Figures 5**, **6**, displayed the accuracy of predicting these compounds. The models constructed for pulp samples displayed good calibration and validation statistics (**Table 3** and **Figure 6**). Thus, the R^2 and RMSE were generally similar to those found in models constructed based on the peels' extracts. In calibration models, the R^2 values ranged between 0.85 and 0.98 along with RMSE values in the range of 0.46 and 0.9. For the validation models, R^2 and RMSE were in the range of 0.7–0.88 and 0.23–0.05, respectively. The highest performance of prediction was mainly observed for quercetin-3-O-rutinoside and cyanidin-3-O-rutinoside of which the R^2-Val were higher than 0.87 with the respective RMSE of 0.23 and 1.21 (**Table 3**). RPD has different interpretations in the literature.

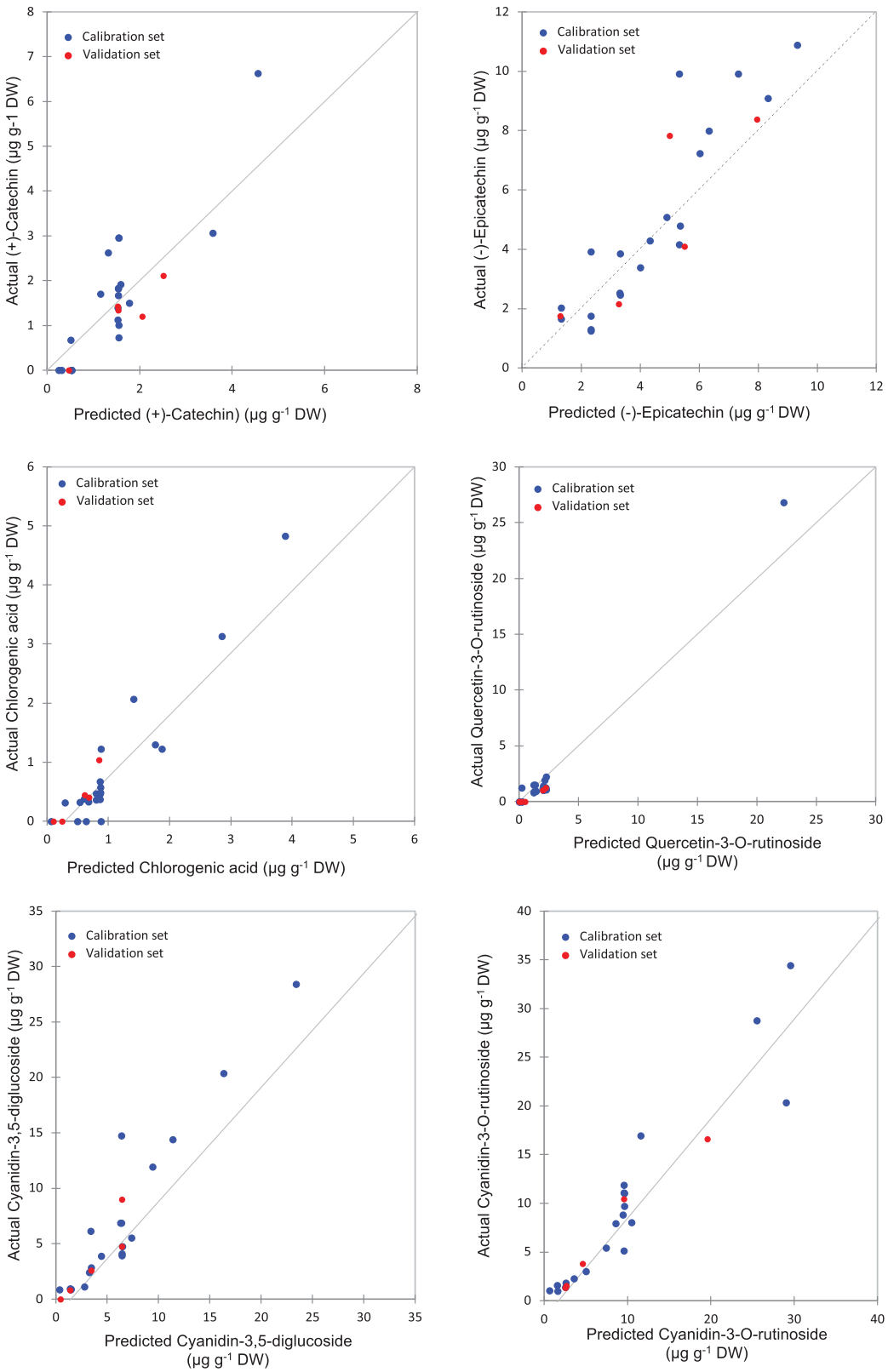

FIGURE 6 | Correlation plots for the prediction of phenolic compounds in the pulp samples using PLSR based on the FT-IR spectra.

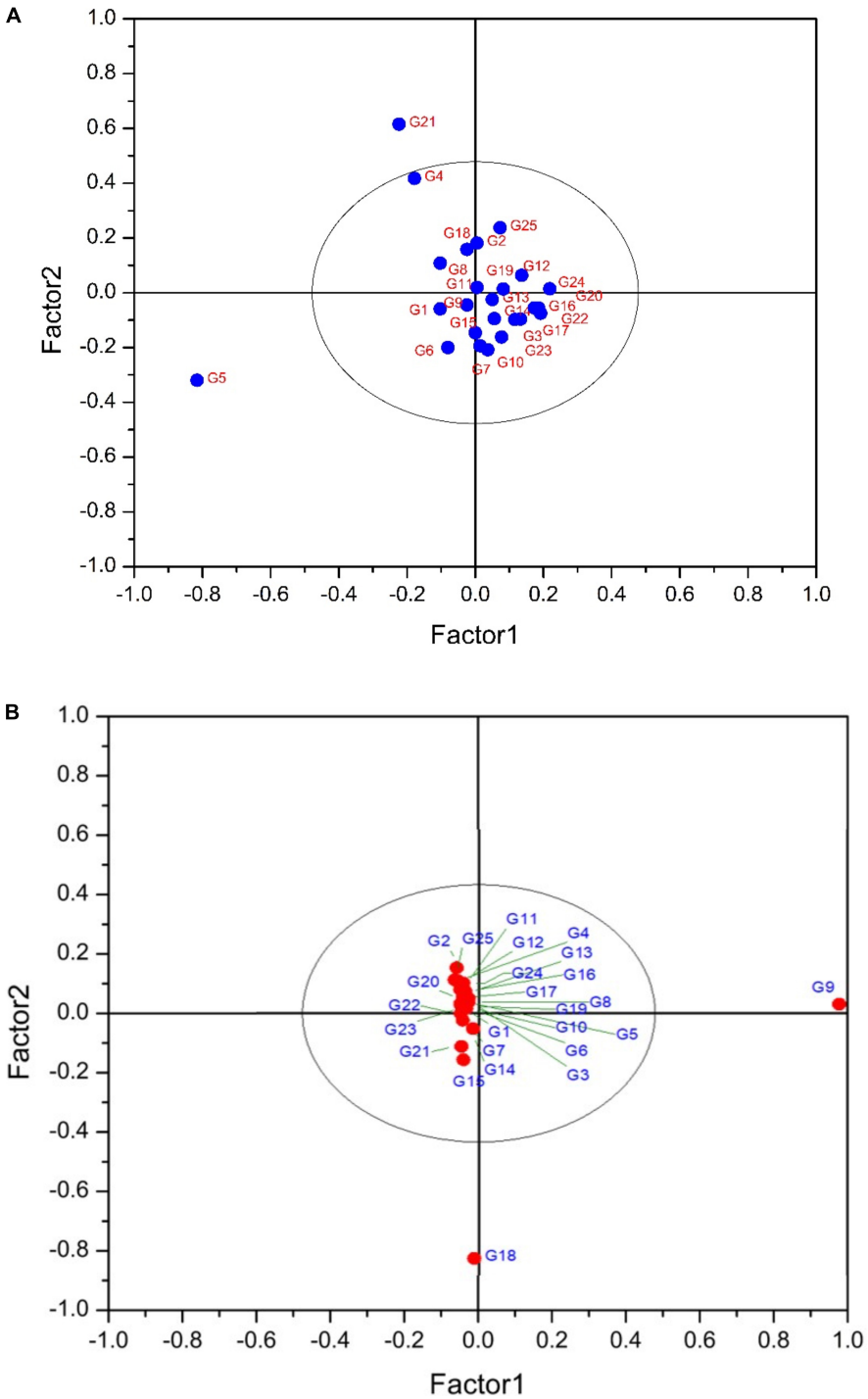

FIGURE 7 | (A) PLS-DA plot showing the distribution of scanned peel samples. The variance explained by the factor1 and 2 are 77.40 and 15.44%, respectively. G1 to G25 refer to the cultivars codes as given in the **Table 1**. **(B)** PLS-DA plot showing the distribution of scanned pulp samples. The variance explained by the factor1 and 2 are 80 and 10.78%, respectively. G1 to G25 refer to the cultivars codes as given in the **Table 1**.

Hence, according to Morgan et al. (1994), an RPD value in the range of 2.5 and 3 seems adequate for screening and an interval of 3–5 is assumed better for quality assurance. On the other hand, Chang et al. (2001) assumed that the RPD greater than 2 is sufficient for a high throughput resolution, while the RPD < 1.4 may not lead to a reliably prediction. The results in **Table 3** showed the RPD in the range of 2.14–3.84 and 1.86–2.62 for peel samples calibration and validation, respectively,

TABLE 4 | Loadings of phenolic compounds in the partial least squares discriminant analysis (PLS-DA) factors for both peel and pulp extracts.

	Peel		Pulp	
	Factor 1	**Factor 2**	**Factor 1**	**Factor 2**
Gallic acid	0.48	0.78	–	–
(+)-Catechin	15.4	10.26	0.11	−0.03
(−)-Epicatechin	20.28	−11.33	−0.89	3.98
Chlorogenic acid	1.11	−3.36	−0.59	0.85
Quercetin-3-O-rutinoside	−30.07	−34.96	−1.27	1.98
Quercetin-3-O-glucoside	6.08	−6.53	−0.51	−0.80
Luteolin-7-O-glucoside	3.20	0.39	−0.24	−0.48
Quercetin	11.21	6.02	–	–
Apigenin	0.59	0.99	–	–
Cyanidin-3,5-diglucoside	153.04	−207.32	−1.30	8.72
Cyanidin-3-O-rutinoside	137.46	−188.69	−2.31	11.34
Pelargonidin-3-O-rutinoside	2.369	−3.81	–	–

whereas, for pulp samples it was in the following ranges 3.52–4.21 and 1.75–2.67, respectively, for calibration and validation. Overall, the abovementioned value seemed acceptable and suggest satisfactory throughput resolution of phenolic acids and flavonoids over both fruit parts. It is noteworthy that quercetin-3-O-glucoside and cyanidin-3,5-diglucoside alongwith cyanidin-3-O-rutinoside, displayed the highest RPD values for calibration step, which were generally greater than 3. For calibration, the same compounds displayed acceptable level for validation step with value greater than 2 for both fruit parts, except quercetin-3-O-glucoside which was not detected over pulp extracts.

Over all, both fruit parts revealed a reliable throughput resolution in predicting the concentrations of phenolic acids and flavonoids in different fig samples. Although the prediction of some compounds seemed to be slightly lower but remains good, since they were detected at a very minor levels and were not identified in all herein involved samples.

In raw material with high moisture content, such as figs (Farahnaky et al., 2009), the use of mid infrared spectroscopy is often reliable since it presents a low overlapping probability with the important bands associated with the measured property (Cozzolino et al., 2021). Based on the findings, the FTIR-ATR spectroscopy could be recommended as a simple and direct technique to assess the phenolic composition of figs, which does not require a tremendous sample pre-treatment or processing allowing for the development of a high throughput analytical method.

Partial Least Squares Discriminant Analysis

Partial least squares discriminant analysis is a linear classification approach that combines the properties of PLSR with the high discrimination feature of a classification method. The principal advantage of Partial Least Squares Discriminant Analysis (PLS-DA) is LVs, which model the main sources of variance within the data, and represent linear combinations of the original variables. Therefore, it allows the graphical presentation and understanding of the special distribution of the different data patterns and relations by LV scores and loadings (Ballabio and Consonni, 2013). **Figures 7A,B** shows that the data are not strongly clustered, particularly for the pulp samples that showed a strong overlapping around the plot origin. Based on **Table 4**, cyanidin-3,5-diglucoside and cyanidin-3-O-rutinoside had the highest loadings on the first and second factor for both fruit parts. This is due to the fact that these compounds are the predominant anthocyanins in fig peel and pulp, as reported by Russo et al. (2014). The distribution of peel samples, revealed one main cluster, with two cultivars, classified each as a single item (**Figure 7A**). Similarly, the pulp samples distribution displayed a single main cluster, with high overlapping intensity. Two cultivars were highly distinguished from the agglomerated samples (**Figure 7B**). The low overlapping level observed in the PLS-DA of peel samples suggest the use of this part of the fruit in future studies as they may offer better discrimination on fig tree cultivars. This makes sense, since the fig peels were reported to held the high levels of PCs compared with the pulp (del Caro and Piga, 2008; Oliveira et al., 2009; Qin et al., 2015).

CONCLUSION

This study is the first work attempting to examine the ability of FTIR-ATR spectroscopy combined with chemometrics to predict phenolic acids and flavonoids in fresh figs, with regard to their partitioning between the fruit peel and pulp. The results demonstrated the great potential of such simple and rapid technique to predict the PCs in the powder samples, with a satisfactory throughput resolution. All PCs in both fruit parts displayed high levels of prediction in both calibration and validation models. Although the prediction of some few compounds seemed to be slightly lower but still remains good, since they were detected at a minor level and were not identified in all herein involved samples. Significant differences were observed between the models built for the two fruit parts. Similar divergence was observed based on the distribution revealed by PLS-DA, where the highest scores were captured by cyanidin-3,5-diglucoside and cyanidin-3-O-rutinoside. Therefore, the FTIR-ATR spectroscopic technique represents, particularly when combined with chemometric approach, a convenient alternative in terms of time and chemical inputs saving for routine analyses of large raw material sample length. This approach can be considered as an affordable methodology, but one of the limitations of this work is that a larger sample length is required and further validation must be performed using samples from other varieties and origins.

DATA AVAILABILITY STATEMENT

The original contributions presented in the study are included in the article/supplementary material, further inquiries can be directed to the corresponding author.

AUTHOR CONTRIBUTIONS

LH: supervision, conceptualization, methodology, software, writing—original draft, resources, formal analysis, data curation, resources and visualization and review and editing. RR: data curation, resources, and visualization. YB: data modeling, software, and data inspection. All authors contributed to the article and approved the submitted version.

REFERENCES

Anjos, O., Campos, M. G., Ruiz, P. C., and Antunes, P. (2015). Application of FTIR-ATR spectroscopy to the quantification of sugar in honey. *Food Chem.* 169, 218–223. doi: 10.1016/j.foodchem.2014.07.138

Armenta, S., Quint, G., Garrigues, S., and De Guardia, M. (2005). A validated and fast procedure for FTIR determination of Cypermethrin and Chlorpyrifos. *Talanta* 67, 634–639. doi: 10.1016/j.talanta.2005.03.008

Arvaniti, O. S., Samaras, Y., Gatidou, G., Thomaidis, N. S., and Stasinakis, A. S. (2019). Review on fresh and dried figs: chemical analysis and occurrence of phytochemical compounds, antioxidant capacity and health effects. *Food Res. Int.* 119, 244–267. doi: 10.1016/j.foodres.2019.01.055

Ballabio, D., and Consonni, V. (2013). Classification tools in chemistry. Part 1: linear models. PLS-DA. *Anal. Methods* 5, 3790–3798. doi: 10.1039/c3ay40582f

Baranowska-Wójcik, E., and Szwajgier, D. (2019). Characteristics and pro-health properties of mini kiwi (*Actinidia arguta*). *Hortic. Environ. Biotechnol.* 60, 217–225. doi: 10.1007/s13580-018-0107-y

Bouafif, H., Koubaa, A., Perré, P., Cloutier, A., and Riedl, B. (2008). Analysis of among-species variability in wood fiber surface using DRIFTS and XPS: effects on esterification efficiency. *J. Wood Chem. Technol.* 28, 296–315. doi: 10.1080/02773810802485139

Bouyanfif, A., Liyanage, S., Hequet, E., Moustaid-Moussa, N., and Abidi, N. (2019). FTIR microspectroscopy reveals fatty acid-induced biochemical changes in C. *elegans*. *Vib. Spectrosc.* 102, 8–15. doi: 10.1016/j.vibspec.2019.03.002

Brereton, R. G., and Lloyd, G. R. (2014). Partial least squares discriminant analysis: taking the magic away. *J. Chemom.* 28, 213–225. doi: 10.1002/cem.2609

Cebi, N., Durak, M. Z., Toker, O. S., Sagdic, O., and Arici, M. (2016). An evaluation of Fourier transforms infrared spectroscopy method for the classification and discrimination of bovine, porcine and fish gelatins. *Food Chem.* 190, 1109–1115. doi: 10.1016/j.foodchem.2015.06.065

Česoniene, L., Jasutiene, I., and Šarkinas, A. (2009). Phenolics and anthocyanins in berries of European cranberry and their antimicrobial activity. *Medicina* 45, 992–999. doi: 10.3390/medicina45120127

Chang, C.-W., Laird, D. A., Mausbach, M. J., and Hurburgh, C. R. (2001). Near-infrared reflectance spectroscopy-principal components regression analyses of soil properties. *Soil Sci. Soc. Am. J.* 65, 480–490. doi: 10.2136/SSSAJ2001.652480X

Chiang, H., Song, R., Mou, B., Li, K. P., Chiang, P., Wang, D., et al. (1999). Fourier transform Raman spectroscopy of carcinogenic polycyclic aromatic hydrocarbons in biological systems: binding to Heme proteins. *J. Raman Spectrosc.* 30, 551–555. doi: 10.1002/(sici)1097-4555(199907)30:7<551::aid-jrs417>3.0.co;2-i

Cozzolino, D., Dao, A., Phan, T., Netzel, M. E., and Smyth, H. (2021). The use of vibrational spectroscopy to predict Vitamin C in Kakadu plum powders (*Terminalia ferdinandiana* Exell, Combretaceae). *J. Sci. Food Agric.* 101, 3208–3213. doi: 10.1002/jsfa.10950

de Nardo, T., Shiroma-Kian, C., Halim, Y., Francis, D., and Rodriguez-Saona, L. E. (2009). Rapid and simultaneous determination of lycopene and β-carotene contents in tomato juice by infrared spectroscopy. *J. Agric. Food Chem.* 57, 1105–1112. doi: 10.1021/jf802920z

del Caro, A., and Piga, A. (2008). Polyphenol composition of peel and pulp of two Italian fresh fig fruits cultivars (*Ficus carica* L.). *Eur. Food Res. Technol.* 226, 715–719. doi: 10.1007/s00217-007-0581-4

Dong, D., Zhao, C., Zheng, W., Wang, W., Zhao, X., and Jiao, L. (2013). Analyzing strawberry spoilage via its volatile compounds using Longpath Fourier transform infrared spectroscopy. *Sci. Rep.* 3:2585. doi: 10.1038/srep02585

Farahnaky, A., Ansari, S., and Majzoobi, M. (2009). Effect of glycerol on the moisture sorption isotherms of figs. *J. Food Eng.* 93, 468–473. doi: 10.1016/j.jfoodeng.2009.02.014

Genskowsky, E., Puente, L. A., Pérez-Álvarez, J. A., Fernández-López, J., Muñoz, L. A., and Viuda-Martos, M. (2016). Determination of polyphenolic profile, antioxidant activity and antibacterial properties of maqui [*Aristotelia chilensis* (Molina) Stuntz] a Chilean blackberry. *J. Sci. Food Agric.* 96, 4235–4242. doi: 10.1002/jsfa.7628

Goodhue, D., Lewis, W., and Thompson, R. (2006). "PLS, small sample size, and statistical power in MIS research," in *Proceedings of the Annual Hawaii International Conference on System Sciences*, (Piscataway, NJ: IEEE). doi: 10.1109/HICSS.2006.381

Harvey, T. J., Gazi, E., Henderson, A., Snook, R. D., Clarke, N. W., Brown, M., et al. (2009). Factors influencing the discrimination and classification of prostate cancer cell lines by FTIR microspectroscopy. *Analyst* 134, 1083–1091. doi: 10.1039/b903249e

Harzallah, A., Bhouri, A. M., Amri, Z., Soltana, H., and Hammami, M. (2016). Phytochemical content and antioxidant activity of different fruit parts juices of three figs (*Ficus carica* L .) varieties grown in Tunisia. *Ind. Crops Prod.* 83, 255–267. doi: 10.1016/j.indcrop.2015.12.043

Haytowitz, D. B., Wu, X., and Bhagwat, S. (2018). *USDA Database for the Flavonoid Content of Selected Foods Release 3.3*. Beltsville, MD: USDA, Agricultural Research Service.

Hirri, A., Bassbasi, M., Souhassou, S., Kzaiber, F., and Oussama, A. (2016). Prediction of polyphenol fraction in virgin olive oil using mid-infrared attenuated total reflectance attenuated total reflectance accessory-mid-infrared coupled with partial least squares regression. *Int. J. Food Properties* 19, 1504–1512. doi: 10.1080/10942912.2015.1059854

Hssaini, L., Charafi, J., Hanine, H., Ennahli, S., Mekaoui, A., Mamouni, A., et al. (2019). Comparative analysis and physio-biochemical screening of an ex-situ fig (*Ficus carica* L.) collection. *Hortic. Environ. Biotechnol.* 60, 671–683. doi: 10.1007/s13580-019-00170-4

Hssaini, L., Hanine, H., Razouk, R., Ennahli, S., Mekaoui, A., Ejjilani, A., et al. (2020a). Assessment of genetic diversity in Moroccan fig (*Ficus carica* L.) collection by combining morphological and physicochemical descriptors. *Genet. Resour. Crop Evol.* 67, 457–474. doi: 10.1007/s10722-019-00838-x

Hssaini, L., Hanine, H., Razouk, R., Ennahli, S., Mekaoui, A., Guirrou, I., et al. (2020b). Diversity screening of fig (*Ficus carica* L.) germplasm through integration of morpho-agronomic and biochemical traits. *Int. J. Fruit Sci.* 20, 939–958. doi: 10.1080/15538362.2019.1700871

Jacob, S. J. P., Prasad, V. L. S., Sivasankar, S., and Muralidharan, P. (2017). Biosynthesis of silver nanoparticles using dried fruit extract of *Ficus carica* – Screening for its anticancer activity and toxicity in animal models. *Food Chem. Toxicol.* 109, 951–956. doi: 10.1016/j.fct.2017.03.066

Kamiloglu, S., and Capanoglu, E. (2013). Investigating the in vitro bioaccessibility of polyphenols in fresh and sun-dried figs (*Ficus carica* L.). *Int. J. Food Sci. Technol.* 48, 2621–2629. doi: 10.1111/ijfs.12258

Karaman, I., Qannari, E. M., Martens, H., Hedemann, M. S., Knudsen, K. E., and Kohler, A. (2013). Comparison of Sparse and Jack-knife partial least squares regression methods for variable selection. *Chemom. Intell. Lab. Syst.* 122, 65–77. doi: 10.1016/j.chemolab.2012.12.005

Koch, C., Posch, A. E., Goicoechea, H. C., Herwig, C., and Lendl, B. (2014). Multi-analyte quantification in bioprocesses by Fourier-transform-infrared spectroscopy by partial least squares regression and multivariate curve resolution ג. *Anal. Chim. Acta* 807, 103–110. doi: 10.1016/j.aca.2013.10.042

Lee, L. C., and Jemain, A. A. (2019). Predictive modelling of colossal ATR-FTIR spectral data using PLS-DA: empirical differences between PLS1-DA and PLS2-DA algorithms. *Analyst* 144, 2670–2678. doi: 10.1039/c8an02074d

Liang, N., Lu, X., Hu, Y., and Kitts, D. D. (2016). Application of attenuated total reflectance-fourier transformed infrared (ATR-FTIR) spectroscopy to determine the chlorogenic acid isomer profile and antioxidant capacity of coffee beans. *J. Agric. Food Chem.* 64, 681–689. doi: 10.1021/acs.jafc.5b05682

Lu, X., Wang, J., Al-Qadiri, H. M., Ross, C. F., Powers, J. R., Tang, J., et al. (2011). Determination of total phenolic content and antioxidant capacity of onion

(*Allium cepa*) and shallot (*Allium oschaninii*) using infrared spectroscopy. *Food Chem.* 129, 637–644. doi: 10.1016/j.foodchem.2011.04.105

Mamera, M., van Tol, J. J., Aghoghovwia, M. P., and Kotze, E. (2020). Sensitivity and calibration of the ft-ir spectroscopy on concentration of heavy metal ions in river and borehole water sources. *Appl. Sci. (Switzerland)* 10, 1–16. doi: 10.3390/app10217785

Masek, A., Chrzescijanska, E., Kosmalska, A., and Zaborski, M. (2014). Characteristics of compounds in hops using cyclic voltammetry, UV-VIS, FTIR and GC-MS analysis. *Food Chem.* 156, 353–361. doi: 10.1016/j.foodchem.2014.02.005

Mehmood, T., and Ahmed, B. (2016). The diversity in the applications of partial least squares: an overview. *J. Chemom.* 30, 4–17. doi: 10.1002/cem.2762

Morgan, J. E., Campbell, L. D., Edney, M. J., and Williams, P. C. (1994). Analysis of feed barley by near infrared reflectance technology. *J. Near Infrared Spectrosc.* 2, 33–41. doi: 10.1255/jnirs.29

Movasaghi, Z., Rehman, S., and Rehman, I. (2018). Fourier transform infrared (FTIR) spectroscopy of biological tissues. *Appl. Spectrosc. Rev.* 43:4928. doi: 10.1080/05704920701829043

Nadeem, M., and Zeb, A. (2018). Impact of maturity on phenolic composition and antioxidant activity of medicinally important leaves of *Ficus carica* L. *Physiol. Mol. Biol. Plants* 24, 881–887. doi: 10.1007/s12298-018-0550-3

Nickless, E. M., Holroyd, S. E., Stephens, J. M., Gordon, K. C., and Wargent, J. J. (2014). Analytical FT-Raman spectroscopy to chemotype *Leptospermum scoparium* and generate predictive models for screening for dihydroxyacetone levels in floral nectar. *J. Raman Spectrosc.* 45, 890–894. doi: 10.1002/jrs.4576

Notions, P. (2010). Partial least squares regression and projection on latent structure regression (PLS Regression). *Wiley Interdiscip. Rev. Comput. Stat.* 2, 97–106. doi: 10.1002/wics.51

Oh, S. Y., Yoo, D. I., Shin, Y., and Seo, G. (2005). FTIR analysis of cellulose treated with sodium hydroxide and carbon dioxide. *Carbohydr. Res.* 340, 417–428. doi: 10.1016/j.carres.2004.11.027

Oliveira, A. P., Valentão, P., Pereira, J. A., Silva, B. M., Tavares, F., Andrade, P. B., et al. (2009). *Ficus carica* L .: metabolic and biological screening. *Food Chem. Toxicol.* 47, 2841–2846. doi: 10.1016/j.fct.2009.09.004

Paczkowska, M., Lewandowska, K., Bednarski, W., Mizera, M., Podborska, A., Krause, A., et al. (2015). Application of spectroscopic methods for identification (FT-IR, Raman spectroscopy) and determination (UV, EPR) of quercetin-3-O-rutinoside. Experimental and DFT based approach. *Spectrochim. Acta Part A Mol. Biomol. Spectrosc.* 140, 132–139. doi: 10.1016/j.saa.2014.12.050

Palmeira, L., Pereira, C., Dias, M. I., Abreu, R. M. V., Corrêa, R. C. G., Pires, T. C. S. P., et al. (2019). Nutritional, chemical and bioactive profiles of different parts of a Portuguese common fig (*Ficus carica* L.) variety. *Food Res. Int.* 126:108572. doi: 10.1016/j.foodres.2019.108572

Paluszkiewicz, C., and Kwiatek, W. M. (2001). Analysis of human cancer prostate tissues using FTIR microspectroscopy and SRIXE techniques. *J. Mol. Struct.* 565-566, 329–334.

Prabakaran, S., Ramu, L., Veerappan, S., Pemiah, B., and Kannappan, N. (2017). Effect of different solvents on volatile and non-volatile constituents of red bell pepper (*Capsicum annuum* L.) and their in vitro antioxidant activity. *J. Food Meas. Charact.* 11, 1531–1541. doi: 10.1007/s11694-017-9532-3

Qin, H., Zhou, G., Peng, G., Li, J., and Chen, J. (2015). Application of ionic liquid-based ultrasound-assisted extraction of five phenolic compounds from fig (*Ficus carica* L.) for HPLC-UV. *Food Anal. Methods* 8, 1673–1681. doi: 10.1007/s12161-014-0047-9

Robb, C. S., Geldart, S. E., Seelenbinder, J. A., and Brown, P. R. (2002). Analysis of green tea constituents by HPLC-FTIR. *J. Liquid Chromatogr. Relat. Technol.* 25, 787–801. doi: 10.1081/JLC-120003036

Rothwell, J. A., Perez-Jimenez, J., Neveu, V., Medina-Remón, A., M'Hiri, N., García-Lobato, P., et al. (2013). Phenol-Explorer 3.0: a major update of the Phenol-Explorer database to incorporate data on the effects of food processing on polyphenol content. *Database* 2013:bat070. doi: 10.1093/database/bat070

Russo, F., Caporaso, N., Paduano, A., and Sacchi, R. (2014). Phenolic compounds in fresh and dried figs from Cilento (Italy), by considering Breba crop and full crop, in comparison to Turkish and Greek dried figs. *J. Food Sci.* 79, C1278–C1284. doi: 10.1111/1750-3841.12505

Sarstedt, M., Ringle, C. M., and Hair, J. F. (2017). "Partial least squares structural equation modeling," in *Handbook of Market Research*, eds C. Homburg, M. Klarmann, and A. Vomberg (Cham: Springer International Publishing), 1–40. doi: 10.1007/978-3-319-05542-8_15-1

Schwanninger, M., Rodrigues, J. C., Pereira, H., and Hinterstoisser, B. (2004). Effects of short-time vibratory ball milling on the shape of FT-IR spectra of wood and cellulose. *Vib. Spectrosc.* 36, 23–40. doi: 10.1016/j.vibspec.2004.02.003

Szakonyi, G., and Zelkó, R. (2012). Water content determination of superdisintegrants by means of ATR-FTIR spectroscopy. *J. Pharm. Biomed. Anal.* 63, 106–111. doi: 10.1016/j.jpba.2012.01.023

Tahir, H. E., Xiaobo, Z., Zhihua, L., Jiyong, S., Zhai, X., Wang, S., et al. (2017). Rapid prediction of phenolic compounds and antioxidant activity of Sudanese honey using Raman and Fourier transform infrared (FT-IR) spectroscopy. *Food Chem.* 226, 202–211. doi: 10.1016/j.foodchem.2017.01.024

Tejamukti, E. P., Setyaningsih, W., Irnawati, Yasir, B., Alam, G., and Rohman, A. (2020). Application of FTIR spectroscopy and HPLC combined with multivariate calibration for analysis of Xanthones in Mangosteen extracts. *Sci. Pharm.* 88:35. doi: 10.3390/scipharm88030035

Tenenhaus, M., Pagès, J., Ambroisine, L., and Guinot, C. (2005). PLS methodology to study relationships between hedonic judgements and product characteristics. *Food Qual. Prefer.* 16, 315–325. doi: 10.1016/j.foodqual.2004.05.013

Terpugov, E. L., Degtyareva, O. v., and Savransky, V. v. (2016). Possibility of light-induced Mid-IR emission in situ analysis of plants. *J. Russ. Laser Res.* 37, 507–510. doi: 10.1007/s10946-016-9602-8

Tulukcu, E., Cebi, N., and Sagdic, O. (2019). Chemical fingerprinting of seeds of some salvia species in Turkey by using GC-MS and FTIR. *Foods* 8:118. doi: 10.3390/foods8040118

Vallejo, F., Marín, J. G., and Tomás-barberán, F. A. (2012). Phenolic compound content of fresh and dried figs (*Ficus carica* L .). *Food Chem.* 130, 485–492. doi: 10.1016/j.foodchem.2011.07.032

Vinson, J. A., Hao, Y., Su, X., and Zubik, L. (1998). Phenol antioxidant quantity and quality in foods: vegetables. *J. Agric. Food Chem.* 46, 3630–3634. doi: 10.1021/jf980295o

Viuda-martos, M., Barber, X., Pérez-álvarez, J. A., and Fernández-lópez, J. (2015). Assessment of chemical, physico-chemical, techno-functional and antioxidant properties of fig (*Ficus carica* L .) powder co-products. *Ind. Crops Prod.* 69, 472–479. doi: 10.1016/j.indcrop.2015.03.005

Vongsvivut, J., Heraud, P., Gupta, A., Puri, M., McNaughton, D., and Barrow, C. J. (2013). FTIR microspectroscopy for rapid screening and monitoring of polyunsaturated fatty acid production in commercially valuable marine yeasts and protists. *Analyst* 138, 6016–6031. doi: 10.1039/c3an00485f

Wold, S., Sjöström, M., and Eriksson, L. (2001). PLS-regression: a basic tool of chemometrics. *Chemom. Intell. Lab. Syst.* 58, 109–130. doi: 10.1016/S0169-7439(01)00155-1

Yaman, N., and Velioglu, S. D. (2019). Use of attenuated total reflectance—Fourier transform infrared (ATR-FTIR) spectroscopy in combination with multivariate methods for the rapid determination of the adulteration of grape, carob and mulberry PEKmez. *Foods* 8:231. doi: 10.3390/foods8070231

Yang, J., and Yang, J. Y. (2003). Why can LDA be performed in PCA transformed space? *Pattern Recognit.* 36, 563–566. doi: 10.1016/S0031-3203(02)00048-1

Zheng, X., Hu, Y., Anggreani, E., and Lu, X. (2017). Determination of total phenolic content and antioxidant capacity of blueberries using Fourier transformed infrared (FT-IR) spectroscopy and Raman spectroscopy. *J. Food Meas. Charact.* 11, 1909–1918. doi: 10.1007/s11694-017-9573-7

Conflict of Interest: The authors declare that the research was conducted in the absence of any commercial or financial relationships that could be construed as a potential conflict of interest.

Publisher's Note: All claims expressed in this article are solely those of the authors and do not necessarily represent those of their affiliated organizations, or those of the publisher, the editors and the reviewers. Any product that may be evaluated in this article, or claim that may be made by its manufacturer, is not guaranteed or endorsed by the publisher.

frontiers | Frontiers in Plant Science

ORIGINAL RESEARCH
published: 15 April 2022
doi: 10.3389/fpls.2022.882120

Comparison of Metabolome and Functional Properties of Three Korean Cucumber Cultivars

*Hyo Eun Jo[1], Su Young Son[1] and Choong Hwan Lee[1,2]**

[1]*Department of Bioscience and Biotechnology, Konkuk University, Seoul, South Korea,* [2]*Research Institute for Bioactive-Metabolome Network, Konkuk University, Seoul, South Korea*

Cucumber (*Cucumis sativus* L.) is consumed worldwide and various cultivars have been developed to enhance fruit quality. However, few studies have comprehensively evaluated the quality of various cultivars. We carried out a metabolomics approach to study the three different cucumber cultivars (Chuichung, White Dadagi, and Mini) and their parts (peel and flesh) coupled with antioxidant activities. The amino acids, sugars, flavonoids, carotenoids, and chlorophylls were upregulated in Mini flesh; however, in the case of peel, they were highly expressed in Chuichung. The highest antioxidant activity was observed in the peel of Chuichung and flesh of Mini. Through correlation analysis between metabolites and antioxidant activity, apigenin and quercetin derivatives, chlorophyll a, chlorophyll b, lutein, α-carotene, and β-carotene were found to be significantly positively correlated with antioxidant activity. To understand the metabolism of these compounds, we performed a comprehensive pathway analysis using a metabolomics approach and analysis of associated gene expression. In secondary metabolism, the expression levels of carotenoid-related genes (15-*cis*-phytoene synthase and ζ-carotene desaturase) and chlorophyll-related genes (protochlorophyllide reductase and glutamyl-tRNA reductase) were consistent with the metabolome analysis data. Collectively, carotenoid and chlorophyll metabolism were upregulated in Chuichung peel and Mini flesh, which had the highest antioxidant activity in each part. These bioactive compounds can be used as biomarkers of commercial cucumber fruit quality. Accordingly, this study offers integrative insights into the quality of different cucumber cultivars and explores valuable metabolites and genes that are helpful in improving quality with functional properties.

Keywords: cucumber, fruit quality, metabolomics, antioxidant activity, gene expression, carotenoid and chlorophyll metabolism

OPEN ACCESS

Edited by:
Carlos R. Figueroa, Institute of Biological Sciences, University of Talca, Chile

Reviewed by:
Xuewen Xu, Yangzhou University, China
Umakanta Sarker, Bangabandhu Sheikh Mujibur Rahman Agricultural University, Bangladesh

****Correspondence:***
Choong Hwan Lee
chlee123@konkuk.ac.kr

Specialty section:
This article was submitted to Plant Metabolism and Chemodiversity, a section of the journal Frontiers in Plant Science

Received: *23 February 2022*
Accepted: *29 March 2022*
Published: *15 April 2022*

Citation:
Jo HE, Son SY and Lee CH (2022) Comparison of Metabolome and Functional Properties of Three Korean Cucumber Cultivars. Front. Plant Sci. 13:882120. doi: 10.3389/fpls.2022.882120

INTRODUCTION

Cucumber (*Cucumis sativus*) is a widely cultivated and consumed vegetable around the world. Although over 90% of fresh cucumber fruit is water, it is an important commercial resource because it also contains various bioactive compounds associated with multiple biological properties, including antioxidant, anti-wrinkle, anti-aging, and antimicrobial activities (Kamkaen et al., 2007; Sotiroudis et al., 2010; Nema et al., 2011). In particular, antioxidant activity is

nutritionally important for human health. Previous studies have shown that secondary metabolites, including flavonoids, carotenoids, and chlorophylls, affect antioxidant activity (Heim et al., 2002; Pérez-gálvez et al., 2020). Chlorophylls and carotenoids are pigment molecules that determine the color of cucumber fruit (Wang et al., 2020). Chlorophylls are tetrapyrrole compounds that are green in color, and carotenoids are tetraterpenoids related to yellow, orange-red, and red colors. Cucumber has a unique flavor due to several volatile compounds, known as "cucumber aldehydes," including (*E,Z*)-2,6-nonadienal and (*E*)-2-nonenal (Buescher and Buescher, 2001). This greatly affects consumer preference for cucumber fruit, along with its morphological traits, tastes, and compounds in relation to the activities mentioned above. These are crucial factors in determining the quality of cucumber fruit.

Recently, different cultivars of cucumbers have been developed and introduced into the market to meet the diverse consumer preferences. Studies on the metabolism, transcription, and activity of cucumbers have been conducted; however, integrated research remains limited. Few studies have compared commercial cucumbers in detail by dividing them into peel and flesh. Here, an integrated study into cucumber fruit quality was designed using a metabolomics approach.

South Korea is the 16th largest producer of cucumber in the world, with three major cultivar groups being grown: the Baekdadagi-type, Nakhap-type, and Gasi-type cultivars (Park et al., 2021). In addition, nowadays, the demand for mini vegetables has been increasing due to the increase in single-person households. In this study, we aimed to obtain the insights into the fruit quality of cucumber cultivars by constructing metabolome and transcriptome analysis for three commercial Korean cucumbers (Chuichung, White Dadagi, and Mini). These three cultivars are easily available in the Korean local market. The Chuichung and Mini used in this study belong to the Nakhap-type, and White Dadagi belongs to the Baekdadagi-type. Chuichung (Nakhap-type) and White Dadagi (Baekdadagi-type) have been traditionally eaten in Korea for a long time and they are largely distinguished from each other in morphology. The Mini is a new cultivar recently developed and introduced in Korea. Although the Mini belongs to Nakhap-type, but the size is differ to compare traditional cultivars (Chuichung and White Dadagi). The difference of genome between Nakhap-type and Baekdadagi-type has been reported in previous studies (Song et al., 2021). However, few studies have comprehensively evaluated the quality of these cultivars in terms of metabolomics and bioactivity. Thus, we conducted research based on metabolomics approach to interpret difference in morphology and antioxidant activities. This research was intended to analyze the difference among the three cucumber cultivars that were easily obtained and mainly consumed in Korea. Moreover, we tried to provide morphological characteristics and detailed information, such as metabolites, that contribute to fruit odor, flavor, and antioxidant activity of three different cucumber cultivars.

We performed non-targeted metabolomics analysis using gas chromatography time-of-flight mass spectrometry (GC-TOF-MS), ultrahigh-performance liquid chromatography–linear trap quadrupole-orbitrap–tandem mass spectrometry (UHPLC-LTQ-Orbitrap-MS/MS), and headspace-solid phase microextraction gas chromatography time-of-flight mass spectrometry (HS-SPME-GC-TOF-MS) platforms. In addition, different metabolite contents and differentially expressed genes (DEGs) in different cucumber samples were described in a metabolic pathway map. Applying a combination of integrated metabolomic data and its related gene expression data could help us understand the metabolism and molecular mechanisms of gene regulation through the construction of a single pathway.

This study presents a comprehensive picture of the differences in the chemical composition of the primary, secondary, and volatile compounds and the antioxidant activities of three different commercial cucumber fruit. The aim is to provide insights into the metabolism of different cucumber cultivars to facilitate future improvements in cucumber fruit quality.

MATERIALS AND METHODS

Chemicals and Reagents

HPLC-grade solvents were purchased from Fisher Scientific (Waltham, MA, United States). All standard compounds and analytical-grade reagents used in this study were obtained from Sigma-Aldrich (St. Louis, MO, United States) and Junsei Chemical (Tokyo, Japan).

Sample Preparation

The fruit of three commercial cucumbers (Chuichung, White Dadagi, and Mini) at the ripe stage were purchased from a local market (Seoul, Korea; **Figure 1**). Each cucumber fruit was washed with distilled water and divided into three segments based on length. In this study, intermediate segments were used for further analyses. Furthermore, the peel and flesh of the cucumber were separated using a hand-held vegetable peeler. Each sample was dried using a freeze dryer (Operon, Gimpo, Korea) for 5 days and then ground into a powder with a mortar and pestle. Powdered cucumber peel and flesh were stored at −80°C until metabolite extraction. Three biological replicates of cucumber peel and flesh were used.

Sample Extractions for Antioxidant Assays, Total Phenolic, and Flavonoid Contents Analysis, and Metabolic Profiling

Dried powder samples (100 mg) were extracted with 1 ml of 80% aqueous methanol, including internal standard solution (2-chloro-*L*-phenylalanine, 1 mg/ml in water) using an MM 400 mixer mill (Retsch®; Haan, Germany) at a frequency of 30 s^{-1} for 10 min, followed by 5 min of sonication at 4°C (Hettich Zentrifugen Universal 320; Tuttlingen, Germany). The extracted samples were centrifuged at 15,000 rpm for 10 min at 4°C, and the supernatants were filtered using 0.2-μm polytetrafluoroethylene (PTFE) syringe filters (Chromdisc, Daegu, Korea). The filtered supernatants were completely dried using a speed vacuum concentrator (Biotron, Seoul, Korea) and re-dissolved in 80% methanol to obtain a final concentration

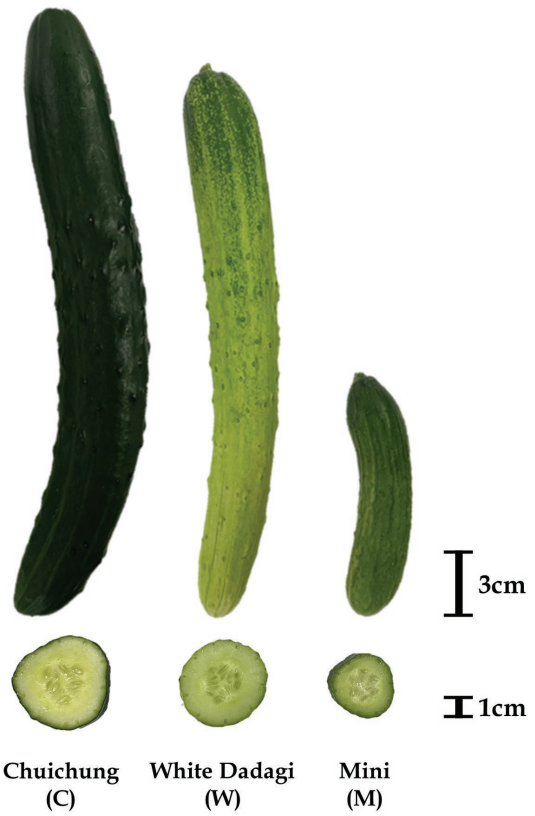

FIGURE 1 | Photographs of representative ripe fruit of the three cucumber cultivars evaluated in this study: Chuichung, White Dadagi, and Mini.

of 10,000 ppm (10 mg/ml) for the bioactivity assays and instrument analyses.

Determination of Antioxidant Activity

Antioxidant activities, including 2,2′-azino-bis (3-ethyl benzothiazoline-6-sulfonic acid; ABTS) and ferric reducing antioxidant power (FRAP) radical scavenging assays, were performed using the methods described by Lee et al. (2016) with some modifications.

ABTS solution (7 mM) was dissolved in a 2.45 mM potassium persulfate solution. Then, the mixture was incubated for 20 min at 60°C in the dark and stored overnight at 4°C. The solution was diluted with distilled water until the absorbance reached 0.7 ± 0.02 at 750 nm using a spectrophotometer (SpectraMax®190; Molecular Devices, San Jose, CA, United States). Sample extracts (10 µl) were mixed with 190 µl of diluted ABTS solution in 96-well plates and incubated for 7 min at 37°C in the dark. The absorbance of the reacted samples was recorded at 750 nm using a spectrophotometer (SpectraMax®190; Molecular Devices, San Jose, CA, United States).

The FRAP solution was mixed with 300 mM acetate buffer (pH 3.6), 10 mM TPTZ(2,4,6-tris(2-pyridyl)-s-triazine; in 40 mM HCl solution), and 20 mM $FeCl_3…6H_2O$ (in distilled water) at a ratio of 10:1:1. The assays were performed by adding 10 µl of the sample extract to 300 µl of the FRAP solution in 96-well plates, followed by incubation for 6 min at 37°C in the dark. The absorbance was measured at 570 nm using a spectrophotometer (SpectraMax®190; Molecular Devices, San Jose, CA, United States).

Analysis for antioxidant activities, such as ABTS and FRAP assay, were conducted in triplicate, and the results were displayed as Trolox equivalent antioxidant capacity (TEAC). The concentration ranges were 0.0156–1 and 0.0156–2 mM in the ABTS and FRAP assays, respectively.

Determination of Total Phenolic and Flavonoid Contents

Total phenolic content (TPC) and total flavonoid content (TFC) were determined using a method described in our previous study (Lee et al., 2016) with some modifications.

To determine the TPC, 20 µl of the sample extracts from each part of the cucumber sample were mixed with 100 µl of 0.2 N Folin–Ciocalteu's phenol reagent in 96-well plates under dark conditions. After incubation for 6 min, 80 µl of 7.5% Na_2CO_3 solution (in distilled water) was added to the mixture. Absorbance was measured at 750 nm using a spectrophotometer (SpectraMax®190; Molecular Devices, San Jose, CA, United States). The results are presented as gallic acid equivalent concentrations, with a concentration range of 3.90625–500 ppm.

To measure TFCs, 180 µl of 90% diethylene glycol (in distilled water), 20 µl of 1 N NaOH, and 20 µl of each sample extract were added to 96-well plates and incubated for 60 min at room temperature in the dark. Lastly, the absorbance was measured at 405 nm using a spectrophotometer (SpectraMax®190; Molecular Devices, San Jose, CA, United States). The results are presented as naringin equivalent concentrations, with a concentration range of 1.5625–200 ppm. All assays were performed in triplicate.

Analysis of Chlorophylls and Carotenoids Contents

The chlorophylls and carotenoids contents were measured according to the procedures described by Xie et al. (2019) and Wang et al. (2020) with some modifications. Dried powder sample (100 mg) was placed in a 15 ml centrifuge tube with 5 ml of solution (9:1 = acetone: 0.1 M NH_4OH). After vortexing, the mixture was sonicated for 15 min and centrifuged at 3,000 rpm for 20 min. Supernatants were collected in a 50 ml tube. The same process was repeated in triplicate, and the supernatants were collected using hexane. The absorbance of the mixed supernatant was measured at 662, 645, and 470 nm using a spectrophotometer (SpectraMax®190; Molecular Devices, San Jose, CA, United States). The measurements were performed using three biological replicates.

The chlorophylls and carotenoids contents were calculated as follows:

$$C_a = 11.75A_{662} - 2.35A_{645}$$

$$C_b = 18.61A_{645} - 3.96A_{662}$$

$$C_{ca} = 1000A_{470} - 2.27C_a - 81.4C_b / 227$$

where C_a, C_b, and C_{ca} indicate the chlorophyll a, chlorophyll b, and total carotenoids content (μg/mL), respectively, and A_{662}, A_{645}, and A_{470} represent the absorbances at 662, 645, and 470 nm, respectively.

Liquid Chromatography-Diode Array Detection (LC-DAD) Analysis for Carotenoids

Carotenoids were extracted from 100 mg of dried powder samples by adding 3 ml of ethanol containing 0.1% ascorbic acid. Mixture vortexed and placed in a water bath at 85°C for 5 min. The carotenoids extract was saponated with 120 μl of 80% potassium hydroxide at 85°C for 10 min. After saponification, the samples were placed on ice and 1.5 ml of cold water was mixed with the sample. β-Apo-8′-carotenal (25 μg/ml) was added as the internal standard. Carotenoids were extracted twice using 1.5 ml of hexane by centrifuging at 1,200 rpm to separate the layers. The supernatants were dried and re-dissolved in 50:50 (v/v) dichloromethane/methanol for analysis. Carotenoids were analyzed using a LC-DAD system, consisting of a Shimadzu Nexera X2 LC-30 AD pump, Shimadzu SIL-30 AC Autosampler, and Shimadzu SPD-20A. Chromatographic separation was performed using a YMC carotenoid C30 column (250 mm × 4.6 mm, 5 μm particle size; YMC, Gyeonggi-do, Korea) with an injection volume of 10 μl. The flow rate was 1 ml/min. The binary solvent system consisted of solvent A (methanol/water (92:8, v/v) with 10 mM ammonium acetate) and solvent B (*tert-butyl* methyl ether). The gradient parameters were set as follows: 0–1 min, 20% B; 1–19 min, 20–100% B; 19–20 min, 100% B; 20–21 min, 100–20% B. Absorbance was measured at a wavelength of 450 nm. Carotenoids were identified by comparing their retention times and absorbance spectra with those of standard carotenoid compounds.

Metabolome Analysis

Gas Chromatography Time-of-Flight Mass Spectrometry Analysis for Primary Metabolites

The dried extracts were re-dissolved in 80% MeOH (10,000 ppm) and filtered using a 0.2-μm PTFE filter (Chromdisc, Daegu, Korea) for GC-TOF-MS analysis. For derivatization, 100 μl of the re-dissolved sample extract (10,000 ppm) was collected in 1.5 ml Eppendorf tubes and completely dried using a speed vacuum concentrator. The derivatization reaction involved oximation and silylation. For oximation, was 50 μl of methoxyamine hydrochloride (20 mg/ml in pyridine) added to the dried extract, and the mixture incubated for 90 min at 30°C. Next, silylation was performed by adding 50 μl of *N*-methyl-*N*-(trimethylsilyl) trifluoroacetamide to the mixture, followed by incubation for 30 min at 37°C. The final concentration of the derivatized sample extract was 10,000 ppm. All samples were filtered using a 0.2-μm PTFE filter (Chromdisc, Daegu, Korea) prior to instrument analyses. After injecting 1 μl into the GC-TOF-MS instrument in splitless mode, GC-TOF-MS analysis was performed using an Agilent 7890A GC system (Agilent Technologies, Palo Alto, CA, United States) coupled with an Agilent 7,693 autosampler (Agilent Technologies) and Pegasus HT TOF-MS (LECO Corp., St. Joseph, MI, United States). The chromatographic separation was conducted by an Rtx-5MS column (30 m × 0.25 mm, 0.25 μm particle size; Restek Corp., St. Joseph, MI, United States) with a helium as carrier gas. The analytical methods and operation parameters were as described in our previous study (Lee et al., 2016). Sample analysis was performed for three biological replicates and two analytical replicates.

Ultrahigh-Performance Liquid Chromatography-Linear Trap Quadrupole-Orbitrap-Tandem Mass Spectrometry Analysis for Secondary Metabolites

The dried extracts were re-dissolved in 80% MeOH (10,000 ppm) and filtered using a 0.2-μm PTFE filter (Chromdisc, Daegu, Korea) for UHPLC-LTQ-Orbitrap-MS/MS analysis. A UHPLC system was equipped with a Vanquish binary pump H system (Thermo Fisher Scientific, Waltham, MA, United States) coupled with an autosampler and column compartment. Chromatographic separation was performed using a Phenomenex KINETEX® C18 column (100 mm × 2.1 mm, 1.7 μm particle size; Torrance, CA, United States) using a mobile phase consisting of 0.1% (v/v) formic acid in water (solvent A) and 0.1% (v/v) formic acid in acetonitrile (solvent B). The gradient condition was designed as follows: 0–1 min, 5% B; 1–10 min, 5–100% B; 10–11 min, 100% B; 11–14 min, 100–5% B. The flow rate, injection volume, column temperature were set at 0.3 ml/min, 5 μl, and 40°C, respectively. Mass spectra were recorded in the full-spectrum mode covering 100–1,000 m/z using an Orbitrap Velos Pro™ system consisting of an ion trap mass spectrometer (Thermo Fisher Scientific) paired with a detector. Mass spectrometry detection designed as follows: capillary temperature, 350°C; and capillary voltage, 2.5 kV in negative mode and 3.7 kV in positive mode. The analytical methods and operation parameters were adopted from a previous study with some modifications (Mun et al., 2021). Sample analysis was performed for three biological replicates and two analytical replicates.

Headspace-Solid Phase Microextraction Gas Chromatography Time-of-Flight Mass Spectrometry Analysis for Volatile Organic Compounds (VOCs)

To extract VOCs from cucumber samples, 5 g of fresh cucumber was ground using liquid nitrogen. The homogenized sample was transferred into a 20 ml SPME glass vial (20 ml) and filled with 2 μl of solution (20% NaCl/Octanal (98:2, v/v)). For volatile collection, headspace-solid phase microextraction (HS-SPME) of the VOCs was performed using 50/30 μm divinylbenzene/carboxen™/polydimethylsiloxane (DVB-CAR-PDMS) StableFlex™ fiber (Sigma-Aldrich, St. Louis, MO, United States). The SPME fiber, preheated at 270°C for 1 min, was injected into the SPME vial and exposed to the headspace for 20 min at 60°C. Then, the fiber was introduced into the injector port of a GC–MS

instrument (7890A GC-5975C MSD; Agilent) equipped with a DB-FFAP column (30 m × 0.25 mm, 0.25 μm film; J&W Scientific, Folsom, CA, United States). The injector (splitless mode) temperature was set at 250°C and extraction of VOCs was performed by exposing the SPME fiber to the headspace of sample supernatants for 30 min at 37°C. The oven temperature was initially set at 50°C for 2 min and increased to 300°C at a rate of 10°C min^{-1}. After reaching 300°C, the temperature was held for 3 min. The temperature of the transfer line was set 240°C. After the extraction, fiber was removed from holder and desorbed at the GC port for 1 min at 270°C. The analytical method for VOCs was followed by Singh and Lee (2018) with some modifications. The sample analysis was performed using two analytical replicates.

Data Processing and Multivariate Statistical Analysis

The GC-TOF-MS and HS-SPME-GC-TOF-MS raw data files were converted into NetCDF (*.cdf) format using the LECO ChromaTOF software (version 4.44). In addition, the UHPLC-LTQ-orbitrap-MS/MS raw data files were converted to NetCDF (*.cdf) format using Thermo Xcalibur software (version 2.1; Thermo Fisher Scientific). After conversion, NetCDF files were processed using the metAlign software package for peak detection, retention time correction, and alignment. The processed data were then used for SIMCA-P + 12.0 (Umetrics, Umea, Sweden) for principal component analysis (PCA) and partial least squares-discriminant analysis (PLS-DA). To select the significantly different metabolites among the samples, variable importance in the projection (VIP > 0.7) values based on a partial least squares-discriminant analysis (PLS-DA) score plot were applied. In addition, the significance test ($p < 0.05$) between biological and analytical replicates was performed by analysis of variance (ANOVA) and Duncan's multiple-range tests using PASW Statistics 18 software (SPSS, Inc., Chicago, IL, United States). Selected metabolites were tentatively identified by comparison with various data, including mass fragment patterns, retention times, and the mass spectra of data for standard compounds under the same conditions from published papers and commercial databases, such as the National Institutes of Standards and Technology (NIST) Library (version 2.0, 2011, FairCom, Gaithersburg, MD, United States), and Wiley 9. A correlation map was obtained using the PASW Statistics software (version 18.0; SPSS Inc., Chicago, IL, United States).

RNA Extraction and Transcriptome Analysis

For RNA isolation, fresh cucumber samples were homogenized in liquid nitrogen using a mortar and pestle. The homogenized sample was transferred into Eppendorf tubes filled with TRI reagent solution and stored at −80°C until RNA purification. Library preparation and RNA sequencing were performed using the Illumina Hiseq4000 platform by Macrogen (Seoul, Korea; http://www.macrogen.com; accessed December 25, 2021). Prior to RNA sequencing, a 2,100 Bioanalyzer (Agilent, Böblingen, Germany) was used to determine the total RNA quality and amount separated from the samples. For library preparation, we confirmed that all samples had RNA integrity ≥7.5. Library construction was performed by using the TruSeq Stranded mRNA LT sample prep Kit (Illumina, San Diego, CA, United States) by Macrogen (Seoul, Korea). Raw data were trimmed by filtering according to the following criteria: unpaired reads, empty nucleotides, adaptor-only nucleotides, short reads (<36 bp), and low-quality nucleotides (Q-value: Phred quality value ≤20). Processed reads were aligned to reference genome data (GCF_000004075.3_Cucumber_9930_V3) using HISAT2 (version 2.1.0). After alignment, aligned reads were assembled into transcripts using StringTie (version 2.1.3b). The raw and trimmed data statistics were presented in supplementary table (**Supplementary Tables S7**, **S8**). Mapped data statistics summarized in **Supplementary Table S9**. The expression level of each transcript was normalized to the values of fragments per kilobase of exon per million fragments mapped (FPKM) and log2-transformed for quantile normalization. In addition, in the statistical analysis prior to DEG analysis, genes with a count value of 0 in at least one sample were excluded from the analysis. Therefore, the analysis was conducted on 16,816 genes of the total 23,995 genes excluding 7,179 (**Supplementary Figure S7**). DEGs in each sample were selected as $p \leq 0.05$, $\log_2$ fold change values (FC) ≥2. The count of up and downregulation genes that present significantly differences based on fold change and value of p for each combination is summarized in **Supplementary Figure S8**. In this study, DEGs associated with flavonoid, carotenoid, and chlorophyll metabolic pathways were selectively identified and included in **Figure 2**. In addition, to compare the gene expression associated with the antioxidant activity of cucumber fruit, the main focus was the DEG of the Chuichung and Mini, which had the largest difference in activity in this study. RNA extraction and transcriptome analysis were performed as described by Son et al. (2019) with some modifications. We have submitted the raw sequence data to NCBI (BioProject: PRJNA817515).

RESULTS

Difference in Morphological Features, Level of Bioactive Secondary Metabolites, and Antioxidant Activity in Three Cucumber Cultivars

To evaluate cucumber fruit quality, we examined the morphological characteristics, content of total phenolic and flavonoid compounds, carotenoids and chlorophylls, and antioxidant activities of three different cultivars. **Figure 1** shows photographs of the three cucumber cultivars analyzed in this study. The morphological characteristics of cucumbers are listed in **Table 1**. The weight, length, and width of the cucumber fruit were measured, and these varied depending on the cultivar. These data indicated that cucumber fruit have various morphological characteristics based on their cultivar.

To compare the bioactivities and bioactive secondary metabolite levels of the three cucumbers, we analyzed their antioxidant activities (ABTS and FRAP), TPC, TFC, and

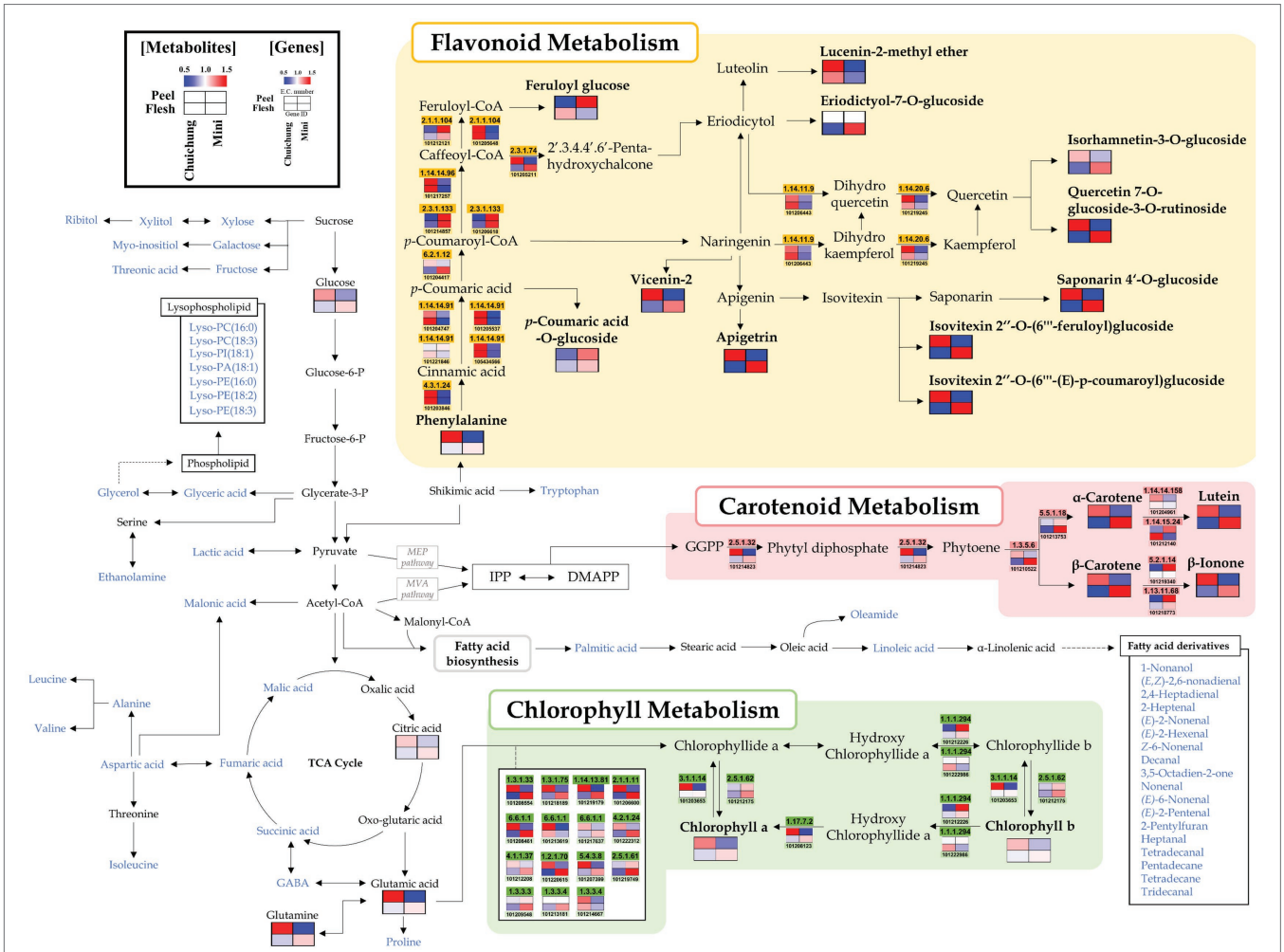

FIGURE 2 | Schematic representation of the flavonoid, carotenoid, and chlorophyll metabolic pathway with metabolite and related gene expression levels in the Chuichung and Mini cultivars. The pathway was modified from the Kyoto Encyclopedia of Genes and Genomes (KEGG) database (http://www.genome.jp/kegg/). The colored squares (blue-to-red) represent the relative abundance. The blue characters represent metabolites detected through the mass spectrometry, and the relative abundance of these metabolites is shown in **Figures 4**, **5**.

carotenoids and chlorophylls contents (**Figure 3**). In the peel, the antioxidant levels determined by ABTS and FRAP assays were significantly higher in Chuichung than in the others. In contrast, in the flesh, antioxidant activities were highest in Mini (**Figures 3A,B**). TPC and TFC were highest in the fruit peel of Chuichung and fruit flesh of Mini (**Figures 3C,D**). Chlorophylls and carotenoids contents also showed the same tendency as antioxidant activities (**Figure 3E–G**). We performed LC-DAD to confirm the relative abundance of each carotenoid compound, including lutein, α-carotene, and β-carotene. Lutein, α-carotene, and β-carotene were the highest in Chuichung peel. However, in the flesh, these compounds were the highest in Mini (**Figure 3H**).

Collectively, we observed that the levels of antioxidant activities and bioactive compound contents (carotenoids and chlorophylls) of cucumber fruit types showed different patterns in the peel and flesh. The content of carotenoids and chlorophylls, TFC, TPC, and antioxidant activity levels were the highest in the fruit peel of Chuichung and fruit flesh of Mini. All of these were confirmed to be statistically significant.

Comparative Evaluation of Different Cucumber Cultivars Based On Metabolite Profiles

To analyze the global metabolites in the three different cucumbers, metabolite profiling was performed using HS-SPME-GC-TOF-MS, GC-TOF-MS, and UHPLC-LTQ-Orbitrap-MS/MS. To evaluate significantly discriminated metabolites derived from cucumber, we performed multivariate analyses including PCA and PLS-DA. The results revealed that the three commercial cucumbers were distinguished from each other and clustered depending on their type (**Supplementary Figures S1, S2**). The PLS-DA score plot also showed a similar pattern to that of the PCA score plot (**Figures 4A–C** and **Figures 5A–C**). To investigate distinctive metabolites among the different types

TABLE 1 | Data on the morphological characterization of the three cucumber cultivars.

No.	Cultivars	Abbreviation	Morphological characterization			
			Weight (g)		Length (cm)	Width (cm)
			Peel	Flesh		
1	Chuichung	C	28.46 ± 0.50[a]	222.79 ± 2.33[a]	29.9 ± 0.79[a]	3.86 ± 0.15[a]
2	White Dadagi	W	30.41 ± 1.65[a]	212.42 ± 20.02[a]	24.2 ± 0.26[b]	3.73 ± 0.21[a]
3	Mini	M	10.30 ± 0.79[b]	50.51 ± 6.23[b]	11.0 ± 0.26[c]	2.73 ± 0.32[b]

The different alphabets (a, b, c) within the morphological characterization columns indicate values that are significantly distinguished according to the Duncan multiple-range test at value of $p < 0.05$.

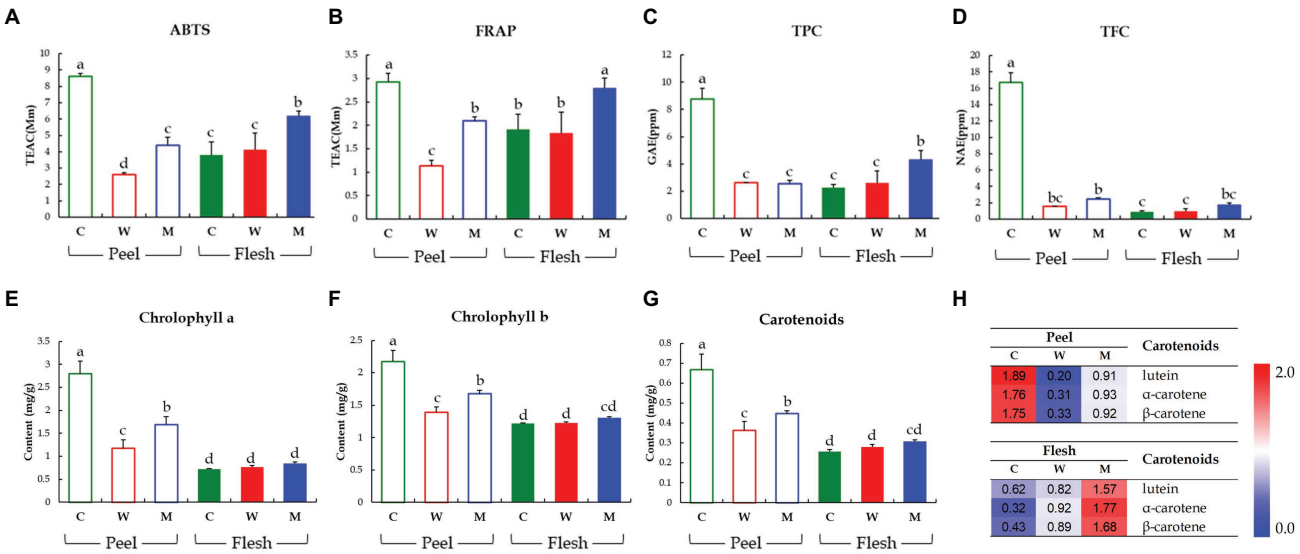

FIGURE 3 | Results of antioxidant activities including ABTS assay (**A**) and FRAP assay (**B**), TPCs (**C**), TFCs (**D**), chlorophylls contents (**E, F**), and carotenoid analysis (**G, H**). Different letters in the bar graph indicate significant difference by ANOVA followed by Duncan's multiple-range test ($p < 0.05$). ABTS, 2,2′-azino-bis (3-ethylbenzothiazoline-6-sulfonic acid); FRAP, ferric reducing antioxidant power; TEAC, trolox equivalent antioxidant capacity; GAE, gallic acid equivalent concentration; NAE, naringin equivalent concentration; C, Chuichung; W, White Dadagi; M, Mini.

of cucumbers, we selected significantly discriminated metabolites based on the VIP value (>0.7) derived from the PLS-DA model and $p < 0.05$.

In the peel, the PLS-DA model derived from GC-TOF-MS, UHPLC-LTQ-Orbitrap-MS/MS, and HS-SPME-GC-TOF-MS datasets, three cucumber samples showed distinct patterns of PLS1 and PLS2 (**Figures 4A–C**). Notably, the PLS-DA model for UHPLC-LTQ-Orbitrap-MS/MS data showed that Chuichung was clearly distinguished from the others by PLS1 (36.21%), concurrent with the antioxidant activity (**Figure 4B**). A total of 80 distinguished metabolites were identified, of which 34, 21, and 25 metabolites were identified by GC-TOF-MS, UHPLC-LTQ-Orbitrap-MS/MS, and HS-SPME-GC-TOF-MS, respectively (**Supplementary Tables S1–S3**). These identified metabolites were categorized into the following metabolite classes: 14 amino acids, nine organic acids, eight sugar derivatives, 10 flavonoids, 11 lipids (three fatty acids, one fatty acid amide, and seven lysophospholipids), and 25 volatile compounds (16 aldehydes, three alcohols, two alkanes, two sesquiterpenoids, and two others).

In the flesh, the PLS-DA model for GC-TOF-MS, UHPLC-LTQ-Orbitrap-MS/MS, and HS-SPME-GC-TOF-MS datasets also displayed clearly distinguished patterns among the three different cucumbers by PLS1 and PLS2, respectively (**Figures 5A–C**). Contrary to the peel, the PLS-DA model for UHPLC-LTQ-Orbitrap-MS/MS data showed that Mini was clearly distinct from the others by PLS1 (28.36%; **Figures 5B**). A total of 69 distinguished metabolites were identified, of which 29, 15, and 25 metabolites were identified by GC-TOF-MS, UHPLC-LTQ-Orbitrap-MS/MS, and HS-SPME-GC-TOF-MS, respectively (**Supplementary Tables S4–S6**). These identified metabolites included 12 amino acids, nine organic acids, seven sugar derivatives, 10 flavonoids, three lipids (two fatty acids and one lysophospholipids), and 25 volatile compounds (16 aldehydes, three alcohols, two alkanes, two sesquiterpenoids, and two others).

For the visualization of significantly different metabolites, all metabolites were displayed on a heat scale (**Figures 4D–F**). Each column is expressed as a fold change calculated from

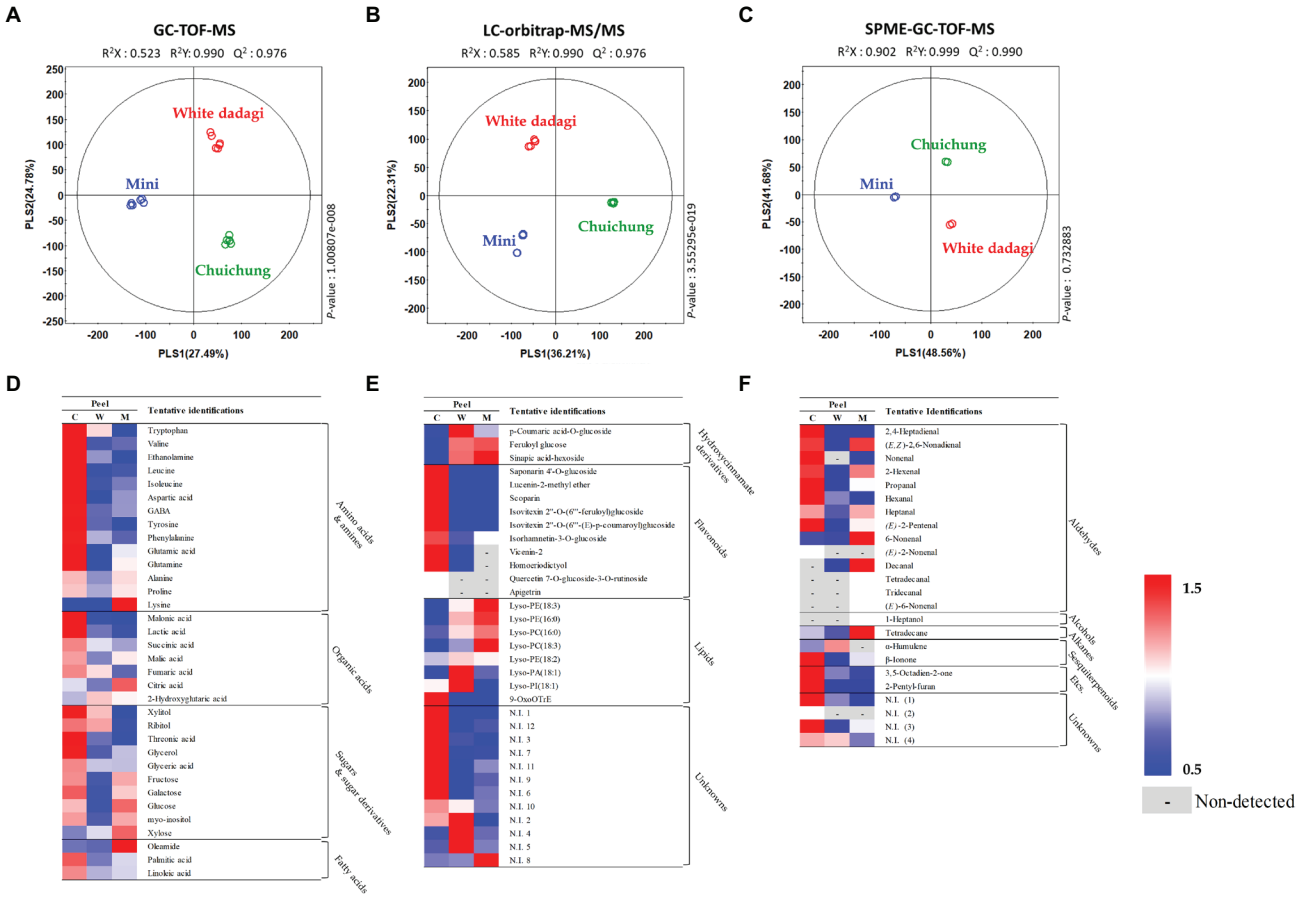

FIGURE 4 | Partial least squares-discriminant analysis (PLS-DA; **A–C**) score plots for metabolites in three different cucumber peel based on GC-TOF-MS **(A)**, UHPLC-LTQ-Orbitrap-MS/MS **(B)**, and HS-SPME-GC-TOF-MS **(C)** dataset. Heat map analysis of different cucumber peel based on GC-TOF-MS **(D)**, UHPLC-LTQ-Orbitrap-ESI-MS/MS **(E)**, and HS-SPME-GC-TOF-MS **(F)** data. Heat map representation of the relative abundance of significantly discriminant metabolites (VIP > 0.7, $p < 0.05$) based on PLS-DA model. Peel of Chuichung (○), White Dadagi (○), and Mini (○) samples. GC-TOF-MS, gas chromatography time-of-flight mass spectrometry; UHPLC-LTQ-Orbitrap-MS/MS, ultrahigh-performance liquid chromatography–linear trap quadrupole-orbitrap–tandem mass spectrometry; HS-SPME-GC-TOF-MS, headspace-solid phase microextraction gas chromatography time-of-flight mass spectrometry; VIP, variable importance projection; PLS-DA, partial least squares-discriminant analysis.

the average peak area of each type of cucumber. In the peel, the levels of primary metabolites, such as amino acids (tryptophan, valine, ethanolamine, leucine, isoleucine, aspartic acid, GABA, tyrosine, phenylalanine, glutamic acid, and glutamine), organic acids (malonic acid, lactic acid, succinic acid, malic acid, and fumaric acid), and sugar derivatives (xylitol, ribitol, threonic acid, glycerol, glyceric acid, galactose, and myo-inositol), were relatively higher in Chuichung than in other cucumbers (**Figure 4D**). The levels of secondary metabolites were showed different metabolite pattern according to cucumber cultivars. Most of flavonoid compounds (saponarin 4'-*O*-glucoside, vicenin-2, lucenin-2-methyl ether, scoparin, isovitexin 2″-*O*-(6‴-feruloyl)glucoside, isovitexin 2″-O-(6‴-(E)-p-coumaroyl) glucoside, isorhamnetin-3-O-glucoside, and homoeriodictyol) were relatively higher in Chuichung than in other cucumbers. In particular, quercetin 7-O-glucoside-3-O-rutinoside and apigetrin were detected in only Chuichung. Hydroxycinnamate derivatives and lipids were observed the lowest level in Chuichung (**Figure 4E**). Volatile compounds also showed significantly different patterns according to the fruit cultivars. In this study, 24 volatile compounds were tentatively identified as a compound have significantly differences among the peel of the three cucumber cultivars. Fourteen of 24 volatile compounds belonged to the aldehyde. In particular, aldehyde including 2,4-heptadienal, nonenal, propanal, hexanal, and *(E)*-2-pentenal showed clearly higher level in Chuichung than other cultivars. However, 6-nonenal and decanal showed higher level in Mini than others. Specifically, *(E)*-2-nonenal was only detected in Chuichung and tridecanal, tetradecanal, and *(E)*-6-nonenal were detected only in Mini (**Figure 4F**).

In the flesh, the levels of the most of primary metabolites, such as some amino acids (GABA, serine, glutamic acid, aspartic acid, glycine, and ethanolamine), organic acids (citric acid, lactic acid, succinic acid, malic acid, fumaric acid, and 2-hydroxyglutaric acid), and sugar derivatives (xylose, xylitol, ribitol, fructose, galactose, glucose, myo-inositol, glyceric acid,

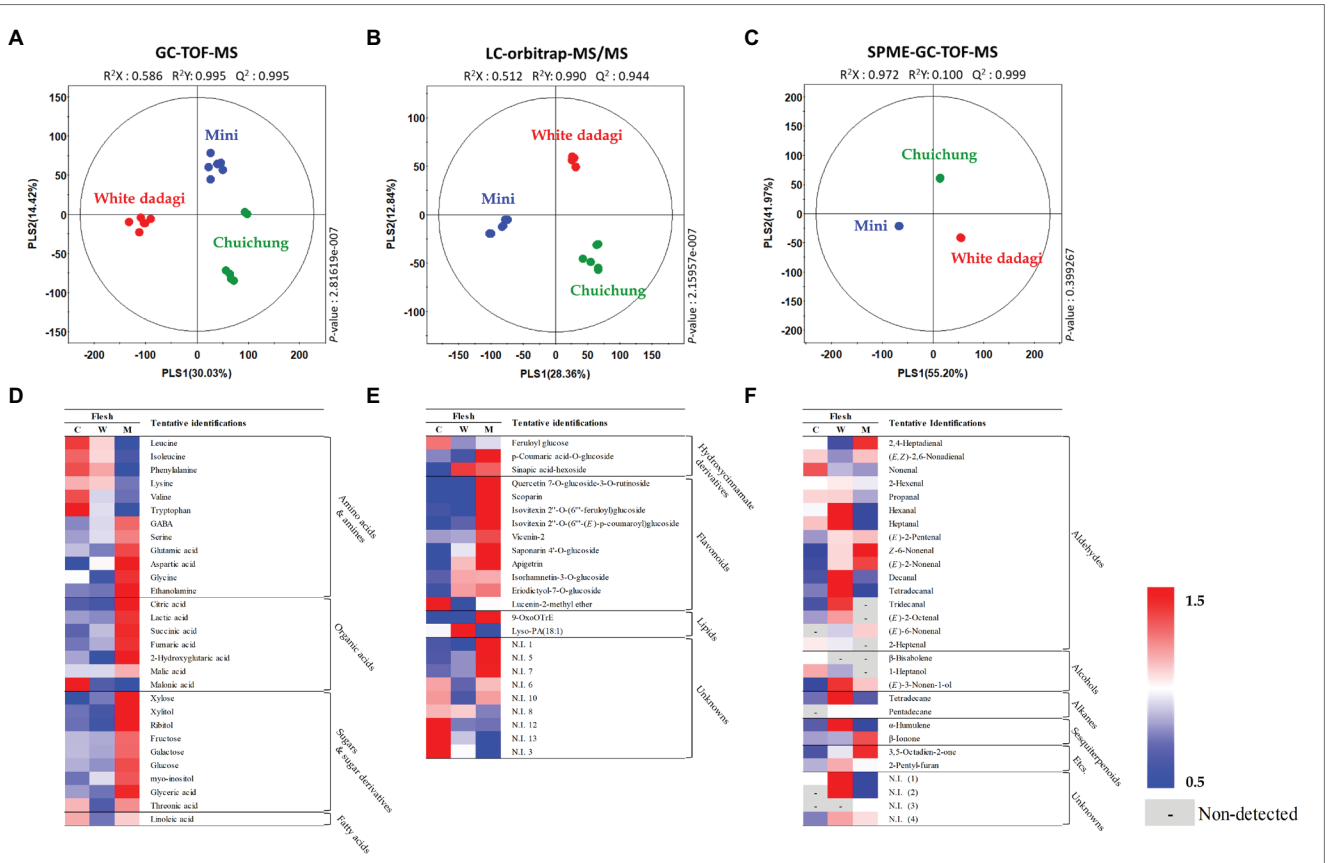

FIGURE 5 | Partial least squares-discriminant analysis (PLS-DA; **A**–**C**) score plots for metabolites in three different cucumber flesh based on GC-TOF-MS (**A**), UHPLC-LTQ-Orbitrap-MS/MS (**B**), and HS-SPME-GC-TOF-MS (**C**) data set. Heat map analysis of different cucumber flesh based on GC-TOF-MS (**D**), UHPLC-LTQ-Orbitrap-ESI-MS/MS (**E**), and HS-SPME-GC-TOF-MS (**F**) data. Heat map representation of the relative abundance of significantly discriminant metabolites (VIP > 0.7, $p < 0.05$) based on PLS-DA model. Flesh of Chuichung (○), White Dadagi (○), and Mini (○) samples. GC-TOF-MS, gas chromatography time-of-flight mass spectrometry; UHPLC-LTQ-Orbitrap-MS/MS, ultrahigh-performance liquid chromatography–linear trap quadrupole-orbitrap–tandem mass spectrometry; HS-SPME-GC-TOF-MS, headspace-solid phase microextraction gas chromatography time-of-flight mass spectrometry; VIP, variable importance projection; PLS-DA, partial least squares-discriminant analysis.

and threonic acid), were observed that higher abundance in Mini than in other cucumbers (**Figure 5D**). The level of secondary metabolite also showed different patterns by cultivars. Most of flavonoid compounds including quercetin 7-O-glucoside-3-O-rutinoside, scoparin, isovitexin 2″-O-(6‴-feruloyl)glucoside, isovitexin 2″-O-(6‴-*(E)*-*p*-coumaroyl)glucoside, vicenin-2, saponarin 4'-O-glucoside, and apigetrin were showed that relatively higher level in Mini than in other cucumbers (**Figure 5E**). Volatile compounds showed significantly different patterns according to the fruit cultivars. In this study, 29 volatile compounds were tentatively identified as a compound have significantly differences among the flesh of the three cucumber cultivars. Among VOCs, the most detected aldehyde, such as 2,4-heptadienal, *(E,Z)*-2,6-nonadienal, *(E)*-2-pentenal, *(Z)*-6-nonenal, *(E)*-2-nonenal, and *(E)*-6-nonenal, were showed the highest level in Mini. On the other hand, 2-hexenal, hexanal, heptanal, decanal, tetradecanal, tridecanal, and *(E)*-2-octenal were observed that higher level in White Dadagi than others. Nonenal and 2-heptenal were represented the highest pattern in Chuichung (**Figure 5F**).

Integrated Pathway Mapping for Discriminant Metabolites and DEGs In Chuichung and Mini Cultivars

To identify the compounds that contribute to antioxidant activity, we conducted a correlation analysis between metabolites and activities with Chuichung and Mini, which showed the most characteristic patterns in each part (**Supplementary Figure S3**). In both peel and flesh, apigenin and quercetin derivatives, chlorophyll a, chlorophyll b, lutein, α-carotene, and β-carotene were significantly positively correlated with the antioxidant activity.

Moreover, we performed a comprehensive metabolic pathway analysis through an metabolomics and DEGs analysis data to understand the detailed biosynthesis of positively correlated secondary metabolites with antioxidant activity (**Figure 2**).

According to pathway analysis, α-carotene, β-carotene, and lutein presented high relative abundance in Chuichung peel, whereas in flesh, they were higher on Mini. Moreover, β-ionone, a carotenoid-derived volatile compound, exhibited the same pattern. The expression patterns of 15-*cis*-pytoene synthase (EC 2.5.1.32) and ζ-carotene desaturase (EC 1.3.5.6), which

are involved in the synthesis of precursors of these carotenoids, were consistent with the measured carotenoids contents. The chlorophyll a and chlorophyll b contents showed the same tendency as carotenoids. Most genes related to chlorophyll synthesis and regulation, such as protochlorophyllide reductase (EC 1.3.1.33), magnesium protoporphyrin IX monomethyl ester (oxidative) cyclase (EC 1.14.13.81), magnesium protoporphyrin O-methyltransferase (EC 2.1.1.11), magnesium chelatase subunit D (EC 6.6.1.1), glutamyl-tRNA reductase (EC 1.2.1.70), glutamate-1-semialdehyde 2,1-aminomutase (EC 5.4.3.8), heme oxygenase (biliverdin-producing, ferredoxin; EC 1.14.15.20), porphobilinogen synthase (EC 4.2.1.24), uroporphyrinogen decarboxylase (EC 4.1.1.37), chlorophyllase (EC 3.1.1.14), and 7-hydroxymethyl chlorophyll a reductase (EC 1.17.7.2), showed higher expression levels in Chuichung peel and Mini flesh. Flavonoids, such as apigenin derivatives (apigetrin, saponarin 4'-*O*-glucoside, isovitexin 2″-*O*-(feruloyl)-glucoside, and isovitexin 2″-*O*-(6″-(*E*)-*p*-coumaroyl)-glucoside) and quercetin derivatives (isorhamnetin-3-*O*-glucoside and quercetin-7-*O*-glucoside-3-*O*-rutinoside), were observed at a relatively higher abundance in Chuichung peel and in Mini flesh. Phenylalanine, a precursor of flavonoid biosynthesis, showed the same pattern. However, unlike carotenoid and chlorophyll metabolism, flavonoid-related genes were highly expressed in the peels of both cucumber cultivars.

DISCUSSION

Cucumber is consumed around the world for its flavor, important nutrients, and bioactive compounds. In addition, cucumber is also used in therapeutic medicine and cosmetic fields. Currently, various cultivars of cucumbers have been developed to appeal to consumers by enhancing fruit quality. The fruit quality of cucumbers is determined by various factors, such as morphological traits, flavors, and biological properties (Cuthbertson et al., 2012). However, few studies have comprehensively investigated the quality of various cultivars. In this study, we performed the comprehensive research to compare the fruit quality among different cucumber cultivars: Chuichung and White Dadagi, which are mainly consumed in Korea, and Mini, was recently developed in Korea.

Comparison of Odor In Cucumber Fruit

In the peel, most alcohols (2,4-heptadienal, (*E,Z*)-2,6-nonadienal, nonenal, 2-hexenal, propanal, hexanal, heptanal, (*E*)-2-pentenal, and (*E*)-2-nonenal) were higher in Chuichung than in the others. In addition, the volatiles β-ionone, 3,5-octadien-2-one, and 2-pentyl-furan showed higher patterns in Chuichung than in the others. White Dadagi showed the lowest relative abundance of VOCs, except for α-humulene (**Figure 4F**). In the flesh, most alcohols (2-hexenal, propanal, hexanal, heptanal, (*E*)-2-pentenal, (*E*)-2-nonenal, decanal, tetradecanal, tridecanal, and (*E*)-2-octanal), 2-pentyl-furan, and α-humulene were present at higher levels in White Dadagi than in the other groups (**Figure 5F**). In agreement with our results, similar classes of VOCs have been reported in cucumber (Chen et al., 2015; Wei et al., 2016). The volatiles 2,4-heptadienal, nonenal, 2-hexenal, and 3,5-octadien-2-one have been reported to be important contributors to green and fresh odors. Heptanal, (*E*)-2-pentenal, and 2-pentyl-furan are known to have fruity odors. In addition, β-ionone has a flower-like odor (Chen et al., 2015; Wei et al., 2016). Therefore, it can be inferred that Chuichung peel has an abundant and diverse odor compared to other cucumber cultivars; however, White Dadagi flesh has more varied types of odors than the other cultivars. Volatile (*E,Z*)-2,6-nonadienal, which is derived from the 9-hydroperoxides of linolenic acid, has been associated with a cucumber-like odor and has been reported as the major volatile component of cucumber aroma (Grosch and Schwarz, 1971). In both the peel and flesh, the relative proportions of (*E,Z*)-2,6-nonadienal were found to be comparatively higher in Chuichung and Mini than in White Dadagi (**Figures 4F, 5F**). Collectively, the characteristic odors of cucumber can be found in Chuichung and Mini.

Comparison of Taste and Nutritional Compounds In Cucumber Fruit

Cucumber fruit mainly have sweet and bitter tastes. Previous studies have shown that the amino acid content determines various factors affecting the taste, flavor, nutrition, and palatability of fruit (Youn et al., 2007). The glycine and serine contents determine the sweetness of fruit, whereas valine, leucine, isoleucine, and phenylalanine confer a bitter taste (Keutgen and Pawelzik, 2008). In our study, in the peel, the sweet taste-related metabolites, such as glycine, serine, and sugar derivatives, and bitter taste-related metabolites, including valine, leucine, isoleucine, and phenylalanine, were higher in Chuichung (**Figure 4D**). In the flesh, some amino acids related to bitter taste were higher in Chuichung; however, compounds related to sweet taste were higher in Mini (**Figure 5D**).

Cucumber fruit also contain various nutritionally and functionally important secondary metabolites (Mukherjee et al., 2013). According to their research, flavonoids, carotenoids, and chlorophylls are important secondary metabolites of cucumber fruit.

Flavonoids are polyphenolic secondary metabolites that have been identified in many plants (Tadmor et al., 2010). Fruit and vegetable polyphenols are phenolics including coumarins, phenolic acids, like hydroxybenzoic acids (Sarker and Oba, 2020c) and hydroxycinnamic acids (Sarker, 2018), flavonoids, such as flavonols (Sarker and Oba, 2019), flavones (Sarker and Oba, 2020d), flavanols (Sarker and Oba, 2020b), flavanones (Sarker et al., 2020), isoflavones, anthocyanins, chalcones and non-flavonoids, such as tannins, lignans, and stilbenes, with strong radical quenching ability (Sarker and Oba, 2020e). In this study, we identified apigenin and quercetin derivatives. Apigenin and quercetin are flavones and flavanols, respectively, which are water-soluble pigments contained in vegetables and are generally reported to have a pale yellow color (Alihosseini and Sun, 2011; Awika, 2017). Flavonoids are considered antioxidants because they can remove free radicals, inhibit lipid oxidation, or chelate metal ions (Tripoli et al., 2007). The reason for the increased scavenging activity of flavonoids is

mainly due to the C2−C3 double bond with the 4-oxo group of C-rings, but is also affected by the number of hydroxyl groups on the B-rings (Borges Bubols et al., 2013).

Carotenoids are tetraterpenoids, namely, α-carotene, β-carotene, (Sarker and Oba, 2021), xanthophylls like neoxanthin, violaxanthin, zeaxanthin, lutein (Sarker and Oba, 2020a), lycopene, etc. having strong antioxidants capacity (Sarker and Oba, 2018a,b, 2020e) which are responsible for yellow, orange-red, and red colors (Miller et al., 2014; Aadil et al., 2019). These compounds are likely to be involved in the prevention or protection of severe human health disorders, such as heart disease, cancer, and macular degeneration (Agarwal and Rao, 2000; Fiedor and Burda, 2014). Carotenoids are composed of a 40-carbon skeleton of isoprene units covalently linked together, forming multiple conjugated double bonds. The biggest feature of this structure is the long series of conjugated double bonds that form the central part of the molecule. It gives them a compound shape, chemical reactivity, and light-absorbing properties (Miller et al., 2014. Carotenoids with these structural characteristics are known to be effective antioxidants because of their ability to remove free radicals (Pérez-gálvez et al., 2020).

Chlorophylls are tetrapyrrole metabolites that indicates green color present in plants and serves to convert light energy into chemical energy in plants through a process known as photosynthesis (Ares et al., 2021). Chlorophylls have a characteristic central structure similar to the heme structure of hemoglobin constituting blood (Pérez-gálvez et al., 2020). Therefore, chlorophyll supplies oxygen to the blood and helps detoxify human organisms. Other health-promoting effects caused by its antioxidant and anti-inflammatory activities have also been reported in previous studies (Perez-Galvez et al., 2017).

These metabolites are crucial for pigments and antioxidant compounds in cucumber (Lanfer-Marquez et al., 2005; Złotek et al., 2014; Lai et al., 2015; Wang et al., 2020). Previous studies have reported that the contents of chlorophylls, carotenoids, and flavonoids are much higher in dark-green cucumbers than in light-green cucumbers (Wang et al., 2020). In addition, Mun et al. (2021) reported that the levels of flavonoids, carotenoids, and antioxidant activity were relatively high in fruit of cultivars that were smaller than the conventional cultivars of general size.

In our study, after separating the skin and flesh, the relative abundance levels of these metabolites and antioxidant activity were analyzed according to cultivar. Similarly, these compounds were relatively higher in the peel of Chuichung, which had the darkest color (**Figures 3E–H, 4E**). In the flesh, although the color difference of each cucumber was not observed as clearly as in the peel, the contents of chlorophyll b and carotenoids were significantly higher in Mini, which had a relatively darker color (**Figures 3F–H**, **5E**). Therefore, we found that the compounds involved in the taste and nutrition of fruit differed depending on the cultivar and that secondary metabolites associated with various activities showed relatively high levels in Chuichung peel and Mini flesh. This result was consistent with our results from the antioxidant activity assay (**Figures 3A,B**). Comprehensively considering our results, based on our metabolite profiling and functional studies, we assumed that the color of cucumbers was associated with antioxidant activity. The association between fruit color and antioxidant activity has also been reported in previous studies (Hua et al., 2018; Shi et al., 2018).

Metabolism of Bioactive Compounds In Cucumber Fruit

Antioxidant activity prevents and suppresses various diseases and aging by removing free radicals (Masaki, 2010; Song et al., 2010; Fiedor and Burda, 2014). Thus, cucumber fruit can be used in various food and cosmetic industries. Therefore, this is an important factor in evaluating cucumber fruit quality. In the present study, the patterns of antioxidant activity showed contradictory phenomena in the peel and flesh. Therefore, we conducted a correlation analysis to understand the different patterns of bioactivity in the peel and flesh and performed a correlation analysis between secondary metabolites and antioxidant activity. According to our results, we estimated that flavonoids, chlorophylls, and carotenoids had a significantly positive correlation with antioxidant activity in both the peel and flesh (**Supplementary Figure S3**).

We performed an integrated metabolic pathway analysis to understand the biosynthesis mechanism of bioactive compounds (**Figure 2**). Based on pathway analysis, we observed differences in the metabolism of bioactive compounds between Chuichung and Mini, which were the most distinguished in the results of UHPLC-LTQ-orbitrap-MS/MS analysis and antioxidant activity.

The mechanism of flavonoid synthesis and related genes have been described in previous studies (Dao et al., 2011; Zhang et al., 2020). Genes including phenylalanine ammonia lyase (*PAL*; EC 4.3.1.24), *trans*-cinnamate-4-monooxygenase (*C4H*; EC 1.14.14.91), four coumarate-CoA-ligases (*4CL*; EC 6.2.1.12), chalcone synthase (*CHS*; EC 2.3.1.74), naringenin, and 2-oxoglutarate 3-dioxygenase (*F3H*; EC 1.14.11.9) are known to play an important role in the flavonoid synthesis pathway (Dao et al., 2011; Zhang et al., 2020). *PAL*, *C4H*, *4CL*, and *CHS* catalyze the conversion of phenylalanine to naringenin chalcone. Subsequently, *chalcone isomerase (CHI)* catalyzes the conversion of naringenin chalcone to naringenin, which is then converted to dihydrokaempferol by *F3H* (Yu et al., 2021). Our study identified 14 DEGs involved in flavonoid metabolism. The 14 DEGs were displayed in the flavonoid pathway analysis (**Supplementary Table S10**; **Figure 5**). We found that *CHS* and *4CL* were upregulated in Chuichung peel and Mini flesh, and tentatively identified flavonoids, such as apigetrin, quercetin derivatives, and isovitexin derivatives, that were also upregulated in Chuichung peel and Mini flesh (**Figure 2**). This indicated that *CHS* was significantly more expressed in Chuichung peel and Mini flesh, which led to the upregulation of flavonoids. However, *C4H* was upregulated in Mini peel and Chuichung flesh, and *PAL* and *F3H* showed higher expression levels in Chuichung in both peel and flesh. Wang et al. (2020) reported that *CHS* and *4CL* play key roles in the synthesis of flavonoids and are significantly more expressed in dark-green cucumbers than in light-green

cucumbers. Wang et al. (2020) also conducted research on genes that play a key role in the synthesis of flavonoids and reported that *CHS* and *4CL* are significantly more highly expressed in dark-green cucumbers than in light-green cucumbers. This result was consistent with our results. Therefore, in this study, it was found that various key genes regulating flavonoid synthesis mechanisms, including *PAL*, *C4H*, *4CL*, *CHS*, and *F3H*, were expressed differently in each type of cucumber.

The carotenoid synthesis mechanism has been previously described (Rodríguez-Concepción, 2010; Grassi et al., 2013). In addition, previous studies have shown that several genes, such as geranylgeranyl diphosphate synthase (*GGPPS*; EC 2.5.1.29), phytoene synthase (*PSY*; EC 2.5.1.32), and ζ-carotene desaturase (*ZDS*; EC 1.3.5.6), are involved in the carotenoid synthesis pathway (Rodríguez-Concepción, 2010; Grassi et al., 2013). Carotenoids are mainly biosynthesized from isopentenyl diphosphate (IPP) and dimethylallyl diphosphate (DMAPP) *via* the methylerythritol 4-phosphate (MEP) pathway in plastids (Rodríguez-Concepción, 2010; Grassi et al., 2013). Geranylgeranyl diphosphate (GGPP) was synthesized using *GGPPS*. Then, the two GGPP molecules start to condense to produce phytoene by *PSY*. Subsequently, phytoene desaturase (*PDS*; EC 1.3.5.5) and *ZDS* catalyze similar dehydrogenation reactions by introducing four double bonds in phytoene to form lycopene, which is a precursor of α-carotene, β-carotene, and lutein. In this study, 21 DEGs involved in carotenoid metabolism were identified. Among these, seven were selected to visualize the integrated carotenoid pathway analysis (**Supplementary Table S10; Figure 2**). The expression of DEGs in the synthesis of carotenoids, genes associated with phytoene and lycopene synthase, *PSY* and *ZDS*, were highly upregulated in Chuichung peel and Mini flesh. These results are consistent with the higher abundance of carotenoids in Chuichung peel and Mini flesh. β-ionone, a carotenoid-derived volatile compound, also showed the same pattern as the other carotenoid compounds (**Figure 2**). Therefore, it seems that the gene expression of *PSY* and *ZDS* is a key mechanism regulating the production of carotenoids, and these key genes may accelerate carotenoid synthesis in Chuichung peel and Mini flesh. It was reported by Rodrigo et al. (2004) that increased *PSY* and *ZDS* gene expression plays an important role in enhancing the production of carotenoids in this pathway.

Genes involved in chlorophyll synthesis have been found in plant leaf and fruit, and chlorophyll synthesis mechanisms have been well studied (Lai et al., 2015; Wen et al., 2015). Genes including glutamyl-tRNA reductase 2 (*HemA*; EC 1.2.1.70), delta-aminolevulinic acid dehydratase (*HemB*; EC 4.2.1.24), uroporphyrinogen decarboxylase (*HemE*; EC 4.1.1.37), magnesium chelatase subunit chlH (*chlH*; EC 6.6.1.1), magnesium protoporphyrin IX methyltransferase (*chlM*; EC 2.1.1.11), chlorophyll(ide) b reductase (*NOL*; EC 1.1.1.294), and protochlorophyllide oxidoreductase (*por*; EC 1.3.1.33) are known to play important roles in the chlorophyll biosynthesis pathway (Tanaka and Tanaka, 2006, 2007). *HemA* is an enzyme that participates in chlorophyll biosynthesis in the plastids. It catalyzes the biosynthesis of 5-aminolevulinic acid from glutamyl-tRNA (Eckhardt et al., 2004). ChlH catalyzes the conversion of protoporphyrin IX to Mg-protoporphyrin IX. Magnesium protoporphyrin IX monomethyl ester formation catalyzes magnesium protoporphyrin IX in the chlorophyll synthesis pathway by *chlM* (Wang et al., 2017). *Por* is an important enzyme that catalyzes protochlorophyllide to generate chlorophyllide, which is a critical intermediate step in the conversion of chlorophyll (Kwon et al., 2017). In this study, 31 DEGs associated with chlorophyll metabolism were identified. Twenty of the 31 DEGs were displayed in the chlorophyll pathway analysis (**Supplementary Table S10**; **Figure 2**). With regards to the expression of DEGs in the chlorophyll synthesis pathway, most of the genes, including *HemA*, *HemB*, *HemE*, *chlH*, *chlM*, *chlE*, *CLH, DVR*, and *por*, were upregulated in Chuichung peel and Mini flesh. These results are consistent with the higher abundance of chlorophyll a and chlorophyll b in Chuicung peel and Mini flesh (**Figure 2**). This suggests that the expression of various key genes, including *HemA*, *HemB*, *HemE*, *chlH*, *chlM*, *chlE*, *CLH*, *DVR*, and *por*, is crucial for regulating the production of chlorophylls, and these genes may accelerate chlorophyll synthesis in Chuichung peel and Mini flesh. A previous study (Tanaka and Tanaka, 2007) found that the expression levels of the aforementioned genes play an important role in improving chlorophyll production in the pathway mechanism.

The present study evaluated various genes involved in flavonoid, carotenoid, and chlorophyll metabolisms. In the flavonoid pathway analysis, we proposed that *CHS* is a key gene for the regulation of flavonoid compounds. Analysis of the carotenoid and chlorophyll pathways confirmed that the expression patterns of genes involved in the synthesis of precursors corresponded to metabolite patterns. Therefore, from the results of this study, we could infer that the synthesis of a phytoene, a precursor of carotenoids, and chlorophyllide a, a precursor of chlorophylls, occurs differently depending on the cultivar and part of cucumbers, which leads to differences in fruit activity. This biosynthetic pathway analysis provides insight into disparities in metabolism distribution.

CONCLUSION

This study demonstrates that the metabolomics approach is effective for investigating different cultivars that have various quality parameters. We conducted metabolomics study to evaluate three different cucumber cultivars (Chuichung, White Dadagi, and Mini) and their parts (peel and flesh). Although amino acids, sugars, flavonoids, carotenoids, and chlorophylls were found to be upregulated in Mini flesh, in the case of peel, these were expressed at higher levels in Chuichung. In addition, antioxidant activity was high in both Chuichung peel and Mini flesh. To interpret the different tendencies of bioactivity in their parts, we performed a comprehensive pathway analysis about the flavonoids, carotenoids, and chlorophylls, which had significantly positive correlation with antioxidant activity, using an integrated metabolomics and transcriptomics approach. The expression levels of flavonoid-related genes (*CHS* and *4CL*), carotenoid-related genes (*PSY* and *ZDS*), and chlorophyll-related

genes (*HemA*, *HemB*, *HemE*, *chlH*, *chlM*, *chlE*, *CLH*, *DVR*, and *por*) were indicated the same tendency with the metabolome analysis data. As a result, we could estimate that flavonoid, carotenoid, and chlorophyll metabolism were upregulated in Chuichung peel and Mini flesh. These findings provide an insight of various commercial cucumbers and help explore valuable metabolites and genes associated with improving cucumber fruit quality. Also, these results provide valuable information of different characteristics in various cucumber cultivars, which can be considered while purchasing and consuming the cucumber fruit.

DATA AVAILABILITY STATEMENT

The datasets presented in this study can be found in online repositories. The names of the repository/repositories and accession number(s) can be found at: National Center for Biotechnology Information (NCBI) BioProject database under accession number PRJNA817515.

AUTHOR CONTRIBUTIONS

HJ, SS, and CL conceived of and designed the study. HJ collected the phenotypic data, analyzed the data, and wrote the manuscript. SS assisted with data analysis and reviewed the manuscript. All authors have contributed to the manuscript and approved the submitted version.

FUNDING

This paper resulted from the Konkuk University research support program.

SUPPLEMENTARY MATERIAL

The Supplementary Material for this article can be found online at: https://www.frontiersin.org/articles/10.3389/fpls.2022.882120/full#supplementary-material

REFERENCES

Aadil, R. M., Roobab, U., Sahar, A., Rahman, U. u., and Khalil, A. A. (2019). "Functionality of bioactive nutrients in beverages", in *Nutrients in Beverages: Volume 12: The Science of Beverages*. eds. A. M. Grumezescu and B. Holban (Cambridge, MA: Academic Press), 237–276.

Agarwal, S., and Rao, A. V. (2000). Tomato lycopene and its role in human health and chronic diseases. *CMAJ* 163, 739–744.

Alihosseini, F., and Sun, G. (2011). "17 - antibacterial colorants for textiles," in *Woodhead Publishing Series in Textiles Sun Protection and Health*. ed. N. Pan (Sawston: Woodhead Publishing), 376–403.

Ares, A. M., Bernal, J. L., Nozal, M. J., and Bernal, J. (2021). "Chapter 6 - analysis of herbal bioactives," in *Aromatic Herbs in Food*. ed. F. Galanakis (Cambridge, MA: Academic Press), 201–232.

Awika, J. M. (2017). "Chapter 3 - Sorghum: its unique nutritional and health-promoting attributes," in *Food Science, Technology and Nutrition*. eds. J. R. N. Taylor and J. M. B. T.-G.-F. A. G. Awika (Sawston: Woodhead Publishing), 21–54.

Borges Bubols, G., da Rocha Vianna, D., Medina-Remon, A., von Poser, G., Maria Lamuela-Raventos, R., Lucia Eifler-Lima, V., et al. (2013). The antioxidant activity of Coumarins and flavonoids. *Mini-Reviews Med. Chem.* 13, 318–334. doi: 10.2174/1389557511313030002

Buescher, R. H., and Buescher, R. W. (2001). Production and stability of (E, Z)-2, 6-nonadienal, the major flavor volatile of cucumbers. *J. Food Sci.* 66, 357–361. doi: 10.1111/j.1365-2621.2001.tb11346.x

Chen, S., Zhang, R., Hao, L., Chen, W., and Cheng, S. (2015). Profiling of volatile compounds and associated gene expression and enzyme activity during fruit development in two cucumber cultivars. *PLoS One* 10, 1–22. doi: 10.1371/journal.pone.0119444

Cuthbertson, D., Andrews, P. K., Reganold, J. P., Davies, N. M., and Lange, B. M. (2012). Utility of metabolomics toward assessing the metabolic basis of quality traits in apple fruit with an emphasis on antioxidants. *J. Agric. Food Chem.* 60, 8552–8560. doi: 10.1021/jf3031088

Dao, T. T. H., Linthorst, H. J. M., and Verpoorte, R. (2011). Chalcone synthase and its functions in plant resistance. *Phytochem. Rev.* 10, 397–412. doi: 10.1007/s11101-011-9211-7

Eckhardt, U., Grimm, B., and Hörtensteiner, S. (2004). Recent advances in chlorophyll biosynthesis and breakdown in higher plants. *Plant Mol. Biol.* 56, 1–14. doi: 10.1007/s11103-004-2331-3

Fiedor, J., and Burda, K. (2014). Potential role of carotenoids as antioxidants in human health and disease. *Nutrients* 6, 466–488. doi: 10.3390/nu6020466

Grassi, S., Piro, G., Lee, J. M., Zheng, Y., Fei, Z., Dalessandro, G., et al. (2013). Comparative genomics reveals candidate carotenoid pathway regulators of ripening watermelon fruit. *BMC Genom.* 14:781. doi: 10.1186/1471-2164-14-781

Grosch, W., and Schwarz, J. M. (1971). Linoleic and linolenic acid as precursors of the cucumber flavor. *Lipids* 6, 351–352. doi: 10.1007/BF02531828

Heim, K. E., Tagliaferro, A. R., and Bobilya, D. J. (2002). Flavonoid antioxidants: chemistry, metabolism and structure-activity relationships. *J. Nutr. Biochem.* 13, 572–584. doi: 10.1016/S0955-2863(02)00208-5

Hua, Q., Chen, C., Tel Zur, N., Wang, H., Wu, J., Chen, J., et al. (2018). Metabolomic characterization of pitaya fruit from three red-skinned cultivars with different pulp colors. *Plant Physiol. Biochem.* 126, 117–125. doi: 10.1016/j.plaphy.2018.02.027

Kamkaen, N., Mulsri, N., and Treesak, C. (2007). Screening of Some tropical vegetables for anti-tyrosinase activity. *Thai Pharm. Heal. Sci. J.* 2, 15–19. Available at: http://www.fao.org/ag/Ags/agsi/ENZYMEFINAL/Enzymatic Browning.Html.

Keutgen, A. J., and Pawelzik, E. (2008). Contribution of amino acids to strawberry fruit quality and their relevance as stress indicators under NaCl salinity. *Food Chem.* 111, 642–647. doi: 10.1016/j.foodchem.2008.04.032

Kwon, C. T., Kim, S. H., Song, G., Kim, D., and Paek, N. C. (2017). Two NADPH: Protochlorophyllide Oxidoreductase (POR) isoforms play distinct roles in environmental adaptation in Rice. *Rice* 10, 1–14. doi: 10.1186/s12284-016-0141-2

Lai, B., Hu, B., Qin, Y. H., Zhao, J. T., Wang, H. C., and Hu, G. B. (2015). Transcriptomic analysis of Litchi chinensis pericarp during maturation with a focus on chlorophyll degradation and flavonoid biosynthesis. *BMC Genom.* 16, 225–218. doi: 10.1186/s12864-015-1433-4

Lanfer-Marquez, U. M., Barros, R. M. C., and Sinnecker, P. (2005). Antioxidant activity of chlorophylls and their derivatives. *Food Res. Int.* 38, 885–891. doi: 10.1016/j.foodres.2005.02.012

Lee, M. Y., Singh, D., Kim, S. H., Lee, S. J., and Lee, C. H. (2016). Ultrahigh pressure processing produces alterations in the metabolite profiles of Panax ginseng. *Molecules* 21, 1–16. doi: 10.3390/molecules21060816

Masaki, H. (2010). Role of antioxidants in the skin: anti-aging effects. *J. Dermatol. Sci.* 58, 85–90. doi: 10.1016/j.jdermsci.2010.03.003

Miller, D. D., Li, T., and Liu, R. H. B. (2014). *Antioxidants and Phytochemicals*, Amsterdam: Elsevier.

Mukherjee, P. K., Nema, N. K., Maity, N., and Sarkar, B. K. (2013). Phytochemical and therapeutic potential of cucumber. *Fitoterapia* 84, 227–236. doi: 10.1016/j.fitote.2012.10.003

Mun, H. I., Kwon, M. C., Lee, N. R., Son, S. Y., Song, D. H., and Lee, C. H. (2021). Comparing metabolites and functional properties of various tomatoes using mass spectrometry-based metabolomics approach. *Front. Nutr.* 8, 1–10. doi: 10.3389/fnut.2021.659646

Nema, N. K., Maity, N., Sarkar, B., and Mukherjee, P. K. (2011). Cucumis sativus fruit-potential antioxidant, anti-hyaluronidase, and anti-elastase agent. *Arch. Dermatol. Res.* 303, 247–252. doi: 10.1007/s00403-010-1103-y

Park, G., Choi, Y., Jung, J. K., Shim, E. J., Kang, M. Y., Sim, S. C., et al. (2021). Genetic diversity assessment and cultivar identification of cucumber (Cucumis sativus l.) using the fluidigm single nucleotide polymorphism assay. *Plan. Theory* 10, 1–13. doi: 10.3390/plants10020395

Perez-Galvez, A., Viera, I., and Roca, M. (2017). Chemistry in the bioactivity of chlorophylls: an overview. *Curr. Med. Chem.* 24, 4515–4536. doi: 10.2174/0929867324666170714102619

Pérez-gálvez, A., Viera, I., and Roca, M. (2020). Carotenoids and chlorophylls as antioxidants. *Antioxidants* 9, 1–39. doi: 10.3390/antiox9060505

Rodrigo, M. J., Marcos, J. F., and Zacarías, L. (2004). Biochemical and molecular analysis of carotenoid biosynthesis in flavedo of orange (*Citrus sinensis* L.) during fruit development and maturation. *J. Agric. Food Chem.* 52, 6724–6731. doi: 10.1021/jf049607f

Rodríguez-Concepción, M. (2010). Supply of precursors for carotenoid biosynthesis in plants. *Arch. Biochem. Biophys.* 504, 118–122. doi: 10.1016/j.abb.2010.06.016

Sarker, U. (2018). Drought stress enhances nutritional and bioactive compounds, phenolic acids and antioxidant capacity of Amaranthus leafy vegetable. *BMC Plant Biol.* 18, 258–215. doi: 10.1186/s12870-018-1484-1

Sarker, U., Hossain, M. N., Iqbal, M. A., and Oba, S. (2020). Bioactive components and radical scavenging activity in selected advance lines of salt-tolerant vegetable Amaranth. *Front. Nutr.* 7, 1–15. doi: 10.3389/fnut.2020.587257

Sarker, U., and Oba, S. (2018a). Catalase, superoxide dismutase and ascorbate-glutathione cycle enzymes confer drought tolerance of Amaranthus tricolor. *Sci. Rep.* 8, 16496–16413. doi: 10.1038/s41598-018-34944-0

Sarker, U., and Oba, S. (2018b). Drought stress effects on growth, ROS markers, compatible solutes, Phenolics, flavonoids, and antioxidant activity in Amaranthus tricolor. *Appl. Biochem. Biotechnol.* 186, 999–1016. doi: 10.1007/s12010-018-2784-5

Sarker, U., and Oba, S. (2019). Antioxidant constituents of three selected red and green color Amaranthus leafy vegetable. *Sci. Rep.* 9, 18233–18211. doi: 10.1038/s41598-019-52033-8

Sarker, U., and Oba, S. (2020a). Leaf pigmentation, its profiles and radical scavenging activity in selected Amaranthus tricolor leafy vegetables. *Sci. Rep.* 10, 18617–18610. doi: 10.1038/s41598-020-66376-0

Sarker, U., and Oba, S. (2020b). Nutraceuticals, phytochemicals, and radical quenching ability of selected drought-tolerant advance lines of vegetable amaranth. *BMC Plant Biol.* 20, 564–516. doi: 10.1186/s12870-020-02780-y

Sarker, U., and Oba, S. (2020c). Phenolic profiles and antioxidant activities in selected drought-tolerant leafy vegetable amaranth. *Sci. Rep.* 10, 18287–18211. doi: 10.1038/s41598-020-71727-y

Sarker, U., and Oba, S. (2020d). Polyphenol and flavonoid profiles and radical scavenging activity in leafy vegetable Amaranthus gangeticus. *BMC Plant Biol.* 20, 499–412. doi: 10.1186/s12870-020-02700-0

Sarker, U., and Oba, S. (2020e). The response of salinity stress-Induced A. tricolor to growth, anatomy, physiology, non-enzymatic and enzymatic antioxidants. *Front. Plant Sci.* 11, 1–14. doi: 10.3389/fpls.2020.559876

Sarker, U., and Oba, S. (2021). Color attributes, betacyanin, and carotenoid profiles, bioactive components, and radical quenching capacity in selected *Amaranthus gangeticus* leafy vegetables. *Sci. Rep.* 11, 1–14. doi: 10.1038/s41598-021-91157-8

Shi, Q., Zhang, Z., Su, J., Zhou, J., and Li, X. (2018). Comparative analysis of pigments, phenolics, and antioxidant activity of Chinese jujube (*Ziziphus jujuba* mill.) during fruit development. *Molecules* 23, doi:10.3390/molecules23081917. doi: 10.3390/molecules23081917

Singh, D., and Lee, C. H. (2018). Intraspecies volatile interactions affect growth rates and exometabolomes in Aspergillus oryzae KCCM 60345. *J. Microbiol. Biotechnol.* 28, 199–209. doi: 10.4014/jmb.1711.11005

Son, S. Y., Park, Y. J., Jung, E. S., Singh, D., Lee, Y. W., Kim, J. G., et al. (2019). Integrated metabolomics and transcriptomics unravel the metabolic pathway variations for different sized beech mushrooms. *Int. J. Mol. Sci.* 20. doi: 10.3390/ijms20236007

Song, W., Derito, C. M., Liu, M. K., He, X., Dong, M., and Liu, R. H. (2010). Cellular antioxidant activity of common vegetables. *J. Agric. Food Chem.* 58, 6621–6629. doi: 10.1021/jf9035832

Song, K., Shin, Y., Jung, M., Subramaniyam, S., Lee, K. P., Oh, E. A., et al. (2021). Chromosome-scale genome assemblies of two Korean cucumber inbred lines. *Front. Genet.* 12, 1–5. doi: 10.3389/fgene.2021.733188

Sotiroudis, G., Melliou, E., Sotiroudis, T. G., and Chinou, I. (2010). Chemical analysis, antioxidant and antimicrobial activity of three Greek cucumber (*Cucumis sativus*) cultivars. *J. Food Biochem.* 34, 61–78. doi: 10.1111/j.1745-4514.2009.00296.x

Tadmor, Y., Burger, J., Yaakov, I., Feder, A., Libhaber, S. E., Portnoy, V., et al. (2010). Genetics of flavonoid, carotenoid, and chlorophyll pigments in melon fruit rinds. *J. Agric. Food Chem.* 58, 10722–10728. doi: 10.1021/jf1021797

Tanaka, A., and Tanaka, R. (2006). Chlorophyll metabolism. *Curr. Opin. Plant Biol.* 9, 248–255. doi: 10.1016/j.pbi.2006.03.011

Tanaka, R., and Tanaka, A. (2007). Tetrapyrrole biosynthesis in higher plants. *Annu. Rev. Plant Biol.* 58, 321–346. doi: 10.1146/annurev.arplant.57.032905.105448

Tripoli, E., Guardia, M.La, Giammanco, S., Majo, D.Di, and Giammanco, M. (2007). Citrus flavonoids: molecular structure, biological activity and nutritional properties: a review. *Food Chem.* 104, 466–479. doi:10.1016/j.foodchem.2006.11.054.

Wang, M., Chen, L., Liang, Z., He, X., Liu, W., Jiang, B., et al. (2020). Metabolome and transcriptome analyses reveal chlorophyll and anthocyanin metabolism pathway associated with cucumber fruit skin color. *BMC Plant Biol.* 20, 386–313. doi: 10.1186/s12870-020-02597-9

Wang, Z., Hong, X., Hu, K., Wang, Y., Wang, X., Du, S., et al. (2017). Impaired magnesium protoporphyrin IX methyltransferase (ChlM) impedes chlorophyll synthesis and plant growth in rice. *Front. Plant Sci.* 8, 1–18. doi: 10.3389/fpls.2017.01694

Wei, G., Tian, P., Zhang, F., Qin, H., Miao, H., Chen, Q., et al. (2016). Integrative analyses of nontargeted volatile profiling and transcriptome data provide molecular insight into VOC diversity in cucumber plants (*Cucumis sativus*). *Plant Physiol.* 172, 603–618. doi: 10.1104/pp.16.01051

Wen, C. H., Lin, S. S., and Chu, F. H. (2015). Transcriptome analysis of a subtropical deciduous tree: autumn leaf senescence gene expression profile of formosan gum. *Plant Cell Physiol.* 56, 163–174. doi: 10.1093/pcp/pcu160

Xie, J., Yao, S., Ming, J., Deng, L., and Zeng, K. (2019). Variations in chlorophyll and carotenoid contents and expression of genes involved in pigment metabolism response to oleocellosis in citrus fruits. *Food Chem.* 272, 49–57. doi: 10.1016/j.foodchem.2018.08.020

Youn, A.-R., Park, P.-J., Choi, H.-R., Kim, B.-S., and Cha, H.-S. (2007). Physicochemical characteristics of Rubus coreanus Miquel during maturation. *Korean J. Food Sci. Technol.* 39, 476–479.

Yu, Z. W., Zhang, N., Jiang, C. Y., Wu, S. X., Feng, X. Y., and Feng, X. Y. (2021). Exploring the genes involved in biosynthesis of dihydroquercetin and dihydromyricetin in Ampelopsis grossedentata. *Sci. Rep.* 11, 15596–15514. doi: 10.1038/s41598-021-95071-x

Zhang, Q., Wang, L., Liu, Z., Zhao, Z., Zhao, J., Wang, Z., et al. (2020). Transcriptome and metabolome profiling unveil the mechanisms of Ziziphus jujuba mill. Peel coloration. *Food Chem.* 312:125903. doi: 10.1016/j.foodchem.2019.125903

Złotek, U., Świeca, M., and Jakubczyk, A. (2014). Effect of abiotic elicitation on main health-promoting compounds, antioxidant activity and commercial quality of butter lettuce (Lactuca sativa L.). *Food Chem.* 148, 253–260. doi: 10.1016/j.foodchem.2013.10.031

Conflict of Interest: The authors declare that the research was conducted in the absence of any commercial or financial relationships that could be construed as a potential conflict of interest.

Publisher's Note: All claims expressed in this article are solely those of the authors and do not necessarily represent those of their affiliated organizations, or those of the publisher, the editors and the reviewers. Any product that may be evaluated in this article, or claim that may be made by its manufacturer, is not guaranteed or endorsed by the publisher.

frontiers | Frontiers in Plant Science

TYPE Perspective
PUBLISHED 20 October 2022
DOI 10.3389/fpls.2022.937927

OPEN ACCESS

EDITED BY
Itay Maoz,
Agricultural Research Organization (ARO), Israel

REVIEWED BY
Vera Quecini,
Embrapa Uva e Vinho, Brazil
Noam Reshef,
Cornell University, United States

*CORRESPONDENCE
Stefania Savoi
stefania.savoi@unito.it
José Tomás Matus
tomas.matus@uv.es

SPECIALTY SECTION
This article was submitted to Plant Metabolism and Chemodiversity, a section of the journal Frontiers in Plant Science

RECEIVED 06 May 2022
ACCEPTED 09 September 2022
PUBLISHED 20 October 2022

CITATION
Savoi S, Santiago A, Orduña L and Matus JT (2022) Transcriptomic and metabolomic integration as a resource in grapevine to study fruit metabolite quality traits.
Front. Plant Sci. 13:937927.
doi: 10.3389/fpls.2022.937927

Transcriptomic and metabolomic integration as a resource in grapevine to study fruit metabolite quality traits

Stefania Savoi[1]*, Antonio Santiago[2], Luis Orduña[2] and José Tomás Matus[2]*

[1]Department of Agricultural, Forest and Food Sciences, University of Turin, Grugliasco, Italy, [2]Institute for Integrative Systems Biology (I2SysBio), Universitat de València-CSIC, Paterna, Spain

Transcriptomics and metabolomics are methodologies being increasingly chosen to perform molecular studies in grapevine (*Vitis vinifera* L.), focusing either on plant and fruit development or on interaction with abiotic or biotic factors. Currently, the integration of these approaches has become of utmost relevance when studying key plant physiological and metabolic processes. The results from these analyses can undoubtedly be incorporated in breeding programs whereby genes associated with better fruit quality (e.g., those enhancing the accumulation of health-promoting compounds) or with stress resistance (e.g., those regulating beneficial responses to environmental transition) can be used as selection markers in crop improvement programs. Despite the vast amount of data being generated, integrative transcriptome/metabolome meta-analyses (i.e., the joint analysis of several studies) have not yet been fully accomplished in this species, mainly due to particular specificities of metabolomic studies, such as differences in data acquisition (i.e., different compounds being investigated), unappropriated and unstandardized metadata, or simply no deposition of data in public repositories. These meta-analyses require a high computational capacity for data mining *a priori*, but they also need appropriate tools to explore and visualize the integrated results. This perspective article explores the universe of omics studies conducted in *V. vinifera*, focusing on fruit-transcriptome and metabolome analyses as leading approaches to understand berry physiology, secondary metabolism, and quality. Moreover, we show how omics data can be integrated in a simple format and offered to the research community as a web resource, giving the chance to inspect potential gene-*to*-gene and gene-*to*-metabolite relationships that can later be tested in hypothesis-driven research. In the frame of the activities promoted by the COST Action CA17111 INTEGRAPE, we present the first grapevine transcriptomic and metabolomic integrated database (TransMetaDb) developed within the Vitis Visualization (VitViz)

10.3389/fpls.2022.937927

platform (https://tomsbiolab.com/vitviz). This tool also enables the user to conduct and explore meta-analyses utilizing different experiments, therefore hopefully motivating the community to generate Findable, Accessible, Interoperable and Reusable (F.A.I.R.) data to be included in the future.

KEYWORDS

omics integration, Vitviz, database, integrape, *Vitis vinifera*

Introduction

There has been more than 15 years of omics studies accumulated in grapevine (*Vitis vinifera* L.) to understand processes related to its development and interaction with the environment. The vast amount of data generated has allowed us to understand this species singularity in terms of its adaptive traits, but has also permitted us to explore its diversity, especially related to plant performance (e.g., stress resistance, vigor, yield, etc.) and fruit quality. This data includes genome assemblies of many different cultivars and clones of *V. vinifera* and their wild American or Asian-related species and, in decreasing order of the number of published studies, transcriptomic, metabolomic, proteomic, and ionomic data (Figure 1 and Supplementary Table 1).

A significant achievement in the grapevine omics era was the release of two independent genome sequences in 2007, with one being accomplished by a French-Italian Public Consortium (Jaillon et al., 2007), and the second through an Italian-American Collaboration (Velasco et al., 2007). Grapevine then became the first fruit genome to be sequenced and the fourth among plants after

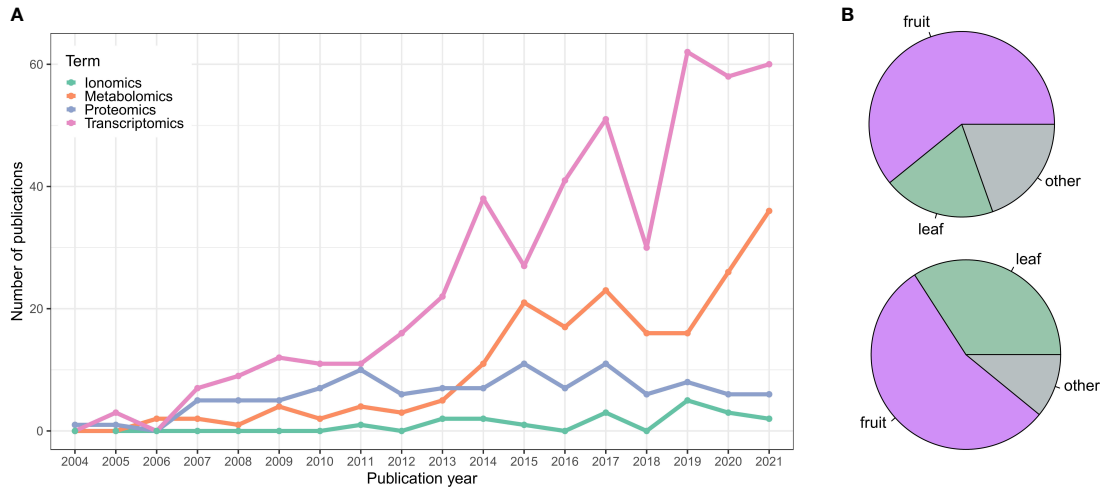

FIGURE 1
(A) Publication trend of grapevine omics studies. Data was collected from NCBI using different queries and keywords for each category to be as comprehensive as possible and retrieve most of the works. Transcriptomics query: 1) RNA-Seq (excluding microarray data): (transcriptom*[Title/Abstract] OR transcript profiling[Title/Abstract] OR mRNA expression[Title/Abstract] OR RNA-Seq[Title/Abstract] OR RNASeq[Title/Abstract] OR RNA Sequencing[Title/Abstract] OR RNA-Sequencing[Title/Abstract]) AND (grapevine[Title/Abstract] OR grape[Title/Abstract] OR Vitis[Title/Abstract] OR V. vinifera[Title/Abstract]). 2) Microarray: (microarray[Title/Abstract] OR Affymetrix[Title/Abstract] OR CombiMatrix[Title/Abstract] OR NimbleGen[Title/Abstract]) AND (grapevine[Title/Abstract] OR grape[Title/Abstract] OR Vitis[Title/Abstract] OR V. vinifera[Title/Abstract]). Proteomics query: (proteom*[Title/Abstract] OR protein profiling[Title/Abstract]) AND (grapevine[Title/Abstract] OR grape[Title/Abstract] OR Vitis [Title/Abstract] OR V. vinifera[Title/Abstract]). Metabolomics query: (metabolom*[Title/Abstract] OR metabolite profiling[Title/Abstract] OR metabolite analyses[Title/Abstract] OR metabolic response[Title/Abstract]) AND (grapevine[Title/Abstract] OR grape[Title/Abstract] OR Vitis[Title/Abstract] OR V. vinifera[Title/Abstract]). Ionomics query: (ionom*[Title/Abstract] OR elemental profiling[Title/Abstract] OR mineral elements[Title/Abstract] OR cations[Title/Abstract]) AND (grapevine[Title/Abstract] OR grape[Title/Abstract] OR Vitis[Title/Abstract] OR V. vinifera[Title/Abstract]). Only the studies published until 12/2021 were considered. Data were manually curated to remove outliers. **(B)** Pie chart showing the percentage of transcriptomics (*top panel*) and metabolomics (*bottom panel*) studies focusing on fruit tissues, leaves or other grapevine organs.

Arabidopsis thaliana (Arabidopsis Genome Initiative, 2000), rice [*Oryza sativa* subsp. indica and subsp. japonica (Goff et al., 2002; Yu et al., 2002)] and poplar (*Populus trichocarpa*) (Tuskan et al., 2006). Since then, the grapevine community has witnessed an increase of high-throughput next-generation sequencing techniques (e.g., long-read sequencing of RNA and DNA) and the availability of updated grapevine genome assemblies of the reference PN40024 (Canaguier et al., 2017; unpublished data), with updated gene functional annotations incorporated in the recently developed Grape Gene Reference Catalogue (Navarro-Payá et al., 2022). We have observed a cascade of genome sequences of *V. vinifera* top-quality wine-making cultivars, and genomes of *Vitis* species important for breeding purposes (da Silva et al., 2013; Venturini et al., 2013; Chin et al., 2016; Minio et al., 2019a; Minio et al., 2019b Vondras et al., 2019; Zhou et al., 2019; Massonnet et al., 2020; Magris et al., 2021). In parallel with genomic/transcriptomic advances, the technological improvement of analytical techniques such as high-resolution liquid and gas chromatography coupled to mass spectrometry, in terms of sensitivity, accuracy, and resolution, has led to a massive amount of metabolomic data from heterogeneous experimental designs, many of which are not public to date.

Comprehensive studies pointing to the expression of the transcriptome or the abundance of the so-far known grape metabolites have boosted the understanding of grapevine physiology in the context of crop and fruit improvement. However, data/metadata interpretation generally encounters difficulties of reusability, for example in meta-analysis studies, either due to high variability and heterogeneity of the associated data or to the presence of partial, misleading, or incomplete experimental descriptions. These descriptors should typically include detailed information on the experimental set-up, report the plant materials used and adopt standardized cultivar names, organs, and developmental stages. Although this comprehensive praxis is highly recommended, in most cases, we notice that even raw data is not entirely available in public databases. Different guidelines have been generated to fill this gap, focusing on harmonizing plant and experiment descriptors. These include standard ontologies, lists of tools, and systematic information for describing omics analyses and tutorials for data submission in public repositories. These guidelines have been recently adopted by the viti-oenology community, sponsored by the COST Action CA17111 INTEGRAPE, in order to adhere to the *findable*, *accessible*, *interoperable* and *reusable* (F.A.I.R) principles (Wilkinson et al., 2016). A section specifically related to grape and wine metabolomics has been recently published (Savoi et al., 2021a) to encourage the grapevine community to follow these guidelines and share metabolomic data in open repositories such as MetaboLights (Haug et al., 2020). These efforts were made because, contrary to the wave of transcriptomic data available online, unfortunately, only very few metabolomic studies are so far accessible to the public.

History of omics studies in grapevine

Transcriptomics

The first records of high-throughput grapevine transcriptomic studies date back to 2005, exploring the changes in gene expression during berry development. Terrier et al. (2005) generated 50-mers oligoarrays bearing a set of approximately 3,200 unigenes from *Vitis vinifera* from nine berry developmental stages to provide the first global picture of the genetic program of grape berry development. The authors were able to discriminate differences in gene expression between hard green and soft green berries at the onset of ripening (veraison), pointing out that remarkable changes may occur within a short period and that 25% of the transcripts were significantly activated or repressed between the green and the ripening phases. In a second study (da Silva et al., 2005), the authors retrieved all the available *Vitis* sequences deposited in GenBank representing numerous *Vitis* species, cultivars, organs, plant developmental stages, and stress treatments. The analysis concluded that each stage of development was characterized by distinct gene expression patterns, including numerous stage-specific transcripts. Interestingly, they identified a MADS-box gene as a putative regulator of grape berry development. A third study (Waters et al., 2005) used the same technology to explore gene expression patterns throughout grape berry development revealing sets of genes with distinctive or similar expression profiles over the course of berry development. Finally, another pioneering study (Grimplet et al., 2007) used a brand new Affymetrix GeneChip® *Vitis vinifera* oligonucleotide microarray to study tissue-specific mRNA expression in berry skin, flesh, and seeds in well-watered and water deficit plants at fruit maturity, listing a repertoire of expressed genes, highlighting those modulated by drought stress. In particular, stress modulated around 13% of the genes, mainly in the pulp and skin. In synthesis, these groundbreaking studies paved the way for future grapevine transcriptomic works developing compendiums of gene expression, studying gene profiles during grape berry development and setting the first milestone in understanding grapevine physiology.

The first grapevine study that specifically employed RNA sequencing using the Illumina platform corresponds to that of Zenoni et al. (2010). The authors focused on three stages of berry development indicated as post-setting, veraison, and ripening, to gain insight into the wide range of transcriptional responses associated with the development of fruits. They detected the expression of 17,324 genes during berry development, of which 6,695 were expressed in a stage-specific manner. Moreover, they identified alternative splicing events for 385 genes suggesting a considerable transcript complexity in developing berries. The

grapevine expression atlas of the cultivar (cv.) 'Corvina' (Fasoli et al., 2012) was later released based on the Nimblegen microarray platform (29,000 genes spotted) representing the first wide study of global gene expression in a complete repertoire of grape organs, including 54 reproductive and vegetative tissues at different developmental stages. This work highlighted a fundamental transcriptome reprogramming during maturation with the activation of a mature/woody developmental program, which was mainly inactive during the vegetative/green stage. Subsequent studies also focused on berry development, ripening, and post-harvest of different cultivars (Pilati et al., 2007; Lijavetzky et al., 2012; Sweetman et al., 2012; Cramer et al., 2014; Gouthu et al., 2014; Pilati et al., 2014; Guo et al., 2016; Zenoni et al., 2016; Ghan et al., 2017; Massonnet et al., 2017; Shangguan et al., 2017; Balic et al., 2018; Fasoli et al., 2018; Savoi et al., 2019; Cramer et al., 2020; Guo et al., 2020; Savoi et al., 2021b; Theine et al., 2021). At the same time, other studies considered the development of tendrils and inflorescences (Díaz-Riquelme et al., 2014), buds (Díaz-Riquelme et al., 2012; Pucker et al., 2020; Shangguan et al., 2020), flower (Sreekantan et al., 2010; Grimplet et al., 2017; Vannozzi et al., 2021), leaf (Pervaiz et al., 2016), fruits of seeded/seedless cultivars (Nwafor et al., 2014; Royo et al., 2016) and roots from *V. vinifera* and *Vitis* rootstocks (Cookson et al., 2013; Corso et al., 2015; Cochetel et al., 2017; Livigni et al., 2019). Further studies investigated the plant responses to ozonated water applications (Campayo et al., 2021), the circadian cycle (Carbonell-Bejerano et al., 2014b; Rienth et al., 2014a), the interaction with abiotic stresses such as temperature (Liu et al., 2012; Carbonell-Bejerano et al., 2013; Xin et al., 2013; Rienth et al., 2014b; Rienth et al., 2016), light (Pontin et al., 2010; Carbonell-Bejerano et al., 2014a) and water availability (Perrone et al., 2012; Dal Santo et al., 2016b).

Regarding pathogens, grapevine is highly susceptible to a range of fungal diseases such as downy mildew (*Plasmopara viticola*) and powdery mildew (*Erysiphe necator*), and the bunch or noble rot (*Botrytis cinerea*). Therefore, several efforts have been made to study these interactions by performing transcriptomic analyses, although most of these have been performed on leaves (Fung et al., 2008; Polesani et al., 2010; Wu et al., 2010; Weng et al., 2014; Amrine et al., 2015; Li et al., 2015).

A few studies have used transcriptomics to better understand the impact of agronomic practices such as defoliation (Pastore et al., 2013; Zenoni et al., 2017) or cluster thinning (Pastore et al., 2011) on fruit quality, showing that these techniques, when applied at the appropriate phenological stage, can improve the quality of ripening fruits, in term of sugars and colors. Moreover, an increasing interest in the transcriptome profiles of other *Vitis* species has been asserted. A complete list of all transcriptomic grapevine studies in fruits is available in Supplementary Table 1A.

Thanks to the large number of public experiments, several transcriptome-related tools have been developed to explore this type of data. The Vitis Co-expression database 'VTCdb' (Wong et al., 2013) offered an online platform for exploring potential regulatory networks by addressing gene co-expression. The VTCdb was replaced by 'VTC-Agg' in Wong, 2020, by gene rank of correlations and aggregate networks, being constructed from 1,359 microarray samples (33 experiments). More recent applications include 'AggGCN', present in the VitViz platform (unpublished), which offers condition-dependent and independent aggregated networks from all SRA-located RNA-seq experiments, and 'VESPUCCI' (Moretto et al., 2016; Moretto et al., 2022), a cross-platform expression compendium that was carefully constructed by collecting, homogenizing, and re-annotating the metadata of publicly available microarray and RNA-Seq data (271 experiments). The GRape Expression Atlas 'GREAT' (unpublished) allows to query, visualize and analyze genes of interest with interactive heatmaps or expression tables by inferring public RNA-seq data (about 2,000 samples) from *Vitis vinifera*. Finally, 'OneGenE' (One Gene network Expansion) (Pilati et al., 2021) is a transcriptomic data mining tool that finds direct correlations between genes, thus producing association networks by using a causality-based method.

Metabolomics

The use of plant metabolite profiling as a new tool for gene functional analyses and plant phenotyping has been incorporated in the last two decades (Fiehn et al., 2000). However, given the vast diversity of plant metabolites, metabolomic approaches are often based on separately analyzing different classes of metabolites having similar physical or chemical properties or functional groups. Hence metabolome studies are based on applying different analytical methods, including variable extraction protocols and instruments. A complete list of metabolomic studies in grapevine is available in Supplementary Table 1B.

The first metabolomic profiling study comprehensively reporting important grape secondary metabolites was achieved by Mattivi et al. (2006), where 91 grape cultivars were characterized for different polyphenols (focusing on the type and amount of flavonols and anthocyanins) at ripening on the berry skins. In particular and on average, the main flavonols found in red and white grapes differed in abundance order, and interestingly, the delphinidin-like flavonols were missing in all white cultivars, suggesting that the genes coding for flavonoid 3′,5′-hydroxylases were not expressed in these cases. A further study identified a hundred grape polyphenols by UHPLC/QTOF, providing a compendium of grape flavonols, anthocyanins, and stilbenes (Flamini et al., 2015). Other studies examined anthocyanin profiles in berry skins during the progress of ripening (Castellarin et al., 2006), the polyphenolic composition of PIWI grape cultivars (from the German fungus-resistant cv. 'Pilzwiderstandsfähige') (Ehrhardt

et al., 2014; Gratl et al., 2021), or of wild American genotypes (Narduzzi et al., 2015; Ruocco et al., 2017). Cultivar-specific compositions of polyphenols have also been assessed, for instance, in 'Muscat' cultivars with anthocyanin profiles driving the main divergence between red and white cultivars, followed by flavonols and flavanols discriminating among the white accessions (Degu et al., 2015). Additionally, the responses to several stresses (Degu et al., 2016), the changes in the flavonoid profiles by early mechanical leaf removal (VanderWeide et al., 2018), or the stimulatory effect of kaolin application in leaves (Conde et al., 2016) have also been accomplished. Metabolomic analyses have also been performed to compare the primary metabolites of fruits (Dai et al., 2013; Cuadros-Inostroza et al., 2016; Zhao et al., 2016) and leaves (Harb et al., 2015; Conde et al., 2018). Other studies have focused on the analysis of the volatile compounds in roots (Lawo et al., 2011), leaves (Weingart et al., 2012), and berries (Vrhovsek et al., 2014).

Research has also been carried out to study the berry late-ripening program in skin, flesh, and seed (Vondras et al., 2017) or to understand the role of drought conditions affecting several metabolic pathways (Hochberg et al., 2013; Griesser et al., 2015; Hochberg et al., 2015b; Herrera et al., 2017; Pinasseau et al., 2017). In addition, the effect of temperature (Hochberg et al., 2015a) and light (Reshef et al., 2017; Reshef et al., 2018) have also been investigated.

Like for transcriptomics, metabolomic approaches have also been deployed to understand plant-pathogen interactions. For example, the identification of biomarkers of defense response to *Plasmopara viticola* has been a trending topic (Adrian et al., 2017; Chitarrini et al., 2017; Negrel et al., 2018; Ciubotaru et al., 2021), as well as the action of *Botrytis cinerea* on the fruit metabolism (Hong et al., 2012; Negri et al., 2017).

In recent years, metabolomics in grapevine has been coupled to transcriptome analyses to understand in detail the physiological mechanisms of berry ripening and the interaction with biotic or abiotic stresses. This topic will be further discussed later on.

Proteomics

Approximately one-hundred grapevine proteomic studies can be found in the literature (a complete list of proteomic studies in grapevine is available in Supplementary Table 1C). The first extensive study on grapevine proteomics analyzed the mesocarp (flesh)-allocated proteins of ripe berries in six different cultivars using two-dimensional electrophoresis followed by MALDI-TOF peptide mass fingerprinting (Sarry et al., 2004). The authors determined the composition of 67 major proteins in ripe fruits and provided new evidence on the metabolism of sugar and organic acids in fruits. A second extensive work studied the proteomic dynamic changes during berry development and ripening in the mesocarp of cv. 'Nebbiolo' by profiling 101 proteins over seven time points (Giribaldi et al., 2007). The authors found that the majority of proteins were linked to metabolism, energy and protein synthesis and fate. In the same year, another study investigated the impact of two major abiotic stresses, water deficit and salt stress, on the shoot proteome of two cultivars, cv. 'Chardonnay' and cv. 'Cabernet Sauvignon', showing that the protein concentration varied mainly in response to the cultivars, then with time, and lastly with the abiotic stress (Vincent et al., 2007).

The knowledge of the grapevine berry proteome has been improved over the years by different studies focusing on skin proteome dynamics throughout berry ripening (Deytieux et al., 2007; Negri et al., 2008a; Martínez-Esteso et al., 2011a), on the identification of the different proteins present in skin, flesh or seed (Tian et al., 2015), on plasma membrane protein expression either during berry ripening (Zhang et al., 2008) or at maturity (Negri et al., 2008b), on the changes of the vacuolar proteome during ripening (Kuang et al., 2019), on single-berry proteome during development and ripening (Martínez-Esteso et al., 2011b; Martínez-Esteso et al., 2013) or in the protein expression profiles of grape berry during postharvest withering process (Di Carli et al., 2011).

Proteomics has also been employed to identify proteins associated with flavor volatile compounds found in fruits, such as proteins involved in the phenylpropanoid pathway, terpene synthesis, fatty acid derived volatiles and esters (Kambiranda et al., 2016; Kambiranda et al., 2018), or with the effects of ABA treatments on ripening *Vitis vinifera* berries (Giribaldi et al., 2010), sunlight exposure (Niu et al., 2013) and water deficit (Cramer et al., 2013). In addition, many other studies have tested proteome changes in plant-pathogen responses. For example, several studies investigated the leaf response to biotic stress, such as *Plasmopara viticola* (Milli et al., 2012; Figueiredo et al., 2017; Nascimento-Gavioli et al., 2017; Santos et al., 2020; Liu et al., 2021), while another study identified potential protein markers in berries affected by noble rot (Lorenzini et al., 2015).

Ionomics

So far, only a few ionomic studies have been performed in grapevine. In 2011 the first ionomic work was published, describing the accumulation pattern of 42 mineral elements in cv. 'Chardonnay' berries during development and ripening (Bertoldi et al., 2011). The authors described that seven elements accumulate prior to veraison, other eighteen accumulate mainly prior to veraison but also during ripening, and seventeen progressively during growth and ripening. With regard to distribution, eight, sixteen and eighteen elements specifically accumulated in seeds, skin and flesh, respectively. In another study, the concentration of 34 mineral elements in grapevine berries was determined by ICP-MS in cv. 'Corvina'

berries, harvested from eleven vineyards, to trace their geographical origin (Pii et al., 2017). Moreover, the analysis of cations such as K^+, Mg^{2+}, Ca^{2+}, NH_4^+ in berries at different developmental stages showed the diversity of their concentration in several cultivars, providing additional information for the selection of genotypes able to cope with the adverse effects of climate change on fruit quality (Bigard et al., 2020). Finally, the ionomic signature was also studied in leaves identifying a mineral element-based response to *Xylella fastidiosa* (De La Fuente et al., 2013) and the changes in mineral distribution after *Plasmopara viticola* infection (Cesco et al., 2020). A complete list of ionomic grapevine studies is available in Supplementary Table 1D.

Multi-omics integration of transcriptomics and metabolomics

In addition to single-omic studies, integrative omics analyses can be applied to provide a deeper understanding of the regulatory processes controlling different molecular phenotypes. To date, around sixty multi-omic studies combine transcriptomics and metabolomics, to study either the early and late responses to abiotic stresses, such as water and salinity stress (Cramer et al., 2007), the molecular mechanisms involved in berry development (Deluc et al., 2007; Fortes et al., 2011; Degu et al., 2014; Fasoli et al., 2018; Griesser et al., 2020) and over-ripening (i.e., post-harvest withering; Zenoni et al., 2016; Zenoni et al., 2020), or the changes in polyphenol and aromatic compound content in ripening berries (Costantini et al., 2015; Malacarne et al., 2015; Costantini et al., 2017). Other integrated approaches have studied berry responses during ripening to water deficit (Deluc et al., 2009; Savoi et al., 2016; Savoi et al., 2017; Yang et al., 2020), light (Suzuki et al., 2015; Sun et al., 2019; He et al., 2020; Zhang K et al., 2021) or temperature (Lecourieux et al., 2017). A few additional studies have also studied the 'genotype by environment' (GxE) interaction (i.e., the effect of terroir) on the plasticity of red and white grapes (Dal Santo et al., 2013; Anesi et al., 2015; Dal Santo et al., 2016a; Dal Santo et al., 2018).

The integration of transcript and metabolite data has contributed to the biological understanding of grape cultivar differences for fruit composition. For example, Degu et al. (2014) identified a cultivar-dependent regulation of specialized metabolism towards fruit maturation when comparing the cv. 'Shiraz' and 'Cabernet Sauvignon', the former displaying a higher upregulation of the entire polyphenol pathway, favoring the accumulation of piceid and *p*-coumaroylated anthocyanins. Moreover, in a post-harvest withering study, the expression of stilbene biosynthesis genes increased after harvest in a genotype-dependent manner, matching the varietal accumulation differences (Zenoni et al., 2016).

The integration of multi-omic datasets has been helpful in the identification of putative candidate genes regulating the accumulation of secondary metabolites in fruits. In this regard, a nudix hydrolase was identified as a component of a terpene synthase-independent pathway, enhancing monoterpene biosynthesis together with other genes potentially involved in terpenoid metabolism, such as cytochrome P450 hydroxylases, epoxide hydrolases, and glucosyltransferases (Costantini et al., 2015). Transcript and metabolite analyses determined that the biosynthesis of anthocyanins was a consistent hallmark of noble rot in white-skinned cv. 'Sémillon' (Blanco-Ulate et al., 2015), an unexpected response due to the absence of functional alleles of the MYBA1-A2 anthocyanin-regulators. This phenomenon led to the hypothesis of novel regulators controlling berry skin pigment production, which were later found by Matus et al. (2017) and D'Incà et al. (2021). The use of metabolomics (stilbenoid-oriented) and transcriptomics, coupled to the genome-wide exploration of transcription factor binding sites through DAP-seq, allowed Orduña et al. (2022) to identify new candidate genes coding for resveratrol modifying enzymes including laccasses, glycosyltransferases and *O*-methyl-transferases, potentially producing viniferin, piceid and pterostilbene, respectively. Finally, Savoi et al. (2016) associated the up-regulation of the *MYB24* transcription factor with the observed increased biosynthesis of three key monoterpenes under water deficit in white grapes, leading to the hypothesis of its capacity to regulate terpene synthase (*TPS*) gene expression. Indeed, this MYB24-*TPS* regulatory relationship was recently confirmed by Zhang C et al. (2021), who also integrated several omics including transcriptomics, metabolomics, and DAP-seq.

Numerous works have applied integrative methods to address responses to pathogen infection, most being conducted in fruits or leaves. For example, the leaf analysis of 'Regent' and 'Trincadeira' cultivars, respectively resistant and susceptible to mildew, has provided information on the different metabolic pathways related to the defense process (Figueiredo et al., 2008). The work of Malacarne et al. (2011) combined metabolic and transcriptional profiles in a segregating population for resistance to *Plasmopara viticola*, while Maia et al. (2020) suggested several gene/metabolite biomarkers of fungal/oomycetes-associated disease susceptibility in eleven *Vitis* genotypes. In addition, combined approaches have been employed to study berries infected with the fungus *Botrytis cinerea* (Agudelo-Romero et al., 2015; Blanco-Ulate et al., 2015), and also to determine how the interaction with this same pathogen at flowering influences quiescence and egressed infection (Haile et al., 2017; Haile et al., 2020). Recently, a few studies have examined the defense responses in susceptible and resistant grape cultivars (Eisenmann et al., 2019; Chitarrini et al., 2020), while others have examined the transcriptional, hormonal, and metabolic changes under powdery mildew infection caused by *Erysiphe*

necator in leaves and berries (Pagliarani et al., 2020; Pimentel et al., 2021).

To date, only three publications integrate transcriptomics, proteomics, and metabolomics in a single study. By overlapping genes, proteins, and metabolites, Zamboni et al. (2010) identified stage-specific biomarkers for berry development and withering. Moreover, multi-omic datasets were integrated to test the uniqueness of three red-skinned and two white-skinned cultivars at berry maturity, providing a detailed indication of genotype differences (Ghan et al., 2015). Finally, multi-omic analyses have been employed in the study of leaf responses to copper stress, providing agronomic knowledge to improve vineyard management and favor the breeding of copper-resistant grape cultivars (Chen et al., 2021).

An illustration of data integration and meta-analysis using the TransMetaDb app

Moving forward from single-omic studies and *gene-to-gene* network exploring tools, the construction of *gene-to-metabolite* networks *via* integrative approaches represents a promising strategy for identifying novel gene functions and unprecedent links between genes and metabolites (Hirai et al., 2005; Saito et al., 2008). This concept has been reviewed in grapevine (Wong and Matus, 2017; Matus et al., 2019), stating the need for appropriate tools to visualize the integration of multi-omic datasets. The first tool developed for data integration in grapevine was 'VitisNet' (Grimplet et al., 2009; Grimplet et al., 2012), which allowed the multiple combinations of omics data by overlapping user data to 247 curated grapevine molecular networks, reporting more than 16,000 genes; unfortunately, this tool is no longer accessible. A second developed tool was 'VitisCyc' (Naithani et al., 2014), a grape-specific database for browsing and visualizing metabolic pathways end enzymatic reactions, compounds, genes and proteins, and for comparing metabolic networks with other publicly-available resources from other plant species (this tool is now hosted in the Gramene database; Tello-Ruiz et al., 2021).

To date, there is no visualization tool in grape to explore the correlation of transcriptomics and metabolomics data, and even less to combine them in meta-analyses. Within the COST Action CA17111 INTEGRAPE, we have developed TransMetaDb (Figure 2), an application available in the *Vitis Visualization* (VitViz) platform (https://tomsbiolab.com/vitviz), to freely explore the correlation between metabolites and genes in multiple transcriptomics/metabolomics integrated datasets. The Integrated Transcriptomics and Metabolomics Database Application (TransMetaDb) was developed in the *Shiny R* environment and offers a user-friendly interface to explore transcriptomic data (i.e., differentially expressed genes and co-expression modules) and its correlation to metabolites quantified in the same conditions. The App takes an Excel or comma/tab-separated file as an input, with only one column containing the 12X.v2 VCost.v3 gene IDs of interest, and an optional second column with the gene names/symbols, whose purpose is to provide a descriptive name for the user-provided genes. The output is a downloadable heatmap or table, with all the genes of interest by row, compared with the different metabolites on each column. Each cell contains the Pearson's correlation coefficient (PCC) value and its *p*-value in brackets, calculated using the student asymptotic method. The identification of gene candidates related to metabolite phenotypic traits has often been inferred from association measures, such as the commonly-used PCC method (to measure linear correlation between two variables). Although alternative measures can be employed, PCC is still the standard for initial exploration of *gene-to-gene* and *gene-to-metabolite* networks (Nikiforova et al., 2005; Mao et al., 2009). This is a first general approach to discover functions in a set of genes and metabolites of interest. On a second tab, the App allows the user to explore co-expression clustered modules, downloading a table with all gene-module categories.

So far, three studies have been uploaded to the App; Savoi et al. (2016) and Savoi et al. (2017) focused on the impact of drought on fruit secondary metabolism and have a similar experimental design, the same metabolomic method, with all data being publicly available. A third study detailed a transcriptomic and metabolomic temporal map of berry development in two cultivars for three consecutive years (Fasoli et al., 2018). This data was first reanalyzed; briefly, the transcriptomic data was re-aligned using STAR v. 2.7.3a (Dobin et al., 2013) against the PN40024 12X.v2 assembly, and a raw gene count matrix was extracted using the latest VCost.v3 annotation (Canaguier et al., 2017) and *featureCounts* (Liao et al., 2014). Gene expression was normalized with FPKM (Fragments per kilobase per million mapped reads) as this normalization method takes into account both sequencing depth of libraries and gene length, allowing the comparison of expression between different genes across different samples (other normalization methods will be applied in the future, such as TMM).

Clustering of gene expression and metabolite profiles can serve for mining useful information from noisy data, identifying cohorts of genes that control metabolism and understanding how metabolic pathways can be rewired in development and stress. Detection of functional gene modules by classical clustering methods, such as *K*-means or mean-shift, have been outperformed in transcriptomic studies by a modification of the algorithm, e.g., the fuzzy *k*-means applied in the *fclust* R package (Ferraro et al., 2019), or by correlation networks using for instance the Weighted Gene Correlation Network Analysis (WGCNA) R package (Langfelder and Horvath, 2008). In TransMetaDb, genes have been clustered in eigen modules

FIGURE 2
Omics integration in two studies that investigated the effect of a long-lasting water deficit on the metabolism of white (cv. 'Tocai friulano') and red (cv. 'Merlot') cultivars during berry development and ripening (Savoi et al., 2016; 2017). **(A)** Methods scheme of the analyses performed for each of the independent studies and the combination of them (i.e., study integration or meta-analysis). Genes with low expression are filtered-out before WGCNA analysis. **(B, C)** Results obtained from the analyses depicted in **(A)**, where **(B)** Improvement of statistical significance and/or correlation between genes and metabolites for the combination of both studies. P-value representation is only shown when the value exceeds the 0.05 threshold. **(C)** Improvement of statistical significance and/or correlation between gene modules and metabolites for the combination of both studies. A $-\log_{10}$(p-value) scale is provided where a higher value represents a greater statistical significance. The red dashed line depicts $-\log_{10}$(p-value) corresponding to a 0.05 threshold. **(D)** Visual interface of the TransMetaDb App, found at the *Vitis* Visualization (VitViz) platform (https://tomsbiolab.com/vitviz). The resulting example heatmap is shown in **(E)**.

(ME) by applying WGCNA, and metabolites have been associated to these modules in the same way as for genes. As explained in Langfelder and Horvath (2008), WGCNA works by generating a network (or adjacency matrix) from the biological data and then performing a hierarchical clustering. In order to build the adjacency matrix, an intermediate co-expression similarity matrix is defined using the biological data by computing co-expression measures between genes. Once the co-expression similarity matrix is constructed, it is transformed in the adjacency matrix using a beta power value that is chosen by the user in order to generate an adjacency matrix, and that satisfies the scale-free network topology where the distribution of node degree is adjusted to a potential law (i.e., high number of nodes with a low number of edges and few nodes with a high number of edges). For doing this analysis, the blockwiseModules function was used with a deepSplit of 4, a mergeCutHeight of 0.1

and a beta power of 30 for the integration of the 'Tocai friulano' and 'Merlot' studies and a power of 11, deepSplit of 4 and a mergeCutHeight of 0.2 for Fasoli et al. (2018). Following *WGCNA* authors' recommendation, the deepSplit and mergeCutHeight parameters were adapted to obtain a number of eigen modules and a number of genes per eigen module adaptable for subsequent analysis with a minimum module size of 40 genes. Transcripts and metabolites were integrated in gene-*to*-metabolite and eigen module-*to*-metabolite matrices for each of the individual and combined studies.

While exploring the WGCNA results of the combined studies we observed that the Pearson correlation coefficients (PCC) and/or the significance (*p*-values) of specific eigen module (ME, Figure 2B) or gene-metabolite (Figure 2C), often increased. This is expected, because as the sample is larger the error is lower and the sample correlation converges to the population parameter, in the same way as increasing the number of replicates improves the inferences that can be made about a population. For example, in the combined eigen module "white", PCC and *p*-values of linalool, geraniol, and α-terpineol were higher and more significant in the 'Tocai friulano'+'Merlot' set, just like the association between these same three terpenes (present in the white cultivar only) and the genes *MYB24* and *TPS35* (Savoi et al., 2016; Zhang C et al., 2021). Moreover, the addition of an anthocyanin-free dataset (i.e., Tocai) to the data belonging to an anthocyanin-pigmented cultivar (i.e., Merlot) also improved the transcript-metabolite correlations between different pigments and related genes as the 'no expression' and 'no pigment accumulation' is a positive correlation in itself. The five glycosylated anthocyanins (only present in the red cultivar) and the anthocyanin-related genes *UFGT* (Boss et al., 1996) and *MYBA1* (Kobayashi et al., 2004) showed increased correlation and/or increased significance in the meta-analysis compared to individual studies (where the correlation was already high). This improvement is due to the coherent behavior of the selected proteins as they correspond to the latest enzyme of the pathway and the master regulator of anthocyanin accumulation, respectively, representing a perfect case of expected correlation. Finally, we observed the same trend for the light-induced carotenoid zeaxanthin and the light/UV signaling gene *HYH* (HY5 HOMOLOGUE; (Loyola et al., 2016). These results clearly imply that meta-analyses of integrated transcriptomic/metabolomic datasets improves the strength of correlation metrics in the same way as adding new samples in the construction of a gene co-expression network increases the network performance until it reaches a plateau (Wong, 2020).

We plan to increase the number of combined transcriptomic and metabolomic datasets in TransMeta Db, based on the quality of the metadata. Metabolic data will be compared in the following submitted studies to see which metabolites can be combined. If this data has been acquired by different platforms, or if it is presented in different units, one possibility would be to scale the data (e.g., Z-score) before integration. Nevertheless, this effort would certainly push the community to improve the annotation of their experiments in public repositories so their data can be fully interoperable. Once more studies have been uploaded, we also expect to showcase alternative correlation metrics using other compatible software and pipelines.

Data availability statement

The datasets presented in this study can be found in online repositories. The names of the repository/repositories and accession number(s) can be found in the article/Supplementary Material.

Author contributions

SS and JM conceived the study and wrote the manuscript. AS and LO contributed with the reanalysis of the transcriptomic and metabolomic data set and by building the TransMetaDb app found in the VitViz platform. All authors contributed to the article and approved the submitted version.

Funding

This publication is based upon work from COST Action CA17111 INTEGRAPE, supported by COST (European Cooperation in Science and Technology) and COST grant ECOST-STSM-Request-CA17111-48997 awarded to SS. This work was also supported by Grants PGC2018-099449-A-I00, PID2021-128865NB-I00 and by the Ramón y Cajal program grant RYC-2017-23645, all awarded to JM, and to the FPI scholarship PRE2019-088044 granted to LO from the Ministerio de Ciencia, Innovación y Universidades (MCIU, Spain), Agencia Estatal de Investigación (AEI, Spain), and Fondo Europeo de Desarrollo Regional (FEDER, European Union).

Acknowledgments

We thank Anne-Marie Digby (University of Verona) for manuscript revision. We apologize to all authors whose work has not been cited owing to space constraints.

Conflict of interest

The authors declare that the research was conducted in the absence of any commercial or financial relationships that could be construed as a potential conflict of interest.

Publisher's note

All claims expressed in this article are solely those of the authors and do not necessarily represent those of their affiliated organizations, or those of the publisher, the editors and the reviewers. Any product that may be evaluated in this article, or claim that may be made by its manufacturer, is not guaranteed or endorsed by the publisher.

Supplementary material

The Supplementary Material for this article can be found online at: https://www.frontiersin.org/articles/10.3389/fpls.2022.937927/full#supplementary-material

SUPPLEMENTARY TABLE 1

List of **(A)** transcriptomics, **(B)** metabolomics, **(C)** proteomics, and **(D)** ionomics studies retrieved from the literature. Data was collected from NCBI using different queries and keywords. Only the studies published until 12/2021 were considered. Data were manually curated to remove clear outliers.

References

Adrian, M., Lucio, M., Roullier-Gall, C., Héloir, M.-C., Trouvelot, S., Daire, X., et al. (2017). Metabolic fingerprint of PS3-induced resistance of grapevine leaves against *Plasmopara viticola* revealed differences in elicitor-triggered defenses. *Front. Plant Sci.* 8. doi: 10.3389/fpls.2017.00101

Agudelo-Romero, P., Erban, A., Rego, C., Carbonell-Bejerano, P., Nascimento, T., Sousa, L., et al. (2015). Transcriptome and metabolome reprogramming in *Vitis vinifera* cv. trincadeira berries upon infection with *Botrytis cinerea*. *J. Exp. Bot.* 66, 1769–1785. doi: 10.1093/jxb/eru517

Amrine, K. C. H., Blanco-Ulate, B., Riaz, S., Pap, D., Jones, L., Figueroa-Balderas, R., et al. (2015). Comparative transcriptomics of central Asian *Vitis vinifera* accessions reveals distinct defense strategies against powdery mildew. *Hortic. Res.* 2, 1–11. doi: 10.1038/hortres.2015.37

Anesi, A., Stocchero, M., Dal Santo, S., Commisso, M., Zenoni, S., Ceoldo, S., et al. (2015). Towards a scientific interpretation of the terroir concept: plasticity of the grape berry metabolome. *BMC Plant Biol.* 15, 191. doi: 10.1186/s12870-015-0584-4

Arabidopsis Genome Initiative (2000). Analysis of the genome sequence of the flowering plant arabidopsis thaliana. *Nature* 408, 796–815. doi: 10.1038/35048692

Balic, I., Vizoso, P., Nilo-Poyanco, R., Sanhueza, D., Olmedo, P., Sepúlveda, P., et al. (2018). Transcriptome analysis during ripening of table grape berry cv. Thompson seedless. *PloS One* 13, e0190087. doi: 10.1371/journal.pone.0190087

Bertoldi, D., Larcher, R., Bertamini, M., Otto, S., Concheri, G., and Nicolini, G. (2011). Accumulation and distribution pattern of macro- and microelements and trace elements in *Vitis vinifera* l. cv. Chardonnay berries. *J. Agric. Food Chem.* 59, 7224–7236. doi: 10.1021/jf2006003

Bigard, A., Romieu, C., Sire, Y., and Torregrosa, L. (2020). Vitis vinifera l. diversity for cations and acidity is suitable for breeding fruits coping with climate warming. *Front. Plant Sci.* 11. doi: 10.3389/fpls.2020.01175

Blanco-Ulate, B., Amrine, K. C. H., Collins, T. S., Rivero, R. M., Vicente, A. R., Morales-Cruz, A., et al. (2015). Developmental and metabolic plasticity of white-skinned grape berries in response to *Botrytis cinerea* during noble rot. *Plant Physiol.* 169, 2422–2443. doi: 10.1104/pp.15.00852

Boss, P. K., Davies, C., and Robinson, S. P. (1996). Expression of anthocyanin biosynthesis pathway genes in red and white grapes. *Plant Mol. Biol.* 32, 565–569. doi: 10.1007/BF00019111

Campayo, A., Savoi, S., Romieu, C., López-Jiménez, A. J., Serrano de la Hoz, K., Salinas, M. R., et al. (2021). The application of ozonated water rearranges the vitis vinifera l. leaf and berry transcriptomes eliciting defence and antioxidant responses. *Sci. Rep.* 11, 8114. doi: 10.1038/s41598-021-87542-y

Canaguier, A., Grimplet, J., Di Gaspero, G., Scalabrin, S., Duchêne, E., Choisne, N., et al. (2017). A new version of the grapevine reference genome assembly (12X.v2) and of its annotation (VCost.v3). *Genom Data* 14, 56–62. doi: 10.1016/j.gdata.2017.09.002

Carbonell-Bejerano, P., Diago, M.-P., Martínez-Abaigar, J., Martínez-Zapater, J. M., Tardáguila, J., and Núñez-Olivera, E. (2014a). Solar ultraviolet radiation is necessary to enhance grapevine fruit ripening transcriptional and phenolic responses. *BMC Plant Biol.* 14, 183. doi: 10.1186/1471-2229-14-183

Carbonell-Bejerano, P., Rodríguez, V., Royo, C., Hernáiz, S., Moro-González, L. C., Torres-Viñals, M., et al. (2014b). Circadian oscillatory transcriptional programs in grapevine ripening fruits. *BMC Plant Biol.* 14, 78. doi: 10.1186/1471-2229-14-78

Carbonell-Bejerano, P., Santa María, E., Torres-Pérez, R., Royo, C., Lijavetzky, D., Bravo, G., et al. (2013). Thermotolerance responses in ripening berries of *Vitis vinifera* l. cv Muscat Hamburg. *Plant Cell Physiol.* 54, 1200–1216. doi: 10.1093/pcp/pct071

Castellarin, S. D., Di Gaspero, G., Marconi, R., Nonis, A., Peterlunger, E., Paillard, S., et al. (2006). Colour variation in red grapevines (*Vitis vinifera* l.): genomic organisation, expression of flavonoid 3'-hydroxylase, flavonoid 3',5'-hydroxylase genes and related metabolite profiling of red cyanidin-/blue delphinidin-based anthocyanins in berry skin. *BMC Genomics* 7, 12. doi: 10.1186/1471-2164-7-12

Cesco, S., Tolotti, A., Nadalini, S., Rizzi, S., Valentinuzzi, F., Mimmo, T., et al. (2020). *Plasmopara viticola* infection affects mineral elements allocation and distribution in *Vitis vinifera* leaves. *Sci. Rep.* 10, 18759. doi: 10.1038/s41598-020-75990-x

Chen, M., Fang, X., Wang, Z., Shangguan, L., Liu, T., Chen, C., et al. (2021). Multi-omics analyses on the response mechanisms of 'Shine muscat' grapevine to low degree of excess copper stress (Low-ECS). *Environ. Pollut.* 286, 117278. doi: 10.1016/j.envpol.2021.117278

Chin, C.-S., Peluso, P., Sedlazeck, F. J., Nattestad, M., Concepcion, G. T., Clum, A., et al. (2016). Phased diploid genome assembly with single-molecule real-time sequencing. *Nat. Methods* 13, 1050–1054. doi: 10.1038/nmeth.4035

Chitarrini, G., Riccadonna, S., Zulini, L., Vecchione, A., Stefanini, M., Larger, S., et al. (2020). Two-omics data revealed commonalities and differences between Rpv12- and Rpv3-mediated resistance in grapevine. *Sci. Rep.* 10, 12193. doi: 10.1038/s41598-020-69051-6

Chitarrini, G., Soini, E., Riccadonna, S., Franceschi, P., Zulini, L., Masuero, D., et al. (2017). Identification of biomarkers for defense response to *Plasmopara viticola* in a resistant grape variety. *Front. Plant Sci.* 8. doi: 10.3389/fpls.2017.01524

Ciubotaru, R. M., Franceschi, P., Zulini, L., Stefanini, M., Škrab, D., Rossarolla, M. D., et al. (2021). Mono-locus and pyramided resistant grapevine cultivars reveal early putative biomarkers upon artificial inoculation with *Plasmopara viticola*. *Front. Plant Sci.* 12. doi: 10.3389/fpls.2021.693887

Cochetel, N., Escudié, F., Cookson, S. J., Dai, Z., Vivin, P., Bert, P.-F., et al. (2017). Root transcriptomic responses of grafted grapevines to heterogeneous nitrogen availability depend on rootstock genotype. *J. Exp. Bot.* 68, 4339–4355. doi: 10.1093/jxb/erx224

Conde, A., Neves, A., Breia, R., Pimentel, D., Dinis, L.-T., Bernardo, S., et al. (2018). Kaolin particle film application stimulates photoassimilate synthesis and modifies the primary metabolome of grape leaves. *J. Plant Physiol.* 223, 47–56. doi: 10.1016/j.jplph.2018.02.004

Conde, A., Pimentel, D., Neves, A., Dinis, L.-T., Bernardo, S., Correia, C. M., et al. (2016). Kaolin foliar application has a stimulatory effect on phenylpropanoid and flavonoid pathways in grape berries. *Front. Plant Sci.* 7. doi: 10.3389/fpls.2016.01150

Cookson, S. J., Clemente Moreno, M. J., Hevin, C., Nyamba Mendome, L. Z., Delrot, S., Trossat-Magnin, C., et al. (2013). Graft union formation in grapevine induces transcriptional changes related to cell wall modification, wounding, hormone signalling, and secondary metabolism. *J. Exp. Bot.* 64, 2997–3008. doi: 10.1093/jxb/ert144

Corso, M., Vannozzi, A., Maza, E., Vitulo, N., Meggio, F., Pitacco, A., et al. (2015). Comprehensive transcript profiling of two grapevine rootstock genotypes contrasting in drought susceptibility links the phenylpropanoid pathway to enhanced tolerance. *J. Exp. Bot.* 66, 5739–5752. doi: 10.1093/jxb/erv274

Costantini, L., Kappel, C. D., Trenti, M., Battilana, J., Emanuelli, F., Sordo, M., et al. (2017). Drawing links from transcriptome to metabolites: the evolution of aroma in the ripening berry of moscato bianco (*Vitis vinifera* l.). *Front. Plant Sci.* 8. doi: 10.3389/fpls.2017.00780

Costantini, L., Malacarne, G., Lorenzi, S., Troggio, M., Mattivi, F., Moser, C., et al. (2015). New candidate genes for the fine regulation of the colour of grapes. *J. Exp. Bot.* 66, 4427–40. doi: 10.1093/jxb/erv159

Cramer, G. R., Cochetel, N., Ghan, R., Destrac-Irvine, A., and Delrot, S. (2020). A sense of place: transcriptomics identifies environmental signatures in Cabernet sauvignon berry skins in the late stages of ripening. *BMC Plant Biol.* 20, 41. doi: 10.1186/s12870-020-2251-7

Cramer, G. R., Ergül, A., Grimplet, J., Tillett, R. L., Tattersall, E. A. R., Bohlman, M. C., et al. (2007). Water and salinity stress in grapevines: early and late changes in transcript and metabolite profiles. *Funct. Integr. Genomics* 7, 111–34. doi: 10.1007/s10142-006-0039-y

Cramer, G. R., Ghan, R., Schlauch, K. A., Tillett, R. L., Heymann, H., Ferrarini, A., et al. (2014). Transcriptomic analysis of the late stages of grapevine (*Vitis vinifera* cv. Cabernet sauvignon) berry ripening reveals significant induction of ethylene signaling and flavor pathways in the skin. *BMC Plant Biol.* 14, 1–21. doi: 10.1186/s12870-014-0370-8

Cramer, G. R., Sluyter, S. C. V., Hopper, D. W., Pascovici, D., Keighley, T., and Haynes, P. A. (2013). Proteomic analysis indicates massive changes in metabolism prior to the inhibition of growth and photosynthesis of grapevine (*Vitis vinifera* l.) in response to water deficit. *BMC Plant Biol.* 13, 1–22. doi: 10.1186/1471-2229-13-49

Cuadros-Inostroza, A., Ruíz-Lara, S., González, E., Eckardt, A., Willmitzer, L., and Peña-Cortés, H. (2016). GC–MS metabolic profiling of Cabernet sauvignon and merlot cultivars during grapevine berry development and network analysis reveals a stage- and cultivar-dependent connectivity of primary metabolites. *Metabolomics* 12, 39. doi: 10.1007/s11306-015-0927-z

Dai, Z. W., Léon, C., Feil, R., Lunn, J. E., Delrot, S., and Gomès, E. (2013). Metabolic profiling reveals coordinated switches in primary carbohydrate metabolism in grape berry (*Vitis vinifera* l.), a non-climacteric fleshy fruit. *J. Exp. Bot.* 64, 1345–1355. doi: 10.1093/jxb/ers396

Dal Santo, S., Fasoli, M., Negri, S., D'Incà, E., Vicenzi, N., Guzzo, F., et al. (2016a). Plasticity of the berry ripening program in a white grape variety. *Front. Plant Sci.* 7. doi: 10.3389/fpls.2016.00970

Dal Santo, S., Palliotti, A., Zenoni, S., Tornielli, G. B., Fasoli, M., Paci, P., et al. (2016b). Distinct transcriptome responses to water limitation in isohydric and anisohydric grapevine cultivars. *BMC Genomics* 17, 815. doi: 10.1186/s12864-016-3136-x

Dal Santo, S., Tornielli, G. B., Zenoni, S., Fasoli, M., Farina, L., Anesi, A., et al. (2013). The plasticity of the grapevine berry transcriptome. *Genome Biol.* 14, r54. doi: 10.1186/gb-2013-14-6-r54

Dal Santo, S., Zenoni, S., Sandri, M., Lorenzis, G. D., Magris, G., Paoli, E. D., et al. (2018). Grapevine field experiments reveal the contribution of genotype, the influence of environment and the effect of their interaction (G×E) on the berry transcriptome. *Plant J.* 93, 1143–1159. doi: 10.1111/tpj.13834

da Silva, F. G., Iandolino, A., Al-Kayal, F., Bohlmann, M. C., Cushman, M. A., Lim, H., et al. (2005). Characterizing the grape transcriptome. analysis of expressed sequence tags from multiple *Vitis* species and development of a compendium of gene expression during berry development. *Plant Physiol.* 139, 574–597. doi: 10.1104/pp.105.065748

da Silva, C., Zamperin, G., Ferrarini, A., Minio, A., Molin, A. D., Venturini, L., et al. (2013). The high polyphenol content of grapevine cultivar tannat berries is conferred primarily by genes that are not shared with the reference genome. *Plant Cell* 25, 4777–4788. doi: 10.1105/tpc.113.118810

Degu, A., Ayenew, B., Cramer, G. R., and Fait, A. (2016). Polyphenolic responses of grapevine berries to light, temperature, oxidative stress, abscisic acid and jasmonic acid show specific developmental-dependent degrees of metabolic resilience to perturbation. *Food Chem.* 212, 828–836. doi: 10.1016/j.foodchem.2016.05.164

Degu, A., Hochberg, U., Sikron, N., Venturini, L., Buson, G., Ghan, R., et al. (2014). Metabolite and transcript profiling of berry skin during fruit development elucidates differential regulation between Cabernet sauvignon and Shiraz cultivars at branching points in the polyphenol pathway. *BMC Plant Biol.* 14, 188. doi: 10.1186/s12870-014-0188-4

Degu, A., Morcia, C., Tumino, G., Hochberg, U., Toubiana, D., Mattivi, F., et al. (2015). Metabolite profiling elucidates communalities and differences in the polyphenol biosynthetic pathways of red and white Muscat genotypes. *Plant Physiol. Biochem.* 86, 24–33. doi: 10.1016/j.plaphy.2014.11.006

De La Fuente, L., Parker, J. K., Oliver, J. E., Granger, S., Brannen, P. M., Santen, E., et al. (2013). The bacterial pathogen *Xylella fastidiosa* affects the leaf ionome of plant hosts during infection. *PloS One* 8, e62945. doi: 10.1371/journal.pone.0062945

Deluc, L. G., Grimplet, J., Wheatley, M. D., Tillett, R. L., Quilici, D. R., Osborne, C., et al. (2007). Transcriptomic and metabolite analyses of Cabernet sauvignon grape berry development. *BMC Genomics* 8, 1–42. doi: 10.1186/1471-2164-8-429

Deluc, L. G., Quilici, D. R., Decendit, A., Grimplet, J., Wheatley, M. D., Schlauch, K. A., et al. (2009). Water deficit alters differentially metabolic pathways affecting important flavor and quality traits in grape berries of Cabernet sauvignon and Chardonnay. *BMC Genomics* 10, 212. doi: 10.1186/1471-2164-10-212

Deytieux, C., Geny, L., Lapaillerie, D., Claverol, S., Bonneu, M., and Donèche, B. (2007). Proteome analysis of grape skins during ripening. *J. Exp. Bot.* 58, 1851–1862. doi: 10.1093/jxb/erm049

Díaz-Riquelme, J., Grimplet, J., Martínez-Zapater, J. M., and Carmona, M. J. (2012). Transcriptome variation along bud development in grapevine (*Vitis vinifera* l.). *BMC Plant Biol.* 12, 181. doi: 10.1186/1471-2229-12-181

Díaz-Riquelme, J., Martínez-Zapater, J. M., and Carmona, M. J. (2014). Transcriptional analysis of tendril and inflorescence development in grapevine (*Vitis vinifera* l.). *PloS One* 9 (3), e92339. doi: 10.1371/journal.pone.0092339

Di Carli, M., Zamboni, A., Pè, M. E., Pezzotti, M., Lilley, K. S., Benvenuto, E., et al. (2011). Two-dimensional differential in gel electrophoresis (2D-DIGE) analysis of grape berry proteome during postharvest withering. *J. Proteome Res.* 10, 429–446. doi: 10.1021/pr1005313

D'Incà, E., Cazzaniga, S., Foresti, C., Vitulo, N., Bertini, E., Galli, M., et al. (2021). VviNAC33 promotes organ de-greening and represses vegetative growth during the vegetative-to-mature phase transition in grapevine. *New Phytol.* 231 (2), 726–746. doi: 10.1111/nph.17263

Dobin, A., Davis, C. A., Schlesinger, F., Drenkow, F., Zaleski, C., Jha, S., et al. (2013)STAR: ultrafast universal RNA-seq aligner. *Bioinformatics* 29 (1), 15–21 doi: 10.1093/bioinformatics/bts635.

Ehrhardt, C., Arapitsas, P., Stefanini, M., Flick, G., and Mattivi, F. (2014). Analysis of the phenolic composition of fungus-resistant grape varieties cultivated in Italy and Germany using UHPLC-MS/MS. *J. Mass Spectrometry* 49, 860–869. doi: 10.1002/jms.3440

Eisenmann, B., Czemmel, S., Ziegler, T., Buchholz, G., Kortekamp, A., Trapp, O., et al. (2019). Rpv3–1 mediated resistance to grapevine downy mildew is associated with specific host transcriptional responses and the accumulation of stilbenes. *BMC Plant Biol.* 19, 343. doi: 10.1186/s12870-019-1935-3

Fasoli, M., Richter, C. L., Zenoni, S., Bertini, E., Vitulo, N., Santo, S. D., et al. (2018). Timing and order of the molecular events marking the onset of berry ripening in grapevine. *Plant Physiol.* 178, 1187–1206. doi: 10.1104/pp.18.00559

Fasoli, M., Santo, S. D., Zenoni, S., Tornielli, G. B., Farina, L., Zamboni, A., et al. (2012). The grapevine expression atlas reveals a deep transcriptome shift driving the entire plant into a maturation program. *Plant Cell* 24, 3489–3505. doi: 10.1105/tpc.112.100230

Ferraro, M. ,. B., Giordani, P., and Serafini, A. (2019). Fclust: An r package for fuzzy clustering. *R J.* 11 (1), 198. doi: 10.32614/RJ-2019-017

Fiehn, O., Kopka, J., Dörmann, P., Altmann, T., Trethewey, R. N., and Willmitzer, L. (2000). Metabolite profiling for plant functional genomics. *Nat. Biotechnol.* 18, 1157–1161. doi: 10.1038/81137

Figueiredo, A., Fortes, A. M., Ferreira, S., Sebastiana, M., Choi, Y. H., Sousa, L., et al. (2008). Transcriptional and metabolic profiling of grape (*Vitis vinifera* l.) leaves unravel possible innate resistance against pathogenic fungi. *J. Exp. Bot.* 59, 3371–3381. doi: 10.1093/jxb/ern187

Figueiredo, A., Martins, J., Sebastiana, M., Guerreiro, A., Silva, A., Matos, A. R., et al. (2017). Specific adjustments in grapevine leaf proteome discriminating resistant and susceptible grapevine genotypes to *Plasmopara viticola*. *J. Proteomics* 152, 48–57. doi: 10.1016/j.jprot.2016.10.012

Flamini, R., De Rosso, M., and Bavaresco, L. (2015). Study of grape polyphenols by liquid chromatography-high-resolution mass spectrometry (UHPLC/QTOF) and suspect screening analysis. *J. Analytical Methods Chem.* 2015, e350259. doi: 10.1155/2015/350259

Fortes, A. M., Agudelo-Romero, P., Silva, M. S., Ali, K., Sousa, L., Maltese, F., et al. (2011). Transcript and metabolite analysis in trincadeira cultivar reveals novel information regarding the dynamics of grape ripening. *BMC Plant Biol.* 11, 149. doi: 10.1186/1471-2229-11-149

Fung, R. W. M., Gonzalo, M., Fekete, C., Kovacs, L. G., He, Y., Marsh, E., et al. (2008). Powdery mildew induces defense-oriented reprogramming of the transcriptome in a susceptible but not in a resistant grapevine. *Plant Physiol.* 146, 236–249. doi: 10.1104/pp.107.108712

Ghan, R., Petereit, J., Tillett, R. L., Schlauch, K. A., Toubiana, D., Fait, A., et al. (2017). The common transcriptional subnetworks of the grape berry skin in the late stages of ripening. *BMC Plant Biol.* 17, 94. doi: 10.1186/s12870-017-1043-1

Ghan, R., Van Sluyter, S. C., Hochberg, U., Degu, A., Hopper, D. W., Tillet, R. L., et al. (2015). Five omic technologies are concordant in differentiating the biochemical characteristics of the berries of five grapevine (*Vitis vinifera* l.) cultivars. *BMC Genomics* 16, 946. doi: 10.1186/s12864-015-2115-y

Giribaldi, M., Gény, L., Delrot, S., and Schubert, A. (2010). Proteomic analysis of the effects of ABA treatments on ripening *Vitis vinifera* berries. *J. Exp. Bot.* 61, 2447–2458. doi: 10.1093/jxb/erq079

Giribaldi, M., Perugini, I., Sauvage, F.-X., and Schubert, A. (2007). Analysis of protein changes during grape berry ripening by 2-DE and MALDI-TOF. *PROTEOMICS* 7, 3154–70. doi: 10.1002/pmic.200600974

Goff, S. A., Ricke, D., Lan, T.-H., Presting, G., Wang, R., Dunn, M., et al. (2002). A draft sequence of the rice genome (*Oryza sativa* l. ssp. japonica). *Science* 296, 92–100. doi: 10.1126/science.1068275

Gouthu, S., O'Neil, S. T., Di, Y., Ansarolia, M., Megraw, M., and Deluc, L. G. (2014). A comparative study of ripening among berries of the grape cluster reveals an altered transcriptional programme and enhanced ripening rate in delayed berries. *J. Exp. Bot.* 65, 5889–5902. doi: 10.1093/jxb/eru329

Gratl, V., Sturm, S., Zini, E., Letschka, T., Stefanini, M., Vezzulli, S., et al. (2021). Comprehensive polyphenolic profiling in promising resistant grapevine hybrids including 17 novel breeds in northern Italy. *J. Sci. Food Agric.* 101, 2380–2388. doi: 10.1002/jsfa.10861

Griesser, M., Savoi, S., Supapvanich, S., Dobrev, P., Vankova, R., and Forneck, A. (2020). Phytohormone profiles are strongly altered during induction and symptom development of the physiological ripening disorder berry shrivel in grapevine. *Plant Mol. Biol* 103, 141–157. doi: 10.1007/s11103-020-00980-6

Griesser, M., Weingart, G., Schoedl-Hummel, K., Neumann, N., Becker, M., Varmuza, K., et al. (2015). Severe drought stress is affecting selected primary metabolites, polyphenols, and volatile metabolites in grapevine leaves (Vitis vinifera cv. pinot noir). *Plant Physiol. Biochem.* 88, 17–26. doi: 10.1016/j.plaphy.2015.01.004

Grimplet, J., Cramer, G. R., Dickerson, J. A., Mathiason, K., Hemert, J. V., and Fennell, A. Y. (2009). VitisNet: "Omics" integration through grapevine molecular networks. *PloS One* 4, e8365. doi: 10.1371/journal.pone.0008365

Grimplet, J., Deluc, L. G., Tillett, R. L., Wheatley, M. D., Schlauch, K. A., Cramer, G. R., et al. (2007). Tissue-specific mRNA expression profiling in grape berry tissues. *BMC Genomics* 8, 187. doi: 10.1186/1471-2164-8-187

Grimplet, J., Hemert, J. V., Carbonell-Bejerano, P., Díaz-Riquelme, J., Dickerson, J., Fennell, A., et al. (2012). Comparative analysis of grapevine whole-genome gene predictions, functional annotation, categorization and integration of the predicted gene sequences. *BMC Res. Notes* 5, 213. doi: 10.1186/1756-0500-5-213

Grimplet, J., Tello, J., Laguna, N., and Ibáñez, J. (2017). Differences in flower transcriptome between grapevine clones are related to their cluster compactness, fruitfulness, and berry size. *Front. Plant Sci.* 8. doi: 10.3389/fpls.2017.00632

Guo, D. L., Wang, Z., Pei, M.-S., Guo, L.-L., and Yu, Y.-H. (2020). Transcriptome analysis reveals mechanism of early ripening in kyoho grape with hydrogen peroxide treatment. *BMC Genomics* 21, 784. doi: 10.1186/s12864-020-07180-y

Guo, D.-L., Xi, F.-F., Yu, Y.-H., Zhang, X.-Y., Zhang, G.-H., and Zhong, G.-Y. (2016). Comparative RNA-seq profiling of berry development between table grape 'Kyoho' and its early-ripening mutant 'Fengzao'. *BMC Genomics* 17, 795. doi: 10.1186/s12864-016-3051-1

Haile, Z. M., Malacarne, G., Pilati, S., Sonego, P., Moretto, M., Masuero, D., et al. (2020). Dual transcriptome and metabolic analysis of *Vitis vinifera* cv. pinot noir berry and *Botrytis cinerea* during quiescence and egressed infection. *Front. Plant Sci.* 10. doi: 10.3389/fpls.2019.01704

Haile, Z. M., Pilati, S., Sonego, P., Malacarne, G., Vrhovsek, U., Engelen, K., et al. (2017). Molecular analysis of the early interaction between the grapevine flower and *Botrytis cinerea* reveals that prompt activation of specific host pathways leads to fungus quiescence. *Plant Cell Environ.* 40, 1409–28. doi: 10.1111/pce.12937

Harb, J., Alseekh, S., Tohge, T., and Fernie, A. R. (2015). Profiling of primary metabolites and flavonols in leaves of two table grape varieties collected from semiarid and temperate regions. *Phytochemistry* 117, 444–55. doi: 10.1016/j.phytochem.2015.07.013

Haug, K., Cochrane, K., Nainala, V. C., Williams, M., Chang, J., Jayaseelan, K. V., et al. (2020). MetaboLights: a resource evolving in response to the needs of its scientific community. *Nucleic Acids Res.* 48, D440–D444. doi: 10.1093/nar/gkz1019

Herrera, J. C., Hochberg, U., Degu, A., Sabbatini, P., Lazarovitch, N., Castellarin, S. D., et al. (2017). Grape metabolic response to postveraison water deficit is affected by interseason weather variability. *J. Agric. Food Chem.* 65, 5868–5878. doi: 10.1021/acs.jafc.7b01466

He, L., Xu, X.-Q., Wang, Y., Chen, W.-K., Sun, R.-Z., Cheng, G., et al. (2020). Modulation of volatile compound metabolome and transcriptome in grape berries exposed to sunlight under dry-hot climate. *BMC Plant Biol.* 20, 59. doi: 10.1186/s12870-020-2268-y

Hirai, M. Y., Klein, M., Fujikawa, Y., Yano, M., Goodenowe, D. B., Yamazaki, Y., et al. (2005). Elucidation of gene-to-gene and metabolite-to-gene networks in arabidopsis by integration of metabolomics and transcriptomics. *J. Biol. Chem.* 280, 25590–25595. doi: 10.1074/jbc.M502332200

Hochberg, U., Batushansky, A., Degu, A., Rachmilevitch, S., and Fait, A. (2015a). Metabolic and physiological responses of Shiraz and Cabernet sauvignon (*Vitis vinifera* l.) to near optimal temperatures of 25 and 35 °C. *Int. J. Mol. Sci.* 16, 24276–24294. doi: 10.3390/ijms161024276

Hochberg, U., Degu, A., Cramer, G. R., Rachmilevitch, S., and Fait, A. (2015b). Cultivar specific metabolic changes in grapevines berry skins in relation to deficit irrigation and hydraulic behavior. *Plant Physiol. Biochem.* 88, 42–52. doi: 10.1016/j.plaphy.2015.01.006

Hochberg, U., Degu, A., Toubiana, D., Gendler, T., Nikoloski, Z., Rachmilevitch, S., et al. (2013). Metabolite profiling and network analysis reveal coordinated changes in grapevine water stress response. *BMC Plant Biol.* 13, 184. doi: 10.1186/1471-2229-13-184

Hong, Y.-S., Martinez, A., Liger-Belair, G., Jeandet, P., Nuzillard, J.-M., and Cilindre, C. (2012). Metabolomics reveals simultaneous influences of plant defence system and fungal growth in *Botrytis cinerea*-infected *Vitis vinifera* cv. Chardonnay berries. *J. Exp. Bot.* 63, 5773–5785. doi: 10.1093/jxb/ers228

Jaillon, O., Aury, J. M., Noel, B., Policriti, A., Clepet, C., Casagrande, A., et al. (2007). The grapevine genome sequence suggests ancestral hexaploidization in major angiosperm phyla. *Nature* 449, 463–467. doi: 10.1038/nature06148

Kambiranda, D., Basha, S. M., Singh, R. K., He, H., Calvin, K., and Mercer, R. (2016). In depth proteome analysis of ripening muscadine grape berry cv. carlos reveals proteins associated with flavor and aroma compounds. *J. Proteome Res.* 15, 2910–2923. doi: 10.1021/acs.jproteome.5b01064

Kambiranda, D., Basha, S. M., Singh, R., Snowden, J., and Mercer, R. (2018). Proteome profile of american hybrid grape cv. blanc du Bois during ripening reveals proteins associated with flavor volatiles and ethylene production. *PROTEOMICS* 18, 1700305. doi: 10.1002/pmic.201700305

Kobayashi, S., Goto-Yamamoto, N., and Hirochika, H. (2004). Retrotransposon-induced mutations in grape skin color. *Science* 304, 982–982. doi: 10.1126/science.1095011

Kuang, L., Chen, S., Guo, Y., and Ma, H. (2019). Quantitative proteome analysis reveals changes in the protein landscape during grape berry development with a focus on vacuolar transport proteins. *Front. Plant Sci.* 10. doi: 10.3389/fpls.2019.00641

Langfelder, P., and Horvath, S. (2008). WGCNA: an r package for weighted correlation network analysis. *BMC Bioinf.* 9, 559. doi: 10.1186/1471-2105-9-559

Lawo, N. C., Weingart, G. J. F., Schuhmacher, R., and Forneck, A. (2011). The volatile metabolome of grapevine roots: First insights into the metabolic response upon phylloxera attack. *Plant Physiol. Biochem.* 49, 1059–1063. doi: 10.1016/j.plaphy.2011.06.008

Lecourieux, F., Kappel, C., Pieri, P., Charon, J., Pillet, J., Hilbert, G., et al. (2017). Dissecting the biochemical and transcriptomic effects of a locally applied heat treatment on developing Cabernet sauvignon grape berries. *Front. Plant Sci.* 8. doi: 10.3389/fpls.2017.00053

Liao, Y., Smyth, G. K., and Shi, W. (2014)featureCounts: an efficient general purpose program for assigning sequence reads to genomic features. *Bioinformatics* 30 (7), 923–930 doi: 10.1093/bioinformatics/btt656.

Lijavetzky, D., Carbonell-Bejerano, P., Grimplet, J., Bravo, G., Flores, P., Fenoll, J., et al. (2012). Berry flesh and skin ripening features in *Vitis vinifera* as assessed by transcriptional profiling. *PloS One* 7, e39547. doi: 10.1371/journal.pone.0039547

Liu, G.-T., Wang, J.-F., Cramer, G., Dai, Z.-W., Duan, W., Xu, H.-G., et al. (2012). Transcriptomic analysis of grape (*Vitis vinifera* l.) leaves during and after recovery from heat stress. *BMC Plant Biol.* 12, 174. doi: 10.1186/1471-2229-12-174

Liu, G.-T., Wang, B.-B., Lecourieux, D., Li, M.-J., Liu, M.-B., Liu, R.-Q., et al. (2021). Proteomic analysis of early-stage incompatible and compatible interactions between grapevine and p. *viticola. Hortic. Res.* 8, 1–21. doi: 10.1038/s41438-021-00533-y

Livigni, S., Lucini, L., Sega, D., Navacchi, O., Pandolfini, T., Zamboni, A., et al. (2019). The different tolerance to magnesium deficiency of two grapevine rootstocks relies on the ability to cope with oxidative stress. *BMC Plant Biol.* 19, 148. doi: 10.1186/s12870-019-1726-x

Li, X., Wu, J., Yin, L., Zhang, Y., Qu, J., and Lu, J. (2015). Comparative transcriptome analysis reveals defense-related genes and pathways against downy mildew in *Vitis amurensis* grapevine. *Plant Physiol. Biochem.* 95, 1–14. doi: 10.1016/j.plaphy.2015.06.016

Lorenzini, M., Millioni, R., Franchin, C., Zapparoli, G., Arrigoni, G., and Simonato, B. (2015). Identification of potential protein markers of noble rot infected grapes. *Food Chem.* 179, 170–174. doi: 10.1016/j.foodchem.2015.01.112

Loyola, R., Herrera, D., Mas, A., Wong, D. C. J., Höll, J., Cavallini, E., et al. (2016). The photomorphogenic factors UV-b RECEPTOR 1, ELONGATED HYPOCOTYL 5, and HY5 HOMOLOGUE are part of the UV-b signalling pathway in grapevine and mediate flavonol accumulation in response to the environment. *J. Exp. Bot.* 67, 5429–5445. doi: 10.1093/jxb/erw307

Magris, G., Jurman, I., Fornasiero, A., Paparelli, E., Schwope, R., Marroni, F., et al. (2021). The genomes of 204 *Vitis vinifera* accessions reveal the origin of European wine grapes. *Nat. Commun.* 12, 7240. doi: 10.1038/s41467-021-27487-y

Maia, M., Ferreira, A. E. N., Nascimento, R., Monteiro, F., Traquete, F., Marques, A. P., et al. (2020). Integrating metabolomics and targeted gene expression to uncover potential biomarkers of fungal/oomycetes-associated disease susceptibility in grapevine. *Sci. Rep.* 10, 15688. doi: 10.1038/s41598-020-72781-2

Malacarne, G., Costantini, L., Coller, E., Battilana, J., Velasco, R., Vrhovsek, U., et al. (2015). Regulation of flavonol content and composition in (Syrah×Pinot noir) mature grapes: integration of transcriptional profiling and metabolic quantitative trait locus analyses. *J. Exp. Bot.* 66, 4441–4453. doi: 10.1093/jxb/erv243

Malacarne, G., Vrhovsek, U., Zulini, L., Cestaro, A., Stefanini, M., Mattivi, F., et al. (2011). Resistance to *Plasmopara viticola* in a grapevine segregating population is associated with stilbenoid accumulation and with specific host transcriptional responses. *BMC Plant Biol.* 11, 114. doi: 10.1186/1471-2229-11-114

Mao, L., Van Hemert, J. L., Dash, S., and Dickerson, J. A. (2009). Arabidopsis gene co-expression network and its functional modules. *BMC Bioinf.* 10 (1), 346. doi: 10.1186/1471-2105-10-346

Martínez-Esteso, M. J., Casado-Vela, J., Sellés-Marchart, S., Elortza, F., Pedreño, M. A., and Bru-Martínez, R. (2011a). iTRAQ-based profiling of grape berry exocarp proteins during ripening using a parallel mass spectrometric method. *Mol. Biosyst.* 7, 749–765. doi: 10.1039/C0MB00194E

Martínez-Esteso, M. J., Sellés-Marchart, S., Lijavetzky, D., Pedreño, M. A., and Bru-Martínez, R. (2011b). A DIGE-based quantitative proteomic analysis of grape berry flesh development and ripening reveals key events in sugar and organic acid metabolism. *J. Exp. Bot.* 62, 2521–2569. doi: 10.1093/jxb/erq434

Martínez-Esteso, M. J., Vilella-Antón, M. T., Pedreño, M. Á., Valero, M. L., and Bru-Martínez, R. (2013). iTRAQ-based protein profiling provides insights into the central metabolism changes driving grape berry development and ripening. *BMC Plant Biol.* 13, 167. doi: 10.1186/1471-2229-13-167

Massonnet, M., Cochetel, N., Minio, A., Vondras, A. M., Lin, J., Muyle, A., et al. (2020). The genetic basis of sex determination in grapes. *Nat. Commun.* 11, 2902. doi: 10.1038/s41467-020-16700-z

Massonnet, M., Fasoli, M., Tornielli, G. B., Altieri, M., Sandri, M., Zuccolotto, P., et al. (2017). Ripening transcriptomic program in red and white grapevine varieties correlates with berry skin anthocyanin accumulation. *Plant Physiol.* 174, 2376–2396. doi: 10.1104/pp.17.00311

Mattivi, F., Guzzon, R., Vrhovsek, U., Stefanini, M., and Velasco, R. (2006). Metabolite profiling of grape: flavonols and anthocyanins. *J. Agric. Food Chem.* 54, 7692–7702. doi: 10.1021/jf061538c

Matus, J. T., Cavallini, E., Loyola, R., Höll, J., Finezzo, L., Dal Santo, S., et al. (2017). A group of grapevine MYBA transcription factors located in chromosome 14 control anthocyanin synthesis in vegetative organs with different specificities compared with the berry color locus. *Plant J.* 91 (2), 220–36. doi: 10.1111/tpj.13558

Matus, J. T., Ruggieri, V., Romero, F. J., Moretto, M., and Wong, D. C. J. (2019). "Status and prospects of systems biology in grapevine research," in *The grape genome, compendium of plant genomes*. Eds. D. Cantu and M. A. Walker (Cham: Springer International Publishing), 137–166. doi: 10.1007/978-3-030-18601-2_8

Milli, A., Cecconi, D., Bortesi, L., Persi, A., Rinalducci, S., Zamboni, A., et al. (2012). Proteomic analysis of the compatible interaction between *Vitis vinifera* and *Plasmopara viticola*. *J. Proteomics* 75, 1284–1302. doi: 10.1016/j.jprot.2011.11.006

Minio, A., Massonnet, M., Figueroa-Balderas, R., Castro, A., and Cantu, D. (2019a). Diploid genome assembly of the wine grape carménère. *G3 Genes|Genomes|Genetics* 9, 1331–1337. doi: 10.1534/g3.119.400030

Minio, A., Massonnet, M., Figueroa-Balderas, R., Vondras, A. M., Blanco-Ulate, B., and Cantu, D. (2019b). Iso-seq allows genome-independent transcriptome profiling of grape berry development. *G3: Genes Genomes Genet.* 9, 755–767. doi: 10.1534/g3.118.201008

Moretto, M., Sonego, P., Pilati, S., Malacarne, G., Costantini, L., Grzeskowiak, L., et al. (2016). VESPUCCI: Exploring patterns of gene expression in grapevine. *Front. Plant Sci.* 7. doi: 10.3389/fpls.2016.00633

Moretto, M., Sonego, P., Pilati, S., Matus, J. T., Costantini, L., Malacarne, G., et al. (2022). A COMPASS for VESPUCCI: A FAIR way to explore the grapevine transcriptomic landscape. *Front. Plant Sci.* 13. doi: 10.3389/fpls.2022.815443

Naithani, S., Raja, R., Waddell, E. N., Elser, J., Gouthu, S., Deluc, L. G., et al. (2014). VitisCyc: a metabolic pathway knowledgebase for grapevine (Vitis vinifera). *Front. Plant Sci.* 5. doi: 10.3389/fpls.2014.00644

Narduzzi, L., Stanstrup, J., and Mattivi, F. (2015). Comparing wild American grapes with *Vitis vinifera:* a metabolomics study of grape composition. *J. Agric. Food Chem.* 63, 6823–6834. doi: 10.1021/acs.jafc.5b01999

Nascimento-Gavioli, M. C. A., Agapito-Tenfen, S. Z., Nodari, R. O., Welter, L. J., Sanchez Mora, F. D., Saifert, L., et al. (2017). Proteome of *Plasmopara viticola*-infected *Vitis vinifera* provides insights into grapevine Rpv1/Rpv3 pyramided resistance to downy mildew. *J. Proteomics Braz. Proteomics* 151, 264–274. doi: 10.1016/j.jprot.2016.05.024

Navarro-Payá, D., Santiago, A., Orduña, L., Zhang, C., Amato, A., D'Inca, E., et al. (2022). The grape gene reference catalogue as a standard resource for gene selection and genetic improvement. *Front. Plant Sci.* 12. doi: 10.3389/fpls.2021.803977

Negrel, L., Halter, D., Wiedemann-Merdinoglu, S., Rustenholz, C., Merdinoglu, D., Hugueney, P., et al. (2018). Identification of lipid markers of *Plasmopara viticola* infection in grapevine using a non-targeted metabolomic approach. *Front. Plant Sci.* 9. doi: 10.3389/fpls.2018.00360

Negri, S., Lovato, A., Boscaini, F., Salvetti, E., Torriani, S., Commisso, M., et al. (2017). The induction of noble rot (*Botrytis cinerea*) infection during postharvest withering changes the metabolome of grapevine berries (*Vitis vinifera* l., cv. garganega). *Front. Plant Sci.* 8. doi: 10.3389/fpls.2017.01002

Negri, A. S., Prinsi, B., Rossoni, M., Failla, O., Scienza, A., Cocucci, M., et al. (2008a). Proteome changes in the skin of the grape cultivar barbera among different stages of ripening. *BMC Genomics* 9, 378. doi: 10.1186/1471-2164-9-378

Negri, A. S., Prinsi, B., Scienza, A., Morgutti, S., Cocucci, M., and Espen, L. (2008b). Analysis of grape berry cell wall proteome: A comparative evaluation of extraction methods. *J. Plant Physiol.* 165, 1379–1389. doi: 10.1016/j.jplph.2007.10.011

Nikiforova, V. J., Daub, C. O., Hesse, H., Willmitzer, L., and Hoefgen, R. (2005). Integrative gene-metabolite network with implemented causality deciphers informational fluxes of sulphur stress response. *J. Exp. Bot.* 56 (417), 1887–1896. doi: 10.1093/jxb/eri179

Niu, N., Cao, Y., Duan, W., Wu, B., and Li, S. (2013). Proteomic analysis of grape berry skin responding to sunlight exclusion. *J. Plant Physiol.* 170, 748–757. doi: 10.1016/j.jplph.2012.12.020

Nwafor, C. C., Gribaudo, I., Schneider, A., Wehrens, R., Grando, M. S., and Costantini, L. (2014). Transcriptome analysis during berry development provides insights into co-regulated and altered gene expression between a seeded wine grape variety and its seedless somatic variant. *BMC Genomics* 15, 1030. doi: 10.1186/1471-2164-15-1030

Orduña, L., Li, M., Navarro-Payá, D., Zhang, C., Santiago, A., Romero, P., et al. (2022). Direct regulation of shikimate, early phenylpropanoid and stilbenoid pathways by subgroup 2 R2R3-MYBs in grapevine. *Plant J* 110 (2), 529–547. doi: 10.1111/tpj.15686

Pagliarani, C., Moine, A., Chitarra, W., Meloni, G. R., Abbà, S., Nerva, L., et al. (2020). The molecular priming of defense responses is differently regulated in grapevine genotypes following elicitor application against powdery mildew. *Int. J. Mol. Sci.* 21, 6776. doi: 10.3390/ijms21186776

Pastore, C., Zenoni, S., Fasoli, M., Pezzotti, M., Tornielli, G. B., and Filippetti, I. (2013). Selective defoliation affects plant growth, fruit transcriptional ripening program and flavonoid metabolism in grapevine. *BMC Plant Biol.* 13, 30. doi: 10.1186/1471-2229-13-30

Pastore, C., Zenoni, S., Tornielli, G. B., Allegro, G., Dal Santo, S., Valentini, G., et al. (2011). Increasing the source/sink ratio in *Vitis vinifera* (cv sangiovese) induces extensive transcriptome reprogramming and modifies berry ripening. *BMC Genomics* 12, 631. doi: 10.1186/1471-2164-12-631

Perrone, I., Pagliarani, C., Lovisolo, C., Chitarra, W., Roman, F., and Schubert, A. (2012). Recovery from water stress affects grape leaf petiole transcriptome. *Planta* 235, 1383–1396. doi: 10.1007/s00425-011-1581-y

Pervaiz, T., Haifeng, J., Haider, M. S., Cheng, Z., Cui, M., Wang, M., et al. (2016). Transcriptomic analysis of grapevine (cv. summer black) leaf, using the illumina platform. *PloS One* 11, e0147369. doi: 10.1371/journal.pone.0147369

Pii, Y., Zamboni, A., Dal Santo, S., Pezzotti, M., Varanini, Z., and Pandolfini, T. (2017). Prospect on ionomic signatures for the classification of grapevine berries according to their geographical origin. *Front. Plant Sci.* 8. doi: 10.3389/fpls.2017.00640

Pilati, S., Brazzale, D., Guella, G., Milli, A., Ruberti, C., Biasioli, F., et al. (2014). The onset of grapevine berry ripening is characterized by ROS accumulation and lipoxygenase-mediated membrane peroxidation in the skin. *BMC Plant Biol.* 14, 87. doi: 10.1186/1471-2229-14-87

Pilati, S., Malacarne, G., Navarro-Payá, D., Tomè, G., Riscica, L., Cavecchia, V., et al. (2021). Vitis OneGenE: a causality-based approach to generate gene networks in vitis vinifera sheds light on the laccase and dirigent gene families. *Biomolecules* 11, 1744. doi: 10.3390/biom11121744

Pilati, S., Perazzolli, M., Malossini, A., Cestaro, A., Demattè, L., Fontana, P., et al. (2007). Genome-wide transcriptional analysis of grapevine berry ripening reveals a set of genes similarly modulated during three seasons and the occurrence of an oxidative burst at vèraison. *BMC Genomics* 8, 428. doi: 10.1186/1471-2164-8-428

Pimentel, D., Amaro, R., Erban, A., Mauri, N., Soares, F., Rego, C., et al. (2021). Transcriptional, hormonal, and metabolic changes in susceptible grape berries

under powdery mildew infection. *J. Exp. Bot.* 72, 6544–6569. doi: 10.1093/jxb/erab258

Pinasseau, L., Vallverdú-Queralt, A., Verbaere, A., Roques, M., Meudec, E., Le Cunff, L., et al. (2017). Cultivar diversity of grape skin polyphenol composition and changes in response to drought investigated by LC-MS based metabolomics. *Front. Plant Sci.* 8. doi: 10.3389/fpls.2017.01826

Polesani, M., Bortesi, L., Ferrarini, A., Zamboni, A., Fasoli, M., Zadra, C., et al. (2010). General and species-specific transcriptional responses to downy mildew infection in a susceptible (*Vitis vinifera*) and a resistant (V. riparia) grapevine species. *BMC Genomics* 11, 117. doi: 10.1186/1471-2164-11-117

Pontin, M. A., Piccoli, P. N., Francisco, R., Bottini, R., Martinez-Zapater, J. M., and Lijavetzky, D. (2010). Transcriptome changes in grapevine (*Vitis vinifera* l.) cv. Malbec leaves induced by ultraviolet-b radiation. *BMC Plant Biol.* 10, 224. doi: 10.1186/1471-2229-10-224

Pucker, B., Schwandner, A., Becker, S., Hausmann, L., Viehöver, P., Töpfer, R., et al. (2020). RNA-Seq time series of *Vitis vinifera* bud development reveals correlation of expression patterns with the local temperature profile. *Plants* 9, 1548. doi: 10.3390/plants9111548

Reshef, N., Agam, N., and Fait, A. (2018). Grape berry acclimation to excessive solar irradiance leads to repartitioning between major flavonoid groups. *J. Agric. Food Chem.* 66, 3624–3636. doi: 10.1021/acs.jafc.7b04881

Reshef, N., Walbaum, N., Agam, N., and Fait, A. (2017). Sunlight modulates fruit metabolic profile and shapes the spatial pattern of compound accumulation within the grape cluster. *Front. Plant Sci.* 8. doi: 10.3389/fpls.2017.00070

Rienth, M., Torregrosa, L., Kelly, M. T., Luchaire, N., Pellegrino, A., Grimplet, J., et al. (2014a). Is transcriptomic regulation of berry development more important at night than during the day? *PloS One* 9, e88844. doi: 10.1371/journal.pone.0088844

Rienth, M., Torregrosa, L., Luchaire, N., Chatbanyong, R., Lecourieux, D., Kelly, M. T., et al. (2014b). Day and night heat stress trigger different transcriptomic responses in green and ripening grapevine (*Vitis vinifera*) fruit. *BMC Plant Biol.* 14, 108. doi: 10.1186/1471-2229-14-108

Rienth, M., Torregrosa, L., Sarah, G., Ardisson, M., Brillouet, J.-M., and Romieu, C. (2016). Temperature desynchronizes sugar and organic acid metabolism in ripening grapevine fruits and remodels their transcriptome. *BMC Plant Biol.* 16, 164. doi: 10.1186/s12870-016-0850-0

Royo, C., Carbonell-Bejerano, P., Torres-Pérez, R., Nebish, A., Martínez, Ó., Rey, M., et al. (2016). Developmental, transcriptome, and genetic alterations associated with parthenocarpy in the grapevine seedless somatic variant corinto bianco. *J. Exp. Bot.* 67, 259–273. doi: 10.1093/jxb/erv452

Ruocco, S., Stefanini, M., Stanstrup, J., Perenzoni, D., Mattivi, F., and Vrhovsek, U. (2017). The metabolomic profile of red non-v. vinifera genotypes. *Food Research International* 98, 10–19. doi: 10.1016/j.foodres.2017.01.024

Saito, K., Hirai, M. Y., and Yonekura-Sakakibara, K. (2008). Decoding genes with coexpression networks and metabolomics – 'majority report by precogs. *Trends Plant Sci.* 13, 36–43. doi: 10.1016/j.tplants.2007.10.006

Santos, R. B., Nascimento, R., V. Coelho, A., and Figueiredo, A. (2020). Grapevine–downy mildew rendezvous: proteome analysis of the first hours of an incompatible interaction. *Plants* 9, 1498. doi: 10.3390/plants9111498

Sarry, J.-E., Sommerer, N., Sauvage, F.-X., Bergoin, A., Rossignol, M., Albagnac, G., et al. (2004). Grape berry biochemistry revisited upon proteomic analysis of the mesocarp. *Proteomics* 4, 201–15. doi: 10.1002/pmic.200300499

Savoi, S., Arapitsas, P., Duchêne, É., Nikolantonaki, M., Ontañón, I., Carlin, S., et al. (2021a). Grapevine and wine metabolomics-based guidelines for FAIR data and metadata management. *Metabolites* 11, 757. doi: 10.3390/metabo11110757

Savoi, S., Herrera, J. C., Forneck, A., and Griesser, M. (2019). Transcriptomics of the grape berry shrivel ripening disorder. *Plant Mol. Biol.* 100, 285–301. doi: 10.1007/s11103-019-00859-1

Savoi, S., Torregrosa, L., and Romieu, C. (2021b). Transcripts switched off at the stop of phloem unloading highlight the energy efficiency of sugar import in the ripening v. vinifera fruit. *Hortic. Res.* 8, 1–15. doi: 10.1038/s41438-021-00628-6

Savoi, S., Wong, D. C. J., Arapitsas, P., Miculan, M., Bucchetti, B., Peterlunger, E., et al. (2016). Transcriptome and metabolite profiling reveals that prolonged drought modulates the phenylpropanoid and terpenoid pathway in white grapes (*Vitis vinifera* l.). *BMC Plant Biol.* 16, 67. doi: 10.1186/s12870-016-0760-1

Savoi, S., Wong, D. C. J., Degu, A., Herrera, J. C., Bucchetti, B., Peterlunger, E., et al. (2017). Multi-omics and integrated network analyses reveal new insights into the systems relationships between metabolites, structural genes, and transcriptional regulators in developing grape berries (*Vitis vinifera* l.) exposed to water deficit. *Front. Plant Sci.* 8. doi: 10.3389/fpls.2017.01124

Shangguan, L., Chen, M., Fang, X., Xie, Z., Gong, P., Huang, Y., et al. (2020). Comparative transcriptome analysis provides insight into regulation pathways and temporal and spatial expression characteristics of grapevine (*Vitis vinifera*) dormant buds in different nodes. *BMC Plant Biol.* 20, 390. doi: 10.1186/s12870-020-02583-1

Shangguan, L., Mu, Q., Fang, X., Zhang, K., Jia, H., Li, X., et al. (2017). RNA-Sequencing reveals biological networks during table grapevine ('Fujiminori') fruit development. *PloS One* 12, e0170571. doi: 10.1371/journal.pone.0170571

Sreekantan, L., Mathiason, K., Grimplet, J., Schlauch, K., Dickerson, J. A., and Fennell, A. Y. (2010). Differential floral development and gene expression in grapevines during long and short photoperiods suggests a role for floral genes in dormancy transitioning. *Plant Mol. Biol.* 73, 191–205. doi: 10.1007/s11103-010-9611-x

Sun, R.-Z., Cheng, G., Li, Q., Zhu, Y.-R., Zhang, X., Wang, Y., et al. (2019). Comparative physiological, metabolomic, and transcriptomic analyses reveal developmental stage-dependent effects of cluster bagging on phenolic metabolism in Cabernet sauvignon grape berries. *BMC Plant Biol.* 19, 583. doi: 10.1186/s12870-019-2186-z

Suzuki, M., Nakabayashi, R., Ogata, Y., Sakurai, N., Tokimatsu, T., Goto, S., et al. (2015). Multiomics in grape berry skin revealed specific induction of the stilbene synthetic pathway by ultraviolet-c irradiation. *Plant Physiol.* 168, 47–59. doi: 10.1104/pp.114.254375

Sweetman, C., Wong, D. C., Ford, C. M., and Drew, D. P. (2012). Transcriptome analysis at four developmental stages of grape berry (*Vitis vinifera* cv. Shiraz) provides insights into regulated and coordinated gene expression. *BMC Genomics* 13, 691. doi: 10.1186/1471-2164-13-691

Tello-Ruiz, M. K., Naithani, S., Gupta, P., Olson, A., Wei, S., Preece, J., et al. (2021). Gramene 2021: harnessing the power of comparative genomics and pathways for plant research. *Nucleic Acids Res.* 49, D1452–D1463. doi: 10.1093/nar/gkaa979

Terrier, N., Glissant, D., Grimplet, J., Barrieu, F., Abbal, P., Couture, C., et al. (2005). Isogene specific oligo arrays reveal multifaceted changes in gene expression during grape berry (*Vitis vinifera* l.) development. *Planta* 222, 832–847. doi: 10.1007/s00425-005-0017-y

Theine, J., Holtgräwe, D., Herzog, K., Schwander, F., Kicherer, A., Hausmann, L., et al. (2021). Transcriptomic analysis of temporal shifts in berry development between two grapevine cultivars of the pinot family reveals potential genes controlling ripening time. *BMC Plant Biol.* 21, 327. doi: 10.1186/s12870-021-03110-6

Tian, B., Harrison, R., Morton, J., and Deb-Choudhury, S. (2015). Proteomic analysis of sauvignon blanc grape skin, pulp and seed and relative quantification of pathogenesis-related proteins. *PloS One* 10, e0130132. doi: 10.1371/journal.pone.0130132

Tuskan, G. A., DiFazio, S., Jansson, S., Bohlmann, J., Grigoriev, I., Hellsten, U., et al. (2006). The genome of black cottonwood, *Populus trichocarpa* (Torr. & Gray). *Science* 313, 1596–1604. doi: 10.1126/science.1128691

VanderWeide, J., Medina-Meza, I. G., Frioni, T., Sivilotti, P., Falchi, R., and Sabbatini, P. (2018). Enhancement of fruit technological maturity and alteration of the flavonoid metabolomic profile in merlot (*Vitis vinifera* l.) by early mechanical leaf removal. *J. Agric. Food Chem.* 66, 9839–9849. doi: 10.1021/acs.jafc.8b02709

Vannozzi, A., Palumbo, F., Magon, G., Lucchin, M., and Barcaccia, G. (2021). The grapevine (*Vitis vinifera* l.) floral transcriptome in pinot noir variety: identification of tissue-related gene networks and whorl-specific markers in pre- and post-anthesis phases. *Hortic. Res.* 8, 1–20. doi: 10.1038/s41438-021-00635-7

Velasco, R., Zharkikh, A., Troggio, M., Cartwright, D. A., Cestaro, A., Pruss, D., et al. (2007). A high quality draft consensus sequence of the genome of a heterozygous grapevine variety. *PloS One* 2, e1326. doi: 10.1371/journal.pone.0001326

Venturini, L., Ferrarini, A., Zenoni, S., Tornielli, G. B., Fasoli, M., Santo, S. D., et al. (2013). *De novo* transcriptome characterization of *Vitis vinifera* cv. corvina unveils varietal diversity. *BMC Genomics* 14, 41. doi: 10.1186/1471-2164-14-41

Vincent, D., Ergül, A., Bohlman, M. C., Tattersall, E. A. R., Tillett, R. L., Wheatley, M. D., et al. (2007). Proteomic analysis reveals differences between *Vitis vinifera* l. cv. Chardonnay and cv. Cabernet sauvignon and their responses to water deficit and salinity. *J. Exp. Bot.* 58, 1873–1892. doi: 10.1093/jxb/erm012

Vondras, A. M., Commisso, M., Guzzo, F., and Deluc, L. G. (2017). Metabolite profiling reveals developmental inequalities in pinot noir berry tissues late in ripening. *Front. Plant Sci.* 8. doi: 10.3389/fpls.2017.01108

Vondras, A. M., Minio, A., Blanco-Ulate, B., Figueroa-Balderas, R., Penn, M. A., Zhou, Y., et al. (2019). The genomic diversification of grapevine clones. *BMC Genomics* 20, 972. doi: 10.1186/s12864-019-6211-2

Vrhovsek, U., Lotti, C., Masuero, D., Carlin, S., Weingart, G., and Mattivi, F. (2014). Quantitative metabolic profiling of grape, apple and raspberry volatile compounds (VOCs) using a GC/MS/MS method. *J. Chromatogr. B Metabolomics II* 966, 132–9. doi: 10.1016/j.jchromb.2014.01.009

Waters, D. L. E., Holton, T. A., Ablett, E. M., Lee, L. S., and Henry, R. J. (2005). cDNA microarray analysis of developing grape (*Vitis vinifera* cv. Shiraz) berry skin. *Funct. Integr. Genomics* 5, 40–58. doi: 10.1007/s10142-004-0124-z

Weingart, G., Kluger, B., Forneck, A., Krska, R., and Schuhmacher, R. (2012). Establishment and application of a metabolomics workflow for identification and profiling of volatiles from leaves of *Vitis vinifera* by HS-SPME-GC-MS. *Phytochemical Anal.* 23, 345–58. doi: 10.1002/pca.1364

Weng, K., Li, Z.-Q., Liu, R.-Q., Wang, L., Wang, Y.-J., and Xu, Y. (2014). Transcriptome of *Erysiphe necator*-infected *Vitis pseudoreticulata* leaves provides insight into grapevine resistance to powdery mildew. *Hortic. Res.* 1, 1–12. doi: 10.1038/hortres.2014.49

Wilkinson, M. D., Dumontier, M., Aalbersberg, I., Appleton, G., Axton, M., Baak, A., et al. (2016). The FAIR guiding principles for scientific data management and stewardship. *Sci. Data* 3, 160018. doi: 10.1038/sdata.2016.18

Wong, D. C. J. (2020). Network aggregation improves gene function prediction of grapevine gene co-expression networks. *Plant Mol. Biol.* 103, 425–41. doi: 10.1007/s11103-020-01001-2

Wong, D. C. J., and Matus, J. T. (2017). Constructing integrated networks for identifying new secondary metabolic pathway regulators in grapevine: Recent applications and future opportunities. *Front. Plant Sci.* 8. doi: 10.3389/fpls.2017.00505

Wong, D. C., Sweetman, C., Drew, D. P., and Ford, C. M. (2013). VTCdb: a gene co-expression database for the crop species vitis vinifera (grapevine). *BMC Genomics* 14, 882. doi: 10.1186/1471-2164-14-882

Wu, J., Zhang, Y., Zhang, H., Huang, H., Folta, K. M., and Lu, J. (2010). Whole genome wide expression profiles of *Vitis amurensis* grape responding to downy mildew by using solexa sequencing technology. *BMC Plant Biol.* 10, 234. doi: 10.1186/1471-2229-10-234

Xin, H., Zhu, W., Wang, L., Xiang, Y., Fang, L., Li, J., et al. (2013). Genome wide transcriptional profile analysis of *Vitis amurensis* and *Vitis vinifera* in response to cold stress. *PloS One* 8, e58740. doi: 10.1371/journal.pone.0058740

Yang, B., He, S., Liu, Y., Liu, B., Ju, Y., Kang, D., et al. (2020). Transcriptomics integrated with metabolomics reveals the effect of regulated deficit irrigation on anthocyanin biosynthesis in Cabernet sauvignon grape berries. *Food Chem.* 314, 126170. doi: 10.1016/j.foodchem.2020.126170

Yu, J., Hu, S., Wang, J., Wong, G. K.-S., Li, S., Liu, B., et al. (2002). A draft sequence of the rice genome (*Oryza sativa* l. *ssp. indica). Sci.* 296, 79–92. doi: 10.1126/science.1068037

Zamboni, A., Carli, M. D., Guzzo, F., Stocchero, M., Zenoni, S., Ferrarini, A., et al. (2010). Identification of putative stage-specific grapevine berry biomarkers and omics data integration into networks. *Plant Physiol.* 154, 1439–1459. doi: 10.1104/pp.110.160275

Zenoni, S., Amato, A., D'Incà, E., Guzzo, F., and Tornielli, G. B. (2020). Rapid dehydration of grape berries dampens the post-ripening transcriptomic program and the metabolite profile evolution. *Horticulture Res.* 7, 1–15. doi: 10.1038/s41438-020-00362-5

Zenoni, S., Dal Santo, S., Tornielli, G. B., D'Incà, E., Filippetti, I., Pastore, C., et al. (2017). Transcriptional responses to pre-flowering leaf defoliation in grapevine berry from different growing sites, years, and genotypes. *Front. Plant Sci.* 8. doi: 10.3389/fpls.2017.00630

Zenoni, S., Fasoli, M., Guzzo, F., Santo, S. D., Amato, A., Anesi, A., et al. (2016). Disclosing the molecular basis of the postharvest life of berry in different grapevine genotypes. *Plant Physiol.* 172, 1821–1843. doi: 10.1104/pp.16.00865

Zenoni, S., Ferrarini, A., Giacomelli, E., Xumerle, L., Fasoli, M., Malerba, G., et al. (2010). Characterization of transcriptional complexity during berry development in *Vitis vinifera* using RNA-seq. *Plant Physiol.* 152, 1787–95. doi: 10.1104/pp.109.149716

Zhang, C., Dai, Z., Ferrier, T., Orduña, L., Santiago, A., Peris, A., et al. (2021). The grape MYB24 mediates the coordination of light-induced terpene and flavonolaccumulation in response to berry anthocyanin sunscreen depletio. *BioRxiv*. doi: 10.1101/2021.12.16.472692

Zhang, K., Li, W., Ju, Y., Wang, X., Sun, X., Fang, Y., et al. (2021). Transcriptomic and metabolomic basis of short- and long-term post-harvest UV-c application in regulating grape berry quality development. *Foods* 10, 625. doi: 10.3390/foods10030625

Zhang, J., Ma, H., Feng, J., Zeng, L., Wang, Z., and Chen, S. (2008). Grape berry plasma membrane proteome analysis and its differential expression during ripening. *J. Exp. Bot.* 59, 2979–90. doi: 10.1093/jxb/ern156

Zhao, L., Chanon, A. M., Chattopadhyay, N., Dami, I. E., and Blakeslee, J. J. (2016). Quantification of carbohydrates in grape tissues using capillary zone electrophoresis. *Front. Plant Sci.* 0. doi: 10.3389/fpls.2016.00818

Zhou, Y., Minio, A., Massonnet, M., Solares, E., Lv, Y., Beridze, T., et al. (2019). The population genetics of structural variants in grapevine domestication. *Nat. Plants* 5, 965–979. doi: 10.1038/s41477-019-0507-8

Advantages of publishing in Frontiers

OPEN ACCESS
Articles are free to read for greatest visibility and readership

FAST PUBLICATION
Around 90 days from submission to decision

HIGH QUALITY PEER-REVIEW
Rigorous, collaborative, and constructive peer-review

TRANSPARENT PEER-REVIEW
Editors and reviewers acknowledged by name on published articles

Frontiers
Avenue du Tribunal-Fédéral 34
1005 Lausanne | Switzerland

Visit us: www.frontiersin.org
Contact us: frontiersin.org/about/contact

REPRODUCIBILITY OF RESEARCH
Support open data and methods to enhance research reproducibility

DIGITAL PUBLISHING
Articles designed for optimal readership across devices

FOLLOW US
@frontiersin

IMPACT METRICS
Advanced article metrics track visibility across digital media

EXTENSIVE PROMOTION
Marketing and promotion of impactful research

LOOP RESEARCH NETWORK
Our network increases your article's readership